BRAIN DISEASE MECHANISMS - EDITOR'S PICKS 2021

EDITED BY: Detlev Boison
PUBLISHED IN: Frontiers in Molecular Neuroscience

frontiers Research Topics

ISSN 1664-8714
ISBN 978-2-88971-063-8
DOI 10.3389/978-2-88971-063-8

About Frontiers

Frontiers is more than just an open-access publisher of scholarly articles: it is a pioneering approach to the world of academia, radically improving the way scholarly research is managed. The grand vision of Frontiers is a world where all people have an equal opportunity to seek, share and generate knowledge. Frontiers provides immediate and permanent online open access to all its publications, but this alone is not enough to realize our grand goals.

Frontiers Journal Series

The Frontiers Journal Series is a multi-tier and interdisciplinary set of open-access, online journals, promising a paradigm shift from the current review, selection and dissemination processes in academic publishing. All Frontiers journals are driven by researchers for researchers; therefore, they constitute a service to the scholarly community. At the same time, the Frontiers Journal Series operates on a revolutionary invention, the tiered publishing system, initially addressing specific communities of scholars, and gradually climbing up to broader public understanding, thus serving the interests of the lay society, too.

Dedication to Quality

Each Frontiers article is a landmark of the highest quality, thanks to genuinely collaborative interactions between authors and review editors, who include some of the world's best academicians. Research must be certified by peers before entering a stream of knowledge that may eventually reach the public - and shape society; therefore, Frontiers only applies the most rigorous and unbiased reviews.
Frontiers revolutionizes research publishing by freely delivering the most outstanding research, evaluated with no bias from both the academic and social point of view. By applying the most advanced information technologies, Frontiers is catapulting scholarly publishing into a new generation.

What are Frontiers Research Topics?

Frontiers Research Topics are very popular trademarks of the Frontiers Journals Series: they are collections of at least ten articles, all centered on a particular subject. With their unique mix of varied contributions from Original Research to Review Articles, Frontiers Research Topics unify the most influential researchers, the latest key findings and historical advances in a hot research area! Find out more on how to host your own Frontiers Research Topic or contribute to one as an author by contacting the Frontiers Editorial Office: frontiersin.org/about/contact

BRAIN DISEASE MECHANISMS - EDITOR'S PICKS 2021

Topic Editor:
Detlev Boison, Robert Wood Johnson Medical School, United States

Citation: Boison, D., ed. (2021). Brain Disease Mechanisms - Editor's Picks 2021. Lausanne: Frontiers Media SA. doi: 10.3389/978-2-88971-063-8

Table of Contents

05 ***Clinical Imaging of Choroid Plexus in Health and in Brain Disorders: A Mini-Review***
Violaine Hubert, Fabien Chauveau, Chloé Dumot, Elodie Ong, Lise-Prune Berner, Emmanuelle Canet-Soulas, Jean-François Ghersi-Egea and Marlène Wiart

13 ***Parkin Promotes Mitophagic Cell Death in Adult Hippocampal Neural Stem Cells Following Insulin Withdrawal***
Hyunhee Park, Kyung Min Chung, Hyun-Kyu An, Ji-Eun Gim, Jihyun Hong, Hanwoong Woo, Bongki Cho, Cheil Moon and Seong-Woon Yu

31 ***Exogenous Ketone Supplementation Decreased the Lipopolysaccharide-Induced Increase in Absence Epileptic Activity in Wistar Albino Glaxo Rijswijk Rats***
Zsolt Kovács, Dominic P. D'Agostino, David M. Diamond and Csilla Ari

43 ***Dexamethasone in Glioblastoma Multiforme Therapy: Mechanisms and Controversies***
Marta Cenciarini, Mario Valentino, Silvia Belia, Luigi Sforna, Paolo Rosa, Simona Ronchetti, Maria Cristina D'Adamo and Mauro Pessia

56 ***Stimulation of Sphingosine Kinase 1 (SPHK1) Is Beneficial in a Huntington's Disease Pre-clinical Model***
Alba Di Pardo, Giuseppe Pepe, Salvatore Castaldo, Federico Marracino, Luca Capocci, Enrico Amico, Michele Madonna, Susy Giova, Se Kyoo Jeong, Bu-Mahn Park, Byeong Deog Park and Vittorio Maglione

67 ***Cancer Stem Cells in Neuroblastoma: Expanding the Therapeutic Frontier***
Hisham F. Bahmad, Farah Chamaa, Sahar Assi, Reda M. Chalhoub, Tamara Abou-Antoun and Wassim Abou-Kheir

84 ***Post-translational Regulation of GLT-1 in Neurological Diseases and Its Potential as an Effective Therapeutic Target***
Allison R. Peterson and Devin K. Binder

95 ***Sex-Dependent Changes in miRNA Expression in the Bed Nucleus of the Stria Terminalis Following Stress***
Maria Mavrikaki, Lorena Pantano, David Potter, Maximilian A. Rogers-Grazado, Eleni Anastasiadou, Frank J. Slack, Sami S. Amr, Kerry J. Ressler, Nikolaos P. Daskalakis and Elena Chartoff

109 ***CSF Cholinergic Index, a New Biomeasure of Treatment Effect in Patients With Alzheimer's Disease***
Azadeh Karami, Maria Eriksdotter, Ahmadul Kadir, Ove Almkvist, Agneta Nordberg and Taher Darreh-Shori

124 ***Evaluation of Biochemical and Epigenetic Measures of Peripheral Brain-Derived Neurotrophic Factor (BDNF) as a Biomarker in Huntington's Disease Patients***
Ashley Gutierrez, Jody Corey-Bloom, Elizabeth A. Thomas and Paula Desplats

135 ***Dysregulation of RNA-Binding Proteins in Amyotrophic Lateral Sclerosis***
Yuan Chao Xue, Chen Seng Ng, Pinhao Xiang, Huitao Liu, Kevin Zhang, Yasir Mohamud and Honglin Luo

146 ***Circulating microRNAs Profile in Patients With Transthyretin Variant Amyloidosis***
Gian Luca Vita, M'Hammed Aguennouz, Francesca Polito, Rosaria Oteri, Massimo Russo, Luca Gentile, Cristina Barbagallo, Marco Ragusa, Carmelo Rodolico, Rosa Maria Di Giorgio, Antonio Toscano, Giuseppe Vita and Anna Mazzeo

frontiers in Molecular Neuroscience

MINI REVIEW
published: 12 February 2019
doi: 10.3389/fnmol.2019.00034

Clinical Imaging of Choroid Plexus in Health and in Brain Disorders: A Mini-Review

*Violaine Hubert[1], Fabien Chauveau[2,3], Chloé Dumot[1,4], Elodie Ong[1,4], Lise-Prune Berner[4], Emmanuelle Canet-Soulas[1], Jean-François Ghersi-Egea[5] and Marlène Wiart[1,3]**

[1] Univ-Lyon, CarMeN Laboratory, Inserm U1060, INRA U1397, Université Claude Bernard Lyon 1, INSA Lyon, Charles Mérieux Medical School, Oullins, France, [2] CNRS UMR5292, INSERM U1028, BIORAN Team, Lyon Neuroscience Research Center, Université Claude Bernard Lyon 1, Lyon, France, [3] CNRS, Lyon, France, [4] HCL, Lyon, France, [5] CNRS UMR5292, INSERM U1028, Fluid Team and BIP Facility, Lyon Neuroscience Research Center, Université Claude Bernard Lyon 1, Lyon, France

The choroid plexuses (ChPs) perform indispensable functions for the development, maintenance and functioning of the brain. Although they have gained considerable interest in the last years, their involvement in brain disorders is still largely unknown, notably because their deep location inside the brain hampers non-invasive investigations. Imaging tools have become instrumental to the diagnosis and pathophysiological study of neurological and neuropsychiatric diseases. This review summarizes the knowledge that has been gathered from the clinical imaging of ChPs in health and brain disorders not related to ChP pathologies. Results are discussed in the light of pre-clinical imaging studies. As seen in this review, to date, most clinical imaging studies of ChPs have used disease-free human subjects to demonstrate the value of different imaging biomarkers (ChP size, perfusion/permeability, glucose metabolism, inflammation), sometimes combined with the study of normal aging. Although very few studies have actually tested the value of ChP imaging biomarkers in patients with brain disorders, these pioneer studies identified ChP changes that are promising data for a better understanding and follow-up of diseases such as schizophrenia, epilepsy and Alzheimer's disease. Imaging of immune cell trafficking at the ChPs has remained limited to pre-clinical studies so far but has the potential to be translated in patients for example using MRI coupled with the injection of iron oxide nanoparticles. Future investigations should aim at confirming and extending these findings and at developing translational molecular imaging tools for bridging the gap between basic molecular and cellular neuroscience and clinical research.

Keywords: choroid plexus, imaging, central nervous system, blood-CSF barrier, inflammation, neurological disease

OPEN ACCESS

Edited by:
Taher Darreh-Shori, Karolinska Institutet (KI), Sweden

Reviewed by:
Alessandra Pelagalli, University of Naples Federico II, Italy
Naguib Mechawar, McGill University, Canada
Ignacio Torres-Aleman, Spanish National Research Council (CSIC), Spain
Fernanda Marques, University of Minho, Portugal

***Correspondence:**
Marlène Wiart
marlene.wiart@univ-lyon1.fr

Received: *12 November 2018*
Accepted: *25 January 2019*
Published: *12 February 2019*

Citation:
Hubert V, Chauveau F, Dumot C, Ong E, Berner L-P, Canet-Soulas E, Ghersi-Egea J-F and Wiart M (2019) Clinical Imaging of Choroid Plexus in Health and in Brain Disorders: A Mini-Review. Front. Mol. Neurosci. 12:34. doi: 10.3389/fnmol.2019.00034

Abbreviations: AD, Alzheimer's disease; ASD, autism spectrum disorders; BCSFB, blood-CSF barrier; ChP, choroid plexus; CRPS, complex regional pain syndrome; CSF, cerebrospinal fluid; CT, computed tomography; IIH, idiopathic intracranial hypertension; MRI, magnetic resonance imaging; MS, multiple sclerosis; PET, positron emission tomography; US, ultrasound.

INTRODUCTION

The choroid plexuses (ChPs) are small structures located in the lateral, third, and fourth brain ventricles. They are formed by numerous villi organized as a tight epithelium enclosing a highly vascularized stromal core that contains immune cells and fibroblasts. The ChPs produce the cerebrospinal fluid (CSF), form a protective barrier between the blood and the CSF (the blood-CSF barrier, BCSFB) and secrete various biologically active molecules. Hence, they play a vital role in maintaining the microenvironment in which the brain is located (Ghersi-Egea et al., 2018). The ChPs are also crucial for immune surveillance of the brain and provide a port of entry for immune cells in a range of neurological diseases (Schwartz and Baruch, 2014). The development of therapeutic strategies to protect the BCSFB may be helpful for the management of these diseases and is thus gaining a growing interest (Dragunow, 2013). However, to date, the role of ChP involvement in brain disorders is largely unknown, notably because their deep location inside the brain hampers non-invasive investigations. Imaging tools have become instrumental to the diagnosis and pathophysiological study of neurological and neuropsychiatric diseases. This review summarizes the knowledge gathered through clinical imaging of ChPs in health and neurological or neuropsychiatric disease not related to a primary ChP pathology.

METHODS

Supplementary Figure 1 presents the literature search flow chart. **Supplementary Table 1** shows the summary of included studies. Note that the review does not include primary ChP pathology diseases such as ChP tumors, ventriculomegaly, and hydrocephalus. Results are discussed in the light of pre-clinical imaging studies whenever available.

RESULTS

Morphology

Choroid plexuse size can be quantified with standard computed tomography (CT) and magnetic resonance imaging (MRI) approaches, and with ultrasound (US) in fetal or newborn infants. Contrast agent administration might be used to improve delineation. Madhukar et al. (2012) documented the size of normal ChPs in children between the ages of 0 and 16 years old. This study was intended to provide reference data to allow the detection of abnormal ChP size in developmental diseases, in the continuity of earlier studies that measured ChP size increase due to choroidal angiomatosis in children with Sturge-Weber syndromes (Stimac et al., 1986; Griffiths et al., 1996). However, it did not lead to further publications to date.

While performing an MRI morphometric brain analysis study in patients suffering from type 1 complex regional pain syndrome (CRPS), Zhou et al. (2015) serendipitously found a significant enlargement of ChPs compared with controls. The same phenomenon was observed with MRI in patients with idiopathic intracranial hypertension (IIH) (**Figure 1A**; Lublinsky et al., 2018). Using a different approach based on MRI texture analysis, Chaddad et al. (2017) identified ChPs as one of the regions having the most significant differences between patients with autism spectrum disorders (ASD) and controls. According to the authors, all these effects could result from the activation of several biological processes including the presence of edema and/or proliferation of ChP cells. Dedicated imaging techniques for evaluating CSF production (see below) may help investigate these hypotheses. Besides, if indeed increased ChP size observed by imaging techniques reflects an increase in ChP epithelial cell number, then it is likely that important choroidal functions other than CSF secretion, such as trophic factors and hormone carrier secretion, will be impacted as well.

Advanced MRI techniques such as diffusion-weighted/diffusion tensor imaging (DWI/DTI) can be used to detect microstructural tissue changes. DTI metrics have been measured in the ChPs of human subjects thus showing the feasibility of this imaging technique to characterize the ChPs despite their small size (Grech-Sollars et al., 2015). The apparent diffusion coefficient (ADC), reflecting the molecular motion of water in the interstitial space, was shown to increase with aging in ChPs (Alicioglu et al., 2017). According to the authors, this effect may be related to increased water diffusion across the epithelium via paracellular spaces, thus signaling BCSFB malfunction.

Calcifications

The occurrence of macroscopic calcifications can be detected on CT and on T2*-weighted MRI scans. ChP calcification increases in frequency and extent with age and is usually not associated with a pathology (Yalcin et al., 2016). However, Bersani et al. (1999) suggested a possible association between the size of ChP calcification and the severity of symptoms in schizophrenic patients independently of age, in line with a former study also based on CT-scan (Sandyk, 1993). The cause remains unclear and these results should be considered with caution as they have not been replicated to date.

CSF Production

Because changes in CSF production rate likely contribute to pathological processes, as exemplified in Alzheimer's disease (Silverberg et al., 2001; Serot et al., 2012), a validated imaging biomarker of CSF production may be valuable for investigating the involvement of ChPs in brain diseases. Net CSF flow through the cerebral aqueduct may serve as a marker of CSF production in the lateral ventricles, i.e., by the ChPs (Spijkerman et al., 2018). This flow may be estimated in humans using an phase-contrast MRI technique (Huang et al., 2004); however, the relationship between these measurements and CSF production has been recently questioned (Spijkerman et al., 2018). Of note, CSF production has choroidal and extrachoroidal components. The imaging of extrachoroidal CSF production and extraventricular CSF circulation is outside the scope of this review; however, because it is in close relation with CSF production at the ChPs, we briefly reviewed this literature in the **Supplementary Data 1**.

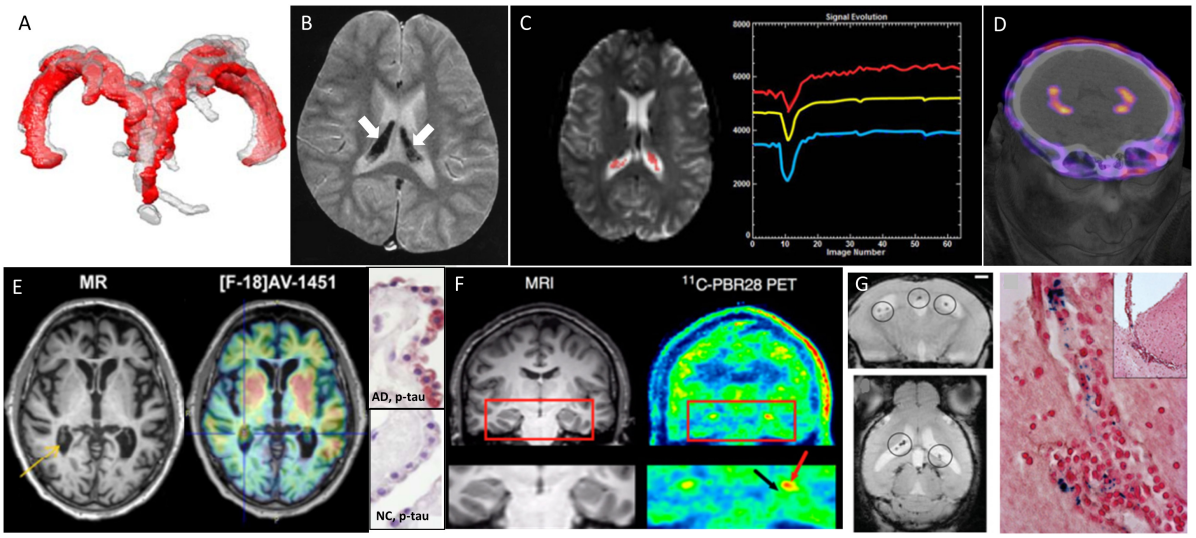

FIGURE 1 | Examples of different clinical imaging techniques available for investigating the involvement of ChPs in brain disorders. **(A)** 3D reconstruction of ChP located within lateral ventricles space [red, before lumbar puncture (LP), and gray, after LP] in a patient with idiopathic intracranial hypertension (Lublinsky et al., 2018); **(B)** ChP iron deposition (arrows on hypointense signals) detected by susceptibility-weighted MRI in a patient who had received both ultrasmall superparamagnetic particles of iron oxide (USPIOs) 2 years earlier and multiple blood transfusions since (Daldrup-Link, 2017); **(C)** signal-time curves extracted in the ChP from dynamic susceptibility contras-enhanced MRI data: the yellow curve represents the mean signal calculated from all the pixels in the ChP volume, while the blue and red curves represent, respectively, the curve with lowest and highest baseline. After first passage of the gadolinium bolus (signal drop), the choroidal signals visually exceed the baseline which indicates gadolinium chelate extravasation into the ChP stroma (Bouzerar et al., 2013); **(D)** PET/CT images showing the normal ChP uptake of [^{68}Ga]-DOTA-E-[c(RGDfK)]$_2$ targeting $\alpha_v\beta_3$ integrin (*This research was originally published in JNM.* Lopez-Rodriguez et al., 2016); **(E)** *in vivo* imaging using the Tau tracer [^{18}F]AV-1451 showing high retention in AD patient and post-mortem ChP histopathology showing immunoreactivity in epithelial cells (pink color) with antibodies against pan-Tau in AD but not in normal control (NC) (Ikonomovic et al., 2016); **(F)** MRI and translocator protein (TSPO) labeling [^{11}C]PBR28 PET images in a patient with left-sided temporal lobe epilepsy showing higher uptake in ipsilateral than in contralateral side in the ChP of lateral ventricles (red arrow) and hippocampus (black arrow) (*This research was originally published in JNM.* Hirvonen et al., 2012); **(G)** *in vivo* MRI using the very small particles of iron oxide (VSOP) and post-mortem Prussian Blue staining in a rat model of multiple sclerosis: VSOP (circles) was detected in the inflamed ChP at peak disease (Millward et al., 2013).

Iron Deposits

Choroid plexuses are involved in iron exchanges between the blood and the brain (Morris et al., 1992; Deane et al., 2004; Rouault et al., 2009). They secrete transferrin (Leitner and Connor, 2012) and serve as an iron storage tissue (Lu et al., 1995; Rouault et al., 2009). MRI is a powerful tool to detect excessive iron in the brain. Several teams have reported iron deposition in ChPs of patients with transfusion-induced iron overload (**Figure 1B**; Kira et al., 2000; Qiu et al., 2014; Hasiloglu et al., 2017). Age-associated iron deposits were also documented in ChPs of mouse lemur, a non-human primate model of pathological brain aging (Joseph-Mathurin et al., 2013). The authors showed that immunization against Aβ worsened ChP iron deposits and suggested that MRI of human subjects immunized against Aβ should be evaluated to determine whether iron accumulation also occurred in humans.

Capillary Perfusion and Permeability

The ChP blood flow is about fivefold higher than the cerebral blood flow (Maktabi et al., 1990). In contrast to the blood-brain barrier (BBB), the ChP capillaries are fenestrated and permeable, allowing free communication between the ChP stroma and the peripheral blood for molecules of different sizes. In physiological conditions, macromolecules with molecular weights up to ∼800 kDa or size ∼12 nm may diffuse into the ChP stroma (Strazielle and Ghersi-Egea, 2013). As a consequence, conventional contrast agents used in clinical MRI and CT (<2 kDa) diffuse into the stroma of ChPs, leading to homogenous enhancement (Guermazi et al., 2000). This physiological enhancement may be used to normalize abnormal brain enhancements (Miller et al., 2016; Vakil et al., 2017; Kim et al., 2018). In turn, Azuma et al. (2018) proposed a 4-point scale to score physiological enhancement of circumventricular organs including ChPs, on MRI, with the aim of recognizing abnormal enhancement in future investigations. Furthermore, ChP capillary permeability and perfusion may be quantified by dynamic contrast-enhanced/dynamic susceptibility contrast enhanced MRI (DCE/DSC-MRI) (**Figure 1C**; Artzi et al., 2013; Bouzerar et al., 2013; Vakil et al., 2017). This latter approach was used to show that ChP capillary permeability and perfusion decreased with aging (Bouzerar et al., 2013). In a mouse model of AD, stromal leakage of an iodinated liposome (size: 100–150 nm) was found in ChPs using microCT (Tanifum et al., 2014). However, the quantification of this leakage did not significantly differ compared to aged-matched control wild-type animals, thus suggesting that this phenomenon was independent from the pathology. Hence further studies are needed to determine whether the measurement of capillary perfusion and/or permeability at ChPs might serve as a biomarker in neurodegenerative diseases.

BCSFB Permeability

The BCSFB at the ChPs is formed by the epithelium whose cells are sealed with tight junctions. As a consequence, no enhancement is seen in the CSF after contrast medium administration, unless the BCSFB is damaged. In patients, reports of contrast medium leakage into the brain ventricles are scarce (excluding cases of hemorrhage; Phatouros et al., 1999). A case of contrast leakage mimicking intraventricular hemorrhage was recently described in an ischemic stroke patient who had been treated with intravenous thrombolysis (IVT) (Park et al., 2017). A study investigating a small series of ischemic stroke patients undergoing mechanical thrombectomy in combination with IVT reported a blood-CSF arachnoid barrier disruption only (Renu et al., 2017). In pre-clinical ischemic stroke studies, two teams have reported MRI contrast medium leakage into the ventricles early after reperfusion (Nagahiro et al., 1994; Batra et al., 2010), in line with a previous study showing an increase in BCSFB permeability in rat models of focal cerebral ischemia (Ennis and Keep, 2006). Other brain pathologies that have been shown to display intraventricular conventional contrast medium extravasation in small animal models include Wernicke's encephalopathy (Nixon et al., 2008), meningitis (Ichikawa et al., 2010), and experimental autoimmune encephalomyelitis (EAE), an animal model of multiple sclerosis (MS) (Wuerfel et al., 2010; Waiczies et al., 2012).

In turn, BCSFB integrity represents a hurdle for delivering drugs to the brain. The assessment of the drug-permeability barrier at the level of the ChP epithelium is therefore a desirable aim to understand cerebral pharmacokinetics. Non-metabolized radiotracers transported by both P-glycoprotein (ABCB1, also known as multidrug resistance protein) and multidrug resistant associated proteins (MRPs and ABCCs) have been used to this aim: the radiolabeled drug localized to ChPs with no detectable activity in adjacent CSF whether in healthy (Rao et al., 1999) or in epileptic subjects (Langer et al., 2007), such showing the efficacy of the BCSFB to prevent drug entry into the CSF. As MRPs rather than P-glycoprotein are expressed in ChPs both in rodent and humans (Gazzin et al., 2008), it is likely that the former plays a special role as biochemical barrier at ChPs. Another pre-clinical example is represented by the presence of ^{64}Cu-labeled fusion protein etanercept (a TNF antagonist) into both the CSF and the ChPs following intravenous perispinal administration (Tobinick et al., 2009), thus demonstrating the potential of such techniques to investigate drug-concentration in both compartments.

Receptor Imaging

In the literature, there are a number of PET studies that mention ChP non-specific uptake due to radiotracer extravasation or binding to calcification, which were thus excluded from this mini-review. A few studies, however, suggested specific ChP uptake of tracers targeting $\alpha_v\beta_3$ integrins (**Figure 1D**; Minamimoto et al., 2015; Lopez-Rodriguez et al., 2016) or serotonin receptors (5-HTRs) (Ettrup et al., 2016; Schankin et al., 2016). An fMRI study also reported an increased BOLD signal in ChPs of volunteers administered with a 5-HT_{2C} receptor agonist (Anderson et al., 2002). This is in line with the known expression of these receptors in ChPs. Altogether these data suggest that imaging ChP receptors is feasible in humans.

Proteinopathies

Proteinopathies can be explored with PET radiotracers targeted at aggregated proteins; yet, in these brain imaging studies, ChPs are usually disregarded because signal enhancement is thought to reflect non-specific uptake, also called "off-target binding" (Lowe et al., 2016). However, in the case of the recently developed Tau radiotracer flortaucipir (also known as [^{18}F]AV-1451 or [^{18}F]-T807), elevated ChP binding has attracted considerable interest because of ChP proximity (and potential signal contamination) to hippocampus, a key region for staging tauopathy in Alzheimer's disease (AD) (Pontecorvo et al., 2017; Lee et al., 2018). At the moment, there are conflicting reports on the substrate of this radiotracer uptake in ChPs: while off-target binding to leptomeningeal melanocytes (adjacent to the lateral ventricles; Marquie et al., 2017), or to ChP calcifications (Lowe et al., 2016), have been suggested by autoradiographic studies, Ikonomovic et al. (2016) reported the histological detection of Tau protein aggregates in ChP epithelial cells, thus suggesting a possible "on-target" binding (**Figure 1E**). Therefore there is still an open debate regarding the interpretation of ChP signals in PET studies of proteinopathies.

In addition, the accumulation of aggregated proteins within epithelial cells may alter the ChP metabolic activity. Daouk et al. hypothesized that dynamic PET imaging with ^{18}F-FDG could be useful to assess glucose metabolism as a marker of ChP epithelium activity in elderly adults, with a view to early diagnosis of AD. The FDG uptake in ChPs decreased with increasing disease severity, thereby providing the proof-of-concept that PET-FDG is feasible and useful to study ChP functional behavior in AD patients (Daouk et al., 2016).

Immune Responses

The ChP stroma contains immune cells such as macrophages, neutrophils, dendritic cells, B and T cells and serves as a gateway for immune cell trafficking into the CSF (Ghersi-Egea et al., 2018). PET imaging of translocator protein 18 kDa (TSPO) is the method of choice for clinically evaluating neuroinflammation (Kreisl et al., 2016) as it is overexpressed in activated microglia/macrophages. In patients with unilateral temporal lobe epilepsy, a higher uptake of the TSPO radiotracer [^{11}C]PBR28 was observed in the ChPs ipsilateral to the seizure focus (**Figure 1F**; Hirvonen et al., 2012). In a mouse model of chronic systemic inflammation, Drake et al. (2011) showed with histological experiments an intense recruitment of activated immune cells at ChPs, while in their parallel human study, they did not examine a potential uptake of the TSPO radiotracer ^{11}C-PK11195 in ChPs of patients at risk of stroke, probably because of the expected "off-target" effect.

Alternatively, neuroinflammation may be assessed with MRI by labeling cells with a contrast agent. Reticuloendothelial MRI contrast media (such as superparamagnetic particles of iron oxide or SPIO) are taken up by phagocytic cells following their intravenous administration. SPIO-enhanced MRI has been extensively used to monitor phagocytic cells in

subjects with neuroinflammatory diseases (Chauveau et al., 2011; Gkagkanasiou et al., 2016). With regard to ChPs, only pre-clinical data have been published to date. An accumulation of contrast material was observed in the ChPs of animal models of ischemic stroke (Wiart et al., 2007; Desestret et al., 2009; Henning et al., 2009) and EAE (Wuerfel et al., 2010; Millward et al., 2013, 2017). These results were obtained using contrast agents of various formulations and size (∼1000 kDa for Gadofluorine M and 7–150 nm for SPIOs). Contrast agents were found in the stroma (**Figure 1G**) with evidence of internalization by phagocytic cells (Wuerfel et al., 2010; Millward et al., 2017). Of note, the very small SPIOs (VSOP) were also found in the endothelium (Millward et al., 2013) and epithelium (Millward et al., 2017). Altogether, these data confirm ChPs involvement in neuroinflammatory diseases and suggest that SPIO-enhanced MRI might represent a powerful tool to study immune activation. Although clinical MRI studies have been conducted using ultrasmall (<50-nm) SPIO (USPIO) in patients with ischemic stroke (Cho et al., 2007; Nighoghossian et al., 2007) and MS (Tourdias et al., 2012), to the best of our knowledge, none has specifically examined the ChPs. Retrospective analysis of those data might help determine whether these pre-clinical observations have a translation in the clinical field.

SUMMARY AND FUTURE DIRECTIONS

Despite an increasing interest, the ChPs are still relatively understudied using neuroimaging. One reason for this lack of data is the small size of ChPs, which may be even more problematic in neurodegenerative diseases due to atrophy (Serot et al., 2003). Another reason is the unspecific ChP uptake of clinically approved contrast agents in physiological conditions, thus complicating image interpretation in pathological conditions. In addition, partial volume effects and/or spill-over from adjacent tissues may biased the quantitative values measured in ChPs. For all these reasons, ChPs are still viewed as challenging structures to image.

Despite these limitations, there is a growing body of evidence showing that ChP imaging is feasible and valuable.

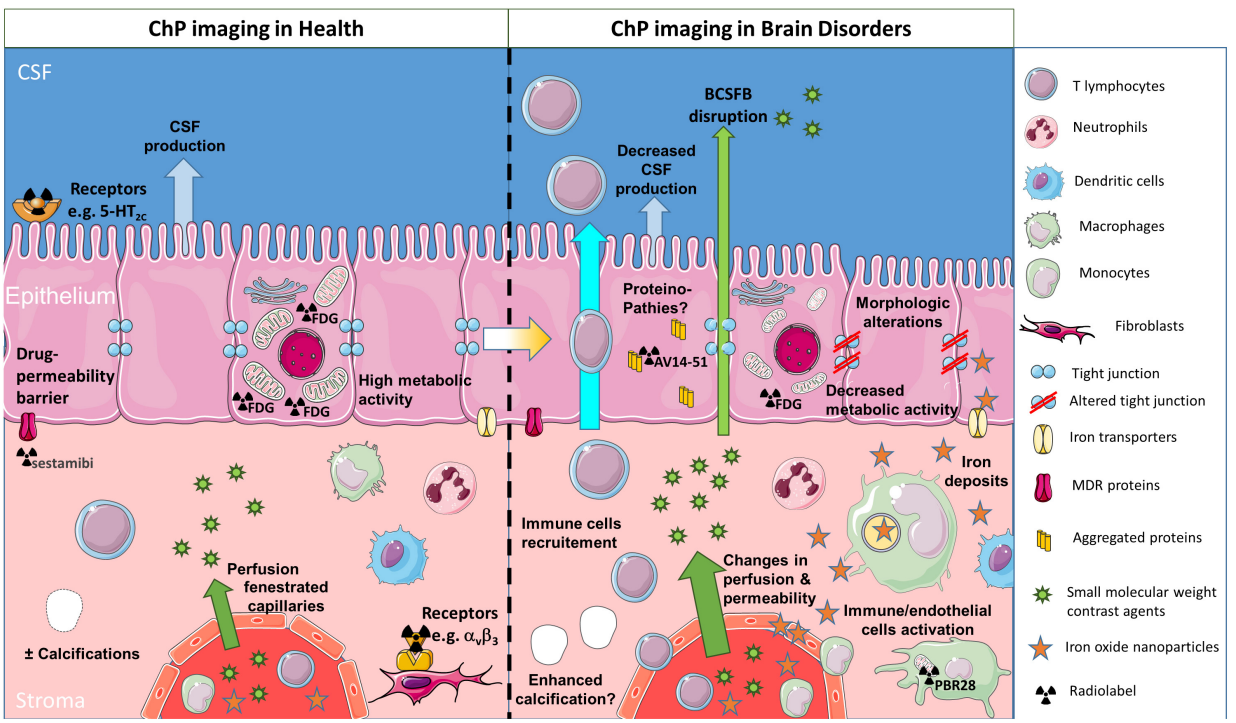

FIGURE 2 | Schematic of different clinical imaging techniques available for investigating the involvement of ChPs in brain disorders. ChP volume and the presence of calcification may be assessed through conventional imaging techniques such as CT and MRI. CSF production may be evaluated with phase-sensitive MRI sequences. ChP capillary perfusion and permeability may be quantified with MRI using dynamic imaging coupled to small molecular weight contrast agents such as gadolinium chelates. Nuclear medicine techniques such as PET give access to: (i) the occurrence of receptors on stromal or epithelial cells (both at the basal or at the apical side) and (ii) epithelial cell metabolism, thanks to dedicated radiotracers. All of these morphological and functional features present a progressive degradation throughout the aging process which might get aggravated in neurological diseases. In addition, in pathological conditions, the extravasation of small molecular weight contrast agents into CSF may allow to image blood-CSF barrier disruption. In inflammatory conditions, reticuloendothelial MRI contrast agents such as iron oxide nanoparticles may get access to the ChP stroma and accumulate into endothelial, stromal, and/or epithelial cells. Alternatively, activation of stromal immune cells (whether resident or infiltrating) may be observed with TSPO-targeted PET radiotracers. Finally, the presence of aggregated proteins due to proteinopathies might be detected with dedicated PET tracers, although this is still debated due to "off-target" binding. ChPs, choroid plexuses; CSF, cerebrospinal fluid; BCSFB, blood-cerebrospinal fluid barrier; MDR, multidrug-resistant; CT, computed tomography; MRI, magnetic resonance imaging; PET, positron emission tomography; TSPO, translocator protein 18 kDa (this figure was prepared with Servier Medical Art).

Figure 2 presents imaging strategies that may be used to obtain information about ChPs morphology and function. To date, most clinical imaging studies of ChPs have used human subjects free from neurological disease to show the interest of different ChPs imaging biomarkers, sometimes combined with the study of normal neurodevelopment or aging. Very few have actually tested the value of ChP imaging biomarkers in patients with neurodiseases; but these pioneer studies gave promising results in CRPS, IIH, ASD, schizophrenia, epilepsy, and AD. Future investigation should aim at confirming and extending these findings, evaluating their clinical relevance, and using them to investigate the involvement of ChPs in brain disorders.

Retrospective analysis of neuroimaging databases with a focus on ChPs might provide some answers in this respect. Morphological and functional changes in ChPs may be readily estimated by MRI, CT, and PET imaging, all approaches being relatively widespread in clinical trials that make use of neuroimaging. The questions that need to be answered are related to the potential of the different imaging techniques to differentiate between normal and pathological conditions, to follow-up disease progression and to monitor the effects of therapy. In addition, the study of inflammation at the ChPs may bring some new insights into the role of these structures in neuro-inflammatory disorders.

There are obvious limitations to retrospective studies, especially for the study of ChPs, since by definition they were not optimized to image such small structures. In the future, prospective studies should thus be properly designed, by making use of the latest technological developments such as hybrid imaging with PET/MR and the development of dedicated imaging tools. In parallel, further pre-clinical investigation is needed to elucidate the biological correlates of ChPs imaging biomarkers.

CONCLUSION

In summary, the clinical assessment of ChP alterations associated with brain disorders using neuroimaging methods may be the necessary step to effective therapeutic targeting of these conditions. The development of translational imaging approaches dedicated to the evaluation of ChP morphology and function could play a crucial role, by bridging the gap between basic molecular and cellular neuroscience and clinical research.

AUTHOR CONTRIBUTIONS

MW conceived the review focus, conducted the literature review, and overviewed drafting of the manuscript. VH, EC-S, FC, CD, EO, L-PB, and J-FG-E reviewed the literature in their respective fields of expertise, i.e., neuroscience, neuroimaging, neurology, neuroradiology, and plexus choroid research, and finalized the manuscript. All authors approved final version of manuscript.

FUNDING

This research was supported by grants from the French National Research Agency (ANR): NanoBrain (ANR-15-CE18-0026-01), CESAME (ANR-10-IBHU-0003), Cyclops (ANR-15-CE17-0020-01), and RHU MARVELOUS (ANR-16-RHUS-0009).

ACKNOWLEDGMENTS

The authors would like to thank Hervé Boutin for fruitful discussions about ChP imaging with PET.

SUPPLEMENTARY MATERIAL

The Supplementary Material for this article can be found online at: https://www.frontiersin.org/articles/10.3389/fnmol.2019.00034/full#supplementary-material

REFERENCES

Alicioglu, B., Yilmaz, G., Tosun, O., and Bulakbasi, N. (2017). Diffusion-weighted magnetic resonance imaging in the assessment of choroid plexus aging. *Neuroradiol. J.* 30, 490–495. doi: 10.1177/1971400917714280

Anderson, I. M., Clark, L., Elliott, R., Kulkarni, B., Williams, S. R., and Deakin, J. F. (2002). 5-HT(2C) receptor activation by m-chlorophenylpiperazine detected in humans with fMRI. *Neuroreport* 13, 1547–1551. doi: 10.1097/00001756-200208270-00012

Artzi, M., Aizenstein, O., Abramovitch, R., and Bashat, D. B. (2013). MRI multiparametric hemodynamic characterization of the normal brain. *Neuroscience* 240, 269–276. doi: 10.1016/j.neuroscience.2013.03.004

Azuma, M., Hirai, T., Kadota, Y., Khant, Z. A., Hattori, Y., Kitajima, M., et al. (2018). Circumventricular organs of human brain visualized on post-contrast 3D fluid-attenuated inversion recovery imaging. *Neuroradiology* doi: 10.1007/s00234-018-2023-3 [Epub ahead of print].

Batra, A., Latour, L. L., Ruetzler, C. A., Hallenbeck, J. M., Spatz, M., Warach, S., et al. (2010). Increased plasma and tissue MMP levels are associated with BCSFB and BBB disruption evident on post-contrast FLAIR after experimental stroke. *J. Cereb. Blood Flow Metab.* 30, 1188–1199. doi: 10.1038/jcbfm.2010.1

Bersani, G., Garavini, A., Taddei, I., Tanfani, G., and Pancheri, P. (1999). Choroid plexus calcification as a possible clue of serotonin implication in schizophrenia. *Neurosci. Lett.* 259, 169–172. doi: 10.1016/S0304-3940(98)00935-5

Bouzerar, R., Chaarani, B., Gondry-Jouet, C., Zmudka, J., and Baledent, O. (2013). Measurement of choroid plexus perfusion using dynamic susceptibility MR imaging: capillary permeability and age-related changes. *Neuroradiology* 55, 1447–1454. doi: 10.1007/s00234-013-1290-2

Chaddad, A., Desrosiers, C., and Toews, M. (2017). Multi-scale radiomic analysis of sub-cortical regions in MRI related to autism, gender and age. *Sci. Rep.* 7:45639. doi: 10.1038/srep45639

Chauveau, F., Cho, T. H., Berthezene, Y., Nighoghossian, N., and Wiart, M. (2011). Imaging inflammation in stroke using magnetic resonance imaging. *Int. J. Clin. Pharmacol. Ther.* 48, 718–728. doi: 10.5414/CPP48718

Cho, T. H., Nighoghossian, N., Wiart, M., Desestret, V., Cakmak, S., Berthezene, Y., et al. (2007). USPIO-enhanced MRI of neuroinflammation at the sub-acute stage of ischemic stroke: preliminary data. *Cerebrovasc. Dis.* 24, 544–546. doi: 10.1159/000111222

Daldrup-Link, H. E. (2017). Ten things you might not know about iron oxide nanoparticles. *Radiology* 284, 616–629. doi: 10.1148/radiol.2017162759

Daouk, J., Bouzerar, R., Chaarani, B., Zmudka, J., Meyer, M. E., and Baledent, O. (2016). Use of dynamic (18)F-fluorodeoxyglucose positron emission tomography to investigate choroid plexus function in Alzheimer's disease. *Exp. Gerontol.* 77, 62–68. doi: 10.1016/j.exger.2016.02.008

Deane, R., Zheng, W., and Zlokovic, B. V. (2004). Brain capillary endothelium and choroid plexus epithelium regulate transport of transferrin-bound and free iron into the rat brain. *J. Neurochem.* 88, 813–820. doi: 10.1046/j.1471-4159.2003.02221.x

Desestret, V., Brisset, J. C., Moucharrafie, S., Devillard, E., Nataf, S., Honnorat, J., et al. (2009). Early-stage investigations of ultrasmall superparamagnetic iron oxide-induced signal change after permanent middle cerebral artery occlusion in mice. *Stroke* 40, 1834–1841. doi: 10.1161/STROKEAHA.108.531269

Dragunow, M. (2013). Meningeal and choroid plexus cells—novel drug targets for CNS disorders. *Brain Res.* 1501, 32–55. doi: 10.1016/j.brainres.2013.01.013

Drake, C., Boutin, H., Jones, M. S., Denes, A., McColl, B. W., Selvarajah, J. R., et al. (2011). Brain inflammation is induced by co-morbidities and risk factors for stroke. *Brain Behav. Immun.* 25, 1113–1122. doi: 10.1016/j.bbi.2011.02.008

Ennis, S. R., and Keep, R. F. (2006). The effects of cerebral ischemia on the rat choroid plexus. *J. Cereb. Blood Flow Metab.* 26, 675–683. doi: 10.1038/sj.jcbfm.9600224

Ettrup, A., Svarer, C., McMahon, B., da Cunha-Bang, S., Lehel, S., Moller, K., et al. (2016). Serotonin 2A receptor agonist binding in the human brain with [(11)C]Cimbi-36: test-retest reproducibility and head-to-head comparison with the antagonist [(18)F]altanserin. *Neuroimage* 130, 167–174. doi: 10.1016/j.neuroimage.2016.02.001

Gazzin, S., Strazielle, N., Schmitt, C., Fevre-Montange, M., Ostrow, J. D., Tiribelli, C., et al. (2008). Differential expression of the multidrug resistance-related proteins ABCb1 and ABCc1 between blood-brain interfaces. *J. Comp. Neurol.* 510, 497–507. doi: 10.1002/cne.21808

Ghersi-Egea, J. F., Strazielle, N., Catala, M., Silva-Vargas, V., Doetsch, F., and Engelhardt, B. (2018). Molecular anatomy and functions of the choroidal blood-cerebrospinal fluid barrier in health and disease. *Acta Neuropathol.* 135, 337–361. doi: 10.1007/s00401-018-1807-1

Gkagkanasiou, M., Ploussi, A., Gazouli, M., and Efstathopoulos, E. P. (2016). USPIO-enhanced MRI neuroimaging: a review. *J. Neuroimaging* 26, 161–168. doi: 10.1111/jon.12318

Grech-Sollars, M., Hales, P. W., Miyazaki, K., Raschke, F., Rodriguez, D., Wilson, M., et al. (2015). Multi-centre reproducibility of diffusion MRI parameters for clinical sequences in the brain. *NMR Biomed.* 28, 468–485. doi: 10.1002/nbm.3269

Griffiths, P. D., Blaser, S., Boodram, M. B., Armstrong, D., and Harwood-Nash, D. (1996). Choroid plexus size in young children with Sturge-Weber syndrome. *AJNR Am. J. Neuroradiol.* 17, 175–180.

Guermazi, A., De Kerviler, E., Zagdanski, A. M., and Frija, J. (2000). Diagnostic imaging of choroid plexus disease. *Clin. Radiol.* 55, 503–516. doi: 10.1053/crad.1999.0476

Hasiloglu, Z. I., Asik, M., Ure, E., Ertem, F., Apak, H., and Albayram, S. (2017). The utility of susceptibility-weighted imaging to evaluate the extent of iron accumulation in the choroid plexus of patients with beta-thalassaemia major. *Clin. Radiol.* 72, 903.e1–903.e7. doi: 10.1016/j.crad.2017.04.008

Henning, E. C., Ruetzler, C. A., Gaudinski, M. R., Hu, T. C., Latour, L. L., Hallenbeck, J. M., et al. (2009). Feridex preloading permits tracking of CNS-resident macrophages after transient middle cerebral artery occlusion. *J. Cereb. Blood Flow Metab.* 29, 1229–1239. doi: 10.1038/jcbfm.2009.48

Hirvonen, J., Kreisl, W. C., Fujita, M., Dustin, I., Khan, O., Appel, S., et al. (2012). Increased *in vivo* expression of an inflammatory marker in temporal lobe epilepsy. *J. Nucl. Med.* 53, 234–240. doi: 10.2967/jnumed.111.091694

Huang, T. Y., Chung, H. W., Chen, M. Y., Giiang, L. H., Chin, S. C., Lee, C. S., et al. (2004). Supratentorial cerebrospinal fluid production rate in healthy adults: quantification with two-dimensional cine phase-contrast MR imaging with high temporal and spatial resolution. *Radiology* 233, 603–608. doi: 10.1148/radiol.2332030884

Ichikawa, H., Ishikawa, M., Fukunaga, M., Ishikawa, K., and Ishiyama, H. (2010). Quantitative evaluation of blood-cerebrospinal fluid barrier permeability in the rat with experimental meningitis using magnetic resonance imaging. *Brain Res.* 1321, 125–132. doi: 10.1016/j.brainres.2010.01.050

Ikonomovic, M. D., Abrahamson, E. E., Price, J. C., Mathis, C. A., and Klunk, W. E. (2016). [F-18]AV-1451 PET retention in choroid plexus: more than "off-target" binding. *Ann. Neurol.* 80, 307–308. doi: 10.1002/ana.24706

Joseph-Mathurin, N., Dorieux, O., Trouche, S. G., Boutajangout, A., Kraska, A., Fontes, P., et al. (2013). Amyloid beta immunization worsens iron deposits in the choroid plexus and cerebral microbleeds. *Neurobiol. Aging* 34, 2613–2622. doi: 10.1016/j.neurobiolaging.2013.05.013

Kim, S., Kim, D., Kim, S. H., Park, M. A., Chang, J. H., and Yun, M. (2018). The roles of (11)C-acetate PET/CT in predicting tumor differentiation and survival in patients with cerebral glioma. *Eur. J. Nucl. Med. Mol. Imaging* 45, 1012–1020. doi: 10.1007/s00259-018-3948-9

Kira, R., Ohga, S., Takada, H., Gondo, K., Mihara, F., and Hara, T. (2000). MR choroid plexus sign of iron overload. *Neurology* 55:1340. doi: 10.1212/WNL.55.9.1340

Kreisl, W. C., Lyoo, C. H., Liow, J. S., Wei, M., Snow, J., Page, E., et al. (2016). (11)C-PBR28 binding to translocator protein increases with progression of Alzheimer's disease. *Neurobiol. Aging* 44, 53–61. doi: 10.1016/j.neurobiolaging.2016.04.011

Langer, O., Bauer, M., Hammers, A., Karch, R., Pataraia, E., Koepp, M. J., et al. (2007). Pharmacoresistance in epilepsy: a pilot PET study with the P-glycoprotein substrate R-[(11)C]verapamil. *Epilepsia* 48, 1774–1784. doi: 10.1111/j.1528-1167.2007.01116.x

Lee, C. M., Jacobs, H. I. L., Marquie, M., Becker, J. A., Andrea, N. V., Jin, D. S., et al. (2018). 18F-flortaucipir binding in choroid plexus: related to race and hippocampus signal. *J. Alzheimers Dis.* 62, 1691–1702. doi: 10.3233/JAD-170840

Leitner, D. F., and Connor, J. R. (2012). Functional roles of transferrin in the brain. *Biochim. Biophys. Acta* 1820, 393–402. doi: 10.1016/j.bbagen.2011.10.016

Lopez-Rodriguez, V., Galindo-Sarco, C., Garcia-Perez, F. O., Ferro-Flores, G., Arrieta, O., and Avila-Rodriguez, M. A. (2016). PET-based human dosimetry of the dimeric alphavbeta3 integrin ligand 68Ga-DOTA-E-[c(RGDfK)]2, a potential tracer for imaging tumor angiogenesis. *J. Nucl. Med.* 57, 404–409. doi: 10.2967/jnumed.115.161653

Lowe, V. J., Curran, G., Fang, P., Liesinger, A. M., Josephs, K. A., Parisi, J. E., et al. (2016). An autoradiographic evaluation of AV-1451 Tau PET in dementia. *Acta Neuropathol. Commun.* 4:58. doi: 10.1186/s40478-016-0315-6

Lu, J., Kaur, C., and Ling, E. A. (1995). Expression and upregulation of transferrin receptors and iron uptake in the epiplexus cells of different aged rats injected with lipopolysaccharide and interferon-gamma. *J. Anat.* 187(Pt 3), 603–611.

Lublinsky, S., Kesler, A., Friedman, A., Horev, A., and Shelef, I. (2018). Quantifying response to intracranial pressure normalization in idiopathic intracranial hypertension via dynamic neuroimaging. *J. Magn. Reson. Imaging* 47, 913–927. doi: 10.1002/jmri.25857

Madhukar, M., Choudhary, A. K., Boal, D. K., Dias, M. S., and Iantosca, M. R. (2012). Choroid plexus: normal size criteria on neuroimaging. *Surg. Radiol. Anat.* 34, 887–895. doi: 10.1007/s00276-012-0980-5

Maktabi, M. A., Heistad, D. D., and Faraci, F. M. (1990). Effects of angiotensin II on blood flow to choroid plexus. *Am. J. Physiol.* 258(2 Pt 2), H414–H418. doi: 10.1152/ajpheart.1990.258.2.H414

Marquie, M., Verwer, E. E., Meltzer, A. C., Kim, S. J. W., Aguero, C., Gonzalez, J., et al. (2017). Lessons learned about [F-18]-AV-1451 off-target binding from an autopsy-confirmed Parkinson's case. *Acta Neuropathol. Commun.* 5:75. doi: 10.1186/s40478-017-0482-0

Miller, W. P., Mantovani, L. F., Muzic, J., Rykken, J. B., Gawande, R. S., Lund, T. C., et al. (2016). Intensity of MRI gadolinium enhancement in cerebral adrenoleukodystrophy: a biomarker for inflammation and predictor of outcome following transplantation in higher risk patients. *AJNR Am. J. Neuroradiol.* 37, 367–372. doi: 10.3174/ajnr.A4500

Millward, J. M., Ariza de Schellenberger, A., Berndt, D., Hanke-Vela, L., Schellenberger, E., Waiczies, S., et al. (2017). Application of europium-doped very small iron oxide nanoparticles to visualize neuroinflammation with mri and fluorescence microscopy. *Neuroscience* doi: 10.1016/j.neuroscience.2017.12.014 [Epub ahead of print].

Millward, J. M., Schnorr, J., Taupitz, M., Wagner, S., Wuerfel, J. T., and Infante-Duarte, C. (2013). Iron oxide magnetic nanoparticles highlight early involvement of the choroid plexus in central nervous system inflammation. *ASN Neuro* 5:e00110. doi: 10.1042/AN20120081

Minamimoto, R., Jamali, M., Barkhodari, A., Mosci, C., Mittra, E., Shen, B., et al. (2015). Biodistribution of the (1)(8)F-FPPRGD(2) PET radiopharmaceutical in cancer patients: an atlas of SUV measurements. *Eur. J. Nucl. Med. Mol. Imaging* 42, 1850–1858. doi: 10.1007/s00259-015-3096-4

Morris, C. M., Keith, A. B., Edwardson, J. A., and Pullen, R. G. (1992). Uptake and distribution of iron and transferrin in the adult rat brain. *J. Neurochem.* 59, 300–306. doi: 10.1111/j.1471-4159.1992.tb08904.x

Nagahiro, S., Goto, S., Korematsu, K., Sumi, M., Takahashi, M., and Ushio, Y. (1994). Disruption of the blood-cerebrospinal fluid barrier by transient cerebral ischemia. *Brain Res.* 633, 305–311. doi: 10.1016/0006-8993(94)91553-9

Nighoghossian, N., Wiart, M., Cakmak, S., Berthezene, Y., Derex, L., Cho, T. H., et al. (2007). Inflammatory response after ischemic stroke: a USPIO-enhanced MRI study in patients. *Stroke* 38, 303–307. doi: 10.1161/01.STR.0000254548.30258.f2

Nixon, P. F., Jordan, L., Zimitat, C., Rose, S. E., and Zelaya, F. (2008). Choroid plexus dysfunction: the initial event in the pathogenesis of Wernicke's encephalopathy and ethanol intoxication. *Alcohol. Clin. Exp. Res.* 32, 1513–1523. doi: 10.1111/j.1530-0277.2008.00723.x

Park, M. G., Kim, M. K., Kim, B. K., Baik, S. K., and Park, K. P. (2017). A case of contrast leakage mimicking intraventricular hemorrhage in a patient with intravenous thrombolysis. *J. Stroke Cerebrovasc. Dis.* 26, e14–e17. doi: 10.1016/j.jstrokecerebrovasdis.2016.09.041

Phatouros, C. C., Halbach, V. V., Malek, A. M., Meyers, P. M., Dowd, C. F., and Higashida, R. T. (1999). Intraventricular contrast medium leakage during ethanol embolization of an arteriovenous malformation. *AJNR Am. J. Neuroradiol.* 20, 1329–1332.

Pontecorvo, M. J., Devous, M. D. Sr., Navitsky, M., Lu, M., Salloway, S., Schaerf, F. W., et al. (2017). Relationships between flortaucipir PET tau binding and amyloid burden, clinical diagnosis, age and cognition. *Brain* 140, 748–763. doi: 10.1093/brain/aww334

Qiu, D., Chan, G. C., Chu, J., Chan, Q., Ha, S. Y., Moseley, M. E., et al. (2014). MR quantitative susceptibility imaging for the evaluation of iron loading in the brains of patients with beta-thalassemia major. *AJNR Am. J. Neuroradiol.* 35, 1085–1090. doi: 10.3174/ajnr.A3849

Rao, V. V., Dahlheimer, J. L., Bardgett, M. E., Snyder, A. Z., Finch, R. A., Sartorelli, A. C., et al. (1999). Choroid plexus epithelial expression of MDR1 P glycoprotein and multidrug resistance-associated protein contribute to the blood-cerebrospinal-fluid drug-permeability barrier. *Proc. Natl. Acad. Sci. U.S.A.* 96, 3900–3905. doi: 10.1073/pnas.96.7.3900

Renu, A., Laredo, C., Lopez-Rueda, A., Llull, L., Tudela, R., San-Roman, L., et al. (2017). Vessel wall enhancement and blood-cerebrospinal fluid barrier disruption after mechanical thrombectomy in acute ischemic stroke. *Stroke* 48, 651–657. doi: 10.1161/STROKEAHA.116.015648

Rouault, T. A., Zhang, D. L., and Jeong, S. Y. (2009). Brain iron homeostasis, the choroid plexus, and localization of iron transport proteins. *Metab. Brain Dis.* 24, 673–684. doi: 10.1007/s11011-009-9169-y

Sandyk, R. (1993). Choroid plexus calcification as a possible marker of hallucinations in schizophrenia. *Int. J. Neurosci.* 71, 87–92. doi: 10.3109/00207459309000595

Schankin, C. J., Maniyar, F. H., Seo, Y., Kori, S., Eller, M., Chou, D. E., et al. (2016). Ictal lack of binding to brain parenchyma suggests integrity of the blood-brain barrier for 11C-dihydroergotamine during glyceryl trinitrate-induced migraine. *Brain* 139(Pt 7), 1994–2001. doi: 10.1093/brain/aww096

Schwartz, M., and Baruch, K. (2014). The resolution of neuroinflammation in neurodegeneration: leukocyte recruitment via the choroid plexus. *EMBO J.* 33, 7–22. doi: 10.1002/embj.201386609

Serot, J. M., Bene, M. C., and Faure, G. C. (2003). Choroid plexus, aging of the brain, and Alzheimer's disease. *Front. Biosci.* 8:s515–s521.

Serot, J.-M., Zmudka, J., and Jouanny, P. (2012). A possible role for CSF turnover and choroid plexus in the pathogenesis of late onset Alzheimer's disease. *J. Alzheimers Dis.* 30, 17–26. doi: 10.3233/JAD-2012-111964

Silverberg, G. D., Heit, G., Huhn, S., Jaffe, R. A., Chang, S. D., Bronte-Stewart, H., et al. (2001). The cerebrospinal fluid production rate is reduced in dementia of the Alzheimer's type. *Neurology* 57, 1763–1766. doi: 10.1212/WNL.57.10.1763

Spijkerman, J. M., Geurts, L. J., Siero, J. C. W., Hendrikse, J., Luijten, P. R., and Zwanenburg, J. J. M. (2018). Phase contrast MRI measurements of net cerebrospinal fluid flow through the cerebral aqueduct are confounded by respiration. *J. Magn. Reson. Imaging* 49, 433–444. doi: 10.1002/jmri.26181

Stimac, G. K., Solomon, M. A., and Newton, T. H. (1986). CT and MR of angiomatous malformations of the choroid plexus in patients with Sturge-Weber disease. *AJNR Am. J. Neuroradiol.* 7, 623–627.

Strazielle, N., and Ghersi-Egea, J. F. (2013). Physiology of blood-brain interfaces in relation to brain disposition of small compounds and macromolecules. *Mol. Pharm.* 10, 1473–1491. doi: 10.1021/mp300518e

Tanifum, E. A., Starosolski, Z. A., Fowler, S. W., Jankowsky, J. L., and Annapragada, A. V. (2014). Cerebral vascular leak in a mouse model of amyloid neuropathology. *J. Cereb. Blood Flow Metab.* 34, 1646–1654. doi: 10.1038/jcbfm.2014.125

Tobinick, E. L., Chen, K., and Chen, X. (2009). Rapid intracerebroventricular delivery of Cu-DOTA-etanercept after peripheral administration demonstrated by PET imaging. *BMC Res. Notes* 2:28. doi: 10.1186/1756-0500-2-28

Tourdias, T., Roggerone, S., Filippi, M., Kanagaki, M., Rovaris, M., Miller, D. H., et al. (2012). Assessment of disease activity in multiple sclerosis phenotypes with combined gadolinium- and superparamagnetic iron oxide-enhanced MR imaging. *Radiology* 264, 225–233. doi: 10.1148/radiol.12111416

Vakil, P., Elmokadem, A. H., Syed, F. H., Cantrell, C. G., Dehkordi, F. H., Carroll, T. J., et al. (2017). Quantifying intracranial plaque permeability with dynamic contrast-enhanced mri: a pilot study. *AJNR Am. J. Neuroradiol.* 38, 243–249. doi: 10.3174/ajnr.A4998

Waiczies, H., Millward, J. M., Lepore, S., Infante-Duarte, C., Pohlmann, A., Niendorf, T., et al. (2012). Identification of cellular infiltrates during early stages of brain inflammation with magnetic resonance microscopy. *PLoS One* 7:e32796. doi: 10.1371/journal.pone.0032796

Wiart, M., Davoust, N., Pialat, J. B., Desestret, V., Moucharaffie, S., Cho, T. H., et al. (2007). MRI monitoring of neuroinflammation in mouse focal ischemia. *Stroke* 38, 131–137. doi: 10.1161/01.STR.0000252159.05702.00

Wuerfel, E., Infante-Duarte, C., Glumm, R., and Wuerfel, J. T. (2010). Gadofluorine M-enhanced MRI shows involvement of circumventricular organs in neuroinflammation. *J. Neuroinflammation* 7:70. doi: 10.1186/1742-2094-7-70

Yalcin, A., Ceylan, M., Bayraktutan, O. F., Sonkaya, A. R., and Yuce, I. (2016). Age and gender related prevalence of intracranial calcifications in CT imaging; data from 12,000 healthy subjects. *J. Chem. Neuroanat.* 78, 20–24. doi: 10.1016/j.jchemneu.2016.07.008

Zhou, G., Hotta, J., Lehtinen, M. K., Forss, N., and Hari, R. (2015). Enlargement of choroid plexus in complex regional pain syndrome. *Sci. Rep.* 5:14329. doi: 10.1038/srep14329

Conflict of Interest Statement: MW has a research contract with AMAG for the study of neuroinflammation using Ferumoxytol.

The remaining authors declare that the research was conducted in the absence of any commercial or financial relationships that could be construed as a potential conflict of interest.

frontiers in Molecular Neuroscience

ORIGINAL RESEARCH
published: 22 February 2019
doi: 10.3389/fnmol.2019.00046

Parkin Promotes Mitophagic Cell Death in Adult Hippocampal Neural Stem Cells Following Insulin Withdrawal

*Hyunhee Park[1], Kyung Min Chung[1], Hyun-Kyu An[1], Ji-Eun Gim[1], Jihyun Hong[1], Hanwoong Woo[1], Bongki Cho[1], Cheil Moon[1] and Seong-Woon Yu[1,2]**

[1] Department of Brain and Cognitive Sciences, Daegu Gyeongbuk Institute of Science and Technology, Daegu, South Korea,
[2] Neurometabolomics Research Center, Daegu Gyeongbuk Institute of Science and Technology, Daegu, South Korea

Regulated cell death (RCD) plays a fundamental role in human health and disease. Apoptosis is the best-studied mode of RCD, but the importance of other modes has recently been gaining attention. We have previously demonstrated that adult rat hippocampal neural stem (HCN) cells undergo autophagy-dependent cell death (ADCD) following insulin withdrawal. Here, we show that Parkin mediates mitophagy and ADCD in insulin-deprived HCN cells. Insulin withdrawal increased the amount of depolarized mitochondria and their colocalization with autophagosomes. Insulin withdrawal also upregulated both mRNA and protein levels of Parkin, gene knockout of which prevented mitophagy and ADCD. c-Jun is a transcriptional repressor of Parkin and is degraded by the proteasome following insulin withdrawal. In insulin-deprived HCN cells, Parkin is required for Ca^{2+} accumulation and depolarization of mitochondria at the early stages of mitophagy as well as for recognition and removal of depolarized mitochondria at later stages. In contrast to the pro-death role of Parkin during mitophagy, Parkin deletion rendered HCN cells susceptible to apoptosis, revealing distinct roles of Parkin depending on different modes of RCD. Taken together, these results indicate that Parkin is required for the induction of ADCD accompanying mitochondrial dysfunction in HCN cells following insulin withdrawal. Since impaired insulin signaling is implicated in hippocampal deficits in various neurodegenerative diseases and psychological disorders, these findings may help to understand the mechanisms underlying death of neural stem cells and develop novel therapeutic strategies aiming to improve neurogenesis and survival of neural stem cells.

Keywords: autophagy-dependent cell death, c-Jun, hippocampal neural stem cells, mitophagy, Parkin

OPEN ACCESS

Edited by:
Vsevolod V. Gurevich,
Vanderbilt University, United States

Reviewed by:
Alicia M. Pickrell,
Virginia Tech, United States
Ralf J. Braun,
University of Bayreuth, Germany
Matteo Bordi,
University of Rome Tor Vergata, Italy

****Correspondence:***
Seong-Woon Yu
yusw@dgist.ac.kr

Received: *18 October 2018*
Accepted: *05 February 2019*
Published: *22 February 2019*

Citation:
Park H, Chung KM, An H-K, Gim J-E, Hong J, Woo H, Cho B, Moon C and Yu S-W (2019) Parkin Promotes Mitophagic Cell Death in Adult Hippocampal Neural Stem Cells Following Insulin Withdrawal. Front. Mol. Neurosci. 12:46. doi: 10.3389/fnmol.2019.00046

INTRODUCTION

Regulated cell death (RCD) is an evolutionarily conserved process and is tightly controlled by various intracellular signals and extracellular cues (Danial and Korsmeyer, 2004; Galluzzi et al., 2018). RCD is essential for normal development and maintenance of tissue homeostasis (Ellis et al., 1991; Coucouvanis and Martin, 1995). Therefore, dysregulation of RCD underlies a variety of human diseases, such as cancer, neurodegeneration, and autoimmunity.

RCD is currently categorized into 12 distinct cell death subroutines, with intrinsic and extrinsic apoptosis, necroptosis, and autophagy-dependent cell death (ADCD) as main subroutines based on morphological and biochemical criteria (Galluzzi et al., 2018). Cell shrinkage, membrane blebbing, nuclear DNA fragmentation, chromatin condensation, and activation of caspases are hallmarks of apoptosis (Galluzzi et al., 2007). Morphologically, necrosis is characterized by a rapid collapse of the plasma membrane and uncontrolled release of cytoplasmic components (Rello et al., 2005). Recent progress in the understanding of the regulatory mechanisms of necrosis suggests its regulatable nature, and has led to the coining of the term "necroptosis" (Galluzzi and Kroemer, 2008; Moriwaki et al., 2016).

Autophagy ("*self-eating*" in Greek) is a lysosome-dependent catabolic process characterized morphologically by an increased formation of autophagic vesicles (autophagosomes and autolysosomes) (Yang and Klionsky, 2010). Autophagy is essential for turnover and removal of dysfunctional or toxic intracellular components (Shintani and Klionsky, 2004). Autophagy can also recycle obsolete cellular constituents (Mizushima and Komatsu, 2011). Thereby, autophagy generally has protective and adaptive functions in response to cellular stress. Autophagy is mediated by the autophagy-related (Atg) genes (Klionsky et al., 2011). It begins by phagophore formation and elongation to generate double-membraned autophagosomes. For this process, microtubule-associated proteins 1A/1B light chain 3B (LC3, the mammalian homologue of the yeast Atg8 protein) is cleaved by Atg4 to produce LC3-I, which is a cytosolic form of LC3 (Satoo et al., 2009). When autophagosome formation is triggered, LC3-I is conjugated to phosphatidylethanolamine to form LC3-II, which is then recruited to the expanding phagophore membranes to facilitate autophagosome formation (Ichimura et al., 2000). Autophagosomes then mature into autolysosomes through fusion with the lysosomes for degradation and recycling of the autophagy cargos. An increase in the amount of LC3-II or in the number of LC3 puncta in autophagic vesicles can serve as an indicator of increased autophagy flux (Klionsky et al., 2016). p62 (sequestosome 1/SQSTM1) is a ubiquitin-binding autophagy adaptor protein, which becomes incorporated into the autophagosomes together with the delivered cargos for autophagic degradation (Pankiv et al., 2007). Thus, the degradation of p62 is regarded as another index of autophagy flux (Ichimura et al., 2008).

Contrary to the general notion of autophagy as a survival mechanism, there are reports that excessive or prolonged autophagy can induce cell death (Tsujimoto and Shimizu, 2005). Together with frequent observation of autophagy in cells undergoing RCD, these findings led to the concept of ADCD. ADCD, previously also known as autophagic cell death, was first proposed based on widespread morphological association of autophagy with cell death, but without implication of the causative role of autophagy in cell death (Tsujimoto and Shimizu, 2005). Therefore, it is still contentious whether autophagy plays a causative role in cell death, especially in mammals. Taking this controversy into account, ADCD is suggested as a type of RCD that requires autophagic machinery without participation of other cell death pathways (Galluzzi et al., 2018).

Insulin/insulin-like growth factor (IGF) family proteins are vital extracellular cues for the differentiation and survival of neural stem cells (NSCs) in the hippocampus (Åberg et al., 2000; Lichtenwalner et al., 2001). As such, adult hippocampal NSCs, abbreviated as HCN cells following the original description of their isolation, depend on insulin/IGF for survival in *in vitro* culture (Palmer et al., 1997). Interestingly, we found that insulin-deprived HCN cells undergo ADCD rather than apoptosis despite their intact apoptotic capability (Yu et al., 2008; Baek et al., 2009). Further study revealed that glycogen synthase kinase-3β (GSK3-3β) mediates ADCD in HCN cells (Yu et al., 2008; Baek et al., 2009; Ha et al., 2015). Pharmacological or genetic inactivation of GSK-3β decreased ADCD, while over-expression of the wild-type (WT) or constitutively active form of GSK-3β facilitated ADCD without apoptosis induction (Ha et al., 2015). Because a rise in the intracellular Ca^{2+} level is known to trigger autophagy (Høyer-Hansen et al., 2007), we next focused on the regulation of ADCD by Ca^{2+}. In insulin-deprived HCN cells, intracellular Ca^{2+} level increases, mainly owing to its release from the endoplasmic reticulum (ER) mediated by the type 3 ryanodine receptor (RyR3) (Chung et al., 2016). RyR3-mediated increase in cytosolic Ca^{2+} activates AMP-activated protein kinase (AMPK), which leads to a novel phosphorylation of p62 and promotes mitophagy (Ha et al., 2017). Further study is needed to understand how mitophagy is regulated in insulin-deprived HCN cells.

Parkin is an E3 ubiquitin ligase, and more than 100 mutations in the Parkin-encoding *PARK2* gene are known to cause an autosomal recessive form of Parkinson's disease (PD) (Dawson and Dawson, 2010). PD is characterized mainly by an array of motor impairments associated with progressive death of dopaminergic neurons in the substantia nigra pars compacta (Dauer and Przedborski, 2003). PD also affects a number of neuronal systems and causes various non-motor symptoms including neuropsychiatric manifestations and cognitive deficits such as early premotor dysfunction (Meissner et al., 2011). The relevance of Parkin in these cognitive symptoms is not well understood. An emerging role of Parkin is regulation of mitophagy (Narendra et al., 2008). Mitophagy is a particular mode of autophagy that removes damaged or dysfunctional mitochondria and thereby helps maintain mitochondrial quality and homeostasis (Lemasters, 2005). Since mitochondrial dysfunction is implicated in the pathogenesis of PD, the role of Parkin-mediated mitophagy in the regulation of mitochondrial function and dynamics has gained great attention.

Hippocampus is one of the neurogenic regions where new neurons are continuously generated throughout adulthood (Gould et al., 1997; Alvarez-Buylla and Lim, 2004). Adult hippocampal neurogenesis is implicated in hippocampal learning and memory, and is impaired in the aged or injured brain (Shors et al., 2001; Rodríguez et al., 2008). Given their highly dynamic nature and differentiation potential, NSCs residing in the neurogenic niches must be

under tight control in terms of metabolism, mitochondrial homeostasis, and autophagy level. Of relevance to this notion, a recent report on the characteristics of mt-Keima mice, an *in vivo* model of mitophagy, suggested high basal level of mitophagy in the dentate gyrus (DG) areas of the adult hippocampus (Sun et al., 2015). However, it has not been studied whether adult NSCs require Parkin activity for mitophagy.

In the present study, we investigated the role of Parkin in mitophagy in HCN cells; this investigation was prompted by its roles in other cell types and the high rate of on-going mitophagy in the DG. We demonstrate that Parkin is upregulated through degradation of its transcriptional repressor, c-Jun, following insulin withdrawal. Parkin is required for mitophagy and plays a pro-death role during ADCD of HCN cells. On the other hand, Parkin plays an anti-apoptotic role in response to well-known apoptotic stimuli. Our findings suggest distinct functions of Parkin in the regulation of RCD of HCN cells depending on the cellular context.

MATERIALS AND METHODS

Reagents and Antibodies

Antibodies against Parkin (4211), cleaved caspase 3 (9664), poly(ADP-ribose) polymerase (PARP) (9542), c-Jun (9165), and voltage-dependent anion channel (VDAC) (4866), phospho-SAPK/JNK (Thr183/Tyr185) (9251), horseradish peroxidase (HRP)-linked anti-mouse IgG (7076) were purchased from Cell Signaling Technology (Danvers, MA, United States). Antibodies against p62 (P0067, Sigma-Aldrich, Saint Louis, MO, United States), LC3B (100-2220, Novus Biologicals, City of Centennial, CO, United States), HRP-conjugated β-actin (47778, Santa Cruz Biotechnology, Dallas, TX, United States) and goat anti-rabbit IgG (H+L) secondary antibody (31460, Thermo Fisher Scientific, Carlsbad, CA, United States), PTEN-induced putative kinase 1 (PINK1) (BC100-494, Novus Biologicals) and ubiquitin phosphorylated at S65 residue (p-Ub-S65) (ABS1513-I, EMD Millipore, Burlington, MA, United States) were purchased at the indicated companies. Bafilomycin A1 (Baf.A1, Sigma-Aldrich), carbonyl cyanide 3-chlorophenylhydrazone (CCCP, Sigma-Aldrich), staurosporine (STS, Cell Signaling Technology), and necrostatin-1 (Invitrogen, Carlsbad, CA, United States) were purchased from the indicated companies.

Cell Culture

HCN cells were cultured as we previously reported (Chung et al., 2015, 2016). In brief, cells were grown in chemically composed serum free medium containing Dulbecco's modified Eagle's medium/F-12 (12400-024, Thermo Fisher Scientific) supplemented with our own-made N2 components, which we made by mixing individual components including 5 mg/l insulin (Sigma-Aldrich), 16 mg/l putrescine dihydrochloride (Sigma-Aldrich), 100 mg/l transferrin (Sigma-Aldrich), 30 nM sodium selenite (Sigma-Aldrich), and 20 nM progesterone (Sigma-Aldrich). Medium was adjusted to pH 7.2 after adding 1.27 g/l sodium biocarbonate (Sigma-Aldrich). Insulin was omitted to prepare I(−) medium. In this paper, I(+) and I(−) denote insulin-containing and insulin-deprived media, respectively.

Cell Death Assay

HCN cells were seeded in a 96-well plate at a density of 1.0×10^5 cells/ml. To assess cell death, cells were stained with Hoechst 33342 (Invitrogen) and propidium iodide (PI) (Sigma-Aldrich), and were imaged under a fluorescence microscope (Axiovert 40 CFL, Carl Zeiss, Oberkochen, Germany). We used DAPI filter for Hoechst stained cells, and Cy3 filter for PI positive cells. Images were obtained by AxioVision 4 module Multichannel software (Carl Zeiss) and were analyzed by Pixcavator student edition analysis software (Intelligent Perception Co.). The contrast value of the software was adjusted according to the brightness of the image, and total 7,000–8,000 cells were counted per condition and more than 3 experiments were performed. The cell death rates were calculated as follows: Cell death (%) = (PI positive cell number/Hoechst positive cell number) × 100.

Caspase 3 Activity Assay

HCN cells were seeded onto 96-well white plates and caspase 3 activity was measured using a Caspase 3 activity assay kit (Promega, Madison, WI, United States) according to the manufacturer's instructions. A freshly prepared Caspase 3 Glo reagent solution was added to cultured HCN cells, and luminescence was measured in a luminometer (SpectraMax L, Molecular Devices, San Jose, CA, United States) and were analyzed by SoftMax Pro Software (Molecular Devices). Luminescence values were normalized to protein concentration. We calculated the average value by analyzing duplets samples per condition, and performed a total 3 repeat experiment.

Terminal Deoxynucleotidyl Transferase dUTP Nick End Labeling (TUNEL) Assay

Cells were fixed in 4% paraformaldehyde for 25 min at 4°C, washed twice in phosphate-buffered saline (PBS), 5 min each time. After permeabilization with 0.2% Triton X-100 in PBS for 5 min, the assay was performed using TUNEL System kit (G3250, Promega) according to the manufacture's instruction. In brief, 100 μl of equilibration buffer was added to the cells for 5–10 min at room temperature. After that, 50 μl TdT reaction mix was added for 60 min at 37°C. Cells were immersed in 2 × SSC buffer to stop reaction. Hoechst was added to stain nucleus, and the cells were mounted and analyzed by under a confocal microscope (LSM 700, Carl Zeiss).

Western Blotting

HCN cells were harvested and lysed on ice in radioimmunoprecipitation assay (RIPA) buffer (Thermo Fisher Scientific) with 1 × Halt Protease and Phosphatase inhibitor cocktail (Thermo Fisher Scientific), 1 mM phenylmethanesulfonylfluoride, 1 mM dithiothreitol. Lysates were centrifuged 12,000 ×*g* for 10 min and protein concentration was measured using a Pierce BCA protein assay kit (Thermo Fisher Scientific). Usually, 10–20 μg total protein was loaded per well. After electrophoresis, proteins were transferred to

polyvinylidene fluoride membranes in a semidry electrophoretic transfer cell (Bio-Rad, Richmond, CA, United States). The membranes were blocked in blocking buffer consisting of 5% non-fat dry milk in Tris-buffered saline with 0.1% Tween 20 (TBST) for 1 h at room temperature and incubated overnight with diluted primary antibodies. Each primary antibody was diluted in 5% bovine serum Albumin (Thermo Fisher Scientific) or 5% skim milk in TBST. After 3 washes with TBST, membranes were incubated with suitable HRP-conjugated secondary antibodies (10,000 dilution) diluted in blocking buffer for 1 h. After 3 washes with TBST, proteins were detected using Super Signal West Pico PLUS Chemiluminescent Substrate (34580, Thermo Fisher Scientific). SRX 201A (Konica Minolta Medical Imaging, Wayne, NJ, United States) was used to develop films. Obtained images were analyzed using Image J software and each protein level was finally quantified after normalization via β-actin.

Mitochondrial and Cytosolic Fractionation

Subcellular fractionation was performed according to the published protocol (Dimauro et al., 2012) with a slight modification. HCN cells were homogenized by vortexing for 15 min in lysis buffer (250 mM sucrose, 50 mM Tris-HCl, pH 7.4, 5 mM $MgCl_2$, 1 × Halt protease and phosphatase inhibitor cocktail) and kept on ice for 30 min. The homogenate was centrifuged at 600 ×*g* for 15 min and the supernatant (S_0) was further centrifuged at 11,000 ×*g* for 10 min to separate the supernatant (S_1) and pellet (P_1). An equal volume of cold 100% acetone was added to S_1 and the samples were incubated overnight at –20°C to precipitate the proteins. After centrifugation at 12,000 ×*g* for 5 min, the pellet was resuspended in lysis buffer and used as the cytosolic fraction. P_1, which contained the mitochondrial fraction, was resuspended in lysis buffer and centrifuged at 11,000 ×*g* for 10 min; the pellet (P_2) was resuspended in extraction buffer (50 mM Tris-HCl pH 6.8, 1 mM EDTA, 0.5% Triton-X 100, and protease and phosphatase inhibitor cocktails) and sonicated with a Bioruptor KRB-01 (CosmoBio, Japan) on ice 3 times for 10 s with 30 s intervals. We used this fraction as the mitochondrial fraction.

Plasmids and Transfection

Plasmids encoding RFP-LC3, EGFP-LC3, monomeric RFP-GFP tandem fluorescent LC3 (mRFP-GFP-LC3), and GFP-double FYVE domain–containing protein 1 (DFCP1) were purchased from Addgene (Cambridge, MA, United States). DsRed2-Mito was purchased from Takara Bio United States (Mountain View, CA, United States) and Case12-mito from Evrogen (Moscow, Russia). Cells were seeded in a 6-well plate 24 h prior to transfection. Transfection was conducted using Lipofectamine 2000 (Invitrogen) according to the manufacturer's instructions. The Plasmids list is shown in **Table 1**.

Park2 and *Pink1* Knockout

Rat *Park2* single guide RNA (sgRNA), rat *Pink1* sgRNA, and Cas9 were designed by and purchased from Toolgen (Republic of Korea). The target sequence for *Park2* was 5′-ATCACTCGCAGCTGGTCAGCTGG-3′ and the target sequence for *Pink1* was 5′-CCTGACACCGGGCCCGGCTTGGG-3′. HCN cells were transfected with *Park2* sgRNA or *Pink1* sgRNA and Cas9 for 24 h and selected by hygromycin B (InvivoGen, San Diego, CA, United States).

Quantitative Real-Time Reverse Transcription Polymerase Chain Reaction (qRT-PCR)

RNA was isolated from HCN cells using QIAzol lysis reagent (Qiagen, Germantown, MD, United States) and used to synthesize cDNA with an ImProm-II Reverse Transcriptase kit (Promega). A CFX96 Real-Time PCR detection system (Bio-Rad) and TOPreal qPCR 2X premix (Enzynomics, Republic of Korea) were used for real-time PCR with the following primers: rat *Park2* forward (5′-ATG ATA GTG TTT GTC AGG TT-3′) and reverse (5′-AGA CAA AAA AGC TGT GGT AG-3′); rat ring finger protein 19A (*Rnf19a/Dofrin*) forward (5′-ATC TCC AAT CGT CTG CTT CGT CTG-3′) and reverse (5′-CGT TCA GTG CATTCT GGA CAA CTG-3′); rat heme-oxidized IRP2 ubiquitin ligase-1 (*HOIL-1/Rbck1*) forward (5′-ATG GAC GAG AAGACC AAG AAA GCA-3′) and reverse (5′-GTT GAG TGA TGT GTT GCG GGC T-3′); β-actin *(Actb)* forward (5′-AGC CAT GTA CGT AGC CAT CC-3′) and reverse (5′-CTC TCA GCT GTG GTG GTG AA-3′).

Flow Cytometry Analysis

Before harvesting, HCN cells were incubated with 100 nM MitoTracker Deep Red and 50 nM MitoTracker Green (Thermo Fisher Scientific) for 15 min. Harvested cells were washed in cold PBS twice and analyzed using a BD Accuri C6 flow cytometer (BD

TABLE 1 | Information of plasmids.

Plasmid name	Plasmid numbers	Characteristics	Reference
pmRFP-LC3	21075	Encoding a fusion of rat LC3 and mRFP	Kimura et al., 2007
pEGFP-LC3	21073	Encoding a fusion of rat LC3 and EGFP	Kabeya et al., 2000
ptfLC3	21074	Encoding a fusion of rat LC3 and mRFP and EGFP	Kimura et al., 2007
pMXs-puro GFP-DFCP1	38269	Encoding a fusion of *M. musculus* DFCP1 and EGFP	Itakura and Mizushima, 2010
pDsRed2-Mito	632421	Encoding a fusion of *Discosoma* sp. red fluorescent protein (DsRed2) and a mitochondrial targeting sequence of human cytochrome c oxidase subunit VIII (Mito).	
pCase12-mito	FP992	Encoding mitochondria-targeted fluorescent Ca^{2+} sensor Case12	Gorman, 1985

Biosciences, San Jose, CA, United States). MitoTracker Green- and MitoTracker Deep Red-stained cells were detected by FL1 and FL3 channel, respectively. Total 30,000 cells were counted in each condition. For negative control, non-stained cells and single stained cells were counted. Data were analyzed by BD Accuri C6 software.

Immunocytochemistry and Quantification of Relative Fluorescence Intensity or Colocalization Coefficient

Cells were fixed in 4% paraformaldehyde or methanol for 5–10 min, washed in PBS twice, and mounted on a glass slide with mount solution (Dako, Carpinteria, CA, United States). Samples were examined under a confocal microscope (LSM 700, Carl Zeiss). Relative fluorescence intensities of TMRE, Case12-mito, p-Ub-S65 were analyzed using Image J software. The cytosol region excluding nucleus area was drawn with drawing tools and integrated density of this region was measured. The relative fluorescence intensity in each experimental condition was quantified based on the mean value of the I(+) condition.

Colocalization coefficient of mitochondria with LC3 or DFCP1 was analyzed using "colocalization" tool from Zen software (Carl Zeiss) and then quantified using colocalization coefficient following the guideline of the software.

Promoter Activity Assay

pGL3 and pRL-TK vectors (Promega) contain modified coding regions for firefly luciferase and *Renilla* luciferase, respectively. We used firefly luciferase as a reporter for transcriptional activity of *Park2* promoter. *Renilla* luciferase, which was expressed constitutively, served as a control for normalization. Cells were seeded in a 12-well plate 24 h prior to transfection, and pGL3-basic vectors carrying a series of truncated forms of the rat *Park2* promoter region were co-transfected with pRL-TK using Lipofectamine 2000. After transfection for 12 h, the cells were collected in I(-) medium and re-seeded in a 24-well plate. Luciferase assay was conducted by using a Dual-Glo Luciferase Assay System (Promega) according to the manufacturer's instructions. Freshly prepared Dual-Glo luciferase reagent solution was added to the cells and luciferase activity was measured in a white 96-well plate in a SpectraMax L luminometer. We measured and analyzed the data using "photon counting mode" of SoftMax Pro Software. We calculated the relative values of each result based on I(+).

Statistics

Data from at least three independent experiments were expressed as the mean ± standard error (SEM). "n = " represents a number of cells, unless otherwise stated. Statistical significance was determined using the paired t-test for two-group experiments. For experiments with three or more groups, comparisons were made using one-way analysis of variance and Tukey's test. GraphPad Prism 5 (GraphPad Software, San Diego, CA, United States) was used to analyze the data. Differences were considered statistically significant for p-values < 0.05.

RESULTS

Insulin Withdrawal Induces ADCD With Mitochondrial Alterations in HCN Cells

HCN cells depend on insulin for their survival and proliferation (Palmer et al., 1997). Insulin withdrawal significantly increased cell death (**Figure 1A**). Consistent with our previous reports (Yu et al., 2008; Baek et al., 2009) on the non-apoptotic nature of insulin withdrawal-induced death of HCN cells, caspase 3 activity (**Figure 1B**) and the number of activated, cleaved caspase 3 (C.Casp3)-positive cells remained very low despite an increase in cell death, indicating no involvement of apoptosis (**Figures 1C,D**). On the other hand, a robust induction of caspase 3 activation by the well-known prototypical apoptosis inducer STS demonstrates normal apoptotic capability of HCN cells (**Figures 1B–D**). We also confirmed that DNA fragmentation, a marker of apoptosis, did not occur in insulin-deprived HCN cells (**Figure 1E**). 63% of total cells were TUNEL-positive by STS-treatments, but TUNEL-positive cells were not observed in either I(+) or I(-) condition. Also, ineffectiveness of pan caspase inhibitor Z-VAD against insulin withdrawal-induced death of HCN cells have been reported in our previous studies (Chung et al., 2015; Ha et al., 2015). These results support non-apoptotic nature of insulin withdrawal-induced HCN cell death. In addition, insulin-deprived HCN cells did not undergo necrosis. Necrostatin-1, an inhibitor of necroptosis, blocked cell death induced by H_2O_2 but did not prevent cell death induced by insulin withdrawal (**Figure 1F**). We also reported that suppression of autophagy by knockdown of Atg7 prevented HCN cell death following insulin withdrawal, indicating the causative role of autophagy in cell death (Yu et al., 2008). Characterization of cell death mode excluded apoptosis and necroptosis. Therefore, we presumed that PI/Hoechst-based cell death assay approximately measures total cell death under insulin withdrawal condition.

To measure autophagic flux, immunofluorescence assay using mRFP-GFP-LC3 was performed. The GFP, but not RFP signal is readily quenched in acidic conditions, such as within the autolysosomes (Kimura et al., 2007). As a result, autophagosomes and autolysosomes are observed as yellow (RFP^+GFP^+) and red (RFP^+GFP^-) puncta, respectively (Kimura et al., 2007). In insulin-deprived HCN cells, the number of both the yellow and red LC3 puncta increased, indicating an increase in autophagy flux in comparison with I(+) HCN cells (**Figures 1G,H**). In addition, when autophagosome maturation was blocked by treatment with Baf.A1, which inhibits fusion between autophagosomes and lysosomes, accumulation of yellow LC3 puncta in I(-) HCN cells was much higher than without Baf.A1 treatment, confirming a robust biogenesis of autophagic vesicles in I(-) HCN cells (**Figures 1G,H**).

Taken together, insulin withdrawal-induced cell death meets the following criteria: (i) increased autophagic flux is observed (this study; Yu et al., 2008; Baek et al., 2009); (ii) suppression

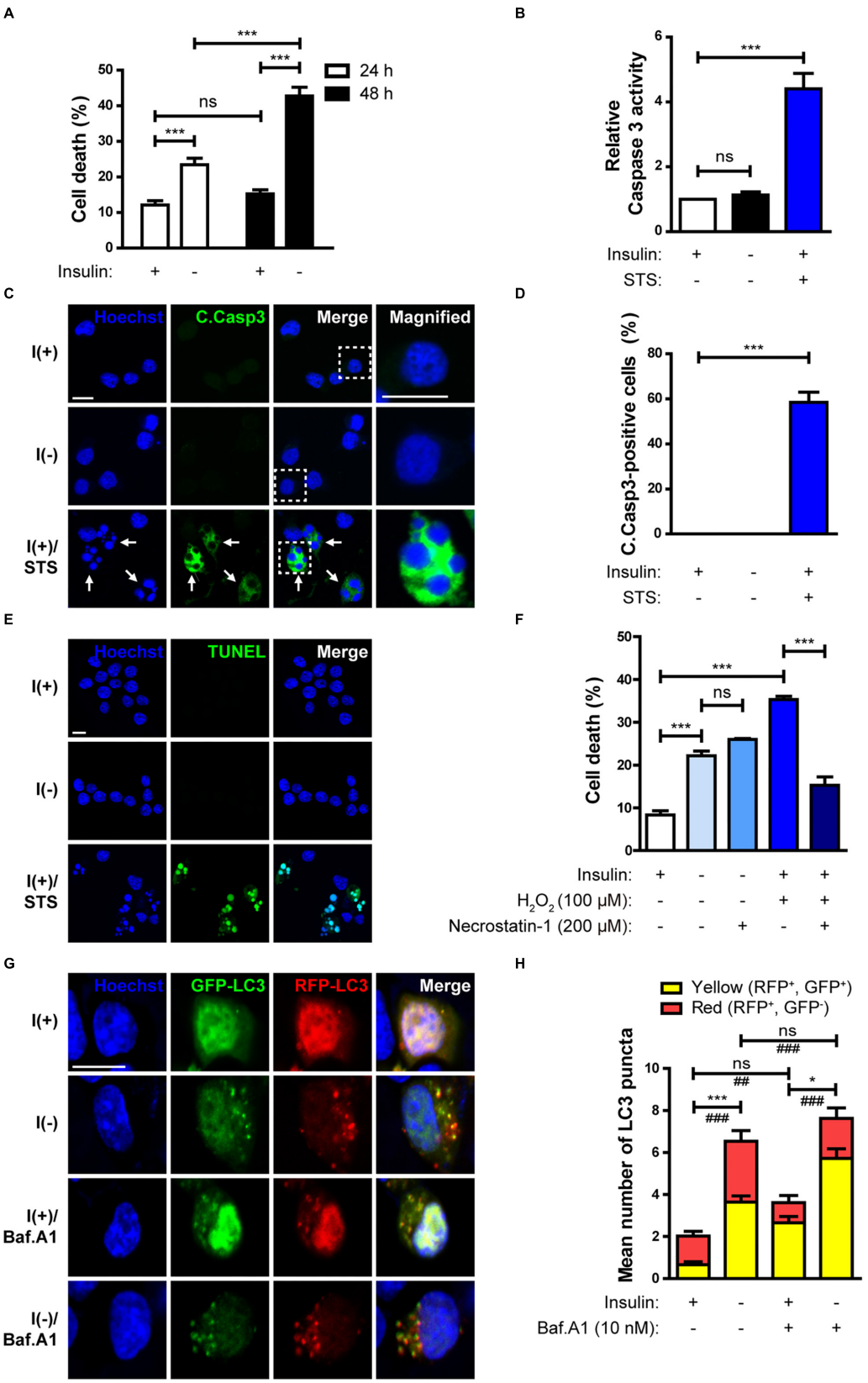

FIGURE 1 | Continued

FIGURE 1 | Insulin withdrawal induces autophagy-dependent cell death (ADCD) in adult hippocampal neural stem (HCN) cells. **(A)** Cell death rates in insulin-deprived HCN cells after insulin withdrawal for 24 and 48 h (n = 3). **(B)** Caspase 3 activity after insulin withdrawal for 24 h. HCN cells were treated with staurosporine (STS; 0.5 μM) for 3 h as a positive control of apoptosis (n = 4). **(C)** Immunocytochemical detection of cleaved caspase 3 (C.Casp3) in HCN cells after insulin withdrawal for 24 h. Cells were treated with STS (0.5 μM, 8 h) (n = 47 cells for I(+), 50 cells for I(-), 56 cells for I(+)/STS from 3 independent experiments). Arrows indicate fragmented nuclei in C.Casp3-positive cells. Scale bars, 10 μm. **(D)** Quantification of C.Casp3-positive cells from **(C)** (n = 47 cells for I(+), 50 cells for I(-), 56 cells for I(+)/STS from 3 independent experiments). **(E)** TUNEL assay in HCN cells after insulin withdrawal for 24 h. Cells were treated with STS (0.5 μM, 8 h) (n = 258 cells for I(+), n = 310 cells for I(-), n = 340 cells for I(+)/STS from 3 independent experiments). Scale bar, 10 μm. **(F)** Cell death rates in insulin-deprived HCN cells treated with necrostatin-1 after insulin withdrawal for 24 h (n = 3). **(G)** Assessment of autophagy flux by mRFP-GFP-LC3 puncta assay after insulin withdrawal for 24 h. Cells were treated with Baf.A1 (10 nM) for 1 h before harvesting. Scale bar, 10 μm. **(H)** Quantification of red and yellow LC3 puncta from **(G)** (n = 47 cells for I(+), 40 cells for I(+)/Baf.A1, 52 cells for I(-), 50 for I(-)/Baf.A1 from 3 independent experiments). $^{*}p < 0.05$, $^{***}p < 0.001$ for the red puncta; $^{\#\#}p < 0.01$, $^{\#\#\#}p < 0.001$ for the yellow puncta; ns, not significant.

of autophagy prevents cell death (Yu et al., 2008); and (iii) alternative cell death pathways such as apoptosis and necrosis are not involved (this study; Yu et al., 2008; Chung et al., 2015; Ha et al., 2015). Thus, from the current and our previous data we concluded that insulin-deprived HCN cells undergo ADCD.

Our previous observation suggests that insulin withdrawal induces an increase in cytosolic Ca^{2+} that originates from the ER (Chung et al., 2016). We hypothesized that this increase may induce mitochondrial Ca^{2+} accumulation. To measure mitochondrial Ca^{2+} level, we co-transfected HCN cells with RFP-LC3 and Case12-mito, which is an indicator of mitochondrial Ca^{2+} level (Takeuchi et al., 2013). Co-transfection with RFP-LC3 and Case12-mito showed an increase in mitochondrial Ca^{2+} levels in autophagy-induced cells following insulin withdrawal (**Figures 2A,B**). Since elevated mitochondrial Ca^{2+} could cause mitochondrial depolarization (Baumgartner et al., 2009), we next examined mitochondrial depolarization by staining HCN cells with MitoTracker Deep Red or TMRE, which are sequestered in healthy, polarized mitochondria, but are excluded from depolarized mitochondria (Scaduto, R. C. Jr. and Grotyohann, 1999). Fluorescence-activated cell sorting (FACS) analysis of HCN cells co-stained with MitoTracker Green (to ensure the equal number of total mitochondria) and MitoTracker Deep Red (for measurement of mitochondria membrane potential) revealed a reduced number of MitoTracker Deep Red–positive cells, indicating an increase in mitochondrial depolarization following insulin withdrawal (**Figure 2C**). This result was confirmed by fluorescence microscopy, which showed lower staining intensity of TMRE in I(−) HCN cells than in I(+) HCN cells (**Figures 2D,E**).

Insulin-Deprived HCN Cells Undergo Excessive Mitophagy

Because we observed mitochondrial Ca^{2+} accumulation and depolarization during ADCD, we next examined whether depolarized mitochondria underwent mitophagy. Co-transfection of HCN cells with GFP-LC3 and DsRed-Mito showed that their overlap was increased by insulin withdrawal **Figures 3A,B,E**). Phosphatidylinositol 3-phosphate (PI3P) is a key signaling lipid for recruitment of autophagy effector proteins to initiate autophagosome generation (Burman and Ktistakis, 2010). DFCP1 contains PI3P-recognizing FYVE domains and binds to PI3P, and thus can serve as a marker of autophagosome nucleation (Axe et al., 2008). Therefore, we assessed translocation of DFCP1 to the vicinity of damaged mitochondria as another measure of mitophagy (Lazarou et al., 2015). I(-) HCN cells showed not only more DFCP1 puncta, but also increased colocalization of DFCP1 and mitochondria in comparison with I(+) HCN cells, confirming the occurrence of mitophagy (**Figures 3C,D,F**).

As an alternative approach to demonstrate the localization of LC3 in mitochondria, we used subcellular fractionation. Successful separation of mitochondrial and cytosolic fractions was verified by Western blotting analysis using VDAC and β-tubulin as respective markers for these fractions. We observed more LC3-II in the mitochondrial fraction of I(-) HCN cells than in that of I(+) cells (**Figures 3G,H**). These results suggest that mitophagy is induced in HCN cells following insulin withdrawal.

Parkin Is Upregulated Through Inhibition of Its Transcriptional Repressor c-Jun in Insulin-Deprived HCN Cells

Parkin-mediated mitophagy has been actively studied (Narendra et al., 2008). However, it remains ill-defined whether Parkin-dependent mitophagy can contribute to cell death. Since we observed mitophagy in insulin-deprived HCN cells undergoing ADCD, we wondered if Parkin is involved in ADCD through regulation of mitophagy. To that end, we first checked Parkin levels in HCN cells following insulin withdrawal. Parkin protein levels were significantly increased 24 and 48 h after insulin withdrawal (**Figures 4A,B**). We compared the time course of Parkin upregulation with that of autophagy flux induction following insulin withdrawal. An increase in Parkin protein amount was first observed as early as 3 h after insulin withdrawal, which coincided well with an increase in autophagy flux (**Figures 4C,D**). Related to its protein levels, its transcript levels also increased significantly following insulin withdrawal (**Figure 4E**). Interestingly, Parkin protein level was decreased when apoptosis was induced by STS, suggesting the potential ADCD-specific role of Parkin in HCN cells (**Figures 4A,B**). Like Parkin, Dorfin, and HOIL-1 are also RING-IBR-RING-finger domain E3 ligases present in the brain (Niwa et al., 2002; Tanaka et al., 2004). Interestingly, their mRNA levels were not altered in response to insulin withdrawal (**Figure 4F**).

Because upregulation of the Parkin mRNA level by insulin withdrawal seemed to play an important role in ADCD of

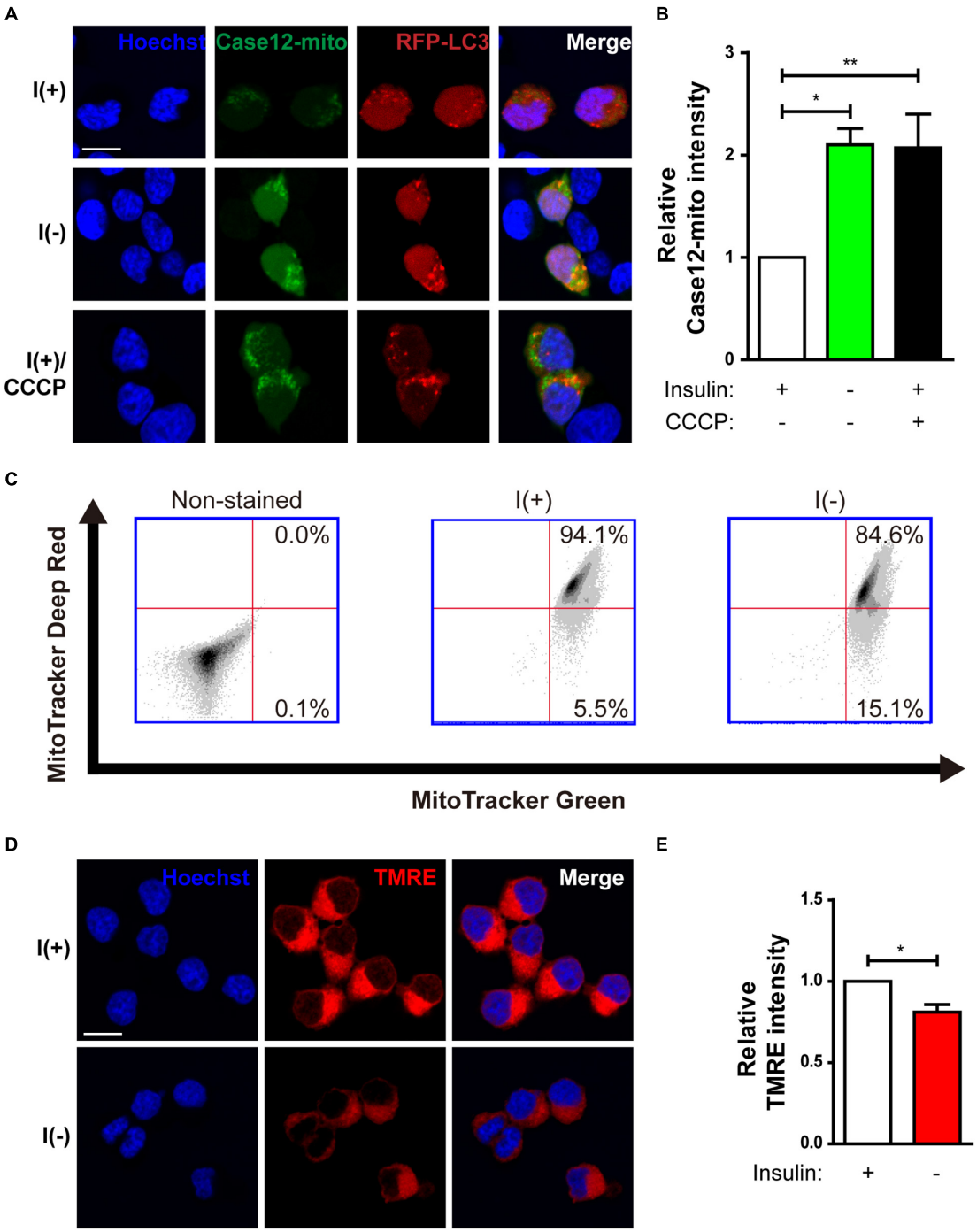

FIGURE 2 | Changes in mitochondria of HCN cells after insulin withdrawal. **(A)** Assessment of mitochondrial Ca^{2+} levels using Case12-mito after insulin withdrawal for 24 h. Scale bar, 10 μm. **(B)** Quantification of fluorescence intensity of Case12-mito in HCN cells (n = 33 cells for I(+), 25 cells for I(-), 36 cells for I(+)/CCCP from 3 independent experiments). **(C)** FACS analysis of HCN cells stained with MitoTracker Green to determine the total number of mitochondria and MitoTracker Deep Red to determine the number of depolarized mitochondria after insulin withdrawal for 24 h. 30,000 cells were analyzed in each experiment. **(D)** Fluorescence imaging analysis of TMRE-stained HCN cells. Scale bar, 10 μm. **(E)** Quantification of fluorescence intensity of TMRE in HCN cells (n = 12 cells from 2 independent experiments). Relative TMRE intensity of fluorescence microscope image was measured by image J. *$p < 0.05$, **$p < 0.01$.

HCN cells, we investigated the regulation of Parkin gene transcription in insulin-deprived HCN cells. First, to delineate the *Park2* promoter region critical for transcription, we cloned a 2.5-kilobase rat *Park2* promoter fragment in the pGL3-luc vector in front of a sequence encoding luciferase and measured *Park2* promoter activity by luciferase assay.

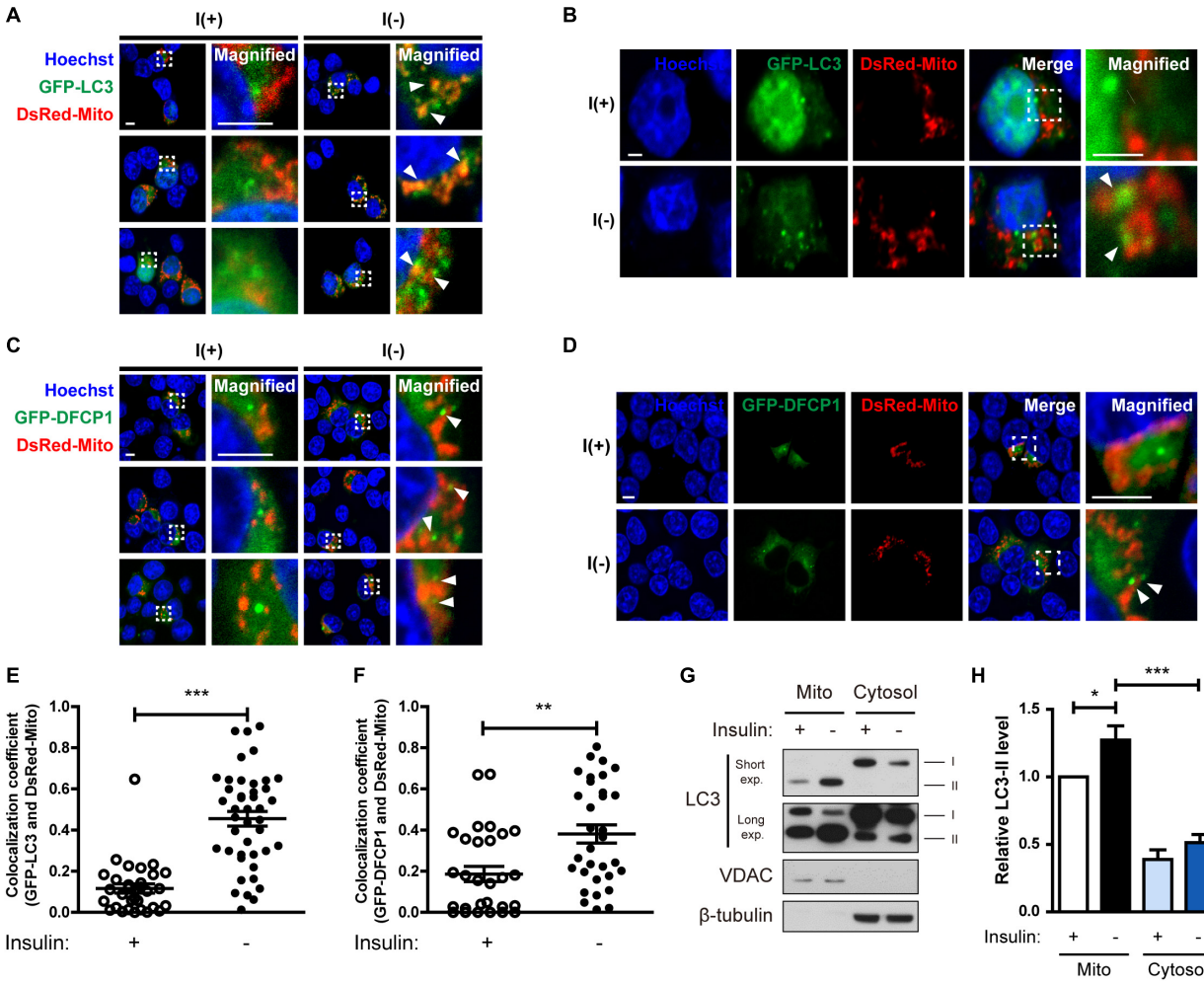

FIGURE 3 | Insulin-deprived HCN cells undergo excessive mitophagy. **(A,B)** Colocalization of GFP-LC3 and DsRed-Mito (arrowheads) after insulin withdrawal for 24 h. Scale bars, 5 μm for **(A)**, 2 μm for **(B)**. **(C,D)** Immunofluorescence of GFP-DFCP1 and DsRed-Mito after insulin withdrawal for 24 h. Arrowheads indicate colocalization of GFP-DFCP1 and DsRed-Mito. Scale bars, 5 μm for **(C)**, 2 μm for **(D)**. **(E)** Quantification of colocalization of LC3 and mitochondria (n = 31 cells for I(+), 42 cells for I(-) from 3 independent experiments). **(F)** Quantification of colocalization of DFCP1 and mitochondria (n = 30 cells for I(+), 33 cells for I(-) from 3 independent experiments). **(G)** Western blotting analysis of mitochondrial translocation of LC3 after insulin withdrawal for 24 h. Mito, mitochondrial fraction; cytosol, cytosolic fraction. The blots shown are representative of four experiments with similar results. **(H)** Quantification of LC3-II levels (n = 4) from **(G)**. $^{*}p < 0.05$, $^{**}p < 0.01$, $^{***}p < 0.001$.

Luciferase expression driven by the cloned *Park2* promoter fragment led to substantial luciferase activity in the basal condition (presence of insulin) in comparison with the empty vector (**Figure 5A**). Activity was further increased by insulin withdrawal (**Figure 5A**). Next, we cloned a series of truncated versions of the *Park2* promoter to find the sequences critical for *Park2* transcription and found that 500 bp upstream of the *Park2* gene is the core promoter region (**Figure 5B**).

Next, we used the PROMO program (Messeguer et al., 2002; Farré et al., 2003) to predict the candidate transcription factors that may participate in both Parkin transcription and autophagy. Binding element analyses predicted several candidate transcription factors, including c-Jun because there were three potential c-Jun-binding sites in the *Park2* promoter region (**Figure 5C**). c-Jun is a transcription factor phosphorylated and activated mainly by c-Jun NH2 terminal kinase (JNK) (Minden et al., 1994). Based on prior reports on c-Jun functions in autophagy inhibition (Yogev and Shaulian, 2010) and *Park2* transcriptional repression (Bouman et al., 2011), we hypothesized that c-Jun decreases Parkin level. To test this hypothesis, we used an ATP-competitive JNK inhibitor, SP60015, to block phosphorylation of c-Jun by JNK. SP600125 treatment increased Parkin mRNA and protein levels in the presence of insulin, suggesting that *Park2* is under transcriptional repression by c-Jun in the I(+) condition when Parkin level is low (**Figures 5D–G**). However, Parkin expression levels was not further increased by SP600125 treatment in insulin-deprived HCN cells (**Figures 5F,G**), probably due to already high Parkin protein level in I(-) HCN cells. Inactivation of the mammalian

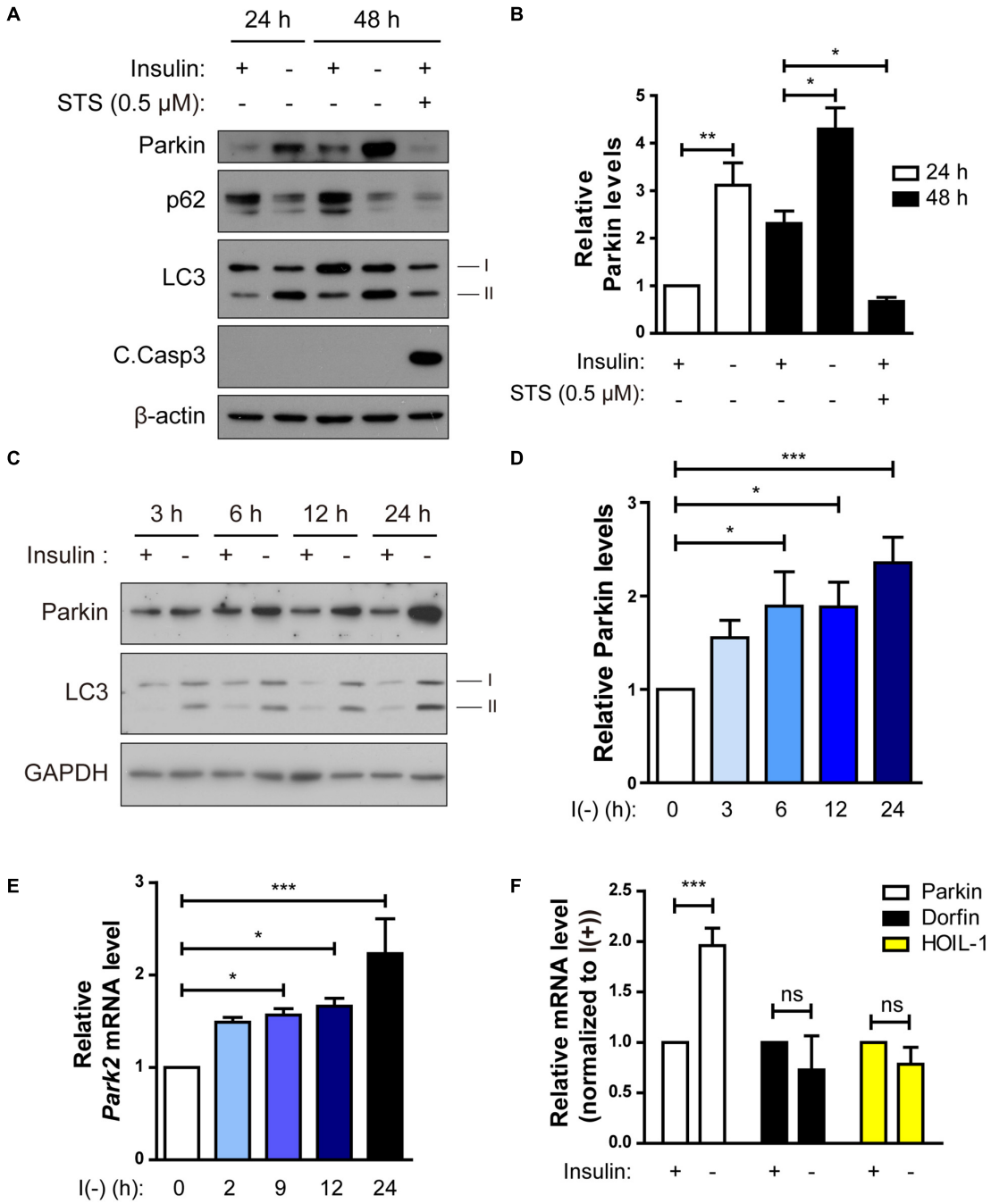

FIGURE 4 | Parkin expression is upregulated following insulin withdrawal. **(A)** Western blotting analysis of Parkin protein level in HCN cells after insulin withdrawal for 24 and 48 h. **(B)** Quantification of Parkin protein level (n = 3 or 4). **(C)** Time course analysis of Parkin protein levels following insulin withdrawal. **(D)** Quantification of Parkin protein levels (n = 5) from **(C)**. **(E)** Time course analysis of mRNA levels of Parkin following insulin withdrawal (n = 4). **(F)** Changes in the mRNA levels of Parkin, Dorfin, and HOIL-1 (n = 3–7). *$p < 0.05$, **$p < 0.01$, ***$p < 0.001$; ns, not significant.

target of rapamycin (mTOR)-Akt pathway in I(-) HCN cells was observed previously (Yu et al., 2008). To test whether the mTOR-Akt cascade is involved in Parkin expression, we checked the Parkin expression levels in I(+) condition with rapamycin, which is an mTOR inhibitor. We observed increased Parkin expression in rapamycin-treated I(+) HCN cells, suggesting the involvement of mTOR-Akt pathway in regulation of Parkin following insulin withdrawal in HCN cells (**Figure 5H**).

If c-Jun is a transcriptional repressor of the *Park2* gene, then its level should decrease following insulin withdrawal to allow the upregulation of the Parkin mRNA level. To validate this notion, we assessed changes in c-Jun protein in the absence of insulin.

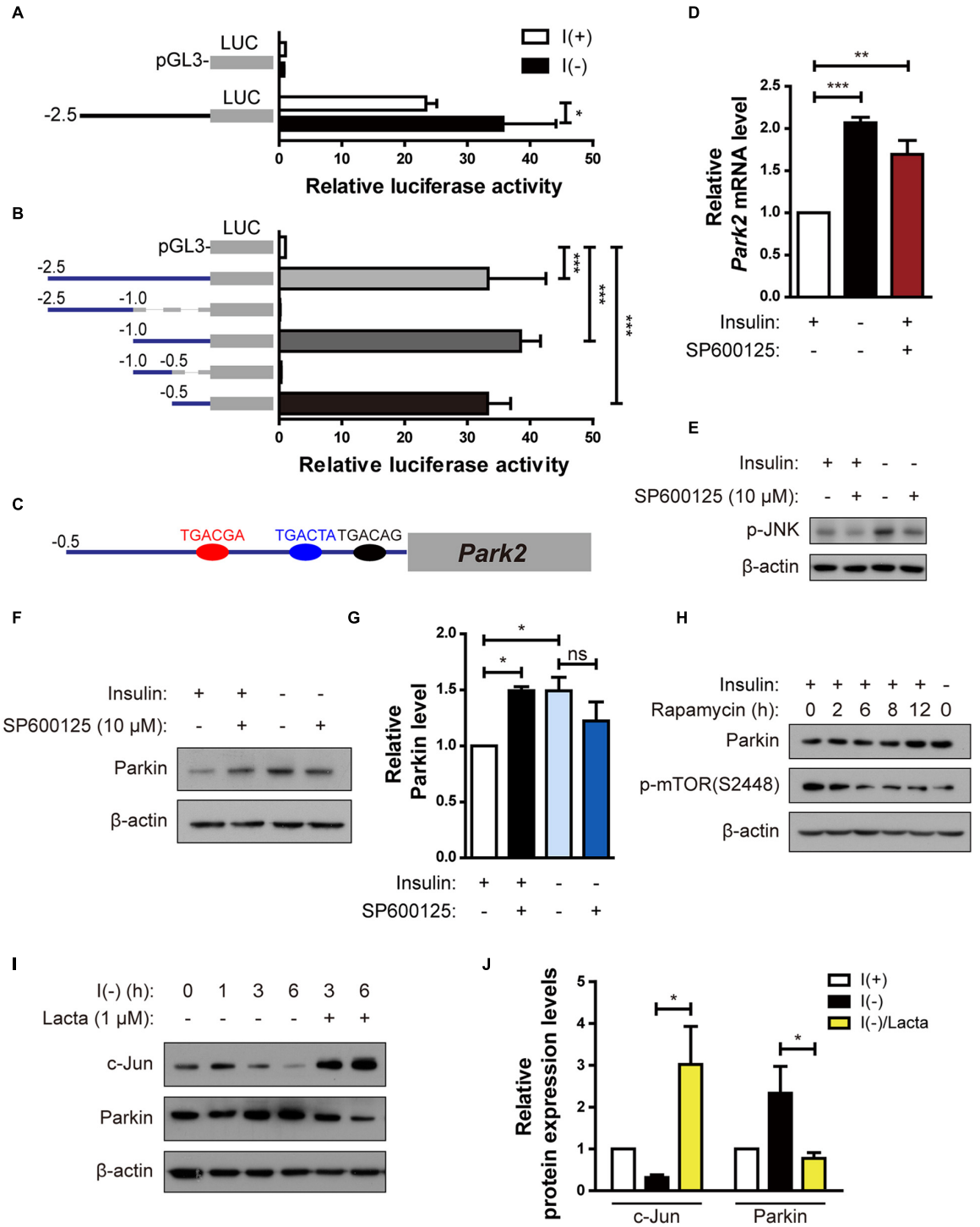

FIGURE 5 | Parkin is upregulated in HCN cells by degradation of c-Jun, a transcriptional repressor, following insulin withdrawal. **(A)** Luciferase activity assay to analyze *Park2* promoter activity after insulin withdrawal for 24 h ($n = 3$). **(B)** Activities of various truncated fragments of the *Park2* promoter in I(+) cells. Promoter activity was measured using a luciferase assay ($n = 3$–7). **(C)** Prediction of c-Jun-binding sites in the *Park2* promoter region. **(D)** Parkin mRNA level in HCN cells treated with SP600125, an ATP-dependent JNK inhibitor, (10 μM) for 8 h in comparison with that in I(-) HCN cells after insulin withdrawal for 24 h ($n = 3$). **(E)** Western blotting analysis of p-JNK levels in HCN cells after insulin withdrawal for 2 h. SP600125 (10 μM) was treated 10 μM for 2 h. The blots shown are representative of three experiments with similar results. **(F)** Western blotting analysis of Parkin protein levels in SP600125 (10 μM, 8 h) -treated HCN cells. The blots shown are representative of five experiments with similar results. **(G)** Quantification of Parkin levels ($n = 5$) from **(F)**. **(H)** Increased Parkin protein levels in HCN cells treated with Rapamycin (20 nM, 2 h), a mTOR inhibitor. **(I)** Time course analysis of c-Jun protein levels following insulin withdrawal in comparison with lactacystin treatment (Lacta, 1 μM). **(J)** Quantification of c-Jun and Parkin protein levels in I(-) HCN cells treated with or without Lacta (1 μM) for 6 h ($n = 3$). $^*p < 0.05$, $^{**}p < 0.01$, $^{***}p < 0.001$.

c-Jun protein amount was reduced in a time-dependent manner with kinetics similar to that of Parkin increase (**Figure 5I**). This gradual decrease in c-Jun level was due to its degradation via the ubiquitin–proteasome system, since the proteasome inhibitor lactacystin prevented c-Jun degradation (**Figures 5I,J**). Lactacystin-mediated blockage of c-Jun degradation decreased the Parkin protein level under insulin withdrawal conditions, confirming the inhibitory role of c-Jun in Parkin expression (**Figures 5I,J**). Taken together, these data reveal that c-Jun is a transcriptional repressor of the *Park2* gene, and proteasome-dependent degradation of c-Jun leads to upregulation of Parkin in insulin-deprived HCN cells.

Parkin Knockout Prevents ADCD in HCN Cells Following Insulin Withdrawal

To investigate the role of Parkin in ADCD of insulin-deprived HCN cells, we over-expressed Parkin, however, there was no significant change in ADCD rate (data not shown). We speculated that Parkin level was already high in insulin-deprived HCN cells and therefor over-expression of Parkin did not induce additional effects. Therefore, we ablated the *Park2* gene in HCN cells by using the CRISPR/Cas9 gene-editing technique and designated the knockout (KO) cells as sgParkin and control cells as sgCon.

Parkin KO attenuated an increase in LC3-II levels following insulin withdrawal (**Figures 6A,B**). Autophagy flux was also decreased in sgParkin cells, as revealed by a decrease in accumulation of LC3-II induced by Baf.A1 (**Figures 6C,D**). Also, ablation of the *Park2* gene reduced cell death in I(-) HCN cells (**Figure 6E**). However, Parkin KO did not prevent, but rather promoted apoptosis, since the two prototypical apoptotic inducers STS and etoposide (ETO) increased cell death rate to a greater extent and led to a more robust activation of caspase 3 and PARP in sgParkin than in sgCon cells (**Figures 6F–H**). These results suggest that Parkin has opposite pro-death or anti-death roles depending on HCN cell death mode. Parkin is essential for insulin withdrawal-triggered mitophagy and plays a pro-death role in ADCD. However, Parkin has anti-apoptotic activity against well-known apoptotic inducers and its deletion renders HCN cells more susceptible to apoptosis.

In the Parkin-dependent mitophagy model, PINK1 is essential for the action of Parkin (Narendra et al., 2010; Youle and Narendra, 2011). PINK1 constitutively shuttles between the cytosol and mitochondria in normal cells but accumulates on the outer membrane of depolarized mitochondria (Narendra et al., 2010). Therefore, we examined whether PINK1 is recruited to mitochondria in I(-) HCN cells. Fluorescence imaging analyses showed an increased accumulation of PINK1 on the mitochondria in I(-) HCN cells (**Figures 7A–C**). To further examine the involvement of PINK1 in mitophagy, we used an anti-p-Ub-S65 antibody. PINK1 is a ubiquitin kinase. Once stabilized on the outer membrane the depolarized mitochondria, PINK1 phosphorylates ubiquitin at S65, which further stimulates the E3 ligase activity of Parkin (Kane et al., 2014). As expected, in accordance with PINK1 accumulation, the signal intensity p-Ub-S65 was substantially increased in I(-) HCN cells (**Figures 7D,E**). In this experiment, the potent depolarizing agent CCCP was used as a positive control to chemically induce mitophagy (**Figures 7A–D**). In addition, ADCD was reduced by PINK1 KO (**Figure 7F**). In conclusion, PINK1 acts upstream of Parkin in insulin-deprived HCN cells, and HCN cells undergo ADCD through PINK1/Parkin-dependent mitophagy.

Parkin KO Rescues Mitochondrial Alterations and Prevents Initiation of Mitophagy in Insulin-Deprived HCN Cells

Next, we examined whether Parkin deletion affects events upstream of mitophagy. Interestingly, mitochondrial Ca^{2+} level was reduced in sgParkin cells (**Figures 8A,B**). Unexpectedly, we found that the ratio of depolarized mitochondria was lower in sgParkin than sgCon cells following insulin withdrawal (**Figure 8C**). These results suggest that Parkin is required for efficient ER-to-mitochondria Ca^{2+} transfer and ensuing depolarization. In accordance with decreases in the mitochondrial Ca^{2+} accumulation and depolarization, subsequent mitophagy-related events, such as mitochondrial translocation of LC3 (**Figures 8D,E,H**) and DFCP1 (**Figures 8F,G,I**), were all attenuated in I(-) sgParkin cells, suggesting that Parkin KO interfered with the initial steps of mitophagy. Our results suggest that Parkin deletion not only impairs the recognition of the depolarized mitochondria and their removal, but also blocks early changes in mitochondrial physiology and prevents initiation of mitophagy. Therefore, mechanistically, Parkin is intimately involved in mitophagy from its very early steps, including ER-to-mitochondria Ca^{2+} transfer and recruitment of the autophagy-initiating/elongating molecules to mitochondria.

DISCUSSION

Parkin can suppress or promote apoptosis depending on cell type and stressor. Our results are more in line with the anti-apoptotic role of Parkin in HCN cells challenged with well-known apoptotic stimuli. In contrast to this pro-survival role, we also found that Parkin promotes ADCD following the removal of insulin, the key survival neurotrophic factor for HCN cells. Currently, it is not known how these opposite roles of Parkin in the control of distinct modes of cell death are regulated. Overall, deregulated Parkin activity and mishandling of depolarized mitochondria will be detrimental to the cells and lead to neurodegeneration through various pathways depending on cell type and degeneration cue.

Although, PD is mainly a movement disorder with motor symptoms, non-motor symptoms such as sleep abnormalities, autonomic failure, and a range of neuropsychiatric symptoms including depression, anxiety, cognitive impairment, dementia, and impulse control disorders are increasingly being recognized as features of PD pathology (Meissner et al., 2011). So far, most therapeutic efforts have been focused on motor control, and alleviation of non-motor symptoms has received less attention. Therefore, there is an unmet need to alleviate non-motor symptoms for better therapeutic design and management of PD. However, currently there is no good

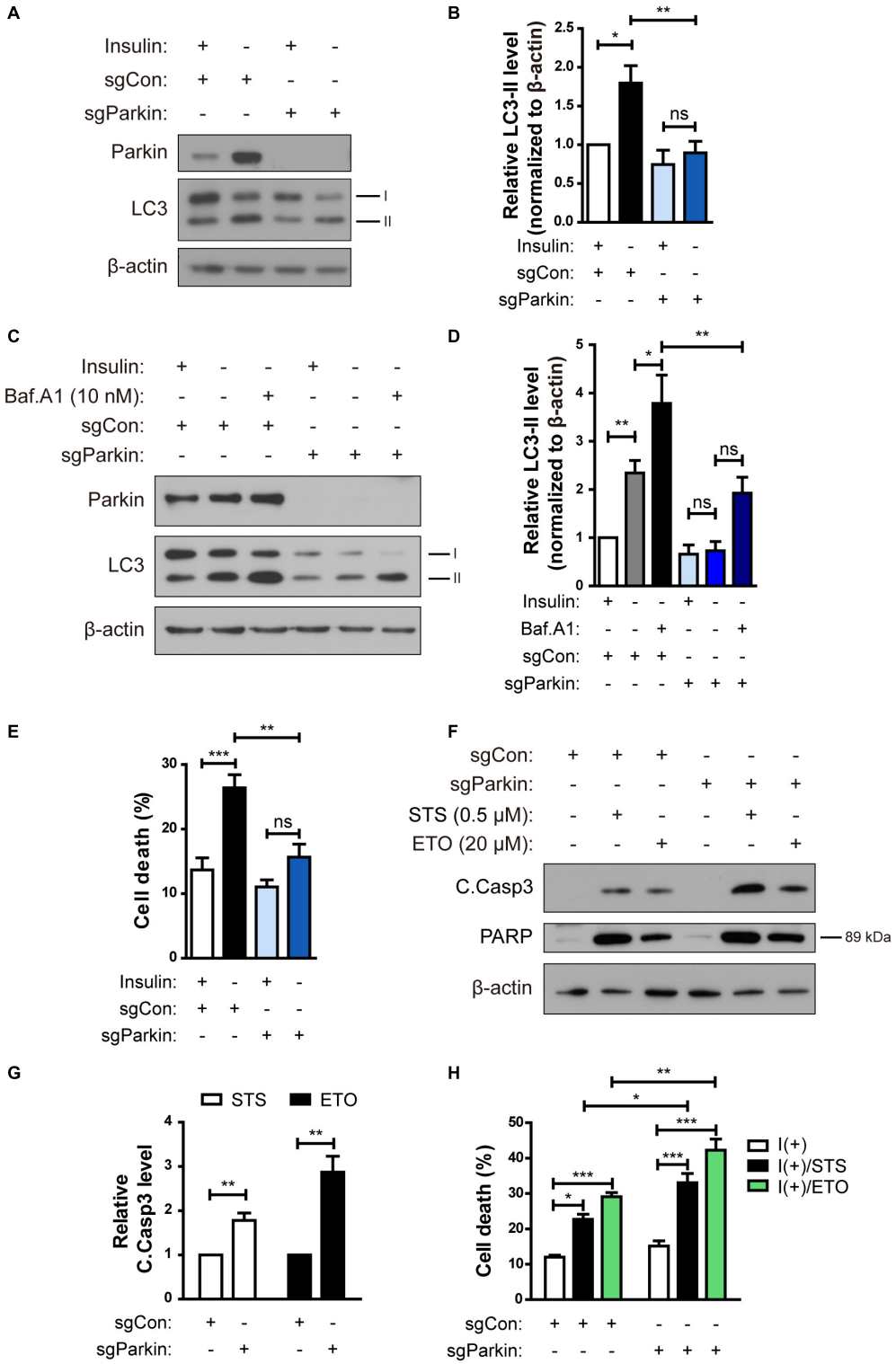

FIGURE 6 | Parkin knockout (KO) prevents ADCD in HCN cells following insulin withdrawal. **(A)** A decrease in autophagy level in sgParkin cells after insulin withdrawal for 24 h. **(B)** Quantification of LC3-II levels ($n = 6$). **(C)** Autophagic flux in sgParkin cells after insulin withdrawal. Cells were treated with Baf.A1 (10 nM) before harvesting. The blots shown are representative of four experiments with similar results. **(D)** Quantification of LC3-II levels ($n = 4$) from **(C)**. **(E)** Cell death rates in sgCon and sgParkin cells after insulin withdrawal for 24 h ($n = 11$). **(F)** Western blotting analysis of C.Casp3, PARP after STS (0.5 μM) or etoposide (ETO) (20 μM) treatment for 8 h. **(G)** Quantification of C.Casp3 level after normalization to β-actin ($n = 5$–7). **(H)** Cell death rates of sgCon and sgParkin cells after STS or ETO treatment for 8 h ($n = 3$). $^*p < 0.05$, $^{**}p < 0.01$, $^{***}p < 0.001$.

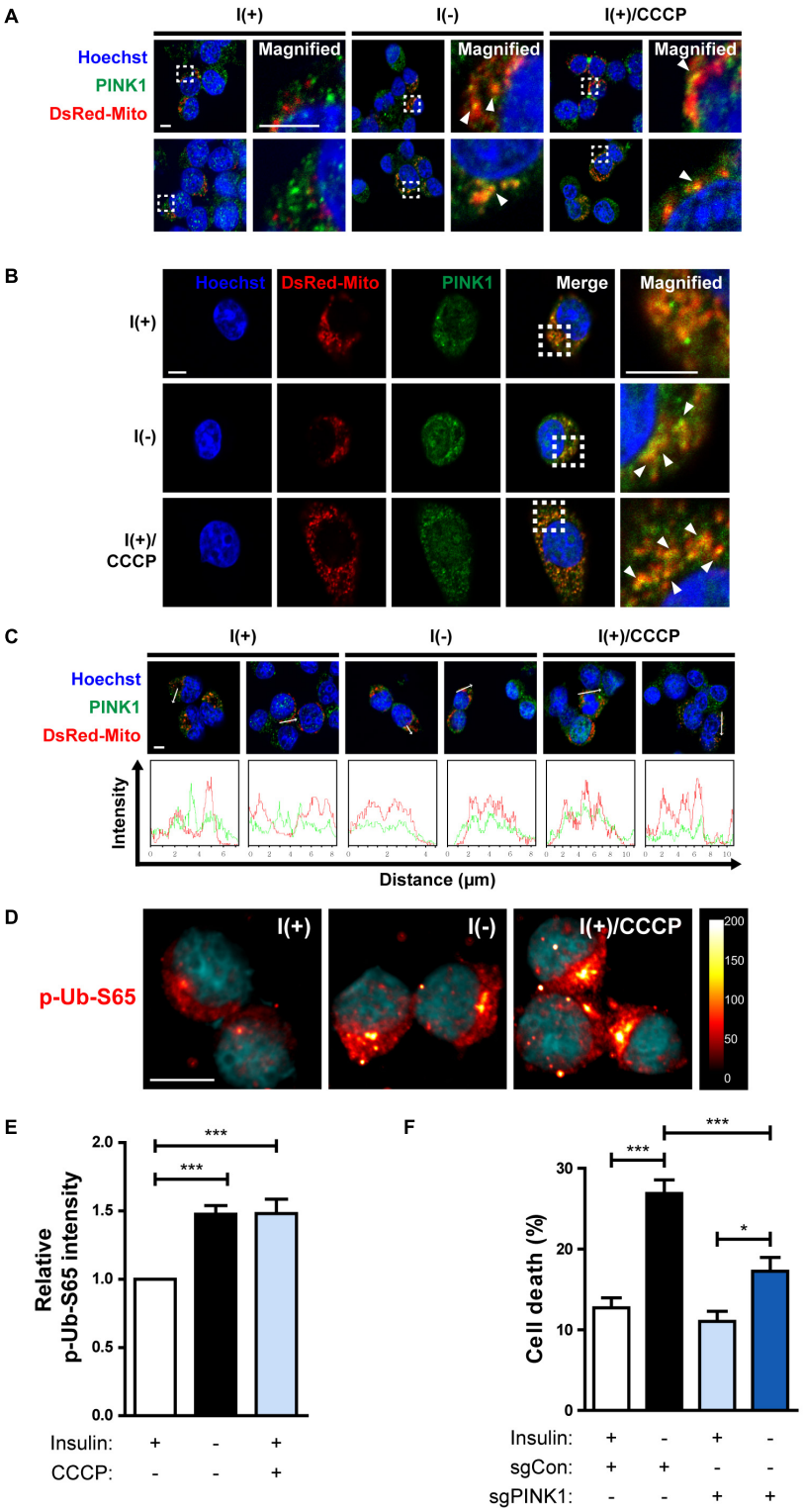

FIGURE 7 | HCN cells undergo PINK1/Parkin-dependent mitophagy following insulin withdrawal. **(A,B)** An increase in colocalization of PINK1 and mitochondria after insulin withdrawal for 24 h. Arrowheads indicate DsRed-Mito and PINK1 colocalization. Scale bars, 5 μm. **(C)** Intensity profile graphs of PINK1 and DsRed-Mito. Scale bar, 5 μm. **(D)** An increase in the level of p-Ub-S65 after insulin withdrawal for 24 h. Cells were treated with CCCP (10 μM) for 0.5 h as a positive control of mitophagy. Blue staining indicates Hoechst, and red staining indicates p-Ub-S65. Intensity is indicated in arbitrary units. Scale bar, 10 μm. **(E)** The mean intensity of p-Ub-S65 was quantified using ImageJ software (n = 33 cells for I(+), 38 cells for I(−), 46 cells for I(+)/CCCP from 3 independent experiments). **(F)** Cell death rates of sgCon and sgPINK1 cells (n = 4). $^{*}p < 0.05$, $^{***}p < 0.001$.

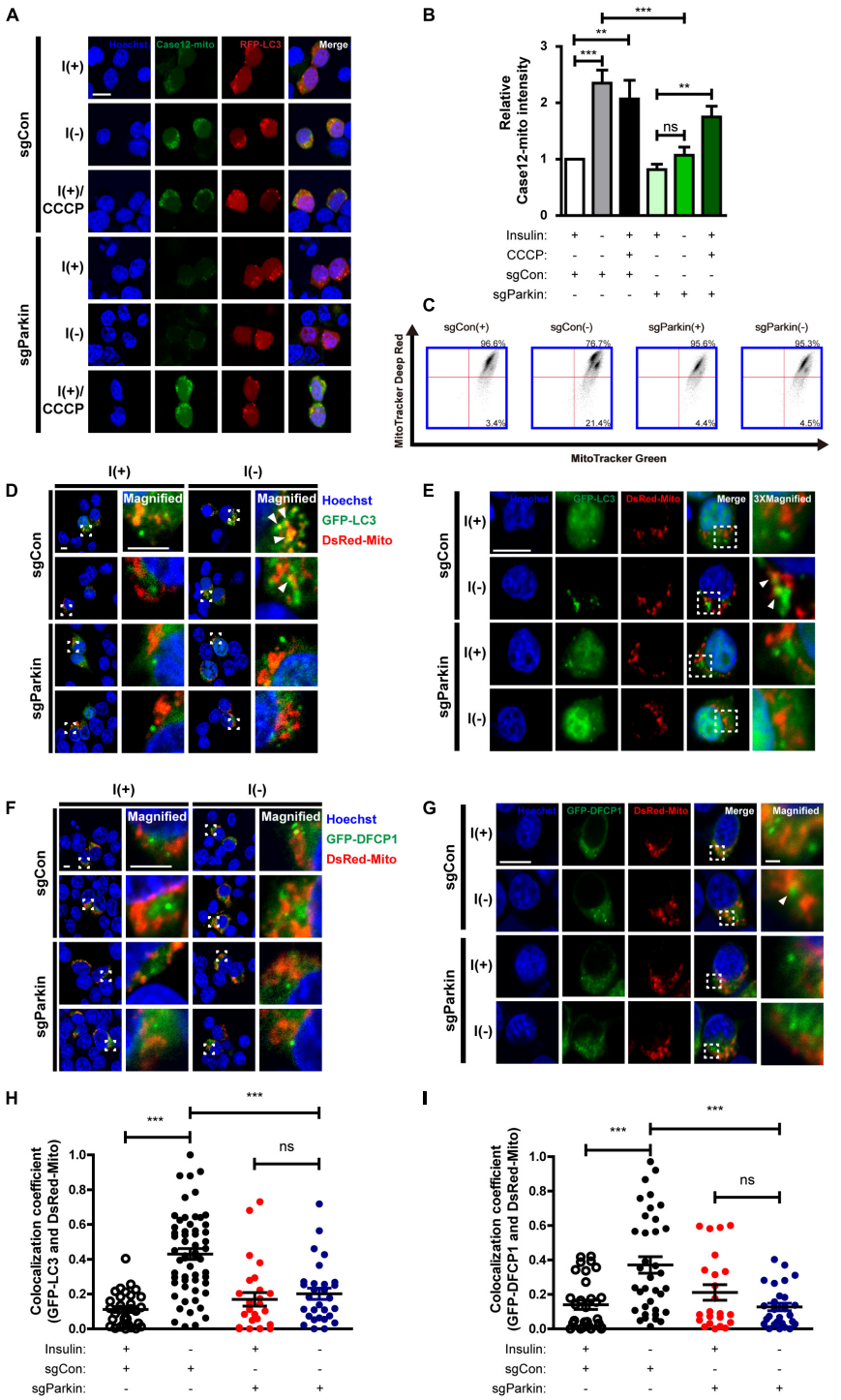

FIGURE 8 | Parkin KO prevents initiation of mitophagy following insulin withdrawal. **(A)** Fluorescence images of Case12-mito in sgParkin cells after insulin withdrawal for 24 h. Scale bar, 5 μm. **(B)** Quantification of fluorescence intensity of Case12-mito (n = 39 cells for sgCon(+), 28 cells for sgCon(-), 36 cells for sgCon(+)/CCCP, 80 cells for sgParkin(+), 73 cells for sgParkin(-), 37 cells for sgParkin(+)/CCCP from 3 independent experiments). **(C)** Double staining with MitoTracker Green and MitoTracker Deep Red to measure the ratio of depolarized mitochondria relative to total mitochondria after insulin withdrawal for 24 h. **(D,E)** Colocalization of LC3 and mitochondria in sgParkin cells after co-transfection with GFP-LC3 and DsRed-Mito. Colocalization was analyzed after insulin withdrawal for 24 h. Arrowheads indicate colocalization of GFP-LC3 and DsRed-Mito. Scale bars, 5 μm for **(D)**, 10 μm for **(E)**. **(F,G)** Colocalization of DFCP1 and mitochondria (arrowheads) in sgParkin cells after insulin withdrawal for 24 h. Scale bars, 5 μm for **(F)**, 10 μm for **(G)**. **(H)** Quantification of colocalization of LC3 and mitochondria (n = 26–52 cells from 3 independent experiments). **(I)** Quantitative analysis of colocalization of DFCP1 and mitochondria (n = 23–36 cells from 3 independent experiments). $^{**}p < 0.01$, $^{***}p < 0.001$; ns, not significant.

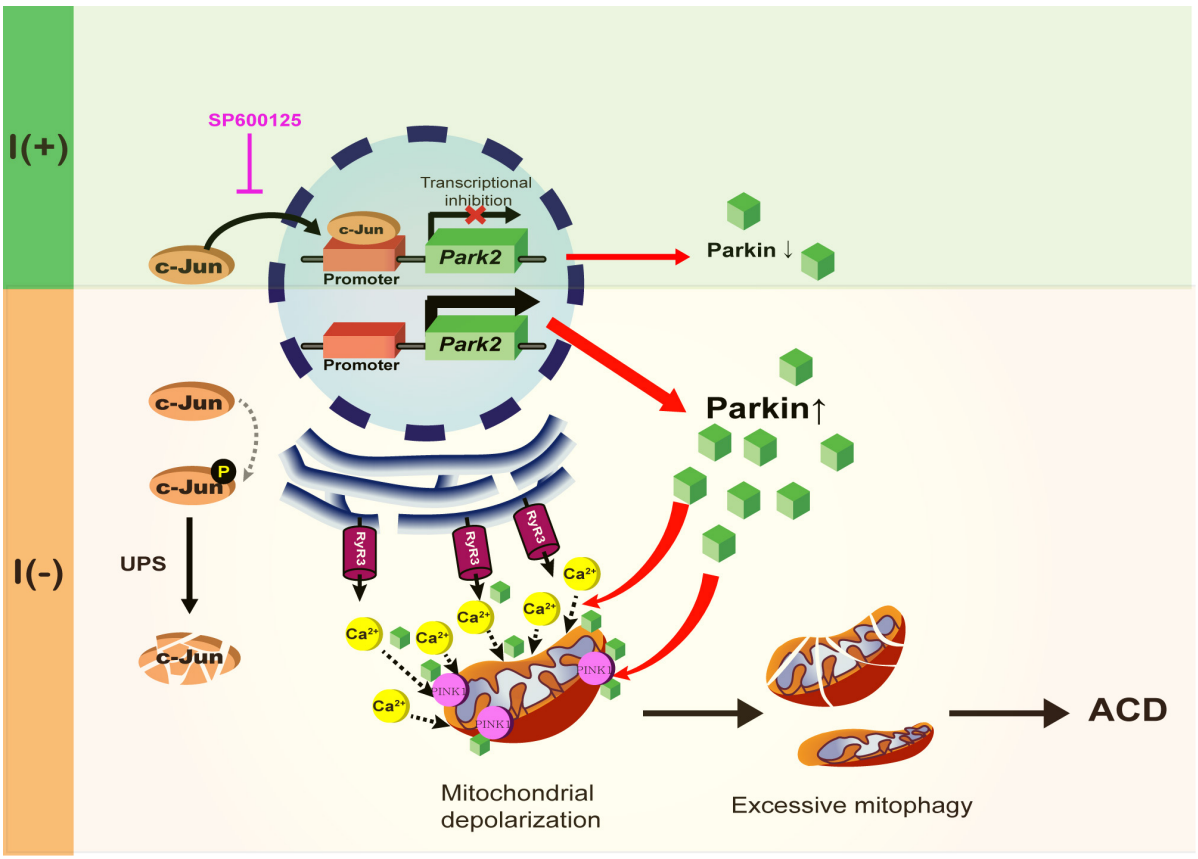

FIGURE 9 | A schematic diagram of Parkin-dependent mitophagy and ADCD. Parkin expression is increased by the degradation of c-Jun, a transcriptional repressor of Parkin in insulin-deprived HCN cells. Insulin withdrawal induced mitochondrial depolarization and recruitment of Parkin and PINK1 to mitochondria, where Parkin is also required for ER-to-mitochondria Ca^{2+} transfer. PINK1/Parkin-dependent mitophagy occurs in HCN cells following insulin withdrawal causing excessive mitophagy and ADCD.

animal or cellular model to help address the neuropsychiatric symptoms of PD. In that regard, our present study on Parkin-mediated mitophagy in HCN cells could contribute to understanding the various roles of Parkin in brain areas other than substantia nigra.

What is the interconnection between mitophagy and conventional autophagy? Although, it may not be easy to distinguish the effects of mitophagy from those of conventional bulk autophagy in the same cell, it is interesting that ablation of Parkin attenuates not only mitophagy, but also conventional autophagy. Parkin may play additional roles in facilitation of conventional autophagy in insulin-deprived HCN cells. Another possibility is that elimination of mitochondria has a greater effect on autophagy than elimination of other intracellular constituents in HCN cells. Since interference with mitophagy by using Mdivi-1 reduced autophagy level in HCN cells, the latter possibility seems plausible. During bulk autophagy, as in nutrient starvation conditions, autophagy can be selective for certain intracellular organelles, such as ribosomes and peroxisomes (Hara-Kuge and Fujiki, 2008; Cebollero et al., 2012). In certain cell types, including HCN cells, mitochondria could be the main cargo for autophagic degradation.

In this study, we also identified a new mode of action of Parkin in regulation of mitophagy. Our data suggest that ER-to-mitochondria Ca^{2+} mobilization triggers Parkin/PINK1-dependent mitophagy and at the same time Parkin is required for this Ca^{2+} mobilization. In line with this idea, a previous study reported that Parkin upregulation increases ER? mitochondria contact to regulate Ca^{2+} transfer (Calì et al., 2013). Upon insulin withdrawal, Parkin mediates Ca^{2+} accumulation in mitochondria and thereby instigates mitochondrial depolarization at the early stage of mitophagy. This may allow recruitment of PINK1 and Parkin and progress of mitophagy. Then, recruited Parkin recognizes and removes dysfunctional mitochondria. According to our model, Parkin is intimately involved from the beginning of mitophagy, and liaises with PINK1 in a mutually cooperative way for the progress of mitophagy. Parkin's role is more than recognition and removal of depolarized mitochondria; it is an initiator and actuator of mitophagy in the context of ADCD. A schematic diagram shown in **Figure 9** summarizes the regulation of Parkin expression and its roles during ADCD.

It is also puzzling how Parkin-mediated selective elimination of dysfunctional mitochondria leads to cell death in insulin-

deprived HCN cells, whereas Parkin-dependent mitophagy promotes and cellular homeostasis according to other studies. Currently, the link between mitophagy and cell death remains under-studied. What mechanisms determine the outcome of Parkin-driven mitophagy, i.e., whether it ensures mitochondrial quality control or facilitates mitophagic cell death? Further studies are warranted to resolve this issue.

AUTHOR CONTRIBUTIONS

S-WY contributed to conception and design, data analysis and interpretation, manuscript writing, and approved the manuscript. HP contributed to conception and design, collection and assembly of data, data analysis and interpretation, and manuscript writing. KMC and H-KA contributed to data collection and analysis. BC and CM contributed to study design, and data analysis and interpretation. J-EG, JH, and HW collected the data.

FUNDING

This work was supported by the National Research Foundation of Korea (NRF) (Grants Nos. 2017R1A2B4004289 and 2018M3C7A1056275) and the DGIST Convergence Science Center Program (18-BD-04) of the Ministry of Science and ICT of Korea.

REFERENCES

Åberg, M. A., Åberg, N. D., Hedbäcker, H., Oscarsson, J., and Eriksson, P. S. (2000). Peripheral infusion of IGF-I selectively induces neurogenesis in the adult rat hippocampus. *J. Neurosci.* 20, 2896–2903.

Alvarez-Buylla, A., and Lim, D. A. (2004). For the long run: maintaining germinal niches in the adult brain. *Neuron* 41, 683–686.

Axe, E. L., Walker, S. A., Manifava, M., Chandra, P., Roderick, H. L., Habermann, A., et al. (2008). Autophagosome formation from membrane compartments enriched in phosphatidylinositol 3-phosphate and dynamically connected to the endoplasmic reticulum. *J. Cell Biol.* 182, 685–701. doi: 10.1083/jcb.200803137

Baek, S.-H., Kim, E.-K., Goudreau, J. L., Lookingland, K. J., Kim, S. W., and Yu, S.-W. (2009). Insulin withdrawal-induced cell death in adult hippocampal neural stem cells as a model of autophagic cell death. *Autophagy* 5, 277–279.

Baumgartner, H. K., Gerasimenko, J. V., Thorne, C., Ferdek, P., Pozzan, T., Tepikin, A. V., et al. (2009). Calcium elevation in mitochondria is the main Ca2+ requirement for mitochondrial permeability transition pore (mPTP) opening. *J. Biol. Chem.* 284, 20796–20803. doi: 10.1074/jbc.M109.025353

Bouman, L., Schlierf, A., Lutz, A., Shan, J., Deinlein, A., Kast, J., et al. (2011). Parkin is transcriptionally regulated by ATF4: evidence for an interconnection between mitochondrial stress and ER stress. *Cell Death Diff.* 18, 769–782. doi: 10.1038/cdd.2010.142

Burman, C., and Ktistakis, N. T. (2010). Regulation of autophagy by phosphatidylinositol 3-phosphate. *FEBS lett.* 584, 1302–1312. doi: 10.1016/j.febslet.2010.01.011

Calì, T., Ottolini, D., Negro, A., and Brini, M. (2013). Enhanced parkin levels favor ER-mitochondria crosstalk and guarantee Ca 2+ transfer to sustain cell bioenergetics. *Mole. Basis Dis.* 1832, 495–508.

Cebollero, E., Reggiori, F., and Kraft, C. (2012). Reticulophagy and ribophagy: regulated degradation of protein production factories. *Int. J. Cell Biol.* 2012:182834. doi: 10.1155/2012/182834

Chung, K. M., Jeong, E.-J., Park, H., An, H.-K., and Yu, S.-W. (2016). Mediation of autophagic cell death by type 3 ryanodine receptor (RyR3) in adult hippocampal neural stem cells. *Front. Cell. Neurosc.* 10:116.

Chung, K. M., Park, H., Jung, S., Ha, S., Yoo, S. J., Woo, H., et al. (2015). Calpain determines the propensity of adult hippocampal neural stem cells to autophagic cell death following insulin withdrawal. *Stem Cells* 33, 3052–3064. doi: 10.1002/stem.2082

Coucouvanis, E., and Martin, G. R. (1995). Signals for death and survival: a two-step mechanism for cavitation in the vertebrate embryo. *Cell* 83, 279–287.

Danial, N. N., and Korsmeyer, S. J. (2004). Cell death: critical control points. *Cell* 116, 205–219.

Dauer, W., and Przedborski, S. (2003). Parkinson's disease: mechanisms and models. *Neuron* 39, 889–909.

Dawson, T. M., and Dawson, V. L. (2010). The role of parkin in familial and sporadic parkinson's disease. *Mov. disord.* 25(Suppl. 1), S32–S39. doi: 10.1002/mds.22798

Dimauro, I., Pearson, T., Caporossi, D., and Jackson, M. J. (2012). A simple protocol for the subcellular fractionation of skeletal muscle cells and tissue. *BMC Res. Notes* 5:513. doi: 10.1186/1756-0500-5-513

Ellis, R. E., Yuan, J., and Horvitz, H. R. (1991). Mechanisms and functions of cell death. *Ann. Rev. Cell Biol.* 7, 663–698.

Farré, D., Roset, R., Huerta, M., Adsuara, J. E., Roselló, L., Albà, M. M., et al. (2003). Identification of patterns in biological sequences at the ALGGEN server: PROMO and MALGEN. *Nucleic Acids Res.* 31, 3651–3653.

Galluzzi, L., and Kroemer, G. (2008). Necroptosis: a specialized pathway of programmed necrosis. *Cell* 135, 1161–1163. doi: 10.1016/j.cell.2008.12.004

Galluzzi, L., Maiuri, M., Vitale, I., Zischka, H., Castedo, M., Zitvogel, L., et al. (2007). Cell death modalities: classification and pathophysiological implications. *Cell Death Diff.* 14, 1237–1243.

Galluzzi, L., Vitale, I., Aaronson, S. A., Abrams, J. M., Adam, D., Agostinis, P., et al. (2018). Molecular mechanisms of cell death: recommendations of the nomenclature committee on cell death 2018. *Cell Death Diff.* 25, 486–541. doi: 10.1038/s41418-017-0012-4

Gorman, C. M. (1985). High efficiency gene transfer into mammalian cells. *DNA clon.* 2, 154–157.

Gould, E., McEwen, B. S., Tanapat, P., Galea, L. A., and Fuchs, E. (1997). Neurogenesis in the dentate gyrus of the adult tree shrew is regulated by psychosocial stress and NMDA receptor activation. *J. Neurosci.* 17, 2492–2498.

Ha, S., Jeong, S.-H., Yi, K., Chung, K. M., Hong, C. J., Kim, S. W., et al. (2017). Phosphorylation of p62 by AMP-activated protein kinase mediates autophagic cell death in adult hippocampal neural stem cells. *J. Biol. Chem.* 292, 13795–13808. doi: 10.1074/jbc.M117.780874

Ha, S., Ryu, H. Y., Chung, K. M., Baek, S.-H., Kim, E.-K., and Yu, S.-W. (2015). Regulation of autophagic cell death by glycogen synthase kinase-3β in adult hippocampal neural stem cells following insulin withdrawal. *Mole. Brain* 8:30. doi: 10.1186/s13041-015-0119-9

Hara-Kuge, S., and Fujiki, Y. (2008). The peroxin Pex14p is involved in LC3-dependent degradation of mammalian peroxisomes. *Exp. Cell Res.* 314, 3531–3541. doi: 10.1016/j.yexcr.2008.09.015

Høyer-Hansen, M., Bastholm, L., Szyniarowski, P., Campanella, M., Szabadkai, G., Farkas, T., et al. (2007). Control of macroautophagy by calcium, calmodulin-dependent kinase kinase-β, and Bcl-2. *Mol. Cell* 25, 193–205.

Ichimura, Y., Kirisako, T., Takao, T., Satomi, Y., Shimonishi, Y., Ishihara, N., et al. (2000). A ubiquitin-like system mediates protein lipidation. *Nature* 408:488.

Ichimura, Y., Kominami, E., Tanaka, K., and Komatsu, M. (2008). Selective turnover of p62/A170/SQSTM1 by autophagy. *Autophagy* 4, 1063–1066.

Itakura, E., and Mizushima, N. (2010). Characterization of autophagosome formation site by a hierarchical analysis of mammalian Atg proteins. *Autophagy* 6, 764–776.

Kabeya, Y., Mizushima, N., Ueno, T., Yamamoto, A., Kirisako, T., Noda, T., et al. (2000). LC3, a mammalian homologue of yeast Apg8p, is localized in autophagosome membranes after processing. *EMBO J.* 19, 5720–5728.

Kane, L. A., Lazarou, M., Fogel, A. I., Li, Y., Yamano, K., Sarraf, S. A., et al. (2014). PINK1 phosphorylates ubiquitin to activate Parkin E3 ubiquitin ligase activity. *J. Cell Biol.* 205:143. doi: 10.1083/jcb.201402104

Kimura, S., Noda, T., and Yoshimori, T. (2007). Dissection of the autophagosome maturation process by a novel reporter protein, tandem fluorescent-tagged LC3. *Autophagy* 3, 452–460.

Klionsky, D. J., Abdelmohsen, K., Abe, A., Abedin, M. J., Abeliovich, H., Acevedo Arozena, A., et al. (2016). Guidelines for the use and interpretation of assays for monitoring autophagy. *Autophagy* 12, 1–222.

Klionsky, D. J., Baehrecke, E. H., Brumell, J. H., Chu, C. T., Codogno, P., Cuervo, A. M., et al. (2011). A comprehensive glossary of autophagy-related molecules and processes. *Autophagy* 7, 1273–1294. doi: 10.4161/auto.7.11.17661

Lazarou, M., Sliter, D. A., Kane, L. A., Sarraf, S. A., Wang, C., Burman, J. L., et al. (2015). The ubiquitin kinase PINK1 recruits autophagy receptors to induce mitophagy. *Nature* 524:309. doi: 10.1038/nature14893

Lemasters, J. J. (2005). Selective mitochondrial autophagy, or mitophagy, as a targeted defense against oxidative stress, mitochondrial dysfunction, and aging. *Rejuvenat. Res.* 8, 3–5.

Lichtenwalner, R., Forbes, M., Bennett, S., Lynch, C., Sonntag, W., and Riddle, D. (2001). Intracerebroventricular infusion of insulin-like growth factor-I ameliorates the age-related decline in hippocampal neurogenesis. *Neuroscience* 107, 603–613.

Meissner, W. G., Frasier, M., Gasser, T., Goetz, C. G., Lozano, A., Piccini, P., et al. (2011). Priorities in parkinson's disease research. *Nat. Rev. Drug Disc.* 10:377. doi: 10.1038/nrd3430

Messeguer, X., Escudero, R., Farré, D., Nuñez, O., Martınez, J., and Albà, M. M. (2002). PROMO: detection of known transcription regulatory elements using species-tailored searches. *Bioinformatics* 18, 333–334.

Minden, A., Lin, A., Smeal, T., Derijard, B., Cobb, M., Davis, R., et al. (1994). c-Jun N-terminal phosphorylation correlates with activation of the JNK subgroup but not the ERK subgroup of mitogen-activated protein kinases. *Mol. Cell. Biol.* 14, 6683–6688.

Mizushima, N., and Komatsu, M. (2011). Autophagy: renovation of cells and tissues. *Cell* 147, 728–741. doi: 10.1016/j.cell.2011.10.026

Moriwaki, K., Bertin, J., Gough, P., Orlowski, G., and Chan, F. K. (2016). Differential roles of RIPK1 and RIPK3 in TNF-induced necroptosis and chemotherapeutic agent-induced cell death. *Cell Death Dis.* 6:e1636. doi: 10.1038/cddis.2015.16

Narendra, D., Tanaka, A., Suen, D.-F., and Youle, R. J. (2008). Parkin is recruited selectively to impaired mitochondria and promotes their autophagy. *J. Cell Biol.* 183, 795–803. doi: 10.1083/jcb.200809125

Narendra, D. P., Jin, S. M., Tanaka, A., Suen, D.-F., Gautier, C. A., Shen, J., et al. (2010). PINK1 is selectively stabilized on impaired mitochondria to activate Parkin. *PLoS Biol.* 8:e1000298. doi: 10.1371/journal.pbio.1000298

Niwa, J.-I., Ishigaki, S., Hishikawa, N., Yamamoto, M., Doyu, M., Murata, S., et al. (2002). Dorfin ubiquitylates mutant SOD1 and prevents mutant SOD1-mediated neurotoxicity. *J. Biol. Chem.* 277, 36793–36798.

Palmer, T. D., Takahashi, J., and Gage, F. H. (1997). The adult rat hippocampus contains primordial neural stem cells. *Mol. Cell. Neurosci.* 8, 389–404.

Pankiv, S., Clausen, T. H., Lamark, T., Brech, A., Bruun, J.-A., Outzen, H., et al. (2007). p62/SQSTM1 binds directly to Atg8/LC3 to facilitate degradation of ubiquitinated protein aggregates by autophagy. *J. Biol. Chem.* 282, 24131–24145.

Rello, S., Stockert, J., Moreno, V. L., Gamez, A., Pacheco, M., Juarranz, A., et al. (2005). Morphological criteria to distinguish cell death induced by apoptotic and necrotic treatments. *Apoptosis* 10, 201–208.

Rodríguez, J. J., Jones, V. C., Tabuchi, M., Allan, S. M., Knight, E. M., LaFerla, F. M., et al. (2008). Impaired adult neurogenesis in the dentate gyrus of a triple transgenic mouse model of Alzheimer's disease. *PloS one* 3:e2935.

Satoo, K., Noda, N. N., Kumeta, H., Fujioka, Y., Mizushima, N., Ohsumi, Y., et al. (2009). The structure of Atg4B–LC3 complex reveals the mechanism of LC3 processing and delipidation during autophagy. *The EMBO J.* 28, 1341–1350. doi: 10.1038/emboj.2009.80

Scaduto, R. C. Jr., and Grotyohann, L. W. (1999). Measurement of mitochondrial membrane potential using fluorescent rhodamine derivatives. *Biophys. J.* 76, 469–477.

Shintani, T., and Klionsky, D. J. (2004). Autophagy in health and disease: a double-edged sword. *Science* 306, 990–995.

Shors, T. J., Miesegaes, G., Beylin, A., Zhao, M., Rydel, T., and Gould, E. (2001). Neurogenesis in the adult is involved in the formation of trace memories. *Nature* 410:372.

Sun, N., Yun, J., Liu, J., Malide, D., Liu, C., Rovira, I. I., et al. (2015). Measuring in vivo mitophagy. *Mol. Cell* 60, 685–696. doi: 10.1016/j.molcel.2015.10.009

Takeuchi, A., Kim, B., and Matsuoka, S. (2013). The mitochondrial Na+-Ca 2+ exchanger, NCLX, regulates automaticity of HL-1 cardiomyocytes. *Sci. Rep.* 3:2766. doi: 10.1038/srep02766

Tanaka, K., Suzuki, T., Hattori, N., and Mizuno, Y. (2004). Ubiquitin, proteasome and parkin. *Mol. Cell Res.* 1695, 235–247.

Tsujimoto, Y., and Shimizu, S. (2005). Another way to die: autophagic programmed cell death. *Cell Death Diff.* 12, 1528–1534.

Yang, Z., and Klionsky, D. J. (2010). Eaten alive: a history of macroautophagy. *Nature Cell Biol.* 12:814. doi: 10.1038/ncb0910-814

Yogev, O., and Shaulian, E. (2010). Jun proteins inhibit autophagy and induce cell death. *Autophagy* 6, 566–567. doi: 10.4161/auto.6.4.11950

Youle, R. J., and Narendra, D. P. (2011). Mechanisms of mitophagy. *Nature Rev. Mol. Cell Biol.* 12:9. doi: 10.1038/nrm3028

Yu, S. W., Baek, S. H., Brennan, R. T., Bradley, C. J., Park, S. K., Lee, Y. S., et al. (2008). Autophagic death of adult hippocampal neural stem cells following insulin withdrawal. *Stem Cells* 26, 2602–2610. doi: 10.1634/stemcells.2008-0153

Conflict of Interest Statement: The authors declare that the research was conducted in the absence of any commercial or financial relationships that could be construed as a potential conflict of interest.

frontiers in Molecular Neuroscience

ORIGINAL RESEARCH
published: 28 February 2019
doi: 10.3389/fnmol.2019.00045

Exogenous Ketone Supplementation Decreased the Lipopolysaccharide-Induced Increase in Absence Epileptic Activity in Wistar Albino Glaxo Rijswijk Rats

*Zsolt Kovács[1], Dominic P. D'Agostino[2,3], David M. Diamond[2,4] and Csilla Ari[4]**

[1] Department of Biology, ELTE Eötvös Loránd University, Savaria University Centre, Szombathely, Hungary, [2] Laboratory of Metabolic Medicine, Department of Molecular Pharmacology and Physiology, Morsani College of Medicine, University of South Florida, Tampa, FL, United States, [3] Institute for Human and Machine Cognition, Ocala, FL, United States, [4] Comparative Neuroscience Research Laboratory, Department of Psychology, University of South Florida, Tampa, FL, United States

It has been demonstrated previously that exogenous ketone supplements such as ketone ester (KE) decreased absence epileptic activity in a well-studied animal model of human absence epilepsy, Wistar Albino Glaxo/Rijswijk (WAG/Rij) rats. It is known that lipopolysaccharide (LPS)-generated changes in inflammatory processes increase absence epileptic activity, while previous studies show that ketone supplement-evoked ketosis can modulate inflammatory processes. Thus, we investigated in the present study whether administration of exogenous ketone supplements, which were mixed with standard rodent chow (containing 10% KE + 10% ketone salt/KS, % by weight, KEKS) for 10 days, can modulate the LPS-evoked changes in absence epileptic activity in WAG/Rij rats. At first, KEKS food alone was administered and changes in spike-wave discharge (SWD) number, SWD time, discharge frequency within SWDs, blood glucose, and beta-hydroxybutyrate (βHB) levels, as well as body weight and sleep-waking stages were measured. In a separate experiment, intraperitoneal (i.p.) injection of LPS (50 μg/kg) alone and a cyclooxygenase 1 and 2 (COX-1 and COX-2) inhibitor indomethacin (10 mg/kg) alone, as well as combined IP injection of indomethacin with LPS (indomethacin + LPS) were applied in WAG/Rij rats to elucidate their influences on SWD number. In order to determine whether KEKS food can modify the LPS-evoked changes in SWD number, KEKS food in combination with IP LPS (50 μg/kg) (KEKS + LPS), as well as KEKS food with IP indomethacin (10 mg/kg) and LPS (50 μg/kg) (KEKS + indomethacin + LPS) were also administered. We demonstrated that KEKS food significantly increased blood βHB levels and decreased not only the spontaneously generated absence epileptic activity (SWD number), but also the LPS-evoked increase in SWD number in WAG/Rij rats. Our results suggest that administration of exogenous ketone supplements (ketogenic foods) may be a promising therapeutic tool in the treatment of epilepsy.

Keywords: ketone supplements, ketosis, LPS, inflammation, absence epilepsy, WAG/Rij rats

OPEN ACCESS

Edited by:
Michele Papa,
Università degli Studi della Campania Luigi Vanvitelli Caserta, Italy

Reviewed by:
Giovanni Cirillo,
Second University of Naples, Italy
Masahito Kawamura,
Jikei University School of Medicine, Japan

****Correspondence:***
Csilla Ari
csari2000@yahoo.com

Received: *25 November 2018*
Accepted: *05 February 2019*
Published: *28 February 2019*

Citation:
Kovács Z, D'Agostino DP, Diamond DM and Ari C (2019) Exogenous Ketone Supplementation Decreased the Lipopolysaccharide-Induced Increase in Absence Epileptic Activity in Wistar Albino Glaxo Rijswijk Rats. Front. Mol. Neurosci. 12:45. doi: 10.3389/fnmol.2019.00045

INTRODUCTION

Ketone bodies (beta-hydroxybutyrate/βHB, acetoacetate, and acetone) are produced mainly in the liver, which may serve as an energy source for different tissues under circumstances when glucose supply is insufficient, such as fasting or after following a ketogenic diet (Hashim and VanItallie, 2014; Achanta and Rae, 2017). It has been demonstrated that administration of exogenous ketone (ketogenic) supplements, such as ketone ester (KE) and ketone salt (KS) generate rapid and sustained increases in the blood level of βHB inducing nutritional ketosis (Poff et al., 2015; Ari et al., 2016; Kesl et al., 2016), which may evoke alleviating effects on different central nervous system (CNS) diseases. For example, exogenous ketone supplement-evoked ketosis shows therapeutic potential in the treatment of epilepsy, Parkinson's disease and Alzheimer's disease (D'Agostino et al., 2013; Hashim and VanItallie, 2014; Newport et al., 2015; Kovács et al., 2017).

Inflammatory processes have a role in the precipitation and aggravation of epileptic activity (Vezzani et al., 2008, 2011). For example, it was demonstrated in a well-investigated animal model of human absence epilepsy of Wistar Albino Glaxo/Rijswijk (WAG/Rij) rats (Kovács et al., 2006, 2011, 2014a; Russo et al., 2014) that lipopolysaccharide (LPS; a cell wall component of gram-negative bacteria) (Vezzani et al., 2011) aggravates absence epileptic activity. LPS increases the expression of Toll-like receptor 4 (TLR4) and the release/expression of proinflammatory cytokines, such as interleukin-1β (IL-1β), cyclooxygenase-2 (COX-2) and, as a consequence, prostaglandins (Mlodzikowska-Albrecht et al., 2007; Vezzani et al., 2011). Prostaglandins may decrease the seizure threshold and prostaglandin E_2 (PGE2) showed a proconvulsant effect (Sayyah et al., 2003). These effects of LPS may enhance cortical excitability for example via modulation of GABAergic, glutamatergic, and adenosinergic systems (Wang and White, 1999; Coenen and Van Luijtelaar, 2003; Kovács et al., 2015b) and, as a consequence, augment absence epileptic activity in WAG/Rij rats (Kovács et al., 2006, 2011, 2014a). The LPS-evoked increase in spike-wave discharge (SWD) number was abolished by a potent inhibitor of prostaglandin synthesis, a cyclooxygenase 1 (COX-1) and COX-2 inhibitor indomethacin. These results suggest the role of the TLR4/COX-2/PGE2 system in the LPS-induced processes leading to PGE2 synthesis, which may enhance SWD generator mechanisms (Kovács et al., 2006, 2011, 2014a).

It has been demonstrated that intragastric administration (gavage) of ketone supplements, such as KE, decreased absence epileptic activity (SWDs) in WAG/Rij rats (Kovács et al., 2017). The exogenous ketone supplement-evoked increase in βHB level may exert its alleviating effects on CNS diseases, among others, via modulation of the inflammatory system (Newman and Verdin, 2014; Youm et al., 2015; Yamanashi et al., 2017), which is implicated in the pathophysiology of absence epilepsy (Kovács et al., 2006, 2011; Van Luijtelaar et al., 2012; Russo et al., 2014). Consequently, we hypothesized that administration of exogenous ketone supplements may modulate not only absence epileptic activity, which spontaneously generated and manifested in SWDs as shown by an electroencephalogram (EEG) (Coenen and Van Luijtelaar, 2003; Kovács et al., 2017), but also the LPS-induced changes in absence epileptic activity in WAG/Rij rats (Kovács et al., 2006, 2014a). Thus, we addressed in the present study whether sub-chronical administration (10 days) of exogenous ketone supplements, which were mixed with standard rodent chow (10% KE + 10% KS, % by weight: KEKS), can modulate spontaneous absence epileptic activity and LPS-evoked increases in SWD number.

Abbreviations: A_1R, adenosine A_1 receptor; $A_{2A}R$, adenosine A_{2A} receptor; ASC, apoptosis-associated speck-like protein containing a caspase recruitment domain; βHB, beta-hydroxybutyrate; CNS, central nervous system; COX, cyclooxygenase; EEG, electroencephalogram; IL-1β, interleukin-1β; i.p., intraperitoneal; K_{ATP} channels, ATP-sensitive potassium channels; KE, ketone ester; KS, ketone salt; LPS, lipopolysaccharide; NF-κB, nuclear factor-κB; NLRP3, NOD-like receptor pyrin domain 3; PGE_2, prostaglandin E_2; PT day, post-treatment control experiment/day; REM sleep, rapid eye movement sleep; ROS, reactive oxygen species; S.E.M., standard error of the mean; SWD, spike-wave discharge; SWS, slow wave sleep; TLR4, Toll-like receptor 4; TNF-α, tumor necrosis factor-α; WAG/Rij, Wistar Albino Glaxo/Rijswijk.

MATERIALS AND METHODS

Animals

Animal treatments and surgery procedures were carried out according to the local ethical rules, guidelines of the Hungarian Act of Animal Care and Experimentation (1998, XXVIII, section 243), European Communities Council Directive 24 November 1986 (86/609/EEC) and EU Directive 2010/63/EU on the use and treatment of animals in experimental laboratories. The experiments were approved by the Animal Care and Experimentation Committee of the Eötvös Loránd University (Savaria Campus) and National Scientific Ethical Committee on Animal Experimentation (Hungary) under license number VA/ÉBNTF02/85-8/2016. All efforts were made to minimize pain and suffering and to reduce the number of animals used.

WAG/Rij male rats ($n = 48$; 10 months old, 325–345 g; breeding colony of WAG/Rij rats at Eötvös Loránd University, Savaria Campus, Szombathely, Hungary) were housed in groups (3–4 animals/group), while they were housed individually after surgery. Standard laboratory conditions were provided during the experiments (12:12 h light-dark cycle: light was on from 8:00 a.m. to 8:00 p.m.; free access to water and food; air-conditioned rooms at $22 \pm 2^{\circ}$C).

Electrode Implantation and EEG Recording

Isoflurane-air mixture (2.0–2.5%) anesthesia was used for electrode implantation for EEG recording (Kovács et al., 2006). Briefly, screw electrodes were implanted into the bone above two cortical areas (primary motor cortex and somatosensory cortex: A 0.8 mm, L 1.8 mm, and A 0.2 mm, L 6.2 mm, respectively) (Paxinos and Watson, 1999) and above the cerebellar cortex (as ground electrode). The reference electrode was a stainless steel plate (3 × 4 mm with one side insulated), which was implanted under the skin and over the masseter muscle. All electrodes and the plate were soldered to a ten-pin socket, which were fixed and attached to the skull by dentacrylate cement (Ivoclar, Liechtenstein). Lidocaine ointment

(5%; EGIS, Hungary) was used for post-operative pain relief (Kovács et al., 2006).

Electroencephalography was recorded by a differential biological amplifier (Bioamp4, Supertech Ltd., Pécs, Hungary) attached to a CED 1401 mkII (Cambridge Electronic Design Ltd., UK) data capture and analysis device between 2:30 p.m. and 5:00 p.m. The bandwidth of the EEG recording was 0.3–150 Hz and the sampling rate was 500 Hz (Kovács et al., 2014a).

Administration of Ketone Supplements and Drugs

Both KE (R,S-1,3-butanediol—acetoacetate diester) and KS (Na^+/K^+-βHB mineral salt) were developed by D'Agostino et al. (2013; University of South Florida/USF, USA) in collaboration with Savind Inc. (Urbana, IL, USA). Ketone salt was mixed into a 50% solution (375 mg/g pure βHB and 125 mg/g of Na^+/K^+ in a 1:1 ratio). As we tested in a pilot study, 20% KEKS in standard rodent chow (KEKS food) was well-palatable for rats without either side effects or decrease in body weight and was able to induce ketosis (10% KE + 10% KS, % by weight; mixed with powdered standard rodent chow and water resulting paste-like consistency food). In order to improve palatability 1% saccharine was added. Moreover, *ad libitum* feeding of rats by ketone-supplemented food is a non-stressful method for ketone supplement-induced ketosis. Thus, in this study we fed the animals with KEKS-containing (20% KEKS) food for 10 days. To ensure freshness and *ad libitum* access, KEKS food was freshly mixed and replaced every day and was placed in a Petri dish on the bottom of the animal's cage.

Based on our previous results on WAG/Rij rats (Kovács et al., 2006, 2014a), the effective doses of LPS (50 μg/kg; Sigma-Aldrich Inc., Hungary, Budapest) and indomethacin (10 mg/kg; Sigma-Aldrich Inc., Hungary, Budapest) were also IP injected alone and in combination. It was demonstrated earlier that 5% (v/v) ethanol solution has no significant effect on absence epileptic activity in WAG/Rij rats (Kovács et al., 2006, 2014a). Thus, 5% ethanol solution was administered to dissolve the indomethacin, whereas LPS was dissolved in saline (Kovács et al., 2006, 2014a).

Experimental Design

Adaptation Period and Pre-treatment Control Days

Rats were assigned into 6 groups (group 1–group 6; **Figure 1**). After the 2 week recovery period, animals were handled daily and were connected to the biological amplifier for 5 days for the adaptation of rats to the experimental procedures (e.g., EEG recording). Moreover, all rats (group 1–group 6) were fed paste-like standard rodent chow (standard rodent chow was mixed with water and 1% saccharine was added, without KEKS) between the 1st and 5th days of the experiments (adaptation to EEG recording and food). Then, to establish the averaged control SWD number (group 1–group 6) and average SWD time, discharge frequency within SWDs and time of sleep-waking stages (group 1), rats were fed by paste-like normal rat food (without KEKS) furthermore on 5 consecutive days between 6th and 10th days of the experiments, and EEG was recorded (5 day control period, pre-treatment control days) (**Figure 1**). In addition, except for the animals of group 1, all rats (group 2–group 6) were injected IP with 0.3 ml saline/100 g body weight (1st injection) followed by the same injection (0.3 ml saline/100 g body weight, 30 min later; 2nd injection) at the 5 day control period.

Treatments by Ketone Supplements, Indomethacin, and Lipopolysaccharide

In group 1 ($n = 8$), after the 5 day control period, animals were fed with KEKS food for 10 consecutive days (between the 11th and 20th days of the experiment) (**Figure 1**). Finally, the 10-day KEKS treatments was followed by two post-treatment control days (PT days; rats were fed by paste-like normal rat food without KEKS) to investigate putative sustained effect of KEKS on SWD number (on 21st and 22nd day of the experiment). EEGs were recorded every day.

After 5 day control periods, animals in groups 2–4 were treated by two IP injections (1st injection was followed by 2nd injection 30 min later) on the 11th day of the experiments (**Figure 1**): indomethacin (10 mg/kg) in 0.3 ml 5% ethanol solution/100 g body weight (1st injection) and 0.3 ml saline/100 g body weight (2nd injection; $n = 8$; group 2); 0.3 ml 5% ethanol solution/100 g body weight (1st injection) and LPS (50 μg/kg) in 0.3 ml saline/100 g body weight (2nd injection; $n = 8$; group 3); combined injection of indomethacin with LPS: indomethacin (10 mg/kg) in 0.3 ml 5% ethanol solution/100 g body weight (1st injection) and LPS (50 μg/kg) in 0.3 ml saline/100 g body weight (2nd injection; $n = 8$; group 4). Similar to group 1, EEGs were recorded every day.

After 5 day control periods, animals of groups 5 and 6 were fed with KEKS food for 10 consecutive days between the 11th and 20th days of the experiment. In addition, these animals received IP 0.3 ml saline/100 g body weight (1st injection) followed by the same injection (0.3 ml saline/100 g body weight, 30 min later; 2nd injection) between the 11th and 18th days and on the 20th day of the experiment (**Figure 1**). On the 19th day of the experiment, when KEKS treatment alone (group 1) significantly changed the SWD number, treatments were as follows in groups 5 and 6: 1st IP injection was 5% ethanol solution and the 2nd injection (saline) contained LPS (50 μg/kg; $n = 8$; group 5). In group 6, the 1st IP injection (5% ethanol solution) contained indomethacin (10 mg/kg) whereas the 2nd injection (saline) contained LPS (50 μg/kg; $n = 8$) on the 19th day of experiment (**Figure 1**). EEGs were recorded every day.

Measuring of Blood Glucose and βHB Levels as Well as Body Weight

Blood βHB (mmol/L) and glucose (mg/dl) levels were measured from blood taken from the tail vein with a glucose and ketone monitoring system (Precision Xtra™, Abbott Laboratories, Abbott Park, IL, USA) (Ari et al., 2016; Kovács et al., 2017), which only measures blood levels of D-βHB. Thus, total blood ketone levels (D-βHB + L-βHB + acetoacetate + acetone) would be higher than we measured. To investigate the effect of KEKS on blood glucose and βHB levels, we measured them on the last

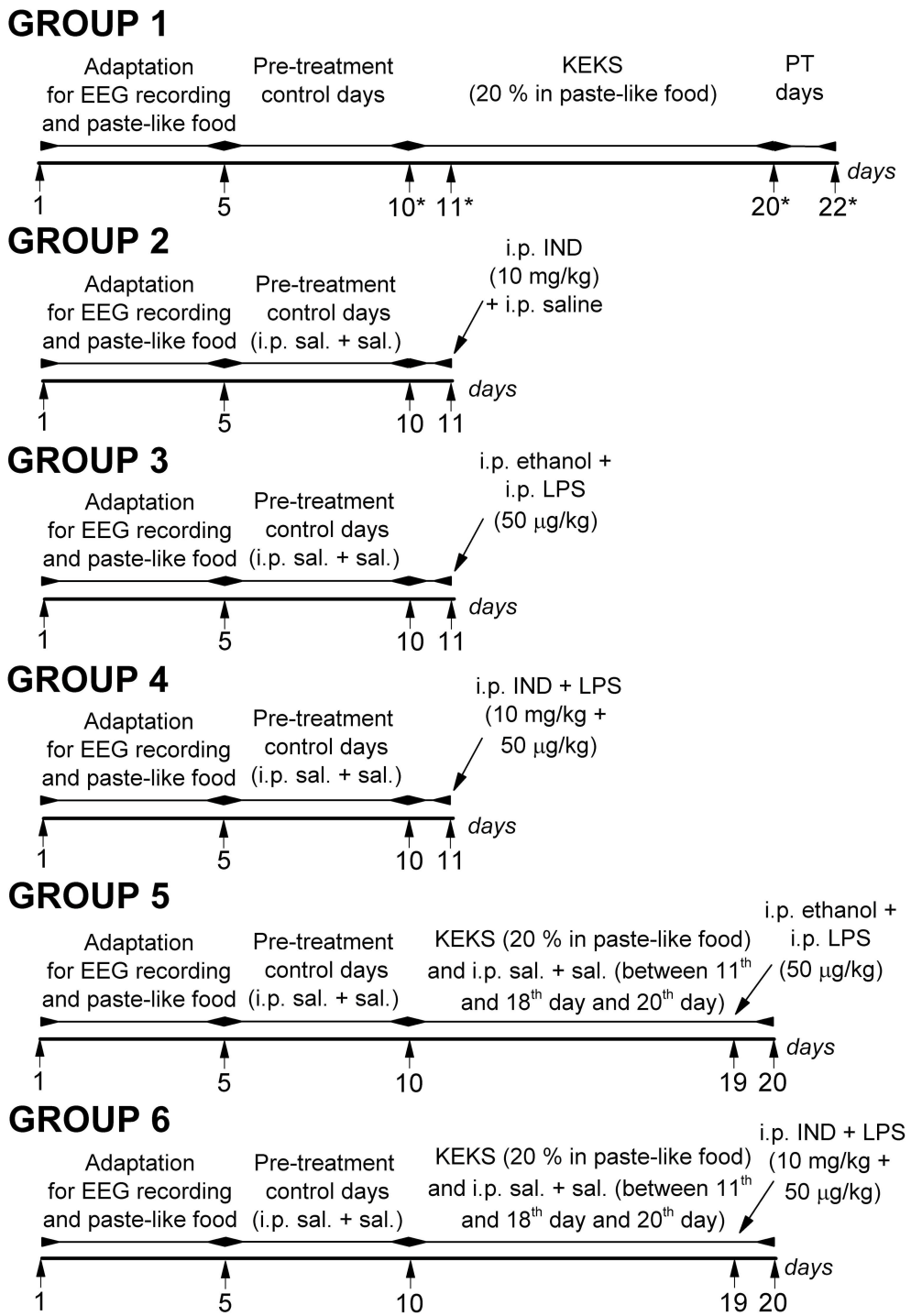

FIGURE 1 | Schematic drawing of the experimental design on 6 animal groups. *Days of blood glucose and βHB level measuring (group 1); IND, indomethacin; i.p. sal. + sal., IP 0.3 ml saline/100 g body weight (1st injection) followed by 0.3 ml saline/100 g body weight (30 min later, 2nd injection); KEKS, ketone ester/KE + ketone salt/KS; LPS, lipopolysaccharide; PT days, post-treatment control days.

(5th) control day (control), on the days of the 1st and the 10th day of KEKS administration and on the 2nd PT day (on the 10th, 11th, 20th, and 22nd days of the experiment, respectively; group 1) (**Figure 1**).

The body weights of the rats were also measured before KEKS administration started (5th control day: control), after the last (10th) KEKS day and on the 2nd PT day (on the 10th, 20th, and 22nd day of the experiment, respectively; group 1).

Evaluation of EEG Recordings and Statistical Analysis

Handling may evoke stress-induced changes in the behavior of WAG/Rij rats for about 30 min, which can modify the SWD number (Coenen and Van Luijtelaar, 2003; Kovács et al., 2006, 2014a). Thus, evaluation of the SWD number, average SWD time, discharge frequency within SWDs and sleep-waking stages were carried out between 30 and 150 min of recording. However, normal behavior and typical SWDs were detected in all animals 30 min after the connection of rats to the biological amplifier similarly to our previous study (Kovács et al., 2017). EEG recordings were split into 60 min sections and were evaluated separately (Kovács et al., 2006). Manual separation of SWDs from the EEG was carried out based on their features: typical SWDs contain a train of asymmetric spikes and slow waves starting and ending with sharp spikes, which SWDs characterized by 7–11 Hz discharge frequency within SWDs and 1–30 s duration (Coenen and Van Luijtelaar, 2003). SWDs were checked by FFT (Fast Fourier Transform) analysis.

It has been demonstrated previously that gavage of ketone supplements (e.g., KE) and ketone supplement-evoked ketosis had no effects on sleep-waking stages, average SWD time and discharge frequency within SWDs (Kovács et al., 2017). However, as we had no data on putative effects of KEKS food on sleep-waking stages, average SWD time and discharge frequency within SWDs, and also because changes in time of sleep-waking stages may alter SWD number in WAG/Rij rats (Coenen and Van Luijtelaar, 2003), we investigated the effect of KEKS food (after 9th day of KEKS administration; 19th day of experiments; group 1) on SWD number, average time of SWDs, discharge frequency within SWDs and sleep-waking stages between 30 and 90 min. Evaluation of sleep-waking stages was performed offline by visual evaluation of the raw EEG. We distinguished wakefulness (passive and active wake), slow wave sleep (SWS; light SWS and deep SWS) and rapid eye movement (REM) sleep in 60 min epochs according to Kovács et al. (2006). The wakefulness stage shows predominantly beta (20–40 Hz) and theta (6–8 Hz) activity (passive/active wake: without/with high slow waves of motor artifacts); light SWS was characterized by sleep spindles (10–16 Hz), theta waves and some slow waves (2–4 Hz); the disappearance of sleep spindles and an increasing ratio of high slow delta waves (0.5–4 Hz) were demonstrated under deep SWS; and REM sleep was characterized by continuous theta activity without any motor artifacts (Kovács et al., 2006).

All results were expressed as means ± standard error of the mean (S.E.M.). In relation to SWD number, average SWD time, discharge frequency within SWDs and sleep-waking stages the pre-treatment control values were the grand average calculated from the results of 5 control days (5 day control period). In case of blood level of glucose, βHB and body weight, the results were calculated from the values measured on the last (5th) control day. Data analysis was performed using GraphPad PRISM version 6.0a. Significance was determined by One- or Two-way analysis of variance (ANOVA) with Tukey's multiple comparisons test and Sidak's multiple comparisons test as was described previously (Ari et al., 2016). Results were considered significant when $p < 0.05$.

RESULTS

Effect of the KEKS Treatment on Absence Epileptic Activity, Sleep-Waking Stages, Blood βHB, and Glucose Levels as Well as Body Weight

KEKS food significantly decreased the SWD number between the 7th and 10th days of the treatment from 30 to 150 min (group 1; **Figure 2**; **Table 1**), compared to control levels. Moreover, SWD numbers returned to near the control levels on the 2nd PT day (**Figure 2**; **Table 1**). In relation to discharge frequency within SWDs, we did not find significant changes on the 9th KEKS treatment day between 30 and 90 min, compared to the control (group 1; **Table 2**). Average SWD duration was similar to the control on the 9th day of KEKS treatment between 30 and 90 min (group 1; **Table 2**). Because average SWD duration did not change after treatment by KEKS, but SWD number decreased (**Figure 2**; group 1), changes in the total time of SWDs were similar to the change in SWD number. Indeed, on the 9th day of KEKS treatment, the total time of SWDs decreased between 30 and 90 min compared to the control (**Table 2**).

The total time of sleep-waking stages did not change on the 9th day of KEKS food administration, compared to the control (group 1; **Table 3**).

Blood βHB level was significantly increased after the 1st and 10th KEKS treatment compared to control levels, whereas βHB level returned to the baseline (control) levels on the 2nd PT day (group 1; **Table 4**). Glucose level was unchanged on the days tested (group 1; **Table 4**).

After KEKS treatment, no significant change in body weight was detected compared to control levels (group 1) (body weight, g ± S.E.M.; on the control day/10th KEKS day: 331.8 ± 5.694/324.8

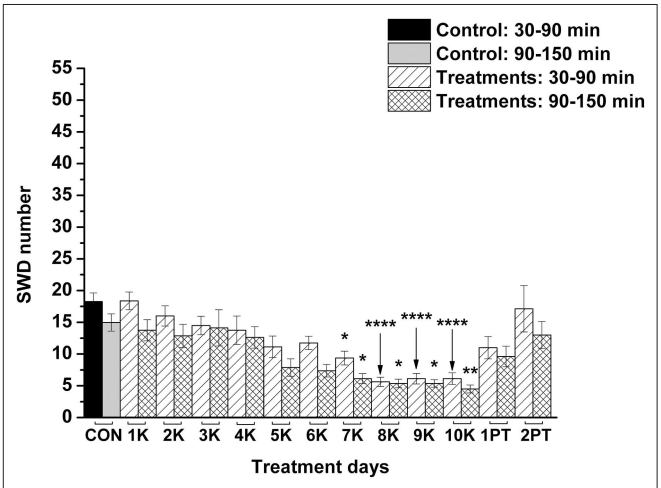

FIGURE 2 | Effect of KEKS food (20% KEKS and 1% saccharin in standard rodent chow; group 1) administration on SWD number. 1K, 1st KEKS food administration; 2K, 2nd KEKS food administration and so on; 1PT, 1st post-treatment control day; 2PT, 2nd post-treatment control day; CON, control; SWD, spike-wave discharge. $^{*}p < 0.05$, $^{**}p < 0.01$, and $^{****}p < 0.0001$.

TABLE 1 | Effect of KEKS food (20% KEKS and 1% saccharin in standard rodent chow; **Figure 2**, group 1) on SWD number.

Treatments (Figure 2; group 1)	SWD number (mean ± S.E.M.; significance level/*p*-value)	
	30–90 min	90–150 min
Control (CON)	18.3 ± 1.352	14.9 ± 1.358
1st KEKS treatment (1K)	18.4 ± 1.388 –/>0.9999	13.8 ± 1.666 –/>0.9999
2nd KEKS treatment (2K)	16.0 ± 1.592 –/>0.9999	12.9 ± 1.817 –/>0.9999
3rd KEKS treatment (3K)	14.5 ± 1.452 –/0.9956	14.1 ± 2.850 –/>0.9999
4th KEKS treatment (4K)	13.8 ± 2.242 –/0.9586	12.6 ± 1.689 –/>0.9999
5th KEKS treatment (5K)	11.1 ± 1.705 –/0.2504	7.9 ± 1.381 –/0.2692
6th KEKS treatment (6K)	11.8 ± 1.048 –/0.4306	7.4 ± 0.981 –/0.1607
7th KEKS treatment (7K)	9.4 ± 1.085 */0.0288	6.1 ± 0.789 */0.0321
8th KEKS treatment (8K)	5.6 ± 0.730 ****/<0.0001	5.4 ± 0.679 */0.0102
9th KEKS treatment (9K)	6.1 ± 0.833 ****/<0.0001	5.4 ± 0.596 */0.0102
10th KEKS treatment (10K)	6.1 ± 0.915 ****/<0.0001	4.5 ± 0.627 **/0.0023
1st Post-treatment day (1PT)	11.0 ± 1.753 –/0.2211	9.6 ± 1.625 –/0.8168
2nd Post-treatment day (2PT)	17.1 ± 3.652 –/>0.9999	13.0 ± 2.129 –/>0.9999

*1st KEKS treatment, 1st day of KEKS food application; SWD, spike-wave discharge. *$p < 0.05$, **$p < 0.01$ and ****$p < 0.0001$.*

± 5.192, $p = 0.823$; on control day/2nd PT day: 331.8 ± 5.694/329.5 ± 5.096, $p = 0.964$). Although food intake was not monitored in this study, the unchanged body weight suggests that KEKS treatment did not exert its effect on epileptic activity by means of insufficient food/energy intake and calorie restriction.

Indomethacin- and Lipopolysaccharide-Evoked Influences on the Absence Epileptic Activity

As we demonstrated previously (Kovács et al., 2006, 2014a), IP indomethacin (10 mg/kg) alone significantly decreased the SWD number between 30 and 150 min compared to the control (group 2; **Figure 3**; **Table 5**). Moreover, IP LPS (50 μg/kg) alone significantly increased the SWD number between 30 and 150 min compared to the control (group 3; **Figure 3**; **Table 5**). Combined IP administration of indomethacin (10 mg/kg) with LPS (50 μg/kg) abolished the effect of LPS alone on SWD number (group 4; **Figure 3**; **Table 5**).

Effect of the KEKS Treatment on Lipopolysaccharide-Evoked Changes in Absence Epileptic Activity

Nevertheless, KEKS treatment decreased the SWD number between the 6th and 8th days of the treatment from 30 to 150 min (group 5 and 6; **Figures 4**, **5**; **Tables 6**, **7**), and administration of KEKS food abolished the aggravating effect of IP LPS (50 μg/kg) on SWD number on the 9th KEKS day (group 5; **Figure 4**; **Table 6**). As **Figure 5** shows, IP indomethacin (10 mg/kg) enhanced the alleviating effect of KEKS treatment on the IP LPS-evoked increase in SWD number on the 9th KEKS day; after combined injection of indomethacin with LPS, a decrease in SWD number was demonstrated between 30 and 150 min (**Figure 5**; **Table 7**), with the influence being significant between 30 and 90 min. One day after the 9th KEKS day (KEKS food administration with IP LPS injection; group 5), the SWD number was not different, compared to the control on the 10th KEKS day (**Figure 4**; **Table 6**). Nevertheless, one day after the 9th KEKS food administration, which was combined with an IP injection of indomethacin and LPS (group 6), the SWD number significantly decreased compared to the control on the 10th KEKS day (**Figure 5**; **Table 7**).

DISCUSSION

Our results provide new evidence that exogenous ketone (KEKS)-supplemented food could decrease the LPS-evoked increase in SWD number. Moreover, we further confirmed our previous results that IP indomethacin alone decreases SWD number and IP LPS alone increases SWD number, whereas combined administration of indomethacin with LPS abolishes the LPS-generated increase in SWD number (Kovács et al., 2006, 2011, 2014a). However, similar to our previous results, when oral gavage of ketone supplements (e.g., KE) was administered to WAG/Rij rats for 7 days (Kovács et al., 2017), 10 days of administering KEKS food also had no significant effects on discharge frequency within SWDs, total time of sleep-waking stages, blood glucose levels or body weight of WAG/Rij animals in the recent study.

It was demonstrated previously that administration of exogenous ketone supplements is a well-tolerated, safe and efficient method to evoke therapeutic ketosis in both animals and humans (Newport et al., 2015; Kesl et al., 2016; Stubbs et al., 2017). After consumption, digestion of exogenous ketone supplements such as KEKS (or KEKS supplemented food) in the small intestine liberates ketone bodies (e.g., βHB and AcAc) (Brunengraber, 1997), which can be transported to the systemic bloodstream and evoke rapidly and then maintain mild therapeutic ketosis (Ari et al., 2016; Kesl et al., 2016; Stubbs et al., 2017). Subsequently, ketone bodies can be transported to the mitochondria of brain cells. In the mitochondria, ketone bodies are converted back to acetyl-CoA, a molecule which enters the Krebs cycle and is then used as an energy source under different circumstances when glucose supply is insufficient, alleviating cell energy metabolism (Newman and Verdin, 2014; Achanta and Rae, 2017). It

TABLE 2 | Effect of KEKS food (20% KEKS and 1% saccharin in standard rodent chow; group 1) on discharge frequency within SWDs, average SWD duration and total time of SWDs on 9th KEKS treatment day between 30 and 90 min.

Treatments (group 1)	Discharge frequency within SWDs (Hz ± S.E.M.; significance level/*p*-value)	Average SWD duration (sec ± S.E.M.; significance level/*p*-value)	Total time of SWDs (sec ± S.E.M.; significance level/*p*-value)
Control	7.6 ± 0.101	6.1 ± 0.334	111.8 ± 3.327
KEKS	7.5 ± 0.092 –/0.3655	5.8 ± 0.354 –/0.6550	35.6 ± 1.525 ****/<0.0001

*SWD, spike-wave discharge. ****p < 0.0001.*

TABLE 3 | Effect of KEKS food (20% KEKS and 1% saccharin in standard rodent chow; group 1) on total time of sleep-waking stages on 9th KEKS treatment day between 30 and 90 min.

Treatments (group 1)	Active wake (sec; mean ± S.E.M.; significance level/*p*-value)	Passive wake (sec; mean ± S.E.M.; significance level/*p*-value)	Light SWS (sec; mean ± S.E.M.; significance level/*p*-value)	Deep SWS (sec; mean ± S.E.M.; significance level/*p*-value)	REM (sec; mean ± S.E.M.; significance level/*p*-value)
Control	678.5 ± 39.002	667.9 ± 14.909	953.2 ± 27.649	1,081.8 ± 43.387	106.9 ± 6.403
KEKS	682.6 ± 38.976 –/0.9407	681.9 ± 14.226 –/0.5046	942.1 ± 16.312 –/0.7358	1145.1 ± 48.361 –/0.3463	112.5 ± 3.524 –/0.4563

REM, rapid eye movement sleep; SWS, slow wave sleep.

was also demonstrated that an exogenous ketone supplement-evoked increase in ketone body/βHB concentration may evoke beneficial effects on different CNS diseases in animal models and/or humans (D'Agostino et al., 2013; Hashim and VanItallie, 2014; Newport et al., 2015; Ari et al., 2016), such as epilepsy (Kovács et al., 2017; Simeone et al., 2018). In relation to the mechanism of action on absence epileptic activity, an increased level of ketone bodies/βHB is able to inhibit glycolysis. Subsequently, this process results in a decrease in cytosolic ATP level near the plasma membrane, which enhances the activity of ATP-sensitive potassium (K_{ATP}) channels hyperpolarizing neuronal membranes (Achanta and Rae, 2017) and decreasing seizure activity (Boison and Steinhäuser, 2018). Moreover, βHB may modulate release of neurotransmitters, among others, by inhibition of histone deacetylase (Sleiman et al., 2016). Indeed, ketosis/βHB enhances the GABAergic effects (e.g., via increased levels/activity of GABA and $GABA_A$ receptors), decreases extracellular glutamate release and increases adenosine level (McNally and Hartman, 2012; Sharma et al., 2015; Achanta and Rae, 2017), which exerts influence by effectively modulating absence epileptic activity (Peeters et al., 1989; D'Alimonte et al., 2009; Kovács et al., 2015a). As we demonstrated previously, after oral gavage of ketone supplements, such as KE, absence epileptic activity was decreased in correlation with the increase in βHB levels in WAG/Rij rats. This likely happens via inhibitory A1 type of adenosine receptors (A_1Rs) (Kovács et al., 2017), because activation of both the A2A type of adenosine receptors ($A_{2A}Rs$) and $GABA_A$ receptors evoked an increase in the SWD number in WAG/Rij rats (D'Alimonte et al., 2009; Kovács et al., 2015a; Lakatos et al., 2016). Activation of A_1Rs may decrease neuronal activity by hyperpolarization of neuronal membranes via synaptic inhibition (e.g., by decreased Ca^{2+} influx) and by modulation of neurotransmitter release (e.g., by decreased glutamate release) (Ciruela et al., 2006; Kovács et al., 2014b). It has been demonstrated that activation of A_1Rs causes hyperpolarization with opening potassium channels (Haas and Greene, 1984) and that a ketogenic diet (ketones) suppresses hyperexcitability of neurons by opening K_{ATP} channels via activation of A_1Rs (Kawamura et al., 2014). An exogenous ketone supplement-evoked increase in βHB concentration may increase the activity of mitochondrial synthesis of ATP in brain cells (Achanta and Rae, 2017; Simeone et al., 2018). ATP may release from cells and metabolize to adenosine by ectonucleotidases (Kovács et al., 2013), an effect (increased extracellular adenosine level) which may evoke opening of K_{ATP} channels via A_1Rs and, consequently, may generate hyperpolarization of the neuronal membrane and decrease neuronal activity (Andoh et al., 2006; Achanta and Rae, 2017; Simeone et al., 2018). All these effects may decrease excess hyperexcitability in the somatosensory cortex (cortical focus of absence epilepsy genesis) (Coenen and Van Luijtelaar, 2003), decreasing SWD number in WAG/Rij rats. Our results suggest that KEKS food-evoked ketosis may also decrease SWD number (**Figure 2**; **Table 1**) *via* increased adenosine levels and by activation of A_1Rs as well as K_{ATP} channels.

It is widely recognized that glial cells have a leading role both in the genesis and modulation of epileptic activity, for example, by modification of inflammatory processes (Boison and Steinhäuser, 2018; Hiragi et al., 2018). Indeed, it has been demonstrated that IP injection of LPS evokes an immune response in the brain by means of TLR4, glycosylphosphatidylinositol-anchored glycoprotein CD14 and accessory protein MD-2 (Vezzani and Granata, 2005; Vezzani et al., 2011). LPS generates the release of

TABLE 4 | Effect of KEKS food (20% KEKS and 1% saccharin in standard rodent chow; group 1) on blood βHB and glucose levels.

Treatments (group 1)	Blood βHB and glucose levels (mean ± S.E.M.; significance level/*p*-value)	
	βHB (mmol/l)	Glucose (mg/dl)
Control (CON)	0.83 ± 0.025	70.88 ± 2.022
1st KEKS treatment (1K)	1.25 ± 0.059 ***/0.0007	66.75 ± 1.924 –/0.3571
10th KEKS treatment (10K)	1.35 ± 0.109 ****/<0.0001	73.88 ± 1.407 –/0.6224
2nd post-treatment day (2PT)	0.80 ± 0.046 –/0.9935	76.13 ± 1.552 –/0.1692

*1st KEKS treatment, 1st day of KEKS food administration; βHB, beta-hydroxybutyrate. ***$p < 0.001$ and ****$p < 0.0001$.*

TABLE 5 | Effect of IP indomethacin and lipopolysaccharide alone, as well as their combined administration on SWD number (**Figure 3**, group 2–4).

Treatments (Figure 3; groups 2–4)	SWD number (mean ± S.E.M.; significance level/*p*-value)	
	30–90 min	90–150 min
Control	17.9 ± 0.306	17.3 ± 0.189
Indomethacin	6.0 ± 0.436 ****/<0.0001	8.4 ± 0.297 ****/<0.0001
Control	18.5 ± 0.413	18.7 ± 0.457
LPS	40.6 ± 1.757 ****/<0.0001	57.4 ± 2.419 ****/<0.0001
Control	17.6 ± 0.408	17.8 ± 0.233
Indomethacin + LPS	16.9 ± 0.488 –/0.6321	17.6 ± 0.528 –/0.9773

*LPS, lipopolysaccharide; SWD, spike-wave discharge. ****$p < 0.0001$.*

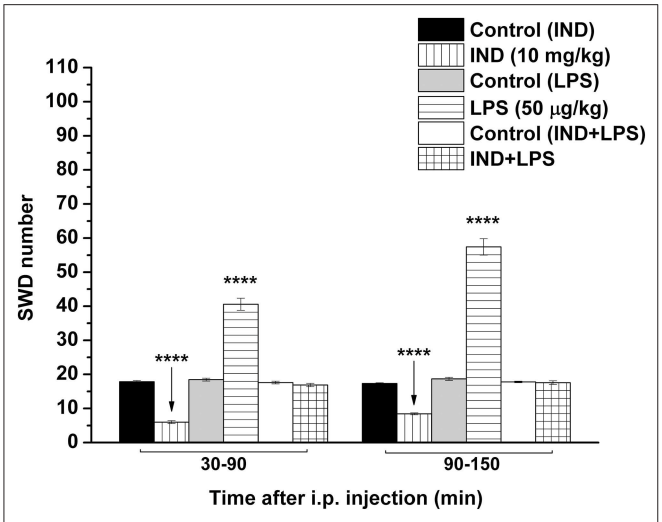

FIGURE 3 | Effect of IP indomethacin (IND: 10 mg/kg), IP lipopolysaccharide (LPS: 50 μg/kg), and combined administration of IP indomethacin (10 mg/kg) and IP LPS (50 μg/kg; IND+LPS) on SWD number (groups 2, 3, and 4, respectively). IND, indomethacin; i.p., intraperitoneal; LPS, lipopolysaccharide; SWD, spike-wave discharge. ****$p < 0.0001$ level of significance.

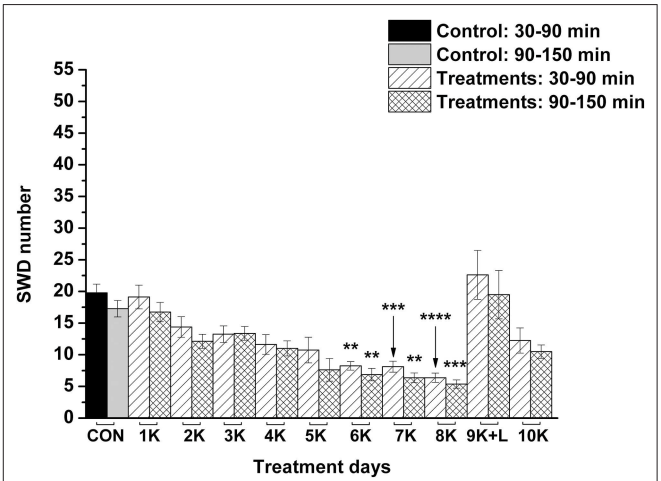

FIGURE 4 | The effect of combined administration of KEKS food (20% KEKS and 1% saccharin in standard rodent chow) with IP LPS (50 μg/kg) on SWD number on the day of 9th KEKS food administration (9K+L; group 5). 1K, 1st KEKS food administration; 2K, 2nd KEKS food administration and so on; 9K+L, combined administration of KEKS food (K) with i.p. LPS (L) on the day of 9th KEKS food administration; CON, control; SWD, spike-wave discharge. **$p < 0.01$, ***$p < 0.001$, and ****$p < 0.0001$.

proinflammatory cytokines such as IL-1β and tumor necrosis factor-α (TNF-α) from activated glial cells by means of the TLR4 pathway (Mlodzikowska-Albrecht et al., 2007; Vezzani et al., 2011). IL-1β and TNF-α may modulate excitatory and inhibitory processes via increased glutamatergic and decreased GABAergic neurotransmission (Vezzani and Granata, 2005; Mlodzikowska-Albrecht et al., 2007; Vezzani et al., 2008, 2011) and may generate an imbalance between excitatory/inhibitory processes in the brain; LPS, IL-1β and prostanoids (e.g., PGE_2) may evoke neuronal hyperexcitability and rapid excitation in the cortex via the TLR4/IL-1 receptor (IL-1R) signaling pathway (Wang and White, 1999; Maroso et al., 2011). As SWDs arise from the hyperexcitable focal cortical zone in WAG/Rij rats, these LPS-induced inflammatory processes above aggravate absence epileptic activity/SWD number via an increase in excitation in the thalamo-cortical/cortico-thalamic circuitry (Coenen and Van Luijtelaar, 2003; Kovács et al., 2006, 2014a). Moreover, enhanced activity of astrocytes by inflammatory processes may evoke increased activity of the adenosine-metabolizing enzyme adenosine kinase (Boison and Steinhäuser, 2018). Under these circumstances, adenosine kinase intensifies the metabolism of adenosine to adenosine monophosphate (Kovács et al., 2014b) and, as a result, it decreases adenosine levels and may increase not only neuronal excitability, but also the SWD number via decreased activity of inhibitory A_1Rs.

NOD-like receptor pyrin domain 3 (NLRP3) inflammasome is a multiprotein complex containing NOD-like receptor (NLRP3), an adaptor protein (ASC: apoptosis-associated speck-like protein

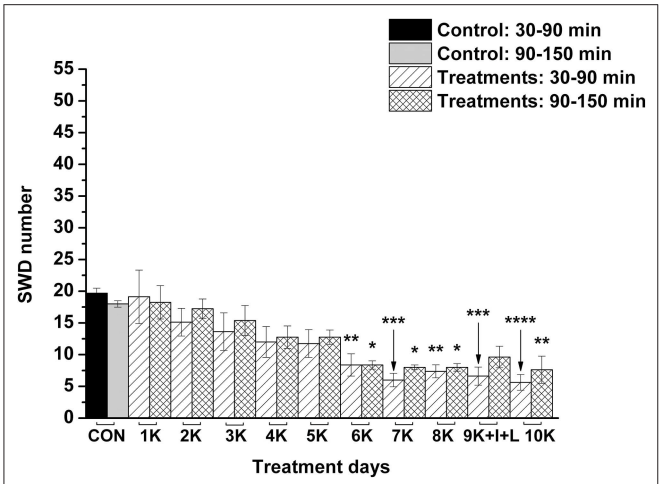

FIGURE 5 | The effect of combined administration of KEKS food (20% KEKS and 1% saccharin in standard rodent chow) with IP indomethacin plus IP LPS (10 mg/kg + 50 μg/kg, respectively) on SWD number on the day of 9th KEKS food administration (9K+I+L; group 6). 1K, 1st KEKS food administration; 2K, 2nd KEKS food administration and so on; 9K+I+L, combined administration of KEKS food (K) with i.p. indomethacin (I) and i.p. LPS (L) on the day of 9th KEKS food administration; CON, control; SWD, spike-wave discharge. $^{*}p < 0.05$, $^{**}p < 0.01$, $^{***}p < 0.001$, and $^{****}p < 0.0001$.

TABLE 6 | Effect of KEKS food on IP lipopolysaccharide-evoked changes in SWD number on the 9th KEKS day (9K+L; **Figure 4**, group 5).

Treatments (Figure 4; group 5)	SWD number (mean ± S.E.M.; significance level/*p*-value)	
	30–90 min	90–150 min
Control (CON)	19.8 ± 1.366	17.3 ± 1.301
1st KEKS treatment (1K)	19.1 ± 1.875 –/>0.9999	16.8 ± 1.532 –/>0.9999
2nd KEKS treatment (2K)	14.4 ± 1.625 –/0.8297	12.1 ± 1.109 –/0.8764
3rd KEKS treatment (3K)	13.3 ± 1.306 –/0.5073	13.4 ± 1.085 –/0.9923
4th KEKS treatment (4K)	11.6 ± 1.558 –/0.1289	11.0 ± 1.195 –/0.5773
5th KEKS treatment (5K)	10.8 ± 2.024 –/0.2122	7.6 ± 1.792 –/0.1358
6th KEKS treatment (6K)	8.3 ± 0.675 **/0.0084	6.9 ± 0.989 **/0.0067
7th KEKS treatment (7K)	8.1 ± 0.875 ***/0.0009	6.4 ± 0.754 **/0.0031
8th KEKS treatment (8K)	6.4 ± 0.730 ****/<0.0001	5.4 ± 0.653 ***/0.0006
9th KEKS + LPS treatment (9K+L)	22.6 ± 3.868 –/>0.9999	19.5 ± 3.827 –/>0.9999
10th KEKS treatment (10K)	12.3 ± 1.989 –/0.2380	10.5 ± 1.052 –/0.4243

1st KEKS treatment, 1st day of KEKS food administration; LPS, lipopolysaccharide; SWD, spike-wave discharge. $^{**}p < 0.01$, $^{***}p < 0.001$, and $^{****}p < 0.0001$.

TABLE 7 | Effect of KEKS food on IP indomethacin plus lipopolysaccharide-evoked changes in SWD number on the 9th KEKS day (9K+I+L; **Figure 5**, group 6).

Treatments (Figure 5; group 6)	SWD number (mean ± S.E.M.; significance level/*p*-value)	
	30–90 min	90–150 min
Control (CON)	19.7 ± 0.783	17.9 ± 0.508
1st KEKS treatment (1K)	19.1 ± 4.223 –/>0.9999	18.3 ± 2.631 –/>0.9999
2nd KEKS treatment (2K)	15.1 ± 2.191 –/0.9819	17.3 ± 1.521 –/>0.9999
3rd KEKS treatment (3K)	13.6 ± 2.964 –/0.7755	15.4 ± 2.375 –/>0.9999
4th KEKS treatment (4K)	12.0 ± 2.435 –/0.3315	12.8 ± 1.770 –/0.9261
5th KEKS treatment (5K)	11.8 ± 2.194 –/0.3626	12.7 ± 1.129 –/0.9261
6th KEKS treatment (6K)	8.4 ± 1.752 **/0.0059	8.4 ± 0.653 */0.0396
7th KEKS treatment (7K)	6.0 ± 1.069 ***/0.0001	8.0 ± 0.378 */0.0335
8th KEKS treatment (8K)	7.4 ± 1.017 **/0.0014	8.1 ± 0.598 */0.0335
9th KEKS + indomethacin + LPS treatment (9K+I+L)	6.6 ± 1.426 ***/0.0004	9.6 ± 1.700 –/0.0794
10th KEKS treatment (10K)	5.6 ± 1.238 ****/<0.0001	7.6 ± 2.138 **/0.0077

1st KEKS treatment, 1st day of KEKS food administration; LPS, lipopolysaccharide; SWD, spike-wave discharge. $^{*}p < 0.05$, $^{**}p < 0.01$, $^{***}p < 0.001$, and $^{****}p < 0.0001$.

containing a caspase recruitment domain) and a cysteine protease (caspase-1) (de Rivero Vaccari et al., 2014; Levy et al., 2015), which has a role in the pathophysiology of several CNS diseases, such as epilepsy (Edye et al., 2014; Simeone et al., 2018). The NLRP3 inflammasome controls caspase-1 activity and release of proinflammatory cytokines (e.g., IL-1β). Several factors, such as reactive oxygen species (ROS) and LPS (e.g., activation of TLR4-induced nuclear factor-κB/NF-κB pathway) have a role in the activation of NLRP3 inflammasome: first, translocation of gene expression regulator NF-κB generates upregulation of NLRP3 and pro-IL-1β expression. Subsequently, activation of inflammasome evokes activation of caspase-1-dependent cleavage of pro-IL-1β to its active form (IL-1β) for secretion (Levy et al., 2015; Patel et al., 2017). It has been demonstrated that βHB can exert its antiinflammatory effects by inhibition of NLRP3 and NLRP3 inflammasome-mediated cytokine production/inflammatory processes, suggesting a strong interaction between stimulation of the immune system and metabolic processes. For example, βHB decreased the expression/level of NLRP3, ASC, caspase-1 and IL-1β (Bae et al., 2016), attenuated the release of IL-1β in human monocytes (Youm et al., 2015), and mitigated stress-induced increases in TNF-α and IL-1β in the hippocampus (Yamanashi et al., 2017). Moreover, βHB attenuates the LPS-evoked increase in IL-1β and TNF-α level, as well as LPS-generated increases in COX-2, IL-1β, and TNF-α mRNA expression in BV-2 cells,

likely via inhibition of NF-κB signaling (Fu et al., 2014). It was also demonstrated that βHB may decrease inflammatory processes (e.g., expression of COX and IL-1β) via its G-protein-coupled receptor 109A (GPR109A or hydroxyl-carboxylic acid receptor 2/HCA2), which evoked inhibitory influence on the NF-κB signaling pathway in microglial cells (Fu et al., 2015; Graff et al., 2016). Thus, it is possible that KEKS food-evoked ketosis/increased βHB level may suppress the LPS-generated inflammatory processes and, as a consequence, may evoke antiepileptic effects in WAG/Rij rats via inhibition of the TLR4/IL-1R/NF-κB signaling pathway and decreasing the release of proinflammatory cytokines/enzymes (e.g., IL-1β and COX-2). This hypothesis is supported by our results, in which IP indomethacin enhanced the antiepileptic influence of KEKS food (**Figures 4**, **5**), likely via inhibition of the COX-2/PGE2 system. Moreover, it has been demonstrated that βHB may decrease production of ROS (Maalouf et al., 2007). As ROS may trigger/enhance inflammasome activation and release of proinflammatory cytokines (Patel et al., 2017), it is also possible that KEKS food-evoked increases in βHB level may decrease activation of NLRP3 inflammasome and the subsequent increase in IL-1β level via modulation of ROS production (Choi and Nakahira, 2011; Bae et al., 2016), effects which may decrease the SWD number. In addition, KEKS food-evoked ketosis may also generate anti-inflammatory/antiepileptic effects via increased extracellular adenosine level: for example, adenosine may decrease LPS-induced cytokine production of microglial cells via A_{2A}Rs (Van der Putten et al., 2009). Nevertheless, adenosine may attenuate the deleterious influence of ROS on brain cells via A_1Rs (Almeida et al., 2003).

It was suggested previously that inflammatory processes and proinflammatory cytokines may have a role in the genesis/modulation of spontaneous absence epileptic activity in WAG/Rij rats (Kovács et al., 2006, 2011; Van Luijtelaar et al., 2012; Russo et al., 2014). For example, antiinflammatory drugs, such as indomethacin and a selective COX-2 inhibitor etoricoxib, may decrease not only the LPS-induced increase in SWD number (indomethacin) but also spontaneous absence seizures (indomethacin and etoricoxib) (Kovács et al., 2006, 2011, 2014a; Citraro et al., 2015), whereas etoricoxib evoked long-lasting antiepileptogenic effects likely by inhibition of background inflammatory processes (Citraro et al., 2015). Based on these and our recent results, it is possible that exogenous ketone supplements exert their alleviating effect on both spontaneous absence epileptic activity (Kovács et al., 2017) (**Figure 2**) and LPS-induced increases in SWD number (**Figure 4**) via inhibition of inflammatory processes. Moreover, our results further supported the hypothesis that inflammation and changes in proinflammatory cytokine/enzyme levels could play a role in the appearance/modulation of absence epileptic activity in WAG/Rij rats, and likely other forms of seizures. For example, it is also well established that pro-inflammatory mediators evoke epileptogenic and ictogenic properties following traumatic brain injury (Webster et al., 2017), and this suggests that the therapeutic potential of ketone supplementation to target these inflammatory pathways may be an effective mitigation strategy for post-traumatic epilepsy, especially with penetrating brain injuries where neuroinflammation and seizure occurrence is very high.

In conclusion, KEKS food-evoked ketosis/βHB may decrease the neuronal activity/cortical excitability, which could decrease spontaneous and LPS-generated increases in absence epileptic activity. βHB may exert its antiepileptic effect via multiple processes by changes in metabolic pathways (e.g., modulating ATP level and activity of K_{ATP} channels), neurotransmitter systems (e.g., increasing adenosine level/release and activity of A_1Rs) and the function/activity of the TLR4/IL-1R/NF-κB/COX pathways (e.g., inhibiting proinflammatory cytokine production and release). Our results suggest that ketogenic foods containing exogenous ketone supplements such as KEKS food not only evoke ketosis but, as a consequence, also alleviate the inflammation-evoked processes in the CNS. Thus, theoretically, administration of exogenous ketogenic supplements (ketogenic foods) may be a promising therapeutic tool/metabolic therapy in the treatment of epilepsy and other inflammation-generated neurodegenerative diseases. Therefore, further studies, such as detailed investigation of influence of LPS administration in combination with different ketone supplemented foods on neuronal and glial cells are needed to reveal the exact mechanism of action of exogenous ketone supplementation-induced ketosis on LPS/inflammation-evoked changes in the CNS.

DATA AVAILABILITY

The datasets generated for this study are available on request to the corresponding author.

AUTHOR CONTRIBUTIONS

ZK: conception and design of experiments, data collection, interpretation of data, and writing manuscript. DPD: revising manuscript. DMD: revising manuscript. CA: data analysis and revising manuscript.

FUNDING

This work was supported by ONR Grant N000141310062 (to DPD), OTKA K124558 Research Grant (to ZK).

ACKNOWLEDGMENTS

We wish to thank Tamás Török (ELTE SEK) for the technical assistance. We thank Quest Nutrition LLC for supporting ongoing studies on this topic (to CA).

REFERENCES

Achanta, L. B., and Rae, C. D. (2017). β-Hydroxybutyrate in the brain: one molecule, multiple mechanisms. *Neurochem. Res.* 42, 35–49. doi: 10.1007/s11064-016-2099-2

Almeida, C. G., de Mendonça, A., Cunha, R. A., and Ribeiro, J. A. (2003). Adenosine promotes neuronal recovery from reactive oxygen species induced lesion in rat hippocampal slices. *Neurosci. Lett.* 339, 127–130. doi: 10.1016/S0304-3940(02)01478-7

Andoh, T., Ishiwa, D., Kamiya, Y., Echigo, N., Goto, T., and Yamada, Y. (2006). A1 adenosine receptor-mediated modulation of neuronal ATP-sensitive K channels in rat substantia nigra. *Brain Res.* 1124, 55–61. doi: 10.1016/j.brainres.2006.09.085

Ari, C., Kovács, Z., Juhasz, G., Murdun, C., Goldhagen, C. R., Koutnik, A. M., et al. (2016). Exogenous ketone supplements reduce anxiety-related behavior in Sprague-Dawley and Wistar Albino Glaxo/Rijswijk rats. *Front. Mol. Neurosci.* 9:137. doi: 10.3389/fnmol.2016.00137

Bae, H. R., Kim, D. H., Park, M. H., Lee, B., Kim, M. J., Lee, E. K., et al. (2016). β-Hydroxybutyrate suppresses inflammasome formation by ameliorating endoplasmic reticulum stress via AMPK activation. *Oncotarget* 7, 66444–66454. doi: 10.18632/oncotarget.12119

Boison, D., and Steinhäuser, C. (2018). Epilepsy and astrocyte energy metabolism. *Glia* 66, 1235–1243. doi: 10.1002/glia.23247

Brunengraber, H. (1997). Potential of ketone body esters for parenteral and oral nutrition. *Nutrition* 13, 233–235. doi: 10.1016/S0899-9007(96)00409-1

Choi, A. M., and Nakahira, K. (2011). Dampening insulin signaling by an NLRP3 'meta-flammasome'. *Nat. Immunol.* 12, 379–380. doi: 10.1038/ni.2028

Ciruela, F., Casadó, V., Rodrigues, R. J., Luján, R., Burgueño, J., Canals, M., et al. (2006). Presynaptic control of striatal glutamatergic neurotransmission by adenosine A1-A2A receptor heteromers. *J. Neurosci.* 26, 2080–2087. doi: 10.1523/JNEUROSCI.3574-05.2006

Citraro, R., Leo, A., Marra, R., De Sarro, G., and Russo, E. (2015). Antiepileptogenic effects of the selective COX-2 inhibitor etoricoxib, on the development of spontaneous absence seizures in WAG/Rij rats. *Brain Res. Bull.* 113, 1–7. doi: 10.1016/j.brainresbull.2015.02.004

Coenen, A. M., and Van Luijtelaar, E. L. (2003). Genetic animal models for absence epilepsy: a review of the WAG/Rij strain of rats. *Behav. Genet.* 33, 635–655. doi: 10.1023/A:1026179013847

D'Agostino, D., Pilla, R., Held, H., Landon, C., Puchowicz, M., Brunengraber, H., et al. (2013). Therapeutic ketosis with ketone ester delays central nervous system oxygen toxicity seizures in rats. *Am. J. Phys. Reg. Integr. Comp. Phys.* 304, 829–836. doi: 10.1152/ajpregu.00506.2012

D'Alimonte, I., D'Auro, M., Citraro, R., Biagioni, F., Jiang, S., Nargi, E., et al. (2009). Altered distribution and function of A2A adenosine receptors in the brain of WAG/Rij rats with genetic absence epilepsy, before and after appearance of the disease. *Eur. J. Neurosci.* 30, 1023–1035. doi: 10.1111/j.1460-9568.2009.06897.x

de Rivero Vaccari, J. P., Dietrich, W. D., and Keane, R. W. (2014). Activation and regulation of cellular inflammasomes: gaps in our knowledge for central nervous system injury. *J. Cereb. Blood Flow Metab.* 34, 369–375. doi: 10.1038/jcbfm.2013.227

Edye, M. E., Walker, L. E., Sills, G. J., Allan, S. M., and Brough, D. (2014). Epilepsy and the inflammasome: targeting inflammation as a novel therapeutic strategy for seizure disorders. *Inflammasome* 1, 36–43. doi: 10.2478/infl-2014-0004

Fu, S. P., Li, S. N., Wang, J. F., Li, Y., Xie, S. S., Xue, W. J., et al. (2014). BHBA suppresses LPS-induced inflammation in BV-2 cells by inhibiting NF-κB activation. *Mediators Inflamm.* 2014:983401. doi: 10.1155/2014/983401

Fu, S. P., Wang, J. F., Xue, W. J., Liu, H. M., Liu, B. R., Zeng, Y. L., et al. (2015). Anti-inflammatory effects of BHBA in both *in vivo* and *in vitro* Parkinson's disease models are mediated by GPR109A-dependent mechanisms. *J. Neuroinflamm.* 12:9. doi: 10.1186/s12974-014-0230-3

Graff, E. C., Fang, H., Wanders, D., and Judd, R. L. (2016). Anti-inflammatory effects of the hydroxycarboxylic acid receptor 2. *Metabolism* 65, 102–113. doi: 10.1016/j.metabol.2015.10.001

Haas, H. L., and Greene, R. W. (1984). Adenosine enhances afterhyperpolarization and accommodation in hippocampal pyramidal cells. *Pflugers Arch.* 402, 244–247. doi: 10.1007/BF00585506

Hashim, S. A., and VanItallie, T. B. (2014). Ketone body therapy: from the ketogenic diet to the oral administration of ketone ester. *J. Lipid Res.* 55, 1818–1826. doi: 10.1194/jlr.R046599

Hiragi, T., Ikegaya, Y., and Koyama, R. (2018). Microglia after seizures and in epilepsy. *Cells* 7:E26. doi: 10.3390/cells7040026

Kawamura, M. Jr., Ruskin, D. N., Geiger, J. D., Boison, D., and Masino, S. A. (2014). Ketogenic diet sensitizes glucose control of hippocampal excitability. *J. Lipid Res.* 55, 2254–2260. doi: 10.1194/jlr.M046755

Kesl, S. L., Poff, A. M., Ward, N. P., Fiorelli, T. N., Ari, C., Van Putten, A. J., et al. (2016). Effects of exogenous ketone supplementation on blood ketone, glucose, triglyceride, and lipoprotein levels in Sprague-Dawley rats. *Nutr. Metab.* 13:9. doi: 10.1186/s12986-016-0069-y

Kovács, Z., Czurkó, A., Kékesi, K. A., and Juhász, G. (2011). Intracerebroventricularly administered lipopolysaccharide enhances spike-wave discharges in freely moving WAG/Rij rats. *Brain Res. Bull.* 85, 410–416. doi: 10.1016/j.brainresbull.2011.05.003

Kovács, Z., D'Agostino, D. P., Dobolyi, A., and Ari, C. (2017). Adenosine A1 receptor antagonism abolished the anti-seizure effects of exogenous ketone supplementation in Wistar Albino Glaxo Rijswijk rats. *Front. Mol. Neurosci.* 10:235. doi: 10.3389/fnmol.2017.00235

Kovács, Z., Dobolyi, A., Juhász, G., and Kékesi, K. A. (2014a). Lipopolysaccharide induced increase in seizure activity in two animal models of absence epilepsy WAG/Rij and GAERS rats and Long Evans rats. *Brain Res. Bull.* 104, 7–18. doi: 10.1016/j.brainresbull.2014.03.003

Kovács, Z., Dobolyi, A., Kékesi, K. A., and Juhász, G. (2013). 5'-nucleotidases, nucleosides and their distribution in the brain: pathological and therapeutic implications. *Curr. Med. Chem.* 20, 4217–4240. doi: 10.2174/09298673113203400003

Kovács, Z., Kékesi, K. A., Dobolyi, Á., Lakatos, R., and Juhász, G. (2015a). Absence epileptic activity changing effects of non-adenosine nucleoside inosine, guanosine and uridine in Wistar Albino Glaxo Rijswijk rats. *Neuroscience* 300, 593–608. doi: 10.1016/j.neuroscience.2015.05.054

Kovács, Z., Kékesi, K. A., Juhász, G., Barna, J., Héja, L., Lakatos, R., et al. (2015b). Non-adenosine nucleoside inosine, guanosine and uridine as promising antiepileptic drugs: a summary of current literature. *Mini Rev. Med. Chem.* 14, 1033–1042. doi: 10.2174/1389557514666141107120226

Kovács, Z., Kékesi, K. A., Juhász, G., and Dobolyi, A. (2014b). The antiepileptic potential of nucleosides. *Curr. Med. Chem.* 21, 788–821. doi: 10.2174/13816128196661311191545O5

Kovács, Z., Kékesi, K. A., Szilágyi, N., Ábrahám, I., Székács, D., Király, N., et al. (2006). Facilitation of spike-wave discharge activity by lipopolysaccharides in Wistar Albino Glaxo/Rijswijk rats. *Neuroscience* 140, 731–742. doi: 10.1016/j.neuroscience.2006.02.023

Lakatos, R. K., Dobolyi, Á., Todorov, M. I., Kékesi, K. A., Juhász, G., Aleksza, M., et al. (2016). Guanosine may increase absence epileptic activity by means of A2A adenosine receptors in Wistar Albino Glaxo Rijswijk rats. *Brain Res. Bull.* 124, 172–181. doi: 10.1016/j.brainresbull.2016.05.001

Levy, M., Thaiss, C. A., and Elinav, E. (2015). Taming the inflammasome. *Nat. Med.* 21, 213–215. doi: 10.1038/nm.3808

Maalouf, M., Sullivan, P. G., Davis, L., Kim, D. Y., and Rho, J. M. (2007). Ketones inhibit mitochondrial production of reactive oxygen species production following glutamate excitotoxicity by increasing NADH oxidation. *Neuroscience* 145, 256–264. doi: 10.1016/j.neuroscience.2006.11.065

Maroso, M., Balosso, S., Ravizza, T., Liu, J., Bianchi, M. E., and Vezzani, A. (2011). Interleukin-1 type 1 receptor/toll-like receptor signalling in epilepsy: the importance of IL-1beta and high-mobility group box 1. *J. Intern. Med.* 270, 319–326. doi: 10.1111/j.1365-2796.2011.02431.x

McNally, M. A., and Hartman, A. L. (2012). Ketone bodies in epilepsy. *J. Neurochem.* 121, 28–35. doi: 10.1111/j.1471-4159.2012.07670.x

Mlodzikowska-Albrecht, J., Steinborn, B., and Zarowski, M. (2007). Cytokines, epilepsy and epileptic drugs-is there a mutual influence? *Pharmacol. Rep.* 59, 129–138.

Newman, J. C., and Verdin, E. (2014). Ketone bodies as signaling metabolites. *Trends Endocrinol. Metab.* 25, 42–52. doi: 10.1016/j.tem.2013.09.002

Newport, M. T., VanItallie, T. B., Kashiwaya, Y., King, M. T., and Veech, R. L. (2015). A new way to produce hyperketonemia: use of ketone ester in a case of Alzheimer's disease. *Alzheimers Dement.* 11, 99–103. doi: 10.1016/j.jalz.2014.01.006

Patel, M. N., Carroll, R. G., Galván-Peña, S., Mills, E. L., Olden, R., Triantafilou, M., et al. (2017). Inflammasome priming in sterile inflammatory disease. *Trends Mol. Med.* 23, 165–180. doi: 10.1016/j.molmed.2016.12.007

Paxinos, G., and Watson, C. (1999). *The Rat Brain Stereotaxic Coordinates*. Orlando, FL: Academic Press.

Peeters, B. W., Van Rijn, C. M., Vossen, J. M., and Coenen, A. M. (1989). Effects of GABA-ergic agents on spontaneous non-convulsive epilepsy, EEG and behaviour, in the WAG/RIJ inbred strain of rats. *Life Sci.* 45, 1171–1176. doi: 10.1016/0024-3205(89)90505-5

Poff, A. M., Ward, N., Seyfried, T. N., Arnold, P., and D'Agostino, D. P. (2015). Non-toxic metabolic management of metastatic cancer in VM mice: novel combination of ketogenic diet, ketone supplementation, and hyperbaric oxygen therapy. *PLoS ONE* 10:e0127407. doi: 10.1371/journal.pone.0127407

Russo, E., Andreozzi, F., Iuliano, R., Dattilo, V., Procopio, T., Fiume, G., et al. (2014). Early molecular and behavioral response to lipopolysaccharide in the WAG/Rij rat model of absence epilepsy and depressive-like behavior, involves interplay between AMPK, AKT/mTOR pathways and neuroinflammatory cytokine release. *Brain Behav. Immun.* 42, 157–168. doi: 10.1016/j.bbi.2014.06.016

Sayyah, M., Javad-Pour, M., and Ghazi-Khansari, M. (2003). The bacterial endotoxin lipopolysaccharide enhances seizure susceptibility in mice: involvement of proinflammatory factors: nitric oxide and prostaglandins. *Neuroscience* 122, 1073–1080. doi: 10.1016/j.neuroscience.2003.08.043

Sharma, A. K., Rani, E., Waheed, A., and Rajput, S. K. (2015). Pharmacoresistant epilepsy: a current update on non-conventional pharmacological and non-pharmacological interventions. *J. Epilepsy Res.* 5, 1–8. doi: 10.14581/jer.15001

Simeone, T. A., Simeone, K. A., Stafstrom, C. E., and Rho, J. M. (2018). Do ketone bodies mediate the anti-seizure effects of the ketogenic diet? *Neuropharmacology* 133, 233–241. doi: 10.1016/j.neuropharm.2018.01.011

Sleiman, S. F., Henry, J., Al-Haddad, R., El Hayek, L., Abou Haidar, E., Stringer, T., et al. (2016). Exercise promotes the expression of brain derived neurotrophic factor (BDNF) through the action of the ketone body β-hydroxybutyrate. *Elife* 5:e15092. doi: 10.7554/eLife.15092

Stubbs, B. J., Cox, P. J., Evans, R. D., Santer, P., Miller, J. J., Faull, O. K., et al. (2017). On the metabolism of exogenous ketones in humans. *Front. Physiol.* 8:848. doi: 10.3389/fphys.2017.00848

Van der Putten, C., Zuiderwijk-Sick, E. A., van Straalen, L., de Geus, E. D., Boven, L. A., Kondova, I., et al. (2009). Differential expression of adenosine A3 receptors controls adenosine A2A receptor-mediated inhibition of TLR responses in microglia. *J. Immunol.* 182, 7603–7612. doi: 10.4049/jimmunol.0803383

Van Luijtelaar, G., Lyashenko, S., Vastyanov, R., Verbeek, G., Oleinik, A., Van Rijn, C., et al. (2012). Cytokines and absence seizures in a genetic rat model. *Neurophysiology* 43, 478–486. doi: 10.1007/s11062-012-9252-6

Vezzani, A., Balosso, S., and Ravizza, T. (2008). The role of cytokines in the pathophysiology of epilepsy. *Brain Behav. Immun.* 22, 797–803. doi: 10.1016/j.bbi.2008.03.009

Vezzani, A., and Granata, T. (2005). Brain inflammation in epilepsy: experimental and clinical evidence. *Epilepsia* 46, 1724–1743. doi: 10.1111/j.1528-1167.2005.00298.x

Vezzani, A., Maroso, M., Balosso, S., Sanchez, M. A., and Bartfai, T. (2011). IL-1 receptor/Toll-like receptor signaling in infection, inflammation, stress and neurodegeneration couples hyperexcitability and seizures. *Brain Behav. Immun.* 25, 1281–1289. doi: 10.1016/j.bbi.2011.03.018

Wang, Y. S., and White, T. D. (1999). The bacterial endotoxin lipopolysaccharide causes rapid inappropriate excitation in rat cortex. *J. Neurochem.* 72, 652–660. doi: 10.1046/j.1471-4159.1999.0720652.x

Webster, K. M., Sun, M., Crack, P., O'Brien, T. J., Shultz, S. R., and Semple, B. D. (2017). Inflammation in epileptogenesis after traumatic brain injury. *J Neuroinflammation* 14:10. doi: 10.1186/s12974-016-0786-1

Yamanashi, T., Iwata, M., Kamiya, N., Tsunetomi, K., Kajitani, N., Wada, N., et al. (2017). Beta-hydroxybutyrate, an endogenic NLRP3 inflammasome inhibitor, attenuates stress-induced behavioral and inflammatory responses. *Sci. Rep.* 7:7677. doi: 10.1038/s41598-017-08055-1

Youm, Y. H., Nguyen, K. Y., Grant, R. W., Goldberg, E. L., Bodogai, M., Kim, D., et al. (2015). The ketone metabolite β-hydroxybutyrate blocks NLRP3 inflammasome-mediated inflammatory disease. *Nat. Med.* 21, 263–269. doi: 10.1038/nm.3804

Conflict of Interest Statement: International Patent # PCT/US2014/031237, University of South Florida, DPD, S. Kesl, and P. Arnold, Compositions and Methods for Producing Elevated and Sustained Ketosis. Non-provisional patents: #62289749, University of South Florida, CA and DPD, Exogenous ketone supplements for reducing anxiety-related behavior; CA, Arnold P, and DPD Technology Title: Elevated Blood Ketone Levels by Ketogenic Diet or Exogenous Ketone Supplements Induced Increased Latency of Anesthetic Induction USF Ref. No. 16A018PR; CA, Arnold P, and DPD Technology Title: Exogenous Ketone Supplementation Improved Motor Function in Sprague-Dawley Rats. USF Ref. No: 16A019; CA, Arnold P, and DPD Technology Title: Lowering of Blood Glucose in Exercising and Non-Exercising Rats Following Administration of Exogenous Ketones and Ketone Formulas. USF Ref. No: 16A049; CA, Arnold P, and DPD Technology Title: Ketone Supplementation Elevates Blood Ketone Level and Improves Motor Function in GLUT1 Deficiency Syndrome Mice. USF Ref. No: 16B116 (provisional patent); CA, Arnold P, and DPD Technology Title: Neuroregeneration improved by ketone. USF Ref. No: 16B128 (provisional patent); CA, DPD, and Dean, J. B Technology Title: Delaying latency to seizure by combinations of ketone supplements. USF Ref. No: 16B138PR. DPD and AC are co-owners of the company Ketone Technologies LLC, providing scientific consulting and public speaking engagements about ketogenic therapies. The company obtained an option agreement from the University of South Florida on the non-provisional patent No. 62/310,302 Methods of increasing latency of anesthetic induction using ketone supplementation. These interests have been reviewed and managed by the University in accordance with its Institutional and Individual Conflict of Interest policies. The authors declare that Csilla Ari received funding from Quest Nutrition LLC. The funder was not involved in the study design or collection, analysis, or interpretation of the data.

frontiers in Molecular Neuroscience

REVIEW
published: 29 March 2019
doi: 10.3389/fnmol.2019.00065

Dexamethasone in Glioblastoma Multiforme Therapy: Mechanisms and Controversies

*Marta Cenciarini[1], Mario Valentino[2], Silvia Belia[3], Luigi Sforna[1], Paolo Rosa[4], Simona Ronchetti[5], Maria Cristina D'Adamo[2] and Mauro Pessia[1,2]**

[1]Section of Physiology and Biochemistry, Department of Experimental Medicine, University of Perugia School of Medicine, Perugia, Italy, [2]Department of Physiology and Biochemistry, Faculty of Medicine and Surgery, University of Malta, Msida, Malta, [3]Department of Chemistry, Biology and Biotechnology, University of Perugia, Perugia, Italy, [4]Department of Medical-Surgical Sciences and Biotechnologies, University of Rome "Sapienza", Polo Pontino, Latina, Italy, [5]Section of Pharmacology, Department of Medicine, University of Perugia School of Medicine, Perugia, Italy

Glioblastoma multiforme (GBM) is the most common and malignant of the glial tumors. The world-wide estimates of new cases and deaths annually are remarkable, making GBM a crucial public health issue. Despite the combination of radical surgery, radio and chemotherapy prognosis is extremely poor (median survival is approximately 1 year). Thus, current therapeutic interventions are highly unsatisfactory. For many years, GBM-induced brain oedema and inflammation have been widely treated with dexamethasone (DEX), a synthetic glucocorticoid (GC). A number of studies have reported that DEX also inhibits GBM cell proliferation and migration. Nevertheless, recent controversial results provided by different laboratories have challenged the widely accepted dogma concerning DEX therapy for GBM. Here, we have reviewed the main clinical features and genetic and epigenetic abnormalities underlying GBM. Finally, we analyzed current notions and concerns related to DEX effects on cerebral oedema, cancer cell proliferation and migration and clinical outcome.

Keywords: GBM, dexamethasone, cerebral oedema, pharmacogenomics, glioblastoma multiforme therapy

OPEN ACCESS

Edited by:
Vittorio Maglione, Mediterranean Neurological Institute (IRCCS), Italy

Reviewed by:
Giuseppe Giannini, Sapienza University of Rome, Italy
Stefania Crispi, Institute of Bioscience and Bioresources, National Research Council, Italy

****Correspondence:***
Mauro Pessia
mauro.pessia@um.edu.mt;
mauro.pessia@unipg.it

Received: *16 January 2019*
Accepted: *26 February 2019*
Published: *29 March 2019*

Citation:
Cenciarini M, Valentino M, Belia S, Sforna L, Rosa P, Ronchetti S, D'Adamo MC and Pessia M (2019) Dexamethasone in Glioblastoma Multiforme Therapy: Mechanisms and Controversies. Front. Mol. Neurosci. 12:65. doi: 10.3389/fnmol.2019.00065

INTRODUCTION

Glioblastoma multiforme (GBM) is the most aggressive form of brain tumor, accounting for 54% of all gliomas (Dolecek et al., 2012). The estimated number of annual new cases of GBM are: Japan 2,200, UK 2,531, France 3,000, Germany 3,500, USA 18,000. Globally, over 100,000 patients die each year as a result of this type of brain cancer. It is highly invasive and not amenable to current treatment such as surgical management, chemo- and radio-therapy (Furnari et al., 2007) and affected individuals have very poor life expectancy (Miller and Perry, 2007). The highly aggressive course and poor response to treatments likely result from uncontrolled cellular proliferation, migration, presence of a cancer stem-like cell population, neo-angiogenesis and severe brain oedema.

GBM-induced cerebral oedema is currently treated with corticosteroids due to their ability to decrease the permeability of the blood brain barrier (BBB; Salvador et al., 2014). Dexamethasone (DEX) represents the drug of choice among the synthetic glucocorticoids (GCs) by virtue of its minimal mineralocorticoid activity, long half-life and high potency (Kostaras et al., 2014). By evaluating the typical features of GBM aggressiveness, several studies have shown positive effects of DEX on GBM cells both *in vitro* and cancer volume, *in vivo* (Guerin et al., 1992; Wolff et al., 1997;

Kaup et al., 2001; Villeneuve et al., 2008; Piette et al., 2009; Fan et al., 2014) although, the mechanisms accounting for these actions remain unclear. Strikingly, contradictory evidence has been published generating controversies that are still debated. As a resource for those interested in this issue, we have reviewed relevant critical articles from various research groups describing DEX actions in GBM and discussed proposed mechanisms and controversies.

GLIOBLASTOMA MULTIFORME: CLINICAL AND MOLECULAR FEATURES

GBM is known as grade IV astrocytoma according to the World Health Organization (WHO) classification. "Primary GBM" accounts for some 90% of cases, arises *de novo* and affects older patients. "Secondary GBM" develops from preceding low-grade astrocytomas and is more common in patients that are ≤45 years old (Crespo et al., 2015; Louis et al., 2016). Neurological signs depend on the location of the tumor within the brain and can be either focal or generalized. Frequently, symptoms include headache, seizures, cognitive dysfunction, ataxia, vomiting, vision disturbance. Unusual symptoms such as syncope, vertigo, hypoesthesia or psychiatric manifestations could result in misdiagnosis and mistreatment. In some instances, GBM infiltrate the brain as finger-like tentacles making surgical resection of the tumor very difficult, especially when it develops near eloquent regions of the brain. GBM could be considered a non-metastatic cancer, as it rarely spreads from the primary site to other remote tissues of the body thanks to the confining properties of the BBB (Beauchesne, 2011). Another typical feature is the presence of hypoxic and necrotic regions within the cancer mass (Lara-Velazquez et al., 2017). Microscopic analyses showed a central large necrotic core that takes up to 80% of tumor mass and multiple thrombotic foci surrounded by pseudopalisading cells migrating towards more oxygenated areas (Rong et al., 2006; Amberger-Murphy, 2009; Sforna et al., 2017). Hypoxia induces important changes on tumor cell genome and proteome, which increase its aggressiveness (Amberger-Murphy, 2009). In particular, hypoxia promotes invasiveness, radio- and chemo-resistance, glioma stem cell (GSC) development and angiogenesis (Jensen, 2009; Yang et al., 2012; Sforna et al., 2015). The vascular endothelial growth factor (VEGF) is over-expressed by cancer cells under hypoxia and promotes neo-angiogenesis (Soda et al., 2013; Dubois et al., 2014). Indeed, GBM is a highly vascularized tumor and the degree of vascularization influences prognosis, remarkably (Takano et al., 2010; Dubois et al., 2014).

Histological evaluations have shown extensive variability of cell morphology that is characterized by the coexistence of small cells and multinucleated giant cells (Meyer-Puttlitz et al., 1997; Kleihues, 1998). A growing body of evidence supports the notion that GBM cell heterogeneity results also from the presence of GSCs, a small subpopulation of tumor cells that show features of self-renewal, resistance to radiotherapy (RT) and chemotherapy, ability to differentiate *in vitro* and promote tumor recurrence. These properties are shared in part with neuronal stem cells (NSCs; Reya et al., 2001; Bao et al., 2006; Vescovi et al., 2006; Park and Rich, 2009; Rosen and Jordan, 2009; Frank et al., 2010; Heddleston et al., 2010). Of note is that, GSCs are also responsible for the angiogenic potential of the tumor by expressing high levels of VEGF (Bao et al., 2006; Li et al., 2009). Initially, the term multiforme referred to a broad spectrum in cellular heterogeneity. However, in addition to the histological features, GBM is characterized by several genetic and epigenetic alterations. Thus, multiforme currently refers to the latter multifaceted features of the cancer (DeAngelis and Mellinghoff, 2011; Stoyanov et al., 2018). Indeed, genomic investigations resulted in the identification of a number of genetic abnormalities underlying the molecular transcriptional subtypes of GBM. Verhaak et al. (2010) proposed the classification of GBM into four distinct subtypes: classical, mesenchymal, proneural and neural.

The classical subtype is characterized by amplification or mutation in the *epidermal growth factor receptor* (EGFR) and deletion mutations in the *cyclin-dependent kinase inhibitor 2A* (*CDKN2A*) gene, coding for the p16INK4A and p14arf protein tumor suppressors. Genomic amplification of EGFR is observed in 97% of the classical subtype, which leads to the four-fold increase in EGFR expression. The most common point mutation results in the deletion variant EGFRvIII, lacking exons 2–7, which encode the extracellular domain. The EGFRvIII alteration prevents EGF binding and confers ligand-independent signaling, thereby activating pathways other than those controlled by the wild-type EGFR.

The mesenchymal subtype is featured by deletions of a region at 17q11.2 containing the gene NF1 (*neurofibromin*). Moreover, genes in the *tumor necrosis factor* (TNF) super family pathway are highly expressed in this subtype, potentially as a consequence of higher overall necrosis (Verhaak et al., 2010; DeAngelis and Mellinghoff, 2011; Lara-Velazquez et al., 2017).

The proneural subtype is characterized by high levels of *platelet-derived growth factor receptor A* (PDGFRA) expression and point mutations of both *isocitrate dehydrogenase 1* (IDH1) and p53. Although, focal amplifications of the locus at 4q12 harboring the PDGFRA gene were observed in all GBM subtypes, the proneural samples possess a much higher degree. Multiple PDGFRA point mutations have been identified in the Ig-domain, potentially disrupting ligand interaction. Moreover, a rare in frame deletion of the Ig-domain of PDGFRA has been described (Kumabe et al., 1992; Rand et al., 2005). The IDH family includes three enzymes with different locations: IDH1 found in cytosol and peroxisome and IDH2 and IDH3 located in mitochondria. These are involved in the biosynthesis of central metabolites in the tricarboxylic acid (TCA) cycle and catalyze the oxidative decarboxylation of isocitrate to α-ketoglutarate (α-KG), producing NADPH (Leonardi et al., 2012; Miller and Perry, 2007). The proneural subtype is also characterized by point mutations in the IDH1 gene. These mutations produce d-2-hydroxyglutarate (d-2HG), a competitive inhibitor of alpha-ketoglutarate-dependent dioxygenase which induces epigenetic changes, including hypermethylation (Waitkus et al., 2016; Czapski et al., 2018; Lee et al., 2018).

The neural subtype is characterized by expression of neural markers such as *neurofilament light* (NEFL), *gamma-*

aminobutyric acid type A receptor alpha-1 subunit (GABRA1) and the SLC12A5 (K^+/Cl^- *co-transporter 2*).

According to recent WHO guidelines, GBMs could be subdivided into IDH wild-type and IDH-mutant (Louis et al., 2016). GBM/IDH wild-type are more common (∼90%), tend to be more aggressive, and have worse prognosis than GBM/IDH mutant. Mutations in the IDH-encoding gene have been found in ∼10% of GBM (Parsons et al., 2008) and are associated with altered cell metabolism. IDH mutations were mainly found in secondary GBM, which develops from low-grade gliomas (Han and Batchelor, 2017).

IDH1 mutations occur in 50%–80% of grade II and III astrocytoma, oligodendroglioma and secondary GBM. IDH2 mutations occur in the same tumor with less frequency (Hartmann et al., 2009). The most common mutation in IDH1 results in arginine 132 to histidine substitution (R132H). This mutation converts α-KG to the R(−)-2-hydroxyglutarate (2-HG), considered as a potential "*oncometabolite*." It has been shown that accumulation of 2HG affects histone and DNA demethylases resulting in a hypermethylation phenotype with chromatin modifications and gene expression dysregulation (Staedtke et al., 2016; Han and Batchelor, 2017).

The Epigenetic Origin of GBM and Therapeutic Potential of Epigenetic Modifiers Synergized by DEX

Epigenetic modifications refer to changes in gene expression and cellular phenotype without alterations in the DNA sequence. A number of studies over the past years have provided greater knowledge and insight concerning the epigenetic origin of GBM. *Hypermethylation* represents an epigenetic mechanism frequently observed in GBM that occurs at genes involved in cell cycle regulation, DNA repair, apoptosis, angiogenesis and invasion (Alaminos et al., 2005; Tews et al., 2007; Martinez and Esteller, 2010). DNA hypermethylation of promoter regions can silence tumor suppressor genes or pro-apoptotic genes, or even favor the response to chemotherapy and RT in tumor cells (Kanazawa et al., 2019). Remarkably, 90% of high-grade gliomas contained methylated gene promoters. Affected individuals were found to have large amounts of DNA in the plasma and the same methylated promoters present in the tumor were also found in the plasma in 60% of the cases. This represents the first step towards the development of quantitative plasma biomarkers that could be used to monitor glioma status (Weaver et al., 2006). Methylation of the *O6-methylguanine DNA methyltransferase* (MGMT) promoter is frequently observed in secondary GBM, associated with p53 mutations (Nakamura et al., 2001; Martinez and Esteller, 2010). MGMT is involved in DNA repair and its activity is down-regulated by methylation.

Methylation, demethylation and acetylation are among the main epigenetic modifications of histone. Histone methylation and demethylation are involved in reprogramming GBM cell metabolism and occur by action of histone methyltransferases (HMTs) and demethylases (HDMs), respectively (Dong and Cui, 2018). Histone acetyltransferases (HATs) and deacetylases (HDACs) control the acetylation state of histones, modulating chromatin structure and function and promote the transcriptional activation or repression (Bezecny, 2014). HDACs also change non-histone proteins which regulate important cellular functions such as cell-cycle progression, differentiation and apoptosis (Lee et al., 2015). The HDAC family includes four classes: Zn^{2+}-dependent (classes I, II and IV), Zn^{2+}-independent (class III) and nicotinamide-adenine dinucleotide-dependent enzymes (Lee et al., 2017). In GBM, HDACs are considered the main effectors of epigenetic alterations and are implicated in tumorigenesis. Indeed, mutations and alterations of HDAC expression have been identified and associated to GBM pathogenesis and progression (Was et al., 2019). In particular, mutations in both HDAC2 and HDAC9 genes have been found through sequencing of GBM biopsies (Parsons et al., 2008). It has been reported that GBM displays decreased mRNA expression in class II and class IV HDACs. On the other hand, recent studies have shown increased levels of HDAC1, HDAC3, and HDAC6 (Staberg et al., 2017), as well as overexpression of HDAC9 (Yang, 2015).

The reversibility of epigenetic modifications opens new therapeutic perspectives for GBM. As such, the search for new drugs targeting epigenetic modifications has been expanded over the past years. DNA methyltransferase inhibitors (DNMTi) and histone deacetylase inhibitors (HDACi) have been tested in multiple cancers. However, only HDACi have been approved in clinical trials (Romani et al., 2018). HDACi are divided into seven categories: short chain fatty acids, benzamides, cyclic peptides, electrophilic ketones, hydro-xamines, sirtuin inhibitors and other miscellaneous forms (Lee et al., 2015). Their anti-cancer effects include the induction of cell-cycle arrest, differentiation, apoptosis, mitotic cell death and autophagic cell death (Bezecny, 2014). *Vorinostat*, *Romidepsin* and *Valproic Acid* are among the HDCAi that managed to find their way in clinical trials. The efficacy of *Vorinostat* has been tested in primary GBM explants, as well as in murine GBM cell lines, *in vitro* and *in vivo*. The drug induced accumulation of cells in the G2-M phase, increased the expression of p21WAF1, p27KIP1, DR5 and TNFα, and decreased the levels of the pro-growth genes CDK2, CDK4, cyclin D1 and cyclin D2. In addition, it reduced the invasiveness in a number of GBM cell lines with different PTEN and p53 mutations (An et al., 2010; Xu et al., 2011). *Romidepsin* is a class I HDACi and exerts its functions by down-regulating Bcl-xL and up-regulating p21 expression (Lee et al., 2015).

The *Enhancer of Zeste Homolog 2* (EZH2) is a histone-lysine N-methyltransferase enzyme that participates in histone methylation. EZH2 is the functional enzymatic component of the *Polycomb Repressive Complex 2* (PRC2) involved in a wide range of glioma processes, including cell cycle, invasion, GSC maintenance, drug and RT resistance (Yin et al., 2016). A recent study showed the effects of the SAM-competitive EZH2 inhibitor UNC1999 in different stem cell-like glioma cells, named brain tumor-initiating cells (BTICs). By evaluating cell growth, the combination of UNC1999 with DEX exerted a synergistic effect in two different BTICs type and suppressed tumor growth, *in vivo* (Grinshtein et al., 2016). Therefore, therapeutic anti-cancer benefits may result from the combination of drugs which enhance therapeutic efficacy compared to the

mono-therapy approach derived through targeting key pathways in a characteristically synergistic or additive manner. However, a common obstacle shared by all these therapeutic approaches is the low permeability of the BBB. It is hoped that the use of easily penetrating drugs, such as DEX, together with newly selected epigenetic compounds that are able to cross the BBB could contribute to finding a better therapy for GBM.

GBM-INDUCED CEREBRAL OEDEMA

Cerebral oedema is a hallmark of malignant brain tumors that influences the clinical course and the prognosis of the disease (Stummer, 2007; Lin et al., 2016). It represents a major cause of morbidity and mortality in GBM due to the high risk of brain herniation in up to 60% of patients (Silbergeld et al., 1991). Indeed, the accumulation of fluids inside the cerebral parenchyma induces a rapid increase in brain volume leading to a sharp increase in intracranial pressure (ICP), which may cause ischemia, herniation and ultimately death (Papadopoulos et al., 2004). The main processes involved in cerebral oedema are vasogenic and cytotoxic oedema. Vasogenic oedema results from accumulation of fluid in the cerebral parenchyma caused by disruption and increased permeability of the BBB. Cytotoxic oedema results from failure in cell metabolism leading to impairment of the Na^+/K^+ pump (Michinaga and Koyama, 2015). In gray and white matter, astrocytes may swell as a result of cytoplasmic retention of Na^+ ions and water. Typically, GBM-associated cerebral oedema is vasogenic in nature. It is characterized by breakdown of the BBB, resulting in extracellular accumulation of fluid with disruption of homeostasis around the microenvironment of the compromised parenchyma.

The BBB represents a structure that separates the brain parenchyma from the circulatory system, allowing maintenance of central nervous system (CNS) fluid homeostasis and passage of substances to brain cells by mechanisms that rely on simple diffusion or active transport (Campos-Bedolla et al., 2014). It is formed by brain capillary endothelial cells (BCECs) that are supported by neighboring glial cells (microglia and astrocytes; Kaur and Ling, 2008), neurons and perivascular pericytes (Wolburg and Lippoldt, 2002; Zlokovic, 2008; Zozulya et al., 2008). The BCECs are joined together by means of tight junctions (TJs), composed of several proteins, among which are claudins and occludins (Furuse et al., 1993, 1996, 1998; Kubota et al., 1999). These transmembrane proteins bind intracellular proteins such as zonula occludens-1 and -2 (ZO1; ZO2) allowing the coupling of TJs to the cytoskeleton elements of endothelial cells (Stummer, 2007). The TJ formation is promoted by growth factors secreted by astrocytes which therefore play an important role in controlling the unique tightness of the BBB (Wolburg et al., 2012). TJ proteins with altered expression or function affect the tightness of epithelial surfaces, causing BBB hyper-permeability and consequently vasogenic oedema (**Figure 1**). It has been shown that occludin is downregulated and subsequently phosphorylated in human high-grade gliomas, thus causing increased permeability of the TJs as a result of the altered interaction between phosphorylated occludin and ZO1, ZO2 and ZO3 (Rubin and Staddon, 1999; Papadopoulos et al., 2001; Kale et al., 2003). Liebner et al. (2000) have shown that the expression of the TJ protein claudin 1 is lost in the majority of tumor micro vessels and claudin 5 down-regulated in hyperplastic vessels, leading to increased endothelial permeability. GBM cells secrete several factors including VEGF, stromal cell-derived factor-1 (SDF-1α) and Angiopoietin 1 (Ang-1) that increase the proliferation of endothelial cells and promote development of new vessels. To further aggravate the condition, the tumor's vascularization is immature and morphologically abnormal. Indeed, the new vessels are disorganized, deformed, tortuous, partially occluded, excessively leaky and dysfunctional (Hardee and Zagzag, 2012; Dubois et al., 2014; Salmaggi et al., 2004). The main factor that promotes neo-angiogenesis is VEGF, which is up-regulated in brain tumors associated with oedema (Lin and Wang, 2016;

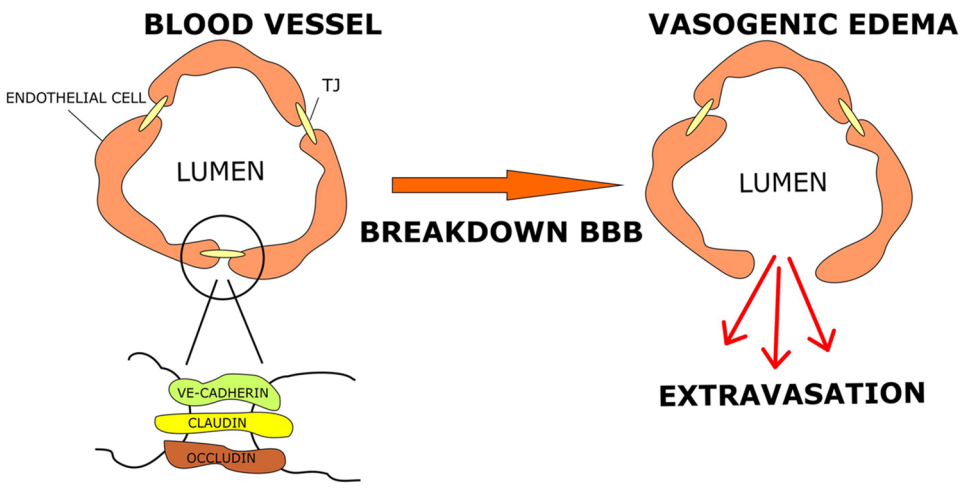

FIGURE 1 | Tumor-related oedema. Brain capillary endothelial cells (BCECs) are connected *via* tight junction (TJ) protein complexes that fuse endothelial cells together. When a brain tumor develops, particularly high-grade gliomas, TJs become permeable due to release of angiogenic factors and changes in protein component. These events cause blood brain barrier (BBB) breakdown and vasogenic oedema.

Lin et al., 2016). VEGF affects the vascular endothelium, stimulating the proliferation and migration of endothelial cells, decreasing the expression of TJ proteins, whilst increasing the hydraulic permeability of vessels (Hardee and Zagzag, 2012; Stokum et al., 2016). Overall, altered TJs in endothelial cells and abnormal vascularization result in fluid buildup in cerebral parenchyma, leading to increased brain volume and ICP (Papadopoulos et al., 2004).

MANAGEMENT OF BRAIN OEDEMA WITH DEX

GCs are steroid hormones produced by the adrenal cortex under the control of the hypothalamic–pituitary–adrenal axis (HPA) that regulate carbohydrate metabolism, inflammatory and immune responses. Their effects are mediated by binding to GC receptor (GR) on a time scale from hours to days (genomic effects). The best known and well characterized isoform of GR is GR-α. The complex GC-GR binds to DNA at particular glucocorticoid responsive elements (GRE) and regulates the transcription of a number of genes (Piette et al., 2006).

GCs reduce oedema by affecting BBB functionality, particularly through modulation of gene expression and function of claudins, occludins, and vascular endothelial (VE)-cadherin that regulate endothelial permeability (Hue et al., 2015). In rodent brain tumors, DEX decreases BBB permeability by up-regulating the expression of occludin (Gu et al., 2009a,b).

The stability of the BBB is regulated by Ang-1 and Ang-2, as well as VEGF (Kaal and Vecht, 2004; Nag et al., 2005). Ang-1 binds to the receptor tyrosine kinase Tie-2 expressed on endothelial cells, whereas, Ang-2 participates in BBB breakdown through vessel destabilization (Maisonpierre et al., 1997). Up-regulation of Ang-1 and down-regulation of VEGF by DEX treatment have been reported in human brain astrocytes and pericytes (Kim et al., 2008). DEX ameliorates oedema not only by influencing the factors that regulate the permeability of the capillary bed, but also by inhibiting their production (**Figure 2**). Indeed in C6 cells, DEX down-regulates VEGF mRNA and protein expression in a dose-dependent manner both in normoxic and hypoxic conditions. This effect was found to be mediated by GR (Finkenzeller et al., 1995; Nauck et al., 1998; Machein et al., 1999).

The ability of DEX to modulate the expression of several potassium channel types in the BBB of glioma has also been demonstrated (Zhang et al., 2007). In particular, DEX treatment increased the expression of calcium-activated K^+ channels in the BBB of rat brain glioma (Gu et al., 2007; Gu et al., 2009b). In the same glioma model, up-regulation of ATP sensitive-K^+ channel (K_{ATP}) expression by DEX has also been reported (Gu et al., 2007). Through up-regulation of these K^+ channel types, DEX could regulate transcellular pathways of brain tumor microvessels controlling BBB permeability. Although DEX seems to reduce oedema formation by modifying the permeability of capillaries within the tumor and enhancing the clearance of extracellular water (Swaroops et al., 2001; Sinha et al., 2004), the mechanisms of its actions are as to date not fully understood.

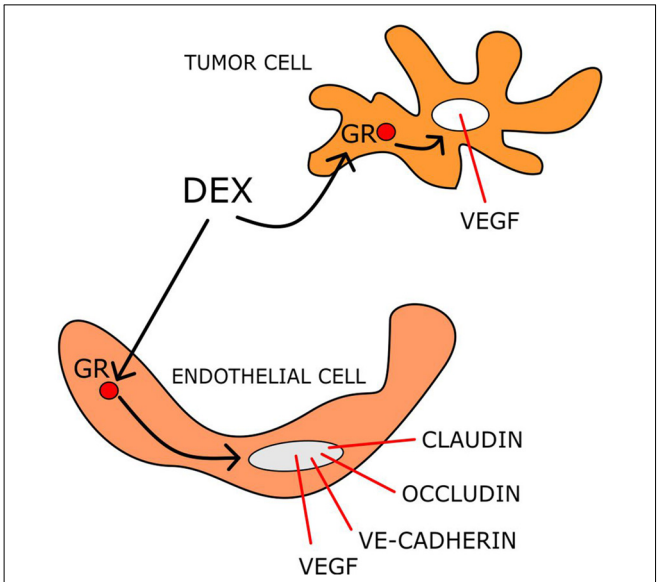

FIGURE 2 | DEX mechanisms reducing tumor-induced brain oedema. DEX acting on both endothelial and tumor cells modulates the transcription of several gene products that control the BBB permeability.

GBM-INDUCED ABNORMAL CELL-PROLIFERATION

Cell proliferation is a physiological process that involves the activation of many signaling pathways. GBM and several genetic abnormalities associated with this cancer alter various signaling pathways that control cell proliferation.

EGFR plays an important role in cell proliferation principally through receptor-mediated activation of PI3K/AKT/mTOR and GRB2/MEK/ERK/MAPK signaling pathways (Chistiakov et al., 2017). Amplification or mutations of EGFR are frequently found in GBM (Maire and Ligon, 2014). Indeed, 30% of GBM cases express the truncated mutant EGFRvIII receptor that is deprived from its extracellular ligand binding site and as a consequence is activated, constitutively (Frederick et al., 2000; Paff et al., 2014). By stimulating the downstream signal transduction pathways promotes tumorigenicity (Wang et al., 2009; Chistiakov et al., 2017). Importantly, the genetic analysis of EGFR in GBM is widely used as a diagnostic biomarker (Maire and Ligon, 2014).

Phosphatase and tensin homolog (PTEN) is a tumor suppressor that dephosphorylates the second messenger phosphatidylinositol 3, 4, 5-triphosphate, inhibits the PI3K/AKT pathway and reduces cyclin D1 accumulation, inducing cell cycle arrest at the G_0/G_1 phase. Mutations in PTEN are found in 20%–40% of cases that are mainly affected by primary GBM. Loss of function mutations in PTEN activate signaling molecules including phosphatidylinositol-dependent kinases (PDKs), serine/threonine kinases, AKT/protein kinase B, S6 kinase, and mTOR, as well as the small GTPases Rac1 and Cdc42 (Alexiou and Voulgaris, 2010). The overall effects resulting from activation of these signaling pathways are increased cell proliferation and tumor growth. In addition to cell

proliferation, the PI3K/Akt/mTOR pathway regulates apoptosis and angiogenesis. Notably, this pathway is up-regulated in GBM and mediates uncontrolled cell proliferation, tumor growth and multidrug resistance (Zhao et al., 2017). As such, intense investigations are aimed to identify therapeutic strategies to inhibit the PI3K/AKT/mTOR pathway (Ströbele et al., 2015; Li et al., 2016).

Recent studies, have highlighted the important role of ion channels in GBM cell proliferation and aggressiveness (Sforna et al., 2017; Wong et al., 2018; Yang et al., 2017, 2018; D'Alessandro et al., 2018). In particular, it has been shown that the *swelling-activated Cl^- current* is over-expressed in GBM cell lines (Catacuzzeno et al., 2014; Sforna et al., 2017), and contributes substantially to cell proliferation through activation of JAK2/STAT3 and PI3K/AKT signaling pathways (Wong et al., 2018). Indeed, the inhibition of this Cl^- current reduced cell viability, proliferation and migration. However, cell volume changes are detected by the *Volume Regulated Anion Channel* (VRAC) that is composed of members of the *leucine-rich repeat-containing protein 8* (LRRC8) gene family, LRRC8A–E (Qiu et al., 2014; Voss et al., 2014). Downregulation of LRRC8A expression reduces GBM cell proliferation and increases sensitivity to the clinically used Temozolomide (TMZ) and Carmustine (Rubino et al., 2018).

THE ANTI- AND PRO-PROLIFERATIVE EFFECTS OF DEX

The effects of DEX on GBM cell proliferation depend on cell type, drug concentration and experimental conditions (Piette et al., 2006). The anti-proliferative effect of DEX has been shown in several cell lines (e.g., T98G, A172, 86HG39, F98, GL261, U87; Kaup et al., 2001; Fan et al., 2014). By contrast, Fan et al. (2014) found that DEX did not compromise the vitality of T98G and U251 cells. However, they showed that DEX significantly decreased the percentage of F98 cells in the S-phase favoring the G_0/G_1 phase of cell cycle, thus highlighting its cytostatic effect (Fan et al., 2014). Piette et al. (2009) reported that DEX attenuated cell proliferation, through inhibition of the ERK1/2 MAPK pathway. It has also been shown that DEX interrupted cell cycle progression through down-regulation of cyclin D1 and inhibition of ERK1/2 phosphorylation, without altering the overall expression level of ERK1/2 (Liu et al., 2009). Necrotic death of C6 cells can be induced by serum deprivation and DEX enhanced this cytotoxic effect through GR activation (Morita et al., 1999). In the same cell line, the anti-proliferative effect of DEX was shown to be dose and time dependent and to involve Aquaporin 1 (AQP_1; Guan et al., 2018). Indeed, DEX increased the mRNA and protein expression of AQP_1. Moreover, the effect of DEX on cell proliferation was abolished upon AQP_1 gene silencing (Guan et al., 2018). Surprisingly, by using U373 cells, Gündisch et al. (2012) showed a pro-proliferative effect of DEX (**Table 1**).

In murine xenograph models, *in vivo*, DEX reduced tumor mass (Villeneuve et al., 2008). GL261 cells were implanted in the brains of male C57BL/6 mice and DEX treatment (1 mg/kg) was administered twice daily. After 20 days of treatment, this resulted in a 33% reduction in glioma volume (Villeneuve et al., 2008). Although, DEX did not influence the *in vitro* proliferation of GL261 cells, the decrease in tumor mass could be accounted for its effects on Ang-2 expression (Villeneuve et al., 2008).

TABLE 1 | Effects of DEX on cell proliferation of glioma cell lines.

Cell line	DEX dose	Proliferation inhibition	References
A172 T98G 86HG39	5 nM – 0.5 μM	YES	Kaup et al. (2001)
F98 GL261 U87	1–200 μg/ml	YES	Fan et al. (2014)
T98G U251	1–200 μg/ml	NO	Fan et al. (2014)
U373	0.1 μM	NO	Gündisch et al. (2012)
U373	10 μM	YES	Piette et al. (2009)
C6	0.01 μM	YES	Guan et al. (2018)
C6	0.1 μM	YES	Liu et al. (2009)
GL261	1 μg/ml	NO	Villeneuve et al. (2008)

DEX increases the chemotherapeutic action of several drugs. Indeed, in a human glioma U87 xenograph model, DEX significantly increased the therapeutic effects of carboplatin/gemcitabine combined therapy (Wang et al., 2004). However, the opposite effect of DEX has also been observed, *in vitro*. In particular, the strong apoptotic effect of TMZ in T98G and U87 cells was antagonized by DEX pre-treatment (Das et al., 2004, 2008; Sur et al., 2005). Notably, DEX administration pre-RT reduced the survival of glioma-bearing mice (Pitter et al., 2016).

GBM-INDUCED CELL MIGRATION

The ability of GBM cells to migrate and invade healthy brain tissue is remarkable, and makes GBM cells excellent experimental models for studying migratory processes. Cell invasion comprises four basic steps: detachment of invasive cells from the primary tumor mass, adhesion to the extracellular matrix (ECM), matrix degradation and cell migration (Onishi et al., 2011). Matrix metalloproteinases (MMPs) have been implicated in the degradation of ECM in various physiological and pathological conditions. They are believed to be important factors in tumor invasion through their effects on components of the ECM (Nakada et al., 2003). A decisive role in glioma invasion is played by the gelatinases MMP-2 and MMP-9 and increased expression levels of MMP-2 is associated with glioma invasiveness (Rao, 2003).

Full surgical resection of GBM is impossible as cancer cells migrate actively along brain structures, including white matter tracks, interstitial space of the brain parenchyma, blood vessels and the subarachnoid space (Bellail et al., 2004; Cuddapah et al., 2014). Migration also requires physical contacts that the GBM cells establish with molecules of the vascular walls. It has been shown that bradykinin induces Ca^{2+} release from intracellular stores of GBM cells, promoting cell migration (Montana and Sontheimer, 2011). In addition, GBM cells release large amounts of glutamate in the brain parenchyma that kill neurons effectively and acts as an autocrine and paracrine signal to promote migration of cancer cells by triggering cytoplasmic Ca^{2+} oscillations (Ye and Sontheimer, 1999; Lyons et al., 2007).

To assume their characteristic migratory shape, GBM cells undergo cell volume changes and cytoskeletal remodeling. These processes are strictly dependent on the activity of several ion channel types. Indeed, Cl^- and K^+ channels are over-expressed in GBM cells and facilitate their migratory features. The Cl^- and K^+ ion flux through chloride channels and Ca^{2+}-activated K^+ channels ($K_{Ca1.1}$ and $K_{Ca3.1}$) allows cell volume changes that are essential events for effective GBM cell migration (Turner and Sontheimer, 2014; Catacuzzeno et al., 2015; Rosa et al., 2017). ClC-3 expression is up-regulated in glioma and correlates with WHO histological grade (Wang et al., 2017). Previous studies have shown the important role of ClC-3 in human glioma cells invasion through the application of pharmacological inhibitors or ClC-3 siRNA transfection (Lui et al., 2010; Cuddapah and Sontheimer, 2010). Recently, Wang et al. (2017) reported that knock-down of ClC-3, by using recombinant adenovirus expressing short hairpin RNA targeting human ClC-3 gene, inhibited the migration of U87MG cells significantly and reduced volume-regulated chloride currents in U87MG and SNB19 cells.

Previous studies have shown that hypoxia promotes GBM cell migration and increases tumor aggressiveness (Jensen, 2009; Yang et al., 2012). Extensive hypoxic areas are found within GBM mass that distinguish this tumor from those of low-grade malignancy. A distinctive histological pattern observed within the GBM is the palisade characterized by the presence of occluded vessels, around an extensive necrotic area and migrating cancerous cells (Rong et al., 2006; Amberger-Murphy, 2009). Sforna et al. (2017) reported that the *swelling-activated Cl^- current* is up-regulated during hypoxia, an effect that further facilitates GBM cell migration and brain infiltration (Wong et al., 2018).

EFFECTS OF DEX ON CELL MIGRATION

Scant and inconsistent information is available on the effects of DEX on cell migration and this varies with the cell type under investigation. Inhibitory effects of DEX in migration/invasion of several glioma cell lines (e.g., C6, U251, U373, and A172), have been previously reported (Bauman et al., 1999). DEX inhibited the migration of U87 cells by reducing MMP-2 secretion (Lin et al., 2008). On the other hand, Piette et al. (2009) have shown that DEX treatment significantly reduced the migration and invasion of U373 cells through GR-dependent ERK1/2 MAPK pathway. It should be recalled that in GBM the ERK1/2 MAPK pathway is activated remarkably through EGFR and is linked to cell invasion and migration, as well as proliferation (Huang et al., 2009). Moreover, the isoforms p44 (ERK1) and p42 (ERK2) are stimulated by a wide variety of growth factors and mitogens (Johnson and Lapadat, 2002).

In stark contrast with previous studies, a recent report has shown that DEX facilitated C6 cells migration through up-regulation of AQP_1 expression (Guan et al., 2018).

DEX THERAPY IN GBM

Patients with primary brain tumors are commonly treated with DEX before and after biopsy or resection and during RT. Unfortunately, DEX causes many side effects including myopathy, abnormal glucose metabolism, gastrointestinal complications, irritability, anxiety, insomnia, and is linked to high risk of pneumonia infection (Kostaras et al., 2014). Although, myopathy is reversible upon DEX discontinuation, almost 50% of patients develop disturbed glucose metabolism which persists even after dose reduction (Wen et al., 2006). Most psychiatric complications occur within the 1st week of therapy. The severity of side effects increases with the dose regimen and length of treatment. Thus, it is recommended that DEX therapy be reduced once symptoms commence to improve (Kostaras et al., 2014).

Upon DEX treatment apoptosis of T cell is observed, accounting for its immunosuppressant effects (Dietrich et al., 2011). The potent immunosuppressive actions of GCs could raise the question as to whether these drugs could weaken the body immune response against cancer cells and contribute to the short survival of GBM-affected individuals. However, due to its immunosuppressant activity, DEX interfered with conventional chemotherapies or electric field-based therapy delivered by the NovoTTF-100A (Hughes et al., 2005; Grossman et al., 2011; Wong et al., 2015). This is a new medical device used for chronic treatment of patients with recurrent or progressive GBM that exploit alternating electric fields (termed TTFields).

A number of studies have demonstrated DEX effectiveness in management of patients with brain peri-tumor oedema by ameliorating the symptoms associated with vasogenic oedema and intracranial high pressure within 48 h of treatment (Galicich et al., 1961; Hossmann et al., 1983; Ostergaard et al., 1999; Sinha et al., 2004; Dietrich et al., 2011; Kostaras et al., 2014). An excellent technique for monitoring tumor-related oedema in patients is magnetic resonance imaging (MRI) that allows the evaluation of various water diffusion parameters (Yamasaki et al., 2012; Bode et al., 2006; Kural et al., 2018). Using diffusion tensor imaging, Sinha et al. (2004) examined individuals with intracranial tumors and observed a significant reduction in the mean diffusivity of brain oedema after 48–72 h post-DEX treatment. However, a recent study conducted in 28 patients with different degrees of glioma, brain metastases and neurological deficits, reported that DEX had no significant effect on the volume of peritumoral oedema in 19 patients, while some improvements were observed in the remaining (Kural et al., 2018). Given the very frequent use of DEX in GBM therapy and the controversies concerning its effects there is now a renewed interest to evaluate the correlation between the use of this drug and the overall survival (OS) rate of treated patients. A recent study showed that administration of DEX during RT in patients treated with TMZ, was a poor prognostic indicator of both OS and progression-free survival (PFS). Therefore, DEX treatment before or concomitantly with TMZ was not recommended. However, the OS and PFS were not affected by DEX in patients who received a combination therapy with both TMZ and Bevacizumab (BEV), during RT (Shields et al., 2015). Important observations about the use of DEX in GBM therapy have been provided by Wong et al. (2015). Indeed, they showed that patients treated with higher DEX doses (>4.1 mg daily) had significantly shorter OS than those treated with lower doses

(<4.1 mg daily). DEX-treatment at high doses (6–16 mg/day) resulted in the disappearance of the tumor mass in some patients. Remarkably, the tumor reappeared after 1–4 weeks and was much more aggressive (Buxton et al., 1997; Zaki et al., 2004; Goh et al., 2009). It has also been observed that DEX therapy reduced the OS of a particular subgroup of GBM patients (Dubinski et al., 2018). In this study, 35 patients received preoperative DEX and compared to 78 control patients. The OS value was not different between these two main groups. However, within the subgroup of patients who received DEX, 22 individuals showed DEX-induced leukocytosis (DIL) and had shorter OS that those without DIL. As such, patients with DIL were considered at a high risk of poor outcome (Dubinski et al., 2018).

In patients with cancer, inter-individual differences in drug response influences both the outcome to therapy, as well as the prevalence of adverse effects. Along with the progress in diagnosis, based on tumor molecular characteristics, genomic and proteomic approaches continue to be developed to ameliorate individualized treatment (Shai et al., 2008). Changes in protein expression due to altered gene regulation in drug-target genes can affect the efficacy or toxicity of the drug. This concept applies especially to GCs, as well as to other drugs used in the management of GBM. Indeed, GCs are known to regulate the expression of hundreds of genes, whose dysregulation could favor a poor prognosis for GBM patients. In a study that analysed the type of genes affected by DEX treatment from patient-derived GSC lines several genes associated with cell proliferation and migration were either up-regulated or down-regulated by the drug (Luedi et al., 2017). Importantly, DEX-responsive genes were found to be prognostic of poor outcome in two independent GBM cohorts (Luedi et al., 2017). Both, *in vitro* and *in vivo* evaluation of DEX effects along with the analysis of clinical information from *The Cancer Genome Atlas* (TCGA) cohort, important correlations have been derived between DEX treatment and alterations in gene expression profiles. The comparison between patients with mesenchymal and proneural GBM showed that the former subgroup had significant up-regulation of DEX-controlled gene network as well as pathways closely related to proliferation, invasion, and angiogenesis. The effects of DEX on invasion, proliferation and angiogenesis in GBM patient–derived GSCs with IDH1 wild-type (GSC3) and with IDH1 mutant (GSC6) were very recently evaluated. DEX significantly increased the invasive properties of the GSC3 cell line, both *in vitro* and *in vivo*. Moreover, using both GSC3 and GSC6 lines, the drug promoted proliferation and angiogenesis, *in vivo* (Luedi et al., 2018). The results of this interesting study, have questioned the use of DEX in GBM therapy, highlighting its ability to increase the aggressiveness of the tumor.

CONCLUDING REMARKS

Since 1960, DEX represented the gold standard for treatment to reduce oedema caused by brain tumors, although current literature fails to clearly delineate the mechanism of action. In this review, we have discussed several critical factors regarding the influence of DEX in GBM. Overall, contradictory effects of DEX opposing or favoring GBM aggressiveness have emerged from a number of *in vitro*, *in vivo* and clinical studies. It has been argued that this conflicting data was a result of different experimental conditions (Mealey et al., 1971; Grasso et al., 1977; Pinski et al., 1993; Langeveld et al., 1992; Morita et al., 1999; Piette et al., 2006). Considering this variability and current controversial issues, investigators are focusing on genetic biomarkers and transcriptional signature that are influenced by DEX. Knowledge derived through these studies is highly needed to provide prediction in patient OS. The urge to evaluate other subtypes of GBM that are distinguished by different genetic and epigenetic alterations, the distinct susceptibility to DEX and their changes in the degree of malignancy upon drug exposure is inevitable in future studies. Indeed, establishing the GBM type that can or cannot be treated with DEX along with early diagnosis shall increase patients' life expectancy, considerably.

Pharmacogenomics promise the advent of precision medicine. Thus, to optimize DEX therapy with respect to patients' genotype and ensure maximum efficiency with minimal adverse effects, genome-wide association investigations incorporating genomics and epigenetic approaches, should be considered. The recognition of the various desirable and undesirable pathways that are activated in GBM by GCs could pave the way towards a combinational therapy, consisting in the co-administration of a classical GC with drugs that inhibit the unwanted pathways activated by that specific GC. Furthermore, a road map guiding progress towards development of selective GR agonists and modulators with a more restricted GR activity, which retain efficacy without eliciting unwanted adverse effects should be established (Sundahl et al., 2016). Overall, these strategies could settle the "*DEX issue in GBM*" and allow the prescription of this drug to distinct subsets of patients or through individual therapy depending on one's genetic makeup.

AUTHOR CONTRIBUTIONS

MC, MV, SB, MD and MP contributed to writing the manuscript. LS, PR and SR contributed to revising the manuscript. MP coordinated the writing, revised and submitted the manuscript.

FUNDING

This work was supported by the University of Malta—Research, Innovation and Development Trust (RIDT) and Internal Research Grant. MV was supported by the Alfred Mizzi Foundation, Malta through the RIDT.

ACKNOWLEDGMENTS

We thank Eleanor Harold-Barry for reading and commenting our manuscript.

REFERENCES

Alaminos, M., Dávalos, V., Ropero, S., Setién, F., Paz, M. F., Herranz, M., et al. (2005). EMP3, a myelin-related gene located in the critical 19q13.3 region, is epigenetically silenced and exhibits features of a candidate tumor suppressor in glioma and neuroblastoma. *Cancer Res.* 65, 2565–2571. doi: 10.1158/0008-5472.can-04-4283

Alexiou, G. A., and Voulgaris, S. (2010). The role of the PTEN gene in malignant gliomas. *Neurol. Neurochir. Pol.* 44, 80–86. doi: 10.1016/s0028-3843(14)60408-4

Amberger-Murphy, V. (2009). Hypoxia helps glioma to fight therapy. *Curr. Cancer Drug Targets* 9, 381–390. doi: 10.2174/156800909788166637

An, Z., Gluck, C. B., Choy, M. L., and Kaufman, L. I. (2010). Suberoylanilide hydroxamic acid limits migration and invasion of glioma cells in two and three dimensional culture. *Cancer Lett.* 292, 215–227. doi: 10.1016/j.canlet.2009.12.006

Bao, S., Wu, Q., McLendon, R. E., Hao, Y., Shi, Q., Hjelmeland, A. B., et al. (2006). Glioma stem cells promote radioresistance by preferential activation of the DNA damage response. *Nature* 444, 756–760. doi: 10.1038/nature05236

Bauman, G. S., MacDonald, W., Moore, E., Ramsey, D. A., Fisher, B. J., Amberger, V. R., et al. (1999). Effects of radiation on a model of malignant glioma invasion. *J. Neurooncol.* 44, 223–231. doi: 10.1023/A:1006319417077

Beauchesne, P. (2011). Extra-neural metastases of malignant gliomas: myth or reality? *Cancers* 3, 461–477. doi: 10.3390/cancers3010461

Bellail, A. C., Hunter, S. B., Brat, D. J., Tan, C., and Van Meir, E. G. (2004). Microregional extracellular matrix heterogeneity in brain modulates glioma cell invasion. *Int. J. Biochem. Cell Biol.* 36, 1046–1069. doi: 10.1016/j.biocel.2004.01.013

Bezecny, P. (2014). Histone deacetylase inhibitors in glioblastoma: pre-clinical and clinical experience. *Med. Oncol.* 31:985. doi: 10.1007/s12032-014-0985-5

Bode, M. K., Ruohonen, J., Nieminen, M. T., and Pyhtinen, J. (2006). Potential of diffusion imaging in brain tumors: a review. *Acta Radiol.* 47, 585–594. doi: 10.1080/02841850600580598

Buxton, N., Phillips, N., and Robertson, I. (1997). The case of the disappearing glioma. *J. Neurol. Neurosurg. Psychiatry* 63, 520–521. doi: 10.1136/jnnp.63.4.520

Campos-Bedolla, P., Walter, F. R., Veszelka, S., and Deli, M. A. (2014). Role of the blood-brain barrier in the nutrition of the central nervous system. *Arch. Med. Res.* 45, 610–638. doi: 10.1016/j.arcmed.2014.11.018

Catacuzzeno, L., Caramia, M., Sforna, L., Belia, S., Guglielmi, L., D'Adamo, M. C., et al. (2015). Reconciling the discrepancies on the involvement of large-conductance Ca^{2+}-activated K channels in glioblastoma cell migration. *Front. Cell. Neurosci.* 9:152. doi: 10.3389/fncel.2015.00152

Catacuzzeno, L., Michelucci, A., Sforna, L., Aiello, F., Sciaccaluga, M., Fioretti, B., et al. (2014). Identification of key signaling molecules involved in the activation of the swelling-activated chloride current in human glioblastoma cells. *J. Membr. Biol.* 247, 45–55. doi: 10.1007/s00232-013-9609-9

Chistiakov, D. A., Chekhonin, I. V., and Chekhonin, V. P. (2017). The EGFR variant III mutant as a target for immunotherapy of glioblastoma multiforme. *Eur. J. Pharmacol.* 810, 70–82. doi: 10.1016/j.ejphar.2017.05.064

Crespo, I., Vital, A. L., Gonzalez-Tablas, M., Patino Mdel, C., Otero, A., Lopes, M. C., et al. (2015). Molecular and genomic alterations in glioblastoma multiforme. *Am. J. Pathol.* 185, 1820–1833. doi: 10.1016/j.ajpath.2015.02.023

Cuddapah, V. A., Robel, S., Watkins, S., and Sontheimer, H. (2014). A neurocentric perspective on glioma invasion. *Nat. Rev. Neurosci.* 15, 455–465. doi: 10.1038/nrn3765

Cuddapah, V. A., and Sontheimer, H. (2010). Molecular interaction and functional regulation of ClC-3 by Ca^{2+}/calmodulin-dependent protein kinase II (CaMKII) in human malignant glioma. *J. Biol. Chem.* 285, 11188–11196. doi: 10.1074/jbc.M109.097675

Czapski, B., Baluszek, S., Herold-Mende, C., and Kaminska, B. (2018). Clinical and immunological correlates of long term survival in glioblastoma. *Contemp. Oncol.* 22, 81–85. doi: 10.5114/wo.2018.73893

D'Alessandro, G., Limatola, C., and Catalano, M. (2018). Functional roles of the Ca^{2+}-activated K^+ channel, KCa3.1, in brain tumors. *Curr. Neuropharmacol.* 16, 636–643. doi: 10.2174/0929867324666170713103621

Das, A., Banik, N. L., Patel, S. J., and Ray, S. K. (2004). Dexamethasone protected human glioblastoma U87MG cells from temozolomide induced apoptosis by maintaining Bax:Bcl-2 ratio and preventing proteolytic activities. *Mol. Cancer* 3:36. doi: 10.1186/1476-4598-3-36

Das, A., Banik, N. L., and Ray, S. K. (2008). Modulatory effects of acetazolomide and dexamethasone on temozolomide-mediated apoptosis in human glioblastoma T98G and U87MG cells. *Cancer Invest.* 26, 352–358. doi: 10.1080/07357900701788080

DeAngelis, L. M., and Mellinghoff, I. K. (2011). Virchow 2011 or how to ID(H) human glioblastoma. *J. Clin. Oncol.* 29, 4473–4474. doi: 10.1200/JCO.2011.37.5873

Dietrich, J., Rao, K., Pastorino, S., and Kesari, S. (2011). Corticosteroids in brain cancer patients: benefits and pitfalls. *Expert Rev. Clin. Pharmacol.* 4, 233–242. doi: 10.1586/ecp.11.1

Dolecek, T. A., Propp, J. M., Stroup, N. E., and Kruchko, C. (2012). CBTRUS statistical report: primary brain and central nervous system tumors diagnosed in the United States in 2005–2009. *Neuro Oncol.* 14, v1–v49. doi: 10.1093/neuonc/nos218

Dong, Z., and Cui, H. (2018). Epigenetic modulation of metabolism in glioblastoma. *Semin. Cancer Biol.* doi: 10.1016/j.semcancer.2018.09.002 [Epub ahead of print].

Dubinski, D., Won, S. Y., Gessler, F., Quick-Weller, J., Behmanesh, B., Bernatz, S., et al. (2018). Dexamethasone-induced leukocytosis is associated with poor survival in newly diagnosed glioblastoma. *J. Neurooncol.* 137, 503–510. doi: 10.1007/s11060-018-2761-4

Dubois, L. G., Campanati, L., Righy, C., D'Andrea-Meira, I., Spohr, T. C., Porto-Carreiro, I., et al. (2014). Gliomas and the vascular fragility of the blood brain barrier. *Front. Cell. Neurosci.* 8:418. doi: 10.3389/fncel.2014.00418

Fan, Z., Sehm, T., Rauh, M., Buchfelder, M., Eyupoglu, I. Y., and Savaskan, N. E. (2014). Dexamethasone alleviates tumor-associated brain damage and angiogenesis. *PLoS One* 9:e93264. doi: 10.1371/journal.pone.0093264

Finkenzeller, G., Technau, A., and Marmé, D. (1995). Hypoxia-induced transcription of the vascular endothelial growth factor gene is independent of functional AP-1 transcription factor. *Biochem. Biophys. Res. Commun.* 208, 432–439. doi: 10.1006/bbrc.1995.1356

Frank, N. Y., Schatton, T., and Frank, M. H. (2010). The therapeutic promise of the cancer stem cell concept. *J. Clin. Invest.* 120, 41–50. doi: 10.1172/JCI41004

Frederick, L., Wang, X. Y., Eley, G., and James, C. D. (2000). Diversity and frequency of epidermal growth factor receptor mutations in human glioblastomas. *Cancer Res.* 60, 1383–1387.

Furnari, F. B., Fenton, T., Bachoo, R. M., Mukasa, A., Stommel, J. M., Stegh, A., et al. (2007). Malignant astrocytic glioma: genetics, biology and paths to treatment. *Genes Dev.* 21, 2683–2710. doi: 10.1101/gad.1596707

Furuse, M., Fujimoto, K., Sato, N., Hirase, T., Tsukita, S., and Tsukita, S. (1996). Overexpression of occludin, a tight junction-associated integral membrane protein, induces the formation of intracellular multilamellar bodies bearing tight junction-like structures. *J. Cell Sci.* 109, 429–435.

Furuse, M., Hirase, T., Itoh, M., Nagafuchi, A., Yonemura, S., Tsukita, S., et al. (1993). Occludin: a novel integral membrane protein localizing at tight junctions. *J. Cell Biol.* 123, 1777–1788. doi: 10.1083/jcb.123.6.1777

Furuse, M., Sasaki, H., Fujimoto, K., and Tsukita, S. (1998). A single gene product, claudin-1 or -2, reconstitutes tight junction strands and recruits occludin in fibroblasts. *J. Cell Biol.* 143, 391–401. doi: 10.1083/jcb.143.2.391

Galicich, J. H., French, L. A., and Melby, J. C. (1961). Use of dexamethasone in treatment of cerebral oedema associated with brain tumors. *J. Lancet* 81, 46–53.

Goh, J. J., See, S. J., Ang, E., and Ng, W. H. (2009). Vanishing glioblastoma after corticosteroid therapy. *J. Clin. Neurosci.* 16, 1226–1228. doi: 10.1016/j.jocn.2008.10.029

Grasso, R. J., Johnson, C. E., Boler, R. K., and Moore, N. A. (1977). Combined growth-inhibitory responses and ultrastructural alterations produced by 1,3-bis(2-chloroethyl)-1-nitrosourea and dexamethasone in rat glioma cell cultures. *Cancer Res.* 37, 585–594.

Grinshtein, N., Rioseco, C. C., Marcellus, R., Uehling, D., Aman, A., Lun, X., et al. (2016). Small molecule epigenetic screen identifies novel EZH2 and HDAC inhibitors that target glioblastoma brain tumor-initiating cells. *Oncotarget* 7, 59360–59376. doi: 10.18632/oncotarget.10661

Grossman, S. A., Ye, X., Lesser, G., Sloan, A., Carraway, H., Desideri, S., et al. (2011). Immunosuppression in patients with high-grade gliomas treated with radiation and temozolomide. *Clin. Cancer Res.* 17, 5473–5480. doi: 10.1158/1078-0432.CCR-11-0774

Gu, Y. T., Qin, L. J., Qin, X., and Xu, F. (2009a). The molecular mechanism of dexamethasone-mediated effect on the blood-brain tumor barrier permeability in a rat brain tumor model. *Neurosci. Lett.* 452, 114–118. doi: 10.1016/j.neulet.2008.12.047

Gu, Y. T., Xue, Y. X., Wang, P., Zhang, H., Qin, L. J., and Liu, L. B. (2009b). Dexamethasone enhances calcium-activated potassium channel expression in blood-brain tumor barrier in a rat brain tumor model. *Brain Res.* 1259, 1–6. doi: 10.1016/j.brainres.2008.12.080

Gu, Y. T., Zhang, H., and Xue, Y. X. (2007). Dexamethasone enhances adenosine 5′-triphosphate-sensitive potassium channel expression in the blood-brain tumor barrier in a rat brain tumor model. *Brain Res.* 1162, 1–8. doi: 10.1016/j.brainres.2007.05.053

Guan, Y., Chen, J., Zhan, Y., and Lu, H. (2018). Effects of dexamethasone on C6 cell proliferation, migration and invasion through the upregulation of AQP1. *Oncol. Lett.* 15, 7595–7602. doi: 10.3892/ol.2018.8269

Guerin, C., Wolff, J. E., Laterra, J., Drewes, L. R., Brem, H., and Goldstein, G. W. (1992). Vascular differentiation and glucose transporter expression in rat gliomas: effects of steroids. *Ann. Neurol.* 31, 481–487. doi: 10.1002/ana.410310504

Gündisch, S., Boeckeler, E., Behrends, U., Amtmann, E., Ehrhardt, H., and Jeremias, I. (2012). Glucocorticoids augment survival and proliferation of tumor cells. *Anticancer Res.* 32, 4251–4261.

Han, C. H., and Batchelor, T. T. (2017). Isocitrate dehydrogenase mutation as a therapeutic target in gliomas. *Chin. Clin. Oncol.* 6:33. doi: 10.21037/cco.2017.06.11

Hardee, M. E., and Zagzag, D. (2012). Mechanisms of glioma-associated neovascularization. *Am. J. Pathol.* 181, 1126–1141. doi: 10.1016/j.ajpath.2012.06.030

Hartmann, C., Meyer, J., Balss, J., Capper, D., Mueller, W., Christians, A., et al. (2009). Type and frequency of IDH1 and IDH2 mutations are related to astrocytic and oligodendroglial differentiation and age:a study of 1,010 diffuse gliomas. *Acta Neuropathol.* 118, 469–474. doi: 10.1007/s00401-009-0561-9

Heddleston, J. M., Li, Z., Lathia, J. D., Bao, S., Hjelmeland, A. B., and Rich, J. N. (2010). Hypoxia inducible factors in cancer stem cells. *Br. J. Cancer* 102, 789–795. doi: 10.1038/sj.bjc.6605551

Hossmann, K. A., Hürter, T., and Oschlies, U. (1983). The effect of dexamethasone on serum protein extravasation and oedema development in experimental brain tumors of cat. *Acta Neuropathol.* 60, 223–231. doi: 10.1007/bf00691870

Huang, P. H., Xu, A. M., and White, F. M. (2009). Oncogenic EGFR signaling networks in glioma. *Sci. Signal* 2:re6. doi: 10.1126/scisignal.287re6

Hue, C. D., Cho, F. S., Cao, S., Dale Bass, C. R., Meaney, D. F., and Morrison, B. (2015). Dexamethasone potentiates *in vitro* blood-brain barrier recovery after primary blast injury by glucocorticoid receptor-mediated upregulation of ZO-1 tight junction protein. *J. Cereb. Blood Flow Metab.* 35, 1191–1198. doi: 10.1038/jcbfm.2015.38

Hughes, M. A., Parisi, M., Grossman, S., and Kleinberg, L. (2005). Primary brain tumors treated with steroids and radiotherapy: low CD4 counts and risk of infection. *Int. J. Radiat. Oncol. Biol. Phys.* 62, 1423–1426. doi: 10.1016/j.ijrobp.2004.12.085

Jensen, R. L. (2009). Brain tumor hypoxia: tumorigenesis, angiogenesis, imaging, pseudoprogression and as a therapeutic target. *J. Neurooncol.* 92, 317–335. doi: 10.1007/s11060-009-9827-2

Johnson, G. L., and Lapadat, R. (2002). Mitogen-activated protein kinase pathways mediated by ERK, JNK, and p38 protein kinases. *Science* 298, 1911–1912. doi: 10.1126/science.1072682

Kaal, E. C., and Vecht, C. J. (2004). The management of brain oedema in brain tumors. *Curr. Opin. Oncol.* 16, 593–600. doi: 10.1097/01.cco.0000142076.52721.b3

Kale, G., Naren, A. P., Sheth, P., and Rao, R. K. (2003). Tyrosine phosphorylation of occludin attenuates its interactions with ZO-1, ZO-2, and ZO-3. *Biochem. Biophys. Res. Commun.* 302, 324–329. doi: 10.1016/S0006-291X(03)00167-0

Kanazawa, T., Minami, Y., Jinzaki, M., Toda, M., Yoshida, K., and Sasaki, H. (2019). Predictive markers for MGMT promoter methylation in glioblastomas. *Neurosurg. Rev.* doi: 10.1007/s10143-018-01061-5 [Epub ahead of print].

Kaup, B., Schindler, I., Knüpfer, H., Schlenzka, A., Preiss, R., and Knüpfer, M. M. (2001). Time-dependent inhibition of glioblastoma cell proliferation by dexamethasone. *J. Neurooncol.* 51, 105–110. doi: 10.1023/A:1010684921099

Kaur, C., and Ling, E. A. (2008). Blood brain barrier in hypoxic-ischemic conditions. *Curr. Neurovasc. Res.* 5, 71–81. doi: 10.2174/156720208783565645

Kim, H., Lee, J. M., Park, J. S., Jo, S. A., Kim, Y. O., Kim, C. W., et al. (2008). Dexamethasone coordinately regulates angiopoietin-1 and VEGF: a mechanism of glucocorticoid-induced stabilization of blood-brain barrier. *Biochem. Biophys. Res. Commun.* 372, 243–248. doi: 10.1016/j.bbrc.2008.05.025

Kleihues, P. (1998). Subsets of glioblastoma: clinical and histological vs. *Brain Pathol.* 8, 667–668. doi: 10.1111/j.1750-3639.1998.tb00192.x

Kostaras, X., Cusano, F., Kline, G. A., Roa, W., and Easaw, J. (2014). Use of dexamethasone in patients with high-grade glioma: a clinical practice guideline. *Curr. Oncol.* 21, e493–e503. doi: 10.3747/co.21.1769

Kubota, K., Furuse, M., Sasaki, H., Sonoda, N., Fujita, K., Nagafuchi, A., et al. (1999). Ca^{2+}-independent cell-adhesion activity of claudins, a family of integral membrane proteins localized at tight junctions. *Curr. Biol.* 9, 1035–1038. doi: 10.1016/s0960-9822(99)80452-7

Kumabe, T., Sohma, Y., Kayama, T., Yoshimoto, T., and Yamamoto, T. (1992). Overexpression and amplification of α-PDGF receptor gene lacking exons coding for a portion of the extracellular region in a malignant glioma. *Tohoku J. Exp. Med.* 168, 265–269. doi: 10.1620/tjem.168.265

Kural, C., Atac, G. K., Tehli, O., Solmaz, I., Temiz, C., Hodaj, I., et al. (2018). The evaluation of the effects of steroid treatment on the tumor and peritumoral oedema by DWI and MR spectroscopy in brain tumors. *Neurol. Neurochir. Pol.* 52, 495–504. doi: 10.1016/j.pjnns.2018.03.002

Langeveld, C. H., van Waas, M. P., Stoof, J. C., Sutanto, W., de Kloet, E. R., Wolbers, J. G., et al. (1992). Implication of glucocorticoid receptors in the stimulation of human glioma cell proliferation by dexamethasone. *J. Neurosci. Res.* 31, 524–531. doi: 10.1002/jnr.490310316

Lara-Velazquez, M., Al-Kharboosh, R., Jeanneret, S., Vazquez-Ramos, C., Mahato, D., Tavanaiepour, D., et al. (2017). Advances in brain tumor surgery for glioblastoma in adults. *Brain Sci.* 7:E166. doi: 10.3390/brainsci7120166

Lee, P., Murphy, B., Miller, R., Menon, V., Banik, N. L., Giglio, P., et al. (2015). Mechanisms and clinical significance of histone deacetylase inhibitors: epigenetic glioblastoma therapy. *Anticancer Res.* 35, 615–625.

Lee, D. H., Ryu, H. W., Won, H. R., and Kwon, S. H. (2017). Advances in epigenetic glioblastoma therapy. *Oncotarget* 8, 18577–18589. doi: 10.18632/oncotarget.14612

Lee, E., Yong, R. L., Paddison, P., and Zhu, J. (2018). Comparison of glioblastoma (GBM) molecular classification methods. *Semin. Cancer Biol.* 53, 201–211. doi: 10.1016/j.semcancer.2018.07.006

Leonardi, R., Subramanian, C., Jackowski, S., and Rock, C. O. (2012). Cancer associated isocitrate dehydrogenase mutations inactivate NADPH-dependent reductive carboxylation. *J. Biol. Chem.* 287, 14615–14620. doi: 10.1074/jbc.C112.353946

Li, X., Wu, C., Chen, N., Gu, H., Yen, A., Cao, L., et al. (2016). PI3K/Akt/mTOR signaling pathway and targeted therapy for glioblastoma. *Oncotarget* 7, 33440–33450. doi: 10.18632/oncotarget.7961

Li, Z., Bao, S., Wu, Q., Wang, H., Eyler, C., Sathornsumetee, S., et al. (2009). Hypoxia-inducible factors regulate tumorigenic capacity of glioma stem cells. *Cancer Cell* 15, 501–513. doi: 10.1016/j.ccr.2009.03.018

Liebner, S., Fischmann, A., Rascher, G., Duffner, F., Grote, E. H., Kalbacher, H., et al. (2000). Claudin-1 and claudin-5 expression and tight junction morphology are altered in blood vessels of human glioblastoma multiforme. *Acta Neuropathol.* 100, 323–331. doi: 10.1007/s004010000180

Liu, H., Huang, X., Wang, H., Shen, A., and Cheng, C. (2009). Dexamethasone inhibits proliferation and stimulates SSeCKS expression in C6 rat glioma cell line. *Brain Res.* 1265, 1–12. doi: 10.1016/j.brainres.2009.01.050

Lin, Y. M., Jan, H. J., Lee, C. C., Tao, H. Y., Shih, Y. L., Wei, H. W., et al. (2008). Dexamethasone reduced invasiveness of human malignant glioblastoma cells through a MAPK phosphatase-1(MKP-1) dependent mechanism. *Eur. J. Pharmacol.* 593, 1–9. doi: 10.1016/j.ejphar.2008.06.111

Lin, K. T., and Wang, L. H. (2016). New dimension of glucocorticoids in cancer treatment. *Steroids* 111, 84–88. doi: 10.1016/j.steroids.2016.02.019

Lin, L., Xue, Y., Duan, Q., Sun, B., Lin, H., Huang, X., et al. (2016). The role of cerebral blood flow gradient in peritumoral oedema for differentiation of

glioblastomas from solitary metastatic lesions. *Oncotarget* 7, 69051–69059. doi: 10.18632/oncotarget.12053

Louis, D. N., Perry, A., Reifenberger, G., von Deimling, A., Figarella-Branger, D., Cavenee, W. K., et al. (2016). The 2016 world health organization classification of tumors of the central nervous system: a summary. *Acta Neuropathol.* 131, 803–820. doi: 10.1007/s00401-016-1545-1

Luedi, M. M., Singh, S. K., Mosley, J. C., Hassan, I. S. A., Hatami, M., Gumin, J., et al. (2018). Dexamethasone-mediated oncogenicity *in vitro* and in an animal model of glioblastoma. *J. Neurosurg.* 129, 1446–1455. doi: 10.3171/2017.7.jns17668

Luedi, M. M., Singh, S. K., Mosley, J. C., Hatami, M., Gumin, J., Sulman, E. P., et al. (2017). A dexamethasone-regulated gene signature is prognostic for poor survival in glioblastoma patients. *J. Neurosurg. Anesthesiol.* 29, 46–58. doi: 10.1097/ANA.0000000000000368

Lui, V. C., Lung, S. S., Pu, J. K., Hung, K. N., and Leung, G. K. (2010). Invasion of human glioma cells is regulated by multiple chloride channels including ClC-3. *Anticancer Res.* 30, 4515–4524.

Lyons, S. A., Chung, W. J., Weaver, A. K., Ogunrinu, T., and Sontheimer, H. (2007). Autocrine glutamate signaling promotes glioma cell invasion. *Cancer Res.* 67, 9463–9471. doi: 10.1158/0008-5472.can-07-2034

Machein, M. R., Kullmer, J., Rönicke, V., Machein, U., Krieg, M., Damert, A., et al. (1999). Differential downregulation of vascular endothelial growth factor by dexamethasone in normoxic and hypoxic rat glioma cells. *Neuropathol. Appl. Neurobiol.* 25, 104–112. doi: 10.1046/j.1365-2990.1999.00166.x

Maire, C. L., and Ligon, K. L. (2014). Molecular pathologic diagnosis of epidermal growth factor receptor. *Neuro Oncol.* 16, viii1–viii6. doi: 10.1093/neuonc/nou294

Maisonpierre, P. C., Suri, C., Jones, P. F., Bartunkova, S., Wiegand, S. J., Radziejewski, C., et al. (1997). Angiopoietin-2, a natural antagonist for Tie2 that disrupts *in vivo* angiogenesis. *Science* 277, 55–60.

Martinez, R., and Esteller, M. (2010). The DNA methylome of glioblastoma multiforme. *Neurobiol. Dis.* 39, 40–46. doi: 10.1016/j.nbd.2009.12.030

Mealey, J. Jr., Chen, T. T., and Schanz, G. P. (1971). Effects of dexamethasone and methylprednisolone on cell cultures of human glioblastomas. *J. Neurosurg.* 34, 324–334. doi: 10.3171/jns.1971.34.3.0324

Meyer-Puttlitz, B., Hayashi, Y., Waha, A., Rollbrocker, B., Boström, J., Wiestler, O. D., et al. (1997). Molecular genetic analysis of giant cell glioblastomas. *Am. J. Pathol.* 151, 853–857.

Michinaga, S., and Koyama, Y. (2015). Pathogenesis of brain oedema and investigation into anti-oedema drugs. *Int. J. Mol. Sci.* 16, 9949–9975. doi: 10.3390/ijms16059949

Miller, C. R., and Perry, A. (2007). Glioblastoma. *Arch. Pathol. Lab. Med.* 131, 397–406. doi: 10.1043/1543-2165(2007)131[397:G]2.0.CO;2

Montana, V., and Sontheimer, H. (2011). Bradykinin promotes the chemotactic invasion of primary brain tumors. *J. Neurosci.* 31, 4858–4867. doi: 10.1523/JNEUROSCI.3825-10.2011

Morita, K., Ishimura, K., Tsuruo, Y., and Wong, D. L. (1999). Dexamethasone enhances serum deprivation-induced necrotic death of rat C6 glioma cells through activation of glucocorticoid receptors. *Brain Res.* 816, 309–316. doi: 10.1016/s0006-8993(98)01093-2

Nag, S., Papneja, T., Venugopalan, R., and Stewart, D. J. (2005). Increased angiopoietin2 expression is associated with endothelial apoptosis and blood-brain barrier breakdown. *Lab. Invest.* 85, 1189–1198. doi: 10.1038/labinvest.3700325

Nakada, M., Okada, Y., and Yamashita, J. (2003). The role of matrix metalloproteinases in glioma invasion. *Front. Biosci.* 8, e261–e269. doi: 10.2741/1016

Nakamura, M., Watanabe, T., Yonekawa, Y., Kleihues, P., and Ohgaki, H. (2001). Promoter methylation of the DNA repair gene MGMT in astrocytomas is frequently associated with G:C -->A:T mutations of the TP53 tumor suppressor gene. *Carcinogenesis* 22, 1715–1719. doi: 10.1093/carcin/22.10.1715

Nauck, M., Karakiulakis, G., Perruchoud, A. P., Papakonstantinou, E., and Roth, M. (1998). Corticosteroids inhibit the expression of the vascular endothelial growth factor gene in human vascular smooth muscle cells. *Eur. J. Pharmacol.* 341, 309–315. doi: 10.1016/s0014-2999(97)01464-7

Onishi, M., Ichikawa, T., Kurozumi, K., and Date, I. (2011). Angiogenesis and invasion in glioma. *Brain Tumor Pathol.* 28, 13–24. doi: 10.1007/s10014-010-0007-z

Ostergaard, L., Hochberg, F. H., Rabinov, J. D., Sorensen, A. G., Lev, M., Kim, L., et al. (1999). Early changes measured by magnetic resonance imaging in cerebral blood flow, blood volume and blood-brain barrier permeability following dexamethasone treatment in patients with brain tumors. *J. Neurosurg.* 90, 300–305. doi: 10.3171/jns.1999.90.2.0300

Paff, M., Alexandru-Abrams, D., Hsu, F. P., and Bota, D. A. (2014). The evolution of the EGFRvIII (rindopepimut) immunotherapy for glioblastoma multiforme patients. *Hum. Vaccin. Immunother.* 10, 3322–3331. doi: 10.4161/21645515.2014.983002

Papadopoulos, M. C., Saadoun, S., Binder, D. K., Manley, G. T., Krishna, S., and Verkman, A. S. (2004). Molecular mechanisms of brain tumor oedema. *Neuroscience* 129, 1011–1020. doi: 10.1016/j.neuroscience.2004.05.044

Papadopoulos, M. C., Saadoun, S., Woodrow, C. J., Davies, D. C., Costa-Martins, P., Moss, R. F., et al. (2001). Occludin expression in microvessels of neoplastic and non-neoplastic human brain. *Neuropathol. Appl. Neurobiol.* 27, 384–395. doi: 10.1046/j.0305-1846.2001.00341.x

Park, D. M., and Rich, J. N. (2009). Biology of glioma cancer stem cells. *Mol. Cells* 28, 7–12. doi: 10.1007/s10059-009-0111-2

Parsons, D. W., Jones, S., Zhang, X., Lin, J. C., Leary, R. J., Angenendt, P., et al. (2008). An integrated genomic analysis of human glioblastoma multiforme. *Science* 321, 1807–1812. doi: 10.1126/science.1164382

Piette, C., Deprez, M., Roger, T., Noël, A., Foidart, J. M., and Munaut, C. (2009). The dexamethasone-induced inhibition of proliferation, migration, and invasion in glioma cell lines is antagonized by macrophage migration inhibitory factor (MIF) and can be enhanced by specific MIF inhibitors. *J. Biol. Chem.* 284, 32483–32492. doi: 10.1074/jbc.m109.014589

Piette, C., Munaut, C., Foidart, J. M., and Deprez, M. (2006). Treating gliomas with glucocorticoids: from bedside to bench. *Acta Neuropathol.* 112, 651–664. doi: 10.1007/s00401-006-0100-x

Pinski, J., Halmos, G., Shirahige, Y., Wittliff, J. L., and Schally, A. V. (1993). Inhibition of growth of the human malignant glioma cell line (U87MG) by the steroid hormone antagonist RU486. *J. Clin. Endocrinol. Metab.* 77, 1388–1392. doi: 10.1210/jcem.77.5.8077338

Pitter, K. L., Tamagno, I., Alikhanyan, K., Hosni-Ahmed, A., Pattwell, S. S., Donnola, S., et al. (2016). Corticosteroids compromise survival in glioblastoma. *Brain* 139, 1458–1471. doi: 10.1093/brain/aww046

Qiu, Z., Dubin, A. E., Mathur, J., Tu, B., Reddy, K., Miraglia, L. J., et al. (2014). SWELL1, a plasma membrane protein, is an essential component of volume-regulated anion channel. *Cell* 157, 447–458. doi: 10.1016/j.cell.2014.03.024

Rand, V., Huang, J., Stockwell, T., Ferriera, S., Buzko, O., Levy, S., et al. (2005). Sequence survey of receptor tyrosine kinases reveals mutations in glioblastomas. *Proc. Natl. Acad. Sci. U S A* 102, 14344–14349. doi: 10.1073/pnas.0507200102

Rao, J. S. (2003). Molecular mechanisms of glioma invasiveness: the role of proteases. *Nat. Rev. Cancer* 3, 489–501. doi: 10.1038/nrc1121

Reya, T., Morrison, S. J., Clarke, M. F., and Weissman, I. L. (2001). Stem cells, cancer and cancer stem cells. *Nature* 414, 105–111. doi: 10.1038/35102167

Romani, M., Pistillo, M. P., and Banelli, B. (2018). Epigenetic targeting of glioblastoma. *Front. Oncol.* 8:448. doi: 10.3389/fonc.2018.00448

Rong, Y., Durden, D. L., Van Meir, E. G., and Brat, D. J. (2006). 'Pseudopalisading' necrosis in glioblastoma: a familiar morphologic feature that links vascular pathology, hypoxia, and angiogenesis. *J. Neuropathol. Exp. Neurol.* 65, 529–539. doi: 10.1097/00005072-200606000-00001

Rosa, P., Sforna, L., Carlomagno, S., Mangino, G., Miscusi, M., Pessia, M., et al. (2017). Overexpression of large-conductance calcium-activated potassium channels in human glioblastoma stem-like cells and their role in cell migration. *J. Cell. Physiol.* 232, 2478–2488. doi: 10.1002/jcp.25592

Rosen, J. M., and Jordan, C. T. (2009). The increasing complexity of the cancer stem cell paradigm. *Science* 324, 1670–1673. doi: 10.1126/science.1171837

Rubin, L. L., and Staddon, J. M. (1999). The cell biology of the blood-brain barrier. *Annu. Rev. Neurosci.* 22, 11–28. doi: 10.1146/annurev.neuro.22.1.11

Rubino, S., Bach, M. D., Schober, A. L., Lambert, I. H., and Mongin, A. A. (2018). Downregulation of leucine-rich repeat-containing 8A limits proliferation and

increases sensitivity of glioblastoma to temozolomide and carmustine. *Front. Oncol.* 8:142. doi: 10.3389/fonc.2018.00142

Salmaggi, A., Gelati, M., Pollo, B., Frigerio, S., Eoli, M., Silvani, A., et al. (2004). CXCL12 in malignant glial tumors: a possible role in angiogenesis and cross-talk between endothelial and tumoral cells. *J. Neurooncol.* 67, 305–317. doi: 10.1023/b:neon.0000024241.05346.24

Salvador, E., Shityakov, S., and Förster, C. (2014). Glucocorticoids and endothelial cell barrier function. *Cell Tissue Res.* 355, 597–605. doi: 10.1007/s00441-013-1762-z

Sforna, L., Cenciarini, M., Belia, S., D'Adamo, M. C., Pessia, M., Franciolini, F., et al. (2015). The role of ion channels in the hypoxia-induced aggressiveness of glioblastoma. *Front. Cell. Neurosci.* 8:467. doi: 10.3389/fncel.2014.00467

Sforna, L., Cenciarini, M., Belia, S., Michelucci, A., Pessia, M., Franciolini, F., et al. (2017). Hypoxia modulates the swelling-activated Cl current in human glioblastoma cells: role in volume regulation and cell survival. *J. Cell. Physiol.* 232, 91–100. doi: 10.1002/jcp.25393

Shai, R. M., Reichardt, J. K., and Chen, T. C. (2008). Pharmacogenomics of brain cancer and personalized medicine in malignant gliomas. *Future Oncol.* 4, 525–534. doi: 10.2217/14796694.4.4.525

Shields, L. B., Shelton, B. J., Shearer, A. J., Chen, L., Sun, D. A., Parsons, S., et al. (2015). Dexamethasone administration during definitive radiation and temozolomide renders a poor prognosis in a retrospective analysis of newly diagnosed glioblastoma patients. *Radiat. Oncol.* 10:222. doi: 10.1186/s13014-015-0527-0

Silbergeld, D. L., Rostomily, R. C., and Alvord, E. C. Jr. (1991). The cause of death in patients with glioblastoma is multifactorial: clinical factors and autopsy findings in 117 cases of supratentorial glioblastoma in adults. *J. Neurooncol.* 10, 179–185. doi: 10.1007/bf00146880

Sinha, S., Bastin, M. E., Wardlaw, J. M., Armitage, P. A., and Whittle, I. R. (2004). Effects of dexamethasone on peritumoral oedematous brain: a DT-MRI study. *J. Neurol. Neurosurg. Psychiatry* 75, 1632–1635. doi: 10.1136/jnnp.2003.028647

Soda, Y., Myskiw, C., Rommel, A., and Verma, I. M. (2013). Mechanisms of neovascularization and resistance to anti-angiogenic therapies in glioblastoma multiforme. *J. Mol. Med.* 91, 439–448. doi: 10.1007/s00109-013-1019-z

Staberg, M., Michaelsen, S. R., Rasmussen, R. D., Villingshøj, M., Poulsen, H. S., and Hamerlik, P. (2017). Inhibition of histone deacetylases sensitizes glioblastoma cells to lomustine. *Cell. Oncol.* 40, 21–32. doi: 10.1007/s13402-016-0301-9

Staedtke, V., Bai, R. Y., and Laterra, J. (2016). Investigational new drugs for brain cancer. *Expert Opin. Investig. Drugs* 25, 937–956. doi: 10.1080/13543784.2016.1182497

Stokum, J. A., Gerzanich, V., and Simard, J. M. (2016). Molecular pathophysiology of cerebral oedema. *J. Cereb. Blood Flow Metab.* 36, 513–538. doi: 10.1177/0271678X15617172

Stoyanov, G. S., Dzhenkov, D., Ghenev, P., Iliev, B., Enchev, Y., and Tonchev, A. B. (2018). Cell biology of glioblastoma multiforme: from basic science to diagnosis and treatment. *Med. Oncol.* 35:27. doi: 10.1007/s12032-018-1083-x

Ströbele, S., Schneider, M., Schneele, L., Siegelin, M. D., Nonnenmacher, L., Zhou, S., et al. (2015). A potential role for the inhibition of PI3K signaling in glioblastoma therapy. *PLoS One* 10:e0131670. doi: 10.1371/journal.pone.0131670

Stummer, W. (2007). Mechanisms of tumor-related brain oedema. *Neurosurg. Focus* 22:E8.

Sundahl, N., Clarisse, D., Bracke, M., Offner, F., Berghe, W. V., and Beck, I. M. (2016). Selective glucocorticoid receptor-activating adjuvant therapy in cancer treatments. *Oncoscience* 3, 188–202. doi: 10.18632/oncoscience.315

Sur, P., Sribnick, E. A., Patel, S. J., Ray, S. K., and Banik, N. L. (2005). Dexamethasone decreases temozolomide-induced apoptosis in human gliobastoma T98G cells. *Glia* 50, 160–167. doi: 10.1002/glia.20168

Swaroops, G. R., Kelly, P. A., Holmes, M. C., Shinoda, J., and Whittle, I. R. (2001). The effects of dexamethasone therapy on permeability, blood flow and iNOS expression in experimental glioma. *J. Clin. Neurosci.* 8, 35–39. doi: 10.1054/jocn.2000.0817

Takano, S., Yamashita, T., and Ohneda, O. (2010). Molecular therapeutic targets for glioma angiogenesis. *J. Oncol.* 2010:351908. doi: 10.1155/2010/351908

Tews, B., Roerig, P., Hartmann, C., Hahn, M., Felsberg, J., Blaschke, B., et al. (2007). Hypermethylation and transcriptional downregulation of the CITED4 gene at 1p34.2 in oligodendroglial tumors with allelic losses on 1p and 19q. *Oncogene* 26, 5010–5016. doi: 10.1038/sj.onc.1210297

Turner, K. L., and Sontheimer, H. (2014). Cl^- and K^+ channels and their role in primary brain tumor biology. *Philos. Trans. R. Soc. Lond. B Biol. Sci.* 369:20130095. doi: 10.1098/rstb.2013.0095

Verhaak, R. G., Hoadley, K. A., Purdom, E., Wang, V., Qi, Y., Wilkerson, M. D., et al. (2010). Integrated genomic analysis identifies clinically relevant subtypes of glioblastoma characterized by abnormalities in PDGFRA, IDH1, EGFR, and NF1. *Cancer Cell.* 17, 98–110. doi: 10.1016/j.ccr.2009.12.020

Vescovi, A. L., Galli, R., and Reynolds, B. A. (2006). Brain tumor stem cells. *Nat. Rev. Cancer* 6, 425–436. doi: 10.1038/nrc1889

Villeneuve, J., Galarneau, H., Beaudet, M. J., Tremblay, P., Chernomoretz, A., and Vallières, L. (2008). Reduced glioma growth following dexamethasone or anti-angiopoietin 2 treatment. *Brain Pathol.* 18, 401–414. doi: 10.1111/j.1750-3639.2008.00139.x

Voss, F. K. F., Ullrich, J., Münch, K., Lazarow, D., Lutter, N., Mah, M. A., et al. (2014). Identification of LRRC8 heteromers as an essential component of the volume-regulated anion channel VRAC. *Science* 344, 634–638. doi: 10.1126/science.1252826

Waitkus, M. S., Diplas, B. H., and Yan, H. (2016). Isocitrate dehydrogenase mutations in gliomas. *Neuro Oncol.* 18, 16–26. doi: 10.1093/neuonc/nov136

Wang, H., Jiang, H., Zhou, M., Xu, Z., Liu, S., Shi, B., et al. (2009). Epidermal growth factor receptor vIII enhances tumorigenicity and resistance to 5-fluorouracil in human hepatocellular carcinoma. *Cancer Lett.* 279, 30–38. doi: 10.1016/j.canlet.2009.01.019

Wang, H., Li, M., Rinehart, J. J., and Zhang, R. (2004). Pretreatment with dexamethasone increases antitumor activity of carboplatin and gemcitabine in mice bearing human cancer xenografts: *in vivo* activity, pharmacokinetics, and clinical implications for cancer chemotherapy. *Clin. Cancer Res.* 10, 1633–1644. doi: 10.1158/1078-0432.ccr-0829-3

Wang, B., Xie, J., He, H. Y., Huang, E. W., Cao, Q. H., Luo, L., et al. (2017). Suppression of CLC-3 chloride channel reduces the aggressiveness of glioma through inhibiting nuclear factor-κB pathway. *Oncotarget* 8, 63788–63798. doi: 10.18632/oncotarget.19093

Was, H., Krol, S. K., Rotili, D., Mai, A., Wojtas, B., Kaminska, B., et al. (2019). Histone deacetylase inhibitors exert anti-tumor effects on human adherent and stem-like glioma cells. *Clin. Epigenetics* 11:11. doi: 10.1186/s13148-018-0598-5

Weaver, K. D., Grossman, S. A., and Herman, J. G. (2006). Methylated tumor-specific DNA as a plasma biomarker in patients with glioma. *Cancer Invest.* 24, 35–40. doi: 10.1080/07357900500449546

Wen, P. Y., Schiff, D., Kesari, S., Drappatz, J., Gigas, D. C., and Doherty, L. (2006). Medical management of patients with brain tumors. *J. Neurooncol.* 80, 313–332. doi: 10.1212/01.con.0000464172.50638.21

Wolburg, H., and Lippoldt, A. (2002). Tight junctions of the blood-brain barrier: development, composition and regulation. *Vascul Pharmacol.* 38, 323–337. doi: 10.1016/S1537-1891(02)00200-8

Wolff, J. E., Mölenkamp, G., Hotfilder, M., and Laterra, J. (1997). Dexamethasone inhibits glioma-induced formation of capillary like structures *in vitro* and angiogenesis *in vivo*. *Klin. Padiatr.* 209, 275–277. doi: 10.1055/s-2008-1043962

Wong, R., Chen, W., Zhong, X., Rutka, J. T., Feng, Z. P., and Sun, H. S. (2018). Swelling-induced chloride current in glioblastoma proliferation, migration, and invasion. *J. Cell. Physiol.* 233, 363–370. doi: 10.1002/jcp.25891

Wolburg, H., Noell, S., Fallier-Becker, P., Mack, A. F., and Wolburg-Buchholz, K. (2012). The disturbed blood-brain barrier in human glioblastoma. *Mol. Aspects. Med.* 33, 579–589. doi: 10.1016/j.mam.2012.02.003

Wong, E. T., Lok, E., Gautam, S., and Swanson, K. D. (2015). Dexamethasone exerts profound immunologic interference on treatment efficacy for recurrent glioblastoma. *Br. J. Cancer* 113:1642. doi: 10.1038/bjc.2015.404

Xu, J., Sampath, D., Lang, F. F., Prabhu, S., Rao, G., Fuller, G. N., et al. (2011). Vorinostat modulates cell cycle regulatory proteins in glioma cells and human glioma slice cultures. *J. Neurooncol.* 105, 241–251. doi: 10.1007/s11060-011-0604-7

Yamasaki, F., Kurisu, K., Aoki, T., Yamanaka, M., Kajiwara, Y., Watanabe, Y., et al. (2012). Advantages of high b-value diffusion-weighted imaging to diagnose pseudo-responses in patients with recurrent glioma after bevacizumab treatment. *Eur. J. Radiol.* 81, 2805–2810. doi: 10.1016/j.ejrad.2011.10.018

Yang, Y. (2015). Cancer immunotherapy: harnessing the immune system to battle cancer. *J. Clin. Invest.* 125, 3335–3337. doi: 10.1172/JCI83871

Yang, L., Lin, C., Wang, L., Guo, H., and Wang, X. (2012). Hypoxia and hypoxia-inducible factors in glioblastoma multiforme progression and therapeutic implications. *Exp. Cell Res.* 318, 2417–2426. doi: 10.1016/j.yexcr.2012.07.017

Yang, W. Y., Tan, Z. F., Dong, D. W., Ding, Y., Meng, H., Zhao, Y., et al. (2018). Association of aquaporin—1 with tumor migration, invasion and vasculogenic mimicry in glioblastoma multiforme. *Mol. Med. Rep.* 17, 3206–3211. doi: 10.3892/mmr.2017.8265

Yang, J., Zhang, J. N., Chen, W. L., Wang, G. S., Mao, Q., Li, S. Q., et al. (2017). Effects of AQP5 gene silencing on proliferation, migration and apoptosis of human glioma cells through regulating EGFR/ERK/ p38 MAPK signalling pathway. *Oncotarget* 8, 38444–38455. doi: 10.18632/oncotarget.16461

Ye, Z. C., and Sontheimer, H. (1999). Glioma cells release excitotoxic concentrations of glutamate. *Cancer Res.* 59, 4383–4391.

Yin, Y., Qiu, S., and Peng, Y. (2016). Functional roles of enhancer of zeste homolog 2 in gliomas. *Gene* 576, 189–194. doi: 10.1016/j.gene.2015.09.080

Zaki, H. S., Jenkinson, M. D., Du Plessis, D. G., Smith, T., and Rainov, N. G. (2004). Vanishing contrastenhancement in malignant glioma after corticosteroid treatment. *Acta Neurochir.* 146, 841–845. doi: 10.1007/s00701-004-0282-8

Zhang, H., Gu, Y. T., and Xue, Y. X. (2007). Bradykinin-induced blood-brain tumor barrier permeability increase is mediated by adenosine 5'-triphosphate-sensitive potassium channel. *Brain Res.* 1144, 33–41. doi: 10.1016/j.brainres.2007.01.133

Zhao, H. F., Wang, J., Shao, W., Wu, C. P., Chen, Z. P., To, S. T., et al. (2017). Recent advances in the use of PI3K inhibitors for glioblastoma multiforme: current preclinical and clinical development. *Mol. Cancer* 16:100. doi: 10.1186/s12943-017-0670-3

Zlokovic, B. V. (2008). The blood-brain barrier in health and chronic neurodegenerative disorders. *Neuron* 57, 178–201. doi: 10.1016/j.neuron.2008.01.003

Zozulya, A., Weidenfeller, C., and Galla, H. J. (2008). Pericyte-endothelial cell interaction increases MMP-9 secretion at the blood-brain barrier *in vitro*. *Brain Res.* 1189, 1–11. doi: 10.1016/j.brainres.2007.10.099

Conflict of Interest Statement: The authors declare that the research was conducted in the absence of any commercial or financial relationships that could be construed as a potential conflict of interest.

frontiers in Molecular Neuroscience

ORIGINAL RESEARCH
published: 24 April 2019
doi: 10.3389/fnmol.2019.00100

Stimulation of Sphingosine Kinase 1 (SPHK1) Is Beneficial in a Huntington's Disease Pre-clinical Model

Alba Di Pardo[1], Giuseppe Pepe[1], Salvatore Castaldo[1], Federico Marracino[1], Luca Capocci[1], Enrico Amico[1], Michele Madonna[1], Susy Giova[1], Se Kyoo Jeong[2], Bu-Mahn Park[3], Byeong Deog Park[4] and Vittorio Maglione[1]**

[1]IRCCS, Neuromed, Pozzilli, Italy, [2]Department of Cosmetic Science, Seowon University, Cheongju, South Korea, [3]NeoPharm USA Inc., Engelwood Cliffs, NJ, United States, [4]Dr. Raymond Laboratories, Inc., Englewood Cliffs, NJ, United States

Although several agents have been identified to provide therapeutic benefits in Huntington disease (HD), the number of conventionally used treatments remains limited and only symptomatic. Thus, it is plausible that the need to identify new therapeutic targets for the development of alternative and more effective treatments is becoming increasingly urgent. Recently, the sphingosine-1-phosphate (S1P) axis has been reported to be a valid potential novel molecular target for therapy development in HD. Modulation of aberrant metabolism of S1P in HD has been proved to exert neuroprotective action *in vitro* settings including human HD iPSC-derived neurons. In this study, we investigated whether promoting S1P production by stimulating Sphingosine Kinase 1 (SPHK1) by the selective activator, K6PC-5, may have therapeutic benefit *in vivo* in R6/2 HD mouse model. Our findings indicate that chronic administration of 0.05 mg/kg K6PC-5 exerted an overall beneficial effect in R6/2 mice. It significantly slowed down the progressive motor deficit associated with disease progression, modulated S1P metabolism, evoked the activation of pro-survival pathways and markedly reduced the toxic mutant huntingtin (mHtt) aggregation. These results suggest that K6PC-5 may represent a future therapeutic option in HD and may potentially counteract the perturbed brain function induced by deregulated S1P pathways.

Keywords: HD, K6PC-5, SPHK1, aggregates, neuroprotection

OPEN ACCESS

Edited by:
Chiara Donati,
University of Florence, Italy

Reviewed by:
Paola Giussani,
University of Milan, Italy
Dagmar Meyer zu Heringdorf,
Goethe-Universität Frankfurt am Main, Germany

****Correspondence:***
Alba Di Pardo
alba.dipardo@neuromed.it
Vittorio Maglione
vittorio.maglione@neuromed.it

Received: *08 January 2019*
Accepted: *03 April 2019*
Published: *24 April 2019*

Citation:
Di Pardo A, Pepe G, Castaldo S, Marracino F, Capocci L, Amico E, Madonna M, Giova S, Jeong SK, Park B-M, Park BD and Maglione V (2019) Stimulation of Sphingosine Kinase 1 (SPHK1) Is Beneficial in a Huntington's Disease Pre-clinical Model. Front. Mol. Neurosci. 12:100. doi: 10.3389/fnmol.2019.00100

INTRODUCTION

Huntington's disease (HD) is a fatal inherited brain disorder characterized by progressive striatal and cortical neurodegeneration and associated motor, cognitive and behavioral disturbances (McColgan and Tabrizi, 2017). The disease results from the expansion of a polyglutamine stretch (polyQ; >36 repeats) in the N-terminal region of huntingtin (Htt), a widely expressed protein whose function is still under investigation (Jimenez-Sanchez et al., 2017).

Expansion of the polyQ tract endows mutant Htt (mHtt) with toxic properties, resulting in the development of a number of deleterious effects in both neuronal and non-neuronal cells (Maglione et al., 2005, 2006a,b; Carroll et al., 2015; Jimenez-Sanchez et al., 2017).

Defects in the metabolism of sphingosine-1-phosphate (S1P) have recently emerged as an important factor in the disease pathogenesis (Di Pardo et al., 2017a,b; Pirhaji et al., 2017).

S1P is one the most potent signaling lipids that regulates several molecular events underlying cellular homeostasis and viability (Maceyka et al., 2012) and whose homeostasis is finely governed by the action of number of different highly specialized enzymes (Le Stunff et al., 2002; Morozov et al., 2013). Reduction of S1P levels is associated with different neurodegenerative disorders (Di Pardo and Maglione, 2018b) only recently including HD (Pirhaji et al., 2016, 2017; Di Pardo et al., 2017a,b). Although the molecular mechanism behind the reduction of S1P content is thought to be complex in the case of HD it may be in part due to the reduced levels of the S1P biosynthetic enzyme, sphingosine kinase-1 (SPHK1; Di Pardo et al., 2017a,b), whose activity is normally associated with cell survival (Le Stunff et al., 2002; Morozov et al., 2013). In line with that, stimulation of SPHK1, with the selective activator K6PC-5, exerts beneficial effects and pro-survival actions in *in vitro* models of HD, and importantly also in human iPSC-derived neurons from HD patients (Di Pardo et al., 2017a).

In this study, we demonstrate for the first time that stimulation of SPHK1 is therapeutically effective in R6/2 mice.

The R6/2 mouse model, overexpressing the exon 1 of the human HD gene (*HTT*) with long (141–157) CAG-repeat expansions (Mangiarini et al., 1996), is one of the best-characterized and the most widely used animal models to study the pathogenesis of HD. Motor symptoms usually start at 6 weeks of age and progressively worsen over weeks (Mangiarini et al., 1996; Di Pardo et al., 2014). Despite the wealth of different transgenic HD mice available, the R6/2 line remains one of the most used models for testing novel therapeutic interventions for HD, and many compounds that have been reported effective in these mice have proceeded to clinical trials with mixed results (Chang et al., 2015).

Our data indicate that chronic administration of K6PC-5 exerts an overall therapeutic action in R6/2 mice with amelioration of the forelimb and hindlimb clasping, and prevention of motor deficit progress. Interestingly, from a mechanistic perspective, the treatment with K6PC-5 stimulates S1P metabolism, evokes the activation of pro-survival pathways and autophagic flux and reduces mHtt toxicity which translates into a significant slow-down of the overall disease progression in HD mice.

MATERIALS AND METHODS

Animals

Breeding pairs of the R6/2 line of transgenic mice [strain name: B6CBA-tgN (HDexon1) 62Gpb/1J] with 160 (CAG) repeat expansions were purchased from the Jackson Laboratories and were crossed with female B6CBA wild-type (WT) mice to establish the animal colony. All experimental procedures were approved by the IRCCS Neuromed Animal Care Review Board and by "Istituto Superiore di Sanità" (ISS permit number: 1163/2015-PR) and were conducted according to the 2010/63/EU Directive for animal experiments.

Analyses were carried out in both R6/2 mice and WT littermates, starting from 5 weeks of age. To ensure homogeneity of the experimental cohorts, mice from the same F generation were assigned to experimental groups, such that age and weight were matched.

In vivo Drug Administration

K6PC-5 (provided by NeoPharm) was dissolved in DMSO, further diluted in saline (vehicle) and daily administered, starting at 6 weeks of age, by intraperitoneal (i.p.) injection at a dose of 0.05 mg/kg, whose effectiveness was determined by an explorative pilot study (**Supplementary Figure S1**). Control mice (WT and R6/2) were injected daily with the same volume of vehicle containing DMSO.

Clasping Analysis

The clasping score is determined over 30 s. In particular, mice were suspended by their tails from a height of 50 cm and a limb-clasping response was defined as the withdrawal of any limb to the torso for more than 2 s. The following scores were used: 0, absence of clasping; 0.5, withdrawal of any single limb; 1, withdrawal of any two limbs; 1.5, withdrawal of any three limbs; 2, withdrawal of all four limbs.

Motor Behavior Tests

Motor performance was assessed by the Horizontal Ladder Task and Rotarod tests as described previously (Di Pardo et al., 2018). All tests took place during the light phase of the light-dark cycle and mice were tested before and after the initiation of the treatment as indicated.

All animals used for biochemical and histological experiments were euthanized after 5 weeks of treatment (11 weeks of age). Mice used for life-span analysis were examined once daily until natural death.

Brain Lysate Preparation

Eleven-week-old mice were sacrificed within 1 h from the last treatment by cervical dislocation and brains were removed from the skull, weighed and dissected. Brains were immediately snap-frozen in liquid N2 and pulverized in a mortar with a pestle as previously described (Di Pardo et al., 2018).

Semi-quantitative Analysis of Sphingosine-1-Phosphate (S1P)

To assure that an equal amount of homogenate was analyzed, each tissue lysate sample was serially diluted, and the protein concentration was assessed by NanoDrop Spectrophotometer. Five-hundred nanograms of striatal lysate from vehicle- and K6PC-5 treated R6/2 mice were spotted in quadruplicate on a nitrocellulose membrane. Membranes were incubated with the anti-S1P antibody (LT1002; 1:500; Echelon Biosciences, Cat. N. Z-P300), and with the anti-Actin antibody (1: 5,000; Sigma Aldrich, Cat. N. A5441; see **Supplementary Material**). S1P- and actin-immunopositive spots were visualized by ECL Plus (GE Healthcare) and quantitated with Image Lab Software (Bio-Rad Laboratories).

Quantitative Real Time PCR (qPCR)

Mice were sacrificed by cervical dislocation and brain regions were dissected out, snap frozen in liquid N2 and pulverized in a mortar with a pestle. Total RNA was extracted using the RNeasy kit (Qiagen) according to the manufacturer's instructions. One microgram of total RNA was reverse-transcribed using Superscript II reverse transcriptase (Invitrogen) and oligo-dT primer, and the resulting cDNAs were amplified using Sso Advanced Universal SYBR Green Supermix (Bio-Rad Laboratories, Cat. N. #1725271) following the manufacturers' instructions. Quantitative PCR (qPCR) analysis was performed on a CFX Connect Real-Time System instrument (Bio-Rad Laboratories) as previously described (Di Pardo et al., 2017b). The following primers were used (5′ → 3′): CDase-Fw: GTG TGGCATATTCTCATCTG; CDase-Rv: TAAGGGACACC AATAAAAGC. CerS1-Fw: CACACATCTTTCGGCCCCT; CerS1-Rv: GCGGGTCATGGAAGAAAGGA; CerS2-Fw: GGT GGAGGTAGACCTTTTGTCA; CerS2-Rv: CGGAACTTTTTG AGAAGACTGGG; sphk1-Fw: ACAGTGGGCACCTTCTT TC; sphk1-Rv: CTTCTGCACCAGTGTAGAGGC. Expression of all sphingolipid-metabolizing enzymes was normalized on Cyclophilin-A by using the following primers: CycA-Fw: TCC AAAGACAGCAGAAAACTTTCG; CycA-Rv: TCTTCTTGC TGGTCTTGCCATTCC.

Immunoblottings

Proteins (20 μg) were resolved on 10% SDS-PAGE and immunoblotted with the following antibodies: anti-$S1PR_1$ (1:1,000; Immunological Sciences, Cat. N. AB-83739); anti-$S1PR_5$ (1:1,000; Immunological Sciences, Cat. N. AB-83741); anti-phospho-AKT (1:1,000; Immunological Sciences, Cat. N. AB-10521); anti-AKT (1:1,000; Cell Signaling Cat. N. #2920), anti-phospho-ERK (1:1,000; Immunological Sciences, Cat. N. AB-82379); anti-dopamine- and cAMP-regulated protein 32 (DARPP-32; 1:1,000; Cell Signaling, Cat. N. #2302); anti-brain derived neurotrophic factor (BDNF; 1:1,000; Santa Cruz, Cat. N. sc-546).

For LC3 and Beclin1 analyses, protein lysates (20 μg) were resolved on a 12% SDS-PAGE and immunoblotted with anti-LC3 (1:1,000; Novus, Cat. N. NB100-2331) and anti-Beclin1 (1:1,000; Santa Cruz, Cat. N. sc-11427) antibodies. For protein normalization, anti-Actin (1: 5,000; Sigma Aldrich, Cat. N. A5441) and/or anti-Cyclophilin (Abcam Cat. N. ab16045) were used. Immunoblots were then exposed to specific HRP-conjugated secondary antibodies (Santa Cruz, Cat. N. sc-2004 and sc-2005). Protein bands were visualized by ECL Plus (GE Healthcare) and quantitated with Image Lab Software (Bio-Rad Laboratories). Cell lysate from HUVEC, treated with the autophagy inductor TAT-D11 (10 μM; Shoji-Kawata et al., 2013) was used as positive control.

Analysis of mHtt Aggregates

WT and R6/2 mice were sacrificed by cervical dislocation. Brains were removed and trimmed by removing the olfactory bulbs and spinal cord. The remaining brain was processed and embedded in paraffin wax and 10 μg coronal sections were cut. Four mice/group were used and immunostaining for mHtt aggregates was carried out using a mouse anti-Htt antibody (clone EM48; 1: 150; Immunological Sciences, Cat. N. MAB-94354) as recently described (Di Pardo et al., 2018). For the immunoblotting analyses, cell lysate (30 μg) was resolved on a 10% SDS-PAGE, and entire gel, including the stacking portion, was transblotted over-night at 250 mV in 0.05% SDS and 16% methanol-containing transfer buffer (Di Pardo et al., 2018). The membrane was blocked in 5% non-fat dry milk TBST for 1 h and successively immunoblotted with anti-Htt (clone EM48) antibody (1:1,000). A monoclonal anti-mouse HRP-conjugated antibody (Santa Cruz, Cat. N. sc-2005) was used as a secondary antibody. Protein bands were visualized by ECL Plus (GE Healthcare) and quantified as described above.

Statistics

A Two-way ANOVA followed by a Bonferroni post-test was used to compare treatment groups for the Horizontal Ladder Task and Rotarod tests, as well as for the mouse body weight analysis. A Log-rank test was used to analyze mouse survival. A One-way ANOVA and Two-tailed Unpaired *t*-test was used in all other experiments as indicated. All data were expressed as mean ± SD.

RESULTS

Treatment With K6PC-5 Prevents Motor Dysfunction in R6/2 Mice

K6PC-5 treatment has previously been demonstrated to activate pro-survival pathways in *in vitro* models of HD including human HD patient iPSC-derived neurons (Di Pardo et al., 2017a), however, whether the compound could exert any therapeutic action *in vivo* has never been investigated so far. Here, in order to test the therapeutic potential of K6PC-5, whose potential ability to cross the blood-brain barrier was postulated *in vitro* by the PAMPA assay (see **Supplementary Figure S2**), symptomatic R6/2 mice (6-week-old) and age-matched WT littermate controls were i.p.- injected with 0.05 mg/kg daily, and limb clasping reflex and motor phenotype with movement and coordination were then analyzed.

In contrast to what classically occurs as the disease progresses, R6/2 mice treated with K6PC-5 did not exhibit clasping behavior even at the late stage of the disease (**Figures 1A,B**). K6PC-5 was also therapeutically effective in preventing the worsening of motor functions in these mice. R6/2 mice treated with the compound performed significantly better than vehicle-treated mice during the whole period of the treatment as assessed by Horizontal Ladder Task and Rotarod (**Figures 1C,D**). Interestingly, the beneficial effect of K6PC-5 administration was also detectable when animal body weight (**Figure 1E**) and animal life-span (**Figure 1F**) were assessed. No evidence of adverse effects was observed throughout the period of the treatment.

K6PC-5 Treatment Modulates S1P Metabolism/Axis in HD Mice

Over the last few years, we have extensively demonstrated that the metabolism of different sphingolipids, including

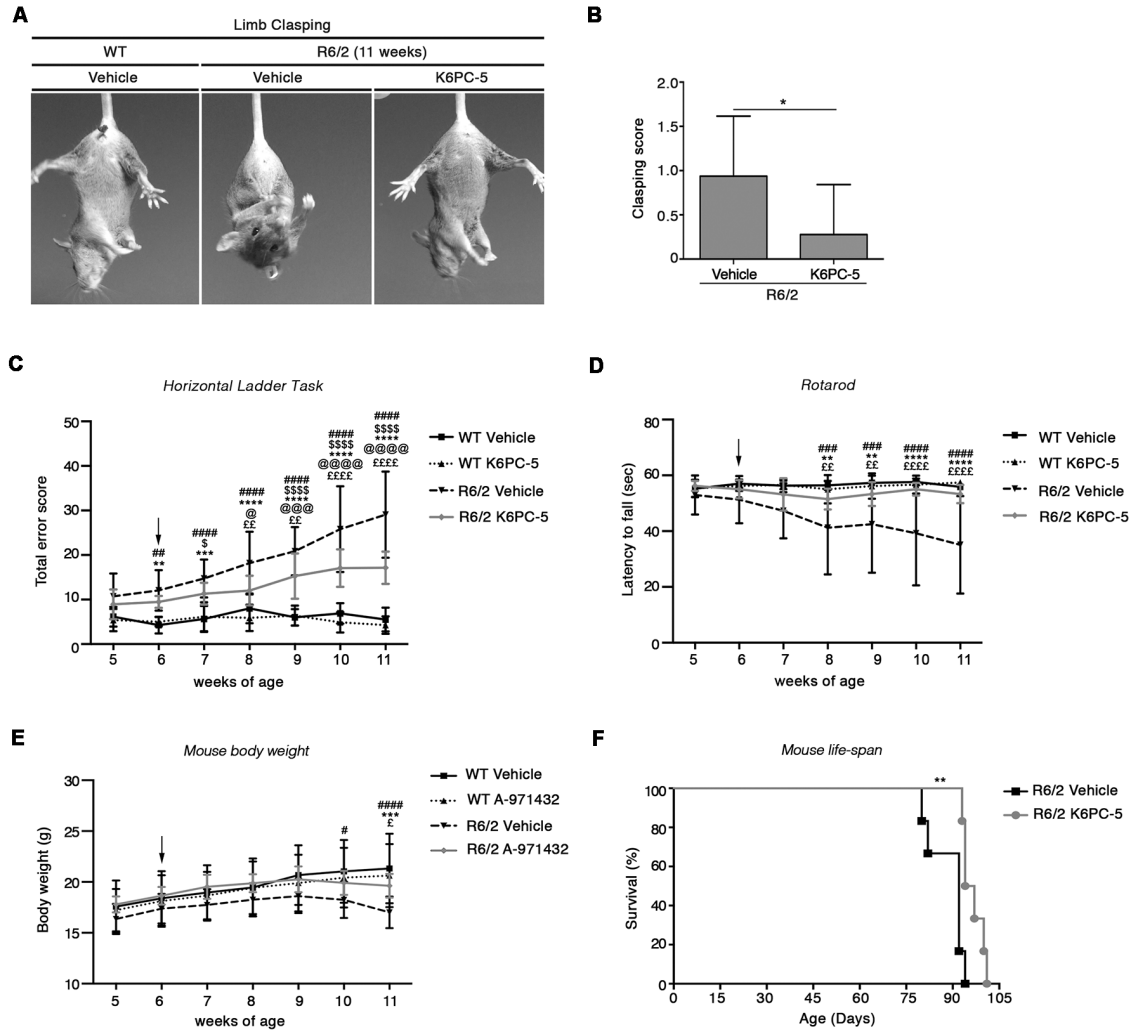

FIGURE 1 | Administration of K6PC-5 ameliorates Huntington's disease (HD) mouse phenotype. **(A,B)** Limb-clasping response at 11 weeks of age HD. Vehicle-treated R6/2 mice, $N = 8$; K6PC-5-treated R6/2 mice, $N = 9$. Values are represented as mean ± SD. $^{*}p < 0.05$ (Un-paired *t*-test). Motor performance assessed by **(C)** Horizontal Ladder Task and **(D)** Rotarod. Vehicle-treated wild-type (WT) mice, $N = 8$; K6PC-5-treated WT mice, $N = 8$; vehicle-treated R6/2 mice, $N = 15$; K6PC-5-treated R6/2 mice, $N = 15$. **(E)** Mouse body weight during the entire period of the treatment. Vehicle-treated WT mice, $N = 8$; K6PC-5-treated WT mice, $N = 8$; vehicle-treated R6/2 mice, $N = 12$; K6PC-5-treated R6/2 mice, $N = 12$. Values are represented as mean ± SD. $^{\#}p < 0.05$; $^{\#\#}p < 0.01$; $^{\#\#\#}p < 0.0001$; $^{\#\#\#\#}p < 0.0001$ (vehicle-treated WT vs. vehicle-treated R6/2 mice). $^{\$}p < 0.05$; $^{\$\$\$\$}p < 0.0001$ (vehicle-treated WT vs. K6PC-5-treated R6/2 mice). $^{**}p < 0.01$; $^{***}p < 0.001$; $^{****}P < 0.0001$ (K6PC-5-treated WT vs. vehicle-treated R6/2 mice). $^{@}p < 0.05$; $^{@@@}p < 0.001$; $^{@@@@}p < 0.0001$ (K6PC-5-treated WT vs. K6PC-5-treated R6/2 mice). $^{£}p < 0.05$; $^{ff}p < 0.01$; $^{££££}p < 0.0001$ (vehicle-treated R6/2 vs. K6PC-5-treated R6/2 mice; Two-Way ANOVA with Bonferroni post-test). **(F)** Kaplan Maier curve of survival HD. Vehicle-treated R6/2 mice, $N = 6$; K6PC-5-treated R6/2 mice, $N = 6$. $^{**}p < 0.01$. Log-rank (Mantel-Cox) test.

S1P, is aberrant in different HD settings ranging from pre-clinical models to human samples from HD patients (Maglione et al., 2010; Di Pardo et al., 2016, 2017a,b; Di Pardo and Maglione, 2017).

Here, we investigated whether the overall therapeutic effectiveness of K6PC-5 might be associated with an overall modulation of S1P metabolism. Semi-quantitative analysis by dot blot, performed with a commercial antibody, that specifically detects S1P (**Supplementary Figure S3**, O'Brien et al., 2009), suggests an increase in the levels of the lipid in the striatal tissues of R6/2 mice after K6PC-5 treatment (**Figure 2A**). Additionally, with the aim of supporting the findings obtained by dot blot, the expression of enzymes (CerS1, CerS2 and CDase), normally involved in the metabolism of ceramide (**Figure 2B**), which serves as a precursor of S1P, was investigated.

Chronic administration of K6PC-5 increased the expression of all three enzymes (**Figures 2C–E**) in striatal tissues from HD mice. Interestingly, mRNA levels of SPHK1 were also increased after treatment (**Figure 2F**).

Furthermore, K6PC-5 treatment correlated with higher protein levels of $S1PR_1$ and $S1PR_5$, two receptors of S1P, mostly abundant in the brain (Soliven et al., 2011; **Figures 3A,B**).

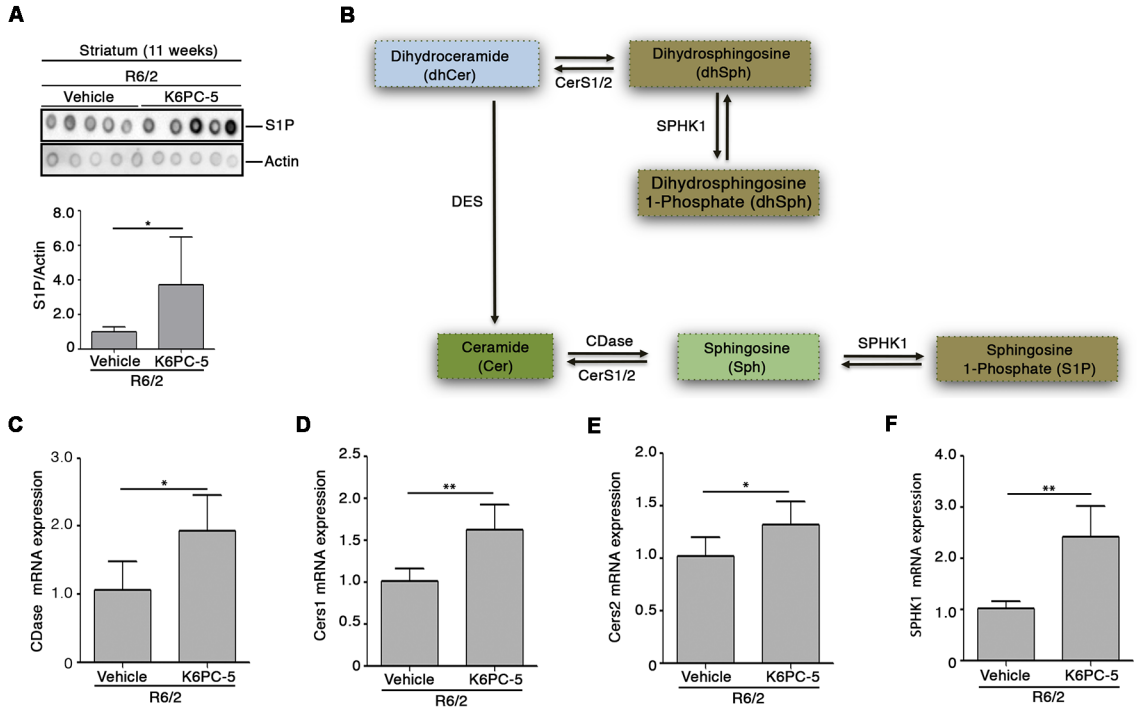

FIGURE 2 | K6PC-5 modulates sphingosine-1-phosphate (S1P) metabolism in the striatum of R6/2 mice. **(A)** Representative cropped dot blotting and densitometric analysis of S1P content in striatal tissues from vehicle- and K6PC-5-treated R6/2 mice at 11 weeks of age. Each spot represents a single animal. Graph represents the average of $N = 7$ vehicle-treated and $N = 5$ K6PC-5-treated R6/2 mice. Data are represented as mean ± SD. $^{*}p < 0.05$ (Unpaired *t*-test). **(B)** Simplified schematic representation of sphingolipid biosynthesis. Ceramide (Cer) may derive either from dihydrosphingosine (dhSph) through the dihydroceramide desaturase (DES) or from the sphingosine (Sph) by CerS1/2. Ceramidase (CDase) converts Cer in sphingosine (Sph), which, in turn, produces S1P through phosphorylation by sphingosine kinase-1 (SPHK1). SPHK1 may also generate dhS1P from dhSph. Quantitative PCR (qPCR) analysis of CDase **(C)**, CerS1/2 **(D,E)**, SPHK1 **(F)**. $N = 5$ for each group of mice. Data are represented as mean ± SD. $^{*}p < 0.05$; $^{**}p < 0.01$ (Unpaired *t*-test).

K6PC-5 Evokes the Activation of Pro-survival Pathways in the Striatum of HD Mice

K6PC-5 has previously been demonstrated to evoke the activation of pro-survival kinases AKT and ERK in multiple HD *in vitro* models, including human iPSC-derived HD neurons (Di Pardo et al., 2017a). Here, we explored the potential that K6PC-5 may have in serving as a neuroprotective agent *in vivo*. Administration of K6PC-5 in R6/2 mice was associated with increased levels of striatal DARPP-32 (**Figure 4A**), a specific marker of medium spiny neurons (Matamales et al., 2009), whose downregulation classically correlates with neurodegeneration in HD (Ehrlich, 2012). Also, K6PC-5 stimulates the phosphorylation of either AKT or ERK, two "classical effectors" whose activation is a prerequisite for neuronal survival also *in vivo* (**Figures 4B,C**).

K6PC-5 Increases Levels of Brain Derived Neurotrophic Factor (BDNF) in Both Striatum and Cortex of R6/2 Mice

Defective expression of BDNF has widely been associated with several brain disorders including HD (Zuccato and Cattaneo, 2009). Developing small molecules to target and/or modulate BDNF production has largely been proposed over the past years (Zuccato and Cattaneo, 2009).

Previous evidence from our group indicates that modulation of S1P axis stimulates the elevation of BDNF levels that are commonly associated with pro-survival effect both in *in vitro* and *in vivo* HD models (Di Pardo et al., 2014, 2018). Interestingly, after administration of K6PC-5, levels of BDNF protein were found markedly elevated in both cortical tissues and in the striatum of R6/2 mice (**Figures 5A,B**).

K6PC-5 Reduces mHtt Aggregation in Brain Tissues From R6/2 Mice

Formation of mHtt aggregates is a pathological hallmark that may conceivably cause neuronal dysfunction in HD (Sánchez et al., 2003; Arrasate et al., 2004). Here we tested the possibility that K6PC-5 treatment may lower mutant Htt toxicity likely modulating its aggregation. Immunohistochemical staining for EM48 highlighted that the size of mHtt aggregates was significantly reduced in both the striatum and cortex of K6PC-5-treated R6/2 mice compared with the controls (**Figures 6A,B** and **Supplementary Figure S4**). This finding was also confirmed by immunoblotting analysis which showed a decrease of EM48-positive SDS-insoluble aggregates in striatal protein lysates (**Figure 6C**).

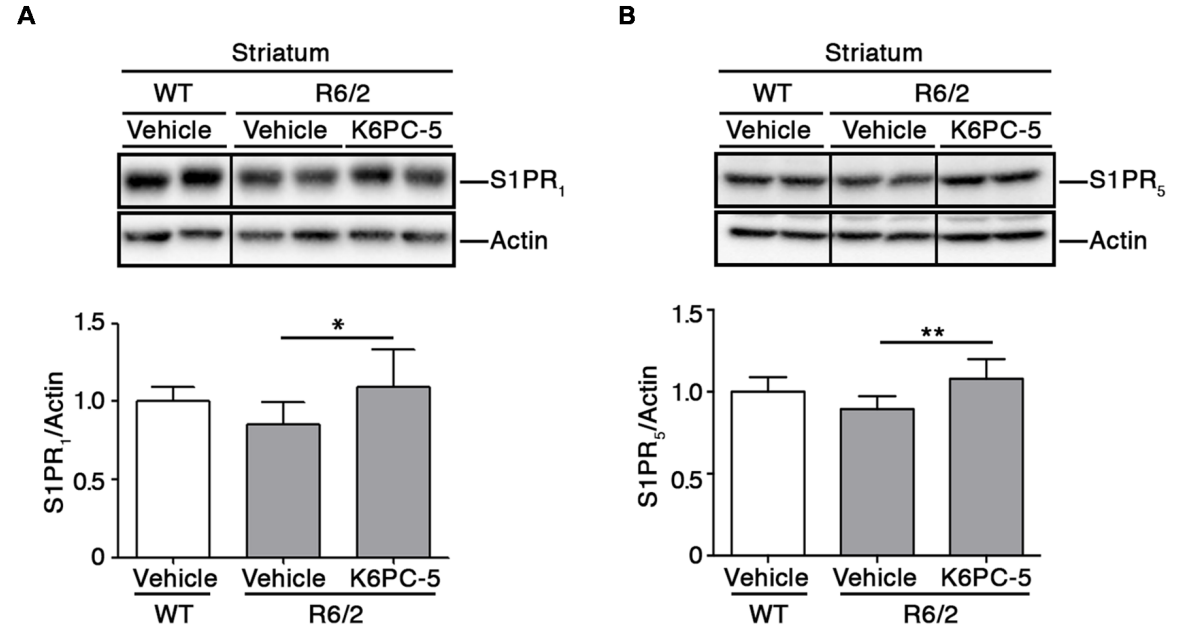

FIGURE 3 | K6PC-5 increases the expression of S1P receptors in the striatum of R6/2 mice. Representative cropped western blotting and densitometric analysis of $S1PR_1$ **(A)** and $S1PR_5$ **(B)** levels in striatal tissues from vehicle-treated WT and vehicle-and K6PC-5-treated R6/2 mice at 11 weeks of age. Non-adjacent samples were separated by a black line. $S1PR_1$: vehicle-treated WT mice, $N = 6$; vehicle-treated R6/2 mice, $N = 7$; K6PC-5-treated R6/2 mice $N = 5$. $S1PR_5$: $N = 7$ for each group of mice. Data are represented as mean ± SD. $^*p < 0.05$; $^{**}p < 0.01$ (One Way ANOVA with Tukey post-test).

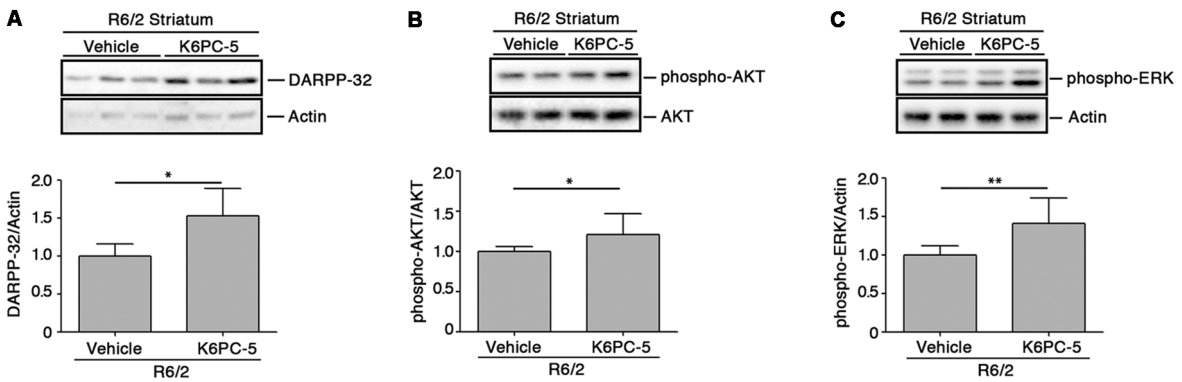

FIGURE 4 | K6PC-5 evokes the activation of pro-survival pathways in the striatum of R6/2 mice. Representative cropped immunoblotting and densitometric analysis of dopamine- and cAMP-regulated protein 32 (DARPP-32; **A**) phospho-AKT/AKT **(B)** and phospho-ERK/Actin **(C)** levels in striatal tissues from vehicle- and K6PC-5-treated R6/2 mice. Phospho-AKT and phospho-ERK: vehicle-treated R6/2 mice, $N = 8$; K6PC-5-treated R6/2 mice, $N = 5$. DARPP-32: vehicle-treated R6/2 mice, $N = 6$; K6PC-5-treated R6/2 mice, $N = 5$. Data are represented as mean ± SD. $^*p < 0.05$; $^{**}p < 0.01$ (Unpaired *t*-test).

Reduction of mHtt Aggregation Is Associated With Modulation of Autophagic Markers

Evidence indicates that S1P may regulate autophagy in different experimental conditions and cell types, including neuronal cells (Karunakaran and van Echten-Deckert, 2017). Increased autophagy has been reported as a molecular mechanism associated with clearance of mHtt aggregation in multiple HD pre-clinical models (Yamamoto et al., 2006; Martin et al., 2015). Here, in order to investigate any correlation between the reduction of mHtt aggregates after K6PC-5 administration and autophagy, protein expression of Beclin1 and LC3, two of the most widely used cellular autophagic markers (Moulis and Vindis, 2017), in striatal tissues from HD mice, was assessed. K6PC-5 administration was associated with an increased expression of Beclin1 (**Figure 7**), whose elevation has been reported to be correlated with an increased autophagic flux (Moulis and Vindis, 2017), with decreased levels of LC3-I and elevation of LC3-II (**Figure 7**), further

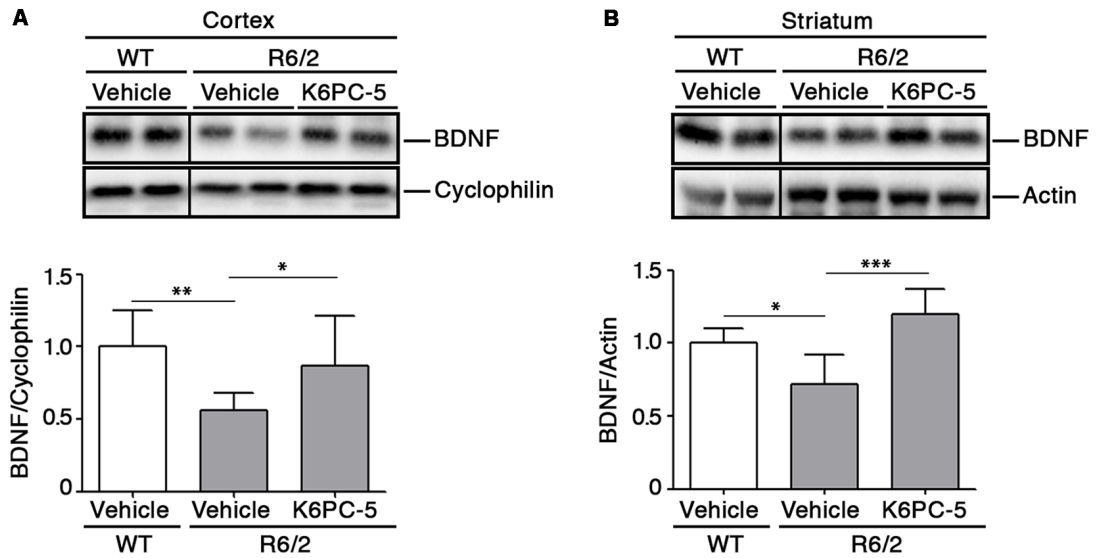

FIGURE 5 | K6PC-5 promotes the elevation of brain derived neurotrophic factor (BDNF) levels in brain tissues from R6/2 mice. Representative cropped western blotting's and densitometric analysis of BDNF protein in cortical **(A)** and striatal **(B)** tissues from the vehicle-treated WT and vehicle- and K6PC-5-treated R6/2 mice at 11 weeks of age. Cortex: $N = 9$ for each group of mice. Striatum: vehicle-treated WT mice, $N = 5$; vehicle-treated R6/2 mice, $N = 5$; K6PC-5-treated R6/2 mice, $N = 6$ Data are represented as mean ± SD. $^{*}p < 0.05$; $^{**}p < 0.01$; $^{***}p < 0.0001$ (One Way ANOVA with Tukey post test).

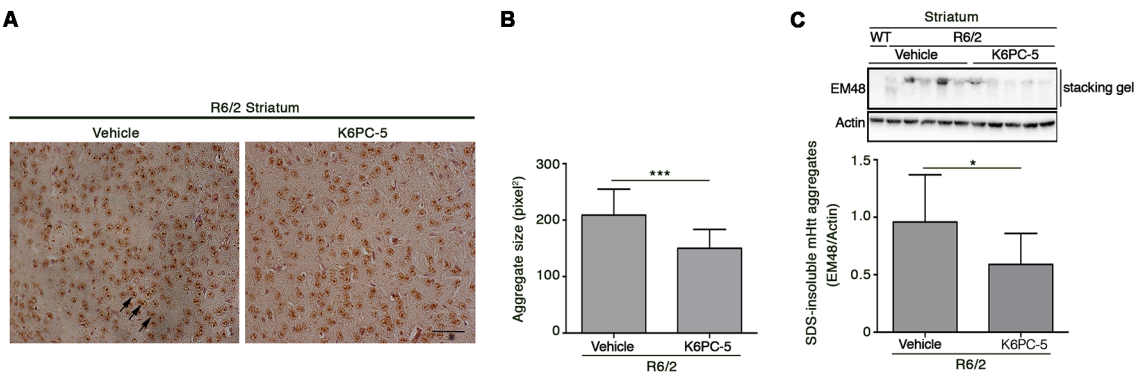

FIGURE 6 | Administration of K6PC-5 ameliorates neuropathology in R6/2 mice. Representative micrograph **(A)** and semi-quantitative analysis of EM48-immunoreactive mutant huntingtin (mHtt) aggregate area **(B)** in the striatum of vehicle- and K6PC-5-treated R6/2 mice at 11 weeks of age. Arrows indicate mHtt aggregates. Scale bar in represents 100 μm. HD, $N = 4 + 4$. Values are represented as mean ± SD. $^{***}p < 0.001$ (Unpaired *t*-test). **(C)** Representative cropped immunoblotting of EM48-positive SDS-insoluble mHtt aggregates in striatal lysate from vehicle- and A-K6PC-5-treated R6/2 mice at 11 weeks of age. Vehicle-treated R6/2 mice, $N = 10$; K6PC-5-treated R6/2 mice, $N = 8$. Values are represented as mean ± SD. $^{*}p < 0.05$ (Unpaired *t*-test).

reinforcing the hypothesis of high autophagic activity after treatment.

DISCUSSION

The complexity and variety of aberrant molecular pathways that are commonly associated with HD have long hampered the development of effective therapies for this disease. Over the last few years, the discovery that sphingolipid metabolism can play a key role in HD pathogenesis and can affect many of the cellular pathways associated with mHtt toxicity, has opened the door to novel potential therapeutic strategies that specifically target the central lipid homeostasis which is tightly regulated to maintain neuronal structure and function (Di Pardo and Maglione, 2018a,b).

Alterations of lipid metabolism have been frequently associated with HD, however the recognition of perturbed sphingolipid metabolism has only very recently become evident in the disease (Maglione et al., 2010; Pirhaji et al., 2016, 2017; Di Pardo et al., 2017a,b).

Aberrant sphingolipid metabolism, with reduced bioavailability of the bioactive lipid S1P, has been reported in multiple HD settings (Pirhaji et al., 2016, 2017; Di Pardo et al., 2017a,b) and, interventions aimed at modulating S1P

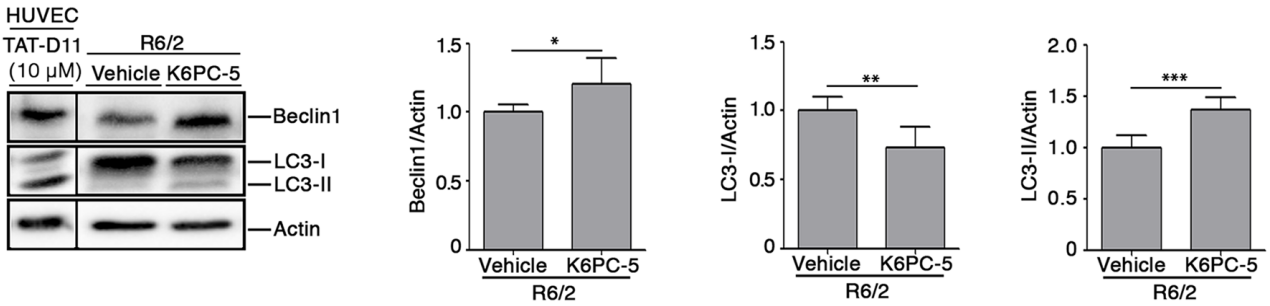

FIGURE 7 | Administration of K6PC-5 modulates autophagic flux in the striatum of R6/2 mice. Representative cropped immunoblotting and densitometric analysis of Beclin1 and LC3-I/-II autophagic markers in striatal tissues from vehicle- and K6PC-5-treated R6/2 mice at 11 weeks of age. Cell lysate from HUVEC, treated with the autophagy inductor TAT-D11 (10 μM; Shoji-Kawata et al., 2013) was used as positive control. All samples were run on the same gel. Non-adjacent samples were separated by a black line. Vehicle-treated R6/2 mice, $N = 6$; K6PC-5-treated R6/2 mice, $N = 6$. Values are represented as mean ± SD. $^{*}p < 0.05$; $^{**}p < 0.01$; $^{***}p < 0.001$ (Unpaired *t*-test).

metabolism/axis have repeatedly been proposed as alternative therapeutic options in the disease (Di Pardo et al., 2014, 2018; Pirhaji et al., 2016; Di Pardo and Maglione, 2017, 2018a; Moruno-Manchon et al., 2017, 2018).

In this study, we reported for the first time, that stimulation of SPHK1 activity is beneficial in a HD animal model. Administration of K6PC-5, a selective activator of SPHK1, exerted an overall beneficial effect on the disease phenotype in R6/2 mice. Besides preventing motor dysfunction, K6PC-5 treatment was associated with conserved body weight and expanded lifespan in this mouse model.

Our results are coherent with a real modulation of S1P pathways in HD, however, the precise molecular mechanisms behind such a therapeutic action remain to be further elucidated. Metabolism of S1P is very complex with several points of regulation including the implication of receptors. Thus, it is conceivable that any modulation of sphingolipid content may determine a global rearrangement of the metabolic pathways.

Reduced content of S1P has previously been associated with HD pathogenesis (Di Pardo et al., 2017a; Pirhaji et al., 2017) and its elevation after K6PC-5 administration likely lies behind the therapeutic action of the compound in R6/2 mice.

The beneficial effect of K6PC-5 seems to be mediated by a number of different molecular mechanisms, however, although only speculative, we believe that an incremented bioavailability of S1P after the treatment may play a pivotal role (**Figure 8**). Changes in the expression of ceramide-metabolizing enzymes (CerS1/2 and CDase) and the incremented expression of SPHK1, probably due to a positive feedback mechanism, may presumably indicate a shift in the sphingolipid rheostat away from ceramide and in favor of S1P. Considering the limitations of the technique applied for determining S1P levels in this study, we believe that qPCR findings represent an indirect indication of the ability of the compound to modulate sphingolipid metabolism and conceivable increase S1P levels in brain tissues.

K6PC-5 increased protein levels of $S1PR_1$ and $S1PR_5$, the latter of which has recently emerged as a therapeutic target in R6/2 mice (Di Pardo et al., 2018). Elevation in the expression of both receptors may be conceivable attributable to higher S1P bioavailability that may somehow stabilize the proteins, promoting then the phosphorylation of pro-survival kinases AKT and ERK. This is particularly important since the alteration in either AKT or ERK seems to be crucial in the pathogenesis of HD and their activation has been proposed as a reasonable event to suppress disease progression (Rai et al., 2019).

Evidence also indicates that increased bioavailability of BDNF predicts benefits in R6/2 mice (Giralt et al., 2011; Giampà et al., 2013). Administration of K6PC-5 in these mice increased levels of BDNF in the cortex and importantly also in the striatum, which normally rely on cortex-synthetized neurotrophin. Thus, it is plausible that K6PC-5 favors the anterograde transport of the BDNF from the cortex to the striatum, which in turn is protected from the loss of striatal neurons, as revealed by increased levels of DARPP-32.

Additional molecular mechanisms underlying the beneficial effect of K6PC-5 may depend on the correlation existing between the S1P biosynthetic enzyme, SPHK1, and the autophagic flux (Lavieu et al., 2006; Moruno Manchon et al., 2015). Coherently, reduced levels and/or activity of SPHK1 have been described to impair endocytic membrane trafficking pathways (Shen et al., 2014) and to inhibit neuronal autophagy in different neurodegenerative conditions (Lee et al., 2014). Its over-expression, instead, stimulates autophagic flux in cells including primary neurons (Lavieu et al., 2006; Moruno Manchon et al., 2015).

In this study, for the first time, we demonstrated that stimulation of SPHK1, by K6PC-5, triggers autophagy *in vivo* in R6/2 mice. This is absolutely in line with the evidence that this enzyme is necessary for promoting the formation of pre-autophagosoms in primary neurons (Moruno Manchon et al., 2015). Change in the expression of Beclin1 and the conversion of LC3-I to LC3-II, all markers classically associated with autophagosomal organization, are clear signs of active autophagic machinery *in vivo*.

Evidence indicates that autophagy may represent a potential therapeutic target in HD pre-clinical models

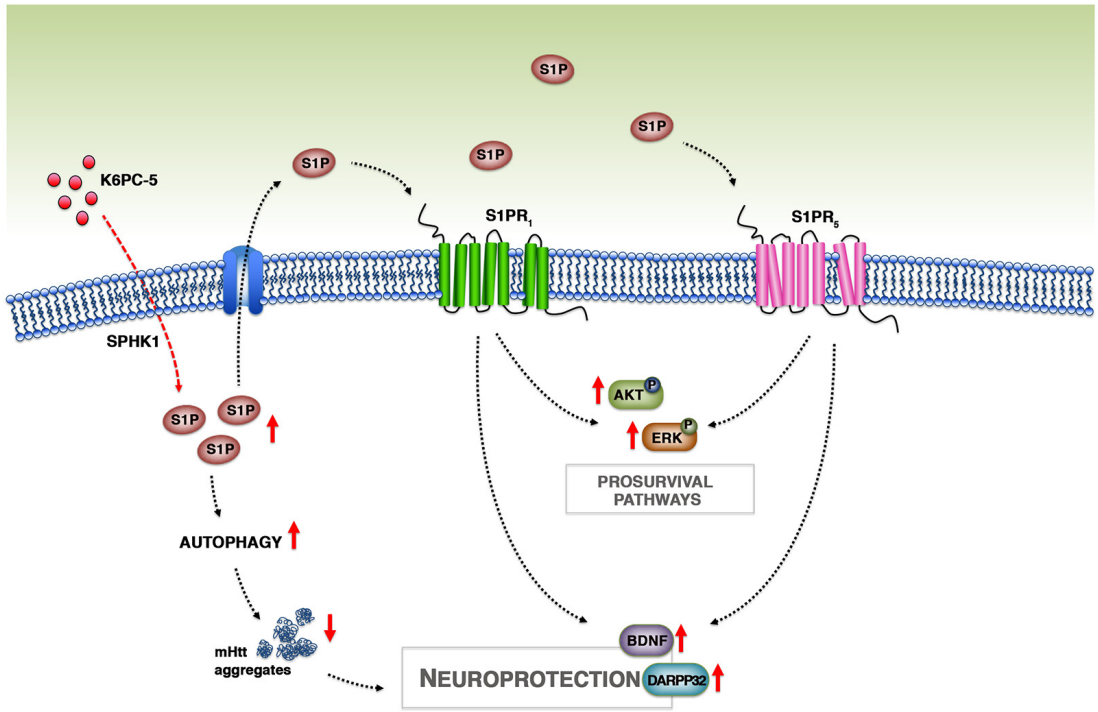

FIGURE 8 | Working model. Treatment with K6PC-5 stimulates the activity of SPHK1 with a subsequent increase in the levels of S1P. S1P may act either intracellularly, by stimulating autophagy and reducing mHtt aggregation, or extracellularly by stabilizing S1PR expression and activating pro-survival pathways.

(Martin et al., 2015) and eventually influence the disease course in HD patients (Metzger et al., 2013). Although in this study, we cannot establish any direct correlation between increased autophagy and reduction of mHtt aggregates, we can speculate that clearance of protein aggregates after administration of K6PC-5 may be associated with boosted autophagy flux. Further studies are necessary to fully clarify this molecular mechanism, however recent evidence demonstrates that overexpression of SPHK1 promotes clearance of mutant Htt exon-1 construct *in vitro* (Moruno Manchon et al., 2015) and suggests a possible link between increased autophagy and reduced mHtt aggregation.

Although we did not have any direct evidence of the ability of K6PC-5 to penetrate the brain, our findings clearly indicate that the compound was able to modulate brain homeostasis. From our perspective, stimulation of SPHK1 exerts a larger array of biological effects by acting on both intracellular (stimulation of the defective sphingolipid metabolism and induction of autophagy) and extracellular pathways (receptor axis and related signaling), with respect to the stimulation of S1P receptors.

What makes our findings attractive is the evidence that S1P metabolism may represent a target for the discovery of novel therapeutic strategies in HD, especially given that drugs working through its related pathways are already in clinical trials for different other pathological conditions (Kunkel et al., 2013; Gonzalez-Cabrera et al., 2014; O'Sullivan and Dev, 2017; Di Pardo and Maglione, 2018a).

In conclusion, with this study we provide further evidence that modulation of S1P metabolism may represent a strong paradigm for pursuing the development of novel and more targeted therapeutic strategy by which it is possible to restore normal sphingolipid metabolism and stimulate S1P axis, which in turn may activate pro-survival pathways and reduce mHtt aggregation with a consequent preservation of neuronal homeostasis in HD brains (**Figure 8**).

ETHICS STATEMENT

All experimental procedures were approved by the IRCCS Neuromed Animal Care Review Board and by "Istituto Superiore di Sanità" (ISS permit number: 1163/2015-PR) and were conducted according to EU Directive 2010/63/EU for animal experiments.

AUTHOR CONTRIBUTIONS

VM and ADP conceived and designed the study, jointly directed the study and co-wrote the manuscript. ADP supervised all *in vivo* experiments. SC, LC, MM and SG managed animal colonies and performed all *in vivo* analyses. FM, EA, GP performed all the biochemical and histological experiments and made manuscript revisions. SJ, B-MP and BP provided

K6PC-5 technology and the PAMPA assay results. All the authors analyzed and discussed the data, revised and approved the manuscript.

FUNDING

This research was funded by the European Huntington's Disease Network (EHDN) Grant number 903 and the Italian Ministry of Health "Ricerca Corrente" funding program, and supported by Fondazione Neuromed.

SUPPLEMENTARY MATERIAL

The Supplementary Material for this article can be found online at: https://www.frontiersin.org/articles/10.3389/fnmol.2019.00100/full#supplementary-material

REFERENCES

Arrasate, M., Mitra, S., Schweitzer, E. S., Segal, M. R., and Finkbeiner, S. (2004). Inclusion body formation reduces levels of mutant huntingtin and the risk of neuronal death. *Nature* 431, 805–810. doi: 10.1038/nature02998

Carroll, J. B., Bates, G. P., Steffan, J., Saft, C., and Tabrizi, S. J. (2015). Treating the whole body in Huntington's disease. *Lancet Neurol.* 14, 1135–1142. doi: 10.1016/S1474-4422(15)00177-5

Chang, R., Liu, X., Li, S., and Li, X. J. (2015). Transgenic animal models for study of the pathogenesis of Huntington's disease and therapy. *Drug Des. Devel. Ther.* 9, 2179–2188. doi: 10.2147/dddt.s58470

Di Pardo, A., Amico, E., Basit, A., Armirotti, A., Joshi, P., Neely, M. D., et al. (2017a). Defective sphingosine-1-phosphate metabolism is a druggable target in Huntington's disease. *Sci. Rep.* 7:5280. doi: 10.1038/s41598-017-05709-y

Di Pardo, A., Basit, A., Armirotti, A., Amico, E., Castaldo, S., Pepe, G., et al. (2017b). *De novo* synthesis of sphingolipids is defective in experimental models of Huntington's disease. *Front. Neurosci.* 11:698. doi: 10.3389/fnins.2017.00698

Di Pardo, A., Amico, E., Favellato, M., Castrataro, R., Fucile, S., Squitieri, F., et al. (2014). FTY720 (fingolimod) is a neuroprotective and disease-modifying agent in cellular and mouse models of Huntington disease. *Hum. Mol. Genet.* 23, 2251–2265. doi: 10.1093/hmg/ddt615

Di Pardo, A., Amico, E., and Maglione, V. (2016). Impaired levels of gangliosides in the corpus callosum of Huntington disease animal models. *Front. Neurosci.* 10:457. doi: 10.3389/fnins.2016.00457

Di Pardo, A., Castaldo, S., Amico, E., Pepe, G., Marracino, F., Capocci, L., et al. (2018). Stimulation of S1PR5 with A-971432, a selective agonist, preserves blood-brain barrier integrity and exerts therapeutic effect in an animal model of Huntington's disease. *Hum. Mol. Genet.* 27, 2490–2501. doi: 10.1093/hmg/ddy153

Di Pardo, A., and Maglione, V. (2017). Glyco-sphingo biology: a novel perspective for potential new treatments in Huntington's disease. *Neural Regen. Res.* 12, 1439–1440. doi: 10.4103/1673-5374.215253

Di Pardo, A., and Maglione, V. (2018a). The S1P axis: new exciting route for treating Huntington's disease. *Trends Pharmacol. Sci.* 39, 468–480. doi: 10.1016/j.tips.2018.02.009

Di Pardo, A., and Maglione, V. (2018b). Sphingolipid metabolism: a new therapeutic opportunity for brain degenerative disorders. *Front. Neurosci.* 12:249. doi: 10.3389/fnins.2018.00249

Ehrlich, M. E. (2012). Huntington's disease and the striatal medium spiny neuron: cell-autonomous and non-cell-autonomous mechanisms of disease. *Neurotherapeutics* 9, 270–284. doi: 10.1007/s13311-012-0112-2

Giampà, C., Montagna, E., Dato, C., Melone, M. A., Bernardi, G., and Fusco, F. R. (2013). Systemic delivery of recombinant brain derived neurotrophic factor (BDNF) in the R6/2 mouse model of Huntington's disease. *PLoS One* 8:e64037. doi: 10.1371/journal.pone.0064037

Giralt, A., Carretón, O., Lao-Peregrin, C., Martín, E. D., and Alberch, J. (2011). Conditional BDNF release under pathological conditions improves Huntington's disease pathology by delaying neuronal dysfunction. *Mol. Neurodegener.* 6:71. doi: 10.1186/1750-1326-6-71

Gonzalez-Cabrera, P. J., Brown, S., Studer, S. M., and Rosen, H. (2014). S1P signaling: new therapies and opportunities. *F1000Prime Rep.* 6:109. doi: 10.12703/p6-109

Jimenez-Sanchez, M., Licitra, F., Underwood, B. R., and Rubinsztein, D. C. (2017). Huntington's disease: mechanisms of pathogenesis and therapeutic strategies. *Cold Spring Harb. Perspect. Med.* 7:a024240. doi: 10.1101/cshperspect.a024240

Karunakaran, I., and van Echten-Deckert, G. (2017). Sphingosine 1-phosphate - A double edged sword in the brain. *Biochim. Biophys. Acta Biomembr.* 1859, 1573–1582. doi: 10.1016/j.bbamem.2017.03.008

Kunkel, G. T., Maceyka, M., Milstien, S., and Spiegel, S. (2013). Targeting the sphingosine-1-phosphate axis in cancer, inflammation and beyond. *Nat. Rev. Drug Discov.* 12, 688–702. doi: 10.1038/nrd4099

Lavieu, G., Scarlatti, F., Sala, G., Carpentier, S., Levade, T., Ghidoni, R., et al. (2006). Regulation of autophagy by sphingosine kinase 1 and its role in cell survival during nutrient starvation. *J. Biol. Chem.* 281, 8518–8527. doi: 10.1074/jbc.m506182200

Lee, H., Lee, J. K., Park, M. H., Hong, Y. R., Marti, H. H., Kim, H., et al. (2014). Pathological roles of the VEGF/SphK pathway in Niemann-Pick type C neurons. *Nat. Commun.* 5:5514. doi: 10.1038/ncomms6514

Le Stunff, H., Peterson, C., Liu, H., Milstien, S., and Spiegel, S. (2002). Sphingosine-1-phosphate and lipid phosphohydrolases. *Biochim. Biophys. Acta* 1582, 8–17. doi: 10.1016/s1388-1981(02)00132-4

Maceyka, M., Harikumar, K. B., Milstien, S., and Spiegel, S. (2012). Sphingosine-1-phosphate signaling and its role in disease. *Trends Cell Biol.* 22, 50–60. doi: 10.1016/j.tcb.2011.09.003

Maglione, V., Cannella, M., Gradini, R., Cislaghi, G., and Squitieri, F. (2006a). Huntingtin fragmentation and increased caspase 3, 8 and 9 activities in lymphoblasts with heterozygous and homozygous Huntington's disease mutation. *Mech. Ageing Dev.* 127, 213–216. doi: 10.1016/j.mad.2005.09.011

Maglione, V., Cannella, M., Martino, T., De Blasi, A., Frati, L., and Squitieri, F. (2006b). The platelet maximum number of A2A-receptor binding sites (Bmax) linearly correlates with age at onset and CAG repeat expansion in Huntington's disease patients with predominant chorea. *Neurosci. Lett.* 393, 27–30. doi: 10.1016/j.neulet.2005.09.037

Maglione, V., Giallonardo, P., Cannella, M., Martino, T., Frati, L., and Squitieri, F. (2005). Adenosine A2A receptor dysfunction correlates with age at onset anticipation in blood platelets of subjects with Huntington's disease. *Am. J. Med. Genet. B Neuropsychiatr. Genet.* 139B, 101–105. doi: 10.1002/ajmg.b.30223

Maglione, V., Marchi, P., Di Pardo, A., Lingrell, S., Horkey, M., Tidmarsh, E., et al. (2010). Impaired ganglioside metabolism in Huntington's disease and neuroprotective role of GM1. *J. Neurosci.* 30, 4072–4080. doi: 10.1523/JNEUROSCI.6348-09.2010

Mangiarini, L., Sathasivam, K., Seller, M., Cozens, B., Harper, A., Hetherington, C., et al. (1996). Exon 1 of the HD gene with an expanded CAG repeat is sufficient to cause a progressive neurological phenotype in transgenic mice. *Cell* 87, 493–506. doi: 10.1016/s0092-8674(00)81369-0

Martin, D. D., Ladha, S., Ehrnhoefer, D. E., and Hayden, M. R. (2015). Autophagy in Huntington disease and huntingtin in autophagy. *Trends Neurosci.* 38, 26–35. doi: 10.1016/j.tins.2014.09.003

Matamales, M., Bertran-Gonzalez, J., Salomon, L., Degos, B., Deniau, J. M., Valjent, E., et al. (2009). Striatal medium-sized spiny neurons: identification by nuclear staining and study of neuronal subpopulations in BAC transgenic mice. *PLoS One* 4:e4770. doi: 10.1371/journal.pone.0004770

McColgan, P., and Tabrizi, S. J. (2017). Huntington's disease: a clinical review. *Eur. J. Neurol.* 25, 24–34. doi: 10.1111/ene.13413

Metzger, S., Walter, C., Riess, O., Roos, R. A., Nielsen, J. E., Craufurd, D., et al. (2013). The V471A polymorphism in autophagy-related gene ATG7 modifies age at onset specifically in Italian Huntington disease patients. *PLoS One* 8:e68951. doi: 10.1371/journal.pone.0068951

Morozov, V. I., Sakuta, G. A., and Kalinski, M. I. (2013). Sphingosine-1-phosphate: distribution, metabolism and role in the regulation of cellular functions. *Ukr. Biokhim. Zh. (1999)* 85, 5–21. doi: 10.15407/ubj85.01.005

Moruno-Manchon, J. F., Uzor, N. E., Ambati, C. R., Shetty, V., Putluri, N., Jagannath, C., et al. (2018). Sphingosine kinase 1-associated autophagy differs between neurons and astrocytes. *Cell Death Dis.* 9:521. doi: 10.1038/s41419-018-0599-5

Moruno-Manchon, J. F., Uzor, N. E., Blasco-Conesa, M. P., Mannuru, S., Putluri, N., Furr-Stimming, E. E., et al. (2017). Inhibiting sphingosine kinase 2 mitigates mutant Huntingtin-induced neurodegeneration in neuron models of Huntington disease. *Hum. Mol. Genet.* 26, 1305–1317. doi: 10.1093/hmg/ddx046

Moruno Manchon, J. F., Uzor, N. E., Dabaghian, Y., Furr-Stimming, E. E., Finkbeiner, S., and Tsvetkov, A. S. (2015). Cytoplasmic sphingosine-1-phosphate pathway modulates neuronal autophagy. *Sci. Rep.* 5:15213. doi: 10.1038/srep15213

Moulis, M., and Vindis, C. (2017). Methods for measuring autophagy in mice. *Cells* 6:E14. doi: 10.3390/cells6020014

O'Brien, N., Jones, S. T., Williams, D. G., Cunningham, H. B., Moreno, K., Visentin, B., et al. (2009). Production and characterization of monoclonal anti-sphingosine-1-phosphate antibodies. *J. Lipid Res.* 50, 2245–2257. doi: 10.1194/jlr.M900048-JLR200

O'Sullivan, S., and Dev, K. K. (2017). Sphingosine-1-phosphate receptor therapies: advances in clinical trials for CNS-related diseases. *Neuropharmacology* 113, 597–607. doi: 10.1016/j.neuropharm.2016.11.006

Pirhaji, L., Milani, P., Dalin, S., Wassie, B. T., Dunn, D. E., Fenster, R. J., et al. (2017). Identifying therapeutic targets by combining transcriptional data with ordinal clinical measurements. *Nat. Commun.* 8:623. doi: 10.1038/s41467-017-00353-6

Pirhaji, L., Milani, P., Leidl, M., Curran, T., Avila-Pacheco, J., Clish, C. B., et al. (2016). Revealing disease-associated pathways by network integration of untargeted metabolomics. *Nat. Methods* 13, 770–776. doi: 10.1038/nmeth.3940

Rai, S. N., Dilnashin, H., Birla, H., Singh, S. S., Zahra, W., Rathore, A. S., et al. (2019). The role of PI3K/Akt and ERK in neurodegenerative disorders. *Neurotox. Res.* 35, 775–795. doi: 10.1007/s12640-019-0003-y

Sánchez, I., Mahlke, C., and Yuan, J. (2003). Pivotal role of oligomerization in expanded polyglutamine neurodegenerative disorders. *Nature* 421, 373–379. doi: 10.1038/nature01301

Shen, H., Giordano, F., Wu, Y., Chan, J., Zhu, C., Milosevic, I., et al. (2014). Coupling between endocytosis and sphingosine kinase 1 recruitment. *Nat. Cell Biol.* 16, 652–662. doi: 10.1038/ncb2987

Shoji-Kawata, S., Sumpter, R., Leveno, M., Campbell, G. R., Zou, Z., Kinch, L., et al. (2013). Identification of a candidate therapeutic autophagy-inducing peptide. *Nature* 494, 201–206. doi: 10.1038/nature11866

Soliven, B., Miron, V., and Chun, J. (2011). The neurobiology of sphingosine 1-phosphate signaling and sphingosine 1-phosphate receptor modulators. *Neurology* 76, S9–S14. doi: 10.1212/WNL.0b013e31820d9507

Yamamoto, A., Cremona, M. L., and Rothman, J. E. (2006). Autophagy-mediated clearance of huntingtin aggregates triggered by the insulin-signaling pathway. *J. Cell Biol.* 172, 719–731. doi: 10.1083/jcb.200510065

Zuccato, C., and Cattaneo, E. (2009). Brain-derived neurotrophic factor in neurodegenerative diseases. *Nat. Rev. Neurol.* 5, 311–322. doi: 10.1038/nrneurol.2009.54

Conflict of Interest Statement: B-MP was employed by company NeoPharm USA Inc. BP was employed by company Dr. Raymond Laboratories Inc., USA.

The remaining authors declare that the research was conducted in the absence of any commercial or financial relationships that could be construed as a potential conflict of interest.

frontiers in Molecular Neuroscience

REVIEW
published: 27 May 2019
doi: 10.3389/fnmol.2019.00131

Cancer Stem Cells in Neuroblastoma: Expanding the Therapeutic Frontier

Hisham F. Bahmad[1†], Farah Chamaa[1†], Sahar Assi[1†], Reda M. Chalhoub[1§], Tamara Abou-Antoun[2‡] and Wassim Abou-Kheir[1*‡]*

[1] Department of Anatomy, Cell Biology and Physiological Sciences, Faculty of Medicine, American University of Beirut, Beirut, Lebanon, [2] Department of Pharmaceutical Sciences, School of Pharmacy, Lebanese American University, Byblos, Lebanon

Neuroblastoma (NB) is the most common extracranial solid tumor often diagnosed in childhood. Despite intense efforts to develop a successful treatment, current available therapies are still challenged by high rates of resistance, recurrence and progression, most notably in advanced cases and highly malignant tumors. Emerging evidence proposes that this might be due to a subpopulation of cancer stem cells (CSCs) or tumor-initiating cells (TICs) found in the bulk of the tumor. Therefore, the development of more targeted therapy is highly dependent on the identification of the molecular signatures and genetic aberrations characteristic to this subpopulation of cells. This review aims at providing an overview of the key molecular players involved in NB CSCs and focuses on the experimental evidence from NB cell lines, patient-derived xenografts and primary tumors. It also provides some novel approaches of targeting multiple drivers governing the stemness of CSCs to achieve better anti-tumor effects than the currently used therapeutic agents.

Keywords: neuroblastoma, cancer stem cells, molecular signatures, therapeutic targets, genetic aberrations

OPEN ACCESS

Edited by:
Michele Papa,
Università degli Studi della Campania Luigi Vanvitelli, Italy

Reviewed by:
Assunta Virtuoso,
Second University of Naples, Italy
Rosa Gomez-Villafuertes,
Complutense University of Madrid, Spain

***Correspondence:**
Tamara Abou-Antoun
tamara.abouantoun@lau.edu.lb
Wassim Abou-Kheir
wa12@aub.edu.lb

[†]These authors have contributed equally to this work as co-first authors

[‡]These authors have contributed equally to this work as joint senior authors

[§]Present address:
Reda M. Chalhoub,
Medical Scientist Training Program, College of Medicine, Medical University of South Carolina, Charleston, SC, United States

Received: *27 February 2019*
Accepted: *07 May 2019*
Published: *27 May 2019*

Citation:
Bahmad HF, Chamaa F, Assi S, Chalhoub RM, Abou-Antoun T and Abou-Kheir W (2019) Cancer Stem Cells in Neuroblastoma: Expanding the Therapeutic Frontier. Front. Mol. Neurosci. 12:131. doi: 10.3389/fnmol.2019.00131

INTRODUCTION

Stem cells are a class of multipotent undifferentiated cells, able to give rise to all cells in a particular tissue, organ or organism. Stem cells are selectively characterized by their endogenous self-renewal ability, continuously maintaining a pool of undifferentiated cells that will further differentiate, during development or following injury, into fully functional cells (Reya et al., 2001). Stem cells were historically further classified into two subtypes: pluripotent embryonic stem cells and adult stem cells. The former arises from a fertilized egg and gives rise to whole-organisms, while the latter represents tissue-specific multipotent cells that reside in adult tissues, and maintain their homeostatic balance (Chen et al., 2015). Mainly, these cells regularly divide to replace old senescent cells, or they get rigorously activated following injury to repair damaged tissues (Gudjonsson and Magnusson, 2005; Daley, 2015).

Abbreviations: ABC, adenosine triphosphate-binding cassette; ABCG2, ATP-binding cassette sub-family G member 2; ALDH1, aldehyde dehydrogenases 1; ATRA, all-trans retinoic acid; BCRP, breast cancer resistance protein; CBHA, carboxycinnamic acid bis-hydroxamide; CSC, cancer stem cell; DLK1, Delta-like 1; EMT, epithelial-to-mesenchymal transition; Fzd6, frizzled receptors 6; G-CSFR, Granulocyte-Colony Stimulation Factor Receptor; HIF, hypoxia-inducible factor; KGN, kartogenin; MDR, multidrug resistance; MDR1, P-glycoprotein; MMP, matrix metalloproteinase; MRP, multidrug resistance proteins; NB, neuroblastoma; NDM29, neuroblastoma differentiation marker 29; PHB1, prohibitin 1; PHB2, prohibitin 2; PLK1, Polo-Like Kinase 1; RA, retinoic acid; RAP, reversible adaptive plasticity; S6RP, S6 ribosomal protein; SFU, sphere-forming units; STAT3, Signal Transducer and Activator of Transcription 3; TIC, tumor-initiating cell.

Recently, a new subpopulation of stem cells was suggested to exist in tumors. This hypothesis originated based on the recurrent clinical course of most cancers, as well as their self-renewal ability and uninhibited growth pattern, two categorical markers of tumorigenesis. This subpopulation of cells is commonly referred to as CSC or TICs. The cancer stem cell was first introduced in leukemias, remarkably distinguishing a population of cells on top of the tumorigenesis hierarchy able to develop and generate malignant hematopoietic colonies (Moore et al., 1973). The heterogenic cellular composition of solid tumors, such as melanoma, further supported the existence of CSCs, thought to be responsible for cancer recurrence after therapy (Menaa et al., 2009). As their nomenclature implies, CSCs possess the ability to self-renew indefinitely, as well as the potential to differentiate into the different types of cells that form the tumor bulk. Nonetheless, while normal stem cells are tightly regulated by tumor-suppressor proteins that control their entry into the cell cycle, cellular division and differentiation, CSCs harbor critical genetic pro-oncogenic mutations that instigate uncontrolled cellular proliferation (Chen et al., 2015), promoting tumor progression and malignancy. Notably, in solid tumors such as gliomas, the self-renewal capacity of CSCs (CD133+ cells) correlated highly with the aggressiveness and clinical grade of these tumors (Singh et al., 2003).

Cancer stem cells are also highly resistant to conventional therapies used to treat cancerous tumors, such as chemotherapy and radiation (Reya et al., 2001; Singh et al., 2003). Despite major advances in the delivery, effectiveness and mechanisms involved in these cancer therapies, cancer recurrence and metastatic growth of an eradicated primary tumor are still serious unfortunate outcomes that are commonly seen in clinical settings. Resistance to chemotherapy and treatment relapse are recently being attributed to our failure to successfully target and suppress these CSCs. While common treatments effectively eliminate a large proportion of differentiated cells within the bulk tumor and hence greatly reducing its size and burden to subclinical levels that cannot be detected using conventional methods, it fails to eradicate the tumor-initiating cells, which further promote tumor growth and progression (Menaa et al., 2009).

The field of CSCs has spurred the attention of many researchers and triggered recent studies to focus on further characterizing these cells, on functional and molecular levels. The identification of molecular markers specific to these cells set the stage for the development of novel therapeutic drugs targeted against them, ultimately aiming at preventing tumor recurrence and treatment resistance. The subpopulation of CSCs is found in many types of malignancies including brain tumors (Dawood et al., 2014), which represent some of the most aggressive cancers found in both children and adults.

Neuroblastoma is the most common extracranial pediatric solid tumor. It often arises in infants and children up to 5 years old (Buhagiar and Ayers, 2015). It originates from embryonic neural crest cells destined to become the sympathetic ganglia of the autonomic nervous system, or the catecholamine-secreting cells of the adrenal glands. Thus, these tumors arise mainly in areas such as the adrenal medulla as well as the neck, chest, and spinal cord, among others (Buhagiar and Ayers, 2015). Interestingly, NB tumors with unfavorable prognosis have been shown to house a population of undifferentiated stem cells, responsible of their superior malignant state (Reya et al., 2001; Singh et al., 2003; Buhagiar and Ayers, 2015). In this review, we go through the latest discoveries that outline the molecular markers of the cancer stem cells in NB, as well as the current platform of CSC targeted novel therapies that achieve a higher therapeutic potential than currently used approaches.

NEUROBLASTOMA CANCER STEM CELLS: MOLECULAR SIGNATURES AND GENETIC ABERRATIONS

Substantial research is aimed at elucidating the molecular signatures of CSCs and specific malignant drivers in order to devise more efficacious therapies. However, the molecular signatures and drivers of malignancy in CSCs seen in solid tumors in general, and NB in particular, are numerous, sometimes overlapping and dynamic. We have previously reported on the RAP in NB that may be rendering it highly malignant and chemotherapy-resistant, a mechanism by which NB CSCs maintain a dynamic ability to revert back-and-forth between anchorage-independent treatment-evasive tumorspheres and anchorage-dependent, adherent cancer cells in response to environmental stressors, such as therapeutic agents, hypoxia, low pH levels and deprivation of growth factors (Chakrabarti et al., 2012).

Pathways that may be dysregulated by the CSCs have been reported to be involved in invasion and metastasis, uncontrolled proliferation, angiogenic potential, therapeutic resistance and self-renewal abilities (Chakrabarti et al., 2012). Ideal therapeutic strategies necessitate targeting several of these malignant pathways, taking into account the RAP character exhibited by this malignant tumor, in order to adequately cripple the cancer and prevent relapse with metastatic disease. The various, extensively studied molecular signatures pertaining to NB CSCs will be elaborated below (**Table 1**).

DLK1 and HIF

The *DLK1* gene encodes Protein Delta Homolog 1, a transmembrane protein which belongs to the *EGF*-like homeotic protein family. This gene is highly expressed in different neuroendocrine tumors, including NB (van Limpt et al., 2000; Kim, 2010) and other nervous system tumors such as gliomas (Yin et al., 2006), and plays a critical role in differentiation processes (Laborda, 2000). *DLK1* expression was shown to be induced by hypoxia, via the *HIF*-dependent mechanism (Kim et al., 2009), in neuronal tumor cells and plays a crucial role in maintaining the tumorigenicity of the CSCs (Kim et al., 2009; Begum et al., 2014). *HIF-1α* and *HIF-2α* both enhance *DLK1* expression, however, only *HIF-2α* is differentially expressed in NB with *MYCN* amplification, whereas *HIF-1α* is ubiquitously expressed (Holmquist-Mengelbier et al., 2006; Kim et al., 2009). *DLK1* also interacts with two molecules, PHB1 and PHB2, the latter of which has a specific and critical role in the self-renewal and clonogenicity of CSCs (Begum et al., 2014). In this sense,

TABLE 1 | Summary table of the major molecular signatures and genetic aberrations attributed to neuroblastoma cancer stem cells.

Molecular/Genetic Signature	References	Results
DLK1	Kim et al., 2009	*DLK1* expression is induced by hypoxia, via HIF-dependent mechanism, in neuronal tumor cells, and plays a crucial role in maintaining the tumorigenicity of the CSCs.
	Holmquist-Mengelbier et al., 2006	*HIF-1*α and *HIF-2*α enhance *DLK1* expression, but only HIF-2α is differentially expressed in NB with *MYCN*-amplification, whereas *HIF-1*α is ubiquitously expressed.
	Begum et al., 2014	*DLK1* interacts with the cytoplasmic domain of *PHB1* and *PHB2* (via Tyrosine339 and Serine355), the latter of which has a specific and critical role in the self-renewal and clonogenicity of CSCs.
CD114/G-CSFR	Hsu et al., 2013	*CD114*+ cells isolated from primary NB tumors are highly tumorigenic and exhibit self-renewal and clonogenic potential, as compared to the *CD114*- population, revealing their stem cell-like phenotype.
	Agarwal et al., 2015	G-CSF acts as an activating growth factor in NB and contributes to the *CD114*+ stem cell population through selective activation and upregulation of *STAT3*.
BMI1	Cui et al., 2007	Development of primary NB tumors is associated with an increased expression of *BMI1* and its down-regulation is associated with an impaired ability of the NB cells to produce tumors in immunodeficient mice.
CD44	Siapati et al., 2011	Inverse correlation exists between *CD44* and *CD24*, which is an established marker of CSCs.
	Jensen et al., 2015; Munchar et al., 2003	*CD44* is a favorable prognostic marker in NB, and lack of *CD44* expression is associated with aggressive and metastatic behavior.
	Rabadan et al., 2013	*CD44* in an inhibitor of metastasis and its downregulation is necessary in NB for the cells to acquire a metastatic potential
CD133	Cournoyer et al., 2012	Isolated NB cells with high *CD133* expression show enhanced ability to form neurospheres relative to cells with low expression of *CD133*.
	Takenobu et al., 2011	NB cells lacking *CD133* show loss of ability to repress differentiation and hence were induced to differentiate.
	Sartelet et al., 2012; Tong et al., 2008	*CD133* levels are significantly increased in NB tumors of more advanced stages.
	Tong et al., 2008	NB patients who have increased levels of *CD133* expression show unfavorable histology and shorter survival time post-surgery.
C-kit (*CD117*)	Lau et al., 2015	Increased c-KIT expression is correlated with poor patient prognosis and outcome in NB
	Walton et al., 2004; Ross and Spengler, 2007	I-type NB cells, which highly resemble CSCs, express the *CD117* stem cell marker.
	Ross et al., 2015	Seven genes are identified to be exclusively elevated in NB CSCs, including *CD133*.
CD24	Jensen et al., 2015	*CD24* expression is found to be elevated in the metastatic NB.
	Siapati et al., 2011	*CD24* is used as a marker for the NB CSCs.
	Hansford et al., 2007	Primary NB cell lines taken from bone marrow metastases reveal that overexpression of *CD24* glycoprotein in cancer cells is associated with accelerated tumor formation and growth.
		CD24 is a candidate unique identifier for CSCs in NB, where a small fraction of CD24+ cells are observed within the high-risk NB tumor-spheres derived from bone marrow aspirate
Fzd6	Cantilena et al., 2011	*Fzd6* positive cells form more neurospheres compared to the Fzd6 negative cells, indicating their potential CSC phenotype.
ALDH1	Flahaut et al., 2016	*ALDH1A2* and *ALDH1A3* are overexpressed in NB CSCs.
		ALDH1A3 expression is significantly correlated with poor patient prognosis and is associated with tumor progression.
	Coulon et al., 2011	Genes crucial to CSC activity, such as *ALDH1A2*, are upregulated in serial sphere passages derived from patient bone marrow metastatic NB cells.
	Hartomo et al., 2015	High *ALDH1A2* expression is found in patients with poor prognosis.
LGR5 (GPR49)	Vieira et al., 2017; Shi et al., 2004	*LGR5* is highly expressed in high grade NB tumors.
	Vieira et al., 2017	*LGR5* acts as upstream of MEK/ERK and Akt pro-survival signaling pathways.
TLX	Chavali et al., 2014	Under hypoxic conditions, TLX activates both *MMP-2* and *OCT-4* genes, stimulating tumor-sphere self-renewal and promoting migratory abilities of NB cells.
		TLX is co-expressed with the migratory neural progenitor markers CD15 and *MMP-2* in xenografts of primary NB cells from patients.
ABCG2	Hirschmann-Jax et al., 2004	Primary NB tumor cells have elevated expression of ABC transporters including *ABCG2*, which are responsible for the efflux of therapeutic drugs and subsequent drug resistance and survival of these cancer cells.
Nestin	Garner and Beierle, 2015	Nestin is one of the first markers used in the description of CSCs in NB tumors.
	Thomas et al., 2004	Overexpression of Nestin is linked to aggressive phenotype of NB tumors.

(Continued)

TABLE 1 | Continued

Molecular/Genetic Signature	References	Results
JARID1B	Kuo et al., 2015	Depletion of *JARID1B* decreases Notch and its ligand, jagged 1 expression, reduces tumor-sphere formation, inhibits invasion, and enhances chemosensitivity to cisplatin.
SPDYA	Lubanska and Porter, 2014	Spy1, a cell cycle regulator encoded by *SPDYA* gene, plays a role in proliferation, self-renewal and differentiation of human NB cells via regulating *CD133*+ cell populations and enhancing neurosphere formation in culture.
		Knockdown of Spy1 causes a decrease in c-MYC expression levels in NB CSCs.
TRPM7	Middelbeek et al., 2015	*TRPM7* overexpression reduces actomyosin-driven cytoskeletal tension which promotes SNAI2 expression, a neural crest specifier, and controls the malignant features of NB cells.
	Lange et al., 2017	FTY-720 inhibits *TRPM7* channel activity kinase signaling and at low concentrations, sensitizes drug-resistant NB cells to antineoplastic drugs.
Lamin A/C	Nardella et al., 2015	Down regulation of Lamin A/C in NB cells enhances self-renewal of CSCs *in vitro* and augments ability to initiate tumors *in vivo*.
	Rauschert et al., 2017	Reintroducing Lamin A/C in NB reduces cell growth kinetics and impairs migration, invasion, anchorage-independent cell growth and promotes cytoskeletal restructuring.
		Introduction of lamin Δ50, known as Progerin, drives NB cells into senescence.
L1-CAM	Rached et al., 2016	*L1-CAM* is a well-established CSC marker in NB and confers chemo- and radio-resistance in aggressive NB tumors.

DLK1 interacts with the PHB complex through its cytoplasmic domain, and Tyrosine339 and Serine355 are specifically required for the maintenance of clonogenicity and tumorigenicity (Kim et al., 2009; Begum et al., 2014).

CD114/G-CSFR

Granulocyte-Colony Stimulation Factor Receptor expression is well-known as a marker of the CSC population in NB. *CD114*+ cells isolated from primary NB tumors were shown to be highly tumorigenic, compared to the *CD114*- population, and exhibited self-renewal and clonogenic potential, revealing their stem cell-like phenotype (Hsu et al., 2013). G-CSF acts as an activating growth factor in NB and contributes to the *CD114*+ stem cell population growth through selective activation and upregulation of *STAT3* (Hsu et al., 2013; Agarwal et al., 2015), a pro-oncogenic transcription factor involved in critical cellular functions, such as growth, division and apoptosis. *STAT3* activates *G-CSFR* transcription in a feed-forward manner, contributing to the maintenance and tumorigenicity of the CSC population (Agarwal et al., 2015). Moreover, *G-CSF-STAT3* signaling loop induces the conversion of differentiated cancer cells into CSCs (Hsu et al., 2013). This signaling pathway is also involved in promoting EMT enhancing the migratory and invasive potential of tumor cells (Agarwal et al., 2015).

BMI1

The oncogene *BMI1* is a transcription factor, member of the polycomb group family that is essential for the self-renewal capacity of stem cells, specifically in the nervous system (Molofsky et al., 2003; Nowak et al., 2006). Development of primary NB tumors is correlated with an increased expression of *BMI1* (Nowak et al., 2006; Cui et al., 2007). On the contrary, *BMI1* down-regulation is associated with an impaired ability of the NB cells to produce tumors in immunodeficient mice (Cui et al., 2007). Moreover, the use of transgenic mice, genetically modified with *MYCN* overexpression, facilitated the monitoring of NB development and revealed an increased expression of *BMI1* (Cui et al., 2007).

Although aggressive NB tumors are associated with *MYCN* amplification, it is important to note that *MYCN* increases the susceptibility of cells to apoptosis (Lutz et al., 1998; Cui et al., 2007) through the *ARF-p53* pathway (Cui et al., 2007). In this context, *BMI1* gene mediates its action by inactivating the apoptotic pathway associated with the *MYN-N* gene amplification, acting as its oncogenic partner (Cui et al., 2007).

CD44

CD44 is a transmembrane glycoprotein involved in cell-cell and cell-ECM interactions (Siapati et al., 2011) and was identified as a CSC marker in numerous pediatric tumors, including NB (Mehrazma et al., 2013). Jensen et al. (2015) showed that metastatic NB was characterized with an increased expression of *CD44* marker, compared to non-metastatic controls. Nonetheless, the lack of *CD44* expression was associated with aggressive and metastatic behavior, as well as unfavorable outcomes (Munchar et al., 2003; Siapati et al., 2011; Rabadan et al., 2013; Nardella et al., 2015). *CD44* is involved in cell-cell adhesion, promoting an antagonistic role vis-a-vis cancer metastasis: its downregulation is thought to be necessary in NB for the cells to acquire a metastatic potential (Rabadan et al., 2013). This was further supported with retrospective studies showing a correlation between increased expression of *CD44* and favorable tumors on histology (Munchar et al., 2003). *In vitro* studies on NB cell lines further investigated the role of *CD44* on cellular morphology: whereas *CD44*- cells had smaller size, lesser neuronal projections, and slower growth, *CD44*+ cells embraced a more flattened morphology and demonstrated a faster growth, with a protein expression

pattern associated with uncontrolled cell cycle progression, immune evasion and lower ability to undergo apoptosis (Siapati et al., 2011). Moreover, one study showed the presence of an inverse correlation between this marker and *CD24* (Siapati et al., 2011), a previously established marker of CSCs (Hansford et al., 2007). The importance of *CD44* as a prognostic marker was challenged by a study conducted by Mehrazma et al. (2013) which failed to prove any correlation between *CD44* expression levels and outcomes in pediatric solid tumors, including NB.

C-kit (CD117)

CD117 is an established marker of stem cells (Hirschmann-Jax et al., 2004; Walton et al., 2004) and proto-oncogene (Lau et al., 2015). It is specifically a factor receptor (Hirschmann-Jax et al., 2004) of the tyrosine kinase type (Lau et al., 2015). It was found that increased *C-kit* expression is correlated with poor patient prognosis and outcome in NB (Lau et al., 2015).

The heterogeneous nature of NB tumors has yielded the identification of 3 different phenotypic cell variants when placed in culture (Ross and Spengler, 2007): two phenotypically stable cell variants – the moderately malignant, weakly substrate-adherent N-type neuroblastic cells and the flattened, substrate-adherent non-neuronal S-type cells (Rettig et al., 1987; Ciccarone et al., 1989) – and a third stable cell type that is "intermediate" between N- and S-type cells, termed "I-type" and recognized to be a highly tumorigenic, malignant NB CSC (Ross et al., 1995). Interestingly, only the latter I-type NB cells, which resemble CSCs the most, express the *CD117* stem cell marker (Walton et al., 2004; Ross and Spengler, 2007).

CD133

CD133, also known as prominin-1, is a 120 kD membrane glycoprotein containing five transmembrane domains. While its specific function remains unknown, this molecule is known to be strictly expressed on protrusions of the plasma membrane of epithelial cells among other cell types (Mizrak et al., 2008). It is well studied as a marker of human hematopoietic stem and progenitor cells (Miraglia et al., 1997; Yin et al., 1997), and of neural stem cells (Mizrak et al., 2008). In addition to its expression in normal stem cells, *CD133* is also often used as a marker of CSCs in a variety of tumors, including NB.

In vitro studies have linked the expression of *CD133* to tumor-initiating capacities in NB cell lines using the neurosphere formation assay, a functional assay that is used to isolate and assess neural stem cells. *CD133*+ cells showed an enhanced ability to form neurospheres compared to *CD133*- cells (Singh et al., 2003; Cournoyer et al., 2012), as well as an increase in average neurosphere size and an enhanced ability of serial passaging, a hallmark of self-renewal (Singh et al., 2003; Cournoyer et al., 2012). Moreover, *CD133*+ NB cells generated a significantly higher number of colonies in anchorage-independent conditions (Cournoyer et al., 2012). Furthermore, *CD133*+ cells injected into the adrenal gland were able to form tumors while low *CD133*- cells failed to do the same (Cournoyer et al., 2012). Many studies have used *CD133* as a stem cell marker in order to track changes in the proportion of this population of cells upon exposure to certain conditions (Bhaskara et al., 2012; Chavali et al., 2014).

The role of this molecule was further investigated in cancer progression and tumorigenesis. *CD133* knockdown experiments revealed significantly increased differentiation patterns within NB cell lines; *CD133* turned out to play a key role inhibiting differentiation partially through regulating signal transduction downstream of RET tyrosine kinase (Takenobu et al., 2011). Moreover, upon exposure of NB CSCs to signals inducing cellular differentiation, *CD133* expression levels were shown to decrease (Takenobu et al., 2011). On the clinical level, *CD133* levels were seen to be significantly increased in tumors of advanced staging (Tong et al., 2008; Sartelet et al., 2012; Mehrazma et al., 2013). Specifically, patients who were found to have increased levels of *CD133* expression also showed unfavorable histology and a shorter survival time post-surgery (Tong et al., 2008). In support of this, a microarray study was performed on several NB cell lines and revealed the presence of seven different genes whose expression was elevated in the highly tumorigenic "I-type" cells, one of which is *CD133* (Ross et al., 2015). The presence of I-cells in NB tumors is currently recognized as an indicator of tumor malignancy (Walton et al., 2004).

CD24

CD24 is a cell adhesion molecule expressed on a variety of cells, such as neural cells and cells of the adrenal medulla, and in several cancers including NB (Akashi et al., 1994). *CD24* expression was found to be elevated in the metastatic NB (Jensen et al., 2015) in one study, and was used as a marker for the NB CSCs in another (Siapati et al., 2011). Additionally, primary NB cell lines taken from bone marrow metastases revealed that overexpression of the *CD24* glycoprotein in cancer cells is associated with accelerated tumor formation and growth (Hansford et al., 2007). Besides, *CD24* had been shown to serve as a candidate unique identifier for CSCs in NB, where a small fraction of $CD24^{+}$ cells were observed within the high-risk NB tumor-spheres derived from bone marrow aspirates (Hansford et al., 2007).

Fzd6

A study examining a possible correlation between expression of frizzled receptors and NB prognosis found that only *Fzd6* was directly linked with poor survival in NB patients. Furthermore, *Fzd6* positive cells within these tumors was found to be localized in the tumor hypoxic areas and expressed nuclear *HIF-2α*. The *Fzd6* positive cells were found to form more neurospheres, and were highly invasive and therapy resistant, compared to the *Fzd6* negative cells, indicating their potential CSC phenotype (Cantilena et al., 2011).

ALDH1 Isoenzymes

Another commonly used marker of stem cells is the subfamily of *ALDH1*, which is composed of *ALDH1A1*, *ALDH1A2*, and *ALDH1A3* isoforms, and are known to be involved in RA synthesis (Koppaka et al., 2012). Specifically, *ALDH1A2* and *ALDH1A3* in NB were found to be overexpressed in a cellular subpopulation of NB, and their roles were further investigated (Flahaut et al., 2016). *ALDH1A2* gene was found

to be upregulated using microarray analysis of serial sphere passages derived from patient bone marrow metastatic NB cells, playing a critical role on the self-renewal and stemness of these cells (Coulon et al., 2011). Notably, an increase in *ALDH1A2* expression in NB tumors was found to be correlated with poorer prognosis (Hartomo et al., 2015).

Similarly, *ALDH1A3* expression was also found to be significantly increased in patients with worse outcome, playing a key role in tumor progression (Flahaut et al., 2016). Most importantly, an increase in ALDH activity is directly related to the tumor's ability to resist conventional drugs and therapies (Abdullah and Chow, 2013; Flahaut et al., 2016).

LGR5 (GPR49)

The stem cell marker *LGR5*, also known as *GPR49*, is a receptor of R-spondins which a promote canonical Wnt signaling and act as growth factors for stem cells (de Lau et al., 2014). This stem cell marker was found to be overexpressed in several types of cancers, such as glioblastoma (Nakata et al., 2013), cervical (Cao et al., 2017), breast (Yang et al., 2015) and colorectal cancers (Hirsch et al., 2014; Yanai et al., 2017). In addition, *LGR5* was found to be overexpressed in high grade NB (Forgham et al., 2015; Vieira et al., 2017), working upstream of the MEK/ERK and Akt pro-survival signaling pathways (Vieira et al., 2017) which are often triggered in primary NB tumors (Opel et al., 2007).

MMP

Highly malignant NB tumors acquire the ability to reach blood vessels and metastasize by releasing matrix metalloproteinases, commonly known as MMPs, which are enzymes that allow the cell to degrade its surrounding extracellular matrix (Chavali et al., 2014). In this context, MMP expression was found to be upregulated in advanced-stage NB tumors and more specifically the *MMP-2* and *MMP-9* (or gelatinase enzymes) (Jiang et al., 2011).

TLX

Nuclear orphan receptor *TLX* (*Drosophila tailless* homolog) maintains self-renewal capabilities of neural stem/progenitor cells (Shi et al., 2004) via hypoxia-mediated mechanisms (Chavali et al., 2011). In NB, it has been demonstrated that under hypoxic conditions, *TLX* can activate both *MMP-2* and *OCT-4* genes, stimulating self-renewal of tumor-spheres and promoting migratory abilities of NB cells (Chavali et al., 2014). In this same study by Chavali et al. (2014) *TLX* was co-expressed with the migratory neural progenitor markers *CD15* and *MMP-2* in xenografts of primary NB cells from patients.

ABCG2

ATP-binding cassette sub-family G member 2 is a marker of neural precursors and is one the first universal markers that were used to identify the CSC population in NB tumors (Ding et al., 2010). *ABCG2* is a member of the *ABC* family of transporter proteins, which are ATP-dependent membrane-spanning proteins involved in the transport of substrates into and out of the cell (Vasiliou et al., 2009). The *ABCG2* transporter was shown to localize in human neural stem/progenitor cells and was proposed to have a crucial role in the maintenance of these cells in an undifferentiated state (Islam et al., 2005).

In a study by Hirschmann-Jax et al. (2004) primary NB tumor cells showed an elevated expression of *ABC* transporters including *ABCG2*, which are responsible for the efflux of therapeutic drugs and therefore for the resistance and survival of these cancer cells. This was further validated by other studies, which showed the role of the *ABCG2* transporter in protecting human neural stem/progenitor cells from toxic substances (Islam et al., 2005).

Even though the specific role of *ABCG2* in cancer progression is not yet known, this protein was shown to be overexpressed in a variety of cancers and numerous reports support its role in the maintenance and tumorigenicity of CSCs. Thus, this marker could have important therapeutic implications in cancer therapies (Ding et al., 2010).

Nestin

Nestin is an intermediate filament protein that is known to be a marker of neural stem/progenitor cells (Suzuki et al., 2010). It is normally expressed in specific subsets of the mammalian CNS during development, but was also detected in a variety of solid tumors, including NB (Krupkova et al., 2011). A study by Krupkova et al. (2011) demonstrated the localization of the Nestin protein in nuclei of tumor cells. Along with *ABCG2*, it is also one of the first markers used in the description of CSCs in NB tumors (Garner and Beierle, 2015). The overexpression of Nestin was shown to be linked to the aggressive phenotype of NB tumors (Thomas et al., 2004).

JARID1B

JARID1B, also known as *PLU1* or *KDM5B*, is a H3K4me3 histone lysine demethylase identified as an oncogene that is overexpressed in many cancer types (Li et al., 2011; Chicas et al., 2012; Sayegh et al., 2013). A study has associated between *JARID1B* and Notch signaling where depletion of *JARID1B* was found to decrease Notch and its ligand jagged 1 expression, reduce tumor-sphere formation, inhibit invasion, and enhance chemosensitivity to cisplatin (Kuo et al., 2015).

SPDYA

Spy1, a cell cycle regulator encoded by *SPDYA* gene, plays a role in proliferation, self-renewal and differentiation of human NB cells via regulating *CD133+* cell populations and enhancing neurospheres formation in culture. This atypical cyclin-like protein Spy1, recently shown to be driving symmetric division of glioma stem cells, is a critical factor in the stem-like properties of NB CSC populations (Lubanska and Porter, 2014). On the other hand, knockdown of Spy1 causes a decrease in *c-MYC* expression levels in NB CSCs, a multifunctional transcription factor involved in cellular proliferation (Lubanska and Porter, 2014). In addition, when Spy1 was over-expressed, it hindered the retinoic acid-induced differentiation of NB CSCs. These interesting findings implicate

a role for this protein in the regulation of *c-MYC* protein expression that may be driving tumor-sphere self-renewal and maintenance in NB tumors.

TRPM7

TRPM7, a mechanically regulated TRP channel with kinase activity, harbors a crucial role in maintaining progenitor-like gene expression program in human NB cell lines (Clark et al., 2006; Middelbeek et al., 2012). This protein is essential in embryogenesis and the maintenance of undifferentiated neural crest progenitors (Jin et al., 2008, 2012). In NB, *TRPM7* overexpression reduces actomyosin-driven cytoskeletal tension which promotes *SNAI2* expression, a neural crest specifier, and controls the malignant features of NB cells (Middelbeek et al., 2015). More recently a study showed that FTY-720 inhibited *TRPM7* channel kinase activation and signaling and at low concentrations, sensitized drug-resistant NB cells to antineoplastic drugs (Lange et al., 2017). As such, FTY-720 may serve as a chemo-sensitizing agent when used in combination therapy.

Lamin A/C

Highly proliferative cancer cells have reduced or no expression of Lamin A/C, a major component of the nuclear lamina. This characteristic was verified by enhanced self-renewal of CSCs *in vitro* and increased ability to initiate tumors *in vivo* upon down regulation of Lamin A/C in NB cells (Nardella et al., 2015). More recently, Rauschert et al. (2017) reported that reintroducing Lamin A/C in NB reduced cell growth kinetics and impaired migration, invasion and anchorage-independent cell growth and led to cytoskeletal restructuring. Moreover, the introduction of lamin Δ50, known as Progerin, drove these NB cells into senescence.

L1-CAM

L1 cell adhesion molecule known as *L1-CAM*, is a well-established CSC marker in various tumors including gliomas (Bao et al., 2008) and NB (Rached et al., 2016) and has been shown to confer chemo- and radio-resistance (Held-Feindt et al., 2012; Rached et al., 2016) in these aggressive cancers. Bao et al. (2008) revealed co-segregation of $CD133^+$ and $L1\text{-}CAM^+$ glioma cells where $CD133^+$ glioma cells expressed higher levels of *L1-CAM* compared to $CD133^-$ glioma cells. The *L1-CAM* over-expressing cells also exhibited upregulation of other stem markers including the transcription factor Olig-2. Furthermore, *L1-CAM* over-expression rendered the cancers highly tumorigenic with increased self-renewal and metastatic potential (Bao et al., 2008). Rached et al. (2016) found that *MYCN*-amplified NB cell line IMR-32, representing NB with poor prognosis and lack of response to treatment, revealed significant overexpression of *L1-CAM* compared to non-*MYCN*-amplified SK-N-SH cells. Moreover, the downregulation of *L1-CAM* transcription using siRNA transfection showed significant inhibition of proliferation, migration, and tumor sphere formation, hence suggesting a role in tumorigenicity and maintenance of the CSC sub-population.

NEUROBLASTOMA CANCER STEM CELLS: FROM GENES TO THERAPIES

Neuroblastoma CSC Pathways and Proteins That Confer Therapeutic Resistance

Neuroblastoma CSCs have been found to exist in patient primary tumors as well as patient-derived xenograft samples and NB cell lines. This CSC sub-population exhibits high resistance to the currently available therapeutic approaches including chemo-, radio-, and small molecule inhibition therapy (**Table 2**). These strategies have been successful at eliminating the bulk, non-stem cancer cells, whereas leaving behind the highly aggressive, stem-like TICs.

Wnt/beta-Catenin Signaling and LRG5

One of the most studied pathways in NB affiliated with therapeutic-resistance is the Wnt/Beta-catenin pathway. Vangipuram et al. (2012) reported an over-expression of genes within the Wnt pathway as well as an increased protein expression of β-Catenin and p-GSK3β in *CD133*+ NB cells compared to $CD133^-$ cells. The increased expression of Wnt pathway activity conferred chemoresistance to the cancer stem-like $CD133^+$ cells, while inhibition of Wnt pathway decreased the viability of these cells, ultimately suggesting a protective role for Wnt signaling in the CSC population of NB (Vangipuram et al., 2012). The involvement of Wnt/β-Catenin pathway in inducing therapeutic resistance was further supported by a recent study which showed pro-apoptotic and anti-proliferative effects in an *in vivo* NB model after GSK3 inhibition (Kunnimalaiyaan et al., 2018). This mechanism has also been suggested in other cancers including Wilms' tumor (Pode-Shakked et al., 2011), colon cancer (Tenbaum et al., 2012), breast cancers (Hallett et al., 2012), pancreatic cancer (Cui et al., 2012) and glioblastoma (Kim et al., 2012).

Leucine-rich repeat-containing G-protein coupled receptors (LRGs) such as LRG5 is important for maintaining Wnt signaling by preventing its ubiquitination and degradation (Hao et al., 2012). Tumor samples from high-risk NB patients not only showed over-expression of Wnt signaling pathway, but also up-regulation of *LRG5* mRNA when grown as tumor-spheres. These tumor-spheres exhibited high expression of Wnt target genes and higher *in vivo* tumorigenicity (Coulon et al., 2011). Moreover, Vieira et al. (2017) demonstrated the important role of *LRG5* in regulating NB survival and proliferation via the MEK/ERK-Wnt/β-Catenin signaling pathways. In fact, MEK/ERK activity has been implicated in the maintenance of embryonic stem cells in the undifferentiated state as well as CSCs in glioma (Kwon et al., 2017), breast cancer (Baker et al., 2018), thyroid cancer (Wang K. et al., 2018), lung cancer (Ning et al., 2018), gastric cancer (Ning et al., 2018), glioblastoma (Wang F. et al., 2018) and rhabdomyosarcoma (Ciccarelli et al., 2016).

Considering the therapeutic implications of these findings, it is tempting to assume that multiple targeting of various

TABLE 2 | Summary table of the major CSC-targeted therapeutic approaches and strategies.

Molecular/Genetic Signature	References	Results
MidKine (MK)	Bilir et al., 2010	Clomipramine and lithium chloride are capable of potentiating vinorelbine cytotoxicity and Midkine, a heparin-binding growth factor, is not a resistance factor for the treatment of neuroblastoma cell lines with the mentioned drugs.
Notch and c-kit	Ayla et al., 2014	Cytotoxic effects of different drugs on neuroblastoma cell lines were not correlated with Notch and c-kit cell signaling.
MDR genes/proteins	Campos-Arroyo et al., 2016	Probenecid co-administered with cisplatin modulate the mRNA and protein expression of the drug efflux transporters MDR1, MRP2 and BCRP
mTOR	Carpentieri et al., 2016	*In vitro* treatment of neuroblastoma cancer cells with mTOR inhibitor (rapamycin) directly differentiates them into osteoblastic and hepatic lineage causing a reversal state of the tumor cells.
Telomerase	Castelo-Branco et al., 2011	Telomerase inhibition exhausts tumor-initiating cells of neural origin.
	Hjelmeland and Rich, 2011	Imetelstat, an oligonucleotide that directly inhibits telomerase activity and is in early clinical development, selectively induces differentiation of neural CSCs and disrupts their growth.
	Wesbuer et al., 2010	Telomerase inhibition increases sensitivity to radiotherapy. Its effect on chemotherapy depends on telomerase activity, the anticancer drug used and the NB cell line.
MAPK	Craig et al., 2016	MAPK inhibition blocks sphere formation in *MYCN*-amplified neuroblastoma cell lines.
Hypoxia	Das et al., 2008	Highly tumorigenic fraction of side population cells migrates to the hypoxic microenvironment in solid tumors *in vivo*.
	Marzi et al., 2007	Treatment of neuroblastoma cell lines with either hypoxia or antiblastic etoposide leads to progressive disappearance of neuronal type cells while maintaining the neural crest stem cells. These cells generate N component cells and fibromuscular progeny. Combination of both modes of treatments cooperated in abolishing the N cells and promoting the conversion to fibromuscular progeny, hence the exhaustion of the tumor.
SLRPs	Farace et al., 2015	Glioblastoma and neuroblastoma CSC-like populations promote increased SLRP activation which induces resistance to temozolomide treatment.
PLK1	Grinshtein et al., 2011	PLK1 inhibitor blocks the growth and survival of neuroblastoma tumor initiating cells in a therapeutic xenograft model.
Proteasome	Hämmerle et al., 2013	Dual therapy of retinoic acid and proteasome inhibitor induced apoptosis, decreased stem cell markers such as Nestin, Sox2 as well as Oct4, and impaired neurosphere formation in neuroblastoma cell lines.
ABDG2 and ABCA3	Hirschmann-Jax et al., 2004	A stable subset of stem cells called "side population (SP)" is identified in primary tumor cells. These SP cells express elevated levels of ABDG2 and ABCA3 and possess increased capacity to expel cytotoxic drugs, thereby developing higher resistance to chemotherapeutic drugs.
G-CSF receptor	Hsu et al., 2013	Isolation of G-CSF receptor-positive subpopulations from primary neuroblastoma tumors or NGP cell line which exhibit high tumorigenicity and capability of both self-renewal as well as differentiation to progeny cells.
Epigenetic modifiers	Ikegaki et al., 2013	Treatment of neuroblastoma cell lines with epigenetic modifiers results in stable malignant stem cell-like NB cells that highly express stem cell markers and have open chromatin structure.
CD133	Khalil et al., 2016	The use of the antiepileptic drug valproic acid (VPA) as a histone deacetylase inhibitor with antitumor activities has limitations. Treatment of four human neuroblastoma cell lines with VPA increased *CD133* expression and displayed higher proliferation of cells with lower sensitivity to cytostatic treatment.
	Vangipuram et al., 2010	*CD133*+ NB cells are more resistant to chemotherapeutic drugs than *CD133*- cells.
DLK1	Kim et al., 2016	The therapeutic effects of β-carotene on CSCs depend on retinoic acid receptor β which interacts with and downregulates the CSC marker *DLK1*.
	Lee et al., 2013	β-carotene treatment strongly reduces cell growth and induces neuronal differentiation along with downregulation of *DLK1* in neuroblastoma CSCs.
	Lim et al., 2014	In a xenograft model, β-carotene treatment induced tumor cell differentiation and suppressed CSC markers such as Oct 3/4 and *DLK1*. It also down-regulated *HIF-1*α expression and its downstream VEGF.
	Park et al., 2012	Mulberry leaf (ML) extract significantly enhanced the differentiation and reduced sphere formation of neuroblastoma stem cell-like population. Moreover, knock-down of *DLK1* enhanced the inhibitory effect of ML on CSCs.
LIN28/Let-7	Lozier et al., 2015	Difluoromethylornithine (DFMO) treatment on NB cell lines reduced LIN28B and MYCN protein levels, increased Let-7 miRNA and decreased neurosphere formation. DFMO treatment *in vivo* decreased the glycolytic metabolic activity by inhibiting ornithine decarboxylase and restored balance to LIN28/Let-7 axis.

(Continued)

TABLE 2 | Continued

Molecular/Genetic Signature	References	Results
Oct4 and Nanog	Monajemzadeh et al., 2014	Neuroblastoma tumors from 47 patients showed high expression of the stem cell markers Oct4 (23 cases) and Nanog (8 cases), but no strong association between them and the prognostic factors.
BRCA1	Morozova et al., 2010	The profiling of 11 NB TIC lines from 6 NB patients using next-generation RNA sequencing and/or human exon arrays showed frequent mis-expression in the genes of the BRCA1 signaling pathway. The Ingenuity Pathways Analysis tool was applied to predict AURKB drug as a potential novel target for NB.
AMPK	Mouhieddine et al., 2015	Treatment of neuroblastoma cell lines with AMPK pathway activator (Metformin) or inhibitor (Ara-a) significantly reduced the CSCs proliferation and survival in a 2D and 3D tumor-sphere model.
PI3/Akt, RAS-Raf-ERK signaling, p38-MAPK, and TGF-β receptors II and III	Naveen et al., 2016	Neuroblastoma cell lines treated with berberine induced neuronal differentiation, inhibited proliferation, restored tumor suppressor proteins, increased epithelial markers and reverted mesenchymal markers. It instigated reversal of EMT by downregulating PI3/Akt and RAS-Raf-ERK signaling, and upregulating p38-MAPK. It also modulated TGF-β receptors II and III.
EGCG	Nishimura et al., 2012	Epigallocatechin gallate (EGCG), the most abundant catechin in green tea, induced growth arrest and apoptosis in neuroblastoma TICs. It also inhibited sphere formation of parental cells but did not affect the growth of serum-free spheres.
γδ T cells	Nishio et al., 2012	Zoledronate, a mevalonate pathway inhibitor, sensitizes neuroblastoma cell line and the enriched TICs to γδ T-cell- mediated cytolysis. Treatment with both was able to inhibit sphere formation *in vitro* and to decelerate the outgrowth of neuroblastoma TICs *in vivo*.
Intercellular interaction	Choi et al., 2013	Perfluorooctanoic acid (PFOA) and perfluorooctanesulfonic acid (PFOS) decreased the expression of E-cadherin and connexin-43 mRNAs in N2a neuronal cells grown in culture as 2D or 3D.
Endosialin/CD248/TEM1	Rouleau et al., 2011	Endosialin is shown to be expressed in neuroblastoma cell lines, including the CSC-like side population, and in human neuroblastoma xenograft tumors suggesting it to be a suitable therapeutic target.
TrKA	Ruggeri et al., 2014	TrkAIII upregulated SOD2 expression, increased mitochondrial SOD2 activity and attenuated the accumulation of mitochondrial free radical ROS, thereby promoting NB cell line resistance to mitochondrial free radical ROS-mediated death and increasing tumor stem cell-like phenotype.
TAS2Rs	Seo et al., 2017	Increased taste receptors TAS2Rs expression in NB cell lines was associated with increased differentiation, neurite elongation and down regulation of CSC markers with suppressed self-renewal characteristics.
DECA-14 and rapamycin	Smith et al., 2010	DECA-14 and rapamycin induced TIC death *in vitro*, reduced NB xenograft tumor growth and decreased self-renewal and tumor-initiation capacity.
TNKS1	Tian et al., 2014	Inhibition of TNKS1 by small molecule inhibitor or by siRNA knockdown decreased CSC markers and cellular migration ability in *CD133*-isolated neuroblastoma cells.
NDM29	Vella et al., 2015	Over-expression of NDM29 by a small molecule increased the susceptibility of NB cells to cisplatin through decreased ABC transporter expression, responsible for drug resistance.
VEGFRs	Zhang et al., 2009	Sunitinib, a kinase inhibitor of platelet derived growth factor receptors and VEGFRs, inhibited tumor cell proliferation and phosphorylation of VEGFRs in NB cell lines derived from patient tumor samples. In a tumor xenograft model, it inhibited tumor growth, angiogenesis and metastasis. Its use with rapamycin demonstrated synergistic cytotoxicity.
N-myc	Zheng et al., 2013	N-myc-amplified NB cells may become enriched with a CSC-like sub-population after long term drug selection with doxorubicin. Treatment with intermittent low doses of vorinostat downregulates stemness gene expression and sensitizes the drug-resistant cells.
Tubulin polymerization and replicative enzymes	Diaz-Carballo et al., 2014	Different small molecules isolated from Cuban propolis were able to selectively target CSCs from NB tumors in a pleiotropic manner. Of these small molecules, flavonoid was detected, and it disrupts tubulin polymerization, four PPAP-like compounds were isolated and DEHP (CZ6) was determined to inhibit replicative enzymes.

tumorigenic pathways may prove beneficial in sensitizing the cancers by eradicating the CSCs within them. In fact, combined targeting of the Wnt signaling with chemotherapy further sensitized the malignant NB cell lines to the treatment, by inducing differentiation. The target genes of the inhibitor, identified by microarray analysis, included *p21*, *p53*, ubiquitin C, *ZBED8*, *MDM2*, *CASP3*, and *FZD1* (Suebsoonthron et al., 2017), thereby explaining the enhanced sensitivity of the malignant NB cell lines to chemotherapy after Wnt signaling inhibition.

ABC Transporters

While therapeutic resistance in NB CSCs may be due to several cellular mechanisms, it is likely to be driven by the common MDR mechanism, which is mediated by the ATP-Binding Cassettes (ABC) drug efflux transporters such as MDR1, several

MRP and BCRP (Gottesman et al., 2002). Various studies have implicated the role of ABC drug efflux transporters in therapeutic resistance of CSCs.

A recent study reported an increased sensitivity of NB stem cells to combined treatment of the antineoplastic drug (cisplatin) with transporter inhibitor (probenecid) (Campos-Arroyo et al., 2016). The combined treatment led to reduced colony forming capacity of the CSCs, increased apoptosis and decreased proliferation. The authors also reported enhanced caspase-3 activity and significant down-regulation of both mRNA and protein expression of MDR1, MRP2 and BCRP (Campos-Arroyo et al., 2016); therefore, suggesting that the transcriptional inhibition of these proteins prevented drug efflux and allowed the drug to remain longer within the CSCs, ultimately inducing the observed apoptotic effect. Moreover, probenecid decreased the side population of the NB CSCs and reduced the percentage of stem marker CD133 as well as EMT markers vimentin and snail (Campos-Arroyo et al., 2016). In brief, if CSCs are forced back into a "non-stem state" by inducing their differentiation or preventing their EMT progression, therapeutic resistance subsides.

Another study by Vella et al. (2015) demonstrated a reduced growth rate of NB nodules and an increased overall survival of the mice in an animal model treated with chemotherapy (cisplatin) combined with a drug that induces NB differentiation (perhexiline). The pharmacologic induction of NDM29 induced NB differentiation and decreased the protein expression of ABC transporters, specifically in TICs/CSCs thereby increasing the chemotherapeutic sensitivity of this malignant, treatment-evasive NB sub-population.

Other studies have also reported similar findings with NB *CD133+* cells exhibiting up-regulated expression of the ABC transporters and leading to their therapeutic resistance. The possible mechanism by which the *CD133+* cells resist the chemo-therapy may be via up-regulation of ABC transporters that efflux the drug out of the cells (Al-Dimassi et al., 2014), thereby hindering the drugs from inducing their apoptotic effects on the CSCs.

Signaling Cascades Involved in Tumorigenesis

AMPK

The AMP-activated protein kinase pathway has been affiliated with driving the malignant behaviors of many tumors including brain cancers (Rehman et al., 2014; Li et al., 2017). Drugs that target this pathway have been investigated to elucidate their role in eliminating cancerous growth. Stem-like TICs within the bulk of tumors have been found to respond to such therapies. A study by Mouhieddine et al. (2015) demonstrated that Metformin, an AMPK activator and Ara-a, an AMPK pathway inhibitor both significantly reduced NB and glioma CSC proliferation and survival in a 2D and 3D tumor-sphere model. The importance of this finding lies in the fact that while the two drugs work antagonistically to each other, their anticancer effects may be due to the inhibitory effects on the mTOR pathway and Akt achieved with Metformin, and the energy deprivation achieved with Ara-a-induced inhibition of AMPK, thereby starving the CSCs. Furthermore, being a nucleoside analog, Ara-a may induce anti-cancer effects by interfering with DNA synthesis in these cells. In fact, the authors report the higher potency of Ara-a on these cancers (Mouhieddine et al., 2015).

MAPK and PI3K/mTOR

Various studies have demonstrated the efficacy of mTOR pathway inhibition on reducing tumor growth and specifically inhibiting proliferation of CSCs. Smith et al. (2010) reported that rapamycin, an mTOR inhibitor, successfully decreased cell viability and proliferation in an *in vitro,* NB patient-derived CSCs model. This activity was mediated by dephosphorylation of mTOR downstream targets $p70^{S6K}$ and S6RP. We further validated this finding in a recent study from our lab, where triciribine and rapamycin were used to study the role of inhibiting two different points of the Akt/mTOR pathway *in vitro* on U251 (glioblastoma) and SH-SY5Y (NB) human cell lines and their CSCs (Bahmad et al., 2018). Both drugs decreased the SFU of glioblastoma and NB cells thus extinguishing their CSC populations (Bahmad et al., 2018). On the other hand, apoptotic markers, such as cleaved PARP and increased sub-2n DNA were observed after rapamycin treatment in NB CSCs (Smith et al., 2010). In addition, it has been reported that NB CSCs infected with mTOR shRNA demonstrated 70–80% growth inhibition compared to mock-infected NB CSCs. Daily *in vivo* rapamycin treatment of mice bearing NB tumors successfully reduced tumor weight by >70% compared to only 43.4% achieved with vinblastine treatment, the standard chemotherapeutic drug used for NB. Tumor-sphere formation in the NB CSCs was also reported to be significantly (7.75-fold) inhibited after rapamycin treatment compared to vehicle-treated CSCs, thereby implicating the CSC-targeting ability of rapamycin (Smith et al., 2010).

As previously well established, *P53* functions to suppress mTOR pathway under stressful conditions in cells. When cells undergo stress, the functional P53 protein triggers transcription of proteins that negatively regulate the IGF/AKT/mTOR pathway to induce cell-cycle arrest, DNA repair, senescence or apoptosis, depending on the stressor and tumor type (Moreno-Smith et al., 2017). As such, combination therapy that stabilizes P53 expression along with mTOR inhibitors may prove more efficacious than single therapy that often leads to resistance. Moreno-Smith et al. (2017) reported on the enhanced effects of temsirolimus (mTOR inhibitor) when combined with *P53* activators (Nutlin 3a, a first-generation and RG7388 a second-generation MDM2 inhibitor) in an *in vivo* model of NB. The combined therapy enhanced the anti-proliferative and pro-apoptotic effects of single-agent therapy, implicating the importance of *P53* stabilization in inducing mTOR inhibition and subsequent cellular apoptosis. This was further tested in an orthotopic, *in vivo* pre-clinical model using both *MYCN*-amplified and non-amplified cell lines. In both cell lines used, the combination therapy was significantly more potent in anti-tumor activity compared to either monotherapy. More importantly, the combination therapy led to long-term cessation

of tumor growth after treatment withdrawal by induced apoptosis (Moreno-Smith et al., 2017).

Hypoxia and Retinoic Acid

The common link between mTOR, PI3K and insulin-like growth factor (IGF) in NB is hypoxia (Påhlman and Mohlin, 2018). In fact, hypoxic regions of NB have been reported to express the hypoxia-inducible factors 1 and 2 (*HIF1* and *HIF2*), which coincidently, confer stem-like features in these cells, including immature, neural-crest like cells with self-renewal potential. In addition, *HIF2* and IGF co-expression is correlated in clinical NB specimens, and *IGF* regulates hypoxic expression of *HIF2* (Påhlman and Mohlin, 2018). Moreover, IGF receptor binding induces PI3K signaling which subsequently drives tumorigenesis such as cancerous growth, survival and differentiation. PI3K and mTOR activation by growth factors also initiates *HIF1* translation, therefore the PI3K/mTOR pathways are putative candidate mediators of IGF-driven *HIF* expression and activity in NB and CSC maintenance and proliferation (Påhlman and Mohlin, 2018).

Inducing differentiation of NB CSCs may render them more sensitive to therapeutic intervention. Retinoic acid is clinically used to induce cancer differentiation in patients that have undergone induction and consolidation chemotherapy for high-risk NB (Duffy et al., 2017). RA (13-*cis*-retinoic acid) is a well-known differentiating agent reported to reduce stemness characteristics in various tumors including NB (Craig et al., 2016). Cimmino et al. (2015) demonstrated that *HIF1A* silencing combined with ATRA treatment led to differentiation and senescence of NB cells into a more benign, glial lineage that would render them therapeutically responsive.

Interestingly, combined RA treatment with proteasome inhibition using MG132 led to growth arrest and differentiation, inhibition of tumor-sphere formation and apoptosis in NB CSCs. Stem markers Nestin, Sox2, and Oct-4 were all reduced with the combination therapy as compared to monotherapy (Hämmerle et al., 2013), exemplifying the importance of differentiation inducers used together with other agents to enhance the anti-CSC effect in the malignant, sub-population of these NB tumors.

Epigenetics

The vast majority of NB tumors in children arise due to somatic mutations, as opposed to germline mutations of the anaplastic lymphoma kinase (ALK) gene in familial neuroblastoma, accounting for 2% of the cases (Mosse et al., 2008). Nonetheless, epigenetic regulation has been the suspected culprit believed to play a critical role driving these malignancies. The heterogeneity of NB tumors is therefore believed to be driven by a combination of somatic mutations and epigenetically-regulated factors. In fact, epigenetic modifications have been reported to induce a stem-like cancer cell in NB (Muñoz et al., 2012; Kobayashi et al., 2013; Toh et al., 2017). Specifically, the epigenetically-induced NB CSCs exhibited high expression of stemness factors and stem cell markers, they had open chromatin structure, increased tumor-initiating ability and metastatic potential. Moreover, they had a highly undifferentiated histological appearance with over-expression of *MYC/MYCN* (Ikegaki et al., 2013).

MYCN has been shown to interact with epigenetic machinery (He et al., 2013) and Duffy et al. (2017) reported that epigenetic regulators, including HDACs and BRD4, were differentially activated in *MYCN*-amplified NB, affecting the RA-induced differentiation in these cells. The authors reported that RA inhibits *HDAC* functioning while *MYCN* overexpression activates it. An important regulator identified in this study was *TGFB1*, a ligand for TGF-β signaling pathway. Pharmacological activation of the TGF-β signaling pathway using KGN, a small molecule that indirectly enhances TGF-β signaling by regulating the activity of SMAD transcriptional effectors, was used in combination with RA to determine the effect of this dual therapy on NB differentiation and malignancy. Both compounds used as sole therapy yielded a modest differentiation response, but in combination, exerted a more potent response and reduced viability in the *MYCN*-amplified NB cells (Duffy et al., 2017), thereby signifying the importance of using combination therapy in *MYCN*-amplified, high-risk NB patients to reach better clinical outcomes.

Others have also shown that *HDAC* inhibition via vorinostat in *MYCN*-amplified NB cells reduced chemo-resistance (DOX response) and *in vitro* invasive potential, inhibited tumor-sphere formation and down-regulated stem marker expression in NB CSCs (Zheng et al., 2013). And yet another group reported on the synergistic effect of combining RA with the *HDAC* inhibitor CBHA in an *in vivo*, human xenograft NB model (Coffey et al., 2001). This was achieved via the inhibition of AKT signaling pathway and survivin (Shah et al., 2013), whose expression usually promote tumor cell proliferation and inhibit apoptosis.

Moreover, combined therapy with *HDAC* inhibitors and ATRA down-regulated c-*Myc*, the neuronal markers *NeuN* and β-3 tubulin, as well as the oncoprotein *BMI1*, and more potently reduced cellular proliferation in NB cell lines (Almeida et al., 2017). Knowing that *BMI1* is a potent stem cell maintenance oncoprotein, this combination therapy may prove effective due to eliminating the CSC sub-population in the aggressive form of NB. As previously reported, *BMI1* is capable of repressing *P53* responses in NB precursors leading to NB initiation (Calao et al., 2012). Furthermore, *BMI1* can directly bind to p53 in a complex with other Polycomb complex proteins, Ring1A or Ring1B, leading to increased p53 ubiquitination and degradation. Another study revealed that *BMI1* expression positively correlated with a nucleotide binding protein BORIS/CTCFL, found to be aberrantly expressed in various malignancies and primarily re-expressed in CSCs (Garikapati et al., 2017). The authors of this study demonstrated an important cross-talk between BORIS/CTCFL and Wnt/β-catenin signaling pathways that led to enhanced expression of stemness proteins and increased EMT markers such as N-CAD, Vimentin and SNAIL. This intricate network of communication between *BMI1*, *BORIS/CTCFL* and *Wnt* signaling plays a crucial role that confers therapeutic resistance and malignancy in the aggressive *MYCN*-amplified NB cell line.

Delta-Like 1

Another important player in hypoxia-induced cancer stemness, as mentioned above, is the *DLK1*, which has been shown to be up-regulated after hypoxia induction in neuronal tumors (Kim et al., 2009). Its protein up-regulation enhances tumor stemness and tumorigenic growth *in vivo*, whereas its silencing drives cellular differentiation and reduces the tumorigenic potential in NB CSCs (Begum et al., 2014).

The combined treatment of NB cells with RA and *DLK1* knock-down led to significantly higher levels of cellular differentiation compared to monotherapy with either agent. Interestingly, the *DLK1* effects seem to be mediated via prohibition *PHB1* and *PHB2* interactions which have previously been reported to play roles in cellular proliferation, apoptosis, transcription, mitochondrial folding and cell signaling (Theiss and Sitaraman, 2011). The authors in Begum et al. (2014) demonstrated that the interaction between *DLK1* and both *PHB1* and *PHB2* via its cytoplasmic domain, bring about NB cell stemness and tumor-sphere self-renewal. They showed that knock-down of either *PHB* or *DLK1* reduces the clonogenic and self-renewal potential of NB CSCs. This interaction was a novel finding and thus, an important avenue to explore in multi-targeted approaches aimed at eliminating the CSCs within the bulk of the tumor along with the differentiated, non-stem cancer cells.

G-CSF/STAT3

Granulocyte-colony stimulation factor receptor positive or *CD114+* NB cells have stem-like characteristics that render them highly tumorigenic, self-renewing, with a treatment evasive phenotype (Hsu et al., 2013). Acting via *STAT3* stimulation and up-regulation, G-CSF presents itself as a very attractive target for NB CSC elimination and for increasing the potential long-term cancer-free survival in children. In fact, Agarwal et al. (2015) demonstrated that anti-G-CSF antibody or *STAT3* inhibition led to depletion of CSC subpopulation within tumors which was correlated with tumor growth inhibition, decreased metastasis, and increased chemo-sensitivity in a pre-clinical NB animal model. Such an observation warrants the consideration of a multi-modality therapeutic approach that targets the G-CSF-STAT3 signaling in the NB CSCs together with the standard chemotherapeutic drugs in order to completely eradicate the high-risk NB.

Gheeya et al. (2009) had previously demonstrated that *STAT3* inhibition using Cucurbitacin I induced an antitumor effect in various solid tumors including NB with and without *MYCN*-amplification. More recently, Honokiol, a biphenolic natural product isolated from the bark and leaves of Magnolia plant, and an inhibitor of the *STAT3* signaling pathway was reported to inhibit cancerous growth in various tumors including NB (Prasad and Katiyar, 2016). Yet another natural inhibitor of *STAT3* called curcumin or turmeric (diferuloylmethane), also known as an inhibitor of *Akt*, *COX2* and *NF-κB* signaling, demonstrated anti-cancer properties which rendered it a chemo-sensitizing agent against various tumors including glioma, NB, cervical carcinoma, epidermal carcinoma, prostate cancer, and colon cancer (Goel and Aggarwal, 2010).

L1-CAM

One of the prominent players in driving tumorigenic invasion and motility is *L1-CAM* (Zaatiti et al., 2018) whose suppression was explored as a therapeutic strategy in various tumors. Bao et al. (2008) reported that shRNA knock-down of *L1-CAM* in $CD133^+$ glioma cells significantly reduced neurosphere self-renewal potential, increased apoptosis, but inhibited proliferation of CSCs. *L1-CAM* silencing suppressed tumor growth and increased survival in an *in vivo* xenograft mouse model (Bao et al., 2008). This silencing was associated with reduced expression of *Olig2*, but increased expression of the *p21* (*WAF1/CIP1*) tumor suppressor, suggesting their possible involvement in the $CD133^+$ driven mechanistic effects in glioma cells.

The CE7 epitope of L1-CAM (CD171) has been explored in the context of CAR-T therapy in NB tumors (Hong et al., 2014; Kunkele et al., 2017) and other cancers, including lung, ovarian (Hong et al., 2016), and renal carcinomas as well as glioblastomas (Hong et al., 2014). One study concluded that CE7 epitope of L1-CAM may be amenable to CAR-T targeted therapy and thus serves as an invaluable tool in adoptive immunotherapy (Hong et al., 2014). Moreover, in a more recent pre-clinical assessment, (Kunkele et al. (2017) tested the safety of targeting the CE7 epitope CD171 with CE7-CAR T cells and determined whether bioactive CAR-T cells may be generated from heavily pretreated NB patients with recurrent or refractory disease. Fortunately, the authors confirmed the efficacy and safety of the CE7 epitope on CD171 to be used as a CAR-T cell target for NB patients with recurrent/refractory disease (Kunkele et al., 2017).

Polo-Like Kinase 1 (PLK1)

Neuroblastoma CSCs have been previously reported to highly express the serine/threonine kinase, Polo-like kinase 1, a known inducer of G2/M-phase transition. Grinshtein et al. (2011) demonstrated that the PLK1 inhibitor, BI 2536 significantly reduced tumor growth in an *in vivo* xenograft therapeutic model of NB CSCs when administered alone or in combination with irinotecan, which is typically used in patients with refractory NB.

More recently, Pajtler et al. (2017) investigated the tumorigenic effects of a PLK1 competitive inhibitor, GSK461364, in both *in vitro* and *in vivo* NB models. This treatment led to significant reduction in cell viability and proliferation and it also induced cell cycle arrest and apoptosis. In addition, the growth of established xenograft tumors in nude mice was significantly delayed, whereas survival time in the treatment group significantly increased (Pajtler et al., 2017). This further highlights the importance of targeting the CSC drivers in an attempt to achieve better anti-tumor effects of the currently used therapeutic agents.

CONCLUSION AND FUTURE DIRECTIONS

A pressing challenge of nervous system tumors in general and NB, specifically, is to overcome the therapy-resistant nature of CSCs. The eminent role they play in aggravating chemoresistance and malignancy magnifies the need to identify (1) the molecular signatures and the genetic aberrations of CSCs in neuroblastoma and (2) the therapeutic intervention that has been used in targeting the stem cell dysregulations. Even though a unique set of CSC markers have not been identified yet, a group of molecules have been associated with a stem-like behavior in cells expressing them, on the molecular, cellular and functional levels. It is foreseeable that targeting the key players that confer stemness to CSCs can substantially eliminate the CSC-like phenotypes. Moreover, combination of multiple targeting strategies provides a potential therapeutic anti-cancer intervention that needs to be further tested and studied. In the field of neuroblastoma, the ongoing efforts in eradicating CSCs may allow for promoting the survival of the children in ways comparable to the progress seen with some leukemias (He et al., 2015; Al-Hussaini et al., 2016; Ruella et al., 2016; Desai et al., 2019).

AUTHOR CONTRIBUTIONS

All authors worked on study conception and design, analyzed and interpreted the data, drafted the manuscript, and read and approved the final draft. HFB and WA-K screened titles for relevance and abstracted the data from the eligible full text articles. TA-A and WA-K critically revised the manuscript with input from the entire team.

ACKNOWLEDGMENTS

We would like to thank all members in WA-K Laboratory (The WAK Lab) and TA-A Laboratory for their help on this work.

REFERENCES

Abdullah, L. N., and Chow, E. K.-H. (2013). Mechanisms of chemoresistance in cancer stem cells. *Clin. Transl. Med.* 2:3. doi: 10.1186/2001-1326-2-3

Agarwal, S., Lakoma, A., Chen, Z., Hicks, J., Metelitsa, L. S., Kim, E. S., et al. (2015). G-CSF promotes neuroblastoma tumorigenicity and metastasis via STAT3-dependent cancer stem cell activation. *Cancer Res.* 75, 2566–2579. doi: 10.1158/0008-5472.can-14-2946

Akashi, T., Shirasawa, T., and Hirokawa, K. (1994). Gene expression of CD24 core polypeptide molecule in normal rat tissues and human tumor cell lines. *Virchows Arch.* 425, 399–406.

Al-Dimassi, S., Abou-Antoun, T., and El-Sibai, M. (2014). Cancer cell resistance mechanisms: a mini review. *Clin. Transl. Oncol.* 16, 511–516. doi: 10.1007/s12094-014-1162-1

Al-Hussaini, M., Rettig, M. P., Ritchey, J. K., Karpova, D., Uy, G. L., Eissenberg, L. G., et al. (2016). Targeting CD123 in acute myeloid leukemia using a T-cell-directed dual-affinity retargeting platform. *Blood* 127, 122–131. doi: 10.1182/blood-2014-05-575704

Almeida, V. R., Vieira, I. A., Buendia, M., Brunetto, A. T., Gregianin, L. J., Brunetto, A. L., et al. (2017). Combined treatments with a retinoid receptor agonist and epigenetic modulators in human neuroblastoma cells. *Mol. Neurobiol.* 54, 7610–7619. doi: 10.1007/s12035-016-0250-3

Ayla, S., Bilir, A., Soner, B. C., Yilmaz-Dilsiz, O., Erguven, M., and Oktem, G. (2014). Notch signaling-related therapeutic strategies with novel drugs in neuroblastoma spheroids. *J. Pediatr. Hematol. Oncol.* 36, 37–44. doi: 10.1097/MPH.0b013e3182755c73

Bahmad, H. F., Mouhieddine, T. H., Chalhoub, R. M., Assi, S., Araji, T., Chamaa, F., et al. (2018). The Akt/mTOR pathway in cancer stem/progenitor cells is a potential therapeutic target for glioblastoma and neuroblastoma. *Oncotarget* 9, 33549–33561. doi: 10.18632/oncotarget.26088

Baker, A., Wyatt, D., Bocchetta, M., Li, J., Filipovic, A., Green, A., et al. (2018). Notch-1-PTEN-ERK1/2 signaling axis promotes HER2+ breast cancer cell proliferation and stem cell survival. *Oncogene* 37, 4489–4504. doi: 10.1038/s41388-018-0251-y

Bao, S., Wu, Q., Li, Z., Sathornsumetee, S., Wang, H., Mclendon, R. E., et al. (2008). Targeting cancer stem cells through L1CAM suppresses glioma growth. *Cancer Res.* 68, 6043–6048. doi: 10.1158/0008-5472.can-08-1079

Begum, A., Lin, Q., Yu, C., Kim, Y., and Yun, Z. (2014). Interaction of delta-like 1 homolog (*Drosophila*) with prohibitins and its impact on tumor cell clonogenicity. *Mol. Cancer Res.* 12, 155–164. doi: 10.1158/1541-7786.mcr-13-0360

Bhaskara, V. K., Mohanam, I., Rao, J. S., and Mohanam, S. (2012). Intermittent hypoxia regulates stem-like characteristics and differentiation of neuroblastoma cells. *PLoS One* 7:e30905. doi: 10.1371/journal.pone.0030905

Bilir, A., Erguven, M., Yazihan, N., Aktas, E., Oktem, G., and Sabanci, A. (2010). Enhancement of vinorelbine-induced cytotoxicity and apoptosis by clomipramine and lithium chloride in human neuroblastoma cancer cell line SH-SY5Y. *J. Neurooncol.* 100, 385–395. doi: 10.1007/s11060-010-0209-6

Buhagiar, A., and Ayers, D. (2015). Chemoresistance, cancer stem cells, and miRNA influences: the case for neuroblastoma. *Anal. Cell. Pathol.* 2015:150634. doi: 10.1155/2015/150634

Calao, M., Sekyere, E. O., Cui, H. J., Cheung, B. B., Thomas, W. D., Keating, J., et al. (2012). Direct effects of Bmi1 on p53 protein stability inactivates oncoprotein stress responses in embryonal cancer precursor cells at tumor initiation. *Oncogene* 32, 3616–3626. doi: 10.1038/onc.2012.368

Campos-Arroyo, D., Maldonado, V., Bahena, I., Quintanar, V., Patino, N., Carlos Martinez-Lazcano, J., et al. (2016). Probenecid sensitizes neuroblastoma cancer stem cells to cisplatin. *Cancer Invest.* 34, 155–166. doi: 10.3109/07357907.2016.1139717

Cantilena, S., Pastorino, F., Pezzolo, A., Chayka, O., Pistoia, V., Ponzoni, M., et al. (2011). Frizzled receptor 6 marks rare, highly tumourigenic stem-like cells in mouse and human neuroblastomas. *Oncotarget* 2, 976–983. doi: 10.18632/oncotarget.410

Cao, H.-Z., Liu, X.-F., Yang, W.-T., Chen, Q., and Zheng, P.-S. (2017). LGR5 promotes cancer stem cell traits and chemoresistance in cervical cancer. *Cell Death Dis.* 8:e3039. doi: 10.1038/cddis.2017.393

Carpentieri, A., Cozzoli, E., Scimeca, M., Bonanno, E., Sardanelli, A. M., and Gambacurta, A. (2016). Differentiation of human neuroblastoma cells toward the osteogenic lineage by mTOR inhibitor. *Cell Death Dis.* 7:e2202. doi: 10.1038/cddis.2016.60

Castelo-Branco, P., Zhang, C., Lipman, T., Fujitani, M., Hansford, L., Clarke, I., et al. (2011). Neural tumor-initiating cells have distinct telomere maintenance and can be safely targeted for telomerase inhibition. *Clin. Cancer Res.* 17, 111–121. doi: 10.1158/1078-0432.ccr-10-2075

Chakrabarti, L., Abou-Antoun, T., Vukmanovic, S., and Sandler, A. D. (2012). Reversible adaptive plasticity: a mechanism for neuroblastoma cell heterogeneity and chemo-resistance. *Front. Oncol.* 2:82. doi: 10.3389/fonc.2012.00082

Chavali, P. L., Saini, R. K., Matsumoto, Y., Agren, H., and Funa, K. (2011). Nuclear orphan receptor TLX induces Oct-3/4 for the survival and maintenance of adult hippocampal progenitors upon hypoxia. *J. Biol. Chem.* 286, 9393–9404. doi: 10.1074/jbc.M110.167445

Chavali, P. L., Saini, R. K., Zhai, Q., Vizlin-Hodzic, D., Venkatabalasubramanian, S., Hayashi, A., et al. (2014). TLX activates MMP-2, promotes self-renewal of tumor spheres in neuroblastoma and correlates with poor patient survival. *Cell Death Dis.* 5:e1502. doi: 10.1038/cddis.2014.449

Chen, X., Ye, S., and Ying, Q. L. (2015). Stem cell maintenance by manipulating signaling pathways: past, current and future. *BMB Rep.* 48, 668–676.

Chicas, A., Kapoor, A., Wang, X., Aksoy, O., Evertts, A. G., Zhang, M. Q., et al. (2012). H3K4 demethylation by Jarid1a and Jarid1b contributes to retinoblastoma-mediated gene silencing during cellular senescence. *Proc. Natl. Acad. Sci. U.S.A.* 109, 8971–8976. doi: 10.1073/pnas.1119836109

Choi, S. K., Kim, J. H., Park, J. K., Lee, K. M., Kim, E., and Jeon, W. B. (2013). Cytotoxicity and inhibition of intercellular interaction in N2a neurospheroids by perfluorooctanoic acid and perfluorooctanesulfonic acid. *Food Chem. Toxicol.* 60, 520–529. doi: 10.1016/j.fct.2013.07.070

Ciccarelli, C., Vulcano, F., Milazzo, L., Gravina, G. L., Marampon, F., Macioce, G., et al. (2016). Key role of MEK/ERK pathway in sustaining tumorigenicity and in vitro radioresistance of embryonal rhabdomyosarcoma stem-like cell population. *Mol. Cancer* 15:16. doi: 10.1186/s12943-016-0501-y

Ciccarone, V., Spengler, B. A., Meyers, M. B., Biedler, J. L., and Ross, R. A. (1989). Phenotypic diversification in human neuroblastoma cells: expression of distinct neural crest lineages. *Cancer Res.* 49, 219–225.

Cimmino, F., Pezone, L., Avitabile, M., Acierno, G., Andolfo, I., Capasso, M., et al. (2015). Inhibition of hypoxia inducible factors combined with all-trans retinoic acid treatment enhances glial transdifferentiation of neuroblastoma cells. *Sci. Rep.* 5:11158. doi: 10.1038/srep11158

Clark, K., Langeslag, M., Van Leeuwen, B., Ran, L., Ryazanov, A. G., Figdor, C. G., et al. (2006). TRPM7, a novel regulator of actomyosin contractility and cell adhesion. *EMBO J.* 25, 290–301. doi: 10.1038/sj.emboj.7600931

Coffey, D. C., Kutko, M. C., Glick, R. D., Butler, L. M., Heller, G., Rifkind, R. A., et al. (2001). The histone deacetylase inhibitor, CBHA, inhibits growth of human neuroblastoma xenografts *in vivo*, alone and synergistically with *all-trans* retinoic acid. *Cancer Res.* 61, 3591–3594.

Coulon, A., Flahaut, M., Muhlethaler-Mottet, A., Meier, R., Liberman, J., Balmas-Bourloud, K., et al. (2011). Functional sphere profiling reveals the complexity of neuroblastoma tumor-initiating cell model. *Neoplasia* 13, 991–1004.

Cournoyer, S., Nyalendo, C., Addioui, A., Belounis, A., Beaunoyer, M., Aumont, A., et al. (2012). Genotype analysis of tumor-initiating cells expressing CD133 in neuroblastoma. *Genes Chromosomes Cancer* 51, 792–804. doi: 10.1002/gcc.21964

Craig, B. T., Rellinger, E. J., Alvarez, A. L., Dusek, H. L., Qiao, J., and Chung, D. H. (2016). Induced differentiation inhibits sphere formation in neuroblastoma. *Biochem. Biophys. Res. Commun.* 477, 255–259. doi: 10.1016/j.bbrc.2016.06.053

Cui, H., Hu, B., Li, T., Ma, J., Alam, G., Gunning, W. T., et al. (2007). Bmi-1 is essential for the tumorigenicity of neuroblastoma cells. *Am. J. Pathol.* 170, 1370–1378. doi: 10.2353/ajpath.2007.060754

Cui, J., Jiang, W., Wang, S., Wang, L., and Xie, K. (2012). Role of Wnt/beta-catenin signaling in drug resistance of pancreatic cancer. *Curr. Pharm. Des.* 18, 2464–2471.

Daley, G. Q. (2015). Stem cells and the evolving notion of cellular identity. *Philos. Trans. R. Soc. Lond. B Biol. Sci.* 370:20140376. doi: 10.1098/rstb.2014.0376

Das, B., Tsuchida, R., Malkin, D., Koren, G., Baruchel, S., and Yeger, H. (2008). Hypoxia enhances tumor stemness by increasing the invasive and tumorigenic side population fraction. *Stem Cells* 26, 1818–1830. doi: 10.1634/stemcells.2007-0724

Dawood, S., Austin, L., and Cristofanilli, M. (2014). Cancer stem cells: implications for cancer therapy. *Oncology* 28, 1101–1107, 1110.

de Lau, W., Peng, W. C., Gros, P., and Clevers, H. (2014). The R-spondin/Lgr5/Rnf43 module: regulator of Wnt signal strength. *Genes Dev.* 28, 305–316. doi: 10.1101/gad.235473.113

Desai, A., Yan, Y., and Gerson, S. L. (2019). Concise reviews: cancer stem cell targeted therapies: toward clinical success. *Stem Cells Transl. Med.* 8, 75–81. doi: 10.1002/sctm.18-0123

Diaz-Carballo, D., Acikelli, A. H., Bardenheuer, W., Gustmann, S., Malak, S., Stoll, R., et al. (2014). Identification of compounds that selectively target highly chemotherapy refractory neuroblastoma cancer stem cells. *Int. J. Clin. Pharmacol. Ther.* 52, 787–801. doi: 10.5414/cp202154

Ding, X. W., Wu, J. H., and Jiang, C. P. (2010). ABCG2: a potential marker of stem cells and novel target in stem cell and cancer therapy. *Life Sci.* 86, 631–637. doi: 10.1016/j.lfs.2010.02.012

Duffy, D. J., Krstic, A., Halasz, M., Schwarzl, T., Konietzny, A., Iljin, K., et al. (2017). Retinoic acid and TGF-β signalling cooperate to overcome MYCN-induced retinoid resistance. *Genome Med.* 9:15. doi: 10.1186/s13073-017-0407-3

Farace, C., Oliver, J. A., Melguizo, C., Alvarez, P., Bandiera, P., Rama, A. R., et al. (2015). Microenvironmental modulation of decorin and lumican in temozolomide-resistant glioblastoma and neuroblastoma cancer stem-like cells. *PLoS One* 10:e0134111. doi: 10.1371/journal.pone.0134111

Flahaut, M., Jauquier, N., Chevalier, N., Nardou, K., Balmas Bourloud, K., Joseph, J. M., et al. (2016). Aldehyde dehydrogenase activity plays a Key role in the aggressive phenotype of neuroblastoma. *BMC Cancer* 16:781. doi: 10.1186/s12885-016-2820-1

Forgham, H., Johnson, D., Carter, N., Veuger, S., and Carr-Wilkinson, J. (2015). Stem cell markers in neuroblastoma-an emerging role for LGR5. *Front. Cell Dev. Biol.* 3:77. doi: 10.3389/fcell.2015.00077

Garikapati, K. R., Patel, N., Makani, V. K. K., Cilamkoti, P., Bhadra, U., and Bhadra, M. P. (2017). Down-regulation of BORIS/CTCFL efficiently regulates cancer stemness and metastasis in MYCN amplified neuroblastoma cell line by modulating Wnt/beta-catenin signaling pathway. *Biochem. Biophys. Res. Commun.* 484, 93–99. doi: 10.1016/j.bbrc.2017.01.066

Garner, E. F., and Beierle, E. A. (2015). Cancer stem cells and their interaction with the tumor microenvironment in neuroblastoma. *Cancers* 8:E5.

Gheeya, J. S., Chen, Q. R., Benjamin, C. D., Cheuk, A. T., Tsang, P., Chung, J. Y., et al. (2009). Screening a panel of drugs with diverse mechanisms of action yields potential therapeutic agents against neuroblastoma. *Cancer Biol. Ther.* 8, 2386–2395.

Goel, A., and Aggarwal, B. B. (2010). Curcumin, the golden spice from Indian saffron, is a chemosensitizer and radiosensitizer for tumors and chemoprotector and radioprotector for normal organs. *Nutr. Cancer* 62, 919–930. doi: 10.1080/01635581.2010.509835

Gottesman, M. M., Fojo, T., and Bates, S. E. (2002). Multidrug resistance in cancer: role of ATP-dependent transporters. *Nat. Rev. Cancer* 2, 48–58. doi: 10.1038/nrc706

Grinshtein, N., Datti, A., Fujitani, M., Uehling, D., Prakesch, M., Isaac, M., et al. (2011). Small molecule kinase inhibitor screen identifies polo-like kinase 1 as a target for neuroblastoma tumor-initiating cells. *Cancer Res.* 71, 1385–1395. doi: 10.1158/0008-5472.can-10-2484

Gudjonsson, T., and Magnusson, M. K. (2005). Stem cell biology and the cellular pathways of carcinogenesis. *APMIS* 113, 922–929. doi: 10.1111/j.1600-0463.2005.apm_371.x

Hallett, R. M., Kondratyev, M. K., Giacomelli, A. O., Nixon, A. M., Girgis-Gabardo, A., Ilieva, D., et al. (2012). Small molecule antagonists of the Wnt/beta-catenin signaling pathway target breast tumor-initiating cells in a Her2/Neu mouse model of breast cancer. *PLoS One* 7:e33976. doi: 10.1371/journal.pone.0033976

Hämmerle, B., Yañez, Y., Palanca, S., Cañete, A., Burks, D. J., Castel, V., et al. (2013). Targeting neuroblastoma stem cells with retinoic acid and proteasome inhibitor. *PLoS One* 8:e76761. doi: 10.1371/journal.pone.0076761

Hansford, L. M., Mckee, A. E., Zhang, L., George, R. E., Gerstle, J. T., Thorner, P. S., et al. (2007). Neuroblastoma cells isolated from bone marrow metastases contain a naturally enriched tumor-initiating cell. *Cancer Res.* 67, 11234–11243. doi: 10.1158/0008-5472.can-07-0718

Hao, H. X., Xie, Y., Zhang, Y., Charlat, O., Oster, E., Avello, M., et al. (2012). ZNRF3 promotes Wnt receptor turnover in an R-spondin-sensitive manner. *Nature* 485, 195–200. doi: 10.1038/nature11019

Hartomo, T. B., Van Huyen Pham, T., Yamamoto, N., Hirase, S., Hasegawa, D., Kosaka, Y., et al. (2015). Involvement of aldehyde dehydrogenase 1A2 in the regulation of cancer stem cell properties in neuroblastoma. *Int. J. Oncol.* 46, 1089–1098. doi: 10.3892/ijo.2014.2801

He, S., Liu, Z., Oh, D.-Y., and Thiele, C. (2013). MYCN and the epigenome. *Front. Oncol.* 3:1. doi: 10.3389/fonc.2013.00001

He, S. Z., Busfield, S., Ritchie, D. S., Hertzberg, M. S., Durrant, S., Lewis, I. D., et al. (2015). A Phase 1 study of the safety, pharmacokinetics and anti-leukemic activity of the anti-CD123 monoclonal antibody CSL360 in relapsed, refractory or high-risk acute myeloid leukemia. *Leuk. Lymphoma* 56, 1406–1415. doi: 10.3109/10428194.2014.956316

Held-Feindt, J., Schmelz, S., Hattermann, K., Mentlein, R., Mehdorn, H. M., and Sebens, S. (2012). The neural adhesion molecule L1CAM confers chemoresistance in human glioblastomas. *Neurochem. Int.* 61, 1183–1191. doi: 10.1016/j.neuint.2012.08.011

Hirsch, D., Barker, N., Mcneil, N., Hu, Y., Camps, J., Mckinnon, K., et al. (2014). LGR5 positivity defines stem-like cells in colorectal cancer. *Carcinogenesis* 35, 849–858. doi: 10.1093/carcin/bgt377

Hirschmann-Jax, C., Foster, A. E., Wulf, G. G., Nuchtern, J. G., Jax, T. W., Gobel, U., et al. (2004). A distinct "side population" of cells with high drug efflux capacity in human tumor cells. *Proc. Natl. Acad. Sci. U.S.A.* 101, 14228–14233. doi: 10.1073/pnas.0400067101

Hjelmeland, A. B., and Rich, J. N. (2011). Molecular targeting of neural cancer stem cells: TTAGGG, you're it! *Clin. Cancer Res.* 17, 3–5. doi: 10.1158/1078-0432.ccr-10-2686

Holmquist-Mengelbier, L., Fredlund, E., Lofstedt, T., Noguera, R., Navarro, S., Nilsson, H., et al. (2006). Recruitment of HIF-1alpha and HIF-2alpha to common target genes is differentially regulated in neuroblastoma: HIF-2alpha promotes an aggressive phenotype. *Cancer Cell* 10, 413–423. doi: 10.1016/j.ccr.2006.08.026

Hong, H., Brown, C. E., Ostberg, J. R., Priceman, S. J., Chang, W.-C., Weng, L., et al. (2016). L1 cell adhesion molecule-specific chimeric antigen receptor-redirected human T cells exhibit specific and efficient antitumor activity against human ovarian cancer in mice. *PLoS One* 11:e0146885. doi: 10.1371/journal.pone.0146885

Hong, H., Stastny, M., Brown, C., Chang, W. C., Ostberg, J. R., Forman, S. J., et al. (2014). Diverse solid tumors expressing a restricted epitope of L1-CAM can be targeted by chimeric antigen receptor redirected T lymphocytes. *J. Immunother.* 37, 93–104. doi: 10.1097/cji.0000000000000018

Hsu, D. M., Agarwal, S., Benham, A., Coarfa, C., Trahan, D. N., Chen, Z., et al. (2013). G-CSF receptor positive neuroblastoma subpopulations are enriched in chemotherapy-resistant or relapsed tumors and are highly tumorigenic. *Cancer Res.* 73, 4134–4146. doi: 10.1158/0008-5472.can-12-4056

Ikegaki, N., Shimada, H., Fox, A. M., Regan, P. L., Jacobs, J. R., Hicks, S. L., et al. (2013). Transient treatment with epigenetic modifiers yields stable neuroblastoma stem cells resembling aggressive large-cell neuroblastomas. *Proc. Natl. Acad. Sci. U.S.A.* 110, 6097–6102. doi: 10.1073/pnas.1118262110

Islam, M. O., Kanemura, Y., Tajria, J., Mori, H., Kobayashi, S., Hara, M., et al. (2005). Functional expression of ABCG2 transporter in human neural stem/progenitor cells. *Neurosci. Res.* 52, 75–82. doi: 10.1016/j.neures.2005.01.013

Jensen, T., Vadasz, S., Phoenix, K., Claffey, K., Parikh, N., and Finck, C. (2015). Descriptive analysis of tumor cells with stem like phenotypes in metastatic and benign adrenal tumors. *J. Pediatr. Surg.* 50, 1493–1501. doi: 10.1016/j.jpedsurg.2015.04.012

Jiang, M., Stanke, J., and Lahti, J. M. (2011). The connections between neural crest development and neuroblastoma. *Curr. Top. Dev. Biol.* 94, 77–127. doi: 10.1016/B978-0-12-380916-2.00004-8

Jin, J., Desai, B. N., Navarro, B., Donovan, A., Andrews, N. C., and Clapham, D. E. (2008). Deletion of Trpm7 disrupts embryonic development and thymopoiesis without altering Mg^{2+} homeostasis. *Science* 322, 756–760. doi: 10.1126/science.1163493

Jin, J., Wu, L. J., Jun, J., Cheng, X., Xu, H., Andrews, N. C., et al. (2012). The channel kinase, TRPM7, is required for early embryonic development. *Proc. Natl. Acad. Sci. U.S.A.* 109, E225–E233. doi: 10.1073/pnas.1120033109

Khalil, M. A., Hrabeta, J., Groh, T., Prochazka, P., Doktorova, H., and Eckschlager, T. (2016). Valproic acid increases CD133 positive cells that show low sensitivity to cytostatics in neuroblastoma. *PLoS One* 11:e0162916. doi: 10.1371/journal.pone.0162916

Kim, Y. (2010). Effect of retinoic acid and delta-like 1 homologue (DLK1) on differentiation in neuroblastoma. *Nutr. Res. Pract.* 4, 276–282. doi: 10.4162/nrp.2010.4.4.276

Kim, Y., Kim, K. H., Lee, J., Lee, Y. A., Kim, M., Lee, S. J., et al. (2012). Wnt activation is implicated in glioblastoma radioresistance. *Lab. Invest.* 92, 466–473. doi: 10.1038/labinvest.2011.161

Kim, Y., Lin, Q., Zelterman, D., and Yun, Z. (2009). Hypoxia-regulated delta-like 1 homologue enhances cancer cell stemness and tumorigenicity. *Cancer Res.* 69, 9271–9280. doi: 10.1158/0008-5472.CAN-09-1605

Kim, Y. S., Kim, E., Park, Y. J., and Kim, Y. (2016). Retinoic acid receptor beta enhanced the anti-cancer stem cells effect of beta-carotene by down-regulating expression of delta-like 1 homologue in human neuroblastoma cells. *Biochem. Biophys. Res. Commun.* 480, 254–260. doi: 10.1016/j.bbrc.2016.10.041

Kobayashi, K., Jakt, L. M., and Nishikawa, S. I. (2013). Epigenetic regulation of the neuroblastoma genes, *Arid3b* and *Mycn*. *Oncogene* 32, 2640–2648. doi: 10.1038/onc.2012.285

Koppaka, V., Thompson, D. C., Chen, Y., Ellermann, M., Nicolaou, K. C., Juvonen, R. O., et al. (2012). Aldehyde dehydrogenase inhibitors: a comprehensive review of the pharmacology, mechanism of action, substrate specificity, and clinical application. *Pharmacol. Rev.* 64, 520–539. doi: 10.1124/pr.111.005538

Krupkova, O Jr, Loja, T., Redova, M., Neradil, J., Zitterbart, K., Sterba, J., et al. (2011). Analysis of nuclear nestin localization in cell lines derived from neurogenic tumors. *Tumour Biol.* 32, 631–639. doi: 10.1007/s13277-011-0162-9

Kunkele, A., Taraseviciute, A., Finn, L. S., Johnson, A. J., Berger, C., Finney, O., et al. (2017). Preclinical assessment of CD171-directed CAR T-cell adoptive therapy for childhood neuroblastoma: CE7 epitope target safety and product manufacturing feasibility. *Clin. Cancer Res.* 23, 466–477. doi: 10.1158/1078-0432.ccr-16-0354

Kunnimalaiyaan, S., Schwartz, V. K., Jackson, I. A., Clark Gamblin, T., and Kunnimalaiyaan, M. (2018). Antiproliferative and apoptotic effect of LY2090314, a GSK-3 inhibitor, in neuroblastoma in vitro. *BMC Cancer* 18:560. doi: 10.1186/s12885-018-4474-7

Kuo, Y. T., Liu, Y. L., Adebayo, B. O., Shih, P. H., Lee, W. H., Wang, L. S., et al. (2015). JARID1B expression plays a critical role in chemoresistance and stem cell-like phenotype of neuroblastoma cells. *PLoS One* 10:e0125343. doi: 10.1371/journal.pone.0125343

Kwon, S. J., Kwon, O. S., Kim, K. T., Go, Y. H., Yu, S. I., Lee, B. H., et al. (2017). Role of MEK partner-1 in cancer stemness through MEK/ERK pathway in cancerous neural stem cells, expressing EGFRviii. *Mol. Cancer* 16:140. doi: 10.1186/s12943-017-0703-y

Laborda, J. (2000). The role of the epidermal growth factor-like protein dlk in cell differentiation. *Histol. Histopathol.* 15, 119–129. doi: 10.14670/HH-15.119

Lange, I., Espinoza-Fuenzalida, I., Ali, M. W., Serrano, L. E., and Koomoa, D. T. (2017). FTY-720 induces apoptosis in neuroblastoma via multiple signaling pathways. *Oncotarget* 8, 109985–109999. doi: 10.18632/oncotarget.22452

Lau, S. T., Hansford, L. M., Chan, W. K., Chan, G. C., Wan, T. S., Wong, K. K., et al. (2015). Prokineticin signaling is required for the maintenance of a de novo population of c-KIT^{+}cells to sustain neuroblastoma progression. *Oncogene* 34, 1019–1034. doi: 10.1038/onc.2014.24

Lee, H. A., Park, S., and Kim, Y. (2013). Effect of beta-carotene on cancer cell stemness and differentiation in SK-N-BE(2)C neuroblastoma cells. *Oncol. Rep.* 30, 1869–1877. doi: 10.3892/or.2013.2643

Li, J., Zhong, L., Wang, F., and Zhu, H. (2017). Dissecting the role of AMP-activated protein kinase in human diseases. *Acta Pharm. Sin. B* 7, 249–259. doi: 10.1016/j.apsb.2016.12.003

Li, Q., Shi, L., Gui, B., Yu, W., Wang, J., Zhang, D., et al. (2011). Binding of the JmjC demethylase JARID1B to LSD1/NuRD suppresses angiogenesis and metastasis in breast cancer cells by repressing chemokine CCL14. *Cancer Res.* 71, 6899–6908. doi: 10.1158/0008-5472.can-11-1523

Lim, J. Y., Kim, Y. S., Kim, K. M., Min, S. J., and Kim, Y. (2014). Beta-carotene inhibits neuroblastoma tumorigenesis by regulating cell differentiation and cancer cell stemness. *Biochem. Biophys. Res. Commun.* 450, 1475–1480. doi: 10.1016/j.bbrc.2014.07.021

Lozier, A. M., Rich, M. E., Grawe, A. P., Peck, A. S., Zhao, P., Chang, A. T., et al. (2015). Targeting ornithine decarboxylase reverses the LIN28/Let-7 axis and inhibits glycolytic metabolism in neuroblastoma. *Oncotarget* 6, 196–206. doi: 10.18632/oncotarget.2768

Lubanska, D., and Porter, L. A. (2014). The atypical cell cycle regulator Spy1 suppresses differentiation of the neuroblastoma stem cell population. *Oncoscience* 1, 336–348. doi: 10.18632/oncoscience.36

Lutz, W., Fulda, S., Jeremias, I., Debatin, K. M., and Schwab, M. (1998). MycN and IFNgamma cooperate in apoptosis of human neuroblastoma cells. *Oncogene* 17, 339–346. doi: 10.1038/sj.onc.1200201

Marzi, I., D'amico, M., Biagiotti, T., Giunti, S., Carbone, M. V., Fredducci, D., et al. (2007). Purging of the neuroblastoma stem cell compartment and tumor

regression on exposure to hypoxia or cytotoxic treatment. *Cancer Res.* 67, 2402–2407. doi: 10.1158/0008-5472.can-06-3208

Mehrazma, M., Madjd, Z., Kalantari, E., Panahi, M., Hendi, A., and Shariftabrizi, A. (2013). Expression of stem cell markers, CD133 and CD44, in pediatric solid tumors: a study using tissue microarray. *Fetal Pediatr. Pathol.* 32, 192–204. doi: 10.3109/15513815.2012.701266

Menaa, F., Houben, R., Eyrich, M., Broecker, E. B., Becker, J. C., and Wischhusen, J. (2009). Stem cells, melanoma and cancer stem cells: the good, the bad and the evil? *G. Ital. Dermatol. Venereol.* 144, 287–296.

Middelbeek, J., Kuipers, A. J., Henneman, L., Visser, D., Eidhof, I., Van Horssen, R., et al. (2012). TRPM7 is required for breast tumor cell metastasis. *Cancer Res.* 72, 4250–4261. doi: 10.1158/0008-5472.can-11-3863

Middelbeek, J., Visser, D., Henneman, L., Kamermans, A., Kuipers, A. J., Hoogerbrugge, P. M., et al. (2015). TRPM7 maintains progenitor-like features of neuroblastoma cells: implications for metastasis formation. *Oncotarget* 6, 8760–8776. doi: 10.18632/oncotarget.3315

Miraglia, S., Godfrey, W., Yin, A. H., Atkins, K., Warnke, R., Holden, J. T., et al. (1997). A novel five-transmembrane hematopoietic stem cell antigen: isolation, characterization, and molecular cloning. *Blood* 90, 5013–5021.

Mizrak, D., Brittan, M., and Alison, M. R. (2008). CD133: molecule of the moment. *J. Pathol.* 214, 3–9. doi: 10.1002/path.2283

Molofsky, A. V., Pardal, R., Iwashita, T., Park, I. K., Clarke, M. F., and Morrison, S. J. (2003). Bmi-1 dependence distinguishes neural stem cell self-renewal from progenitor proliferation. *Nature* 425, 962–967. doi: 10.1038/nature02060

Monajemzadeh, M., Soleimani, V., Vasei, M., Koochakzadeh, L., and Karbakhsh, M. (2014). Expression and prognostic significance of Oct4 and Nanog in neuroblastoma. *APMIS* 122, 734–741. doi: 10.1111/apm.12207

Moore, M. A., Williams, N., and Metcalf, D. (1973). In vitro colony formation by normal and leukemic human hematopoietic cells: characterization of the colony-forming cells. *J. Natl. Cancer Inst.* 50, 603–623.

Moreno-Smith, M., Lakoma, A., Chen, Z., Tao, L., Scorsone, K. A., Schild, L., et al. (2017). p53 non-genotoxic activation and mTORC1 inhibition lead to effective combination for neuroblastoma therapy. *Clin. Cancer Res.* 23, 6629–6639. doi: 10.1158/1078-0432.ccr-17-0668

Morozova, O., Vojvodic, M., Grinshtein, N., Hansford, L. M., Blakely, K. M., Maslova, A., et al. (2010). System-level analysis of neuroblastoma tumor-initiating cells implicates AURKB as a novel drug target for neuroblastoma. *Clin. Cancer Res.* 16, 4572–4582. doi: 10.1158/1078-0432.ccr-10-0627

Mosse, Y. P., Laudenslager, M., Longo, L., Cole, K. A., Wood, A., Attiyeh, E. F., et al. (2008). Identification of ALK as a major familial neuroblastoma predisposition gene. *Nature* 455, 930–935. doi: 10.1038/nature07261

Mouhieddine, T. H., Nokkari, A., Itani, M. M., Chamaa, F., Bahmad, H., Monzer, A., et al. (2015). Metformin and Ara-a effectively suppress brain cancer by targeting cancer stem/progenitor cells. *Front. Neurosci.* 9:442. doi: 10.3389/fnins.2015.00442

Munchar, M. J., Sharifah, N. A., Jamal, R., and Looi, L. M. (2003). CD44s expression correlated with the International Neuroblastoma Pathology Classification (Shimada system) for neuroblastic tumours. *Pathology* 35, 125–129.

Muñoz, P., Iliou, M. S., and Esteller, M. (2012). Epigenetic alterations involved in cancer stem cell reprogramming. *Mol. Oncol.* 6, 620–636. doi: 10.1016/j.molonc.2012.10.006

Nakata, S., Campos, B., Bageritz, J., Bermejo, J. L., Becker, N., Engel, F., et al. (2013). LGR5 is a marker of poor prognosis in glioblastoma and is required for survival of brain cancer stem-like cells. *Brain Pathol.* 23, 60–72. doi: 10.1111/j.1750-3639.2012.00618.x

Nardella, M., Guglielmi, L., Musa, C., Iannetti, I., Maresca, G., Amendola, D., et al. (2015). Down-regulation of the Lamin A/C in neuroblastoma triggers the expansion of tumor initiating cells. *Oncotarget* 6, 32821–32840. doi: 10.18632/oncotarget.5104

Naveen, C. R., Gaikwad, S., and Agrawal-Rajput, R. (2016). Berberine induces neuronal differentiation through inhibition of cancer stemness and epithelial-mesenchymal transition in neuroblastoma cells. *Phytomedicine* 23, 736–744. doi: 10.1016/j.phymed.2016.03.013

Ning, X., Zhang, H., Wang, C., and Song, X. (2018). Exosomes released by gastric cancer cells induce transition of Pericytes into cancer-associated fibroblasts. *Med. Sci. Monit.* 24, 2350–2359.

Nishimura, N., Hartomo, T. B., Pham, T. V., Lee, M. J., Yamamoto, T., Morikawa, S., et al. (2012). Epigallocatechin gallate inhibits sphere formation of neuroblastoma BE(2)-C cells. *Environ. Health Prev. Med.* 17, 246–251. doi: 10.1007/s12199-011-0239-5

Nishio, N., Fujita, M., Tanaka, Y., Maki, H., Zhang, R., Hirosawa, T., et al. (2012). Zoledronate sensitizes neuroblastoma-derived tumor-initiating cells to cytolysis mediated by human gammadelta T cells. *J. Immunother.* 35, 598–606. doi: 10.1097/CJI.0b013e31826a745a

Nowak, K., Kerl, K., Fehr, D., Kramps, C., Gessner, C., Killmer, K., et al. (2006). BMI1 is a target gene of E2F-1 and is strongly expressed in primary neuroblastomas. *Nucleic Acids Res.* 34, 1745–1754. doi: 10.1093/nar/gkl119

Opel, D., Poremba, C., Simon, T., Debatin, K. M., and Fulda, S. (2007). Activation of Akt predicts poor outcome in neuroblastoma. *Cancer Res.* 67, 735–745. doi: 10.1158/0008-5472.can-06-2201

Påhlman, S., and Mohlin, S. (2018). Hypoxia and hypoxia-inducible factors in neuroblastoma. *Cell Tissue Res.* 372, 269–275. doi: 10.1007/s00441-017-2701-1

Pajtler, K. W., Sadowski, N., Ackermann, S., Althoff, K., Schonbeck, K., Batzke, K., et al. (2017). The GSK461364 PLK1 inhibitor exhibits strong antitumoral activity in preclinical neuroblastoma models. *Oncotarget* 8, 6730–6741. doi: 10.18632/oncotarget.14268

Park, S., Kim, J., and Kim, Y. (2012). Mulberry leaf extract inhibits cancer cell stemness in neuroblastoma. *Nutr. Cancer* 64, 889–898. doi: 10.1080/01635581.2012.707280

Pode-Shakked, N., Harari-Steinberg, O., Haberman-Ziv, Y., Rom-Gross, E., Bahar, S., Omer, D., et al. (2011). Resistance or sensitivity of Wilms' tumor to anti-FZD7 antibody highlights the Wnt pathway as a possible therapeutic target. *Oncogene* 30, 1664–1680. doi: 10.1038/onc.2010.549

Prasad, R., and Katiyar, S. K. (2016). "Honokiol, an active compound of magnolia plant, inhibits growth, and progression of cancers of different organs," in *Anti-inflammatory Nutraceuticals and Chronic Diseases*, eds S. C. Gupta, S. Prasad, and B. B. Aggarwal (Cham: Springer), 245–265.

Rabadan, M. A., Usieto, S., Lavarino, C., and Marti, E. (2013). Identification of a putative transcriptome signature common to neuroblastoma and neural crest cells. *Dev. Neurobiol.* 73, 815–827. doi: 10.1002/dneu.22099

Rached, J., Nasr, Z., Abdallah, J., and Abou-Antoun, T. (2016). L1-CAM knockdown radiosensitizes neuroblastoma IMR-32 cells by simultaneously decreasing MycN, but increasing PTEN protein expression. *Int. J. Oncol.* 49, 1722–1730. doi: 10.3892/ijo.2016.3625

Rauschert, I., Aldunate, F., Preussner, J., Arocena-Sutz, M., Peraza, V., Looso, M., et al. (2017). Promoter hypermethylation as a mechanism for Lamin A/C silencing in a subset of neuroblastoma cells. *PLoS One* 12:e0175953. doi: 10.1371/journal.pone.0175953

Rehman, G., Shehzad, A., Khan, A. L., and Hamayun, M. (2014). Role of AMP-activated protein kinase in cancer therapy. *Arch. Pharm.* 347, 457–468. doi: 10.1002/ardp.201300402

Rettig, W. J., Spengler, B. A., Chesa, P. G., Old, L. J., and Biedler, J. L. (1987). Coordinate changes in neuronal phenotype and surface antigen expression in human neuroblastoma cell variants. *Cancer Res.* 47, 1383–1389.

Reya, T., Morrison, S. J., Clarke, M. F., and Weissman, I. L. (2001). Stem cells, cancer, and cancer stem cells. *Nature* 414, 105–111. doi: 10.1038/35102167

Ross, R. A., and Spengler, B. A. (2007). Human neuroblastoma stem cells. *Semin. Cancer Biol.* 17, 241–247. doi: 10.1016/j.semcancer.2006.04.006

Ross, R. A., Spengler, B. A., Domenech, C., Porubcin, M., Rettig, W. J., and Biedler, J. L. (1995). Human neuroblastoma I-type cells are malignant neural crest stem cells. *Cell Growth Differ.* 6, 449–456.

Ross, R. A., Walton, J. D., Han, D., Guo, H. F., and Cheung, N. K. (2015). A distinct gene expression signature characterizes human neuroblastoma cancer stem cells. *Stem Cell Res.* 15, 419–426. doi: 10.1016/j.scr.2015.08.008

Rouleau, C., Smale, R., Sancho, J., Fu, Y. S., Kurtzberg, L., Weber, W., et al. (2011). Endosialin: a novel malignant cell therapeutic target for neuroblastoma. *Int. J. Oncol.* 39, 841–851. doi: 10.3892/ijo.2011.1091

Ruella, M., Barrett, D. M., Kenderian, S. S., Shestova, O., Hofmann, T. J., Perazzelli, J., et al. (2016). Dual CD19 and CD123 targeting prevents antigen-loss relapses after CD19-directed immunotherapies. *J. Clin. Invest.* 126, 3814–3826. doi: 10.1172/jci87366

Ruggeri, P., Farina, A. R., Di Ianni, N., Cappabianca, L., Ragone, M., Ianni, G., et al. (2014). The TrkAIII oncoprotein inhibits mitochondrial free radical

ROS-induced death of SH-SY5Y neuroblastoma cells by augmenting SOD2 expression and activity at the mitochondria, within the context of a tumour stem cell-like phenotype. *PLoS One* 9:e94568. doi: 10.1371/journal.pone.0094568

Sartelet, H., Imbriglio, T., Nyalendo, C., Haddad, E., Annabi, B., Duval, M., et al. (2012). CD133 expression is associated with poor outcome in neuroblastoma via chemoresistance mediated by the AKT pathway. *Histopathology* 60, 1144–1155. doi: 10.1111/j.1365-2559.2012.04191.x

Sayegh, J., Cao, J., Zou, M. R., Morales, A., Blair, L. P., Norcia, M., et al. (2013). Identification of small molecule inhibitors of Jumonji AT-rich interactive domain 1B (JARID1B) histone demethylase by a sensitive high throughput screen. *J. Biol. Chem.* 288, 9408–9417. doi: 10.1074/jbc.M112.419861

Seo, Y., Kim, Y. S., Lee, K. E., Park, T. H., and Kim, Y. (2017). Anti-cancer stemness and anti-invasive activity of bitter taste receptors, TAS2R8 and TAS2R10, in human neuroblastoma cells. *PLoS One* 12:e0176851. doi: 10.1371/journal.pone.0176851

Shah, R. D., Jagtap, J. C., Mruthyunjaya, S., Shelke, G. V., Pujari, R., Das, G., et al. (2013). Sodium valproate potentiates staurosporine-induced apoptosis in neuroblastoma cells via Akt/survivin independently of HDAC inhibition. *J. Cell. Biochem.* 114, 854–863. doi: 10.1002/jcb.24422

Shi, Y., Chichung Lie, D., Taupin, P., Nakashima, K., Ray, J., Yu, R. T., et al. (2004). Expression and function of orphan nuclear receptor TLX in adult neural stem cells. *Nature* 427, 78–83. doi: 10.1038/nature02211

Siapati, E. K., Rouka, E., Kyriakou, D., and Vassilopoulos, G. (2011). Neuroblastoma cells negative for CD44 possess tumor-initiating properties. *Cell. Oncol.* 34, 189–197. doi: 10.1007/s13402-011-0022-z

Singh, S. K., Clarke, I. D., Terasaki, M., Bonn, V. E., Hawkins, C., Squire, J., et al. (2003). Identification of a cancer stem cell in human brain tumors. *Cancer Res.* 63, 5821–5828.

Smith, K. M., Datti, A., Fujitani, M., Grinshtein, N., Zhang, L., Morozova, O., et al. (2010). Selective targeting of neuroblastoma tumour-initiating cells by compounds identified in stem cell-based small molecule screens. *EMBO Mol. Med.* 2, 371–384. doi: 10.1002/emmm.201000093

Suebsoonthron, J., Jaroonwitchawan, T., Yamabhai, M., and Noisa, P. (2017). Inhibition of WNT signaling reduces differentiation and induces sensitivity to doxorubicin in human malignant neuroblastoma SH-SY5Y cells. *Anticancer Drugs* 28, 469–479. doi: 10.1097/cad.0000000000000478

Suzuki, S., Namiki, J., Shibata, S., Mastuzaki, Y., and Okano, H. (2010). The neural stem/progenitor cell marker Nestin is expressed in proliferative endothelial cells, but not in mature vasculature. *J. Histochem. Cytochem.* 58, 721–730. doi: 10.1369/jhc.2010.955609

Takenobu, H., Shimozato, O., Nakamura, T., Ochiai, H., Yamaguchi, Y., Ohira, M., et al. (2011). CD133 suppresses neuroblastoma cell differentiation via signal pathway modification. *Oncogene* 30, 97–105. doi: 10.1038/onc.2010.383

Tenbaum, S. P., Ordonez-Moran, P., Puig, I., Chicote, I., Arques, O., Landolfi, S., et al. (2012). beta-catenin confers resistance to PI3K and AKT inhibitors and subverts FOXO3a to promote metastasis in colon cancer. *Nat. Med.* 18, 892–901. doi: 10.1038/nm.2772

Theiss, A. L., and Sitaraman, S. V. (2011). The role and therapeutic potential of prohibitin in disease. *Biochim. Biophys. Acta* 1813, 1137–1143. doi: 10.1016/j.bbamcr.2011.01.033

Thomas, S. K., Messam, C. A., Spengler, B. A., Biedler, J. L., and Ross, R. A. (2004). Nestin is a potential mediator of malignancy in human neuroblastoma cells. *J. Biol. Chem.* 279, 27994–27999. doi: 10.1074/jbc.M312663200

Tian, X., Hou, W., Bai, S., Fan, J., Tong, H., and Xu, H. (2014). XAV939 inhibits the stemness and migration of neuroblastoma cancer stem cells via repression of tankyrase 1. *Int. J. Oncol.* 45, 121–128. doi: 10.3892/ijo.2014.2406

Toh, T. B., Lim, J. J., and Chow, E. K.-H. (2017). Epigenetics in cancer stem cells. *Mol. Cancer* 16:29. doi: 10.1186/s12943-017-0596-9

Tong, Q. S., Zheng, L. D., Tang, S. T., Ruan, Q. L., Liu, Y., Li, S. W., et al. (2008). Expression and clinical significance of stem cell marker CD133 in human neuroblastoma. *World J. Pediatr.* 4, 58–62. doi: 10.1007/s12519-008-0012-z

van Limpt, V., Chan, A., Caron, H., Sluis, P. V., Boon, K., Hermus, M. C., et al. (2000). SAGE analysis of neuroblastoma reveals a high expression of the human homologue of the Drosophila Delta gene. *Med. Pediatr. Oncol.* 35, 554–558.

Vangipuram, S. D., Buck, S. A., and Lyman, W. D. (2012). Wnt pathway activity confers chemoresistance to cancer stem-like cells in a neuroblastoma cell line. *Tumor Biol.* 33, 2173–2183. doi: 10.1007/s13277-012-0478-0

Vangipuram, S. D., Wang, Z. J., and Lyman, W. D. (2010). Resistance of stem-like cells from neuroblastoma cell lines to commonly used chemotherapeutic agents. *Pediatr. Blood Cancer* 54, 361–368. doi: 10.1002/pbc.22351

Vasiliou, V., Vasiliou, K., and Nebert, D. W. (2009). Human ATP-binding cassette (ABC) transporter family. *Hum. Genomics* 3, 281–290.

Vella, S., Penna, I., Longo, L., Pioggia, G., Garbati, P., Florio, T., et al. (2015). Perhexiline maleate enhances antitumor efficacy of cisplatin in neuroblastoma by inducing over-expression of NDM29 ncRNA. *Sci. Rep.* 5:18144. doi: 10.1038/srep18144

Vieira, G. C., Chockalingam, S., Melegh, Z., Greenhough, A., Malik, S., Szemes, M., et al. (2017). Correction: LGR5 regulates pro-survival MEK/ERK and proliferative Wnt/beta-catenin signalling in neuroblastoma. *Oncotarget* 8:32381. doi: 10.18632/oncotarget.17685

Walton, J. D., Kattan, D. R., Thomas, S. K., Spengler, B. A., Guo, H.-F., Biedler, J. L., et al. (2004). Characteristics of stem cells from human neuroblastoma cell lines and in tumors. *Neoplasia* 6, 838–845.

Wang, F., Wang, A. Y., Chesnelong, C., Yang, Y., Nabbi, A., Thalappilly, S., et al. (2018). ING5 activity in self-renewal of glioblastoma stem cells via calcium and follicle stimulating hormone pathways. *Oncogene* 37, 286–301. doi: 10.1038/onc.2017.324

Wang, K., Ji, W., Yu, Y., Li, Z., Niu, X., Xia, W., et al. (2018). FGFR1-ERK1/2-SOX2 axis promotes cell proliferation, epithelial-mesenchymal transition, and metastasis in FGFR1-amplified lung cancer. *Oncogene* 37, 5340–5354. doi: 10.1038/s41388-018-0311-3

Wesbuer, S., Lanvers-Kaminsky, C., Duran-Seuberth, I., Bolling, T., Schafer, K. L., Braun, Y., et al. (2010). Association of telomerase activity with radio- and chemosensitivity of neuroblastomas. *Radiat. Oncol.* 5:66. doi: 10.1186/1748-717x-5-66

Yanai, H., Atsumi, N., Tanaka, T., Nakamura, N., Komai, Y., Omachi, T., et al. (2017). Intestinal cancer stem cells marked by Bmi1 or Lgr5 expression contribute to tumor propagation via clonal expansion. *Sci. Rep.* 7:41838. doi: 10.1038/srep41838

Yang, L., Tang, H., Kong, Y., Xie, X., Chen, J., Song, C., et al. (2015). LGR5 promotes breast cancer progression and maintains stem-like cells through activation of Wnt/beta-catenin signaling. *Stem Cells* 33, 2913–2924. doi: 10.1002/stem.2083

Yin, A. H., Miraglia, S., Zanjani, E. D., Almeida-Porada, G., Ogawa, M., Leary, A. G., et al. (1997). AC133, a novel marker for human hematopoietic stem and progenitor cells. *Blood* 90, 5002–5012.

Yin, D., Xie, D., Sakajiri, S., Miller, C. W., Zhu, H., Popoviciu, M. L., et al. (2006). DLK1: increased expression in gliomas and associated with oncogenic activities. *Oncogene* 25, 1852–1861. doi: 10.1038/sj.onc.1209219

Zaatiti, H., Abdallah, J., Nasr, Z., Khazen, G., Sandler, A., and Abou-Antoun, T. J. (2018). Tumorigenic proteins upregulated in the MYCN-amplified IMR-32 human neuroblastoma cells promote proliferation and migration. *Int. J. Oncol.* 52, 787–803. doi: 10.3892/ijo.2018.4236

Zhang, L., Smith, K. M., Chong, A. L., Stempak, D., Yeger, H., Marrano, P., et al. (2009). *In vivo* antitumor and antimetastatic activity of sunitinib in preclinical neuroblastoma mouse model. *Neoplasia* 11, 426–435.

Zheng, X., Naiditch, J., Czurylo, M., Jie, C., Lautz, T., Clark, S., et al. (2013). Differential effect of long-term drug selection with doxorubicin and vorinostat on neuroblastoma cells with cancer stem cell characteristics. *Cell Death Dis.* 4:e740. doi: 10.1038/cddis.2013.264

Conflict of Interest Statement: The authors declare that the research was conducted in the absence of any commercial or financial relationships that could be construed as a potential conflict of interest.

frontiers in Molecular Neuroscience

REVIEW
published: 09 July 2019
doi: 10.3389/fnmol.2019.00164

Post-translational Regulation of GLT-1 in Neurological Diseases and Its Potential as an Effective Therapeutic Target

*Allison R. Peterson and Devin K. Binder**

Center for Glial-Neuronal Interactions, Division of Biomedical Sciences, School of Medicine, University of California, Riverside, Riverside, CA, United States

Glutamate transporter-1 (GLT-1) is a Na^+-dependent transporter that plays a key role in glutamate homeostasis by removing excess glutamate in the central nervous system (CNS). GLT-1 dysregulation occurs in various neurological diseases including Huntington's disease (HD), Alzheimer's disease (AD), Parkinson's disease (PD), amyotrophic lateral sclerosis (ALS), and epilepsy. Downregulation or dysfunction of GLT-1 has been a common finding across these diseases but how this occurs is still under investigation. This review aims to highlight post-translational regulation of GLT-1 which leads to its downregulation including sumoylation, palmitoylation, nitrosylation, ubiquitination, and subcellular localization. Various therapeutic interventions to restore GLT-1, their proposed mechanism of action and functional effects will be examined as potential treatments to attenuate the neurological symptoms associated with loss or downregulation of GLT-1.

Keywords: GLT-1, palmitoylation, S-nitrosylation, sumoylation, ubiquitination, post-translational modifications

OPEN ACCESS

Edited by:
Kimberly Frances Raab-Graham, Wake Forest School of Medicine, United States

Reviewed by:
Nien-Pei Tsai, University of Illinois at Urbana–Champaign, United States
Paul Allen Rosenberg, Boston Children's Hospital, Harvard Medical School, United States

***Correspondence:**
Devin K. Binder
dbinder@ucr.edu

Received: *14 January 2019*
Accepted: *14 June 2019*
Published: *09 July 2019*

Citation:
Peterson AR and Binder DK (2019) Post-translational Regulation of GLT-1 in Neurological Diseases and Its Potential as an Effective Therapeutic Target. Front. Mol. Neurosci. 12:164. doi: 10.3389/fnmol.2019.00164

INTRODUCTION

Glutamate transporter-1 (GLT-1), also known as excitatory amino acid transporter 2 (EAAT2), is part of a family of Na^+-dependent transporters that regulate extracellular glutamate homeostasis in the CNS. Na^+-dependent glutamate transporters represent the most significant mechanism of removal of glutamate from the extracellular space and are essential in maintaining low and non-toxic concentrations of glutamate (reviewed in Danbolt, 2001). Glutamate transporter-1 is responsible for glutamate clearance from the synaptic cleft and is essential for maintaining low levels of extracellular glutamate (Levy et al., 1995). GLT-1 is expressed primarily in astrocytes and has been shown to be expressed in axon terminals of neurons (Chen et al., 2004; Furness et al., 2008; Petr et al., 2015; Zhou et al., 2019). Mice that globally lack GLT-1 develop spontaneous seizures associated with high mortality (Tanaka et al., 1997). Mice lacking GLT-1 selectively in the dorsal forebrain survive to adulthood and display transient focal seizures (Sugimoto et al., 2018). These findings revealed the important functional role of GLT-1 in extracellular glutamate modulation.

Glutamate transporter-1 expression has been shown to be altered in many neurological diseases. Huntington's disease (HD) is an autosomal dominant disease that is characterized by degeneration of the striatum and selective cortical degeneration (Jimenez-Sanchez et al., 2017). Downregulation of GLT-1 has been observed in HD and may be responsible for the impaired glutamate uptake and

glutamate toxicity observed in the R6 model of HD (Lievens et al., 2001; Estrada-Sanchez et al., 2009). Similar changes in gene expression patterns associated with transcriptional dysregulation in HD is observed in neuronal GLT-1 KO mice, suggesting neuronal GLT-1 loss in HD may lead to transcriptional dysregulation (Laprairie et al., 2019). Alzheimer's disease (AD) is a neurodegenerative disorder which causes the gradual accumulation of Aβ and Aβ-associated proteins (Selkoe, 2000). Post-mortem tissue from individuals with a clinical history of dementia characteristic of AD show loss of GLT-1 immunoreactivity near amyloid plaques (Jacob et al., 2007). Partial loss of GLT-1 also accelerates cognitive deficit onset in the AβPPswe/PS1ΔE9 mouse model of AD (Mookherjee et al., 2011). Parkinson's disease (PD) is a progressive neurological disorder characterized by tremor, rigidity and akinesia (Lang and Lozano, 1998). L-dopa-induced dyskinesia (LID) is often seen in patients with PD. LID severity is reduced when GLT-1 protein levels are increased in a rat 6-hydroxydopamine model of PD (Chotibut et al., 2017). Amyotrophic lateral sclerosis (ALS) is also a neurodegenerative disorder that causes both progressive and selective loss of motor neurons in the CNS (Tapia, 2014). Loss of GLT-1 has been reported during disease progression in both patients and the G85R-SOD1 mouse model of ALS (Bruijn et al., 1997; Lin et al., 1998). Epilepsy is a condition that is characterized by both recurrent and unprovoked seizures (Hauser et al., 1998). GLT-1 protein levels showed a regional decrease in epilepsy patients with hippocampal sclerosis and cortical dysplasia and in the intrahippocampal kainic acid (IHKA) model of epilepsy (Proper et al., 2002; Hubbard et al., 2016).

Glutamate transporter-1 has become an attractive target for therapeutic intervention due to its dysregulation in neurological diseases. To effectively restore GLT-1 protein levels, the mechanisms which lead to its downregulation should be investigated. Post-translational modulation of GLT-1 has been shown to contribute to its downregulation in various neurological diseases and therefore it is important to understand post-translational mechanisms to develop selective treatment strategies for individual diseases.

EXPRESSION AND ROLES OF GLT-1 IN NEURONS VS. ASTROCYTES

Glutamate transporter-1 is expressed in astrocytes and presynaptic terminals of excitatory neurons. Perisynaptic astrocytic processes (PAPs) express high levels of GLT-1, with approximately 80% of total GLT-1 protein expression found in astrocytes. Neuronal GLT-1 expression accounts for only 5–10% of the total GLT-1 protein expression (Furness et al., 2008). Historically, astrocytic GLT-1 has been thought to be responsible for the majority of glutamate regulation. Interestingly, even though GLT-1 is expressed at low levels in axon terminals, studies from the Danbolt and Rosenberg labs showed that neuronal GLT-1 contributes significantly to glutamate uptake in synaptosomes (Danbolt et al., 2016; Rimmele and Rosenberg, 2016; Zhou et al., 2019). When GLT-1 is deleted in neurons, glutamate uptake capacity (V_{max}) in synaptosomes is significantly reduced by approximately 40% whereas deletion of GLT-1 from astrocytes did not show a significant reduction in synaptosomal glutamate uptake capacity (V_{max}). These results suggest that neuronal GLT-1 transporters, although expressed at low levels, play an important role in glutamate clearance at excitatory synapses where maintaining low levels of extracellular glutamate is critical for proper neuronal function and transmission. Importantly, however, selective ablation of GLT-1 from astrocytes results in lethal spontaneous seizures suggesting that astrocytic GLT-1 protects against fatal epilepsy (Petr et al., 2015). This finding also suggests that astrocytic GLT-1 is vital to maintain low levels of extracellular glutamate in the CNS to prevent glutamate excitotoxicity. Conversely, mice lacking neuronal GLT-1 showed normal survival and no seizures.

Differences in GLT-1 protein expression *in vivo* vs. *in vitro* is an aspect of glutamate transporter regulation that is important to take into consideration prior to exploring GLT-1 dysregulation in models of disease. Primary astrocyte cultures express mostly glutamate aspartate transporter (GLAST), another member of the Na^+-dependent glutamate transporter family, and low levels of GLT-1 (Swanson et al., 1997; Carbone et al., 2012a). Primary astrocyte cultures also maintain a polygonal morphology, dissimilar to astrocytes of brain gray matter, and are considered undifferentiated. Interestingly, astrocytes co-cultured with neurons display a stellate morphology with branched morphology and express GLT-1 and GLAST, suggesting that neurons are responsible for regulating astrocytic glutamate transporters, particularly GLT-1. Expression of glutamate transporters has also been shown to be regulated by cAMP and neuron-conditioned medium (Swanson et al., 1997; Schlag et al., 1998). Neurons can regulate astrocytic glutamate transporters via signaling through soluble factors dependent on neuronal activity (Perego et al., 2000). The activity and cellular localization of expressed glutamate transporters can be regulated by post-translational modifications (PTMs). This review will focus on post-translational regulation of GLT-1 in neurological diseases and we will distinguish cell type-specific GLT-1 regulation if identified in the following studies (**Table 1**).

POST-TRANSLATIONAL REGULATION OF GLT-1

Palmitoylation

Palmitoylation is a post-translational lipid modification that refers to the reversible thioesterification of palmitic acid to cysteine residues (Parenti et al., 1993). Palmitoylation is important for both protein function and regulation while depalmitoylation has been shown to affect protein trafficking and localization (Kong et al., 2013). Protein palmitoylation is important for neuronal development and synaptic function (el-Husseini and Bredt, 2002). Aberrant palmitoylation has been linked to neurological diseases including HD and AD (Vetrivel et al., 2009; Butland et al., 2014).

All proteins associated with the family of Na^+-dependent glutamate transporters have been shown to be palmitoylated including GLT-1 (Kang et al., 2008). Hayden's group at the

TABLE 1 | Glutamate transporter-1 dysregulation in neurological disease models including potential therapeutics to prevent GLT-1 downregulation.

Disease model	GLT-1 post-translational regulation	Potential therapeutic	Therapeutic effect	Citation
SOD1-G93A mouse model of amyotrophic lateral sclerosis (ALS)	Caspase-3 cleaves SUMO1-conjugated GLT-1 leading to accumulation of sumoylated CTE fragments of GLT-1 in astrocyte nuclei during disease progression	Ceftriaxone	Ceftriaxone delayed loss of neurons, muscle strength and increased mouse survival	Rothstein et al., 2005; Foran et al., 2014
YAC128 mouse model of Huntington's disease (HD)	GLT-1 uptake reduced in the striatum and cortex corresponding to a decrease in GLT-1 palmitoylation with no changes in GLT-1 protein expression	–	–	Huang et al., 2010
MPTP mouse model of Parkinson's disease (PD)	Ubiquitin ligase Nedd4-2 mediates the PKC-dependent ubiquitination and degradation of GLT-1	Ceftriaxone	Ceftriaxone decreased behavioral deficits and neurodegeneration	Zhang et al., 2017
Lafora disease (LD) mouse model	Decreased levels of GLT-1 protein expression at the plasma membrane with no change in GLT-1 total protein expression levels suggesting a change in subcellular localization	–	–	Munoz-Ballester et al., 2016
Aβ-42 *in vitro* treatment modeling Alzheimer's disease (AD)	Decreased levels of GLT-1 cell surface expression with no alteration in GLT-1 total protein levels in astrocyte cultures treated with Aβ-42	Vitamin E derivative (Trolox)	Normal levels of detergent-insoluble GLT-1 were restored by pretreatment with Trolox in Aβ-42-treated astrocyte cultures	Scimemi et al., 2013
R6/2 transgenic mouse model of Huntington's disease (HD)	Decreased levels of GLT-1 expression in the cortex and striatum at 13 weeks of age when mice are severely symptomatic	Ceftriaxone	Increased cortical and striatal GLT-1 levels	Sari et al., 2010

Glutamate transporter-1 is SUMO1-conjugated and internalized in the SOD1-G93A model of ALS. GLT-1 expression is decreased in R6/2 model of HD. GLT-1 glutamate uptake and palmitoylation is decreased in the YAC128 model of HD. GLT-1 is degraded following Nedd4-2 mediated ubiquitination in MPTP model of PD. GLT-1 is recruited to the 20S proteasome for degradation via HSP90β in the kainic acid model of TLE. GLT-1 plasma membrane protein levels are decreased in LD mice. GLT-1 cell surface expression is decreased in a model of AD.

University of British Columbia found that reduced GLT-1 palmitoylation is observed in multiple models of HD (Huang et al., 2010). GLT-1 palmitoylation was shown to be significantly reduced in the STHdh-Q111 HD striatal cell line. HD is caused by an expansion in CAG trinucleotide repeats in the gene encoding huntingtin (HTT) where increased repeat length is correlated with severity of disease (Andrew et al., 1993). The STHdh-Q111 cells express a full length mutant HTT with 111 CAG repeats. Since GLT-1 is expressed at low levels in neurons, Hayden's group overexpressed GLT-1 in these cells to examine GLT-1 palmitoylation. [^{3}H] metabolic labeling showed that the HD striatal cells had a significant reduction in GLT-1 palmitoylation compared to the wt STHdh-7Q cell line. These results suggested that there was a reduction in PTM in the presence of the mutant HTT.

Altered GLT-1 palmitoylation can impair GLT-1 glutamate uptake and may be a factor contributing to the enhancement of excitatory transmission observed in HD (Huang et al., 2010; reviewed in Andre et al., 2010). Cysteine 38 is the site of palmitoylation on GLT-1. Huang et al. generated C38s cysteine mutation of GLT-1 to abolish palmitoylation to test the functional effects of altered GLT-1 palmitoylation. A mutation in cysteine 38 eliminates palmitoylation of GLT-1 (GLT-1 C38S). COS cells expressing GLT-1 C38S showed a reduction in glutamate uptake activity compared to wt GLT-1 *in vitro* suggesting palmitoylation of GLT-1 is important for its function. Interestingly, depalmitoylation of GLT-1 was not shown to affect its subcellular localization. Inhibition of GLT-1 palmitoylation in COS cells with the palmitoylation inhibitor, 2-bromopalmitate, also reduced glutamate uptake by approximately 30% but did not affect GLT-1 cell surface expression (Huang et al., 2010).

In a distinct model of HD, whole-brain Western blot analysis revealed that GLT-1 palmitoylation is reduced by approximately 31.8% in the brain of YAC128 mice compared with wt controls (Huang et al., 2010). YAC128 mice show reduced synaptosomal GLT-1 glutamate uptake activity in the cortex and striatum compared to wt controls measured (**Table 2**) (Huang et al., 2010). A selective inhibitor of GLT-1, dihydrokainate (DHK), was used to selectively determine the contribution of GLT-1 to glutamate uptake compared to GLAST. Interestingly, no change in GLT-1 protein expression was observed in the cortex, hippocampus, cerebellum or striatum in the YAC128 mouse model compared to the wt control suggesting a reduction in function not protein expression. Similar to the data observed *in vitro*, GLT-1 expression on membrane compartments in the YAC128 mice brain was not significantly different from wt controls. Together these results suggest that depalmitoylated GLT-1 has reduced function compared to palmitoylated GLT-1 (**Figure 1A**). Changes in GLT-1 palmitoylation can lead to reduced glutamate uptake and could contribute to the excess extracellular glutamate leading to excitotoxicity in HD (Huang et al., 2010).

S-Nitrosylation

S-nitrosylation refers to the attachment of a nitric oxide (NO) to a thiol group of a protein cysteine forming an s-nitrosothiol (SNO). S-nitrosylation plays a role in protein signaling

TABLE 2 | Changes in glutamate uptake in models of neurological disease.

Post-translational modification (PTM)	Model	Experimental paradigm	Glutamate uptake	Citation
Palmitoylation	YAC128 mouse model of PD	Synaptosomal glutamate uptake and synaptosomal DHK-sensitive glutamate uptake measured with ^{3}H-labeled glutamate assay	↓Striatal synaptosomal GLT-1 glutamate uptake compared to wt ↓Cortical synaptosomal glutamate uptake compared to wt	Huang et al., 2010
Palmitoylation	COS cells expressing GLT-1 C38S	^{3}H-labeled glutamate assay	↓Glutamate uptake in COS cells expressing GLT-1 C38S conpared to control	Huang et al., 2010
Nitrosylation	nNOS-/- mice	Synaptosomal glutamate uptake and synaptosomal DHK-sensitive glutamate uptake measured with ^{3}H-labeled glutamate assay	↑Forebrain synaptosomal DHK-sensitive glutamate uptake mnNOS-/-conpared to wt Elimination of NO from S- nitrosocysteine ↑DHK-sensitive glutamate uptake in wt forebrain svnaDtosomes	Raju et al., 2015
Sumoylation	Primary astrocyte culture	^{3}H-labeled glutamate assay	↑DHK-sensitive glutamate uptake in astrocytes overexpressing SENP1 (desumoykting enzyme) compared to control	Foran et al., 2014
Ubiquitination	Primary astrocyte culture	3H-labeled glutamate assay	↑Glutamate uptake in MPP^+-treated astrocytes with Nedd4-2 knockdown	Zhang et al., 2017
Ubiquitination	MPTP-treated mouse model of PD	Synaptosomal glutamate uptake measured with ^{3}H-labeled glutamate assay	↓Striatal synaptosome glutamate uptake compared to wt ↓Midbrain synaptosomal glutamate uptake compared to wt	Zhang et al., 2017

YAC128 mouse model of PD shows a reduction in synaptosomal DHK-sensitive glutamate uptake in the striatum and cortex. COS cells expressing GLT-1 C38S have reduced glutamate uptake compared to wt controls. Elimination of NO in primary synaptosomes increases DHK-sensitive glutamate uptake. DHK-sensitive glutamate uptake is increased in primary astrocytes overexpressing SENP1. Knocking down Nedd4-2 in MPP+-treated astrocyte cultures increases glutamate uptake. Synaptosomal glutamate uptake is decreased in the striatum and midbrain of MPTP-treated mice.

and function (Martinez-Ruiz et al., 2011). Nitrosylation is accomplished via nitric oxide (NO) signaling during glutamatergic neurotransmission while increased S-nitrosylation of proteins has been linked to neuronal death, protein misfolding and pathogenesis in neurodegenerative diseases (Uehara et al., 2006; Cho et al., 2009; Nakamura et al., 2010). NO levels have been shown to be elevated in both epileptic children and animal models of epilepsy, which suggests NO could lead to reactive gliosis and neuronal loss seen in epileptic pathogenesis (Yasuda et al., 2001; Arhan et al., 2011). Neuronal nitric oxide synthase (nNOS) produces NO in the brain and is responsible for S-nitrosylation of proteins involved in glutamate transport.

Glutamate transporter-1 can be targeted for s-nitrosylation at Cys^{373} and Cys^{562}. $nNOS^{-/-}$ mice have an increase in DHK-sensitive glutamate uptake in forebrain synaptosomes compared to wt mice. Interestingly, $nNOS^{-/-}$ mice have similar DHK-insensitive Na^+-dependent glutamate uptake levels when compared to wt suggesting that GLT-1 independent uptake is not affected by NO (Raju et al., 2015). Raju et al. (2015) also showed that eliminating NO in wt synaptosomes by pretreatment with copper and ascorbate increased DHK-sensitive glutamate uptake in wt similar to levels observed in the $nNOS^{-/-}$ mice. This data suggests that nitrosylated GLT-1 has a reduced synaptosomal glutamate uptake capacity (V_{max}).

Exposure of human embryonic kidney (HEK)-293T cells to S-nitrosocysteine promotes S-nitrosylation *in vitro*. Interestingly, treatment of HEK-293T cells with S-nitrosocysteine did not alter GLT-1 expression but it did decrease GLT-1 surface abundance (**Figure 1B**). S-nitrosocysteine treatment of HEK cells reduced DHK-sensitive glutamate uptake capacity (V_{max}) by 84% (Raju et al., 2015). Glutamate uptake activity is able to recover following a gradual decrease in S-nitrosylation (Raju et al., 2015). It is not known whether GLT-1 S-nitrosylation plays a role in neurological diseases but these findings introduce the opportunity for interventions to increase GLT-1 transporter activity. NO signaling is important for normal brain function but in its unregulated mode NO can cause neurotoxicity. There is evidence suggesting that NO may be involved in the pathogenesis of neurological diseases including HD, PD and AD (Boje, 2004). Even though there is currently not evidence of S-nitrosylation of GLT-1 contributing to pathogenesis in neurological diseases, nitrosylation of other proteins have been implicated in disease. For example, S-nitrosylation of peroxiredoxin 2, a neuroprotective antioxidant protein, in human PD brains inhibits is enzymatic activity and neuroprotective function (Fang et al., 2007). Glutamate uptake regulation is disrupted in many neurological diseases and GLT-1 nitrosylation could play a role in its loss of function. The nitrosylation of GLT-1 should be examined in a disease context to determine if it could be partially responsible for glutamate dysregulation.

Sumoylation

Sumoylation is a post-translational modification that is important for various neurological functions including synaptic plasticity, neuronal excitability through ion channel regulation, and axonal transport (van Niekerk et al., 2007; Watanabe et al., 2008; Plant et al., 2011). Sumoylation involves the addition of SUMOs (small ubiquitin-like modifiers) to lysine residues via a covalent bond. Sumoylation of proteins has been shown to change their subcellular localization and expression levels (Shao et al., 2004; Fei et al., 2006).

Glutamate transporter-1 has been shown to be sumoylated under normal physiological conditions in primary astrocytes, wt rat cortex homogenates and non-ALS control post-mortem

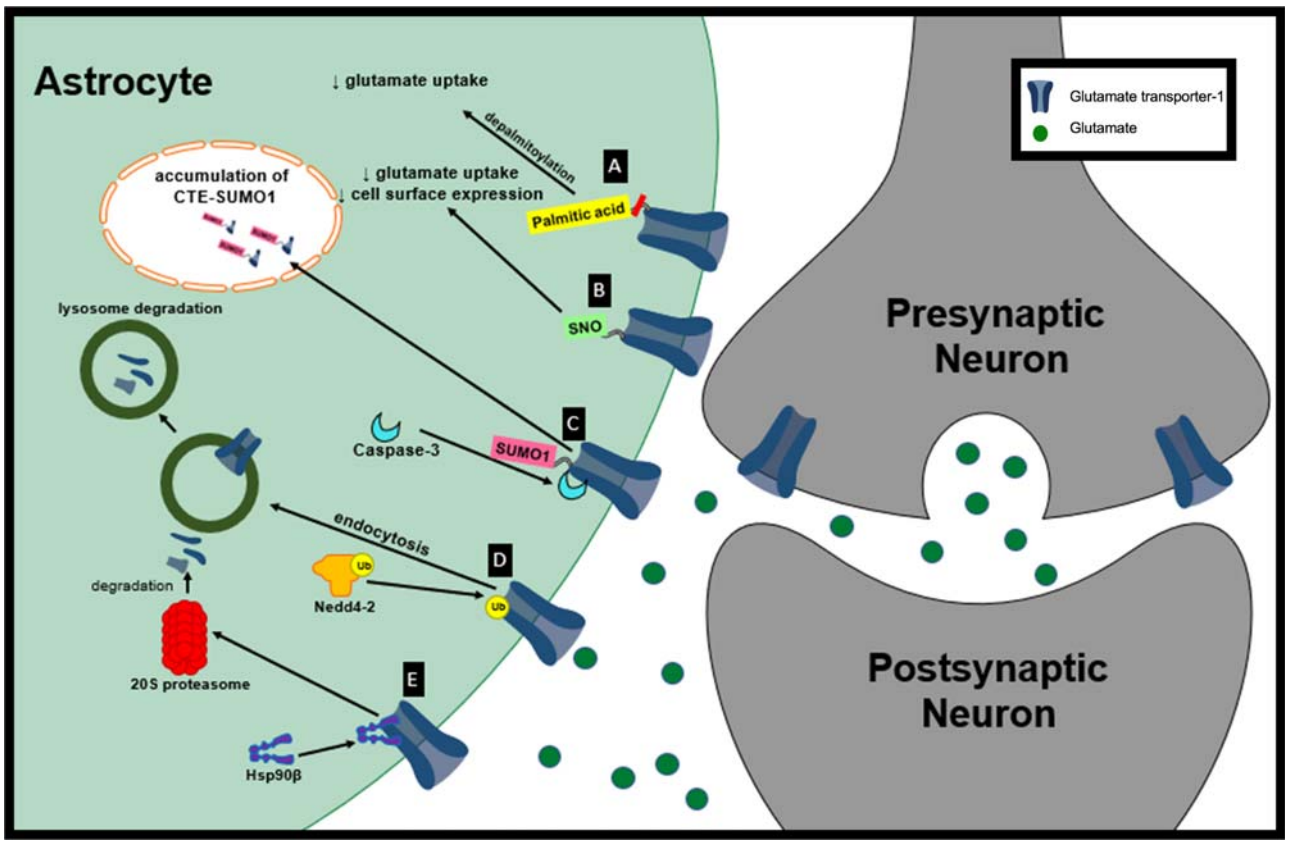

FIGURE 1 | Proposed mechanisms of GLT-1 dysfunction in neurological diseases. **(A)** Depalmitoylation of GLT-1 leads to decreased glutamate uptake by GLT-1. **(B)** S-nitrosylation of GLT-1 leads to decreased glutamate uptake activity and decreased cell surface expression of GLT-1. **(C)** Sumoylated GLT-1 is cleaved by caspase-3 and its cleaved product, CTE SUMO, is internalization and accumulated in subnuclear bodies. **(D)** Nedd4-2 mediates the ubiquitination and lysosomal degradation of GLT-1. **(E)** Hsp90β recruits GLT-1 to 20S proteasome promoting GLT-1 degradation.

tissue with lysine 570 being the primary target for sumoylation of GLT-1 (Fei et al., 2006; Foran et al., 2014). Under oxidative stress, sumoylated GLT-1 cleaved by caspase-3 gives rise to two fragments: truncated EAAT2 and COOH terminus of EAAT2 (CTE) (Boston-Howes et al., 2006). In ALS, although sumoylation of EAAT2 is not altered, it has been hypothesized that sumoylated GLT-1 is targeted for cleavage and internalization by caspase-3 (Boston-Howes et al., 2006; Foran et al., 2014). During disease progression in the SOD1-G93A mouse model of ALS there is increased accumulation of sumoylated CTE fragments in spinal cord astrocyte nuclei (**Figure 1C**). Astrocytes that express CTE-SUMO1 promote motor neuron dysfunction and axonal growth abnormalities. Prolonged expression of CTE-SUMO1 is toxic to astrocytes and causes disturbances in GFAP filament organization (Foran et al., 2011).

Sumoylation of GLT-1 has been shown to dictate its intracellular localization. HEK293T cells transfected with a plasmid encoding GLT-1 express GLT-1 that is localized to the plasma membrane. HEK cells transfected with EAAT2 and a sumoylating enzyme showed an increase in the amount of GLT-1 in the cytoplasm. Similar results were observed when HEK cells were transfected to express GLT-1-SUMO1; these cells displayed considerable GLT-1 clustering inside of cells. Interestingly, primary astrocytes display a large portion of GLT-1 in the cytoplasm that is redistributed to the plasma membrane after treatment with a desumoylating enzyme, suggesting an important role of sumoylation of GLT-1 movement between cellular compartments. In primary astrocyte cultures, desumoylation of GLT-1 with SENP1 leads to an increase in DHK-sensitive glutamate uptake. Desumoylation of EAAT2 in primary astrocytes also dispersed cytoplasmic clusters of EAAT2 (Foran et al., 2014).

The Trotti group at Thomas Jefferson revealed that the extent of sumoylated EAAT2 does not change during the course of ALS progression suggesting that sumoylation is not caused by pathological mechanisms in the SOD1-G93A mouse model (Foran et al., 2014). One possibility could be that changes in caspase-3 regulation cause an increase in EAAT2 cleavage, which leads to the toxic levels of CTE-SUMO1 observed in ALS (Foran et al., 2011). A recent study showed that mutation of the caspase-3 cleavage site in astroglial GLT-1 delays disease progression and extends lifespan in the SOD1-G93A mouse model of ALS (Rosenblum et al., 2017). These results suggest that blocking

the mechanisms responsible for cleavage of sumoylated GLT-1 in neurological diseases could prevent its internalization which would consequently elevate GLT-1 at the plasma membrane.

Ubiquitination

Ubiquitination refers to the multistep enzymatic process leading to the attachment of ubiquitin to a target protein. Ubiquitinated plasma membrane proteins can be recognized and targeted for endocytic removal and degradation (Foot et al., 2017). Nedd4-2 (neuronal precursor cell expressed developmentally down-regulated 4-2) is a member of the Nedd4 family of ubiquitin ligases which catalyzes ubiquitination and degradation (Zhou et al., 2007).

Nedd4-2 has been shown to mediate the ubiquitination and internalization of GLT-1 via protein kinase C (PKC) activation (**Figure 1D**; Garcia-Tardon et al., 2012). Increased extracellular glutamate reduces the concentration of GLT-1 transporters on the cell surface in a dose-dependent manner in primary mixed cultures (glial cells and neurons). The mechanism responsible for the reduction in GLT-1 transporters at the plasma membrane in response to extracellular glutamate is due to the association of the adaptor protein β-arrestin with Nedd4-2 which leads to the increased ubiquitination of GLT-1 (Ibáñez et al., 2016). Elevated levels of extracellular glutamate have been observed in many neurological diseases and could potentially lead to a reduction in GLT-1 at the plasma membrane through this mechanism (Robelet et al., 2004; Soukupova et al., 2015). 1-methyl-4-phenylpyridinium (MPP^+) is a dopaminergic neurotoxin that is used to model PD (Chun et al., 2001). Nedd4-2 interaction with GLT-1 is increased in MPP^+-treated astrocyte cultures along with the ubiquitination of GLT-1 (Zhang et al., 2017). Ubiquitination of GLT-1 by Nedd4-2 in MPP^+ treated astrocytes leads to its internalization and lysosomal degradation. Decreased GLT-1 expression and function in MPP^+ treated cultures can be rescued by lysosome inhibition. Knocking down Nedd4-2, with a shRNA, decreased GLT-1 ubiquitination and increased GLT-1 expression and glutamate uptake activity in MPP+-treated astrocytes, further supporting the significance of Nedd4-2 trafficking of GLT-1 leading to its downregulation (Zhang et al., 2017).

Glutamate transporter-1 expression and glutamate uptake are decreased in the midbrain and striatum in the 1-methyl-4-phenyl-1,2,3,6-tetrahydropyridine (MPTP) mouse model of PD. GLT-1 protein expression was shown to be decreased in the midbrain and striatum in MPTP-treated mice. Synaptosomal glutamate uptake was reduced in the striatum and midbrain of MPTP-treated mice compared to controls. Interestingly, knocking down Nedd4-2 in the MPTP mouse model rescued GLT-1 protein expression and glutamate uptake (Zhang et al., 2017). Zhang et al. (2017) showed that knocking down Nedd4-2 in the MPTP mouse model of PD with a shRNA increases synaptosomal glutamate uptake. These results suggest that preventing the ubiquitination of GLT-1 could lead to reduced hyperexcitability in this model. Interestingly, other studies have shown that downregulation of Nedd4-2 leads to hyperexcitability. For example, Nedd4-2 is known to ubiquitinate voltage-gated sodium channels (Na_vs) in dorsal root ganglion (DRG). Downregulation of Nedd4-2 leads to increased amplitudes of Na_vs currents (Laedermann et al., 2013). Nedd4-2 heterozygous mice have increased motor activity and basal synaptic activity (Yanpallewar et al., 2016). Nedd4-2 inhibition has been shown to rescue GLT-1 protein levels, however, Nedd4-2 is responsible for the ubiquitination and regulation of numerous ion channels in the CNS suggesting that Nedd4-2 inhibition is not a good mechanism to selectively target glutamate uptake. A better approach would be to find a specific molecule that will selectively prevent Nedd4-2 and GLT-1 protein–protein interactions.

Subcellular Localization

Glutamate transporter-1 is not homogenously expressed throughout astrocytes, rather it tends to cluster at processes and astrocytic endfeet (Schreiner et al., 2014). 67% of GLT-1 in the cortex expressed at synapses is in astrocytic processes (Melone et al., 2011).

Changes in GLT-1 subcellular localization have been documented in various neurological diseases. Primary astrocyte cultures from Lafora disease (LD, a form of intractable epilepsy) mice have reduced levels of GLT-1 at the plasma membrane but no alteration in GLT-1 total protein. These astrocytes also showed impairment in glutamate uptake capacity (Munoz-Ballester et al., 2016). Likewise, GLT-1 cell surface expression is reduced in astrocytic cultures exposed to Aβ1–42 with no alteration in GLT-1 total protein levels. Normal levels of GLT-1 can be restored in Aβ1–42 treated astrocyte cultures by pretreating with a vitamin E derivative (Scimemi et al., 2013). These findings suggest that not only reduction of glutamate transporters but GLT-1 mislocalization may play a role in neurological diseases.

THERAPEUTIC STRATEGIES

Dexamethasone

Dexamethasone is a synthetic glucocorticosteroid that has been shown to be a transcriptional enhancer of GLT-1 (**Figure 2A**). Glucocorticoid transcriptional regulation is classically mediated through glucocorticoid receptors (GR) and receptor subtypes are expressed in primary astrocytes (Unemura et al., 2012). Dexamethasone has been reported to elevate GLT-1 transcription, protein levels and activity in cortical and striatal astrocytes *in vitro* (Zschocke et al., 2005; Carbone et al., 2012a). Dexamethasone alone was unable to increase GLT-1 protein levels in cerebellar and midbrain astrocytes but increased GLT-1 expression in cerebellar glia when used in combination with a DNA methyltransferase inhibitor (Zschocke et al., 2005). Downstream signals involved in transcription and *in vivo* models should be further explored to validate dexamethasone as a neuroprotective agent.

Ceftriaxone

Ceftriaxone, a β-lactam antibiotic, has been shown to be increase GLT-1 expression but how ceftriaxone increases glutamate transporter expression is unclear. It is proposed that ceftriaxone elevates the transcription of GLT-1 in astrocytes through the nuclear factor-κB (NF-κB) signaling pathway, although, this is controversial due to evidence showing

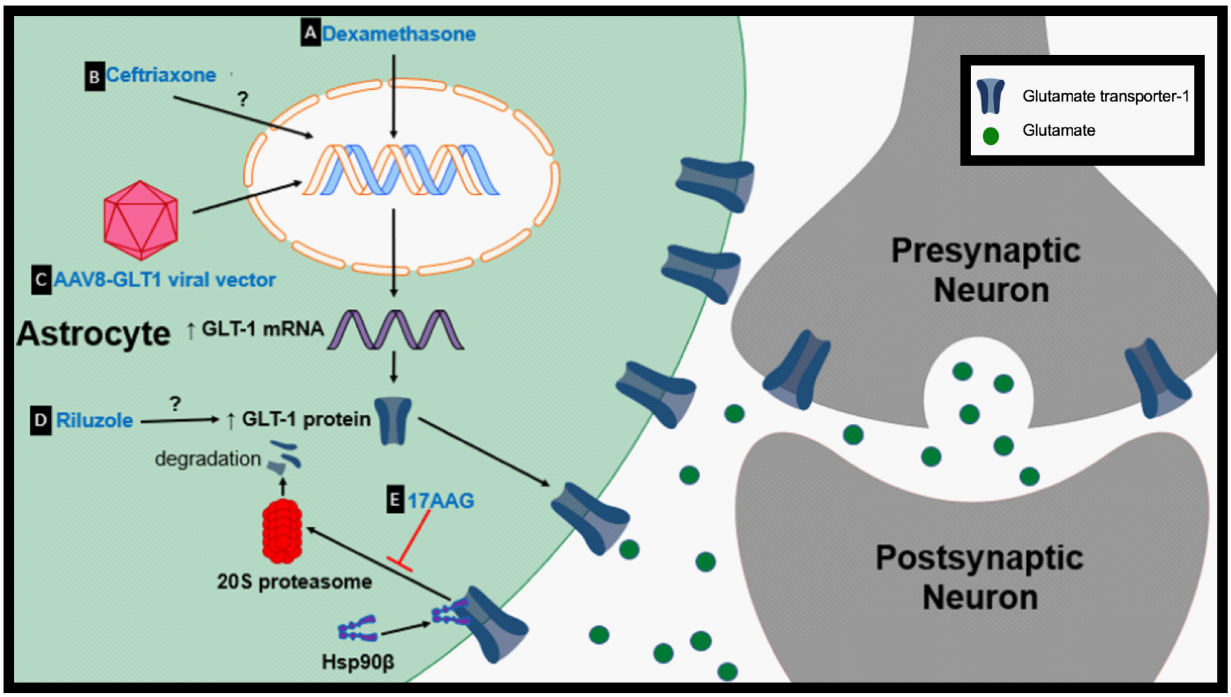

FIGURE 2 | Proposed therapeutic mechanisms to prevent GLT-1 downregulation. **(A)** Dexamethasone is a transcriptional enhancer of GLT-1. **(B)** Ceftriaxone is a transcriptional activator of GLT-1. **(C)** Adeno-associated virus type 8 (AAV-8)-GLT1 vector is used to increase GLT-1 expression under the Gfa2 promoter. **(D)** The mechanism by which riluzole upregulates GLT-1 protein levels is unknown. **(E)** 17AAG prevents the degradation of GLT-1 by inhibition of Hsp90β.

no change in GLT-1 protein expression with treatment in certain models (**Figure 2B**; Lee et al., 2008). For example, ceftriaxone treatment fails to upregulate GLT-1 or modulate glutamate uptake in striatal astrocytes following growth factor withdrawal (Fumagalli et al., 2007). It has also been hypothesized that ceftriaxone may indirectly upregulate GLT-1 through upregulation of an antioxidant defense system (LaCrosse et al., 2017). Since its discovery as a potential transcriptional activator of GLT-1, ceftriaxone's therapeutic effects have been tested in numerous models of neurological diseases. Ceftriaxone successfully upregulated GLT-1 expression in the R6/2 model of HD when cortical and striatal GLT-1 levels are significantly reduced (Sari et al., 2010). Treatment with ceftriaxone prior to onset of epilepsy increased GLT-1 expression and decreased seizure frequency in a genetic mouse model of epilepsy (Zeng et al., 2010). Ceftriaxone increased striatal GLT-1 expression, glutamate uptake, and reduced the abnormal involuntary movements known as l-dopa-induced dyskinesia in the 6-hydroxydopamine model of PD (Chotibut et al., 2017). Ceftriaxone treatment also decreased behavioral deficits and hippocampal neurodegeneration in the MPTP model of PD (Hsu et al., 2015). Ceftriaxone delayed loss of neurons and muscle strength while increasing mouse survival in the G93A mouse model of ALS (Rothstein et al., 2005). Despite promising Stage 2 data, ceftriaxone failed to show efficacy during Stage 3 trials in ALS (Cudkowicz et al., 2014).

Treatment with ceftriaxone has been associated with negative adverse effects which might not be associated with it acting on glutamate transport suggesting that ceftriaxone affects many pathways in the CNS and is not selective to GLT-1. Ceftriaxone treatment has been shown to impair synaptic plasticity in the hippocampus and impair memory recognition (Omrani et al., 2009; Matos-Ocasio et al., 2014). Another study showed that ceftriaxone treatment results in impairment of neuronal circuits and a reduction in EEG theta power (7–9 Hz) in the frontal and parietal cortex (Bellesi et al., 2012). Critical experiments need to be performed to determine whether these adverse effects observed with ceftriaxone treatment are due to increased glutamate transporter protein expression or if they are due to ceftriaxone targeting different pathways. Ceftriaxone's adverse effects in the CNS and mechanisms of action need to be further characterized and addressed in order to determine its potential as a modulator of glutamate uptake. If ceftriaxone does not directly target GLT-1 transcription it might not be an appropriate approach to target glutamate modulation.

AAV8-GLT1

A direct mechanism in which genes can be delivered into cells and expressed under specific promoters can be mediated through adeno-associated virus (AAV) transduction. Recombinant AAVs have the potential to deliver normal copies of a gene that is mutated or absent to treat or prevent particular genetic diseases (Schultz and Chamberlain, 2008). Intraspinal delivery of AAV8-Gfa2-GLT1 results in an increase in astrocytic GLT-1 protein expression (**Figure 2C**; Li et al., 2014). Overexpression of

GLT-1 through AAV8-GLT1 administration following cervical-contusion spinal cord injury (SCI) increased lesion size, phrenic nerve axonal degeneration and denervation (Li et al., 2014). Increasing GLT-1 in cervical-contusion SCI exacerbated pathology, another example of negative effects associated with modulation of glutamate transport.

However, AAV8-GLT1 injection following contusion SCI restored GLT-1 protein levels in the superficial dorsal horn and reversed heat hypersensitivity (Falnikar et al., 2016). Although AAV therapies have not been used to increase GLT-1 expression in neurological diseases, particularly diseases with GLT-1 dysfunction, gene therapy has the capability of modulating glutamate and should be further investigated. In particular, in animal model studies, AAV-induced GLT-1 upregulation can be used to isolate the effects of "pure" GLT1 upregulation from other pharmacologic effects of available drugs.

Riluzole

Riluzole is a neuroprotective agent and is one of only two FDA-approved drug treatments for ALS. Riluzole has been shown to cause several effects including inhibition of voltage-dependent sodium channels and potassium channels (Zona et al., 1998; Urbani and Belluzzi, 2000). Riluzole has been shown to increase Na^+-dependent glutamate uptake in synaptosomes in a dose-dependent manner but the mechanism is unknown (**Figure 2D**; Fumagalli et al., 2007). In striatal astrocyte cultures riluzole upregulated both GLT-1 protein levels and activity following growth factor withdrawal. 6-hydroxydopamine (6-OHDA) causes nigrostriatal degeneration and motor impairments which are characteristic of PD (Deumens et al., 2002). Riluzole treatment decreased ipsiversive rotation when challenged with amphetamine, a characteristic of 6-OHDA-treated animals that is due to loss of dopaminergic transmission, suggesting preservation of the dopaminergic system. Interestingly, riluzole did not affect GLT-1 expression in this model (Carbone et al., 2012b). The mechanisms in which riluzole modulates glutamate levels needs to be further examined to better understand its potential to rescue GLT-1 levels or function.

HSP90 Inhibitors

Heat shock protein 90 (Hsp90) is a chaperone protein involved in proteostasis under normal physiological and pathological states (Schopf et al., 2017). Hsp90 has also been linked to protein degradation (Li et al., 2017). Hsp90 expression is increased in hippocampal formation subfields of mesial temporal lobe epilepsy (MTLE) patients compared to non-epileptic controls (Kandratavicius et al., 2014). Recent findings suggest that astrocytic Hsp90β is increased in patients with drug resistant TLE and hippocampal sclerosis (HS) (Sha et al., 2016). Astrocytic cytoplasmic Hsp90β is increased during the chronic-stage in the IHKA model of epilepsy parallel to reactive astrogliosis. Further examination indicated that specific activation of Hsp90β occurs in reactive astrocytes following an excitotoxic event. Hsp90β overexpression leads to a reduction in GLT-1 protein levels while knocking down Hsp90β increases GLT-1 expression but does not affect GLT-1 mRNA suggesting Hsp90β plays a role in regulating GLT-1 at the post-transcriptional level. The HSP90β inhibitor, 17-allylamino-17-demethoxygeldanamycin (17AAG), disrupts the interaction between Hsp90β and GLT-1 (**Figures 1E**, **2E**). Disrupting Hsp90β's interaction with GLT-1 prevents its recruitment and degradation by the 20S proteasome. 17AAG treatment has been shown to increase DHK-sensitive glutamate uptake in primary astrocyte cultures and hippocampal plasma membrane vesicles (PMVs) of the 17AAG treated mice, reduce epileptic seizures, and reduce astrogliosis in the IHKA model of epilepsy (Sha et al., 2016). Hsp90β is a promising new target that may be partially responsible for GLT-1 dysfunction in many neurological diseases that are accompanied by reactive astrogliosis. In addition, many different Hsp90 inhibitors are in clinical trials for cancer therapy (Jhaveri et al., 2014; Thakur et al., 2016; Cavenagh et al., 2017).

CONCLUSION

Glutamate transporter-1 regulation is a critical component in homeostasis of the glutamatergic system. GLT-1 downregulation is a common occurrence seen across several neurological diseases including HD, AD, Parkinson's disease, ALS, and epilepsy. Here, we have highlighted post-translational modifications (PTMs) that can lead to the reduction of functional GLT-1. PTMs are key mechanisms used to regulate function, localization and degradation of proteins. Under normal physiological conditions, PTMs are essential for allowing cells to respond to stimuli; but in pathogenesis, PTM dysregulation can lead to decreased function and mislocalization of proteins. In this review, we have discussed PTMs of GLT-1 in the context of neurological diseases. Selectively targeting PTMs could reveal novel therapeutics in the context of disease. For example, targeting PTMs, particularly ubiquitination, may be effective in treating particular cancers. Inhibition of the ubiquitin activating enzyme (UAE), using the small molecule inhibitor TAK-243, was shown to have anti-proliferative activity in human cancer cells (Hyer et al., 2018). Identifying changes in GLT-1 PTMs will enable modulation of both localization and function of GLT-1 in neurological diseases. Elucidation of mechanisms underlying GLT-1 dysregulation will allow design of therapeutic strategies not only to target GLT-1 at the transcriptional level but also prevent post-translational mislocalization and degradation.

AUTHOR CONTRIBUTIONS

AP did an exhaustive literature search and generated a complete draft of the review, and prepared the tables and both the figures. DB also reviewed the literature and provided detailed comments and edits to the review and the tables and figures.

REFERENCES

Andre, V. M., Cepeda, C., and Levine, M. S. (2010). Dopamine and glutamate in Huntington's disease: a balancing act. *CNS Neurosci. Ther.* 16, 163–178. doi: 10.1111/j.1755-5949.2010.00134.x

Andrew, S. E., Goldberg, Y. P., Kremer, B., Telenius, H., Theilmann, J., Adam, S., et al. (1993). The relationship between trinucleotide (CAG) repeat length and clinical features of Huntington's disease. *Nat. Genet.* 4, 398–403. doi: 10.1038/ng0893-398

Arhan, E., Serdaroglu, A., Ozturk, B., Ozturk, H. S., Ozcelik, A., Kurt, N., et al. (2011). Effects of epilepsy and antiepileptic drugs on nitric oxide, lipid peroxidation and xanthine oxidase system in children with idiopathic epilepsy. *Seizure* 20, 138–142. doi: 10.1016/j.seizure.2010.11.003

Bellesi, M., Vyazovskiy, V. V., Tononi, G., Cirelli, C., and Conti, F. (2012). Reduction of EEG Theta Power and Changes in Motor Activity in Rats Treated with Ceftriaxone. *PLoS One* 7:e34139. doi: 10.1371/journal.pone.0034139

Boje, K. M. (2004). Nitric oxide neurotoxicity in neurodegenerative diseases. *Front. Biosci.* 9, 763–776. doi: 10.2741/1268

Boston-Howes, W., Gibb, S. L., Williams, E. O., Pasinelli, P., Brown, R. H. Jr., and Trotti, D. (2006). Caspase-3 cleaves and inactivates the glutamate transporter EAAT2. *J. Biol. Chem.* 281, 14076–14084. doi: 10.1074/jbc.m600653200

Bruijn, L. I., Becher, M. W., Lee, M. K., Anderson, K. L., Jenkins, N. A., Copeland, N. G., et al. (1997). ALS-linked SOD1 mutant G85R mediates damage to astrocytes and promotes rapidly progressive disease with SOD1-containing inclusions. *Neuron* 18, 327–338. doi: 10.1016/s0896-6273(00)80272-x

Butland, S. L., Sanders, S. S., Schmidt, M. E., Riechers, S. P., Lin, D. T., Martin, D. D., et al. (2014). The palmitoyl acyltransferase HIP14 shares a high proportion of interactors with huntingtin: implications for a role in the pathogenesis of Huntington's disease. *Hum. Mol. Genet.* 23, 4142–4160. doi: 10.1093/hmg/ddu137

Carbone, M., Duty, S., and Rattray, M. (2012a). Riluzole elevates GLT-1 activity and levels in striatal astrocytes. *Neurochem. Int.* 60, 31–38. doi: 10.1016/j.neuint.2011.10.017

Carbone, M., Duty, S., and Rattray, M. (2012b). Riluzole neuroprotection in a Parkinson's disease model involves suppression of reactive astrocytosis but not GLT-1 regulation. *BMC Neurosci.* 13:38. doi: 10.1186/1471-2202-13-38

Cavenagh, J., Oakervee, H., Baetiong-Caguioa, P., Davies, F., Gharibo, M., Rabin, N., et al. (2017). A phase I/II study of KW-2478, an Hsp90 inhibitor, in combination with bortezomib in patients with relapsed/refractory multiple myeloma. *Br. J. Cancer* 117, 1295–1302. doi: 10.1038/bjc.2017.302

Chen, W., Mahadomrongkul, V., Berger, U. V., Bassan, M., DeSilva, T., Tanaka, K., et al. (2004). The glutamate transporter GLT1a is expressed in excitatory axon terminals of mature hippocampal neurons. *J. Neurosci.* 24, 1136–1148. doi: 10.1523/jneurosci.1586-03.2004

Cho, D. H., Nakamura, T., Fang, J., Cieplak, P., Godzik, A., Gu, Z., et al. (2009). S-nitrosylation of Drp1 mediates beta-amyloid-related mitochondrial fission and neuronal injury. *Science* 324, 102–105. doi: 10.1126/science.1171091

Chotibut, T., Meadows, S., Kasanga, E. A., McInnis, T., Cantu, M. A., Bishop, C., et al. (2017). Ceftriaxone reduces L-dopa-induced dyskinesia severity in 6-hydroxydopamine parkinson's disease model. *Mov. Disord.* 32, 1547–1556. doi: 10.1002/mds.27077

Chun, H. S., Gibson, G. E., DeGiorgio, L. A., Zhang, H., Kidd, V. J., and Son, J. H. (2001). Dopaminergic cell death induced by MPP(+), oxidant and specific neurotoxicants shares the common molecular mechanism. *J. Neurochem.* 76, 1010–1021. doi: 10.1046/j.1471-4159.2001.00096.x

Cudkowicz, M. E., Titus, S., Kearney, M., Yu, H., Sherman, A., Schoenfeld, D., et al. (2014). Safety and efficacy of ceftriaxone for amyotrophic lateral sclerosis: a multi-stage, randomised, double-blind, placebo-controlled trial. *Lancet Neurol.* 13, 1083–1091. doi: 10.1016/S1474-4422(14)70222-4

Danbolt, N. C. (2001). Glutamate uptake. *Prog. Neurobiol.* 65, 1–105.

Danbolt, N. C., Furness, D. N., and Zhou, Y. (2016). Neuronal vs glial glutamate uptake: resolving the conundrum. *Neurochem. Int.* 98, 29–45. doi: 10.1016/j.neuint.2016.05.009

Deumens, R., Blokland, A., and Prickaerts, J. (2002). Modeling Parkinson's disease in rats: an evaluation of 6-OHDA lesions of the nigrostriatal pathway. *Exp. Neurol.* 175, 303–317. doi: 10.1006/exnr.2002.7891

el-Husseini, A.-D., and Bredt, D. S. (2002). Protein palmitoylation: a regulator of neuronal development and function. *Nat. Rev. Neurosci.* 3, 791–802. doi: 10.1038/nrn940

Estrada-Sanchez, A. M., Montiel, T., Segovia, J., and Massieu, L. (2009). Glutamate toxicity in the striatum of the R6/2 Huntington's disease transgenic mice is age-dependent and correlates with decreased levels of glutamate transporters. *Neurobiol. Dis.* 34, 78–86. doi: 10.1016/j.nbd.2008.12.017

Falnikar, A., Tamara, H. J., Poulsen, D. J., and Lepore, A. C. (2016). GLT1 Overexpression reverses established neuropathic pain-related behavior and attenuates chronic dorsal horn neuron activation following cervical spinal cord injury. *Glia* 64, 396–406. doi: 10.1002/glia.22936

Fang, J., Nakamura, T., Cho, D. H., Gu, Z., and Lipton, S. A. (2007). S-nitrosylation of peroxiredoxin 2 promotes oxidative stress-induced neuronal cell death in Parkinson's disease. *Proc. Natl. Acad. Sci. U.S.A.* 104, 18742–18747. doi: 10.1073/pnas.0705904104

Fei, E., Jia, N., Yan, M., Ying, Z., Sun, Q., Wang, H., et al. (2006). SUMO-1 modification increases human SOD1 stability and aggregation. *Biochem. Biophys. Res. Commun.* 347, 406–412. doi: 10.1016/j.bbrc.2006.06.092

Foot, N., Henshall, T., and Kumar, S. (2017). Ubiquitination and the Regulation of Membrane Proteins. *Physiol. Rev.* 97, 253–281. doi: 10.1152/physrev.00012.2016

Foran, E., Bogush, A., Goffredo, M., Roncaglia, P., Gustincich, S., Pasinelli, P., et al. (2011). Motor neuron impairment mediated by a sumoylated fragment of the glial glutamate transporter EAAT2. *Glia* 59, 1719–1731. doi: 10.1002/glia.21218

Foran, E., Rosenblum, L., Bogush, A., Pasinelli, P., and Trotti, D. (2014). Sumoylation of the astroglial glutamate transporter EAAT2 governs its intracellular compartmentalization. *Glia* 62, 1241–1253. doi: 10.1002/glia.22677

Fumagalli, E., Funicello, M., Rauen, T., Gobbi, M., and Tiziana, M. (2007). Riluzole enhances the activity of glutamate transporters GLAST, GLT1 and EAAC1. *Eur. J. Pharmacol.* 578, 171–176. doi: 10.1016/j.ejphar.2007.10.023

Furness, D. N., Dehnes, Y., Akhtar, A. Q., Rossi, D. J., Hamann, M., Grutle, N. J., et al. (2008). A quantitative assessment of glutamate uptake into hippocampal synaptic terminals and astrocytes: new insights into a neuronal role for excitatory amino acid transporter 2 (EAAT2). *Neuroscience* 157, 80–94. doi: 10.1016/j.neuroscience.2008.08.043

Garcia-Tardon, N., Gonzalez-Gonzalez, I. M., Martinez-Villarreal, J., Fernandez-Sanchez, E., Gimenez, C., and Zafra, F. (2012). Protein kinase C (PKC)-promoted endocytosis of glutamate transporter GLT-1 requires ubiquitin ligase Nedd4-2-dependent ubiquitination but not phosphorylation. *J. Biol. Chem.* 287, 19177–19187. doi: 10.1074/jbc.M112.355909

Hauser, W. A., Rich, S. S., Lee, J. R., Annegers, J. F., and Anderson, V. E. (1998). Risk of recurrent seizures after two unprovoked seizures. *N. Engl. J. Med.* 338, 429–434. doi: 10.1056/nejm199802123380704

Hsu, C. Y., Hung, C. S., Chang, H. M., Liao, W. C., Ho, S. C., and Ho, Y. J. (2015). Ceftriaxone prevents and reverses behavioral and neuronal deficits in an MPTP-induced animal model of Parkinson's disease dementia. *Neuropharmacology* 91, 43–56. doi: 10.1016/j.neuropharm.2014.11.023

Huang, K., Kang, M. H., Askew, C., Kang, R., Sanders, S. S., Wan, J., et al. (2010). Palmitoylation and function of glial glutamate transporter-1 is reduced in the YAC128 mouse model of Huntington disease. *Neurobiol. Dis.* 40, 207–215. doi: 10.1016/j.nbd.2010.05.027

Hubbard, J. A., Szu, J. I., Yonan, J. M., and Binder, D. K. (2016). Regulation of astrocyte glutamate transporter-1 (GLT1) and aquaporin-4 (AQP4) expression in a model of epilepsy. *Exp. Neurol.* 283, 85–96. doi: 10.1016/j.expneurol.2016.05.003

Hyer, M. L., Milhollen, M. A., Ciavarri, J., Fleming, P., Traore, T., Sappal, D., et al. (2018). A small-molecule inhibitor of the ubiquitin activating enzyme for cancer treatment. *Nat. Med.* 24, 186–193. doi: 10.1038/nm.4474

Ibáñez, I., Díez-Guerra, J. F., Giménez, C., and Zafra, F. (2016). Activity dependent internalization of the glutamate transporter GLT-1 mediated by β-arrestin 1 and ubiquitination. *Neuropharmacology* 107, 376–386. doi: 10.1016/j.neuropharm.2016.03.042

Jacob, C. P., Koutsilieri, E., Bartl, J., Neuen-Jacob, E., Arzberger, T., Zander, N., et al. (2007). Alterations in expression of glutamatergic transporters and receptors in sporadic Alzheimer's disease. *J. Alzheimers Dis.* 11, 97–116. doi: 10.3233/jad-2007-11113

Jhaveri, K., Chandarlapaty, S., Lake, D., Gilewski, T., Robson, M., Goldfarb, S., et al. (2014). A phase II open-label study of ganetespib, a novel heat shock protein 90 inhibitor for patients with metastatic breast cancer. *Clin. Breast Cancer* 14, 154–160. doi: 10.1016/j.clbc.2013.12.012

Jimenez-Sanchez, M., Licitra, F., Underwood, B. R., and Rubinsztein, D. C. (2017). Huntington's disease: mechanisms of pathogenesis and therapeutic strategies. *Cold Spring Harb. Perspect Med.* 7:a024240. doi: 10.1101/cshperspect.a024240

Kandratavicius, L., Hallak, J. E., Carlotti, C. G. Jr., Assirati, J. A. Jr., and Leite, J. P. (2014). Hippocampal expression of heat shock proteins in mesial temporal lobe epilepsy with psychiatric comorbidities and their relation to seizure outcome. *Epilepsia* 55, 1834–1843. doi: 10.1111/epi.12787

Kang, R., Wan, J., Arstikaitis, P., Takahashi, H., Huang, K., Bailey, A. O., et al. (2008). Neural palmitoyl-proteomics reveals dynamic synaptic palmitoylation. *Nature* 456, 904–909. doi: 10.1038/nature07605

Kong, E., Peng, S., Chandra, G., Sarkar, C., Zhang, Z., Bagh, M. B., et al. (2013). Dynamic palmitoylation links cytosol-membrane shuttling of acyl-protein thioesterase-1 and acyl-protein thioesterase-2 with that of proto-oncogene H-ras product and growth-associated protein-43. *J. Biol. Chem.* 288, 9112–9125. doi: 10.1074/jbc.M112.421073

LaCrosse, A. L., O'Donovan, S. M., Sepulveda-Orengo, M. T., McCullumsmith, R. E., Reissner, K. J., Schwendt, M., et al. (2017). Contrasting the Role of xCT and GLT-1 Upregulation in the Ability of Ceftriaxone to Attenuate the Cue-Induced Reinstatement of Cocaine Seeking and Normalize AMPA Receptor Subunit Expression. *J. Neurosci.* 37, 5809–5821. doi: 10.1523/JNEUROSCI.3717-16.2017

Laedermann, C. J., Cachemaille, M., Kirschmann, G., Pertin, M., Gosselin, R. D., Chang, I., et al. (2013). Dysregulation of voltage-gated sodium channels by ubiquitin ligase NEDD4-2 in neuropathic pain. *J. Clin. Invest.* 123, 3002–3013. doi: 10.1172/JCI68996

Lang, A. E., and Lozano, A. M. (1998). Parkinson's disease. *First of two parts. N. Engl. J. Med.* 339, 1044–1053.

Laprairie, R. B., Petr, G. T., Sun, Y., Fischer, K. D., Denovan-Wright, E. M., and Rosenberg, P. A. (2019). Huntington's disease pattern of transcriptional dysregulation in the absence of mutant huntingtin is produced by knockout of neuronal GLT-1. *Neurochem. Int.* 123, 85–94. doi: 10.1016/j.neuint.2018.04.015

Lee, S. G., Su, Z. Z., Emdad, L., Gupta, P., Sarkar, D., Borjabad, A., et al. (2008). Mechanism of Ceftriaxone Induction of Excitatory Amino Acid Transporter-2 Expression and Glutamate Uptake in Primary Human Astrocytes. *J. Biol. Chem.* 283, 13116–13123. doi: 10.1074/jbc.M707697200

Levy, L. M., Lehre, K. P., Walaas, S. I., Storm-Mathisen, J., and Danbolt, N. C. (1995). Down-regulation of glial glutamate transporters after glutamatergic denervation in the rat brain. *Eur. J. Neurosci.* 7, 2036–2041. doi: 10.1111/j.1460-9568.1995.tb00626.x

Li, K., Nicaise, C., Sannie, D., Hala, T. J., Javed, E., Parker, J. L., et al. (2014). Overexpression of the astrocyte glutamate transporter GLT1 exacerbates phrenic motor neuron degeneration, diaphragm compromise, and forelimb motor dysfunction following cervical contusion spinal cord injury. *J. Neurosci.* 34, 7622–7638. doi: 10.1523/JNEUROSCI.4690-13.2014

Li, Z., Zhou, L., Prodromou, C., Savic, V., and Pearl, L. H. (2017). HECTD3 Mediates an HSP90-Dependent Degradation Pathway for Protein Kinase Clients. *Cell. Rep.* 19, 2515–2528. doi: 10.1016/j.celrep.2017.05.078

Lievens, J. C., Woodman, B., Mahal, A., Spasic-Boscovic, O., Samuel, D., Kerkerian-Le Goff, L., et al. (2001). Impaired glutamate uptake in the R6 Huntington's disease transgenic mice. *Neurobiol. Dis.* 8, 807–821. doi: 10.1006/nbdi.2001.0430

Lin, C. L., Bristol, L. A., Jin, L., Dykes-Hoberg, M., Crawford, T., Clawson, L., et al. (1998). Aberrant RNA processing in a neurodegenerative disease: the cause for absent EAAT2, a glutamate transporter, in amyotrophic lateral sclerosis. *Neuron* 20, 589–602. doi: 10.1016/s0896-6273(00)80997-6

Martinez-Ruiz, A., Cadenas, S., and Lamas, S. (2011). Nitric oxide signaling: classical, less classical, and nonclassical mechanisms. *Free Radic. Biol. Med.* 51, 17–29. doi: 10.1016/j.freeradbiomed.2011.04.010

Matos-Ocasio, F., Hernandez-Lopez, A., and Thompson, K. J. (2014). Ceftriaxone, a GLT-1 transporter activator, disrupts hippocampal learning in rats. *Pharmacol. Biochem. Behav.* 122, 118–121. doi: 10.1016/j.pbb.2014.03.011

Melone, M., Bellesi, M., Ducati, A., Iacoangeli, M., and Conti, F. (2011). Cellular and Synaptic Localization of EAAT2a in Human Cerebral Cortex. *Front. Neuroanat.* 4:151. doi: 10.3389/fnana.2010.00151

Mookherjee, P., Green, P. S., Watson, G. S., Marques, M. A., Tanaka, K., Meeker, K. D., et al. (2011). GLT-1 loss accelerates cognitive deficit onset in an Alzheimer's disease animal model. *J. Alzheimers Dis.* 26, 447–455. doi: 10.3233/JAD-2011-110503

Munoz-Ballester, C., Berthier, A., Viana, R., and Sanz, P. (2016). Homeostasis of the astrocytic glutamate transporter GLT-1 is altered in mouse models of Lafora disease. *Biochim. Biophys. Acta.* 1862, 1074–1083. doi: 10.1016/j.bbadis.2016.03.008

Nakamura, T., Wang, L., Wong, C. C., Scott, F. L., Eckelman, B. P., Han, X., et al. (2010). Transnitrosylation of XIAP regulates caspase-dependent neuronal cell death. *Mol. Cell* 39, 184–195. doi: 10.1016/j.molcel.2010.07.002

Omrani, A., Melone, M., Bellesi, M., Safiulina, V., Aida, T., Tanaka, K., et al. (2009). Up-regulation of GLT-1 severely impairs LTD at mossy fibre–CA3 synapses. *J. Physiol.* 587, 4575–4588. doi: 10.1113/jphysiol.2009.177881

Parenti, M., Viganó, M. A., Newman, C. M., Milligan, G., and Magee, A. I. (1993). A novel N-terminal motif for palmitoylation of G-protein alpha subunits. *Biochem. J.* 291(Pt 2), 349–353. doi: 10.1042/bj2910349

Perego, C., Vanoni, C., Bossi, M., Massari, S., Basudev, H., Longhi, R., et al. (2000). The GLT-1 and GLAST glutamate transporters are expressed on morphologically distinct astrocytes and regulated by neuronal activity in primary hippocampal cocultures. *J. Neurochem.* 75, 1076–1084. doi: 10.1046/j.1471-4159.2000.0751076.x

Petr, G. T., Sun, Y., Frederick, N. M., Zhou, Y., Dhamne, S. C., Hameed, M. Q., et al. (2015). Conditional deletion of the glutamate transporter GLT-1 reveals that astrocytic GLT-1 protects against fatal epilepsy while neuronal GLT-1 contributes significantly to glutamate uptake into synaptosomes. *J. Neurosci.* 35, 5187–5201. doi: 10.1523/JNEUROSCI.4255-14.2015

Plant, L. D., Dowdell, E. J., Dementieva, I. S., Marks, J. D., and Goldstein, S. A. (2011). SUMO modification of cell surface Kv2.1 *potassium channels regulates the activity of rat hippocampal neurons. J. Gen. Physiol.* 137, 441–454. doi: 10.1085/jgp.201110604

Proper, E. A., Hoogland, G., Kappen, S. M., Jansen, G. H., Rensen, M. G., Schrama, L. H., et al. (2002). Distribution of glutamate transporters in the hippocampus of patients with pharmaco-resistant temporal lobe epilepsy. *Brain* 125, 32–43. doi: 10.1093/brain/awf001

Raju, K., Doulias, P. T., Evans, P., Krizman, E. N., Jackson, J. G., Horyn, O., et al. (2015). Regulation of brain glutamate metabolism by nitric oxide and S-nitrosylation. *Sci. Signal* 8:ra68. doi: 10.1126/scisignal.aaa4312

Rimmele, T. S., and Rosenberg, P. A. (2016). GLT-1: the elusive presynaptic glutamate transporter. *Neurochem. Int.* 98, 19–28. doi: 10.1016/j.neuint.2016.04.010

Robelet, S., Melon, C., Guillet, B., Salin, P., and Kerkerian-Le Goff, L. (2004). Chronic L-DOPA treatment increases extracellular glutamate levels and GLT1 expression in the basal ganglia in a rat model of Parkinson's disease. *Eur. J. Neurosci.* 20, 1255–1266. doi: 10.1111/j.1460-9568.2004.03591.x

Rosenblum, L. T., Shamamandri-Markandaiah, S., Ghosh, B., Foran, E., Lepore, A. C., Pasinelli, P., et al. (2017). Mutation of the caspase-3 cleavage site in the astroglial glutamate transporter EAAT2 delays disease progression and extends lifespan in the SOD1-G93A mouse model of ALS. *Exp. Neurol.* 292, 145–153. doi: 10.1016/j.expneurol.2017.03.014

Rothstein, J. D., Patel, S., Regan, M. R., Haenggeli, C., Huang, Y. H., Bergles, D. E., et al. (2005). Beta-lactam antibiotics offer neuroprotection by increasing glutamate transporter expression. *Nature* 433, 73–77. doi: 10.1038/nature03180

Sari, Y., Prieto, A. L., Barton, S. J., Miller, B. R., and Rebec, G. V. (2010). Ceftriaxone-induced up-regulation of cortical and striatal GLT1 in the R6/2 model of Huntington's disease. *J. Biomed. Sci.* 17:62. doi: 10.1186/1423-0127-17-62

Schlag, B. D., Vondrasek, J. R., Munir, M., Kalandadze, A., Zelenaia, O. A., Rothstein, J. D., et al. (1998). Regulation of the glial Na+-dependent glutamate transporters by cyclic AMP analogs and neurons. *Mol. Pharmacol.* 53, 355–369. doi: 10.1124/mol.53.3.355

Schopf, F. H., Biebl, M. M., and Buchner, J. (2017). The HSP90 chaperone machinery. *Nat. Rev. Mol. Cell Biol.* 18:345. doi: 10.1038/nrm.2017.20

Schreiner, A. E., Durry, S., Aida, T., Stock, M. C., Ruther, U., Tanaka, K., et al. (2014). Laminar and subcellular heterogeneity of GLAST and GLT-1 immunoreactivity in the developing postnatal mouse hippocampus. *J. Comp. Neurol.* 522, 204–224. doi: 10.1002/cne.23450

Schultz, B. R., and Chamberlain, J. S. (2008). Recombinant adeno-associated virus transduction and integration. *Mol. Ther.* 16, 1189–1199. doi: 10.1038/mt.2008.103

Scimemi, A., Meabon, J. S., Woltjer, R. L., Sullivan, J. M., Diamond, J. S., and Cook, D. G. (2013). Amyloid-β1-42 slows clearance of synaptically released glutamate by mislocalizing astrocytic GLT-1. *J. Neurosci.* 33, 5312–5318. doi: 10.1523/JNEUROSCI.5274-12.2013

Selkoe, D. J. (2000). The genetics and molecular pathology of Alzheimer's disease: roles of amyloid and the presenilins. *Neurol. Clin.* 18, 903–922.

Sha, L., Wang, X., Li, J., Shi, X., Wu, L., Shen, Y., et al. (2016). Pharmacologic inhibition of Hsp90 to prevent GLT-1 degradation as an effective therapy for epilepsy. *J. Exp. Med.* 214, 547–563. doi: 10.1084/jem.20160667

Shao, R., Zhang, F. P., Tian, F., Anders Friberg, P., Wang, X., Sjoland, H., et al. (2004). Increase of SUMO-1 expression in response to hypoxia: direct interaction with HIF-1alpha in adult mouse brain and heart in vivo. *FEBS Lett.* 569, 293–300. doi: 10.1016/j.febslet.2004.05.079

Soukupova, M., Binaschi, A., Falcicchia, C., Palma, E., Roncon, P., Zucchini, S., et al. (2015). Increased extracellular levels of glutamate in the hippocampus of chronically epileptic rats. *Neuroscience* 301, 246–253. doi: 10.1016/j.neuroscience.2015.06.013

Sugimoto, J., Tanaka, M., Sugiyama, K., Ito, Y., Aizawa, H., Soma, M., et al. (2018). Region-specific deletions of the glutamate transporter GLT1 differentially affect seizure activity and neurodegeneration in mice. *Glia* 66, 777–788. doi: 10.1002/glia.23281

Swanson, R. A., Liu, J., Miller, J. W., Rothstein, J. D., Farrell, K., Stein, B. A., et al. (1997). Neuronal regulation of glutamate transporter subtype expression in astrocytes. *J. Neurosci.* 17, 932–940. doi: 10.1523/jneurosci.17-03-00932.1997

Tanaka, K., Watase, K., Manabe, T., Yamada, K., Watanabe, M., Takahashi, K., et al. (1997). Epilepsy and Exacerbation of Brain Injury in Mice Lacking the Glutamate Transporter GLT-1. *Science* 276, 1699–1702. doi: 10.1126/science.276.5319.1699

Tapia, R. (2014). Cellular and molecular mechanisms of motor neuron death in amyotrophic lateral sclerosis: a perspective. *Front. Cell Neurosci.* 8:241. doi: 10.3389/fncel.2014.00241

Thakur, M. K., Heilbrun, L. K., Sheng, S., Stein, M., Liu, G., Antonarakis, E. S., et al. (2016). A phase II trial of ganetespib, a heat shock protein 90 Hsp90) inhibitor, in patients with docetaxel-pretreated metastatic castrate-resistant prostate cancer (CRPC)-a prostate cancer clinical trials consortium (PCCTC) study. *Invest. New Drugs* 34, 112–118. doi: 10.1007/s10637-015-0307-6

Uehara, T., Nakamura, T., Yao, D., Shi, Z. Q., Gu, Z., Ma, Y., et al. (2006). S-nitrosylated protein-disulphide isomerase links protein misfolding to neurodegeneration. *Nature* 441, 513–517. doi: 10.1038/nature04782

Unemura, K., Kume, T., Kondo, M., Maeda, Y., Izumi, Y., and Akaike, A. (2012). Glucocorticoids decrease astrocyte numbers by reducing glucocorticoid receptor expression in vitro and in vivo. *J. Pharmacol. Sci.* 119, 30–39. doi: 10.1254/jphs.12047fp

Urbani, A., and Belluzzi, O. (2000). Riluzole inhibits the persistent sodium current in mammalian CNS neurons. *Eur. J. Neurosci.* 12, 3567–3574. doi: 10.1046/j.1460-9568.2000.00242.x

van Niekerk, E. A., Willis, D. E., Chang, J. H., Reumann, K., Heise, T., and Twiss, J. L. (2007). Sumoylation in axons triggers retrograde transport of the RNA-binding protein La. *Proc. Natl. Acad. Sci. U.S.A.* 104, 12913–12918. doi: 10.1073/pnas.0611562104

Vetrivel, K. S., Meckler, X., Chen, Y., Nguyen, P. D., Seidah, N. G., Vassar, R., et al. (2009). Alzheimer disease Abeta production in the absence of S-palmitoylation-dependent targeting of BACE1 to lipid rafts. *J. Biol. Chem.* 284, 3793–3803. doi: 10.1074/jbc.M808920200

Watanabe, M., Takahashi, K., Tomizawa, K., Mizusawa, H., and Takahashi, H. (2008). Developmental regulation of Ubc9 in the rat nervous system. *Acta. Biochim. Pol.* 55, 681–686.

Yanpallewar, S., Wang, T., Koh, D. C., Quarta, E., Fulgenzi, G., and Twiss, J. L. (2016). Nedd4-2 haploinsufficiency causes hyperactivity and increased sensitivity to inflammatory stimuli. *Sci. Rep.* 6:32957. doi: 10.1038/srep32957

Yasuda, H., Fujii, M., Fujisawa, H., Ito, H., and Suzuki, M. (2001). Changes in nitric oxide synthesis and epileptic activity in the contralateral hippocampus of rats following intrahippocampal kainate injection. *Epilepsia* 42, 13–20. doi: 10.1046/j.1528-1157.2001.083032.x

Zeng, L. H., Bero, A. W., Zhang, B., Holtzman, D. M., and Wong, M. (2010). Modulation of astrocyte glutamate transporters decreases seizures in a mouse model of Tuberous Sclerosis Complex. *Neurobiol. Dis.* 37, 764–771. doi: 10.1016/j.nbd.2009.12.020

Zhang, Y., He, X., Meng, X., Wu, X., Tong, H., Zhang, X., et al. (2017). Regulation of glutamate transporter trafficking by Nedd4-2 in a Parkinson's disease model. *Cell Death Dis.* 8, e2574–e2574. doi: 10.1038/cddis.2016.454

Zhou, R., Patel, S. V., and Snyder, P. M. (2007). Nedd4-2 catalyzes ubiquitination and degradation of cell surface ENaC. *J. Biol. Chem.* 282, 20207–20212. doi: 10.1074/jbc.m611329200

Zhou, Y., Hassel, B., Eid, T., and Danbolt, N. C. (2019). Axon-terminals expressing EAAT2 (GLT-1; Slc1a2) are common in the forebrain and not limited to the hippocampus. *Neurochem. Int.* 123, 101–113. doi: 10.1016/j.neuint.2018.03.006

Zona, C., Siniscalchi, A., Mercuri, N. B., and Bernardi, G. (1998). Riluzole interacts with voltage-activated sodium and potassium currents in cultured rat cortical neurons. *Neuroscience* 85, 931–938. doi: 10.1016/s0306-4522(97)00604-0

Zschocke, J., Bayatti, N., Clement, A. M., Witan, H., Figiel, M., Engele, J., et al. (2005). Differential promotion of glutamate transporter expression and function by glucocorticoids in astrocytes from various brain regions. *J. Biol. Chem.* 280, 34924–34932. doi: 10.1074/jbc.m502581200

Conflict of Interest Statement: The authors declare that the research was conducted in the absence of any commercial or financial relationships that could be construed as a potential conflict of interest.

frontiers in Molecular Neuroscience

ORIGINAL RESEARCH
published: 04 October 2019
doi: 10.3389/fnmol.2019.00236

Sex-Dependent Changes in miRNA Expression in the Bed Nucleus of the Stria Terminalis Following Stress

Maria Mavrikaki[1], Lorena Pantano[2], David Potter[1], Maximilian A. Rogers-Grazado[3], Eleni Anastasiadou[4], Frank J. Slack[4], Sami S. Amr[3], Kerry J. Ressler[1], Nikolaos P. Daskalakis[1] and Elena Chartoff[1]*

[1] Department of Psychiatry, Harvard Medical School, McLean Hospital, Belmont, MA, United States, [2] Harvard Chan Bioinformatics Core, Harvard School of Public Health, Harvard University, Boston, MA, United States, [3] Translational Genomics Core, Partners Healthcare Personalized Medicine, Cambridge, MA, United States, [4] Department of Pathology, Beth Israel Deaconess Medical Center, Harvard Medical School, Boston, MA, United States

Anxiety disorders disproportionately affect women compared to men, which may arise from sex differences in stress responses. MiRNAs are small non-coding RNAs known to regulate gene expression through actions on mRNAs. MiRNAs are regulated, in part, by factors such as stress and gonadal sex, and they have been implicated in the pathophysiology of multiple psychiatric disorders. Here, we assessed putative sex differences in miRNA expression in the bed nucleus of the stria terminalis (BNST) – a sexually dimorphic brain region implicated in anxiety – of adult male and female rats that had been exposed to social isolation (SI) stress throughout adolescence. To assess the translational utility of our results, we assessed if childhood trauma in humans resulted in changes in blood miRNA expression that are similar to those observed in rats. Male and female Sprague-Dawley rats underwent SI during adolescence or remained group housed (GH) and were tested for anxiety-like behavior in the elevated plus maze as adults. Small RNA sequencing was performed on tissue extracted from the BNST. Furthermore, we re-analyzed an already available small RNA sequencing data set from the Grady Trauma Project (GTP) from men and women to identify circulating miRNAs that are associated with childhood trauma exposure. Our results indicated that there were greater anxiogenic-like effects and changes in BNST miRNA expression in SI versus GH females compared to SI versus GH males. In addition, we found nine miRNAs that were regulated in both the BNST from SI compared to GH rats and in blood samples from humans exposed to childhood trauma. These studies emphasize the utility of rodent models in studying neurobiological mechanisms underlying psychiatric disorders and suggest that rodent models could be used to identify novel sex-specific pharmacotherapies for anxiety disorders.

Keywords: miRNAs, stress, social isolation, small RNA sequencing, BNST, sex differences

OPEN ACCESS

Edited by:
Andrew L. Gundlach, The Florey Institute of Neuroscience and Mental Health, Australia

Reviewed by:
Joanna Dabrowska, Rosalind Franklin University of Medicine and Science, United States
Brian Trainor, University of California, Davis, United States

****Correspondence:***
Maria Mavrikaki
mmavrikaki@mclean.harvard.edu

Received: *21 May 2019*
Accepted: *17 September 2019*
Published: *04 October 2019*

Citation:
Mavrikaki M, Pantano L, Potter D, Rogers-Grazado MA, Anastasiadou E, Slack FJ, Amr SS, Ressler KJ, Daskalakis NP and Chartoff E (2019) Sex-Dependent Changes in miRNA Expression in the Bed Nucleus of the Stria Terminalis Following Stress. Front. Mol. Neurosci. 12:236. doi: 10.3389/fnmol.2019.00236

INTRODUCTION

Early life stressors, particularly at vulnerable developmental periods such as adolescence or childhood, increase the risk for psychiatric disorders in adulthood (Chapman et al., 2004; Gillespie et al., 2009; Khoury et al., 2010; Mehta et al., 2013). Women are twice as likely as men to be diagnosed with mood disorders (Kessler, 2003). Gender differences in the prevalence of mood

disorders are first evident in adolescence (Weintraub et al., 2010), raising the possibility that there are biologically and developmentally based sex differences underlying those disorders.

Adolescent girls report much higher levels of stress associated with negative interpersonal contexts than boys (Hankin et al., 2007). Previous research demonstrated sex-specific effects of adolescent social isolation (SI) on adult stress reactivity, with adult female rats demonstrating more robust adrenal responses to acute and chronic stress compared to corresponding males (Weintraub et al., 2010). Thus, adolescent SI is a translationally relevant stressor that can induce long-term and sex-specific changes in stress reactivity and behavior.

MicroRNAs (miRNAs) are small (∼22 nucleotides; nts) non-coding RNAs that inhibit gene expression (Im and Kenny, 2012; Anastasiadou et al., 2018). Mature miRNAs are processed from genes via a cascade of events that include the enzymes DROSHA and DICER, which act sequentially to convert pri-miRNAs to mature miRNAs (Im and Kenny, 2012). A single miRNA can regulate the expression of hundreds of genes and can itself be regulated by stress and gonadal sex (Sharma and Eghbali, 2014; Pfau et al., 2016). However, there is limited research on stress-regulated miRNAs and miRNA variants that demonstrate sex-specific changes. Nonetheless, some isomiRs, which are miRNAs that vary by one or more nucleotides from the reference miRNA sequence (Tan et al., 2014), have been shown to be differentially expressed in males and females (Guo et al., 2016), but little is known about their regulation or function. As such, it is possible that both stress and sex can differentially induce the expression of both reference miRNAs and isomiRs. The nucleotide differences in isomiRs allow for a range of binding affinities to, or differential selectivity for, mRNAs, which could result in a range of effects on gene expression. IsomiRs can be quantified by next generation sequencing (NGS) (Rubio et al., 2018).

The bed nucleus of the stria terminalis (BNST), part of the extended amygdala, is one of the most complex structures in the central nervous system (Daniel and Rainnie, 2016) and is a sexually dimorphic area that expresses both estrogen and androgen receptors (Lebow and Chen, 2016). The BNST integrates information from stress and reward systems (Doura and Unterwald, 2016; Faria et al., 2016). Previous research demonstrated that activation of the anterodorsal BNST (adBNST) decreases anxiety-like behavior, whereas activation of the oval nucleus of the BNST [part of the adBNST] increases anxiety-like behavior (Kim et al., 2013). The adBNST has high expression levels of corticotropin-releasing factor (CRF) and CRF receptors (Dong et al., 2001), which is essential for stress responses (Erb and Stewart, 1999). To our knowledge, the interaction between sex and adolescent stress on miRNA expression in the adBNST is unknown. Thus, we decided to focus on adBNST as it is an understudied area involved in stress response and demonstrates a sexually dimorphic profile. The present study focused on how stressful (SI) versus non-stressful (group housed, GH) housing conditions during adolescence impacted miRNA expression in the adBNST in early adulthood.

Rodent studies are widely used to assess molecular mechanisms underlying neuropsychiatric disorders; however, there is a need to develop better validated and more useful animal models (Nestler and Hyman, 2010). To achieve this goal, it is essential to compare rodent findings to human data in order to assess their translational utility. In this study, we assessed miRNA expression in the adBNST following SI in rats and we aimed to compare those data to a human stress-related already existing miRNA data set. In addition to the brain and other organs, miRNAs can also be detected in circulating biological fluids such as blood (i.e., circulating miRNAs). Under healthy conditions, miRNA expression profiles remain stable in circulating biological fluids, but can significantly change in response to pathological conditions such as prolonged or severe stress (Chen et al., 2008; Dwivedi, 2014; Grasso et al., 2014). Thus, recent research suggests that miRNAs can not only be used as therapeutic targets, but also as non-invasive diagnostic and predictive biomarkers, which is highly impactful given the ethical and practical limitations in obtaining human brain tissue (Glinge et al., 2017). Given the limitations of research using human brain tissues, it is not surprising that miRNA expression profile in the BNST has not been assessed following SI stress. Although stressful events are not always traumatic, traumatic experiences are always stressful (Willard et al., 2016). Previous research from our group assessed miRNA expression in whole blood in individuals that experienced childhood trauma (Wingo et al., 2015). Blood gene expression may not necessarily map to parallel alterations in the brain itself, although our team findings from animal models of post-traumatic stress disorder (PTSD) have shown convergence between brain and blood gene expression signatures associated with individual differences in the behavioral response to stress at the level of upstream regulators and pathways (Daskalakis et al., 2014; Lori et al., 2018). Here, we re-analyzed a previously published small RNA sequencing data set from men and women (Wingo et al., 2015) to identify circulating miRNAs associated with childhood trauma exposure that overlap with adBNST miRNAs associated with adolescent SI.

In this study, we hypothesized that adolescent SI would produce a more robust anxiogenic phenotype compared to GH conditions in adult females than in males, and increased anxiety would be accompanied by sex-specific changes in miRNA expression in the adBNST. We also hypothesized that childhood trauma experience in humans would induce changes in blood miRNA expression that are similar to those observed in the anxiety-related adBNST in rats (Daskalakis et al., 2018). These studies are important because they probe novel molecular consequences of adolescent social conditions that might lead to improved understanding and development of sex-specific treatments for stress-related disorders.

MATERIALS AND METHODS

Animals

Timed-pregnant female Sprague-Dawley rats (gestation day 15) were purchased from Charles River Laboratories (Wilmington, MA, United States) based on previously published work (Brenhouse et al., 2009; Holland et al., 2014). Once the pregnant dams arrived, they had an additional 7 days to habituate to the

animal colony before giving birth. Although we appreciate that shipment of the pregnant dams can be a stressor, no differences in average litter size (9–12 pups), sex ratio, or weight/health of the pups were noticed in the offspring. After birth, male and female pups were weaned on postnatal day 21 (PD 21) and housed either singly (socially isolated; SI) or in groups of three same-sex littermates (GH; controls). Males and females were housed separately in the same rat colony room, which is on a 12-h light–dark cycle (lights on 7:00 am). All experiments were conducted during the light phase. Rats were treated according to the guidelines recommended by the Animal Care and Use Committee of McLean Hospital and by the National Institutes of Health guide for the care and use of Laboratory animals.

Elevated Plus Maze

After weaning (PD 21), SI and GH rats were maintained under these housing conditions for 6 weeks, as in Butler et al. (2014) and were tested for anxiety-like behavior using the elevated plus maze (EPM) when they reached adulthood (9 weeks old). The EPM was performed as in Knoll et al. (2007). Rats were transported to a holding room with dim white light (LED A19 lamp, 40 W) 1 h before testing. The maze was elevated 85 cm from the ground and consisted of two opposing open arms and two opposing closed arms (40 cm wall height). Rats were placed into the maze facing an open arm (for consistency) and the 5-min sessions were digitally captured by a camera (EverFocus Polestar II, EQ 610) mounted to the ceiling. Digital recordings were analyzed by a viewer blinded to treatment conditions for time spent in open and closed arms, as well as number of entries into open and closed arms. The maze was cleaned thoroughly with 70% ethanol between rats to avoid odors influencing behavior – particularly between males and females. The experiment was performed under red light (between 12:00 amd 3:30 pm) and in the presence of low volume white noise (60 dB). After testing, rats remained in the holding room (range: 1–4 h) until the last rat was tested. The testing order of the rats was randomized by treatment group so that each treatment group contained rats that remained in the holding room for times that spanned the 1–4 h. Rats were then transferred to a different procedure room a few minutes before they were killed for tissue extraction.

Tissue Collection and RNA Extraction

Rats were exposed to CO_2 for 10 s prior to rapid decapitation 1–4 h after completion of the EPM test (time of death was between 3:00 and 5:00 pm). Trunk blood was collected in 15 ml BD Vacutainer PPT plasma preparation tube (BD Biosciences) to assess estradiol levels in female rats (see the **Supplementary Material**) and brains were snap-frozen in isopentane on dry-ice and then stored at −80°C until use. The adBNST was punched from frozen brains as described in Chartoff et al. (2016). Briefly, frozen brains were coronally sectioned on a cryostat (HM 505 E; Microm, Walldorf, Germany) until the anterior BNST was exposed (Bregma 0.00 mm), based on the atlas of Paxinos and Watson (2007). The anterior commissure (ac) and the ventral extension of the lateral ventricle were used as anatomical hallmarks to center the corer between the ac and the ventricle. The corer was right against the boundary of the emerging globus pallidus (GP). Bilateral tissue punches 0.5–0.75 mm in length were taken with a 1-mm internal diameter corer and 1.8-mm outer diameter (Fine Science Tools, Foster City, CA, United States; **Figures 2A,B**; note that the punch looks bigger due to the outer diameter of the corer) and tissue was placed in Eppendorf tubes kept on dry ice and then stored at −80°C. Total RNA was extracted using Trizol reagent (Ambion, Life Technologies) and was treated with a DNA-free kit (Ambion, Life Technologies) to remove genomic DNA contamination according to Mavrikaki et al. (2016). RNA samples were split in two, and half of the samples was processed for small RNA sequencing and the other half was kept at −80°C for the validation of the sequencing using quantitative real-time polymerase chain reaction (qRT-PCR). For the small RNA sequencing female samples, we selected five samples per group that had the highest RNA integrity numbers (RIN) and that represented a range of estradiol levels (high–medium–low levels compared to the mean of the group) to correct for the estrus cycle stage. With these constraints, an *N* of five samples per group was too small to conduct reliable correlational analyses between estradiol levels and miRNA expression.

Small RNA Sequencing

MicroRNA Libraries were prepared using the Bioo Scientific NEXTflex Small RNA-Seq kit v3 per the manufacturer's instructions. Total RNA (215 ng) was used as input and NEXTflex adapters were ligated to the 3′- and 5′-ends of the RNA. After adapter ligations and cleanups, the adapter-ligated RNA entered reverse transcription, resulting in a cDNA first-strand synthesis product. The reverse transcription products were then isolated and amplified by PCR (22 cycles). Successful library production and isolation was confirmed by the Agilent High-Sensitivity Screentape assay. Quantification of libraries was performed using Qubit Picogreen and KAPA qRT-PCR assays. Libraries were normalized, pooled, denatured, and sequenced on the Illumina HiSeq 2500 Rapid v2 platform to generate >10 million (range 11–19 million) 50 bp single end reads per sample.

All samples were processed using the small RNA-seq pipeline implemented in the bcbio-nextgen project[1]. Raw reads were examined for quality issues using FastQC[2] to ensure library generation and sequencing are suitable for further analysis. Adapter sequences, other contaminant sequences such as polyA tails and low-quality sequences with PHRED quality scores <5 were trimmed from reads using cutadapt (Martin, 2011). Trimmed reads were aligned to miRBase v21 (Kozomara and Griffiths-Jones, 2014) to the specific species with seqbuster (Pantano et al., 2010). As well, they were aligned to *Rattus norvegicus* genome (version rn6) using STAR (Dobin et al., 2013). The aligned genomes were used with seqcluster (Pantano et al., 2011) to characterize the whole small RNA transcriptome and classify reads into rRNA, miRNA, repeats, genes, tRNAs, and others from USCC annotation (Mangan et al., 2014). Finally, aligned reads were used with miRDeep2 (Friedlander et al., 2012), an algorithm that assesses the fit of sequenced RNAs to

[1]https://bcbio-nextgen.readthedocs.org/en/latest/

[2]http://www.bioinformatics.babraham.ac.uk/projects/fastqc/

a biological model of miRNA generation and correct folding. Alignments were checked for evenness of coverage, rRNA content, genomic context of alignments (for example, alignments in known transcripts and introns), complexity, and other quality checks using a combination of FastQC, MultiQC (Ewels et al., 2016), and custom code inside bcbio-nextgen pipeline. Data were loaded into R with bcbioSmallRna R package[3] and isomiRs BioC package (Pantano et al., 2016).

Quantitative Real-Time PCR

A total of 50 ng RNA from the same line of samples used for the small RNA sequencing study was used for miRNA-specific reverse transcription using the miScript II RT kit (Qiagen) according to the manufacturer's instructions. qRT-PCR was performed in a 384-well plate using miScript SYBR Green PCR kits (Qiagen) and miScript primer assays (Qiagen) for miR-34c-5p (MS00000238), miR-760-3p (MS00033628), miR-770-3p (MS00028539), miR-140-5p (MS00000406), miR-23b-3p (MS00033341), and RNU6B (MS00033740) using an Applied Biosystems vii7 Real-Time PCR Instrument as previously described (Mavrikaki et al., 2019). miR-23b-3p was compared to RNU6B and was used as a reference gene (**Supplementary Figure 4**). Expression data were analyzed according to the $2^{-\Delta\Delta Ct}$ method (Schmittgen and Livak, 2008).

Comparison of Rat miRNA Data With miRNA Expression Profile in Human Participants in the Grady Trauma Project

To assess the translational utility of our results, we compared differentially expressed miRNAs from the adBNST of SI or GH male and female rats to differentially expressed miRNAs from whole blood taken from humans who had experienced childhood trauma (Wingo et al., 2015). Not all the individuals reporting high levels of trauma exposure in GTP were endorsed high symptoms of or diagnosed for PTSD or depression (**Supplementary Table 7**). To determine the overlap between the rat and the human miRNA lists, we used $p < 0.05$ rather than $p$adj. < 0.05 (as used in the rat study) as a cutoff for differentially expressed rat miRNAs to enhance our ability to identify changes that overlap with human data.

For the human miRNA data, we re-analyzed a previously published small RNA sequencing study (Gene Expression Omnibus GSE74162) (Wingo et al., 2015) from the Grady Trauma Project (GTP) that assessed childhood trauma using the Childhood Trauma Questionnaire (CTQ) (Bernstein et al., 2003). In that study, whole blood RNA samples from 23 subjects who participated in the GTP study were analyzed for miRNA sequencing using Illumina HiSeq 1000 (Wingo et al., 2015). For downstream analyses we kept 1117 miRNAs expressed (>0 counts) in $>25\%$ of the samples. We kept 21 samples for which we had covariate information.

After log-transformation and quantile normalization, we performed a bioinformatic analysis using the limma R-package to assess the effects of childhood trauma on miRNA expression. Childhood trauma was assessed using the total score of CTQ (this score takes into account all five subscales: emotional abuse, physical abuse, sexual abuse, emotional neglect, and physical neglect). We covaried this analysis for confounding effects of adult trauma. We analyzed data from 7 men and 14 women together due to the insufficient sample size. However, we set sex as a covariate in our analysis. In our analysis we also took into account RIN, age, and the type of the four most frequent immune cell types in each sample estimated by the CIBERSORT method (Newman et al., 2015) using RNA expression data from the same individuals (GSE67663; Illumina Human WG-6 v3.0 expression beadchip). To begin to explore if the miRNAs we detected to be associated with childhood trauma are influenced by sex hormones, we used menstrual status as a covariate in our analysis for females.

Statistical Analysis

For the small RNA sequencing study, differential expression (DE) at the gene level was called with DESeq2 (Love et al., 2014) and p-adjusted value was used as a threshold for significant differences. Pathway analysis was performed using DIANA miRPath v.3 (Vlachos et al., 2015). The criteria used were: intersection of at least three miRNAs, p-value threshold 0.05, and MicroT threshold 0.8. For the EPM and qRT-PCR studies, statistical analysis was performed using GraphPad Prism 8. Unpaired t-test was used for comparisons of housing conditions per sex for EPM and two-way ANOVA (housing condition $\times$ miRNA) with repeated measures was used on miRNA for qRT-PCR. *Post hoc* analysis was performed using Fisher's LSD. For human miRNA DE analysis using the limma R-package, we report the DE for the 188 miRNAs that were expressed in both human blood and rat BNST.

RESULTS

Housing Condition During Adolescence Has Sex-Dependent Effects on Anxiety-Like Behavior in Adulthood

Rats underwent adolescent SI (or were GH) for 6 weeks and were then tested for anxiety-like behavior in the EPM when they reached adulthood (**Figure 1A**). SI females had decreased % time spent in the open arms of the EPM compared to GH females [$t(17) = 3.39$, $p < 0.005$; **Figure 1B**], whereas this difference in males was not significant [$t(18) = 1.23$, $p = 0.23$; **Figure 1B**]. Similarly, SI females, but not males, had fewer open arm entries compared to GH rats [females: $t(17) = 4.72$, $p < 0.0005$; males: $t(18) = 1.07$, $p = 0.3$; **Figure 1C**], which taken together suggests a greater anxiogenic effect of SI in females compared to males. Finally, both SI females and males had similar closed arm entries [females: $t(17) = 0.59$, $p = 0.5$; males: $t(18) = 0.47$, $p = 0.6$; **Figure 1D**], suggesting that there was not a general alteration in locomotor activity due to social stress or sex. Of note, GH females tended to spend more time in the open arms than GH males [$t(16) = 1.618$, $p = 0.12$; comparing GH data from **Figure 1B**, male and **Figure 1B**, female], whereas SI females and SI males spent

[3]https://github.com/lpantano/bcbioSmallRna

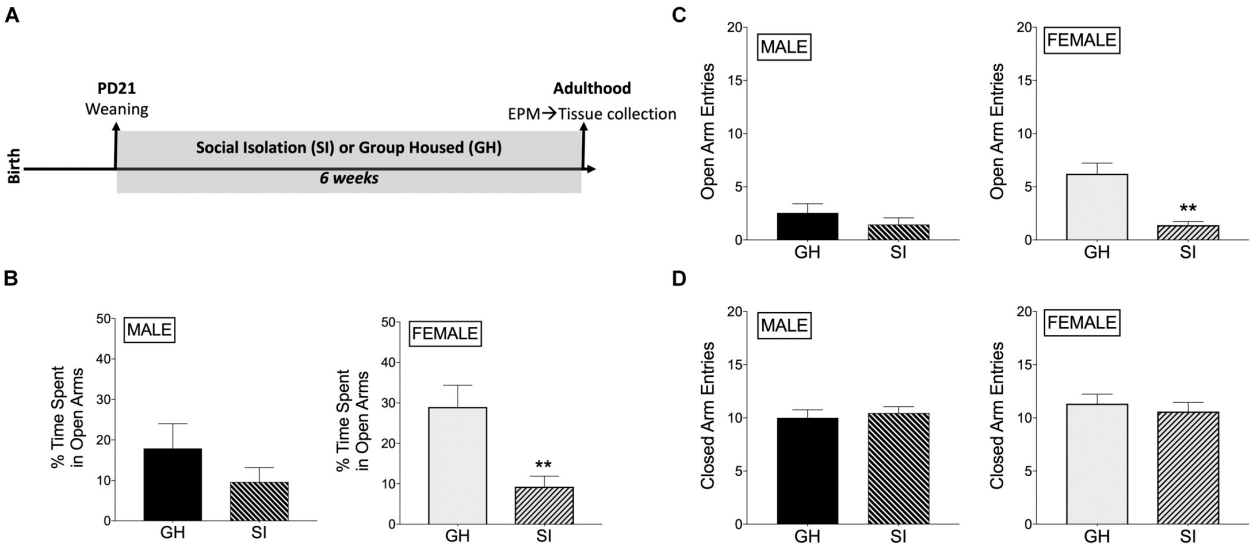

FIGURE 1 | Effects of housing condition during adolescence on anxiety-like behavior in adulthood as measured in the elevated plus maze (EPM). **(A)** Experimental design of the study. **(B)** Male SI and GH rats did not differ in % time spent in open arms (TSOA) [TSOA/(TSOA + closed arm time)], whereas the % TSOA was significantly decreased in SI compared to GH female rats. **(C)** Male SI and GH rats did not differ in the number of open arm entries (OAE), whereas the number of OAE was significantly decreased in SI compared to GH female rats. **(D)** Neither male nor female SI and GH rats differed in the number of closed arm entries. n = 9–11/group; GH, group housed; SI, socially isolated; Asterisks indicate significant difference compared to GH control; $^{**}p < 0.01$.

similar time in the open arms [t(19) = 0.094, p = 0.9; comparing SI data from **Figure 1B**, male and **Figure 1B**, female]. SI did not significantly affect estradiol levels in adulthood [$t(17) = 1.047$, $p = 0.3$; **Supplementary Figure 5**].

Housing Condition During Adolescence Has Sex-Dependent Effects on miRNA Expression in the adBNST in Adulthood

Bioinformatic analysis of the small RNA sequencing results from the adBNST (**Figures 2A,B**) indicated that approximately 80% of the reads corresponded to miRNAs. Principal component analysis (PCA) of all miRNAs measured indicated that most of the samples cluster together and the largest variability is observed in the female samples (**Figure 2C**).

To compare the miRNA expression patterns between male GH vs. SI and female GH vs. SI, we performed a DE analysis. We used DESeq2 at the gene level and set the threshold for significant differences to p-adjusted ($p$adj.) < 0.05. As adBNST is a sexually dimorphic area, we first compared miRNA expression between male and female GH control rats. We found that only rno-miR-3084a/b/d was differentially expressed between male and female GH controls. Thus, we proceeded with the analysis that compared male GH vs. SI and female GH vs. SI. This analysis revealed that a total of 37 miRNAs were differentially expressed in the male, 68 miRNAs were differentially expressed in the female, and 12 miRNAs overlapped and were differentially expressed in both male and female adBNST of SI compared to GH rats ($p$adj. < 0.05; **Figures 2D**, **3A,B** and **Supplementary Table 1**). The majority of those miRNAs were downregulated (10 miRNAs), and two were upregulated in the SI compared to GH condition in both sexes. From the male-specific miRNAs that were differentially expressed in SI compared to GH rats, the majority of those miRNAs (16 miRNAs) were upregulated but others (9 miRNAs) were downregulated (**Supplementary Table 2**). From the female-specific miRNAs that were differentially expressed in SI compared to GH rats, 29 were upregulated and 27 were downregulated (**Supplementary Table 3**). Note that for the miRNA analysis, all isomiRs for each reference miRNA are merged. Our sequencing analysis also identified one novel DE miRNA in both males and females, eight novel DE miRNAs in males only, and five novel DE miRNAs in females only (**Supplementary Table 4**).

Seqbuster of small RNA Seq reads were aligned to rat miRBase v21, which allowed for aligning of sequences to chromosomes. Our results indicate that most of the miRNA precursors that were DE between SI and GH conditions map onto Chromosome 6. Indeed, we found that a cluster on Chromosome 6 in males included rno-miR-329, rno-miR-411, rno-miR-543, and rno-miR-666, and a cluster in females included rno-miR-369, rno-miR-382, and rno-miR-485. Of the differentially expressed (SI vs. GH) miRNAs identified in this study, we found only one miRNA gene in females (miR-98) and one in males (miR-221) that map onto Chromosome X, and none onto Chromosome Y (**Figure 6**).

Pathway Analysis Reveals Sex-Specific Pathway Activation in adBNST Tissue From SI Compared to GH Rats

We used DIANA miRPath v.3 to identify pathways in which DE miRNAs might be involved (**Figure 4**). Based on an analysis, that assesses pathways involved based on mRNA targets, using an intersection of three miRNAs and MicroT Threshold 0.8, we identified two such pathways from differentially

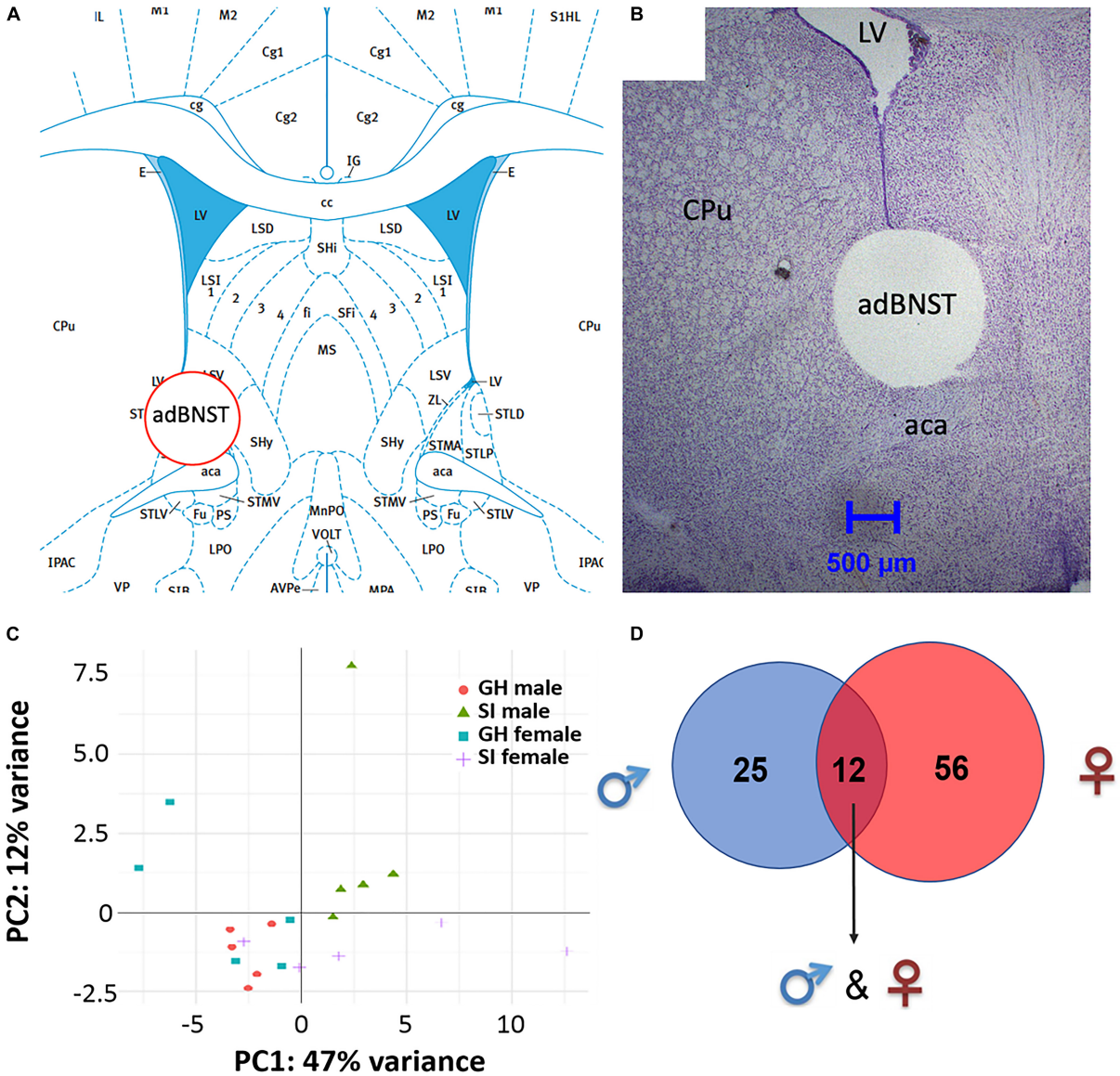

FIGURE 2 | Visualization of the extracted anterodorsal bed nucleus of the stria terminalis (adBNST) and overview of differentially expressed (DE) miRNAs from the adBNST measured using small RNA sequencing. **(A)** Representative coronal brain atlas plate (Paxinos and Watson, 2007) of brain punch location. **(B)** Cresyl violet stained tissue section showing verification of brain punch location of rat adBNST. Note that the internal diameter of the corer used is 1-mm, which is approximately the width and height of the adBNST. Importantly, the outer diameter of the corer is 1.8-mm, which means that the cresyl violet histology pictures show a "hole" that is larger than the actual tissue punch. We processed tissue sections for each brain to examine the accuracy of our BNST punches (both beginning and end of tissue punch), and we discard data from any brains that have off-target BNST punches. Note that for this study, all BNST punches were on-target. **(C)** Principal component analysis showing the first two components of the regularized log2 transformed miRNA abundance data. Every dot represents a sample and they are colored by the condition information (see the legend). **(D)** A Venn diagram that indicates the number of DE miRNAs that reached significance in SI compared to GH controls in the adBNST in males (blue), females (red), or in both sexes (overlap of blue and red). GH, group housed; SI, socially isolated.

expressed miRNAs from both males and females: ECM–receptor interaction and *N*-glycan biosynthesis (**Figure 4A**). Similar analysis revealed four pathways from DE, male-specific miRNAs: hematopoietic cell lineage, GABAergic synapse, microRNAs in cancer, and the PI3K-Akt signaling pathway (**Figure 4B**). Pathway analysis for the DE female-specific miRNAs revealed a total of 16 pathways, including estrogen signaling, cocaine and amphetamine addiction pathways, MAPK signaling, circadian entrainment, axon guidance, and D-glutamine and D-glutamate metabolism (**Figure 4C**).

Validation of miRNA Sequencing Results

To confirm our small RNA sequencing results, we chose representative, DE miRNAs, and performed qRT-PCR on the same RNA samples that we used in the sequencing study as well as on an additional set of samples from rats tested in the EPM

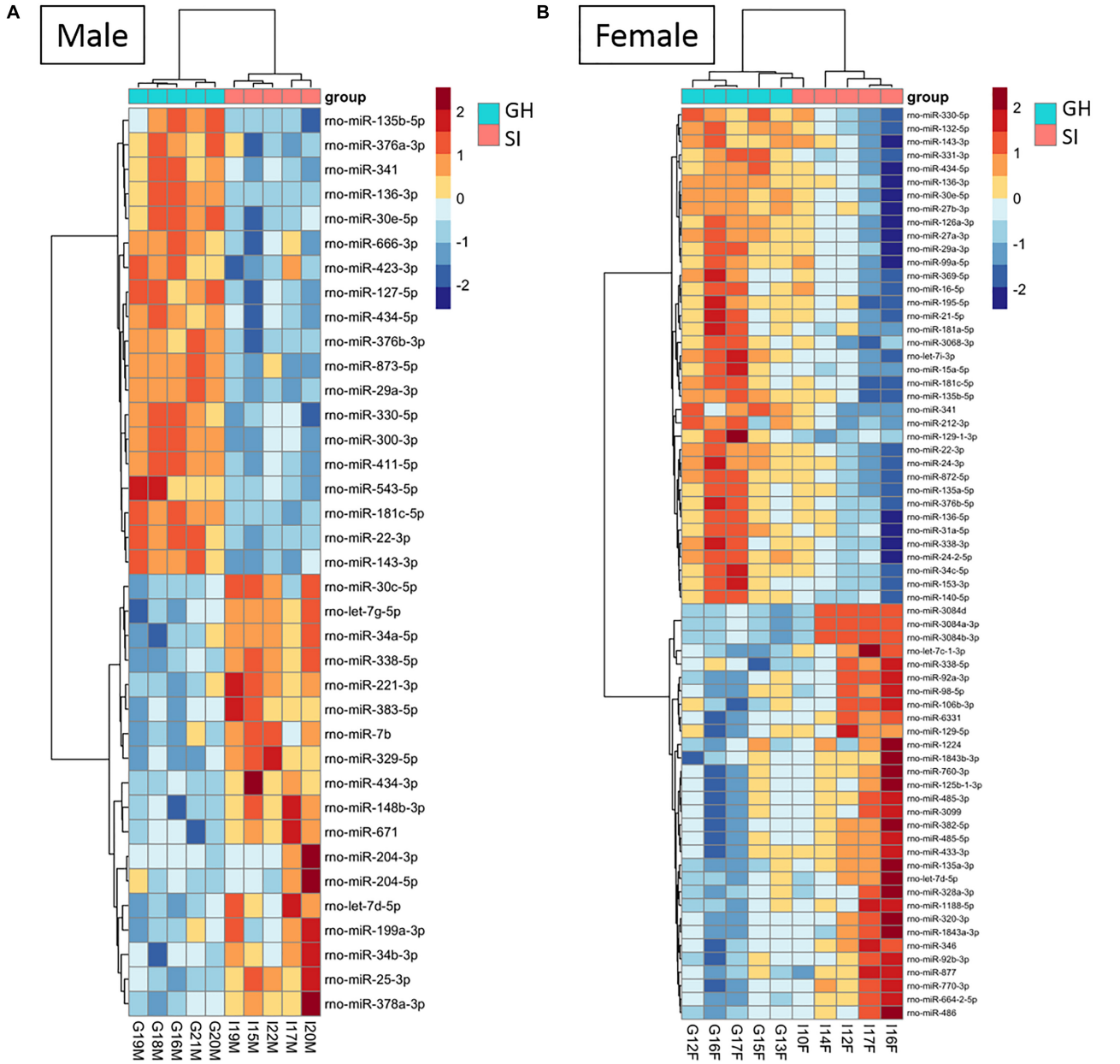

FIGURE 3 | Housing condition during adolescence induces sex-specific miRNA expression in the anterodorsal bed nucleus of the stria terminalis (adBNST) in adulthood. Color represents the miRNA *z*-score expression. The median of the expression is used for each group. DE miRNAs between SI and GH in **(A)** males and **(B)** females; n = 5/group; GH, group housed; SI, socially isolated.

but not in the sequencing study due to space on the sequencing platform. We chose to validate select miRNAs that were DE in females. These were either among the top 10 significantly regulated miRNAs (miR-760-3p and miR-770-3p), or were found within pathways of interest including MAPK signaling and addiction pathways (miR-34c-5p and miR-140-5p). We first identified a miRNA, miR-23b-3p, that was stably expressed across groups in the adBNST in our sequencing study (mean expression 14.03; *SD* 0.098) and confirmed stable expression using qRT-PCR ($p > 0.05$; **Supplementary Figure 4**). Therefore, we proceeded to use miR-23b-3p for normalization across samples. Of the four miRNAs we chose to validate, none were significantly different between SI or GH males in either the sequencing results (**Figure 5A**) or in the qRT-PCR results (**Figure 5C**). In females, all four miRNAs were significantly regulated by housing condition in the sequencing study (housing × miRNA interaction: $F_{(3,24)} = 11.44$, $p < 0.001$; **Figure 5B**). In the female qRT-PCR validation, miRNA expression depended on an interaction between housing and miRNA [$F_{(3,39)} = 4.30$, $p < 0.05$; **Figure 5D**], with *post hoc* analysis showing significant

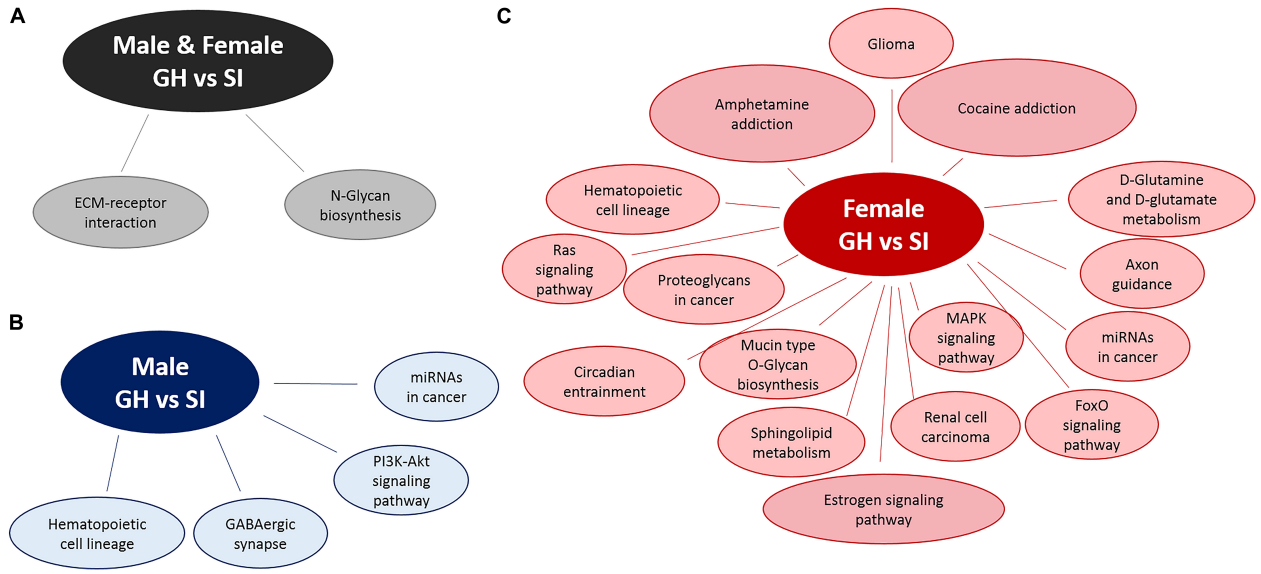

FIGURE 4 | Pathway analysis of DE miRNAs using DIANA miRPath v.3. Pathway analysis for DE miRNAs between SI and GH conditions in **(A)** both males and females, **(B)** males only, and **(C)** females only. GH, group housed; SI, socially isolated.

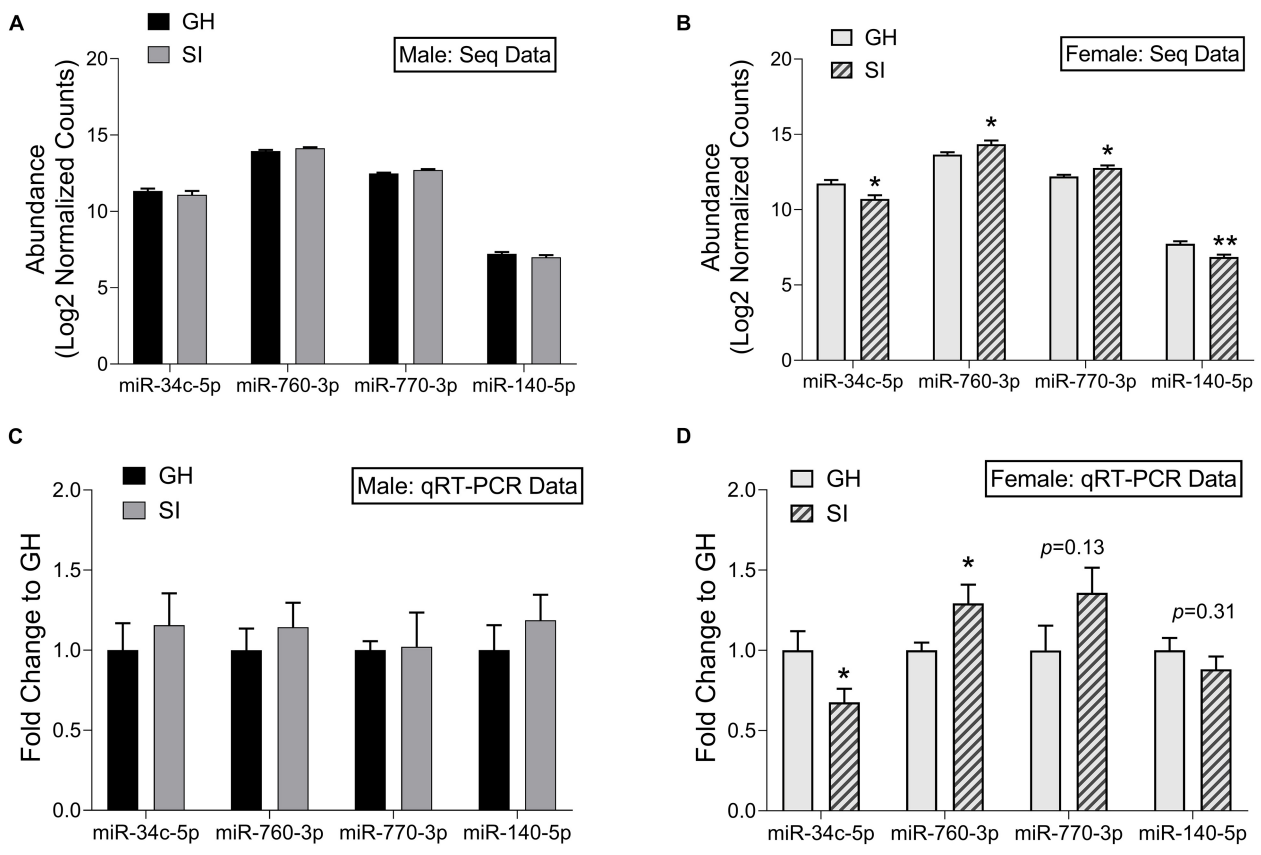

FIGURE 5 | Validation of small RNA sequencing results using qRT-PCR. Log2 normalized counts (abundance) of miRNAs in SI and GH conditions as measured by small RNA sequencing; males **(A)** and females **(B)**. $n = 5$ rats/group. Fold induction (to GH condition) of qRT-PCR results in the adBNST for levels of miRNAs shown in **(A,B)**; Males **(C)** and females **(D)**. $n = 6$–9 rats/group. $^{*}p < 0.05$, $^{**}p < 0.01$, $p = X$ (trend for significance), compared to GH condition for each miRNA. GH, group housed; SI, socially isolated.

differences between SI and GH conditions for miR-34c-5p and miR-760-3p and trends for differences for miR-770-3p and miR-140-5p. In all cases, the direction of regulation matched that of the sequencing results.

Housing Condition During Adolescence Has Sex-Dependent Effects on isomiR Expression in the adBNST in Adulthood

One of the main advantages of using RNA sequencing is its ability to detect changes at a single nucleotide level and detect different miRNA isomers (isomiRs); these include both the reference sequences and also sequences with 1–2 nt variations in the 3p- or 5p-end of the reference miRNA sequence. Using DE analysis, we found a total of 15 isomiRs that were differentially expressed in SI compared to GH males only, 120 isomiRs that were differentially expressed in SI compared to GH females only and five isomiRs that were differentially expressed in SI compared to GH rats of both sexes (**Supplementary Figures 1A,B, 2, 3** for the PCA analysis of all isomiRs measured). Interestingly, in males we identified only seven isomiRs that do not correspond to the reference miRNA sequences (**Supplementary Table 5**). In females, there were 60 isomiRs that did not correspond to reference miRNA sequences and were significantly different between GH and SI (**Supplementary Table 6**). Note that we did not observe any significant differences in isomiR expression when we compared the GH males to the GH females.

Housing Condition During Adolescence in Rats and Childhood Trauma in Humans Induce Similar Changes in miRNAs

Our bioinformatic analysis revealed 15 miRNAs in human blood that were differentially regulated following childhood trauma that are also expressed in the rat adBNST. Of those, nine miRNAs were DE between SI and GH conditions in the rats (**Table 1**). Focusing on miRNAs regulated specifically by childhood trauma in the human samples, we found five miRNAs (miR-106b-3p, miR-181a-5p, miR-125b-1-3p, miR-423-5p, and let-7e-5p) that are DE in SI compared to GH female, and two miRNAs (miR-204-5p and let-7i-5p) DE in SI compared to GH male, and two miRNAs (miR-146a-5p and let-7b-3p) that are DE in SI compared to GH male and female, rat adBNST (**Table 1**). Our analysis showed that the menstrual status of the females did not affect the DE miRNAs.

TABLE 1 | miRNAs regulated by housing condition in rats and by trauma in humans.

miRNA ID	Sex specificity in the rat study	Human study
miR-204-5p	Male only	Childhood trauma
miR-106b-3p	Female only	Childhood trauma
miR-181a-5p	Female only	Childhood trauma
miR-125b-1-3p	Female only	Childhood trauma
miR-423-5p	Female only	Childhood trauma
let-7e-5p	Female only	Childhood trauma
let-7i-5p	Male only	Childhood trauma
miR-146a-5p	Both sexes	Childhood trauma
let-7b-3p	Both sexes	Childhood trauma

Overlapping miRNAs regulated by housing condition in the rat anterodorsal bed nucleus of the stria terminalis (adBNST) and by childhood trauma in human blood samples.

DISCUSSION

This study demonstrates that social housing conditions during adolescence influence anxiety-like behavior in adulthood and produce sex-dependent miRNA signatures in the adBNST, a sexually dimorphic brain region integral to regulating anxiety (Kim et al., 2013; Doura and Unterwald, 2016; Lebow and Chen, 2016). Specifically, females that underwent SI during adolescence showed increased anxiety-like behavior as adults in the EPM compared to GH females, whereas there was no significant effect of adolescent SI on EPM behavior in males. Our small RNA sequencing study and the relevant bioinformatic analysis indicated that the majority of DE miRNAs in the adBNST between SI and GH conditions were sex-specific. In addition, pathway analysis demonstrated that the DE miRNAs are involved in different signaling pathways in males and females. For example, we found that in the female adBNST, miRNAs that are differentially expressed between SI and GH conditions are involved in cocaine and amphetamine addiction pathways as well as in estrogen and MAPK intracellular pathways. However, we found that only one miRNA (rno-miR-3084a/b/d) was differentially expressed between male and female GH controls. By comparing our rat miRNA expression profile based on the different housing conditions with already existing human miRNA data obtained from blood of individuals who experienced trauma (participants in the GTP), we identified nine miRNAs (that are conserved between humans and rats), as stress- and trauma-regulated miRNAs in rats and humans. This finding supports the utility of rodent studies in the effort to better characterize mechanisms underlying human psychopathology.

Adolescent SI has been shown to induce long-lasting effects on stress reactivity and increase anxiety-like behavior in adulthood, an effect that may be sex-specific (McCormick et al., 2004; Weintraub et al., 2010; Skelly et al., 2015). The current study shows that SI compared to GH induced a robust anxiogenic phenotype in female rats, but this effect did not reach significance in male rats. This is supported in the current study by the decreased % time spent in, and entries into, the open arms in females that underwent SI compared to GH conditions. Although we observed similar trends in the males, the effects were not significant. Indeed, our data suggest that it may be GH conditions that are more anxiogenic in males compared to females: quantitatively, GH females spent a greater % of time in the open arms than GH males, an effect that did not reach statistical significance. An early study showed that group housing and overcrowded cages produced a strong stress response in male rats but "calmed" females (Brown and Grunberg, 1995). This effect might be observed in the males due to the social hierarchy, that others have shown that can be anxiogenic in male rodents (Horii et al., 2017). Previous studies using a similar SI paradigm with adolescent onset in male Sprague-Dawley rats

assessed anxiety-like behavior using an EPM and showed that control male rats demonstrate ∼40 s (13%) time spent in open arms (Bledsoe et al., 2011), percent lower than what we observed in the present study (18%). Our results are consistent with previous research showing that adult female rats that underwent adolescent SI demonstrated increased adrenal responses to acute or repeated stress (Weintraub et al., 2010). However, other studies using Long-Evans rats showed that adolescent SI is anxiogenic in male rats (Chappell et al., 2013).

Consistent with the more robust anxiogenic phenotype observed in the SI female rats, we observed greater DE in miRNA expression in the female, compared to the male adBNST. Previous research has shown that adBNST is involved in anxiety-like behavior (Kim et al., 2013; Doura and Unterwald, 2016), which raises the possibility that the observed changes in miRNAs might promote anxiety-like behavior. There was little overlap of miRNA changes between males and females. A previous study by Pfau et al. (2016) using subchronic variable stress followed by small RNA sequencing in the nucleus accumbens (NAc) indicated little overlap of miRNA changes between males and females. In addition, this study also revealed that some miRNAs were up-regulated whereas others were down-regulated following stress (Pfau et al., 2016). Taken together, these findings suggest that males and females process stress differently.

Pathway analysis is a first-choice option to obtain better insight into the underlying biology of differentially expressed genes as it reduces complexity but has increased explanatory power (Khatri et al., 2012). MiRNA-related pathway analysis typically assesses mRNA target predictions (in some cases experimentally proven) followed by a targeted pathway analysis. In this study, we used DIANA miRPath v.3. (Vlachos et al., 2015) to assess pathways in which differentially expressed miRNAs can be involved. DIANA miRPath v.3 assesses miRNA–mRNA target interactions and has incorporated more than 600,000 experimentally supported miRNA targets (Vlachos et al., 2015). As multiple miRNAs have been shown to co-act to regulate molecular pathways, one of the advantages of DIANA miRPath v.3 is that it allows the identification of genes and pathways that are targeted by multiple miRNAs (Vlachos et al., 2015) (in our case minimum of three miRNAs regulating the same target gene). Thus, this type of pathway analysis can provide more biologically relevant results. In females, but not males, we found that DE miRNAs between SI and GH groups were implicated in addiction pathways. This result is intriguing, since SI has been shown to increase drug intake (Bozarth et al., 1989; Raz and Berger, 2010), and it has previously been suggested that miRNAs regulate interactions between stress and drug addiction (Doura and Unterwald, 2016). This finding is also consistent with human literature suggesting there is more of an association of childhood maltreatment and drug dependence in women compared to men (Enoch, 2011). In addition, our results indicate that DE miRNAs between SI and GH conditions in females only are involved in multiple other pathways, including the estrogen signaling pathway, the mitogen-activated protein kinase (MAPK) signaling pathway, the circadian entrainment pathway, and the axon guidance pathway. Further studies that assess the effects of these miRNAs on their relevant mRNA targets are required to confirm their involvement on the aforementioned pathways.

Quantitative real-time polymerase chain reaction (qRT-PCR) is a powerful tool to assess miRNA changes under different experimental conditions, but reliable results depend upon proper normalization to suitable reference genes (Mase et al., 2017). Although RNU6B is typically used for normalization of miRNA expression (Schwarzenbach et al., 2015), it is a small nucleolar RNA rather than a miRNA. Therefore, it lacks the biochemical characteristics of miRNAs (Schwarzenbach et al., 2015). In the current study, our small RNA sequencing results showed that miRNA miR-23b-3p is stably expressed in the adBNST, a finding supported by the small standard deviation (SD = 0.09) in expression among all samples. To validate the sequencing results and the utility of miR-23b-3p as a reference gene in the adBNST, we measured the expression of miR-23b-3p and RNU6B using qRT-PCR and confirmed that miR-23b-3p is stably expressed, thus providing a more biologically relevant approach to normalize miRNA expression in our adBNST samples (**Supplementary Figure 4**). In addition, using qRT-PCR we validated some of the miRNA sequencing results (miR-34c-5p, miR-760-3p, miR-770-3p, and miR-140-5p) and found similar changes to the small RNA sequencing study. These results support the reliability of results obtained using sequencing.

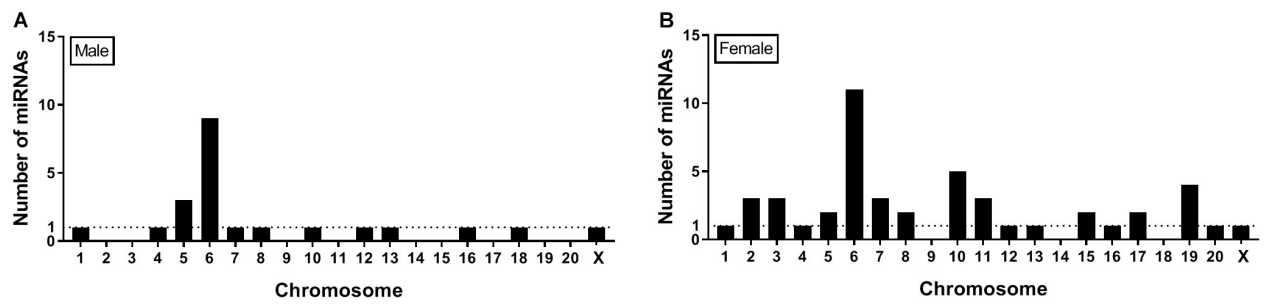

FIGURE 6 | Location on chromosomes of miRNA precursors that are differentially expressed between SI and GH. Seqbuster of small RNA Seq reads were aligned to rat miRBase v21, which allowed for aligning of sequences to chromosomes. Most of the miRNA precursors that are differentially expressed between SI and GH are located on chromosome 6. **(A)** miRNA precursors that are differentially expressed between SI and GH in males only. **(B)** miRNA precursors that are differentially expressed between SI and GH in females only. GH, group housed; SI, socially isolated.

Genes that encode miRNAs are distributed across chromosomes individually or in clusters – typically within 10 Kb of each other (Ghorai and Ghosh, 2014). Our results indicate that most of the miRNA precursors that were DE between SI and GH conditions (9 in males and 11 in females) map onto Chromosome 6 (**Figure 6**), some of them within clusters, which suggests that their expression might be regulated simultaneously. Consistent with this observation, most rat miRNA genes (>60) have been shown to map onto Chromosome 6 (Ghorai and Ghosh, 2014). Of note, more than 50 miRNA genes have been shown to map onto Chromosome X, but no miRNA genes have been identified on Chromosome Y in the rat genome (Ghorai and Ghosh, 2014). These results suggest that most of sex-specific effects on miRNA regulation observed in this study are independent of miRNA gene expression on sex chromosomes, as only two DE miRNAs were found on the X chromosome and none on the Y chromosome.

IsomiRs are mature miRNA isomers that vary in size by one or more nucleotides at the 3′- and/or 5′-end, with the 5′-end known as the "seed region." Depending on where (3′- and/or 5′-end) those variations occur, the stability of the miRNA can be affected. Alternatively, 5′-isomiRs can target different mRNAs compared to the reference miRNA sequence due to shifts in the seed sequence (Tan et al., 2014). IsomiRs can be measured using small RNA sequencing and can differ between sexes (Guo et al., 2016). The current study shows a greater level of isomiR DE in the female compared to the male adBNST between SI and GH conditions (**Supplementary Tables 5**, **6**). These results, together with the overall miRNA analysis, suggest that SI (compared to GH) in females induced more changes in isomiRs compared to the males. Differences in isomiR expression between males and females might be the product of sex differences in the actions of DICER and/or DRHOSHA on isomiRs processing.

Sequencing approaches are also used to identify novel miRNAs, which can be species specific (Huang et al., 2017). In this study, we provide evidence that SI compared to GH housing conditions change the expression of five miRNAs that were not previously identified in the female adBNST, eight in the male adBNST, and one in both male and female adBNST (**Supplementary Table 4**). Future studies are necessary to assess the functional role of those miRNAs.

In a first step to translate our sex-specific and stress-induced miRNA findings to humans, we compared our DE miRNA data with the 15 differentially regulated miRNAs discovered in whole blood following childhood trauma as part of the GTP (Wingo et al., 2015). Importantly, the chronic SI stressor used in the rat studies had an adolescent onset and at least part of the behavioral and biological effects described here were influenced by the developmental aspects of SI during puberty (Varty et al., 1999). Similarly, childhood trauma can have effects on stress-related psychopathology (e.g., PTSD) linked to distinct transcriptional signatures in the blood (Mehta et al., 2013). In a small, but representative subset of the same population (Wingo et al., 2015), we were able to identify blood miRNAs linked to childhood traumatic stress and describe the overlap with the SI signature in rat adBNST. Most of those overlapping miRNAs are regulated by SI in females only (n = 5). However, we also found overlap between male-specific SI-regulated miRNAs (n = 2) as well as miRNAs that are regulated by SI in both males and females (n = 2). The overlapping miRNAs have not been described in a previous human study of PTSD (Daskalakis et al., 2018) and need to be replicated.

It is important to note that one of the limitations of the present study is that SI is a stressor but cannot be considered a traumatic event. Thus, both SI rats and humans that experienced traumatic events experienced stress. However, the intensity of the stressor cannot be considered identical as human individuals experienced more robust stressors. As there are no published studies assessing the effects of SI stress in humans on miRNA expression, the current human study that assessed the effects of childhood trauma on miRNA expression is the most relevant published study to perform a first assessment of the translational utility of our results. This obstacle could had been partially overcome if we had assessed other behaviors in SI rats that are more relevant to traumatic events in humans such as fear conditioning or fear potentiated startle. Importantly, those behaviors include a fear component which could also affect the expression of miRNAs making the effects of SI stress on miRNA expression more difficult to interpret. Our future studies will aim to assess those behaviors on SI rats as well as on overlapping rat-human stress-regulated miRNAs identified in this study.

CONCLUSION

In conclusion, the current study shows that housing conditions (either SI or GH) during adolescence regulate miRNA and isomiR expression in a sex-specific manner in the sexually dimorphic area of the adBNST, raising the possibility that the development of sex-specific pharmacotherapies to treat anxiety-like disorders is essential. Furthermore, this study suggests that the comparison of rat and human miRNA data can reveal translationally relevant information that can be leveraged for treatment and/or diagnostic development.

DATA AVAILABILITY STATEMENT

The datasets generated for this study can be found in the You may view your GSE131289 study at GEO: https://www.ncbi.nlm.nih.gov/geo/query/acc.cgi?acc=GSE131289.

ETHICS STATEMENT

The studies involving human participants were reviewed and approved by the Institutional Review Board of Emory University School of Medicine and Grady Memorial Hospital. The patients/participants provided their written informed consent

to participate in this study. The animal study was reviewed and approved by the Animal Care and Use Committee of McLean Hospital.

AUTHOR CONTRIBUTIONS

MM and EC designed the experiments, analyzed the results, and wrote the manuscript. MM performed the rat studies and the qRT-PCR validation. LP performed the bioinformatic analysis of the small RNA sequencing study and wrote the corresponding part of the manuscript. DP punched the adBNST tissues. MR-G and SA performed the small RNA sequencing study. ND designed and performed the bioinformatic comparison of the rat small RNA sequencing data with the existing human data, wrote the corresponding part of the manuscript, and contributed to the interpretation of those results. KR collected the human data and contributed to the interpretation of the results. EA and FS contributed to the experimental design of the validation of the small RNA sequencing results.

FUNDING

This work was supported by the Jonathan Edward Brooking Fellowship to MM, the Eleanor and Miles Harvard Medical School Fellowship to MM, and the National Institute of Health (DA033526 to EC).

ACKNOWLEDGMENTS

We thank Dr. Aliza Wingo who collected the published human miRNA data that we re-analyzed in this study and Dr. Ioannis Vlachos for providing feedback on using DIANA miRPath v.3. tool.

SUPPLEMENTARY MATERIAL

The Supplementary Material for this article can be found online at: https://www.frontiersin.org/articles/10.3389/fnmol.2019.00236/full#supplementary-material

REFERENCES

Anastasiadou, E., Jacob, L. S., and Slack, F. J. (2018). Non-coding RNA networks in cancer. *Nat. Rev. Cancer* 18, 5–18. doi: 10.1038/nrc.2017.99

Bernstein, D. P., Stein, J. A., Newcomb, M. D., Walker, E., Pogge, D., Ahluvalia, T., et al. (2003). Development and validation of a brief screening version of the Childhood Trauma Questionnaire. *Child Abuse Negl.* 27, 169–190. doi: 10.1016/s0145-2134(02)00541-0

Bledsoe, A. C., Oliver, K. M., Scholl, J. L., and Forster, G. L. (2011). Anxiety states induced by post-weaning social isolation are mediated by CRF receptors in the dorsal raphe nucleus. *Brain Res. Bull.* 85, 117–122. doi: 10.1016/j.brainresbull.2011.03.003

Bozarth, M. A., Murray, A., and Wise, R. A. (1989). Influence of housing conditions on the acquisition of intravenous heroin and cocaine self-administration in rats. *Pharmacol. Biochem. Behav.* 33, 903–907. doi: 10.1016/0091-3057(89)90490-5

Brenhouse, H. C., Napierata, L., Kussmaul, L., Leussis, M., and Andersen, S. L. (2009). Juvenile methylphenidate exposure and factors that influence incentive processing. *Dev. Neurosci.* 31, 95–106. doi: 10.1159/000207498

Brown, K. J., and Grunberg, N. E. (1995). Effects of housing on male and female rats: crowding stresses male but calm females. *Physiol. Behav.* 58, 1085–1089. doi: 10.1016/0031-9384(95)02043-8

Butler, T. R., Carter, E., and Weiner, J. L. (2014). Adolescent social isolation does not lead to persistent increases in anxiety- like behavior or ethanol intake in female long-evans rats. *Alcohol. Clin. Exp. Res.* 38, 2199–2207. doi: 10.1111/acer.12476

Chapman, D. P., Whitfield, C. L., Felitti, V. J., Dube, S. R., Edwards, V. J., and Anda, R. F. (2004). Adverse childhood experiences and the risk of depressive disorders in adulthood. *J. Affect. Disord.* 82, 217–225. doi: 10.1016/j.jad.2003.12.013

Chappell, A. M., Carter, E., McCool, B. A., and Weiner, J. L. (2013). Adolescent rearing conditions influence the relationship between initial anxiety-like behavior and ethanol drinking in male Long Evans rats. *Alcohol. Clin. Exp. Res.* 37(Suppl. 1), E394–E403. doi: 10.1111/j.1530-0277.2012.01926.x

Chartoff, E. H., Ebner, S. R., Sparrow, A., Potter, D., Baker, P. M., and Ragozzino, M. E. (2016). Relative timing between kappa opioid receptor activation and cocaine determines the impact on reward and dopamine release. *Neuropsychopharmacology* 41, 989–1002. doi: 10.1038/npp.2015.226

Chen, X., Ba, Y., Ma, L., Cai, X., Yin, Y., Wang, K., et al. (2008). Characterization of microRNAs in serum: a novel class of biomarkers for diagnosis of cancer and other diseases. *Cell Res.* 18, 997–1006. doi: 10.1038/cr.2008.282

Daniel, S. E., and Rainnie, D. G. (2016). Stress modulation of opposing circuits in the bed nucleus of the stria terminalis. *Neuropsychopharmacology* 41, 103–125. doi: 10.1038/npp.2015.178

Daskalakis, N. P., Cohen, H., Cai, G., Buxbaum, J. D., and Yehuda, R. (2014). Expression profiling associates blood and brain glucocorticoid receptor signaling with trauma-related individual differences in both sexes. *Proc. Natl. Acad. Sci. U.S.A.* 111, 13529–13534. doi: 10.1073/pnas.1401660111

Daskalakis, N. P., Provost, A. C., Hunter, R. G., and Guffanti, G. (2018). Noncoding RNAs: stress, glucocorticoids, and posttraumatic stress disorder. *Biol. Psychiatry* 83, 849–865. doi: 10.1016/j.biopsych.2018.01.009

Dobin, A., Davis, C. A., Schlesinger, F., Drenkow, J., Zaleski, C., Jha, S., et al. (2013). STAR: ultrafast universal RNA-seq aligner. *Bioinformatics* 29, 15–21. doi: 10.1093/bioinformatics/bts635

Dong, H. W., Petrovich, G. D., Watts, A. G., and Swanson, L. W. (2001). Basic organization of projections from the oval and fusiform nuclei of the bed nuclei of the stria terminalis in adult rat brain. *J. Comp. Neurol.* 436, 430–455. doi: 10.1002/cne.1079

Doura, M. B., and Unterwald, E. M. (2016). MicroRNAs Modulate Interactions between Stress and Risk for Cocaine Addiction. *Front. Cell Neurosci.* 10:125. doi: 10.3389/fncel.2016.00125

Dwivedi, Y. (2014). Emerging role of microRNAs in major depressive disorder: diagnosis and therapeutic implications. *Dialog. Clin. Neurosci.* 16, 43–61.

Enoch, M. A. (2011). The role of early life stress as a predictor for alcohol and drug dependence. *Psychopharmacology* 214, 17–31. doi: 10.1007/s00213-010-1916-6

Erb, S., and Stewart, J. (1999). A role for the bed nucleus of the stria terminalis, but not the amygdala, in the effects of corticotropin-releasing factor on stress-induced reinstatement of cocaine seeking. *J. Neurosci.* 19:RC35.

Ewels, P., Magnusson, M., Lundin, S., and Kaller, M. (2016). MultiQC: summarize analysis results for multiple tools and samples in a single report. *Bioinformatics* 32, 3047–3048. doi: 10.1093/bioinformatics/btw354

Faria, M. P., Miguel, T. T., Gomes, K. S., and Nunes-de-Souza, R. L. (2016). Anxiety-like responses induced by nitric oxide within the BNST in mice: role of CRF1 and NMDA receptors. *Horm. Behav.* 79, 74–83. doi: 10.1016/j.yhbeh.2016.01.002

Friedlander, M. R., Mackowiak, S. D., Li, N., Chen, W., and Rajewsky, N. (2012). miRDeep2 accurately identifies known and hundreds of novel microRNA genes in seven animal clades. *Nucleic Acids Res.* 40, 37–52. doi: 10.1093/nar/gkr688

Ghorai, A., and Ghosh, U. (2014). miRNA gene counts in chromosomes vary widely in a species and biogenesis of miRNA largely depends on transcription or post-transcriptional processing of coding genes. *Front. Genet.* 5:100. doi: 10.3389/fgene.2014.00100

Gillespie, C. F., Phifer, J., Bradley, B., and Ressler, K. J. (2009). Risk and resilience: genetic and environmental influences on development of the stress response. *Depress. Anxiety* 26, 984–992. doi: 10.1002/da.20605

Glinge, C., Clauss, S., Boddum, K., Jabbari, R., Jabbari, J., Risgaard, B., et al. (2017). Stability of circulating blood-based microrNAs - pre-analytic methodological considerations. *PLoS One* 12:e0167969. doi: 10.1371/journal.pone.0167969

Grasso, M., Piscopo, P., Confaloni, A., and Denti, M. A. (2014). Circulating miRNAs as biomarkers for neurodegenerative disorders. *Molecules* 19, 6891–6910. doi: 10.3390/molecules19056891

Guo, L., Liang, T., Yu, J., and Zou, Q. (2016). A comprehensive analysis of miRNA/isomiR expression with gender difference. *PLoS One* 11:e0154955. doi: 10.1371/journal.pone.0154955

Hankin, B. L., Mermelstein, R., and Roesch, L. (2007). Sex differences in adolescent depression: stress exposure and reactivity models. *Child Dev.* 78, 279–295. doi: 10.1111/j.1467-8624.2007.00997.x

Holland, F. H., Ganguly, P., Potter, D. N., Chartoff, E. H., and Brenhouse, H. C. (2014). Early life stress disrupts social behavior and prefrontal cortex parvalbumin interneurons at an earlier time-point in females than in males. *Neurosci. Lett.* 566, 131–136. doi: 10.1016/j.neulet.2014.02.023

Horii, Y., Nagasawa, T., Sakakibara, H., Takahashi, A., Tanave, A., Matsumoto, Y., et al. (2017). Hierarchy in the home cage affects behaviour and gene expression in group-housed C57BL/6 male mice. *Sci. Rep.* 7:6991. doi: 10.1038/s41598-017-07233-5

Huang, Y., Ren, H. T., Xiong, J. L., Gao, X. C., and Sun, X. H. (2017). Identification and characterization of known and novel microRNAs in three tissues of Chinese giant salamander base on deep sequencing approach. *Genomics* 109, 258–264. doi: 10.1016/j.ygeno.2017.04.007

Im, H. I., and Kenny, P. J. (2012). MicroRNAs in neuronal function and dysfunction. *Trends Neurosci.* 35, 325–334. doi: 10.1016/j.tins.2012.01.004

Kessler, R. C. (2003). Epidemiology of women and depression. *J. Affect. Disord.* 74, 5–13. doi: 10.1016/s0165-0327(02)00426-3

Khatri, P., Sirota, M., and Butte, A. J. (2012). Ten years of pathway analysis: current approaches and outstanding challenges. *PLoS Comput. Biol.* 8:e1002375. doi: 10.1371/journal.pcbi.1002375

Khoury, L., Tang, Y. L., Bradley, B., Cubells, J. F., and Ressler, K. J. (2010). Substance use, childhood traumatic experience, and posttraumatic stress disorder in an urban civilian population. *Depress. Anxiety* 27, 1077–1086. doi: 10.1002/da.20751

Kim, S. Y., Adhikari, A., Lee, S. Y., Marshel, J. H., Kim, C. K., Mallory, C. S., et al. (2013). Diverging neural pathways assemble a behavioural state from separable features in anxiety. *Nature* 496, 219–223. doi: 10.1038/nature12018

Knoll, A. T., Meloni, E. G., Thomas, J. B., Carroll, F. I., and Carlezon, W. A. Jr. (2007). Anxiolytic-like effects of kappa-opioid receptor antagonists in models of unlearned and learned fear in rats. *J. Pharmacol. Exp. Ther.* 323, 838–845. doi: 10.1124/jpet.107.127415

Kozomara, A., and Griffiths-Jones, S. (2014). miRBase: annotating high confidence microRNAs using deep sequencing data. *Nucleic Acids Res.* 42, D68–D73. doi: 10.1093/nar/gkt1181

Lebow, M. A., and Chen, A. (2016). Overshadowed by the amygdala: the bed nucleus of the stria terminalis emerges as key to psychiatric disorders. *Mol. Psychiatry.* 21, 450–463. doi: 10.1038/mp.2016.1

Lori, A., Maddox, S. A., Sharma, S., Andero, R., Ressler, K. J., and Smith, A. K. (2018). Dynamic patterns of threat-associated gene expression in the amygdala and blood. *Front. Psychiatry* 9:778. doi: 10.3389/fpsyt.2018.00778

Love, M. I., Huber, W., and Anders, S. (2014). Moderated estimation of fold change and dispersion for RNA-seq data with DESeq2. *Genom. Biol.* 15:550.

Mangan, M. E., Williams, J. M., Kuhn, R.M. and Lathe, W.C. 3rd. (2014). The UCSC genome browser: what every molecular biologist should know. *Curr. Protoc. Mol. Biol.* 107, 19.9.1–19.9.36. doi: 10.1002/0471142727.mb1909s107

Martin, M. (2011). Cutadapt removes adapter sequences from high-throughput sequencing reads. *EMBnet* 17, 10–12.

Mase, M., Grasso, M., Avogaro, L., D'Amato, E., Tessarolo, F., Graffigna, A., et al. (2017). Selection of reference genes is critical for miRNA expression analysis in human cardiac tissue. A focus on atrial fibrillation. *Sci. Rep.* 7:41127. doi: 10.1038/srep41127

Mavrikaki, M., Anastasiadou, E., Ozdemir, R. A., Potter, D., Helmholz, C., Slack, F. J., et al. (2019). Overexpression of miR-9 in the nucleus accumbens increases oxycodone self-administration. *Int. J. Neuropsychopharmacol.* 22, 383–393. doi: 10.1093/ijnp/pyz015

Mavrikaki, M., Girardet, C., Kern, A., Faruzzi Brantley, A., Miller, C. A., Macarthur, H., et al. (2016). Melanocortin-3 receptors in the limbic system mediate feeding-related motivational responses during weight loss. *Mol. Metab.* 5, 566–579. doi: 10.1016/j.molmet.2016.05.002

McCormick, C. M., Robarts, D., Gleason, E., and Kelsey, J. E. (2004). Stress during adolescence enhances locomotor sensitization to nicotine in adulthood in female, but not male, rats. *Horm. Behav.* 46, 458–466. doi: 10.1016/j.yhbeh.2004.05.004

Mehta, D., Klengel, T., Conneely, K. N., Smith, A. K., Altmann, A., Pace, T. W., et al. (2013). Childhood maltreatment is associated with distinct genomic and epigenetic profiles in posttraumatic stress disorder. *Proc. Natl. Acad. Sci. U.S.A.* 110, 8302–8307. doi: 10.1073/pnas.1217750110

Nestler, E. J., and Hyman, S. E. (2010). Animal models of neuropsychiatric disorders. *Nat. Neurosci.* 13, 1161–1169. doi: 10.1038/nn.2647

Newman, A. M., Liu, C. L., Green, M. R., Gentles, A. J., Feng, W., Xu, Y., et al. (2015). Robust enumeration of cell subsets from tissue expression profiles. *Nat. Methods* 12, 453–457. doi: 10.1038/nmeth.3337

Pantano, L., Estivill, X., and Marti, E. (2010). SeqBuster, a bioinformatic tool for the processing and analysis of small RNAs datasets, reveals ubiquitous miRNA modifications in human embryonic cells. *Nucleic Acids Res.* 38:e34. doi: 10.1093/nar/gkp1127

Pantano, L., Estivill, X., and Marti, E. (2011). A non-biased framework for the annotation and classification of the non-miRNA small RNA transcriptome. *Bioinformatics* 27, 3202–3203. doi: 10.1093/bioinformatics/btr527

Pantano, L., Friedlander, M. R., Escaramis, G., Lizano, E., Pallares-Albanell, J., Ferrer, I., et al. (2016). Specific small-RNA signatures in the amygdala at premotor and motor stages of Parkinson's disease revealed by deep sequencing analysis. *Bioinformatics* 32, 673–681. doi: 10.1093/bioinformatics/btv632

Paxinos, G., and Watson, C. (2007). *The Rat Brain in Stereotaxic Coordinates*. Amsterdam: Elsevier.

Pfau, M. L., Purushothaman, I., Feng, J., Golden, S. A., Aleyasin, H., Lorsch, Z. S., et al. (2016). Integrative analysis of sex-specific microRNA networks following stress in mouse nucleus accumbens. *Front. Mol. Neurosci.* 9:144. doi: 10.3389/fnmol.2016.00144

Raz, S., and Berger, B. D. (2010). Social isolation increases morphine intake: behavioral and psychopharmacological aspects. *Behav. Pharmacol.* 21, 39–46. doi: 10.1097/FBP.0b013e32833470bd

Rubio, M., Bustamante, M., Hernandez-Ferrer, C., Fernandez-Orth, D., Pantano, L., Sarria, Y., et al. (2018). Circulating miRNAs, isomiRs and small RNA clusters in human plasma and breast milk. *PLoS One* 13:e0193527. doi: 10.1371/journal.pone.0193527

Schmittgen, T. D., and Livak, K. J. (2008). Analyzing real-time PCR data by the comparative C(T) method. *Nat. Protoc.* 3, 1101–1108. doi: 10.1038/nprot.2008.73

Schwarzenbach, H., da Silva, A. M., Calin, G., and Pantel, K. (2015). Data normalization strategies for MicroRNA quantification. *Clin. Chem.* 61, 1333–1342. doi: 10.1373/clinchem.2015.239459

Sharma, S., and Eghbali, M. (2014). Influence of sex differences on microRNA gene regulation in disease. *Biol. Sex Differ.* 5, 3. doi: 10.1186/2042-6410-5-3

Skelly, M. J., Chappell, A. E., Carter, E., and Weiner, J. L. (2015). Adolescent social isolation increases anxiety-like behavior and ethanol intake and impairs fear extinction in adulthood: possible role of disrupted noradrenergic signaling. *Neuropharmacology* 97, 149–159. doi: 10.1016/j.neuropharm.2015.05.025

Tan, G. C., Chan, E., Molnar, A., Sarkar, R., Alexieva, D., Isa, I. M., et al. (2014). 5' isomiR variation is of functional and evolutionary importance. *Nucleic Acids Res.* 42, 9424–9435. doi: 10.1093/nar/gku656

Varty, G. B., Braff, D. L., and Geyer, M. A. (1999). Is there a critical developmental 'window' for isolation rearing-induced changes in prepulse inhibition of the acoustic startle response? *Behav. Brain Res.* 100, 177–183. doi: 10.1016/s0166-4328(98)00129-6

Vlachos, I. S., Zagganas, K., Paraskevopoulou, M. D., Georgakilas, G., Karagkouni, D., Vergoulis, T., et al. (2015). DIANA-miRPath v3.0: deciphering microRNA function with experimental support. *Nucleic Acids Res.* 43, W460–W466. doi: 10.1093/nar/gkv403

Weintraub, A., Singaravelu, J., and Bhatnagar, S. (2010). Enduring and sex-specific effects of adolescent social isolation in rats on adult stress reactivity. *Brain Res.* 1343, 83–92. doi: 10.1016/j.brainres.2010.04.068

Willard, V. W., Long, A., and Phipps, S. (2016). Life stress versus traumatic stress: the impact of life events on psychological functioning in children with and without serious illness. *Psychol. Trauma.* 8, 63–71. doi: 10.1037/tra0000017

Wingo, A. P., Almli, L. M., Stevens, J. S., Klengel, T., Uddin, M., Li, Y., et al. (2015). DICER1 and microRNA regulation in post-traumatic stress disorder with comorbid depression. *Nat. Commun.* 6:10106. doi: 10.1038/ncomms10106

Conflict of Interest: The authors declare that the research was conducted in the absence of any commercial or financial relationships that could be construed as a potential conflict of interest.

frontiers in Molecular Neuroscience

ORIGINAL RESEARCH
published: 11 October 2019
doi: 10.3389/fnmol.2019.00239

CSF Cholinergic Index, a New Biomeasure of Treatment Effect in Patients With Alzheimer's Disease

Azadeh Karami[1]*, *Maria Eriksdotter*[1,2], *Ahmadul Kadir*[1,2], *Ove Almkvist*[1], *Agneta Nordberg*[1,2] and *Taher Darreh-Shori*[1]*

[1]Center for Alzheimer Research, Department of Neurobiology, Care Sciences and Society, Division of Clinical Geriatrics, Karolinska Institutet, Solna, Sweden, [2]Karolinska University Hospital Huddinge, Theme Aging, Stockholm, Sweden

Alzheimer's disease (AD) is a progressive disease with early degeneration of the central cholinergic neurons. Currently, three of four AD drugs act by inhibiting the acetylcholine (ACh) degrading enzyme, acetylcholinesterase (AChE). Efficacy of these drugs depends on available amount of ACh, which is biosynthesized by choline acetyltransferase (ChAT). We investigated whether treatment with a cholinesterase-inhibitor, galantamine, alters the relative levels of AChE to ChAT in cerebrospinal fluid (CSF) and whether levels of these CSF biomarkers correlate with *in vivo* AChE activity and nicotinic binding sites in the brain assessed by positron emission tomography (PET). Protein concentrations and activities of ChAT and AChE were measured in CSF of 18 patients with mild AD prior to and after 3 months of treatment with galantamine ($n = 12$) or placebo ($n = 6$), followed by nine additional months of galantamine treatment in all patients. A Cholinergic index was defined as the ratio of ChAT to AChE in CSF and was evaluated in relation to the *in vivo* AChE activity, the nicotinic binding sites and different measures of cognition. Besides an expected inhibition of AChE activity, galantamine treatment was accompanied by a mild increase in CSF ChAT activity. Thereby, the Cholinergic index was significantly increased in the *Galantamine group* (60% ± 14) after 3 months compared to baseline ($p < 0.0023$) or ($p < 0.0004$). This index remained high in *the Galantamine group* compared to baseline (54% ± 11) at 12 months follow-up, while it showed an increase in *the Placebo group* when they switched to active galantamine treatment (44% ± 14 vs. baseline, 61% ± 14 vs. 3 months, all p-values < 0.05). Furthermore, the *in vivo* brain AChE activity (assessed by PET) correlated with the CSF Cholinergic index at 12 months ($r = 0.98$, $p < 0.001$). The CSF Cholinergic index also correlated with ADAS-Cog and some other neuropsychological tests at 12 months. This is the first study assessing a CSF Cholinergic index in relation to treatment with a cholinesterase inhibitor. The treatment-specific increase in CSF ChAT activity suggests that cholinesterase-inhibitors may also increase the ACh-biosynthesis capacity in the patients. Additional studies are warranted to evaluate the utility of the CSF Cholinergic index as a biomeasure of therapeutic effect in AD.

Keywords: Alzheimer's disease, choline acetyltransferase, acetylcholinesterase, positron emission tomography (PET), cerebrospinal fluid (CSF), red blood cells (RBCs), nicotinic binding sites, galantamine

OPEN ACCESS

Edited by:
Hermona Soreq, Hebrew University of Jerusalem, Israel

Reviewed by:
Rebecca Jane Rylett, University of Western Ontario, Canada
Oksana Lockridge, University of Nebraska Medical Center, United States

***Correspondence:**
Azadeh Karami
azadeh.karami@ki.se
Taher Darreh-Shori
taher.darreh-shori@ki.se

Received: *04 June 2019*
Accepted: *19 September 2019*
Published: *11 October 2019*

Citation:
Karami A, Eriksdotter M, Kadir A, Almkvist O, Nordberg A and Darreh-Shori T (2019) CSF Cholinergic Index, a New Biomeasure of Treatment Effect in Patients With Alzheimer's Disease. Front. Mol. Neurosci. 12:239. doi: 10.3389/fnmol.2019.00239

INTRODUCTION

The central cholinergic pathways have prominent roles in learning and memory. The severity of cholinergic deficits in patients with Alzheimer's disease (AD) correlates with cognitive impairment, which have led to the development of cholinesterase inhibitors (ChEIs). The currently registered ChEIs as AD therapeutics putatively act by inhibiting the degradation of acetylcholine (ACh) in the synaptic cleft by the synaptic acetylcholinesterase (AChE), prolonging ACh's action on its receptors (AChRs; Darreh-Shori and Soininen, 2010).

ChEIs are in use as symptomatic therapy in patients with AD for decades now. Still there are major gaps in our understanding of the *in vivo* biodynamic processes that may account for their limited clinical efficacies, possible disease-modifying effect or development of tolerance against these drugs.

There are three registered ChEIs for symptomatic treatment of dementia, namely donepezil (Winblad et al., 2001; Whitehead et al., 2004), rivastigmine (Rösler et al., 1999) and galantamine (Raskind et al., 2000, 2004; Tariot et al., 2000; Wilcock et al., 2003; Aronson et al., 2009), which have shown both short- and long-term benefits with regard to behavioral and cognitive measurements. The pharmacological properties differ among these ChEIs (Darreh-Shori and Soininen, 2010). Donepezil and galantamine are selective and rapidly reversible inhibitors of AChE, while rivastigmine is a pseudo-irreversible inhibitor of both AChE and its closely related enzyme, butyrylcholinesterase (BChE; Darreh-Shori and Soininen, 2010).

There are large amounts of AChE and BChE activities in blood and plasma. A hematopoietic splice variant of AChE exists in blood, anchored mainly on the red blood cells (RBC AChE) by a glycophosphatidylinositol anchoring protein. Measurement of changes in the RBC AChE activity following treatment with ChEIs has also been used to define the inhibition level of AChE in patients treated with ChEIs (Sramek and Cutler, 2000).

Several reports exist concerning the changes in the AChE and BChE activities and protein levels in blood and cerebrospinal fluid (CSF) following treatment with ChEIs (Nordberg and Svensson, 1998; Darreh-Shori et al., 2006, 2008; Nordberg et al., 2009). In CSF there are two splice variants of AChE, the synaptic (AChE-S) and the stress-associated read-through (AChE-R) variants (Darreh-Shori et al., 2004). Treatment with donepezil or galantamine causes a significant increase in the protein level of AChE-S in CSF of patients (Darreh-Shori et al., 2006, 2008; Nordberg et al., 2009). Through an integration of the changes in the CSF AChE-S protein relative to the corresponding changes in its activity in CSF (Darreh-Shori et al., 2006), we have shown that the CSF increase in the protein expression of AChE reflects at least partially the extent of *in vivo* AChE inhibition in the brain, assessed by positron emission tomography (PET; Darreh-Shori et al., 2008).

Nonetheless, such an increase in the AChE expression may also be a sign of development of a drug tolerance or is signifying a remodeling of the central cholinergic network in response to the prolonged action of ACh at the cholinergic synapses. Indeed, this is a highly plausible disease-modifying outcome since the primary target of the ChEIs is the membrane-anchored synaptic splice variant of AChE protein at the remaining functional cholinergic synapses (Lane and Darreh-Shori, 2015).

To investigate whether the observed increase of AChE protein expression in CSF of patients treated with ChEIs is a sign of drug tolerance or remodeling of the central cholinergic network, it is crucial to simultaneously investigate the changes in the level of the ACh-synthesizing enzyme, choline acetyltransferase (ChAT). This is because a remodeling and/or regeneration of the cholinergic synapses will most likely require extra expression of both ChAT and AChE. In this context, recent reports of the presence of a soluble variant of ChAT in both plasma and CSF has provided a unique opportunity (Vijayaraghavan et al., 2013 Karami et al., 2015) to monitor changes in soluble ChAT for assessing possible improvement of cholinergic neurons in the brain during ChEIs therapy.

In the current study, we hence investigated the changes in AChE and ChAT activities following treatment of a group of patients treated with placebo or galantamine for 3 months followed with galantamine treatment for all in 9–12 months. These changes were also analyzed in relation to available *in vivo* brain PET data, namely the number of nicotinic binding sites and AChE inhibition in different brain regions of the AD patients for up to 1 year.

These objectives are clinically important by providing information about short- and long-term efficacy as well as the underlying mechanism of development of tolerance or delaying the progression of AD during long-term treatment with ChEIs.

MATERIALS AND METHODS

Study Design and Patients

Details of the study have been described elsewhere (Darreh-Shori et al., 2008; Kadir et al., 2008). Briefly, 18 mildly demented AD patients [mean age 69 $\pm$ 2 years, Mini Mental State Examination (MMSE) 26 $\pm$ 1, duration of disease 4 $\pm$ 1 years] were included. A schematic presentation of the study design is shown in **Figure 1A**. The first 3 months of the study was a double-blind placebo-controlled study where six AD patients received placebo and 12 patients received galantamine in flexible doses (16–24 mg daily), followed by 9 months treatment with galantamine for all patients. The patients were recruited at the Danderyd Hospital, and the memory clinic of Karolinska University Hospital Huddinge, Stockholm, Sweden. The diagnosis of AD was made in accordance with the National Institute of Neurological and Communication Disorders and Stroke-AD and Related Disorders Association (NINCDS-ADRDA) criteria (McKhann et al., 1984). Neuropsychological tests were performed throughout the study, at baseline, and after 3 and 12 months follow-up. Blood and CSF samples were obtained at baseline, at 3 and at 12 months.

All patients and their caregivers provided written informed consent to participate in the study, which was conducted according to the Declaration of Helsinki and subsequent revisions. The Ethics Committee of Huddinge University Hospital, Sweden approved the study.

Collection of Blood and CSF Samples

To evaluate cholinesterase activities in RBC and CSF, whole blood and CSF samples were collected from all patients at baseline (pre-drug samples). Whole-blood was collected in standard tubes containing EDTA as anticoagulant. Then, blood was also collected after 3 and 12 months during the study. CSF samples, taken at baseline and after 3 and 12 months of treatment, were collected by lumbar puncture in the L3/L4 or L4/L5 interspace at mornings between 9–12 a.m. All CSF samples were kept frozen in small aliquots at –80°C, until the assay. More detailed information have been given previously (Darreh-Shori et al., 2008; Kadir et al., 2008).

Measurement of CSF ChAT Activity and Protein Concentration

CSF ChAT activity was measured by a colorimetric assay (Vijayaraghavan et al., 2013) in the baseline samples as well as in samples collected after 3 and 12 months follow-up. A modified version of the assay protocol was used, which sequentially quantifies both the activity and amount of ChAT protein, as well as the endogenous choline concentration in biological samples, described in detail below.

ChAT Assay Preparations

The wells of high binding 384-well microtiter plates (Nunc Maxisorb, Denmark) were coated overnight at 4°C with 75 μl of monoclonal anti-human ChAT antibody (MAB3447, R&D System, UK; at 1:250 dilution in carbonate buffer, pH 9.8). The wells for choline standards and their blanks were not coated with the capturing antibody. On the following day, the plates were washed with PBS and tapped dry for the next step (as described below in the assay procedure).

Undiluted CSF samples (10 μl/well) were applied both unmodified (i.e., in native conditions, in triplicates) and as modified denatured samples (also in triplicate). The denatured samples served as controls for both the ChAT activity and the endogenous concentration of choline in the samples. The denatured CSF samples were prepared by heating in a thermal cycler, with three cycles of 8 min at 98°C, and 30 s at 60°C.

Two series of standards were used on each plate, a choline standard sets for quantifying the choline concentration in the wells, and a ChAT protein standard series for quantifying the amount of ChAT protein in the samples. The choline standards were prepared by two-fold serial dilutions of choline chloride solution in TBS buffer (10 mM Tris-HCl, 0.9% sodium chloride, 1 mM EDTA and 0.05% Triton X-100, pH 7.4). The highest choline standard point was 50 μM, and 50 μl/well (in triplicates) of each choline standards were applied into the wells of the microtiter plate. As the ChAT protein standard, a calibrated pooled human plasma sample was used. Like the CSF samples, the ChAT protein standards were applied both as native (unmodified) and as denatured samples (10 μl/well, all in triplicates). The highest ChAT protein standard had a concentration of 1.14 μg/ml, which was prepared by 50 times dilution of the calibrated pooled plasma sample. The denatured standards were prepared as described above for CSF samples.

The ChAT assay requires two master-mix cocktails: ***Cocktail-A*** and ***-B***. The ***Cocktail-A*** was prepared in the TBS buffer, and contained 18.75 μM of choline chloride (C1879, Sigma-Aldrich), 0.75 mM of eserine hemisulfate (E8625, Sigma-Aldrich), 1.25U/mL of phosphotransacetylase (P2783, Sigma-Aldrich), 8.75 mM of acetyl phosphate (P2783, Sigma-Aldrich), and 62.5 μM acetyl-coenzyme A (A2181, Sigma-Aldrich). The Cocktail A was incubated for 10–15 min at 38°C prior to the assay procedure. The ***Cocktail-B*** was prepared in PBS (50 mM phosphate buffered saline, pH 7.4), and contained 0.93 U/ml of choline oxidase (from a 50 U/ml stock, C5896, Sigma-Aldrich), 1/5,000 Streptavidin horseradish peroxidase (P6782 Sigma-Aldrich), 6.3 mM of phenol (P3653, Sigma-Aldrich), and 3 mM of 4-aminoantipyrine (A4382, Sigma-Aldrich). Both cocktails should be prepared freshly.

ChAT Assay Procedure

The unmodified and denatured CSF samples (10 μl/well), the ChAT protein standards (10 μl/well), or the TBS buffer (10 μl/well, as choline-controls) were applied to the wells of the anti-ChAT antibody pre-coated microtiter plate. The choline standards (50 μl/well) were applied to un-coated wells on the plate. Then, 40 μl/well of the Cocktail-A was applied to all wells but the choline standards, using a multichannel pipette. The plate was then sealed and incubated for 2 h in a humid chamber at 38.5°C under gentle shaking. The plate was cooled briefly on ice-water bath and centrifuged gently. The sealing tape was removed and 25 μl/well of the ***Cocktail-B*** was added to all wells, including the wells containing the choline standards. The reaction was then monitored continuously at 1–2 min intervals at 500 nm for changes in absorbance for as long as was deemed necessary (usually 15–30 min) using a Tecan Infinite M1000 microplate reader. This step quantifies both the ChAT activity and the choline concentration in the samples.

After this step, the plate was sealed and incubated overnight at 4°C. On the following day, the plate was washed three times for 5 min with TBS-$T^{0.05\%}$ (10 mM Tris-HCl, pH 7.4, 0.9% sodium chloride, 0.05% Tween 20), and incubated with 100 μl/well of a blocking buffer (TBS-$T^{0.05\%}$ containing 5% BSA and 0.01% sodium azide) for 30 min at 38°C in a humid chamber under gentle shaking. The plate was then washed as before, and incubated for 60 min with 50 μl/well of a working dilution of 1:1,700 of the detecting anti-ChAT antibody (rabbit anti-ChAT polyclonal antibody, PAB 14536, Abnova, Taiwan, prepared in TBS-$T^{0.05\%}$, containing 1% BSA and 0.01% sodium azide) at 38°C in a humid chamber under gentle shaking. Then 25 μl/well of a working solution of a secondary swine anti-rabbit polyclonal antibody (1:2,000, D0306, prepared in TBS-$T^{0.05\%}$, containing 1% BSA and 0.01% sodium azide) was added to the wells and incubated for two more hours at room temperature under gentle shaking. The plate was washed four times with TBS-$T^{0.05\%}$ and one time with 1 M diethanolamine buffer (pH 9.8, containing 1 M magnesium chloride and 0.01% sodium azide). Finally, 75 μl/well of a solution of the alkaline phosphatase substrate [1 mg/mL of p-nitrophenyl phosphate (73724, Sigma-Aldrich), in the diethanolamine buffer]. The absorbance was read at 405 nm until the absorbance of plasma standard reached 2–2.5.

ChAT activity (pmol/min/mL samples) was calculated according to the following formula: **ChAT activity** = $(\mathbf{C}_d - \mathbf{C}_n)/\ \boldsymbol{t}\ ^*\ V_s$, in which C_d and C_n are the measured choline concentrations in the wells (in pmol) containing the denatured and native samples, respectively, t is the incubation time with the ***Cocktail-A*** (in minutes) at 38°C, and V_s is the 10 μl volume of the samples applied into the wells (in mL). The ChAT protein was determined as ng/mL CSF from the second part of the assay protocol, which is similar to a conventional ELISA assay.

The ChAT activity can also be expressed in relation to its protein concentration by dividing the ChAT activity (expressed in pmol/min/mL) to the ChAT protein concentration in the samples (ng/mL). For the simplicity, this parameter will be referred to in the following texts as **functional ChAT activity** ($ChAT_F$). It should be noted that the $ChAT_F$ activity has the unit of pmol/min/ng of ChAT protein. This integration of ChAT activity and protein is necessary for direct comparison between changes in ChAT activity and inhibition of AChE following galantamine (see below).

Measurement of RBC and CSF AChE Activities

The methodological details for measuring RBC and CSF AChE activities have been described previously (Darreh-Shori et al., 2006, 2008).

The RBC AChE activity was measured at baseline, and after 3, 6, 9 and 12 months of treatment with galantamine. The CSF AChE activity was measured at baseline and after 3 and 12 months of follow-up.

CSF-Estimation of AChE Inhibition

The total protein level of the AChE in CSF was measured using a functional-ELISA method previously described in detail for the AChE-R and AChE-S variants (Darreh-Shori et al., 2006, 2008).

The inhibition of the total AChE activity in the CSF of the AD patients was calculated by integrating the CSF AChE activity measured directly by the colorimetric assay with the amount of functionally intact AChE protein in CSF as previously described for the AChE variants' activities (Darreh-Shori et al., 2006, 2008).

In vivo Brain AChE Level by PET

PET was used with the tracer N-[^{11}C] methyl-piperidin-4-yl propionate (^{11}C-PMP), which is an ACh analog, to measure the reduction of cerebral cortical AChE activity in the brain. In the ^{11}C-PMP-PET, the rate constant k_3 for hydrolysis of ^{11}C PMP by AChE according to a kinetic model developed in Kuhl et al. (1999). The methodological details are described in Kadir et al. (2007). The *in vivo* brain AChE activity was determined as k_3 values (min^{-1}) in different brain regions at the follow-up intervals. Thus, the k_3 value has a direct relationship with AChE activity. For cortical regions, the AChE activity was calculated as the average of k_3 values from the "region of interest" (ROI) in the anterior cingulate, frontal, frontal association, parietal, parieto-temporal, temporal, primary visual, sensory motor and temporal medial lobe cortices of the left and right brain hemispheres.

In vivo Brain Level of Nicotinic Acetylcholine Receptors (nAChR) by PET

PET with ^{11}C-nicotine tracer was used to measure the nicotinic binding sites *in vivo* in the brain. The details of ^{11}C-nicotine PET assessment have been described previously (Kadir et al., 2008). Briefly, the number of nicotinic binding sites (k_2*) was calculated in the brain regions using the binding of the tracer (S)(−) ^{11}C-nicotine adjusted for regional cerebral blood flow ($H_2^{15}O$). These measurements were performed at baseline, after 3 weeks, 3 and 12 months of follow-up. The relative changes in the nicotinic binding sites at the follow-ups compared to baseline was calculated using the following formula [%1-$k_2^* = 100-(k_2^{*}{}_{(f)}/k_2^{*}{}_{(b)} \times 100)$, f and b indicate the k_2* values at the follow-ups and the baseline, respectively]. The k_2* has an inverse relationship with the number of nicotinic binding sites in the brain.

Neuropsychological Assessments

To evaluate the effect of galantamine treatment on cognitive function, neuropsychological assessments were performed at baseline (pre-treatment), and after 3 and 12 months of treatment. The details are reported previously (Kadir et al., 2008). Briefly, global cognition was assessed using the MMSE, and the cognitive subscale of the AD Assessment Scale (ADAS-cog). A higher ADAS score indicates a greater degree of cognitive impairment. A battery of neuropsychological tests, addressing different cognitive domains (episodic memory, attention/executive ability, and visuospatial ability) were performed throughout the study. Episodic memory was evaluated using two measures from the Stockholm Gerontology Research Center test of memory for words: (1) the number of correct responses in free recall of words; and (2) the d-prime value (an integration of correct responses and false alarms following decision theory) in recognition of words. Attention domain was assessed using three measures: (1) the number of correct responses in the Digit Symbol response test from the revised Wechsler Adult Intelligence Scale (Wechsler, 1981); (2) the time needed to complete the Trailmaking A; and (3) the number of correct responses in the Trailmaking B test. These measures are known to assess abilities associated with frontal-subcortical brain activity (Cummings, 1993). Visuospatial ability domain was evaluated by recording the number of correct responses in reading and setting a clock. This test reflects parietal lobe function (Cahn-Weiner et al., 1999). To reduce the number of statistical analyses, these data were Z-transformed and the overall composite Z-scores of the three cognitive domains were calculated as described before (Darreh-Shori et al., 2011).

Statistical Analysis

Data are expressed as mean values and standard error of the mean (SEM) or otherwise as stated. The effects of treatment at different time intervals compared to baseline were assessed using repeated measures (RM) analysis of variance (ANOVA) for the double-blind phase as well as open-label phase. The comparison between the groups was done using ANOVA analysis. A significant ANOVA result ($p < 0.05$) was followed by the Bonferroni–Dunn *post hoc* analysis that

tested the significance of results at each time point compared with baseline or between groups. Correlation analyses were performed using correlation *Z*-tests. When deemed necessary, the correlations were asserted using the nonparametric Spearman Rank Correlation and were visualized using simple regression plots.

RESULTS

The Study Design and Groups

The study design and the demographic of the patients are shown schematically in **Figure 1A** and **Table 1**, respectively. The Phase I of the study was 3 months during which the patients received either galantamine (*the Galantamine group*) or placebo (*the Placebo group*). During the Phase II of the study, the patients in *the Galantamine group* continued on galantamine for a total of 12 months. At the beginning of the phase II of the study, *the Placebo group*, however, started on receiving galantamine and continued on this drug for a total of 9 months (*the Placebo-Galantamine* group).

Patient Dropout

Of the initial 18 subjects (**Table 1**), during the double-blind phase, one subject (in *the Galantamine group*) was withdrawn as a result of second-degree atrioventricular block, considered possibly related to galantamine. Overall, 17 subjects completed the double blind Phase I of the study which was for 3 months. During the second phase, i.e., the open-label phase II, three more subjects were withdrawn: one from *the Placebo-Galantamine group* owing to chronic lymphocytic leukemia (an event considered unrelated to galantamine), and the others from the Galantamine arm of the study: one patient due to cardiac arrhythmia and syncope (considered possibly related to galantamine), and one patient as a result of non-compliance. Of the remaining 14 patients, one could not complete the neuropsychological tests at 12 month due to myocardial infarction (which relation to galantamine treatment was considered doubtful). It should be also noted that due to technical issues with PET scan validation and data acquisition, a valid AChE PET scan was available for only 15 patients (five in *the Placebo group* and 10 in *the Galantamine group*) at baseline and 3 months but 11 valid AChE PET scans at 12 months. In case of ^{11}C-nicotine PET scan, data were for similar technical issues available for 17 patients (six in *the Placebo group* and 11 in *the Galantamine group*) at baseline and 3 months but 14 valid ^{11}C-nicotine PET scans at 12 months. Thus, in principle there were a total of four dropout and 14 subjects completed the 12 months study.

Furthermore and particularly relevant to the CSF analyses, at the time of conducting the CSF ChAT measurements there were not enough CSF left either at the 3 months or the 12 months follow-up for some of the patients. Given that the statistical analyses were done on repeated measured analyses only the subjects that had data at baseline, 3 months and/or 12 months could be compared.

Estimated RBC and CSF AChE Inhibition

The descriptive results regarding the changes in the RBC and CSF AChE activities are reported elsewhere (Darreh-Shori et al., 2008). Briefly, a weak to moderate inhibition of RBC AChE activity was observed in *the Galantamine group* at the 3-months follow-up (11 ± 1.4%, $n = 11$). No significant changes in the RBC AChE activity was observed in *the Placebo group* at 3 months. At the 12-month follow-up, however, the RBC AChE inhibition in *the Placebo-Galantamine group* was similar to the inhibition level in *the Galantamine group* (10 ± 4%, $n = 6$ vs. 10 ± 1.3%, $n = 8$, respectively).

The specific changes in the synaptic and read-through AChE splice variants proteins have been reported previously (Darreh-Shori et al., 2008). Here, we estimated the inhibition levels of total AChE activity in CSF by integrating the activity (in nmol/min/mL) and protein levels of AChE (ng/μl), as previously described (Darreh-Shori et al., 2014).

This estimated CSF AChE inhibition is shown in **Figure 1B**. The CSF AChE inhibition was 26 ± 6% and 33 ± 2% in *the Galantamine group* at 3 and 12 months of the study, respectively (all p-values < 0.003, **Figure 1B**). No inhibition of CSF AChE activity was observed in *the Placebo group* at 3 months (**Figure 1B**). In *the Placebo-Galantamine group*, the AChE activity was however inhibited in the CSF by 25 ± 6% at the 12 months follow-up when these patients had been on galantamine treatment for a total of 9 months ($p < 0.02$ compared to baseline, and $p < 0.003$ compared to the 3 months).

Estimated Activity of the Acetylcholine-Synthesizing Enzyme, ChAT in CSF

Functional CSF ChAT Activity

Since the CSF AChE activity was normalized to the AChE protein levels, it was necessary to also integrate the overall ChAT activity (in pmol/min/mL CSF) with its protein in CSF (in ng/mL), to estimate changes in the level of functional ChAT activity (i.e., $ChAT_F$) in CSF.

At 3 months, the $ChAT_F$ activity showed about 30% numerical increase among *the Galantamine group* compared to baseline ($p < 0.099$, $n = 8$, **Figure 1C**), or *the Placebo group* ($n = 5$). Noteworthy, repeated-measure ANOVA includes only four subjects in *the Placebo group* who had 12-months data. These analyses indicated that *the Galantamine group* had 47% higher levels of ChAT than *the Placebo group* ($n = 4$, $p < 0.05$, **Supplementary Figure S1**). Considering that galantamine is a drug without any direct effect on $ChAT_F$ activity, the observed increased in $ChAT_F$ activity might indicate an expected effect of treatment in the stimulation of the cholinergic system.

At 12 months in *the Galantamine group*, the CSF $ChAT_F$ activity did not differ compared to the baseline (**Figure 1C**). Among *the Placebo-Galantamine group* who were initially on placebo treatment, baseline, 3-month and 12-month CSF samples were available from four out of five of the patients. The **Supplementary Figure S1A** illustrates an accordingly modified version of **Figure 1C**. As it is easier to appreciate from the

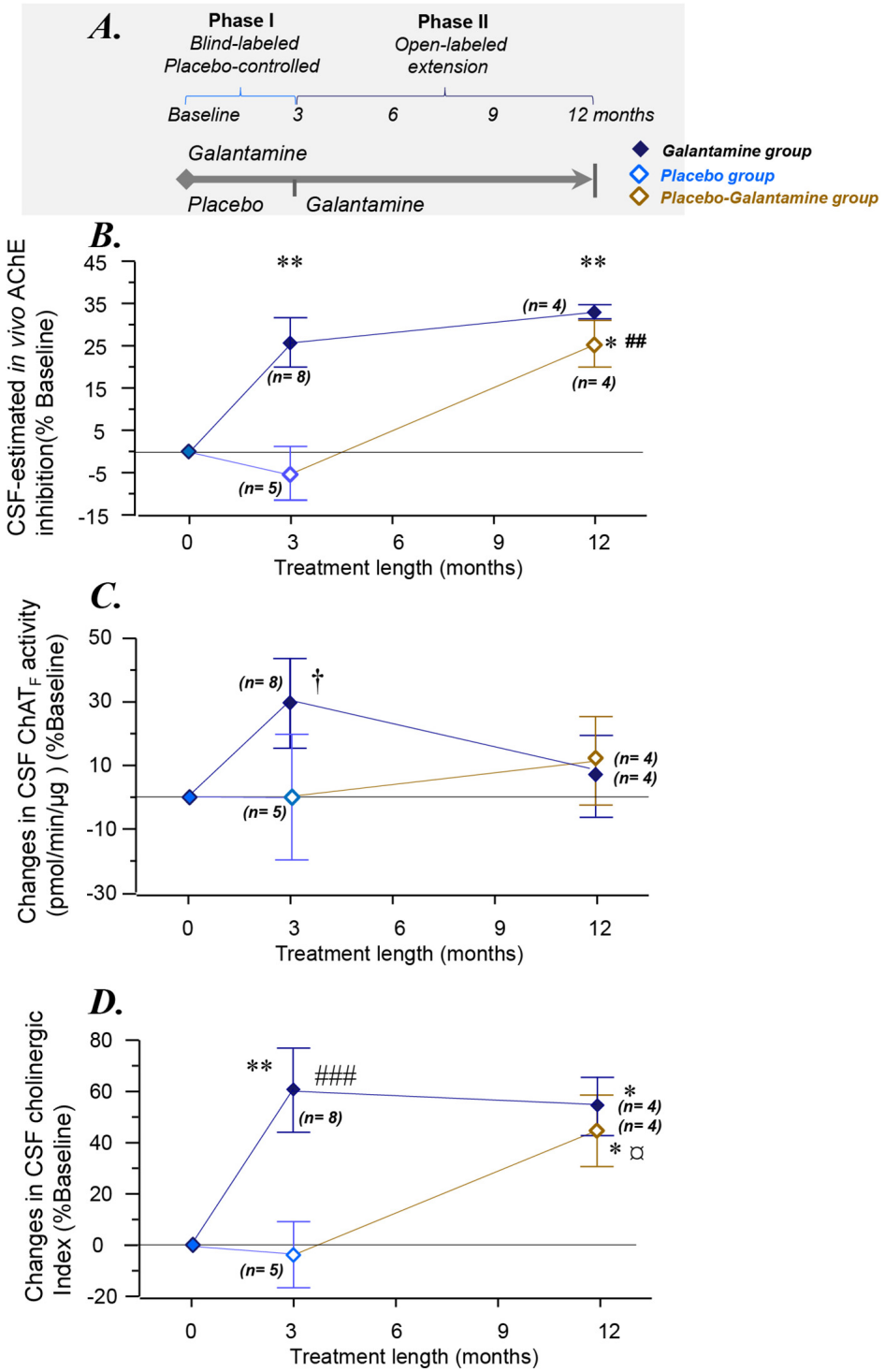

FIGURE 1 | Changes in the overall functional ChAT and AChE activities in CSF. **(A)** Schematic illustration of the galantamine study design (Kadir et al., 2008). **(B)** Changes in the total AChE activity in the CSF. **(C)** Changes in CSF ChAT$_F$ activity. **(D)** Overall changes as a Cholinergic index in CSF after 3–12 months of the study. $^{*}p < 0.05$, and $^{**}p < 0.01$ signify differences compared to baseline. $^{\#\#}p < 0.01$ and $^{\#\#\#}p < 0.001$ signify differences compared to *the Placebo group* at 3 months. $^{\dagger}p < 0.099$ compared to baseline or *the Placebo group*. $^{\circ}p < 0.08$ compared to *the Placebo group* (when $n = 5$, see also **Supplementary Figures S1A,B**). AChE = acetylcholinesterase. ChAT = choline acetyltransferase. CSF ChAT$_F$ activity = the overall functional ChAT activity expressed in pmol/min/µg ChAT protein in the samples. CSF AChE$_F$ activity = the overall functional AChE activity expressed in nmol/min/µg AChE protein in the samples. CSF Cholinergic index = ratio of ChAT$_F$ activity to AChE$_F$ in CSF.

TABLE 1 | Demographic data of the placebo and galantamine-treated groups at baseline.

	Placebo group (n = 6)	Galantamine group (n = 12)	Total (n = 18)
Gender (F/M)	3/3	5/7	8/10
Average age in years (range)	65.8 ± 3.7	70.9 ± 2.7	69.2 ± 2.2
ApoE 4 carriers (+/−)	3/2	7/3	10/5
Duration of disease (years)	2.2 ± 0.7	5.1 ± 1.1	4.1 ± 0.8
Education, mean years (range)	12.8 ± 0.9	10.9 ± 1.1	11.4 ± 0.9
ADAS-cog	19.0 ± 1.1	28.0 ± 3.4	26.2 ± 0.7
MMSE	27.3 ± 0.8	25.6 ± 1.0	26.2 ± 0.7

Values correspond to mean ± SEM. F, females and M, males. MMSE, Mini-Mental State Examination. ADAS-cog/13, Alzheimer's Disease Assessment Scale-cognitive subscale. Although the placebo randomized patients appear younger, having shorter duration of the disease, higher MMSE scores and lower ADAS-cog scores at baseline compared with the galantamine group, no statistical significant difference was observed with regards to age, gender, level of education, duration of disease, MMSE and ADAS-cog scores at baseline (all p > 0.10 except for ADAS-cog, p = 0.09; Kadir et al., 2008).

Supplementary Figure S1A, the CSF $ChAT_F$ activity showed 29% significant increase in *the Placebo-Galantamine group* at the 12 months follow-up compared to their 3 months follow-up ($n = 4$, $p < 0.02$, **Supplementary Figure S1A**).

CSF Cholinergic Index

Cholinergic signaling is most likely regulated through a balance between synthesis, release and degradation of ACh. We hence defined a *CSF Cholinergic index* as a ratio by dividing the functional levels of ChAT (in pmol/min/μg) to that of AChE (in nmol/min/μg) in CSF ($ChAT_F/AChE_F$ activities). Thus, an increase in this ratio means a net increase in ACh levels.

At 3 months, the Cholinergic index differed significantly between *the Galantamine* and *the Placebo* groups (64 ± 14%, $p < 0.0004$). *The Galantamine group* showed also about 60% significant increase when compared to baseline ($p < 0.003$, **Figure 1D**). No significant change was observed in the CSF Cholinergic index in *the Placebo group* at 3 months compared to baseline (4 ± 13%, $p < 0.3$, **Figure 1D**).

At 12 months and in *the Galantamine group*, the Cholinergic index was higher compared to the baseline (54 ± 11%, $p < 0.03$), indicating that in this group the improved cholinergic index was maintained for up to 12 months of galantamine treatment. Most importantly, at the 12 months follow-up, a similar increase in this index was observed in *the Placebo-Galantamine group*. This increase was significant compared to both the baseline (44 ± 14%, $n = 4$, $p < 0.05$, **Figure 1D**) and compared to 3-month levels when these patients were still on placebo treatment (61 ± 14%, $n = 4$, $p < 0.02$, **Figure 1D** and its modified version **Supplementary Figure S1B**).

Correlations Between the *in vivo* Brain AChE Activity (k_3) by PET and the AChE and ChAT Activities in CSF

At baseline, there were no significant correlations between $ChAT_F$ activity or the Cholinergic index in CSF and the *in vivo* brain AChE activity (assessed as k_3) by PET.

At 3 months, the *in vivo* AChE activity (k_3) in the whole brain correlated with the CSF $ChAT_F$ activity ($r = -0.6$, $n = 12$, $p < 0.05$), and the CSF Cholinergic index ($r = -0.7$, $n = 12$, $p < 0.003$), as assessed in all patients as one group.

At 12 months, significant correlations were observed between the *in vivo* AChE activity (k_3) and the $ChAT_F$ activity as well as the Cholinergic index in CSF, which are summarized in **Table 2** and shown graphically in **Figure 2**.

Correlations Between the *in vivo* ^{11}C-Nicotine PET in the Brain and Activities of AChE and ChAT in CSF

At Baseline Prior to Commencing Treatment

At baseline, the CSF AChE activity correlated positively with a number of nicotinic binding sites in the pons ($r = 0.60$, $p < 0.03$) and the left and right primary visual cortex ($r = 0.63$, $p < 0.014$, **Figure 3A**). Two of the brain regions that are relatively less affected by AD, and thereby represent best the normal biodynamic relationship between these cholinergic components. The protein levels of the synaptic AChE-S variant in CSF correlated with the baseline level of number of ^{11}C-nicotinic binding sites in primary visual cortex ($r = 0.81$, $p < 0.0002$, **Figure 3B**), the pons ($r = 0.60$, $p < 0.03$), parietal cortex ($r = 0.59$, $p < 0.033$), cingulate gyrus ($r = 0.56$, $p < 0.045$), and the whole brain ($r = 0.61$, $p < 0.019$, **Figure 3C**).

The functional ChAT activity in CSF at baseline also correlated positively with the number of nicotinic binding sites in left thalamus ($r = 0.60$, $p < 0.025$) and right parieto-temporal cortex ($r = 0.55$, $p < 0.03$). We did not use the CSF Cholinergic index in these analyses since it is composed as a ratio between functional ChAT and AChE activities in CSF.

At 3 months, the number of nicotinic binding sites for the "whole brain regions" showed 11 ± 3% increases in *the Galantamine group* compared to baseline ($p < 0.007$, **Figure 4A**), which at the 12 months follow-up had returned to the levels at baseline (**Figure 4A**).

Analyses between the nicotinic binding sites and the RBC and CSF AChE activity showed positive correlation between the RBC AChE inhibition and the relative increases in the nicotinic binding sites in the majority of the brain regions, in particular in *the Galantamine group* (**Figure 4B** and **Table 3**). Noteworthy, the relative changes in RBC AChE activity among *the Placebo group* showed in contrast an inverse correlation with the number of nicotinic binding in the brain (**Figure 4B**). The latter most likely reflect a basal equilibrium condition between the access to ACh (regulated by AChE activity) and its nAChRs.

At 3 months, similar positive correlations were also observed among *the Galantamine group* between the relative changes in the nicotinic binding sites in the temporal medial lobe and the inhibitions of CSF AChE-S ($r = 0.57$, $p < 0.04$, $n = 13$) and AChE-R variants ($r = 0.60$, $p < 0.03$, $n = 13$).

No significant correlations were observed between $ChAT_F$ activity or the Cholinergic index and the nicotinic binding sites in the brain in *the Galantamine* or *the Placebo group*.

At 12 months, the correlation analyses indicated an inverse association between the RBC AChE inhibition and the relative

TABLE 2 | Correlations between the *in vivo* AChE activity (k_3), cognitive measures, the CSF $ChAT_F$ activity and the Cholinergic Index after 12 months.

		CSF $ChAT_F$ activity		CSF Cholinergic index	
***in vivo* AChE activity in the brain (k_3)**		***r* (*n* = 5)**	***p* < 0.05**	***r* (*n* = 5)**	***p* < 0.05**
Cortical regions	*L*	0.92	**0.023**	0.98	**0.0009**
	R	0.90	**0.040**	0.95	**0.009**
Overall brain regions	*L*	0.92	**0.022**	0.96	**0.007**
	R	0.83	**0.090**	0.84	*0.084*
Average cortical regions		0.93	**0.020**	0.99	**0.0003**
Average overall brain regions		0.94	**0.015**	0.97	**0.004**
Whole brain		*0.96*	**0.0044**	*0.98*	**0.0012**
Cognitive tests		***r* (*n* = 8)**	***p* < 0.05**	***r* (*n* = 8)**	***p* < 0.05**
MMSE Score		*0.7*	**0.03**	*0.6*	*0.1*
ADAS-Cog		*−0.81*	**0.013**	*−0.83*	**0.008**
Neuropsychology tests: Attention Domain		*0.56*	*0.15*	*0.40*	*0.34*
Memory Domain		*0.50*	*0.22*	*0.77*	**0.022**
Visuospatial Domain		*0.85*	**0.0052**	*0.72*	**0.040**

*k_3 = the binding constant calculated as described (Kadir et al., 2008). The k_3 rate constants for the in vivo AChE activity are shown in **Figure 2**. All r-values are correlation coefficient. Some of the correlations are illustrated graphically in **Figure 2** and **Figure 6**. PET, Positron emission tomography; CSF, Cerebrospinal fluid; R and L the right and left brain hemispheres. A large K3 means high in vivo AChE activity. CSF $ChAT_F$ activity refers to choline acetyltransferase activity divided by its protein concentration; Cholinergic Index, refers to ratio of CSF $ChAT_F$ activity/CSF $AChE_F$ activity; MMSE Score, the mini-mental state exam; ADAS-Cog, Alzheimer's Disease Assessment Scale.*

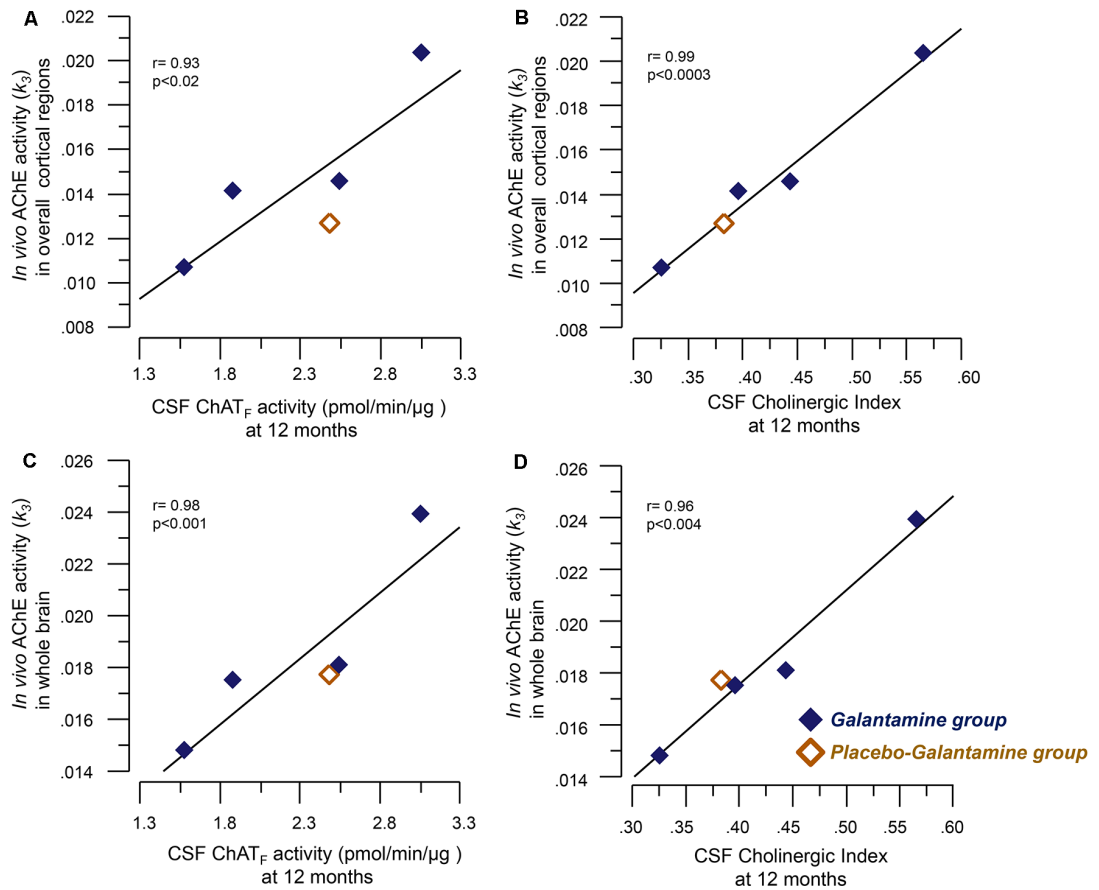

FIGURE 2 | Correlations between the *in vivo* brain AChE activity (k_3) by PET and the CSF cholinergic markers. Panel **(A)** illustrates correlations between the *in vivo* AChE activity (k_3) overall cortical regions and the CSF $ChAT_F$ activity at 12 months. Panel **(B)** shows the corresponding correlation with the Cholinergic index in CSF. Graphs C and D show correlations between the *in vivo* AChE activity (k_3) in the whole brain and CSF $ChAT_F$ activity **(C)** and the Cholinergic index **(D)** in CSF at 9–12 months galantamine treatment. The k_3 value has a direct relationship with AChE activity, i.e., a high k_3 value means a high *in vivo* AChE activity. CSF $ChAT_F$ activity = the overall functional ChAT activity expressed in pmol/min/µg ChAT protein in the samples. CSF $AChE_F$ activity = the overall functional AChE activity expressed in nmol/min/µg AChE protein in the samples. CSF Cholinergic index = ratio of $ChAT_F$ activity to $AChE_F$ in CSF.

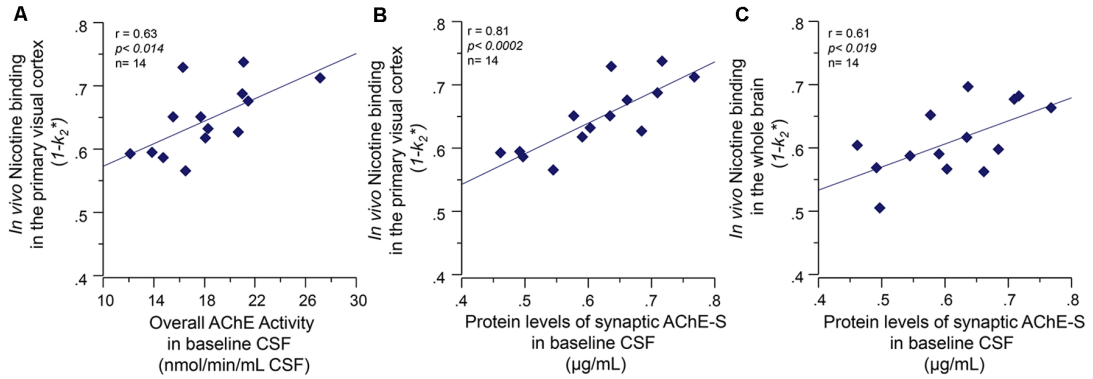

FIGURE 3 | Baseline co-dependency of *in vivo* nicotinic binding sites in the brain and AChE levels in CSF. Positive correlation between the *in vivo* nicotinic binding sites in the primary visual cortex and AChE activity **(A)** and the protein levels of the synaptic AChE-S variant **(B)** in the CSF of the Alzheimer's disease (AD) patients collected at baseline prior to the galantamine treatment. Panel **(C)** illustrates the positive correlation between the CSF AChE-S protein and the *in vivo* ^{11}C-nicotine binding in *the whole-brain* measured by PET. Here, the values are given as $1\text{-}k_2^*$ since k_2^* values have an inverse relationship with ^{11}C-nicotine binding, i.e., a low k_2^* values mean a higher ^{11}C-nicotine binding level. CSF, cerebrospinal fluid; PET, positron emission tomography; AChE-S, synaptic acetylcholinesterase splice variant proteins.

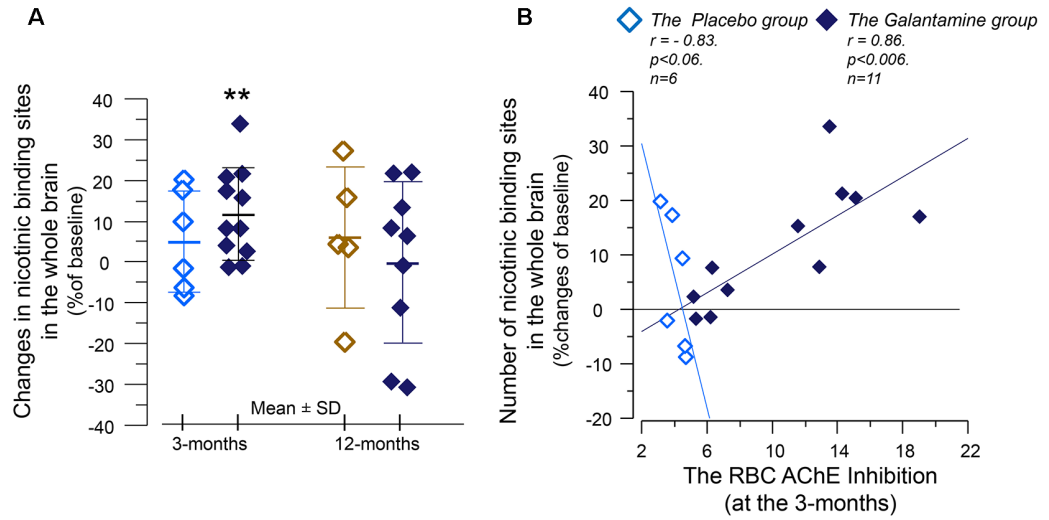

FIGURE 4 | The relative changes of the *in vivo* nicotinic binding sites in the brain and association with changes in the red blood cells (RBCs) AChE activity. **(A)** Changes from baseline in the overall ^{11}C-nicotine PET binding in the brain after 3 months of galantamine or placebo treatment (left panel) as well as after 9–12 months in all patients (right panel). $^{**}p < 0.007$ compared to baseline. **(B)** Correlation between percent changes in the *in vivo* nicotinic binding sites and changes in the RBC AChE activity. The negative correlation among *the Placebo group* indicates that the co-dependency between the number of nicotinic binding sites and the AChE activity that was seen at baseline is still at work among *the Placebo group*. Note that AChE inhibition has inverse relationship with AChE activity. The galantamine treatment instead altered this basal relationship so that the nicotinic binding sites increase in accord with a reduction in (inhibition of) AChE activity by the drug. The *in vivo* nicotinic binding sites were assessed by PET using the ^{11}C-nicotine tracer. Here is shown percent changes in the region of interest of the "Whole brain." All values on both axes are percentages of the individual baseline. Light squares = *the Placebo group*. Dark squares = *the Galantamine group*. PET, positron emission tomography.

changes in the nicotinic binding sites in the brain regions (**Figure 5A** and **Table 3**). Similar inverse correlations were also observed between the inhibition of the CSF AChE and the relative 12-month changes in the nicotinic binding sites (**Figure 5B** and **Table 4**) as well as with absolute number of the nicotinic binding sites in the brain (**Figure 5C**).

A mechanistic biodynamic model is presented in **Figure 5D**, which is based on the overall pattern of findings shown in **Figures 3**, **4B**, **5A–C** as well as **Tables 3**, **4**. Considering that low AChE inhibition (i.e., high AChE activity in synapses) means low concentration and/or short duration of action of ACh in the synaptic cleft (the left part of **Figure 5D**), these findings suggest that the observed physiological equilibrium at the baseline condition between AChE activity and nAChRs (as shown in **Figure 3** for all patients at baseline, and in **Figure 4B** and **Table 3** for *the Placebo group*) was

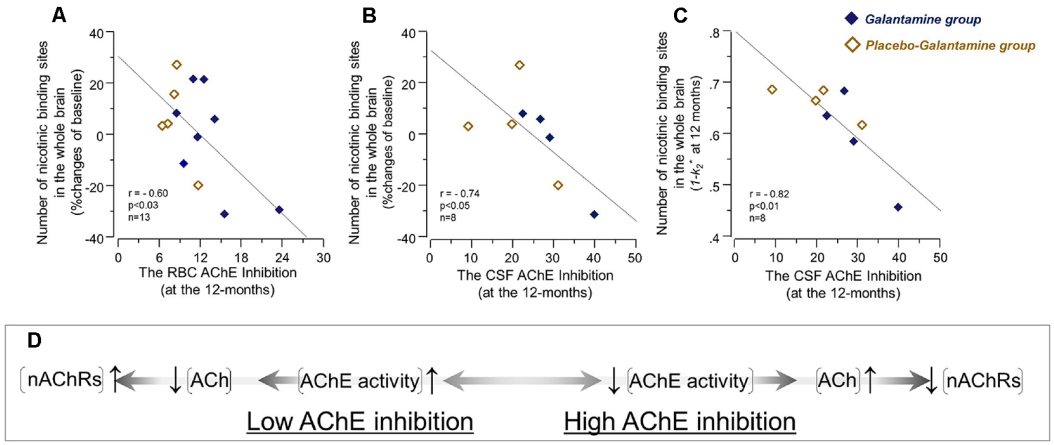

FIGURE 5 | The initial co-dependency between the *in vivo* brain nicotinic binding sites and AChE activity was restored after 9–12 months treatment with galantamine. The graphs show negative correlations between the changes in the *in vivo* ^{11}C-nicotine binding estimated by PET in the whole brain and the percent inhibition of RBC AChE activity **(A)**, and the percent inhibition of total AChE activity in CSF **(B)** following 9–12 months galantamine treatment. In panel **(C)** is shown the negative correlation between the absolute nicotinic binding (1-k_2*) values with the percent AChE inhibition in CSF. In panel **(C)** the ^{11}C-nicotine binding values are given as *1-k_2** since k_2* values have an inverse relationship with this tracer's binding, i.e., a low k_2* values mean a higher ^{11}C-nicotine binding level. The box **(D)** shows schematically a biodynamic model explaining the observed correlation between changes in the nicotinic binding and AChE activity at baseline (as shown in **Figure 3**) and here after 12 months of treatment (note that AChE inhibition shown here in graphs **(A–C)** have inverse relationship with AChE activity). In this model, high AChE inhibition (left-to-right on X-axis) means reduced AChE activity, which consequently means an increase in ACh level or a longer persistent of ACh in the synapses. This is balanced by adjustment of the nAChRs to lower levels (up-to-down on Y-axis). This might point at a protective feed-back mechanism against hyperexcitation state that may occur upon a too high AChE inhibition. Similarly, low AChE inhibition (right-to-left on X-axis) means higher AChE activity, which will reduce ACh levels and/or shorten its duration of action in the synapses. This is balanced by increases in the nAChR levels (down-to-up on Y-axis) to compensate for reduced level/duration of action of ACh. It should be noted that this model will not fit with the observations in *the Galantamine group* after 3 months treatment (as shown in **Figure 4B**), unless a general increase or remodeling of cholinergic-cholinoceptive interfaces is considered in the model, which would require simultaneous increases in both ChAT, AChE and nAChR levels, as was found in the current study. Open orange squares = *the Placebo-Galantamine group*. Dark squares = the *Galantamine group*. CSF, cerebrospinal fluid. PET, positron emission tomography; RBC, red blood cell; ACh, acetylcholine; AChE, acetylcholinesterase; nAChRs, nicotinic ACh receptors.

TABLE 3 | Correlations between the changes in nicotinic binding sites in the brain assessed by PET and the RBC AChE inhibition after 3 and 12 months follow-up.

		The RBC AChE Inhibition					
		3-months				**12-months**	
		Placebo (n = 6)		**Galantamine (n = 11)**		**Overall patients (n = 13)**	
^{11}C- nicotine binding in the brain regions (%1-k_2*)		***r***	***p* < 0.05**	***r***	***p* < 0.05**	***r***	***p* < 0.05**
Cortical regions	*L*	−0.79	0.07	0.61	**0.05**	−0.47	0.1
	R	−0.66	0.17	0.73	**0.009**	−0.51	0.07
Overall brain regions	*L*	−0.86	**0.03**	0.67	**0.02**	−0.53	0.07
	R	−0.66	0.17	0.70	**0.01**	−0.53	0.07
Average L& R cortical		−0.76	0.09	0.70	**0.05**	−0.50	0.08
Average L and R overall brain regions		−0.89	**0.05***	0.71	**0.01**	0.54	0.06
Whole brain		−0.83	0.06*	0.76	**0.005**	−0.60	**0.03**

*All r-values are correlation coefficient. A negative r-value reflects an inverse association between RBC AChE inhibition and the changes in the nicotinic binding sites in the brain. It should be noted that enzyme inhibition has an inverse relation with enzyme activity. Thereby, a negative r-value among the Placebo group means positive association between activity of the enzyme and the changes in the nicotinic binding sites in the brain. Overall, the negative r-value for this group in the table most likely point toward a native biodynamic relationship, meaning that a high ACh degradation (due to low or no inhibition of AChE) might become compensated by an increase in the number of nicotinic receptors to allow neurotransmission. This is because changes in RBC AChE activity or the nicotinic binding sites in the Placebo group during the initial 3 months of study are not caused by galantamine as these patients were on placebo. In contrast, the positive r-values found between these two variables in the Galantamine group indicate that a high AChE inhibition (i.e., a consequently high level and/or long duration of action of ACh within synapses) was accompanied by an increase in the number of nicotinic receptors in the brain. This in turn suggests that such cholinergic stimulation by the drug might induce neuronal and/or synaptic remodeling that requires more ACh receptors and cholinergic enzymes, such as ChAT and AChE to be expressed in the brain as we found in the current study (see also further schematic explanations in **Figure 5D**). Some of these correlations are graphically illustrated in **Figure 4B**. k_2* values for ^{11}C-nicotine binding are exemplified in **Figure 3**. *p-values are based on Spearman Rank Correlation; PET, Positron emission tomography, k_2* = the binding constant. RBC AChE, Red blood cells acetylcholinesterase.*

again restored following the longer-term of 9–12 months of galantamine treatment (as is shown in **Figures 5A–C** and **Table 4**).

At 12 months, no correlations were observed between the nicotinic binding sites in the brain and the CSF $ChAT_F$ activity nor the CSF cholinergic index.

TABLE 4 | Correlations between the number of *in vivo* nicotinic binding sites and the inhibition of CSF AChE-S and AChE-R variants after 12 months.

		AChE-R variant (%Inhibition)		AChE-S variant (%Inhibition)		Total AChE (%Inhibition)	
The nicotinic binding sites in brain region (1-k_2*)		***r* (*n* = 8)**	***p* < 0.05**	***r* (*n* = 8)**	***p* < 0.05**	***r* (*n* = 8)**	***p* < 0.05**
Cortical regions	*L*	−0.70	0.052	−0.67	0.059	−0.73	**0.037**
	R	−0.75	**0.028**	−0.70	**0.050**	−0.77	**0.022**
Overall brain regions	*L*	−0.76	**0.027**	−0.72	**0.043**	−0.78	**0.019**
	R	−0.79	**0.018**	−0.70	0.054	−0.79	**0.016**
Average cortical regions		−0.74	**0.034**	−0.71	**0.049**	−0.76	**0.025**
Average overall brain regions		−0.78	**0.019**	−0.72	**0.044**	−0.80	**0.015**
Whole brain		*−0.79*	**0.017**	*−0.75*	**0.029**	*−0.82*	**0.011**

All r-values are correlation coefficient. Some of the correlations are graphically illustrated in ***Figure 5****. k_2*= the binding constant for the PET tracer. The k_2* values for ^{11}C-nicotine binding are exemplified in* ***Figure 3*** *and* ***Figure 5C****. PET, Positron emission tomography; CSF, Cerebrospinal fluid; AChE-S, Synaptic acetylcholinesterase splice variant protein; AChE-R, Read-through acetylcholinesterase splice variant. The percentages are calculated relative to the patients' baseline value.*

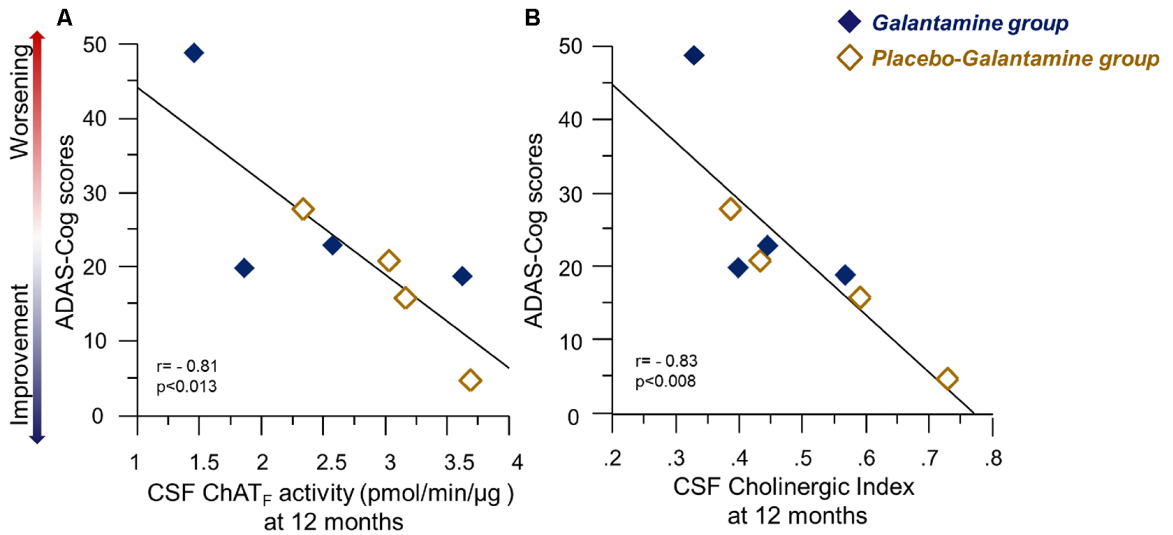

FIGURE 6 | Correlations between ChAT$_F$ activity or the Cholinergic index and the ADAS-Cog test results following 9–12 months of galantamine treatment. Panel **(A)** illustrates correlations between Cognition assessed by ADAS-Cog and the ChAT$_F$ activity in CSF at 12 months. Panel **(B)** shows the corresponding correlation with Cholinergic index in CSF. It should be noted that a high ADAS-Cog score reflects a worse cognitive performance. Thus, the graphs illustrate positive correlation between the CSF cholinergic biomarkers and cognition. Open orange squares = the *Placebo-Galantamine group*. Dark squares = the *Galantamine group*. ChAT = choline acetyltransferase. CSF ChAT$_F$ activity = the overall functional ChAT activity expressed in pmol/min/µg ChAT protein in the samples. CSF Cholinergic Index = ratio of ChAT$_F$ activity to AChE$_F$ in CSF.

Correlations Between Measures of Cognition and AChE and ChAT$_F$ Activity in CSF

Descriptive data concerning changes in cognitive tests are reported in detail in the primary article (Kadir et al., 2008). Briefly, there was a statistically significant improvement in MMSE test at 3 months in *the Galantamine* but not *the Placebo group* compared to baseline. There was also a trend of improvement in ADAS-Cog test in *the Galantamine group* at 3 months (see Figures 5, 6 in Kadir et al., 2008). In the following, we hence focus on the correlations of these cognitive measures and the CSF cholinergic biomarkers.

Neither *at baseline* nor *at 3 months* there were any significant correlations between MMSE scores and the ChAT$_F$ activity or the Cholinergic index in CSF.

At 12 months, there were significant correlations between several measures of cognition and the ChAT$_F$ activity and Cholinergic index in CSF, which are summarized in **Table 2**. The negative correlations between ADAS-Cog and the CSF ChAT$_F$ activity and the Cholinergic index are illustrated in **Figure 6**, which indicate those whose cognitive abilities worsened after 12 months of treatment had a lower ChAT$_F$ activity and Cholinergic index compared to the other patients.

DISCUSSION

Here, we described for the first time the effect of galantamine treatment on CSF levels of two important enzymes that maintain the steady state of ACh in the brain, in particular,

the core-cholinergic enzyme responsible for biosynthesis of ACh, i.e., ChAT. The first 3 months of the study had a double-blinded placebo-controlled protocol, which allowed us to specifically address the biodynamic relationship of AChE and ChAT enzymes in response to galantamine treatment. We showed that specific inhibition of the CSF AChE activity by galantamine treatment was accompanied by a mild increase of the activity of $ChAT_F$ in CSF at 3 months follow-up, with no changes seen in *the Placebo group* regarding the activities of these two enzymes. Furthermore, we found that upon switching from placebo to active treatment a similar pattern of changes in CSF $ChAT_F$ and AChE activities appeared when measured at the 12-months follow-up. We therefore defined a new CSF cholinergic biomeasure by integrating the activities of functional ChAT and AChE in the CSF as a ratio, i.e., the CSF Cholinergic index, for monitoring changes in ACh homeostasis in the CSF (and the brain) following treatment with ChEIs, like galantamine. This Cholinergic index showed a clear increase as response to ChEI-treatment.

In this study, we further assessed the changes in these CSF parameters with the clinical and paraclinical measures in the patients. This way we showed presence of a dynamic pattern of interdependency of the CSF $ChAT_F$ activity, the Cholinergic index and the AChE activity to the *in vivo* AChE inhibition and nicotinic binding sites in several brain regions assessed by PET in AD patients prior to and after treatment with galantamine.

Previously, we have shown that galantamine treatment causes 30%–36% of *in vivo* AChE inhibition in the majority of the regions of the brain, in particular the cortical regions in these patients assessed by PET (Kadir et al., 2008). Here, we found that this *in vivo* AChE inhibition correlated with both CSF $ChAT_F$ activity and the cholinergic index. This is the first study showing that *in vivo* AChE inhibition induces an increase in $ChAT_F$ activity in the CSF of patients following treatment with a ChEI. These findings may indicate that galantamine indirectly affect the activity of the cholinergic neurons as well as the down-stream cholinoceptive neurons. In other words, ChEIs therapy may both prevent degradation of ACh as well as by increasing $ChAT_F$ levels increase the production of ACh.

We further found that galantamine treatment was associated with a 25%–30% inhibition of the total AChE activity in CSF compared to pre-treatment levels and placebo treatment. This is consistent with our previous report showing similar levels of inhibition of the synaptic AChE-S variant in CSF of the galantamine-treated patients (Darreh-Shori et al., 2008).

We then looked at the interdependency of these changes with *in vivo* nicotinic binding sites in the brain assessed by ^{11}C-nicotine PET. Although we found no correlation between the CSF $ChAT_F$ activity and the *in vivo* nicotinic binding sites, significant correlations were observed between the *in vivo* nicotinic binding sites and the RBC and CSF AChE activities in the AD patients. At the baseline condition, we found a positive association between the AChE-S activity and the *in vivo* brain nicotinic binding sites. This was particularly prominent in the primary visual cortex and pons, which are two brain regions known to be relatively less affected by AD. Thus, these findings imply that a high AChE activity is physiologically counterbalanced by high *in vivo* nicotinic binding sites in the brain of AD patients (as depicted schematically in **Figure 5D**), possibly due to low availability and/or short duration of action of ACh. This is consistent with the observations in the AChE over-expressing transgenic mice, in which the high AChE activity seemed to be compensated by an elevation of the number of cortical nAChRs (Svedberg et al., 2002, 2003; Mousavi et al., 2004). These observations hence indicate the presence of a basal physiological equilibrium between ACh and its target receptors, i.e., here the nAChRs. In other words, these findings suggest that under baseline conditions, AD patients with high AChE levels also have a high number of nAChRs in the brain, most likely reflecting a physiological equilibrium (or compensation) between available concentration and/or duration of action of ACh and levels of AChE-S activity in the synaptic clefts.

A comparison at the 3-months follow-up between *the Placebo* and *the Galantamine groups* indicated that the baseline positive association between the AChE activity and the nicotinic binding sites was not altered among *the Placebo group*, while in *the Galantamine-treated group* a reduction in AChE activity (i.e., AChE inhibition) was instead accompanied by an increase in the *in vivo* nicotinic binding sites in the majority of the brain regions. Intuitively, these findings appear unexpected and paradoxical with regards to the pattern of the observations at the baseline. This is because a high AChE inhibition implies less ACh degradation and thereby a prolonged action of ACh on its receptors within the synaptic cleft (as depicted in **Figure 5D**). This in physiological terms should lead to a reduction and not an increase in the numbers of nAChRs (as shown in **Figure 4B**). Thus, the observed mild 11% increase in the *in vivo* nicotinic binding sites in the brain of *the Galantamine-treated* patients can be explained, in a mechanistic view, by an increase in synaptic regeneration and/or synaptic strengthening at the neuronal interfaces between cholinergic and cholinoceptive neurons. This is also in line with the observed increased levels of both $ChAT_F$ and the Cholinergic index in the CSF of these patients in response to a higher *in vivo* brain AChE inhibition. Indeed, the rationale for the use of ChEIs is to stimulate the cholinergic neuronal network. Thus, galantamine-induced AChE inhibition is expected to lead to a more proper cholinergic signaling. This, in turn, might rescue the under-stimulated cholinergic-cholinoceptives neuronal interfaces and/or induce synaptic remodeling and regeneration in the brain. The required time for such re-modulation also coincides with the top level of clinical manifestation of cognitive improvement that is seen within 3–6 months of therapy with ChEIs (Raskind et al., 2000; Tariot et al., 2000). The correlations between RBC AChE activity and the ^{11}C-nicotine PET also suggest that measurement of RBC AChE activity might be of value as a general index for the overall nicotinic receptors in the brain. Indeed, a study has shown that RBC AChE measurement might have the potential as a peripheral biomarker for diagnosis

of familial Alzheimer's and Parkinson's disease dementia (Bawaskar et al., 2015).

At 12 months follow-up, i.e., when all patients were on 9–12 months treatment, the baseline equilibrium seemed to be reestablished, in other words, the positive correlation between the *in vivo* nicotinic binding sites and the AChE activity. Experimental animal studies are also in line with our findings and the described time-dependent biodynamic model of neuronal synaptic plasticity and/or remodeling of the cholinergic and the related neuronal networks. In non-transgenic mice, a similar increase in nAChRs was observed after short-term galantamine treatment in hippocampus, thalamus and several cortical regions compared to saline-treated mice (Svedberg et al., 2004). In contrast, no significant changes were observed in the AChE overexpressing littermate after galantamine treatment (Svedberg et al., 2004). In *APPsw* transgenic mice, galantamine treatment leads to an increase in the protein level of synaptophysin in the cortex compared to saline-treated control (Unger et al., 2006). Synaptophysin together with synaptogyrin seems to play essential roles in synaptic plasticity (Janz et al., 1999). Interestingly, the regulation of synapse formation by synaptophysin appears to be activity-dependent (Tarsa and Goda, 2002).

In addition, both CSF $ChAT_F$ and the Cholinergic index at 12 months showed strong positive correlations with the *in vivo* AChE activity supporting the notion that a new balance between the degradation and production of ACh was established in the brain. Indeed, we found that both CSF $ChAT_F$ and the Cholinergic index also correlated with several cognitive measures at this follow-up time. Similar correlations with MMSE and ADAS-cog have been reported following treatment with encapsulated nerve growth factor releasing implants in nucleus basalis of Meynert of AD patients (Karami et al., 2015), which is another cholinergic enhancing therapeutic strategy. Thus, the CSF $ChAT_F$ and the Cholinergic index may be useful as a monitoring biomeasure following cholinergic enhancing treatments.

In this context, the important questions are how and when treatment with ChEIs (or even with a fully disease-modifying drug) may be able to be manifested as improvement in the CSF cholinergic index, or simply how this index may differ among patients at different stage of the disease. Here, it is crucial to refer to the rational for treatment with ChEIs. These drugs by definition require a certain amount of ACh production (by ChAT) and release into the synapses. In other words, these drugs will not work if the production and release of ACh into synapses is heavily affected or is absent. Given that the cholinergic neurons degenerate early and progressively in the course of AD, it is expected that each remaining cholinergic neuron will with time have fewer synaptic interfaces at its projection sites in the brain that fulfill this criteria as the disease progresses. Thereby, it is plausible that not all of the degenerating synapses of a cholinergic neuron can be stimulated by treatment with ChEIs. This might explain the limited and moderate clinical efficacy observed following treatment with ChEIs. Given that even at mild stage of AD, a substantial number of cholinergic synapses may have already degenerated beyond the rescue point, it is not very surprising that the observed increase in soluble ChAT activity was quite mild in the current study following galantamine treatment. This, in turn, suggests that a higher degree of increase in soluble ChAT should be expected if treatment initiated at milder stage of the disease or even at asymptomatic stages.

This study has several limitations. It was primarily designed as a PET investigation, thus only included a small group of mild AD patients. These features make it necessary to be cautious when interpreting the data, since the small sample size may result in a lack of statistical power, although this might make the significant results even more interesting. Also, relatively large numbers of statistical analyses were performed on the PET measurement in relation to the CSF cholinergic biomarkers and cognitive function, which were not corrected for multiple comparisons. This may render some of the results liable to be obtained by chance. Therefore, we weighted the overall patterns of the results rather than isolated findings. The number of available data at the 12 months follow-up was particularly small because either no CSF sample or PET scan was available for a few of the patients.

In summary, we report for the first time that a cholinesterase inhibitor increases the CSF level of the ACh synthesizing enzyme, choline acetyltransferase. We also report here distinct time and treatment-dependent associations between the CSF $ChAT_F$ activity, the RBC or CSF AChE activity (or inhibition) and the *in vivo* AChE activity and nicotinic binding sites in the brain, measured by PET. The pattern of the findings indicates a time-dependent biodynamic remodeling and/or reorganization, indicative of establishment of a new bio-equilibrium in the function of the cholinergic neuronal interfaces following ChEI-treatment vs. placebo as well as the treatment duration. Altogether, these observations suggest that a neuronal and/or synaptic remodeling occurred in response to stimulation with a ChEI's treatment, which in turn provide a mechanistic basis for the transient stabilization of cognition and delayed progression of the disease observed in AD patients following therapy with ChEIs (Giacobini, 2000, 2001).

DATA AVAILABILITY STATEMENT

The datasets generated for this study are available on request to the corresponding author.

ETHICS STATEMENT

The studies involving human participants were reviewed and approved by The Ethics Committee of Huddinge University Hospital, Sweden. The patients/participants provided their written informed consent to participate in this study.

AUTHOR CONTRIBUTIONS

TD-S and AKarami conceived and designed the CSF experiments; set up and performed the CSF AChE and ChAT assays and performed statistical analysis of the data. AKarami,

TD-S and ME wrote the first draft and did the initial revisions. AN conceived and designed the original galantamine-PET study. AKadir and AN did the *in vivo* AChE and nicotine binding analyses. OA performed the neuropsychological assessments on the patients. All authors read and approved this final draft of the manuscript.

FUNDING

This research was supported by the following foundations: Swedish Research Council (project no. 2016-01806 and 2016-02317); the regional agreement on medical training and clinical research (ALF) between Stockholm County Council and Karolinska Institutet; Loo and Hans Osterman Foundation; KI Foundations; the Åhlén-Foundation; Anér's Foundation, Magnus Bergvalls Foundation; Demensfonden; the foundation for Old Servants (Gamla Tjänarinnor); Gun and Bertil Stohnes Foundation, Odd Fellow, Lindhés advokatbyrå, the foundation for Ragnhild and Einar Lundströms Memory. The original galantamine study was financed by Swedish Research Council (project no. 05817) and Janssen-Cilag (Sweden and USA).

SUPPLEMENTARY MATERIAL

The Supplementary Material for this article can be found online at: https://www.frontiersin.org/articles/10.3389/fnmol.2019.00239/full#supplementary-material.

FIGURE S1 | Changes in the $ChAT_F$ based on patients whose CSF were available both at 3 and 12 months treatment for (RM) ANOVA analysis. The graphs **(A,B)** are a modified version of the corresponding graphs 1C and 1D in **Figure 1**. Here, data from one subject in the placebo (3 months follow-up) is omitted since no CSF at 12 months was left for these patients. Thereby paired analyses could be done on four subjects. This sub-analyses in **(A)** shows that the *Galantamine group* had about 50% higher levels of $ChAT_F$ in CSF than *the Placebo group* at 3 months, (here $n = 4$, $p < 0.05$). At 12 months *the Placebo-Galantamine group* exhibited about 30% significant increase in the CSF $ChAT_F$ activity compared to their own 3 months follow-up ($n = 4$, $p < 0.02$). Panel **(B)** shows similar sub-analyses with regards to changes in the cholinergic index. At 3 months, the actual differences between the *Galantamine group* and *the Placebo group* ($n = 4$) was over 70%. At 12 months, the cholinergic index was increased over 50% in *the Placebo-Galantamine group* compared to their own 3 months follow-up ($n = 4$, $p < 0.02$). $^{*}p < 0.05$ signify differences compared to *the Placebo group* at 3 months. $^{\#}p < 0.02$ signify differences compared to *the Placebo group* at 3 months. CSF $ChAT_F$ activity = the overall functional ChAT activity expressed in pmol/min/μg ChAT protein in the samples.

REFERENCES

Aronson, S., Van Baelen, B., Kavanagh, S., and Schwalen, S. (2009). Optimal dosing of galantamine in patients with mild or moderate Alzheimer's disease. *Drugs Aging* 26, 231–239. doi: 10.2165/00002512-200926030-00004

Bawaskar, H. S., Bawaskar, P. H., and Bawaskar, P. H. (2015). RBC acetyl cholinesterase: a poor man's early diagnostic biomarker for familial alzheimer's and Parkinson's disease dementia. *J. Neurosci. Rural Pract.* 6, 33–38. doi: 10.4103/0976-3147.143187

Cahn-Weiner, D. A., Sullivan, E. V., Shear, P. K., Fama, R., Lim, K. O., Yesavage, J. A., et al. (1999). Brain structural and cognitive correlates of clock drawing performance in Alzheimer's disease. *J. Int. Neuropsychol. Soc.* 5, 502–509. doi: 10.1017/s1355617799566034

Cummings, J. L. (1993). Frontal-subcortical circuits and human behavior. *Arch. Neurol.* 50, 873–880. doi: 10.1001/archneur.1993.00540080076020

Darreh-Shori, T., Hellström-Lindahl, E., Flores-Flores, C., Guan, Z. Z., Soreq, H., and Nordberg, A. (2004). Long-lasting acetylcholinesterase splice variations in anticholinesterase-treated Alzheimer's disease patients. *J. Neurochem.* 88, 1102–1113. doi: 10.1046/j.1471-4159.2003.02230.x

Darreh-Shori, T., Hosseini, S. M., and Nordberg, A. (2014). Pharmacodynamics of cholinesterase inhibitors suggests add-on therapy with a low-dose carbamylating inhibitor in patients on long-term treatment with rapidly reversible inhibitors. *J. Alzheimers Dis.* 39, 423–440. doi: 10.3233/jad-130845

Darreh-Shori, T., Kadir, A., Almkvist, O., Grut, M., Wall, A., Blomquist, G., et al. (2008). Inhibition of acetylcholinesterase in CSF versus brain assessed by 11C-PMP PET in AD patients treated with galantamine. *Neurobiol. Aging* 29, 168–184. doi: 10.1016/j.neurobiolaging.2006.09.020

Darreh-Shori, T., Meurling, L., Pettersson, T., Hugosson, K., Hellstrom-Lindahl, E., Andreasen, N., et al. (2006). Changes in the activity and protein levels of CSF acetylcholinesterases in relation to cognitive function of patients with mild Alzheimer's disease following chronic donepezil treatment. *J. Neural Transm.* 113, 1791–1801. doi: 10.1007/s00702-006-0526-2

Darreh-Shori, T., Modiri, N., Blennow, K., Baza, S., Kamil, C., Ahmed, H., et al. (2011). The apolipoprotein E epsilon4 allele plays pathological roles in AD through high protein expression and interaction with butyrylcholinesterase. *Neurobiol. Aging* 32, 1236–1248. doi: 10.1016/j.neurobiolaging.2009.07.015

Darreh-Shori, T., and Soininen, H. (2010). Effects of cholinesterase inhibitors on the activities and protein levels of cholinesterases in the cerebrospinal fluid of patients with Alzheimer's disease: a review of recent clinical studies. *Curr. Alzheimer Res.* 7, 67–73. doi: 10.2174/156720510790274455

Giacobini, E. (2000). Cholinesterase inhibitors stabilize Alzheimer disease. *Neurochem. Res.* 25, 1185–1190. doi: 10.1023/a:1007679709322

Giacobini, E. (2001). Is anti-cholinesterase therapy of Alzheimer's disease delaying progression? *Aging* 13, 247–254. doi: 10.1007/bf03351483

Janz, R., Südhof, T. C., Hammer, R. E., Unni, V., Siegelbaum, S. A., and Bolshakov, V. Y. (1999). Essential roles in synaptic plasticity for synaptogyrin I and synaptophysin I. *Neuron* 24, 687–700. doi: 10.1016/s0896-6273(00)81122-8

Kadir, A., Darreh-Shori, T., Almkvist, O., Wall, A., Grut, M., Strandberg, B., et al. (2008). PET imaging of the *in vivo* brain acetylcholinesterase activity and nicotine binding in galantamine-treated patients with AD. *Neurobiol. Aging* 29, 1204–1217. doi: 10.1016/j.neurobiolaging.2007.02.020

Kadir, A., Darreh-Shori, T., Almkvist, O., Wall, A., Långström, B., and Nordberg, A. (2007). Changes in brain 11C-nicotine binding sites in patients with mild Alzheimer's disease following rivastigmine treatment as assessed by PET. *Psychopharmacology* 191, 1005–1014. doi: 10.1007/s00213-007-0725-z

Karami, A., Eyjolfsdottir, H., Vijayaraghavan, S., Lind, G., Almqvist, P., Kadir, A., et al. (2015). Changes in CSF cholinergic biomarkers in response to cell therapy with NGF in patients with Alzheimer's disease. *Alzheimer Dement.* 11, 1316–1328. doi: 10.1016/j.jalz.2014.11.008

Kuhl, D., Koeppe, R., Minoshima, S., Snyder, S., Ficaro, E., Foster, N., et al. (1999). *in vivo* mapping of cerebral acetylcholinesterase activity in aging and Alzheimer's disease. *Neurology* 52, 691–699. doi: 10.1212/wnl.52.4.691

Lane, R. M., and Darreh-Shori, T. (2015). Understanding the beneficial and detrimental effects of donepezil and rivastigmine to improve their therapeutic value. *J. Alzheimers Dis.* 44, 1039–1062. doi: 10.3233/jad-142268

McKhann, G., Drachman, D., Folstein, M., Katzman, R., Price, D., and Stadlan, E. M. (1984). Clinical diagnosis of Alzheimer's disease: report of the NINCDS-ADRDA work group under the auspices of department of health and human services task force on Alzheimer's disease. *Neurology* 34, 939–944. doi: 10.1212/wnl.34.7.939

Mousavi, M., Bednar, I., and Nordberg, A. (2004). Selective changes in expression of different nicotinic receptor subtypes in brain and adrenal glands of mice carrying human mutated gene for APP or over-expressing human acetylcholinestrase. *Int. J. Dev. Neurosci.* 22, 545–549. doi: 10.1016/j.ijdevneu.2004.07.005

Nordberg, A., Darreh-Shori, T., Peskind, E., Soininen, H., Mousavi, M., Eagle, G., et al. (2009). Different cholinesterase inhibitor effects on

CSF cholinesterases in Alzheimer patients. *Curr. Alzheimer Res.* 6, 4–14. doi: 10.2174/156720509787313961

Nordberg, A., and Svensson, A.-L. (1998). Cholinesterase inhibitors in the treatment of Alzheimer's disease. *Drug Saf.* 19, 465–480. doi: 10.2165/00002018-199819060-00004

Raskind, M. A., Peskind, E. R., Truyen, L., Kershaw, P., and Damaraju, C. V. (2004). The cognitive benefits of galantamine are sustained for at least 36 months: a long-term extension trial. *Arch. Neurol.* 61, 252–256. doi: 10.1001/archneur.61.2.252

Raskind, M. A., Peskind, E., Wessel, T., and Yuan, W. (2000). Galantamine in AD: a 6-month randomized, placebo-controlled trial with a 6-month extension. *Neurology* 54, 2261–2268. doi: 10.1212/wnl.55.5.744

Rösler, M., Bayer, T., Anand, R., Cicin-Sain, A., Gauthier, S., Agid, Y., et al. (1999). Efficacy and safety of rivastigmine in patients with Alzheimer's disease: international randomised controlled trial Commentary: another piece of the Alzheimer's jigsaw. *BMJ* 318, 633–640. doi: 10.1136/bmj.318.7184.633

Sramek, J. J., and Cutler, N. R. (2000). RBC cholinesterase inhibition: a useful surrogate marker for cholinesterase inhibitor activity in Alzheimer disease therapy? *Alzheimer Dis. Assoc. Disord.* 14, 216–227. doi: 10.1097/00002093-200010000-00006

Svedberg, M. M., Bednar, I., and Nordberg, A. (2004). Effect of subchronic galantamine treatment on neuronal nicotinic and muscarinic receptor subtypes in transgenic mice overexpressing human acetylcholinesterase. *Neuropharmacology* 47, 558–571. doi: 10.1016/j.neuropharm.2004.06.009

Svedberg, M. M., Svensson, A. L., Bednar, I., and Nordberg, A. (2003). Neuronal nicotinic and muscarinic receptor subtypes at different ages of transgenic mice overexpressing human acetylcholinesterase. *Neurosci. Lett.* 340, 148–152. doi: 10.1016/s0304-3940(03)00092-2

Svedberg, M. M., Svensson, A. L., Johnson, M., Lee, M., Cohen, O., Court, J., et al. (2002). Upregulation of neuronal nicotinic receptor subunits α4, β2, and α7 in transgenic mice overexpressing human acetylcholinesterase. *J. Mol. Neurosci.* 18, 211–222. doi: 10.1385/jmn:18:3:211

Tariot, P. N., Solomon, P., Morris, J., Kershaw, P., Lilienfeld, S., Ding, C., et al. (2000). A 5-month, randomized, placebo-controlled trial of galantamine in AD. The galantamine USA-10 study group. *Neurology* 54, 2269–2276. doi: 10.1212/wnl.54.12.2261

Tarsa, L., and Goda, Y. (2002). Synaptophysin regulates activity-dependent synapse formation in cultured hippocampal neurons. *Proc. Natl. Acad. Sci. U S A* 99, 1012–1016. doi: 10.1073/pnas.022575999

Unger, C., Svedberg, M. M., Yu, W. F., Hedberg, M. M., and Nordberg, A. (2006). Effect of subchronic treatment of memantine, galantamine, and nicotine in the brain of Tg2576 (APPswe) transgenic mice. *J. Pharmacol. Exp. Ther.* 317, 30–36. doi: 10.1124/jpet.105.098566

Vijayaraghavan, S., Karami, A., Aeinehband, S., Behbahani, H., Grandien, A., Nilsson, B., et al. (2013). Regulated extracellular choline acetyltransferase activity- the plausible missing link of the distant action of acetylcholine in the cholinergic anti-inflammatory pathway. *PLoS One* 8:e65936. doi: 10.1371/journal.pone.0065936

Wechsler, D. (1981). *Wechsler Adult Intelligence Scale—Revised Manual*. New York, NY: Psychological Corporation.

Whitehead, A., Perdomo, C., Pratt, R. D., Birks, J., Wilcock, G. K., and Evans, J. G. (2004). Donepezil for the symptomatic treatment of patients with mild to moderate Alzheimer's disease: a meta-analysis of individual patient data from randomised controlled trials. *Int. J. Geriatr. Psychiatry* 19, 624–633. doi: 10.1002/gps.1133

Wilcock, G., Howe, I., Coles, H., Lilienfeld, S., Truyen, L., Zhu, Y., et al. (2003). A long-term comparison of galantamine and donepezil in the treatment of Alzheimer's disease. *Drugs Aging* 20, 777–789. doi: 10.2165/00002512-200320150-00009

Winblad, B., Engedal, K., Soininen, H., Verhey, F., Waldemar, G., Wimo, A., et al. (2001). A 1-year, randomized, placebo-controlled study of donepezil in patients with mild to moderate AD. *Neurology* 57, 489–495. doi: 10.1212/wnl.57.3.489

Conflict of Interest: The authors declare that the research was conducted in the absence of any commercial or financial relationships that could be construed as a potential conflict of interest.

frontiers in Molecular Neuroscience

ORIGINAL RESEARCH
published: 23 January 2020
doi: 10.3389/fnmol.2019.00335

Evaluation of Biochemical and Epigenetic Measures of Peripheral Brain-Derived Neurotrophic Factor (BDNF) as a Biomarker in Huntington's Disease Patients

Ashley Gutierrez[1], Jody Corey-Bloom[1], Elizabeth A. Thomas[2†] and Paula Desplats[1,2,3†]*

[1] Department of Neuroscience, School of Medicine, University of California, San Diego, San Diego, CA, United States, [2] Department of Neuroscience, The Scripps Research Institute, La Jolla, CA, United States, [3] Department of Pathology, School of Medicine, University of California, San Diego, San Diego, CA, United States

Huntington's disease (HD) is an autosomal-dominant neurodegenerative movement disorder that presents with prominent cognitive and psychiatric dysfunction. Brain-derived neurotrophic factor (BDNF) plays an important role in the pathophysiology of HD, as well as other neurodegenerative and psychiatric disorders, and epigenetic alterations in the complex BDNF promoter have been associated with its deregulation in pathological conditions. BDNF has gained increased attention as a potential biomarker of disease; but currently, the conflicting results from measurements of BDNF in different biofluids difficult the assessment of its utility as a biomarker for HD. Here, we measured BDNF protein levels in plasma (n = 85) and saliva (n = 81) samples from premanifest and manifest HD patients and normal controls using ELISA assays. We further examined DNA methylation levels of *BDNF* promoter IV using DNA derived from whole blood of HD patients and healthy controls (n = 40) using pyrosequencing. BDNF protein levels were not significantly different in plasma samples across diagnostic groups. Plasma BDNF was significantly correlated with age in control subjects but not in HD patients, nor were significant gender effects observed. Similar to plasma, salivary BDNF was correlated with age only in control subjects, with no gender effects observed. Importantly, we detected significantly lower levels of salivary BDNF in premanifest and manifest HD patients compared to control subjects, with lower BDNF levels being observed in premanifest patients within a predicted 10 years to disease onset. Salivary and plasma BDNF levels were not significantly correlated with one another, suggesting different origins. DNA methylation at four out of the 12 CpG sites studied in promoter IV were significantly altered in HD patients in comparison to controls. Interestingly, methylation at three of these CpG sites was inversely correlated to the Hospital Anxiety and Depression Scale (HADS) scores. *BDNF* promoter methylation was not correlated with motor or cognitive scores in HD patients, and was not associated with sex or age in neither disease nor control groups. Conclusion: Our studies show that BDNF protein levels are

OPEN ACCESS

Edited by:
Enrico Tongiorgi, University of Trieste, Italy

Reviewed by:
Lynn Raymond, The University of British Columbia, Canada
Anthony Hannan, The University of Melbourne, Australia

***Correspondence:**
Paula Desplats
pdesplat@ucsd.edu

† These authors share senior authorship

Received: *30 October 2019*
Accepted: *27 December 2019*
Published: *23 January 2020*

Citation:
Gutierrez A, Corey-Bloom J, Thomas EA and Desplats P (2020) Evaluation of Biochemical and Epigenetic Measures of Peripheral Brain-Derived Neurotrophic Factor (BDNF) as a Biomarker in Huntington's Disease Patients. Front. Mol. Neurosci. 12:335. doi: 10.3389/fnmol.2019.00335

decreased in saliva; and *BDNF* promoter methylation increased in blood in HD subjects when compared to controls. These findings suggest that salivary BDNF measures may represent an early marker of disease onset and DNA methylation at the *BDNF* promoter IV, could represent a biomarker of psychiatric symptoms in HD patients.

Keywords: Huntington's disease, brain-derived neurotrophic factor, DNA methylation, saliva, blood, biomarker, epigenetics, clinical symptoms

INTRODUCTION

Huntington's disease is an inherited, progressive neurodegenerative disorder characterized by chorea, movement dysfunction, cognitive impairment, and behavioral disturbances (The Huntington's Disease Collaborative Research Group, 1993). The prevalence rate of HD in the United States is approximately 5 per 100,000 people (Lanska, 2000; Ho et al., 2001). HD is caused by a CAG trinucleotide repeat expansion in the first exon of the *HTT* gene encoding the HTT (The Huntington's Disease Collaborative Research Group, 1993). Because the gene mutation is known, diagnostic and predictive genetic testing is available for HD; however, biomarkers for HD are still greatly needed to predict disease onset, to assess the diversity and severity of symptoms and to monitor disease progression (Ross et al., 2014). Furthermore, HD biomarkers could serve for monitoring clinical trials of disease-modifying therapeutics (Ross et al., 2014).

A major limitation in the development of biomarkers for CNS disorders is the inaccessibility of brain tissue; therefore, screening of peripheral tissues that may serve as proxy for brain degeneration is crucial. Cerebral spinal fluid (CSF) is thought to represent the biofluid most similar to the brain environment, however, CSF collection is an invasive technique that requires a lumbar puncture, which can be painful and lead to side effects and complications (Evans, 1998). With regards to peripheral sources, investigations in blood have dominated the field for decades, however, other peripheral fluids for biomarker studies have included saliva, urine, and sweat.

One candidate biomarker for HD is BDNF, which plays an important role in survival, growth and differentiation of neurons (Lu, 2003; Greenberg et al., 2009). Decreased levels of BDNF, especially in the striatum, are thought to play a crucial role in HD pathogenesis. A loss of normal huntingtin-mediated *BDNF* gene transcription, and dysregulation of BDNF expression by the mutant form of huntingtin, both contribute to the reduced levels of BDNF in the brain, which has been observed in post-mortem brain tissue from human HD patients (Ferrer et al., 2000; Zuccato et al., 2001), as well as in several transgenic mouse models of HD (Zuccato et al., 2001; Duan et al., 2003; Zhang et al., 2003). Notably, several studies have shown that overexpression of BDNF to the brain ameliorates HD phenotypes in the R6/1 and R6/2 mouse models (Zuccato et al., 2001, 2008; Gharami et al., 2008; Xie et al., 2010), and, in one study, BDNF overexpression *in vivo* was found to rescue HD phenotypes in YAC128 mice (Xie et al., 2010). Moreover, BDNF knock-out mice exhibit many symptoms reminiscent of HD transgenic mice (Canals et al., 2004). These studies suggest therapeutic implications for elevating BDNF levels in this disease.

In addition to widespread expression throughout the CNS (Ma et al., 2012), BDNF is also present in blood (Yamamoto and Gurney, 1990; Radka et al., 1996; Hohlfeld et al., 2006), and studies have shown that BDNF can cross the blood-brain barrier (Pan et al., 1998), suggesting that peripheral measures of BDNF have relevance to brain function and vice versa. However, conflicting literature exists on the levels of BDNF in blood of HD patients, with one study reporting decreased levels of BDNF transcripts in whole blood of HD patients (Krzyszton-Russjan et al., 2013); another showing increased levels of BDNF protein in platelets (Betti et al., 2018) and a third study showing no significant changes in BDNF protein levels in plasma or serum in HD patients (Zuccato et al., 2011) in comparison to healthy control subjects. Here we sought to further investigate blood measures of BDNF in HD patients, as well as exploring BDNF levels in another peripheral fluid, saliva.

With regards to markers of *BDNF* gene activity, analyses have focused on DNA methylation of the *BDNF* promoter in various neurological disorders. Specifically, studies have demonstrated changes in DNA methylation at the BDNF promoter in blood samples from patients with Alzheimer's disease (AD) (Rao et al., 2012; Xie et al., 2017), major depression (Januar et al., 2015; Kang et al., 2015) and schizophrenia (Ikegame et al., 2013). Such studies have suggested that *BDNF* promoter methylation might be a useful peripheral biomarker of disease symptoms observed in these disorders. Based on these findings, we further examined DNA methylation levels at *BDNF* promoter IV in whole blood samples from HD patients and tested for any associations between the *BDNF* DNA methylation levels and clinical presentation in HD patients.

Abbreviations: BDNF, brain-derived neurotrophic factor; HADS, Hospital Anxiety and Depression Scale; HD, Huntington's disease; HTT, Huntingtin protein; MMSE, Mini-Mental State Examination; NA, not applicable; NC, normal control; PM, pre-manifest; TFC, Total Functional Capacity; UHDRS, Motor component of the Unified Huntington's Disease Rating Scale.

MATERIALS AND METHODS

Participants

This study was approved by the University of California, San Diego Institutional Review Board in accordance with the requirements of the Code of Federal Regulations on the Protection of Human Subjects. Informed consent from all subjects was obtained prior to their participation. Patients were recruited from the University of California, San Diego (UCSD) HD Clinical Research Center. HD patient criteria included a definitive diagnosis of HD with family history and an expanded

trinucleotide CAG repeat of 40 or more. Normal controls had no reported history of neurological or psychiatric disorders, and no use of psychoactive substances or medications. Demographic information was collected at the time of saliva collection, including sex, age, and CAG repeat length. This information is provided in **Table 1**. Patients were assessed for cognitive and motor function using the MMSE (score range 0–30) (Gluhm et al., 2013), the Total Motor Score from the UHDRS (score range 0–124), and TFC (range 0–13). Patients were assessed for anxiety and depression symptoms using the HADS. The predicted age to onset of disease symptoms was calculated using the HD conditional onset probability calculator, according to Langbehn, and using the default probability to onset of 0.6[1] (Langbehn et al., 2010).

Saliva Collection

All donors were asked to refrain from smoking, eating, drinking, or oral hygiene procedures for at least 1 h prior to samples collection, and then rinsed their mouth thoroughly with water 15–20 min prior to sample collection. Saliva samples were collected between 10:00 am and 4 pm. using the passive drool method according to previously established protocols (Granger et al., 2012). Roughly two to three milliliters of unstimulated whole saliva were obtained. Samples were immediately frozen at −20°C at the time of collection, then stored at −80°C. At the time of use, saliva samples were thawed and centrifuged at 10,000 *g* for 10 min at 4°C to remove insoluble material and cellular debris. Supernatants were collected and used for all assays.

Plasma Collection

Blood was drawn by venipuncture into 2 ml lavender/EDTA tubes. EDTA/whole blood was mixed well by inversion and spun at 900 × *g* for 15 min. The top plasma layer was transferred into 4 × 1 ml aliquots and snap frozen and stored at −80°C.

[1]http://edwild.com/205-huntingtons-disease-conditional-onset-probability-calculator/

TABLE 1 | Characterization of cases included in this study.

	HD	PM	NC
Plasma			
N	21	30	33
Female:Male	13:8	17:13	17:16
Age (years) ± SD	56.8 ± 11.1	41.2 ± 12.9	50.9 ± 14.6
CAG repeat	43.1 ± 3.07	42.0 ± 2.93	NA
Saliva			
N	20	23	38
Female:Male	11:9	10/13	22/16
Age (years) ± SD	54.5 ± 12.7	43.6 ± 14.5	48.1 ± 14.2
CAG repeat	43.9 ± 2.91	42.3 ± 11.2	NA
DNA methylation			
N	10	11	18
Female:Male	6:4	6/5	12/6
Age (years) ± SD	58.2 ± 12.5	41.8 ± 10.6	55.2 ± 22.3
CAG repeat	43.5 ± 2.67	43.6 ± 2.87	NA

HD, Huntington's disease; PM, Pre-manifest; NC, Normal controls; NA, Not applicable.

BDNF Measurements

Brain derived neurotrophic factor levels in plasma were measured using a commercially available kit according to our previous studies (Corey-Bloom et al., 2017). BDNF levels in saliva were measured using a sandwich ELISA modified from a protocol optimized for salivary BDNF (Mandel et al., 2011). A 96-well microtiter plate was incubated overnight at 4°C with a monoclonal mouse anti-human BDNF (100 ul; clone 35928; Calbiochem, San Diego, CA, United States), diluted to 1 μg/ml in filter-sterilized PBS, pH 7.4. The plate was manually washed three times with TBS + 3% tween (TBST), allowing the plate to soak for 1 min each time. Wells were blocked with 300 μl of 3% BSA in PBST for 2.5 h at room temperature. Standards ranging from 15.6 to 500 pg/ml were prepared fresh for each assay using a full-length, homodimeric recombinant BDNF (rBDNF; Peprotech, Rocky Hill, NJ, United States). Following blocking, the plate was washed five times and 50 ul of sample (diluted 1:1 in blocking solution), was added to the wells and assayed in triplicate. The plate was incubated for 2.5 h at RT with agitation and then washed five times. Subsequently, a polyclonal chicken anti-human BDNF (100 ul; 2.5 μg/ml; Promega) was added to the plate and incubated for 2.5 h. The plate was washed five times with PBST, then anti-chicken IgY-HRP (1 μg/ml; Promega) was added to each well for a 1-h incubation at RT. After the final wash, TMB (tetramethylbenzidine; Promega) substrate was added to each well, followed by quenching with 1M HCl and quantified by reading at 450 nm. The amount of BDNF in each sample was calculated using the regression equation from the standard curve for the plasma samples. For the saliva samples, the amount of BDNF is expressed as a relative amount based on absorbance. All assays were performed by operators blinded to the clinical state of the participant.

Quantification of DNA Methylation at BDNF Promoter

We interrogated 12 CpG sites at promoter IV of the *BDNF* gene by pyrosequencing (performed by EpigenDx) using the probe ADS221-FS2re that covers the region chr11:27723246–27723191 and includes six CpG sites; and the probe Ads3858-FS mapped to chr11:27723144–27723076 and including another six CpG sites. Briefly, DNA was extracted from 1 mL of whole blood from n = 18 control subjects and n = 21 HD cases using QIAamp DNA Blood Midi Kit (Qiagen) as per manufacturer's protocol. DNA (500 ng) was bisulfite-converted with the EZ DNA Methylation−Gold® Kit (Zymo Research, CA, United States). Bisulfite−treated DNA (25 ng) was amplified using HotStarTaq DNA Polymerase (Qiagen, CA, United States) and the following standard PCR conditions. One primer was biotin-labeled and HPLC purified in order to purify the final PCR product using sepharose beads. PCR product was bound to Streptavidin Sepharose HP (GE Healthcare Life Sciences), after which the immobilized PCR products were purified, washed, denatured with a 0.2 μM NaOH solution, and rewashed

using the Pyrosequencing Vacuum Prep Tool (Pyrosequencing, Qiagen), as per the manufacturer's protocol. Next, 0.5 μM of sequencing primer was annealed to the purified single stranded PCR products. 10 μL of the PCR products were sequenced by Pyrosequencing on the PSQ96 HS System (Pyrosequencing, Qiagen) following the manufacturer's instructions.

The methylation status of each CpG site was determined individually as an artificial C/T SNP using QCpG software (Pyrosequencing, Qiagen). The methylation level at each CpG site was calculated as the percentage of the methylated alleles divided by the sum of all methylated and unmethylated alleles. The mean methylation level was calculated using methylation levels of all measured CpG sites within the targeted region of each gene. Each experiment included non-CpG cytosines as internal controls to detect incomplete bisulfite conversion of the input DNA. In addition, a series of unmethylated and methylated DNA are included as controls in each PCR. Furthermore, PCR bias testing was performed by mixing unmethylated control DNA with *in vitro* methylated DNA at different ratios (0, 5, 10, 25, 50, 75, and 100%), followed by bisulfite modification, PCR, and Pyrosequencing analysis. The methylation level at each CpG site was calculated as the ratio of C (methylated cytosine) relative to T (unmethylated cytosine). Mean percent methylation was calculated as the average of individual CpGs.

Statistics

All statistical analyses were performed using Graphpad software (Prism) or JASP Stats. The distribution of the data values in each diagnostic group was tested for normality using the Kolmogorov–Smirnov normality test. BDNF values in all groups showed a normal distribution. Outliers within each plasma and saliva diagnostic groups were determined using Iglewicz and Hoaglin's test for multiple outliers using a z cutoff = 3.5. For the plasma data, this analysis resulted in removing one outlier in the HD group. For the saliva data, this analysis resulted in removing three outliers in the normal control group. Differences between diagnostic groups were determined using One-way ANOVA followed by Dunnett's post-test comparing all groups to the normal control group or when comparing two groups, a Student's t test was used. The effects of sex and age on the diagnostic differences in BDNF levels were determined by ANCOVA. Linear regression analysis (Spearman correlation) was used to compare BDNF levels against age and the clinical variables, which were not normally distributed. For clinical correlations, PM and HD patients were combined. P-values were adjusted for multiple test comparisons using a Bonferroni correction. Sex differences were determined using Student's t test (unpaired; two-tailed). Statistical significance was defined by a P value of less than or equal to 0.05.

RESULTS

Study Cohort

The samples [plasma (n = 85), saliva (n = 81), and whole blood (n = 39)] used in this study correspond to HD patients and healthy controls recruited from the University of California, San Diego (UCSD) HD Clinical Research Center over a period of 3 years. HD patient criteria included a definitive diagnosis of HD with family history and an expanded trinucleotide CAG repeat of 40 or more, giving them "gene (+)" status. Gene (+) patients consisted of both premanifest patients (PM), who were asymptomatic; and manifest, symptomatic HD patients (designated "HD"; **Table 1**). There were no significant differences in sex ratios or age between the HD and control groups. The patients providing plasma, saliva or whole blood samples were separate cohorts with only approximately 25% of subjects contributing more than one sample type.

BDNF Levels in Plasma of HD Patients

We quantified BDNF protein in plasma from HD patients using a commercially available BDNF ELISA kit (Promega). This kit showed excellent reproducibility in a subset of plasma samples that were tested approximately 1 year apart (r = 0.797; p = 0.0004; **Supplementary Figure S1**). We did not detect any sex differences in BDNF levels (p = 0.3468 unpaired t-test; **Figure 1A**). BDNF levels in plasma were positively correlated with age in control subjects (Pearson r = 0.500; p = 0.006; **Table 2**), although this association was absent in HD patients (Pearson r = 0.1945; p = 0.1714; **Table 2**).

Comparing across diagnostic groups, we did not detect any significant differences in BDNF levels between PM nor HD patients in comparison to control subjects ($p > 0.05$, one-way ANOVA; **Figure 1B**). Plasma BDNF levels were not correlated with CAG repeat length nor with any clinical measure, including the MMSE, TFC, total motor score (MOTOR), and the HADS (**Table 2**).

BDNF Levels in Saliva of HD Patients

We next explored the use of saliva as an alternative peripheral non-invasive biofluid for BDNF measurements. We used a modified ELISA method optimized for saliva measurements in human saliva samples, as previously described (Mandel et al., 2011). We did not detect sex differences in the levels of BDNF in saliva (p = 0.7324 unpaired t-test; **Figure 2A**), but, similar to plasma, salivary BDNF was positively correlated with age in controls subjects (Pearson r = 0.387; p = 0.021; **Table 3**). However, neither age nor sex were significant covariates in the diagnostic comparisons of BDNF levels (ANCOVA, p = 0.212 and p = 0.328 for age and sex, respectively). Comparing salivary BDNF levels across diagnostic groups, we detected a significant decrease in salivary BDNF in both PM and HD patients compared to control subjects ($p < 0.01$ and $p < 0.05$ for PM and HD, respectively One-way ANOVA; **Figure 2B**). We next calculated the predicted age to onset of PM patients according to Langbehn et al. (2010) to determine if BDNF levels might be different in those patients closer to disease onset. We found a significant decrease in BDNF levels in those patients who had a predicted age to onset of <10 years, compared to those with a predicted onset of >10 years (**Figure 2C**).

As with the plasma BDNF data, we looked for possible correlations between salivary BDNF levels and clinical measures.

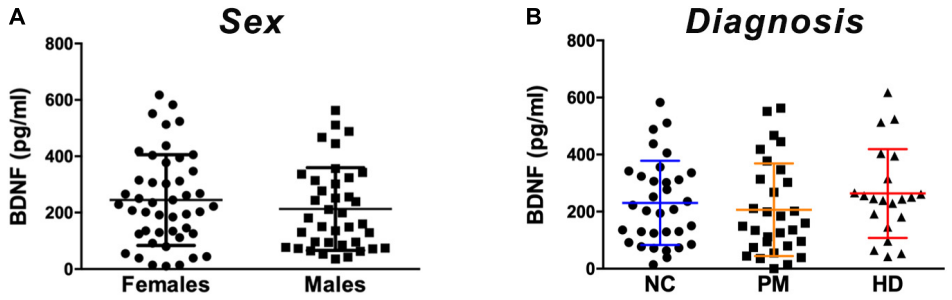

FIGURE 1 | Plasma BDNF levels according to sex and diagnostic group. BDNF levels in plasma (50 ul) were determined by ELISA. **(A)** BDNF levels did not differ by sex among subjects included in our study as per Student's *t* test, unpaired; two-tailed. **(B)** No significant differences were detected according to diagnostic group between premanifest (PM), manifest HD (HD), and normal controls (NC) as per One-way ANOVA. Data is shown as individual BDNF levels ± SD.

TABLE 2 | Correlations between plasma BDNF levels and clinical data in HD patients and control subjects.

	Age	CAG	HADS	TFC	MMSE	MOTOR
HD						
Pearson *r*	0.1945	−0.04949	0.0619	−0.1804	−0.09626	0.2247
95% confidence interval	−0.09404 to 0.4529	−0.3310 to 0.2401	−0.2677 to 0.3786	−0.4412 to 0.1085	−0.3722 to 0.1953	−0.06263 to 0.4777
P value (two−tailed)	0.1714	0.7329	0.7081	0.2053	0.5061	0.1129
P value summary	ns	ns	ns	ns	ns	ns
NC						
Pearson *r*	**0.500**	NA	−0.094	NA	NA	NA
95% confidence interval	0.1142 to 0.6920	NA	−0.5618 to 0.4235	NA	NA	NA
P value (two-tailed)	**0.006**	NA	0.736	NA	NA	NA
P value summary	**	NA	ns	NA	NA	NA

*NC, normal controls; HD patients included premanifest (PM) and manifest HD patients; HADS, Hospital Anxiety and Depression Scale; TFC, Total Functional Capacity; MMSE, Mini-Mental State Examination; MOTOR, the Unified Huntington's Disease Rating Scale Motor component. Bold lettering denotes significant p values. **P = 0.006.*

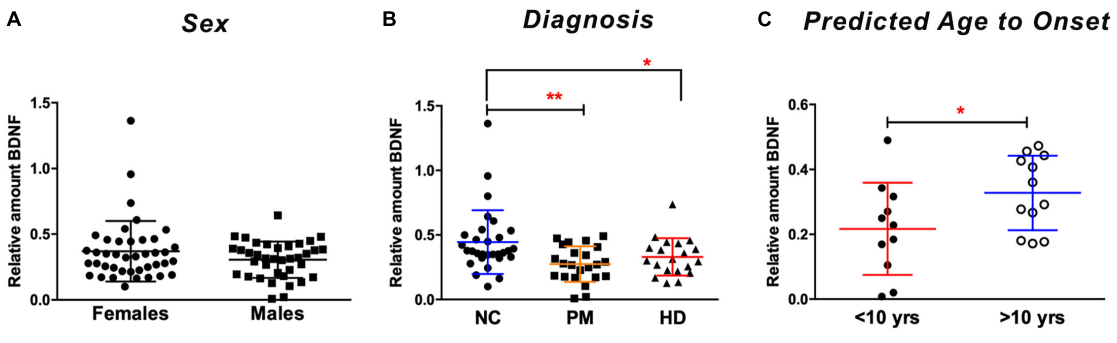

FIGURE 2 | Salivary BDNF levels according to sex and diagnostic group. BDNF levels in saliva (50 ul) were determined by ELISA. **(A)** No significant differences in BDNF were observed by sex (Student's *t* test, unpaired; two-tailed). **(B)** BDNF levels are lower in premanifest (PM) and manifest HD (HD) cases when compared to normal controls (NC). *$p < 0.05$; **$p < 0.01$ in comparison to NC group as per One-way ANOVA. **(C)** BDNF levels are significantly lower in subjects who are >10 years from their predicted age of onset compared to those who are <10 years from predicted onset. *$p = 0.05$. Predicted age to onset was calculated using the Langbehn formula (Langbehn et al., 2010). Data is shown as individual BDNF levels ± SD.

Similar to what we observed in plasma, salivary BDNF levels in patients did not correlate with clinical scores including MMSE; TFC; total motor score or HADS score (**Table 3**).

A subgroup of subjects ($n = 20$) from all cohorts that provided a saliva sample for this study also provided a blood sample, hence we investigate the correlation between BDNF levels in plasma and saliva. We did not detect a significant correlation between plasma and salivary levels (Pearson $r = -0.218$; $p = 0.435$; data not shown), suggesting that the BDNF protein detected in the saliva is not originating nor transported from the blood.

DNA Methylation Alterations at BDNF Promoter IV

As a measure of *BDNF* gene activity, we quantified methylation levels in DNA isolated from whole blood samples from $n = 21$

TABLE 3 | Correlations between salivary BDNF levels and clinical data.

	Saliva					
	Age	**Age of Onset**	**HADS**	**TFC**	**MMSE**	**MOTOR**
HD						
Pearson *r*	−0.1857	−0.2189	−0.05931	−0.1844	−0.04182	0.1952
95% confidence interval	−0.4635 to 0.1254	−0.6031 to 0.2477	−0.3762 to 0.2700	−0.4798 to 0.1486	−0.3654 to 0.2908	−0.1376 to 0.4884
P value (two-tailed)	0.2391	0.3537	0.7273	0.2746	0.8087	0.2469
P value summary	ns	ns	ns	ns	ns	ns
NC						
Pearson *r*	**0.387**	NA	−0.210	NA	NA	NA
95% confidence interval	0.05432 to 0.5686	NA	−0.6066 to 0.2699	NA	NA	NA
P value (two-tailed)	**0.021**	NA	0.387	NA	NA	NA
P value summary	*	NA	ns	NA	NA	NA

*NC, normal controls; HD patients included premanifest (PM) and manifest HD patients; HADS, Hospital Anxiety and Depression Scale; TFC, Total Functional Capacity; MMSE, Mini-Mental State Examination; MOTOR, the Unified Huntington's Disease Rating Scale Motor component. Bold lettering denotes significant p values. *P = 0.021.*

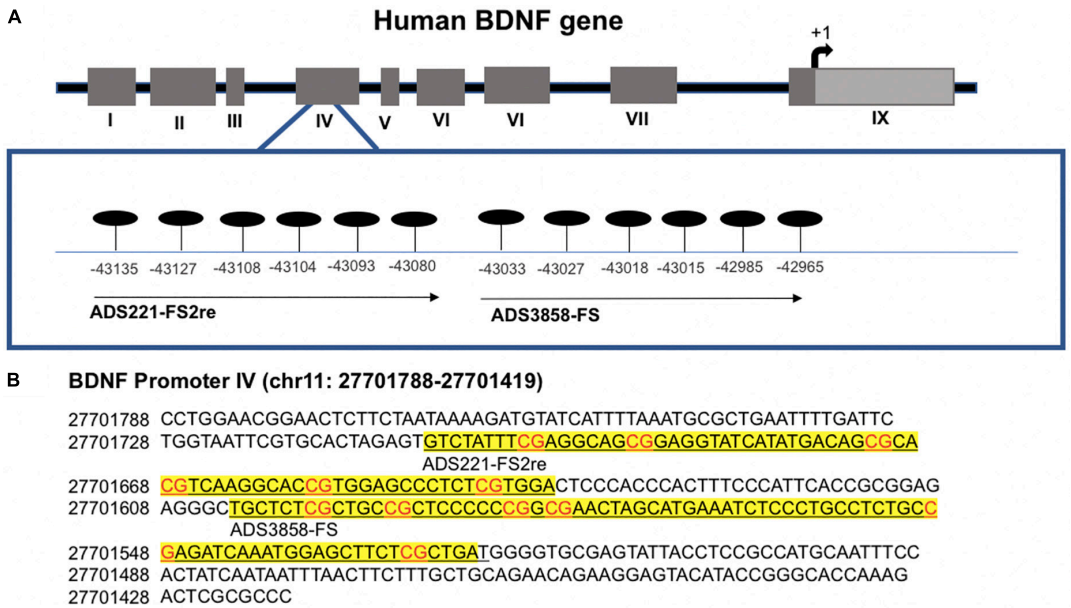

FIGURE 3 | Methylation sites in the BDNF promoter IV region. **(A)** Schematic representation of human BDNF gene indicating alternative promoters. CpG sites analyzed are detailed in enlarged box. Position is in relation to transcription start site. **(B)** Detailed sequence of BDNF promoter IV. Underlined text in yellow boxes indicate regions analyzed with each probe by pyrosequencing. Genomic position is based on chromone build GRCh37.p13 primary assembly.

HD patients and n = 18 normal controls (**Table 1**) by pyrosequencing. For the initial analysis, both HD and PM cases were combined to increase sample size and statistical power. We focused on 12 CpG sites in promoter IV of the *BDNF* gene (**Figure 3**) as this region has been previously reported as differentially methylated in Alzheimer's disease and other neurological conditions (Rao et al., 2012; Ikegame et al., 2013; Januar et al., 2015; Kang et al., 2015; Xie et al., 2017). The mean methylation levels for each CpG tested is shown in **Table 4** for both HD patients and healthy control subjects. We found that four CpG sites were differentially methylated in HD patients, three of the sites showing increased methylation (CpG 444, CpG 445, and CpG 446) and one site, CpG 437, showing decreased methylation levels in comparison to control subjects (**Table 4** and **Figure 4**). For these four CpG sites, we further separated the HD cases into different stages (PM, late pre-manifest (LPM) and manifest HD), and compared methylation levels across stages. We did not observe significant changes in methylation in the early stages of disease, however, progressive increases in methylation at sites 444, 445, and 446 were observed across all stages (**Supplementary Figure S2**). We did not detect a correlation between promoter IV DNA methylation levels to age nor an effect of gender, supporting that these epigenetic changes observed in HD patients are likely associated with the presence of the *HTT* mutation (**Table 5** and **Supplementary Figure S3**).

TABLE 4 | DNA methylation status at selected CpG sites from BDNF promoter IV.

CpG site	Genomic position Chr11	Methylation (%)[1]		*p*-value[2]
		NC	HD Gene (+)	
436	27701529	1.2 (0.0 – 4.6)	1.3 (0.0 – 5.1)	0.89
437	27701549	4.1 (3.1 – 5.5)	2.9 (0.0 – 5.9)	0.032*
438	27701579	1.0 (0.0 – 4.2)	1.0 (0.0 – 4.1)	0.849
439	27701582	3.9 (0.0 – 5.7)	3.1 (0.0 – 7.7)	0.196
440	27701591	2.4 (0.0 – 4.4)	2.3 (0.0 – 5.8)	0.889
441	27701597	1.5 (0.0 – 3.8)	1.7 (0.0 – 4.2)	0.706
444	27701644	1.1 (0.0 – 3.5)	2.3 (0.0 – 7.0)	0.028*
445	27701657	0.9 (0.0 – 3.5)	2.1 (0.0 – 5.3)	0.023*
446	27701668	0.3 (0.0 – 2.6)	1.4 (0.0 – 3.7)	0.002**
447	27701672	2.9 (0.0 – 6.9)	2.9 (0.0 – 6.5)	0.961
448	27701691	5.3 (0.0 – 8.9)	6.4 (3.5 – 11.3)	0.079
449	27701699	3.2 (2.0 – 6.3)	3.7 (0.0 – 6.1)	0.312

*[1]Methylation levels are expressed as a mean percentage and (min–max) values. [2]As per Student's t test (unpaired; two-tailed). Significant differences are denoted by asterisks, * and **, for the shown p-values.*

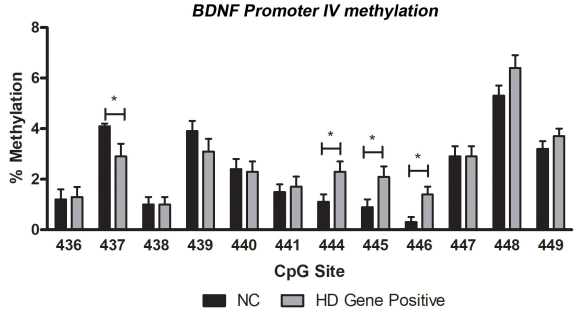

FIGURE 4 | DNA methylation levels of BDNF promoter IV in blood. Methylation was quantified by pyrosequencing and expressed as mean percent methylation representing the averaged value of cases (HD Gene+) or control subjects (NC) for each of individual CpG. Data represents mean value ± SEM. *$p < 0.05$ as per two-tailed Student's *t*-test.

We next tested whether methylation status at these four sites were correlated with BDNF levels in plasma or saliva. For subjects providing whole blood for the DNA methylation analysis, we were able to match subsets to plasma and saliva data ($n = 20$ and $n = 16$ for plasma and saliva, respectively), although these samples were not taken on the same day. We did not detect significant correlations between plasma BDNF and DNA methylation levels for any of the CpGs tested (Spearman r value range = −0.06 to 0.322; uncorrected p-value range = 0.12 to 0.99). In contrast, we observed a negative correlation between salivary BDNF levels and DNA methylation at site #444 (Spearman $r = -0.489$; $p = 0.049$) and #446 (Spearman $r = -0.298$; $p = 0.044$); although the p-values were no longer significant after a multiple test correction ($p = 0.176$ and $p = 0.196$ for site #444 and #446, respectively).

Correlations Between BDNF Promoter IV Methylation and Clinical Data

The analysis of the correlation between DNA methylation levels at the four CpG sites significantly altered in in HD patients with clinical symptoms and disease data showed interesting results. Methylation levels at CpG sites 444, 445, and 456 were inversely correlated to anxiety and depression (Spearman r = -0454 to -0483; $p < 0.05$), as determined by the HADS, a widely used measure of anxiety and depression in patients (**Table 5**). In contrast, methylation at CpG site 437, which was decreased in HD patients, was not correlated to the HADS score (**Table 5**), suggesting that the increases in methylation at CpG sites 444, 445, and 456 might be especially relevant. We did not detect significant correlations between methylation levels and motor or cognitive symptoms, including MMSE, the UHDRS and the TFC (**Table 5**).

Control subjects also were tested for depression symptoms using the HADS index and surprisingly, there was no significant difference between HADS score in HD patients vs. controls (20.8 ± 4.3 vs. 16.6 ± 2.8; $p = 0.43$; Student's t test; two-tailed; unpaired). Correlations between HADS scores and methylation at all 12 CpGs was assessed separately in control subjects and significant correlations were observed for methylation at CpG sites 436, 438, and 447, however, only the p-value for the correlation to site 436 survived multiple tests correction (Pearson $r = -0.671$; corrected p-value = 0.027; data not shown).

DISCUSSION

Multiple lines of evidence indicate that reduced BDNF expression plays a crucial role in HD pathogenesis (Zuccato et al., 2001, 2008; Gharami et al., 2008; Xie et al., 2010), suggesting that peripheral detection of BDNF levels and/or gene activity might represent a relevant biomarker for HD patients. Hence, in this study, we explored BDNF levels and markers of BDNF gene activity in peripheral fluids, including plasma, whole blood and saliva in patients. With respect to plasma, we did not detect significant changes in plasma BDNF across diagnostic groups. Our results are consistent with previous findings showing no change in plasma or serum levels of BDNF in patients with HD (Zuccato et al., 2011). Although other studies have reported decreased levels of BDNF transcripts in whole blood of HD

TABLE 5 | Correlations between BDNF promoter IV methylation and clinical measures in HD patients.

	Age	CAG	MMSE	MOTOR	TFC	HADS
Site 444						
Pearson *r*	−0.1823	0.2772	−0.2358	−0.1612	0.1574	−0.5179
95% confidence interval	−0.5693 to 0.2708	−0.1756 to 0.6332	−0.6059 to 0.2182	−0.5544 to 0.2908	−0.2944 to 0.5517	−0.7761 to −0.1109
P value (two-tailed)	0.4289	0.2239	0.3034	0.4852	0.4955	0.0162
P value summary	ns	ns	ns	ns	ns	*
Site 445						
Pearson *r*	−0.1862	0.141	−0.1579	−0.179	0.1387	−0.533
95% confidence interval	−0.5720 to 0.2670	−0.3096 to 0.5399	−0.5520 to 0.2939	−0.5670 to 0.2739	−0.3117 to 0.5383	−0.7843 to −0.1315
P value (two-tailed)	0.419	0.5421	0.4942	0.4374	0.5487	0.0128
P value summary	ns	ns	ns	ns	ns	*
Site 446						
Pearson *r*	−0.09932	0.2046	−0.2974	−0.1395	0.1238	−0.5048
95% confidence interval	−0.5093 to 0.3474	−0.2492 to 0.5847	−0.6462 to 0.1542	−0.5388 to 0.3110	−0.3253 to 0.5274	−0.7690 to −0.09335
P value (two-tailed)	0.6684	0.3737	0.1905	0.5465	0.5928	0.0196
P value summary	ns	ns	ns	ns	ns	*
Site 437						
Pearson *r*	−0.2749	0.1826	−0.07029	−0.2762	0.1962	0.2656
95% confidence interval	−0.6317 to 0.1780	−0.2705 to 0.5695	−0.4873 to 0.3728	−0.6325 to 0.1766	−0.2574 to 0.5789	−0.2006 to 0.6337
P value (two-tailed)	0.2279	0.4283	0.7621	0.2255	0.394	0.2578
P value summary	ns	ns	ns	ns	ns	ns

*MMSE, Mini-Mental State Examination; the Unified Huntington's Disease Rating Scale Motor component (Motor); TFC, Total Functional Capacity; p-values shown are corrected for multiple comparisons. *$p < 0.05$.*

patients (Krzyszton-Russjan et al., 2013), and increased levels of BDNF protein in platelets from HD patients (Betti et al., 2018). Given the heterogeneous cell types found in whole blood, it is possible that BDNF levels could be altered in a cell-specific manner, which might explain these discrepancies. Other studies have shown that BDNF levels in plasma are different between females and males (Lommatzsch et al., 2005); however, we did not find significant sex differences in plasma BDNF in our cohort, regardless of disease status. We did detect significant positive correlations between both plasma and salivary BDNF and age, which is in contrast to previous studies in the literature that have found either no effect (Jiang et al., 2019) or modest decreased levels of BDNF with age in blood (Lommatzsch et al., 2005; Ziegenhorn et al., 2007). Importantly, however, we did not find that age was a significant covariate in analyzing the differences in BDNF levels between HD patients and controls.

In addition to plasma, we measured BDNF in saliva, which has been gaining recent attention as an alternative peripheral biofluid for biomarker studies (Kaufman and Lamster, 2002). Saliva has several advantages over blood, including its non-invasive nature, less sample processing and the ability to carry out sample collection in any setting, including at home. Here, we report a significant decrease of salivary BDNF in premanifest HD patients compared to control subjects, suggesting its potential application as an early marker of disease in pre-symptomatic mutation carriers. However, we did not detect any significant correlations between salivary or plasma BDNF levels with any clinical measure, including MMSE, TFC, HADS, or motor symptom scores.

We did not observe significant correlations between plasma and salivary BDNF levels, suggesting that salivary BDNF is not coming from the blood via known routes including transcellular transport, passive intracellular diffusion or active transport. BDNF in saliva could arise from expression in white blood cells, which are known to be present in saliva. Support for this idea comes from the fact that we did observe a significant negative correlation between salivary BDNF levels and whole blood DNA methylation at the *BDNF* promoter IV, although the *p*-value for this association did not survive multiple test correction, and white blood cells make up the majority of nucleated cells in whole blood. It is known that promoter methylation can directly regulate transcription (Razin and Cedar, 1991), hence, this correlation might provide a relevant basis for BDNF investigations in saliva. Additional studies using a larger cohort providing matched whole blood and saliva samples will be important to validate this finding. A further possibility is that BDNF is released into the saliva by the nerves innervating the salivary glands. This later possibility suggests that salivary BDNF may represent a better surrogate for brain tissue than plasma; a notion supported by previous observations of reduced BDNF protein levels in the brain of HD mouse models and human HD patients (Ferrer et al., 2000; Zuccato et al., 2001; Duan et al., 2003; Zhang et al., 2003; Corey-Bloom et al., 2017). Future studies should address the source of salivary BDNF, not only to understand fundamental mechanisms involved in the transportation of this protein, but also to better define the use of BDNF as a reliable disease biomarker for HD. Additionally, given that restoring BDNF levels may have therapeutic effects in HD (Zuccato et al., 2001; Gharami et al., 2008; Xie et al., 2010), BDNF measures might also represent a biomarker for monitoring novel therapeutics.

Studies have investigated DNA methylation alterations of the *BDNF* promoter, mainly forms I and IV, to serve as an epigenetic biomarker of disease states in association with neurodegenerative and neuropsychiatric pathology. In particular, changes in DNA methylation at BDNF promoters I and IV have been detected in Alzheimer's disease (AD) (Rao et al., 2012; Xie et al., 2017), major depression (Januar et al., 2015; Kang et al., 2015), and schizophrenia (Ikegame et al., 2013), but such changes have not yet been explored in HD. Here, we report changes in DNA methylation at four CpG sites at promoter IV of the *BDNF* gene in HD patients compared to normal controls, with three site showing increased methylation and one site decreased in methylation. Interestingly, the three CpGs that showed increased methylation in HD cases are in close proximity, suggesting these sites may represent a functional unit that modulates BDNF transcription (Lovkvist et al., 2016).

Although chorea, consisting of involuntary and abnormal movements, is the most characteristic symptom of HD, this disease is also associated with cognitive and psychiatric manifestations that have a major impact on patients and family caregivers. Psychiatric symptoms including anxiety, social withdrawal, depression and impulsivity can often be present early in the disease and can significantly contribute to the overall disability (Sturrock and Leavitt, 2010). Notably, while BDNF promoter methylation was not correlated to motor and cognitive clinical symptoms, methylation at the three sites that showed increased levels in HD patients, was inversely correlated to HADS scores, which is a widely used self-report instrument for measuring anxiety and depression in somatically ill patients (Zigmond and Snaith, 1983; Brennan et al., 2010). This finding is highly relevant in light of previous studies showing associations between BDNF promoter methylation in psychiatric disorders, including schizophrenia and depression, as mentioned above, with one study specifically suggesting that BDNF promoter methylation could be used as a biomarker of depression (Januar et al., 2015). Although increased methylation at promoters usually represses transcription, BDNF is encoded by a highly complex gene harboring six promoters; hence it is likely that promoter regulation is complex and could involve other epigenetic regulators, such as histone modifications. Indeed, reduced levels of H3K4me3 and arginine methylation of H2A/H4R3 (mediated by PRMT5) at the BNDF promoter II have been reported in HD brains (Vashishtha et al., 2013; Ratovitski et al., 2015). Here again, although PRMT5-induced H4R2methylation is associated with gene silencing; chromatin immunoprecipitation experiments showed that this modification is also present in active genes; thus, PRMT5 may act as a positive regulator of BDNF as well; further illustrating the complexity of BDNF epigenetic regulation (Chen and Chen, 2017). Further studies are needed to unravel the epigenetic regulation of BDNF expression and may reveal a more intricate interplay between DNA methylation and salivary BDNF in association with depression symptoms.

DNA methylation is highly associated with aging, and the methylation status at particular genomic sites can be used as an epigenetic clock of aging. Methylation patterns are also distinctive in females and males; not only at the X and Y chromosomes but across autosomal chromosomes as well (Nishioka et al., 2012; Chan and Ye, 2017; Ihara et al., 2018). We tested for association of methylation at BDNF promoter IV with age and sex of the study participants. We did not find a significant correlation between DNA methylation and age, regardless of diagnosis. Although previous studies have reported sex differences in BDNF methylation potentially mediated by estrogen signaling (Chan and Ye, 2017), we did not observe significant differences in methylation between females and males, however, we did see trends toward increased levels methylation at certain loci in female controls. We cannot rule that the lack of association between age/sex and BDNF methylation at the promoter IV in our study is due to the small cohort size analyzed.

A limitation of our study is the use of DNA isolated from whole blood to quantify methylation. DNA methylation profiles are cell specific, therefore detection in blood may be confounded by the heterogeneous composition of the sample. Nonetheless, the mean methylation values we observed in our study, although small, are in good agreement with data reported for the same CpG sites in previous studies (Ikegame et al., 2013).

In summary, our findings demonstrate that salivary BDNF protein is lower in both PM and HD patients compared to controls. Within the PM group, we show that BDNF levels are significantly lower in those patients within 10 years to their predicted age to onset, suggesting the possibility that salivary BDNF could represent an early, non-invasive biomarker of disease onset. The increase in *BDNF* promoter methylation observed in the blood of HD patients and the correlation to psychiatric symptoms in HD may also be relevant for future biomarker utility.

DATA AVAILABILITY STATEMENT

The raw data supporting the conclusions of this manuscript will be made available by the authors, without undue reservation, to any qualified researcher.

ETHICS STATEMENT

The studies involving human participants were reviewed and approved by the University of California, San Diego, Institutional Review Board. The patients/participants provided their written informed consent to participate in this study.

AUTHOR CONTRIBUTIONS

AG performed the experimental work, analyzed the data, and contributed to manuscript writing. JC-B provided blood and saliva samples, performed clinical evaluation of participants, and contributed to experimental design and manuscript preparation. ET performed the experimental work, analyzed the data, and contributed to experimental design and manuscript preparation. PD designed the methylation analysis, performed the data analysis, and contributed to overall experimental design and manuscript preparation.

FUNDING

This work was partially supported by grants from the National Institutes of Health # NS111655 to ET and # NS104013 to PD.

ACKNOWLEDGMENTS

We want to thank participants and their families for their invaluable collaboration. We also thank Ameera Samaher Haque and Aeri Kim for excellent assistance on obtaining samples and compiling clinical and demographic information used in the analysis.

SUPPLEMENTARY MATERIAL

The Supplementary Material for this article can be found online at: https://www.frontiersin.org/articles/10.3389/fnmol.2019.00335/full#supplementary-material

REFERENCES

Betti, L., Palego, L., Unti, E., Mazzucchi, S., Kiferle, L., Palermo, G., et al. (2018). Brain-derived neurotrophic factor (BDNF) and serotonin transporter (SERT) in platelets of patients with mild Huntington's Disease: relationships with social cognition symptoms. *Arch. Ital. Biol.* 156, 27–39. doi: 10.12871/00039829201813

Brennan, C., Worrall-Davies, A., McMillan, D., Gilbody, S., and House, A. (2010). The hospital anxiety and depression scale: a diagnostic meta-analysis of case-finding ability. *J. Psychosom. Res.* 69, 371–378. doi: 10.1016/j.jpsychores.2010.04.006

Canals, J. M., Pineda, J. R., Torres-Peraza, J. F., Bosch, M., Martín-Ibañez, R., Muñoz, M. T., et al. (2004). Brain-derived neurotrophic factor regulates the onset and severity of motor dysfunction associated with enkephalinergic neuronal degeneration in Huntington's disease. *J. Neurosci.* 24, 7727–7739. doi: 10.1523/jneurosci.1197-04.2004

Chan, C. B., and Ye, K. (2017). Sex differences in brain-derived neurotrophic factor signaling and functions. *J. Neurosci. Res.* 95, 328–335. doi: 10.1002/jnr.23863

Chen, K. W., and Chen, L. (2017). Epigenetic regulation of BDNF gene during development and Diseases. *Int. J. Mol. Sci.* 18:E571. doi: 10.3390/ijms18030571

Corey-Bloom, J., Aikin, A. M., Gutierrez, A. M., Nadhem, J. S., Howell, T. L., Thomas, E. A., et al. (2017). Beneficial effects of glatiramer acetate in Huntington's disease mouse models: evidence for BDNF-elevating and immunomodulatory mechanisms. *Brain Res.* 1673, 102–110. doi: 10.1016/j.brainres.2017.08.013

Duan, W., Guo, Z., Jiang, H., Ware, M., Li, X. J., Mattson, M. P., et al. (2003). Dietary restriction normalizes glucose metabolism and BDNF levels, slows disease progression, and increases survival in huntingtin mutant mice. *Proc. Natl. Acad. Sci. U.S.A.* 100, 2911–2916. doi: 10.1073/pnas.0536856100

Evans, R. W. (1998). Complications of lumbar puncture. *Neurol. Clin.* 16, 83–105. doi: 10.1016/s0733-8619(05)70368-6

Ferrer, I., Goutan, E., Marín, C., Rey, M. J., and Ribalta, T. (2000). Brain-derived neurotrophic factor in Huntington disease. *Brain Res.* 866, 257–261. doi: 10.1016/s0006-8993(00)02237-x

Gharami, K., Xie, Y., An, J. J., Tonegawa, S., and Xu, B. (2008). Brain-derived neurotrophic factor over-expression in the forebrain ameliorates Huntington's disease phenotypes in mice. *J. Neurochem.* 105, 369–379. doi: 10.1111/j.1471-4159.2007.05137.x

Gluhm, S., Goldstein, J., Brown, D., Van Liew, C., Gilbert, P. E., Corey-Bloom, J., et al. (2013). Usefulness of the montreal cognitive assessment (MoCA) in Huntington's disease. *Mov. Disord.* 28, 1744–1747. doi: 10.1002/mds.25578

Granger, D. A., Fortunato, C. K., Beltzer, E. K., Virag, M., Bright, M. A., Out, D., et al. (2012). Focus on methodology: salivary bioscience and research on adolescence: an integrated perspective. *J. Adolesc.* 35, 1081–1095. doi: 10.1016/j.adolescence.2012.01.005

Greenberg, M. E., Xu, B., Lu, B., and Hempstead, B. L. (2009). New insights in the biology of BDNF synthesis and release: implications in CNS function. *J. Neurosci.* 29, 12764–12767. doi: 10.1523/JNEUROSCI.3566-09.2009

Ho, L. W., Carmichael, J., Swartz, J., Wyttenbach, A., Rankin, J., Rubinsztein, D. C., et al. (2001). The molecular biology of Huntington's disease. *Psychol. Med.* 31, 3–14. doi: 10.1016/b978-0-12-801893-4.00001-8

Hohlfeld, R., Kerschensteiner, M., Stadelmann, C., Lassmann, H., and Wekerle, H. (2006). The neuroprotective effect of inflammation: implications for the therapy of multiple sclerosis. *Neurol. Sci.* 27(Suppl. 1), S1–S7.

Ihara, K., Fuchikami, M., Hashizume, M., Okada, S., Kawai, H., Obuchi, S., et al. (2018). The influence of aging on the methylation status of brain-derived neurotrophic factor gene in blood. *Int. J. Geriatr. Psychiatry* 33, 1312–1318. doi: 10.1002/gps.4927

Ikegame, T., Bundo, M., Sunaga, F., Asai, T., Nishimura, F., Yoshikawa, A., et al. (2013). DNA methylation analysis of BDNF gene promoters in peripheral blood cells of schizophrenia patients. *Neurosci. Res.* 77, 208–214. doi: 10.1016/j.neures.2013.08.004

Januar, V., Ancelin, M. L., Ritchie, K., Saffery, R., and Ryan, J. (2015). BDNF promoter methylation and genetic variation in late-life depression. *Transl. Psychiatry* 5:e619. doi: 10.1038/tp.2015.114

Jiang, L., Zhang, H., Wang, C., Ming, F., Shi, X., Yang, M., et al. (2019). Serum level of brain-derived neurotrophic factor in Parkinson's disease: a meta-analysis. *Prog. Neuropsychopharmacol. Biol. Psychiatry.* 88, 168–174. doi: 10.1016/j.pnpbp.2018.07.010

Kang, H. J., Kim, J. M., Bae, K. Y., Kim, S. W., Shin, I. S., Kim, H. R., et al. (2015). Longitudinal associations between BDNF promoter methylation and late-life depression. *Neurobiol. Aging* 36, 1764.e1–1764.e7. doi: 10.1016/j.neurobiolaging.2014.12.035

Kaufman, E., and Lamster, I. B. (2002). The diagnostic applications of saliva - A review. *Critical Rev. Oral Biol. Med.* 13, 197–212. doi: 10.1177/154411130201300209

Krzyszton-Russjan, J., Zielonka, D., Jackiewicz, J., Kuśmirek, S., and Bubko, I. (2013). A study of molecular changes relating to energy metabolism and cellular stress in people with Huntington's disease: looking for biomarkers. *J Bioenerg. Biomembr.* 45, 71–85. doi: 10.1007/s10863-012-9479-3

Langbehn, D. R., Hayden, M. R., and Paulsen, J. S. (2010). CAG-repeat length and the age of onset in Huntington disease (HD): a review and validation study of statistical approaches. *Am. J. Med. Genet B Neuropsychiatr. Genet.* 153b, 397–408. doi: 10.1002/ajmg.b.30992

Lanska, D. J. (2000). George Huntington (1850-1916) and hereditary chorea. *J. Hist. Neurosci.* 9, 76–89. doi: 10.1076/0964-704x(200004)9:1;1-2;ft076

Lommatzsch, M., Zingler, D., Schuhbaeck, K., Schloetcke, K., Zingler, C., Schuff-Werner, P., et al. (2005). The impact of age, weight and gender on BDNF levels in human platelets and plasma. *Neurobiol. Aging* 26, 115–123. doi: 10.1016/j.neurobiolaging.2004.03.002

Lovkvist, C., Dodd, I. B., Sneppen, K., and Haerter, J. O. (2016). DNA methylation in human epigenomes depends on local topology of CpG sites. *Nucleic Acids Res.* 44, 5123–5132. doi: 10.1093/nar/gkw124

Lu, B. (2003). BDNF and activity-dependent synaptic modulation. *Learn. Mem.* 10, 86–98. doi: 10.1101/lm.54603

Ma, B., Savas, J. N., Chao, M. V., and Tanese, N. (2012). Quantitative analysis of BDNF/TrkB protein and mRNA in cortical and striatal neurons using alpha-tubulin as a normalization factor. *Cytometry A* 81, 704–717. doi: 10.1002/cyto.a.22073

Mandel, A. L., Ozdener, H., and Utermohlen, V. (2011). Brain-derived neurotrophic factor in human saliva: ELISA optimization and biological correlates. *J. Immunoassay Immunochem.* 32, 18–30. doi: 10.1080/15321819.2011.538625

Nishioka, M., Bundo, M., Kasai, K., and Iwamoto, K. (2012). DNA methylation in schizophrenia: progress and challenges of epigenetic studies. *Genome Med.* 4:96. doi: 10.1186/gm397

Pan, W., Banks, W. A., Fasold, M. B., Bluth, J., and Kastin, A. J. (1998). Transport of brain-derived neurotrophic factor across the blood-brain

barrier. *Neuropharmacology* 37, 1553–1561. doi: 10.1016/s0028-3908(98)00141-5

Radka, S. F., Holst, P. A., Fritsche, M., and Altar, C. A. (1996). Presence of brain-derived neurotrophic factor in brain and human and rat but not mouse serum detected by a sensitive and specific immunoassay. *Brain Res.* 709, 122–301.

Rao, J. S., Keleshian, V. L., Klein, S., and Rapoport, S. I. (2012). Epigenetic modifications in frontal cortex from Alzheimer's disease and bipolar disorder patients. *Transl. Psychiatry* 2:e132. doi: 10.1038/tp.2012.55

Ratovitski, T., Arbez, N., Stewart, J. C., Chighladze, E., and Ross, C. A. (2015). PRMT5- mediated symmetric arginine dimethylation is attenuated by mutant huntingtin and is impaired in Huntington's disease (HD). *Cell Cycle* 14, 1716–1729. doi: 10.1080/15384101.2015.1033595

Razin, A., and Cedar, H. (1991). DNA methylation and gene expression. *Microbiol. Rev.* 55, 451–458.

Ross, C. A., Aylward, E. H., Wild, E. J., Langbehn, D. R., Long, J. D., Warner, J. H., et al. (2014). Huntington disease: natural history, biomarkers and prospects for therapeutics. *Nat. Rev. Neurol.* 10, 204–216. doi: 10.1038/nrneurol.2014.24

Sturrock, A., and Leavitt, B. R. (2010). The clinical and genetic features of Huntington disease. *J. Geriatr. Psychiatry Neurol.* 23, 243–259. doi: 10.1177/0891988710383573

The Huntington's Disease Collaborative Research Group (1993). A novel gene containing a trinucleotide repeat that is expanded and unstable on Huntington's disease chromosomes. The Huntington's Disease Collaborative Research Group. *Cell* 72, 971–983. doi: 10.1016/0092-8674(93)90585-e

Vashishtha, M., Ng, C. W., Yildirim, F., Gipson, T. A., Kratter, I. H., Bodai, L., et al. (2013). Targeting H3K4 trimethylation in Huntington disease. *Proc. Natl. Acad. Sci. U.S.A.* 110, E3027–E3036. doi: 10.1073/pnas.1311323110

Xie, B., Xu, Y., Liu, Z., Liu, W., Jiang, L., Zhang, R., et al. (2017). Elevation of peripheral BDNF promoter methylation predicts conversion from amnestic mild cognitive impairment to Alzheimer's disease: a 5-Year longitudinal study. *J. Alzheimers Dis.* 56, 391–401. doi: 10.3233/JAD-160954

Xie, Y., Hayden, M. R., and Xu, B. (2010). BDNF overexpression in the forebrain rescues Huntington's disease phenotypes in YAC128 mice. *J. Neurosci.* 30, 14708–14718. doi: 10.1523/JNEUROSCI.1637-10.2010

Yamamoto, H., and Gurney, M. E. (1990). Human platelets contain brain-derived neurotrophic factor. *J. Neurosci,.* 10, 3469–3478. doi: 10.1523/jneurosci.10-11-03469.1990

Zhang, Y., Li, M., Drozda, M., Chen, M., Ren, S., Mejia Sanchez, R. O., et al. (2003). Depletion of wild-type huntingtin in mouse models of neurologic diseases. *J. Neurochem.* 87, 101–106. doi: 10.1046/j.1471-4159.2003.01980.x

Ziegenhorn, A. A., Schulte-Herbrüggen, O., Danker-Hopfe, H., Malbranc, M., Hartung, H. D., Anders, D., et al. (2007). Serum neurotrophins–a study on the time course and influencing factors in a large old age sample. *Neurobiol. Aging.* 28, 1436–1445. doi: 10.1016/j.neurobiolaging.2006.06.011

Zigmond, A. S., and Snaith, R. P. (1983). The hospital anxiety and depression scale. *Acta Psychiatr. Scand* 67, 361–370.

Zuccato, C., Ciammola, A., Rigamonti, D., Leavitt, B. R., Goffredo, D., Conti, L., et al. (2001). Loss of huntingtin-mediated BDNF gene transcription in Huntington's disease. *Science* 293, 493–498. doi: 10.1126/science.1059581

Zuccato, C., Marullo, M., Conforti, P., MacDonald, M. E., Tartari, M., Cattaneo, E., et al. (2008). Systematic assessment of BDNF and its receptor levels in human cortices affected by Huntington's disease. *Brain Pathol.* 18, 225–238. doi: 10.1111/j.1750-3639.2007.00111.x

Zuccato, C., Marullo, M., Vitali, B., Tarditi, A., Mariotti, C., Valenza, M., et al. (2011). Brain-derived neurotrophic factor in patients with Huntington's disease. *PLoS One.* 6:e22966. doi: 10.1371/journal.pone.0022966

Conflict of Interest: The authors declare that the research was conducted in the absence of any commercial or financial relationships that could be construed as a potential conflict of interest.

frontiers in Molecular Neuroscience

REVIEW
published: 29 May 2020
doi: 10.3389/fnmol.2020.00078

Dysregulation of RNA-Binding Proteins in Amyotrophic Lateral Sclerosis

Yuan Chao Xue[1,2], *Chen Seng Ng*[1,2], *Pinhao Xiang*[1,2], *Huitao Liu*[1,3], *Kevin Zhang*[1,2], *Yasir Mohamud*[1,2] *and Honglin Luo*[1,2]*

[1]Centre for Heart and Lung Innovation, St. Paul's Hospital, Vancouver, BC, Canada, [2]Department of Pathology and Laboratory Medicine, University of British Columbia, Vancouver, BC, Canada, [3]Department of Experimental Medicine, University of British Columbia, Vancouver, BC, Canada

Genetic analyses of patients with amyotrophic lateral sclerosis (ALS) have revealed a strong association between mutations in genes encoding many RNA-binding proteins (RBPs), including *TARDBP*, *FUS*, *hnRNPA1*, *hnRNPA2B1*, *MATR3*, *ATXN2*, *TAF15*, *TIA-1*, and *EWSR1*, and disease onset/progression. RBPs are a group of evolutionally conserved proteins that participate in multiple steps of RNA metabolism, including splicing, polyadenylation, mRNA stability, localization, and translation. Dysregulation of RBPs, as a consequence of gene mutations, impaired nucleocytoplasmic trafficking, posttranslational modification (PTM), aggregation, and sequestration by abnormal RNA foci, has been shown to be involved in neurodegeneration and the development of ALS. While the exact mechanism by which dysregulated RBPs contribute to ALS remains elusive, emerging evidence supports the notion that both a loss of function and/or a gain of toxic function of these ALS-linked RBPs play a significant role in disease pathogenesis through facilitating abnormal protein interaction, causing aberrant RNA metabolism, and by disturbing ribonucleoprotein granule dynamics and phase transition. In this review article, we summarize the current knowledge on the molecular mechanism by which RBPs are dysregulated and the influence of defective RBPs on cellular homeostasis during the development of ALS. The strategies of ongoing clinical trials targeting RBPs and/or relevant processes are also discussed in the present review.

Keywords: aggregation, gene mutations, nucleocytoplasmic transport, RNA-binding proteins, RNA metabolism

OPEN ACCESS

Edited by:
Mauro Cozzolino, Institute of Traslational Pharmacology (CNR), Italy

Reviewed by:
Riccardo Cristofani, University of Milan, Italy
Marcello Ceci, University of Tuscia, Italy
Epaminondas Doxakis, Biomedical Research Foundation of the Academy of Athens (BRFAA), Greece

***Correspondence:**
Honglin Luo
honglin.luo@hli.ubc.ca

Received: *06 March 2020*
Accepted: *22 April 2020*
Published: *29 May 2020*

Citation:
Xue YC, Ng CS, Xiang P, Liu H, Zhang K, Mohamud Y and Luo H (2020) Dysregulation of RNA-Binding Proteins in Amyotrophic Lateral Sclerosis. Front. Mol. Neurosci. 13:78. doi: 10.3389/fnmol.2020.00078

INTRODUCTION

Amyotrophic lateral sclerosis (ALS), a devastating neurodegenerative disease that primarily targets motor neurons, is categorized into two forms, familial (genetically inherited) and sporadic (without apparent family history). Familiar ALS (fALS) is responsible for ∼5% to 10% of all ALS cases, whereas sporadic ALS (sALS) is the major form of the disease accounting for 90% to 95% of all cases (Brown and Al-Chalabi, 2017; van Es et al., 2017). Since the first identification of *SOD1* as a causative gene for ALS, the list of genetic mutations associated with ALS has grown rapidly. Up to date, more than 30 genes have been recognized as potential causal drivers for ALS (Al-Chalabi et al., 2017). Among them, many encode RNA-binding proteins (RBPs), such as transactivation response DNA-binding protein 43 (TDP-43) and fused in sarcoma/translocated in sarcoma (FUS/TLS).

As key regulators of RNA metabolism, RBPs play a vital role in maintaining the normal function of neuronal systems (Nussbacher et al., 2019). Under physiological conditions, these ALS-linked RBPs are involved in almost all aspects of RNA metabolism, including transcription, alternate splicing, mRNA transport, and stability. Although the exact functions and mechanisms of action of these RBPs are still largely unclear, current evidence suggests a central role for RBPs in the maintenance of neuronal integrity. Defects in RBPs have emerged as a significant contributing factor to the pathogenesis of ALS (Nussbacher et al., 2019). More notably, cytoplasmic mislocalization, aggregation, and fragmentation of RBPs, in particular TDP-43 (termed TDP-43 proteinopathies), have been regarded as a pathological hallmark of ALS or frontotemporal dementia (FTD, a disease sharing many genetic and pathological features with ALS; Neumann et al., 2006; Mackenzie et al., 2010). In this review article, we summarize the current understanding of how RBPs are dysregulated and the role of disrupted RBPs in ALS development. We also highlight the emerging therapeutic intervention by targeting these ALS-implicated RBPs.

MECHANISMS LEADING TO DYSREGULATION OF RBPs IN ALS

As alluded to above, mutations in genes encoding many RBPs are highly associated with ALS. In addition, dysregulation of RBPs as a result of compromised nucleocytoplasmic trafficking, posttranslational modification (PTM), aggregation, and sequestration by abnormal RNAs also contributes significantly to disease pathogenesis. This section will briefly discuss these underlying mechanisms resulting in RBP dysregulation in ALS.

Gene Mutations

Genetic analyses of ALS patients have identified more than 100 ALS-related gene variants, including many genes encoding RBPs, such as TDP-43, FUS, heterogeneous nuclear ribonucleoproteins (hnRNP) A1, hnRNPA2/B1, matrin 3 (MATR3), ataxin 2 (ATXN2), TATA-box binding protein–associated factor 15 (TAF15), T-cell–restricted intracellular antigen 1 (TIA-1), and Ewing sarcoma breakpoint region 1 (EWSR1; Al-Chalabi et al., 2017; Nguyen et al., 2018). As shown in **Figure 1**, these RBPs share some common structural domains. For example, TDP-43, hnRNPA1, hnRNPA2/B1, and TIA-1 all contain the RNA recognition motif (RRM) and the glycine (Gly)-rich prion-like domain. FUS, TAF15, and EWSR1, belonging to the thyrotroph embryonic factor (TEF) family of RBPs, share the N-terminal Gly-rich and glutamine-glycine-serine-tyrosine (QGSY)–rich prion-like domains, the RRM and zinc finger domains that facilitate RNA and DNA interactions, and the C-terminal arginine-glycine-glycine (RGG) domains that stabilize RNA and protein bindings. MATR3 harbors two RRM and two zinc-finger domains. The structure of ATXN2 is relatively unique, containing the N-terminal polyglutamine (polyQ) repeats, the like-Sm protein (LsM) and Lsm-associated domains (LsmAD) that promote RNA bindings, and the poly(A)-binding protein-interacting motif (PAMs). Except for gene mutations in *ATXN2* and *MATR3*, ALS-relevant genetic mutations in RBPs commonly occur in Gly-rich, QGSY-rich, and RGG domains (Kapeli et al., 2017). These gene mutations could lead to loss of function and/or gain of toxic function (will discuss in detail later in this review), contributing to the development of the disease.

Posttranslational Modification

In addition to gene mutations, PTM also serves as an important mechanism for regulating protein structure and function. Aberrant PTM of RBPs is commonly observed in ALS. For example, TDP-43 is extensively posttranslationally modified, including phosphorylation, ubiquitination, acetylation, and sumoylation in both fALS and sALS (Buratti, 2018). Among them, phosphorylation of TDP-43 is the most common PTM of this protein and described as a marker of pathological ALS inclusions (Hasegawa et al., 2008). Several protein kinases have been identified to be responsible for its phosphorylation, including casein kinase (Nonaka et al., 2016), cycle 7-related protein kinase (Liachko et al., 2013), and tau tubulin kinase 1/2 (Liachko et al., 2014). Calcineurin was found to be a phosphatase that regulates TDP-43 phosphorylation (Liachko et al., 2016). Although the exact role of TDP-43 phosphorylation in disease progression remains incompletely understood, clinical data appear to support a function in neurodegeneration (Buratti, 2018).

Another key PTM associated with pathological TDP-43 is the generation of the C-terminal fragments (CTFs), which accumulate in the brains of patients with ALS or FTD and are considered a pathological feature of these diseases (Neumann et al., 2006). Several mechanisms have been proposed for their production, including proteolytic cleavage mediated by cellular proteases such as caspases and calpains, alternative splicing of the TDP-43 gene, and alternate in-frame translation (Buratti, 2018). The CTFs of TDP-43 mislocalize to the cytoplasm due to the removal of nuclear localization signal (NLS) and are prone to form aggregates as compared to the full-length TDP-43 because of the presence of Gly-rich prion-like domain. However, the relative contribution of these CTFs to disease progression remains controversial as transgenic animals expressing CTFs show only subtle motor or behavioral alterations, failing to fully recapitulate those observed in ALS or FTD patients (Berning and Walker, 2019). Methylation is another common type of PTM for RBPs. Methylation often occurs on R residues in RGG motifs of hnRNPs and TEF family of RBPs (i.e., FUS, TAF15, and EWSR1) through the action of protein arginine methyltransferases (Hofweber and Dormann, 2019). Methylation modification is a critical regulator for RBP liquid–liquid phase separation (LLPS) and dynamics of ribonucleoprotein (RNP) granules. Ribonucleoprotein granules, including stress granules (SGs) and processing bodies, are membrane-free, dense cytosolic aggregation of RBPs/RNA and common sites for mRNA storage/degradation (Buchan and Parker, 2009). Disrupted LLPS homeostasis and RNP granule dynamics have been implicated in neurodegeneration. Studies using *in vitro* systems found that R-methylation on ALS-related RBPs, such as hnRNPA2 and FUS, reduces LLPS *via* inhibiting R-aromatic interaction (Hofweber et al., 2018; Qamar et al., 2018; Ryan et al., 2018). In addition to methylation,

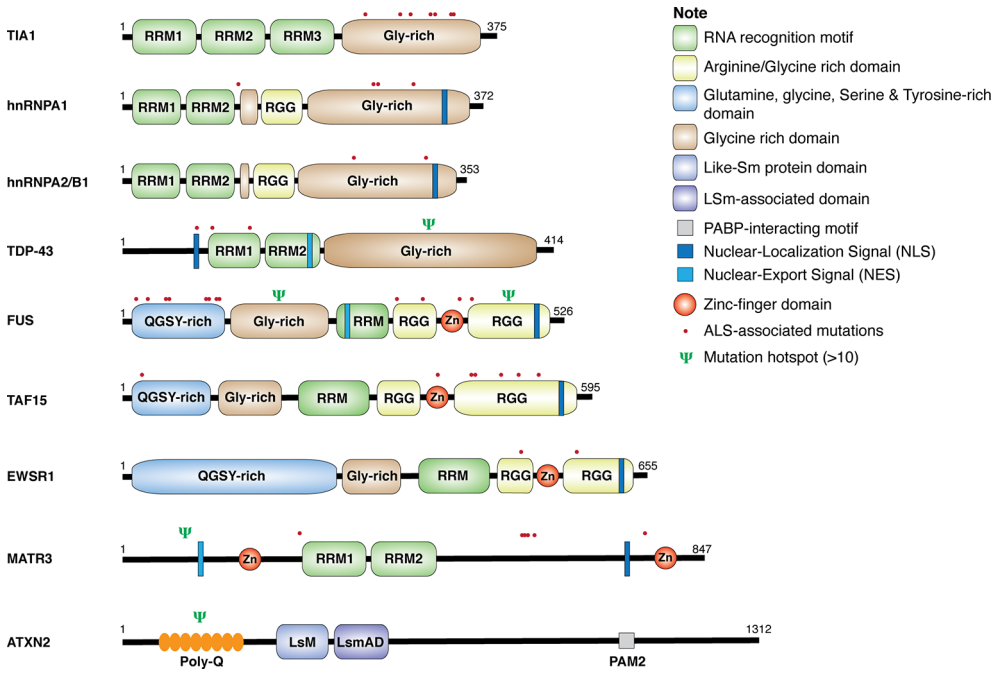

FIGURE 1 | Structure and mutations in RNA-binding proteins (RBPs). Schematic diagram for amyotrophic lateral sclerosis (ALS)-associated RBPs. The location of single point mutations for each RBP is indicated as red dot, and the psi symbol denotes the location of multiple mutations associated with ALS-related motor neuron diseases.

phosphorylation has also been shown to either enhance or suppress RBP phase separation and/or RNP granule dynamics (Hofweber and Dormann, 2019).

Disrupted Nucleocytoplasmic Trafficking

RBPs have predominant localizations within the nucleus to perform RNA processing and metabolism. However, many RBPs are abnormally aggregated in the cytoplasm in ALS. As mentioned above, the CTFs of TDP-43 are mainly found in the cytoplasmic aggregates due to the lack of the NLS. In addition, the presence of ALS-related missense mutations within NLS or PTM sites of these RBPs constitutes another mechanism responsible for their cytoplasmic accumulation (Kim and Taylor, 2017). However, gene mutations and fragmentations cannot explain all cases of the observed mislocalization of RBPs.

Emerging evidence proposes impaired nucleocytoplasmic trafficking as a key mechanism for RBP mislocalization in ALS. Although the precise mechanism remains elusive, studies suggest a role for the hexanucleotide repeat expansion mutation in chromosome 9 open reading frame 72 (*C9orf72*) gene, the most common genetic cause of ALS and FTD (DeJesus-Hernandez et al., 2011; Renton et al., 2011), in such effects. It was found that dipeptide repeats (DPRs) produced from the *C9ORF72* expansion mutant accumulate within the nuclear pore complex to disturb its integrity, leading to compromised nucleocytoplasmic transport (Freibaum et al., 2015; Jovicic et al., 2015; Zhang et al., 2015; Shi et al., 2017). Interestingly, a recent study reported that expression of C9ORF72-derived DPR poly-GA (glycine–alanine), but not poly-GR (glycine–proline) and poly-PR (proline–arginine), disturbs nucleocytoplasmic transport (Vanneste et al., 2019), suggesting a DPR-specific role in the regulation of nucleocytoplasmic trafficking. Further investigations revealed that many nucleocytoplasmic transport factors are recruited and sequestrated in the SGs upon stress or treatment with mutant proteins implicated in ALS (Zhang et al., 2018). Importantly, it was found that inhibition of SG formation attenuates the defects in nucleocytoplasmic trafficking and alleviates neurodegeneration in C9orf72-*ALS Drosophila* models (Zhang et al., 2018). Recent evidence has also identified a mechanism for the observed cytoplasmic mislocalization of wild-type FUS in ALS (Tyzack et al., 2019). It was found that FUS directly binds to the mRNA of splicing factor proline and glutamine rich (SFPQ). The authors proposed that translocation of SFPQ transcripts to the cytoplasm drives nuclear export of FUS (Tyzack et al., 2019).

Aggregation and Sequestration by Abnormal RNA Foci

Protein aggregation is a common event in neurodegenerative diseases, including ALS. Several mechanisms have been recognized to contribute to protein aggregation in ALS, including self-aggregation, altered RNP granule dynamics, sequestration by aberrant RNA foci, and defects in protein quality control system (Conlon and Manley, 2017; Morriss and Cooper, 2017).

Like RNP granules, protein aggregates are formed through LLPS of weak interaction among RBPs and/or RNAs (Hofweber and Dormann, 2019). Many RBPs contain intrinsically disordered low complexity domains (LCDs) that can lead to self-aggregation, especially when abnormally mislocalized, overexpressed, or posttranslationally modified. Interestingly, it was recently reported that factors involved in nuclear import also have a role in phase transition of RBPs (Guo et al., 2018). It was shown that expression of nuclear-import receptors inhibits and reverses aberrant phase separations of RBPs, including TDP-43, FUS, hnRNPA1, hnRNPA2, TAF-15, and EWSR, to restore RBP homeostasis and rescue neurodegeneration caused by ALS-related FUS and hnRNPA1 (Guo et al., 2018). In addition, RBPs can be recruited into RNP granules through interaction with other proteins within the granules. Alternatively, abnormal RNA foci may also lead to RBP aggregations. The GGGGCC repeat RNA of *C9ORF72* can fold into G-quadruplexes and/or form stable hairpin-like secondary structures. These RNA structures sequester ALS-associated RBPs, such as TDP-43, and promote protein aggregation. *In vivo* and *in vitro* models further demonstrate that enrichment of these abnormal RNA foci can induce misprocessing of RNA transcripts that are commonly regulated by many RBPs (Conlon and Manley, 2017; Morriss and Cooper, 2017). Finally, malfunction of the protein quality control system also has a role in the accumulation of RBP aggregates. Many ALS-related mutations in genes, such as *TBK1*, *p62*, *OPTN*, *VCP*, and *UBQLN2*, are involved in autophagy and ubiquitin-proteasome degradation (Al-Chalabi et al., 2017). As a consequence of gene mutations and increased proteasomal and lysosomal load due to an excess production of abnormal protein products, the function of the protein quality control system is impaired, resulting in the buildup of RBP aggregates (Cipolat Mis et al., 2016).

DISRUPTED CELLULAR HOMEOSTASIS CAUSED BY ALS-ASSOCIATED RBPs

Dysregulation of RBP influences various aspects of the RNA metabolism, resulting in diverse molecular phenotypes, such as disrupted transcription and RNA splicing, abnormal RNA transport, altered mRNA stability, and protein translation. Possible mechanisms involve the loss of function and/or toxic gain of function of these RBPs through aberrant protein interactions, aggregate formation, perturbation of RNP granule dynamics, and phase transition (**Figure 2**). The following sections will discuss the known/speculated disease mechanisms in genes, including *TARDBP*, *FUS*, *hnRNPA1*, *hnRNPA2/B1*, *TIA1*, *TAF15*, *MATR3*, and *EWSR1*.

TARDBP/TDP-43

TDP-43 is encoded by the *TARDBP* gene and belongs to the large family of hnRNPs (Kapeli et al., 2017). TDP-43 participates in multiple steps of RNA processing with its role in splicing being best characterized. For example, research has suggested a role for TDP-43 in cryptic splicing, which is impaired in ALS (Ling et al., 2015). The expression of TDP-43 can be autoregulated at the level of mRNA stability *via* a negative-feedback loop (Ayala et al., 2011). Under normal conditions, TDP-43 plays a vital role in maintaining the function of the central nervous system (CNS). For example, TDP-43 has been shown to regulate many mRNAs encoding proteins implicated in CNS development, survival, and synaptic transmission and neural plasticity (Polymenidou et al., 2011; Tollervey et al., 2011; Alami et al., 2014; Ling, 2018). Knockout of TDP-43 in mice is embryonic lethal, and conditional or partial loss of TDP-43 in neural cells results in progressive motor neuron degeneration and motor function impairment (Wu et al., 2012; Iguchi et al., 2013; Yang et al., 2014).

TARDBP was first identified as a causative gene for ALS in 2008 (Kabashi et al., 2008; Sreedharan et al., 2008; Van Deerlin et al., 2008). Since then, more than 50 mutations in *TDP-43* have been found in ALS patients, accounting for ∼5% of fALS and ∼1% of sALS (Taylor et al., 2016). These mutations are predominantly clustered in the Gly-rich domain, an LCD domain critical for protein aggregation and phase transition (Franzmann and Alberti, 2019). Transgenic animals expressing mutant TDP-43 were shown to develop ALS-like pathological and clinical features (Lutz, 2018). Although *TDP-43* mutations are rare, TDP-43 proteinopathies, characterized by cytoplasmic mislocalization, aggregation, and cleavage of TDP-43 accompanied by its nuclear clearance, are found in the affected regions of the CNS in up to 97% of all ALS cases, except for those fALS caused by *SOD1* or *FUS* mutations (Neumann et al., 2006; Mackenzie et al., 2010), suggesting a broader involvement for TDP-43 dysregulation in ALS. In addition to the CNS, mislocalization and aggregation of TDP-43 have also been observed in peripheral tissues, such as in the peripheral blood mononuclear cells, in both fALS (De Marco et al., 2017) and sALS (Arosio et al., 2020). The mechanisms for TDP-43 toxicity in ALS are proposed to be both a loss of function (nuclear depletion of TDP-43) and a gain of toxic function, supported by evidence that both knockout and overexpression of wild-type or mutant TDP-43 recapitulate disease phenotypes (Butti and Patten, 2018). Recent studies have established a mechanism by which aberrant RNA splicing caused by mutant TDP-43 or depletion of nuclear TDP-43 contributes to ALS through a loss of function and/or a gain of function (Deshaies et al., 2018; Fratta et al., 2018; Sivakumar et al., 2018). TDP-43 has also been implicated in the DNA damage response, and loss of nuclear TDP-43 causes defects in DNA repair associated with ALS (Mitra et al., 2019). Moreover, dysregulated or mislocalized TDP-43 has been shown to interfere with cellular translational process. For instance, it was discovered that ALS-linked cytoplasmic TDP-43 interacts with receptor for activated C kinase 1 (RACK1), a ribosomal scaffold protein, on polyribosomes, resulting in a global inhibition of protein synthesis (Russo et al., 2017). It was also shown that mutant TDP-43 (A315T) enhances direct binding and translation of several mRNAs, including *Dennd4a* and *Camta1* that are known to be involved in neurodegeneration (Neelagandan et al., 2019).

Fused in Sarcoma/Translocated in Sarcoma

Similar to TDP-43, FUS is a DNA/RBP and has primarily nuclear localization, but mislocalizes to the cytoplasm in response to

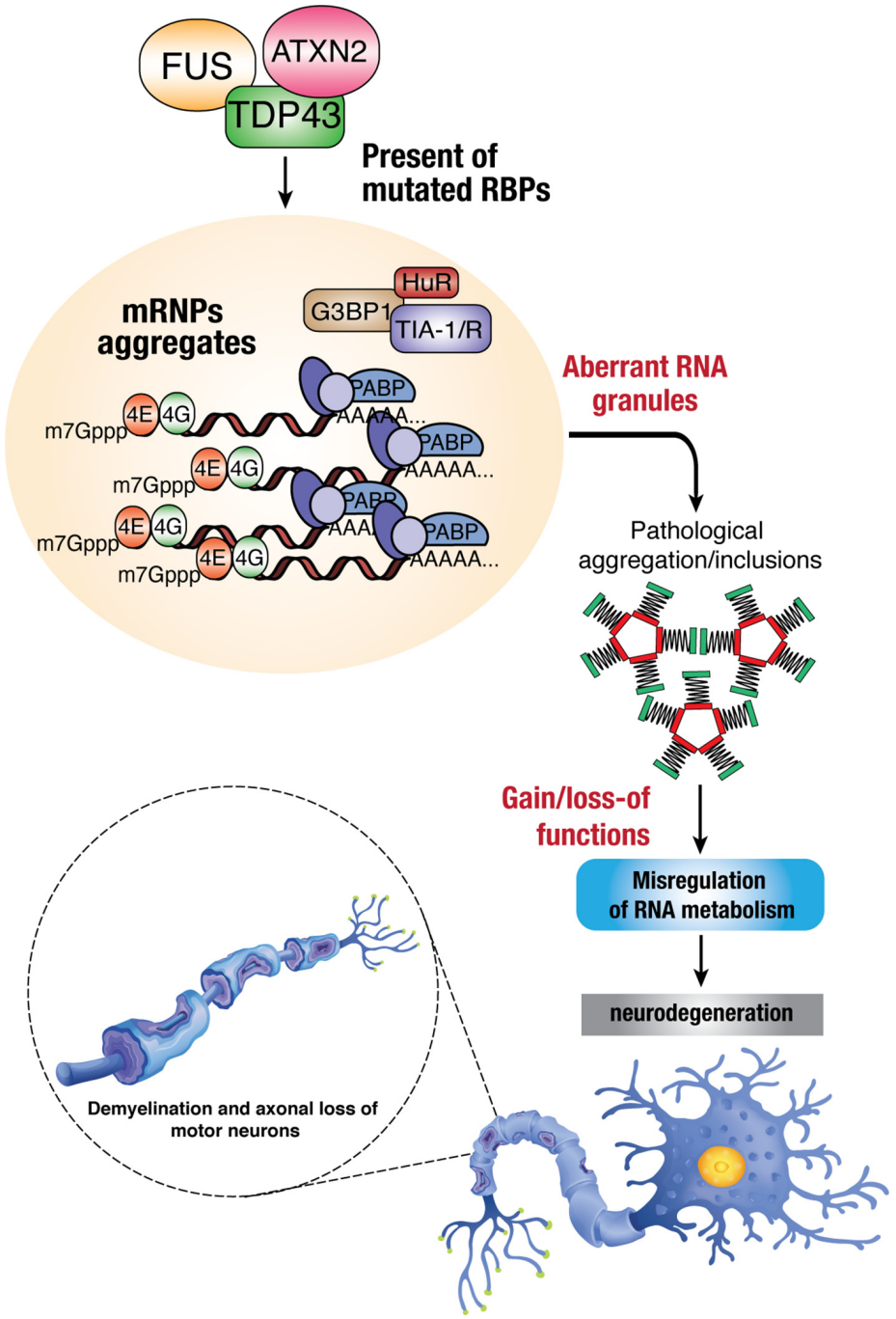

FIGURE 2 | Dysregulation of RBPs in ALS. Mutations in RBPs may result in mislocalization within the cells due to disruption in nucleocytoplasmic trafficking, which can lead to the formation of toxic protein aggregates within cytoplasmic inclusions. The accumulation of these aberrant RNA granules enhances the toxicity/pathological effects in mis-regulating normal RNA metabolism and thus leading to neurodegenerative phenotypes such as demyelination, axonal loss, and death of motor neurons.

stress (Kapeli et al., 2017). FUS also plays multiple functions in RNA metabolism by binding to the target RNAs through its RRM domain (Lagier-Tourenne et al., 2012). Mutations in FUS gene were identified as a genetic driver for ALS in 2009 (Kwiatkowski et al., 2009; Vance et al., 2009). Since then, more than 70 mutations were reported in ALS patients. The majority of these mutations are localized within the NLS, QGSY-rich and RGG1 domains, leading to altered cellular localization and increased aggregation tendency. *FUS* mutations are responsible for ∼5% of fALS and less than 1% of sALS cases (Taylor

et al., 2016). Unlike TDP-43 pathology that can be detected in almost all ALS cases (Mackenzie et al., 2007), cytoplasmic FUS inclusion/aggregation is uncommon and observed only in *FUS*-related fALS (Vance et al., 2009) and a very small subset of sALS (Deng et al., 2010). Thus, the contribution of FUS to ALS did not receive as much attention as that of TDP-43. However, a recent study found that cytoplasmic FUS in a diffused form is widely present in ALS, suggesting that it may have a broader role in ALS than previously recognized (Tyzack et al., 2019). This speculation warrants future investigations.

Unlike TDP-43, the function of FUS does not appear to be essential for embryonic development. Global or motor neuron–specific knockout of *FUS* gene in mice does not cause motor deficits (Sharma et al., 2016), whereas transgenic mice expressing wild-type or mutant *FUS* were shown to develop severe motor impairments and exhibit progressive neurological symptoms, suggesting a mechanism of toxic gain of function rather than loss of function in *FUS*-linked ALS pathogenesis (Qiu et al., 2014; Scekic-Zahirovic et al., 2017; López-Erauskin et al., 2018). Although the exact mechanisms of FUS toxicity are still unclear, recent studies began to unravel the involvement of defective RNA binding and splicing, disrupted protein translation, and impaired DNA damage response. ALS–associated mutant FUS has been shown to have altered RNA binding profiles (Hoell et al., 2011), related to the alteration of its subcellular localization (Dormann et al., 2010; Deshpande et al., 2019). Mutant FUS can also cause splicing defects in genes involved in dendritic growth and synaptic functions (Qiu et al., 2014). In addition, ALS-related mutant FUS was found to suppress protein translation at both global and local (axon regions) levels and disrupt the nonsense-mediated decay, both of which are associated with motor neuron pathogenesis seen in human (Kamelgarn et al., 2018; López-Erauskin et al., 2018). Moreover, defects in DNA damage repair were also proposed to be a mechanism underlying *FUS*-induced ALS pathogenesis. It was reported that DNA damage repair is impaired in human induced pluripotent stem cell (iPSC)—derived motor neurons that carry *FUS* mutations, leading to the formation of cytoplasmic aggregates and neurodegeneration (Naumann et al., 2018; Wang et al., 2018). Finally, a recent study revealed that activation of antiviral immune response is sufficient to induce the formation and persistency of cytoplasmic FUS-containing aggregates, contributing to onset and progression of FUS proteinopathy (Shelkovnikova et al., 2019).

hnRNPA1 and hnRNPA2/B1

hnRNPA1 and hnRNPA2/B1 are two essential RBPs in the family of hnRNPs. Like other RBPs, hnRNPA1 and hnRNPA2/B1 are typically nuclear localized but accumulate in the cytoplasm under stress conditions (Kapeli et al., 2017). hnRNPA1 and hnRNPA2/B1 share similar functions in the regulation of mRNA maturation, splicing, translation, and stability, but they play a differential role in transcriptional regulation (Kapeli et al., 2017). While knockout of *hnRNPA1* is embryonic lethal, and heterozygous mice display defects in muscle development (Liu et al., 2017), knockdown of hnRNPA2/B1 in mice globally disrupts alternative splicing and causes impaired cognitive function (Berson et al., 2012). Genetic analysis identified several ALS-related mutations in both *hnRNPA1* and *hnRNPA2/B1* (Kim et al., 2013; Couthouis et al., 2014; Liu et al., 2016; Naruse et al., 2018); however, the incidence is low (<1%; Taylor et al., 2016). Although the consequence of these mutations is largely unclear, some evidence suggests that mutations within the LCD could lead to increased cytoplasmic accumulation of hnRNPA1 through misfolding and fibrilization that stabilize the proteins (Kim et al., 2013; Gilpin et al., 2015; Molliex et al., 2015; Liu et al., 2016). It was also reported that altered *hnRNPA1* splicing induced by mutant or nuclear depletion of TDP-43 results in the production of an aggregation-prone mutant form of hnRNPA1, contributing to disease progression (Deshaies et al., 2018; Sivakumar et al., 2018). Furthermore, mutations of genes are expected to cause a disruption of protein synthesis as both hnRNPA1 and hnRNPA2/B1 have been implicated in protein translation (Kosturko et al., 2006; Cammas et al., 2007). Finally, iPSC-derived motor neurons expressing ALS-linked hnRNPA2/B1 mutant were shown to have a higher level of cell death and increased stress responses (Martinez et al., 2016).

Others RBPs, Including TIA-1, MATR3, ATXN2, TAF15, and EWSR1

TIA-1 is a critical component of SGs and has multiple functions in RNA metabolism, including mRNA splicing, translational repression, and mRNA silencing. TIA-1 is mainly localized to the nucleus; however, under cellular stress, it translocates to the cytoplasm, where it nucleates SGs and suppresses mRNA translation (Rayman and Kandel, 2017). A number of ALS-related missense mutations in *TIA-1* gene have been identified, all of which manifest in the Gly-rich domain (Mackenzie et al., 2017). Mutations of *TIA-1* gene were shown to alter LLPS and impair SG disassembly *in vitro* (Mackenzie et al., 2017). Nonetheless, because of their rare occurrence in patients, the causality between mutations in *TIA-1* and the pathogenesis of ALS is still debated (Baradaran-Heravi et al., 2018; van der Spek et al., 2018).

MATR3 is a DNA/RBP that interacts with TDP-43. Similar to other RBPs, MATR3 is involved in different steps of RNA processing, including gene transcription, alternative splicing, mRNA export, and stability (Malik et al., 2018). *MATR3* mutations were first reported to be linked to ALS in 2014 (Johnson et al., 2014). Like *TIA-1*, mutations in *MATR3* are rare (<1%) among ALS patients (Taylor et al., 2016). Studies from two recent articles showed that mice expressing mutant *MATR3* (*S85C* or *F115C*) develop motor dysfunction, accompanied by decreased numbers of motor neurons and activation of microglia and astrocytes in the spinal cord (Moloney et al., 2018; Zhang et al., 2019). Mechanistically, it was found that ALS-linked mutations of this gene decrease mRNA nuclear export and inhibit SG formation (Boehringer et al., 2017). S85C mutation of MATR3 was also shown to disrupt the normal function of MATR3 in mediating phase separation and formation of intranuclear droplets (Gallego-Iradi et al., 2019). Contrary to other ALS-related RBPs, wild-type or mutant MATR3 is

primarily localized to the nucleus even under stress or in ALS postmortem tissues (Johnson et al., 2014; Gallego-Iradi et al., 2015), and the accumulation of MATR3 in the nucleus as opposed to its location in the cytoplasm mediates neurotoxicity (Malik et al., 2018).

ATXN2 is an RBP belonging to the like-Sm (LSm) family and participates in the regulation of RNA metabolism. The *ATXN2* gene normally has ∼22–23 glutamine (CAG) repeats. Intermediate-size polyQ expansions (24–34 repeats) have been discovered to be significantly associated with the risk of developing ALS (Elden et al., 2010; Sproviero et al., 2017). ATXN2 plays a critical role in regulating TDP-43 and FUS toxicity through direct protein–protein interaction, and reduction of ATXN2 levels has been shown to inhibit TDP-43–mediated neurotoxicity (Elden et al., 2010; Farg et al., 2013; Becker et al., 2017). Both *in vitro* and knock-in mouse studies demonstrated that polyQ expansion mutants increase the insolubility of ATXN2 and its interacting protein PABPC1, causing neurodegeneration (Damrath et al., 2012).

Mutant forms of both *TAF15* and *EWSR1* have also been identified in ALS patients (Couthouis et al., 2011, 2012; Ticozzi et al., 2011). Similar to other RBPs, TAF15 and EWSR1 normally reside in the nucleus, but translocate to the cytoplasm upon stress (Neumann et al., 2011; Marko et al., 2012). Expression of disease-related variants of TAF15 and EWSR1 in primary neurons from mouse spinal cord has been reported to cause the formation of cytoplasmic foci. Cytoplasmic TAF15 and EWSR1 aggregates were also detected in some spinal cord neurons of patients with sALS (Couthouis et al., 2011, 2012). Overexpression of wild-type and mutant *TAF15* and *EWSR*1 has been shown to enhance protein aggregation and shorten life span in *Drosophila* (Couthouis et al., 2011, 2012).

DEVELOPMENT OF NOVEL THERAPEUTICS BY TARGETING RBPs

Early studies on ALS therapy have been mostly focused on SOD1. However, SOD1 mutations account for approximately only 20% of fALS and approximately 2% to 3% of all ALS cases (Taylor et al., 2016). Given the recognized importance of RBPs in ALS, RBPs have emerged as critical therapeutic targets for the treatment of ALS.

Antisense Oligonucleotide

Antisense oligonucleotides (ASOs) are synthetic single-stranded oligonucleotides that can specifically bind to and accelerate the degradation of the target mRNA *via* the nuclear endonuclease RNase H. ASO-based gene silencing has been previously tested on mutant *SOD1* (m*SOD1*), and the results are promising (Smith et al., 2006; Miller et al., 2013; McCampbell et al., 2018). It was found that direct delivery of m*SOD1*-targeted ASOs to the CNS effectively reduces the levels of mSOD1 and significantly delays disease progression and prolongs survival in SOD^{G93A} animal models (Smith et al., 2006; McCampbell et al., 2018) and mSOD1-linked ALS patients (Miller et al., 2013). Recently, this technique has been utilized to target ATXN2, a key regulator of TDP-43 neurotoxicity, for degradation (Becker et al., 2017). It was shown that administration of *ATXN2*-targeted ASOs to the CNS of a mouse model with TDP-43 proteinopathy attenuates TDP-43 pathology and improves motor function (Becker et al., 2017). Moreover, ASO-based strategies have also been successfully used to silence *GGGGCC* repeat expansion of *C9orf72*, thereby inhibiting RBPs sequestration by abnormal RNA foci (Donnelly et al., 2013; Sareen et al., 2013).

Small Molecules

Small molecules serve as another strategy for ALS treatment by modulating the function and abundance of RBPs. For instance, small molecules that specifically bind to the RRMs (RRM1 and RRM2) of TDP-43 preventing pathogenic interaction of TDP-43 and RNAs led to motor function improvement *in vivo* (*Drosophila*, François-Moutal et al., 2019). In addition, inhibition of tankyrase, a poly(ADP-ribose) polymerase, through small molecules was shown to reduce the accumulation of cytoplasmic TDP-43, FUS, or HNRNPA2/B1 aggregates and associated pathologies (McGurk et al., 2018; Fang et al., 2019; Marrone et al., 2019). Various small molecule activators of autophagy, a major cellular pathway for disposing of misfolded protein aggregates and damaged organelles, have also been tested in mutant *TDP-43* transgenic mice and in mutant *FUS Drosophila* models (Wang et al., 2012; Barmada et al., 2014; Marrone et al., 2019). It was shown that application of these autophagy inducers increases the clearance of protein aggregates and improves motor functions and pathologies. Finally, studies using chemical inhibitors to lessen nuclear export of TDP-43 demonstrated a neuroprotective effect (Haines et al., 2015).

Chaperones

Molecular chaperones, such as heat shock proteins (HSPs), function to assist proper protein folding and prevent misfolded proteins from aggregation. In addition, chaperones can also guide terminally misfolded proteins to the proteolytic system for degradation (Xiao et al., 2010). In the study of ALS treatment, modified yeast HSP104 was discovered to rescue TDP-43 and FUS proteotoxicity by promoting aggregate dissolution (Jackrel et al., 2014). Moreover, HSPB8, a small HSP, was reported to promote autophagic clearance of misfolded mutant TDP-43 and SOD1, as well as DPRs of C9orf72 (Crippa et al., 2016). Notably, a randomized phase II clinical trial is undertaken to examine the therapeutic value of colchicine, which induces the expression of HSPB8 and several autophagy modulators, in ALS (Mandrioli et al., 2019).

Antibodies

Antibody-based therapies have been widely explored for the treatment of neurodegenerative diseases, including ALS. There was a recent study showing beneficial effects of antibodies targeting TDP-43 in ALS (Pozzi et al., 2019). In this study, a single-chain antibody against the RRM1 of TDP-43, a domain involved in protein aggregation and interaction with p65 nuclear factor κB, was generated and delivered into the CNS of TDP-43 mutant transgenic mice through a viral vector. It was found that antibody treatment in these mice significantly reduces neuroinflammation, cognitive impairment, and motor defects (Pozzi et al., 2019).

CONCLUSION

The contribution of dysfunctional RBPs in both fALS and sALS has been greatly appreciated over the last decade since the recognition of *TDP-43* as an ALS causal gene and TDP-43 proteinopathy as a hallmark for ALS. The ALS-implicated RBPs share structural and functional similarity. Dysregulated or mutant RBPs have been shown to cause disease phenotype through common protein pathologies, including increased aggregation tendency, cytoplasmic mislocalization, and irregular LLPS and SG dynamics. However, current evidence also points to a distinct function and unique mechanism for individual RBPs in the pathogenesis of ALS. A better understanding of the molecular mechanisms underlying the pathological role of these RBPs in ALS development will lead to a novel avenue for therapeutic intervention for this devastating disease.

AUTHOR CONTRIBUTIONS

All authors contributed to the writing of this article.

FUNDING

This work was supported by the Canadian Institutes of Health Research (PJT 159546) and the ALS Society of Canada. YM is the recipient of a Doctoral Fellowship from the ALS Canada-Brain Canada. YM and YX are the recipients of UBC Four Year Fellowship. YX is also supported by the UBC ECOSCOPE program. KZ is the recipient of the Faculty of Medicine Summer Student Research program. PX is the recipient of the NSERC Undergraduate Student Research program. CN and HLi are supported by the MITACS Accelerate program.

REFERENCES

Alami, N. H., Smith, R. B., Carrasco, M. A., Williams, L. A., Winborn, C. S., Han, S. S. W., et al. (2014). Axonal transport of TDP-43 mRNA granules is impaired by ALS-causing mutations. *Neuron* 81, 536–543. doi: 10.1016/j.neuron.2013.12.018

Al-Chalabi, A., van den Berg, L. H., and Veldink, J. (2017). Gene discovery in amyotrophic lateral sclerosis: implications for clinical management. *Nat. Rev. Neurol.* 13, 96–104. doi: 10.1038/nrneurol.2016.182

Arosio, A., Cristofani, R., Pansarasa, O., Crippa, V., Riva, C., Sirtori, R., et al. (2020). HSC70 expression is reduced in lymphomonocytes of sporadic ALS patients and contributes to TDP-43 accumulation. *Amyotroph. Lateral Scler. Frontotemporal. Degener.* 21, 51–62. doi: 10.1080/21678421.2019.1672749

Ayala, Y. M., De Conti, L., Avendaño-Vázquez, S. E., Dhir, A., Romano, M., D'Ambrogio, A., et al. (2011). TDP-43 regulates its mRNA levels through a negative feedback loop. *EMBO J.* 30, 277–288. doi: 10.1038/emboj.2010.310

Baradaran-Heravi, Y., Dillen, L., Nguyen, H. P., Van Mossevelde, S., Baets, J., De Jonghe, P., et al. (2018). No supportive evidence for TIA1 gene mutations in a European cohort of ALS-FTD spectrum patients. *Neurobiol. Aging* 69, 293.e9–293.e11. doi: 10.1016/j.neurobiolaging.2018.05.005

Barmada, S. J., Serio, A., Arjun, A., Bilican, B., Daub, A., Ando, D. M., et al. (2014). Autophagy induction enhances TDP43 turnover and survival in neuronal ALS models. *Nat. Chem. Biol.* 10, 677–685. doi: 10.1038/nchembio.1563

Becker, L. A., Huang, B., Bieri, G., Ma, R., Knowles, D. A., Jafar-Nejad, P., et al. (2017). Therapeutic reduction of ataxin-2 extends lifespan and reduces pathology in TDP-43 mice. *Nature* 544, 367–371. doi: 10.1038/nature22038

Berning, B. A., and Walker, A. K. (2019). The pathobiology of TDP-43 C-terminal fragments in ALS and FTLD. *Front. Neurosci.* 13:335. doi: 10.3389/fnins.2019.00335

Berson, A., Barbash, S., Shaltiel, G., Goll, Y., Hanin, G., Greenberg, D. S., et al. (2012). Cholinergic-associated loss of hnRNP-A/B in Alzheimer's disease impairs cortical splicing and cognitive function in mice. *EMBO Mol. Med.* 4, 730–742. doi: 10.1002/emmm.201100995

Boehringer, A., Garcia-Mansfield, K., Singh, G., Bakkar, N., Pirrotte, P., and Bowser, R. (2017). ALS associated mutations in Matrin 3 alter protein-protein interactions and impede mRNA nuclear export. *Sci. Rep.* 7:14529. doi: 10.1038/s41598-017-14924-6

Brown, R. H. Jr., and Al-Chalabi, A. (2017). Amyotrophic lateral sclerosis. *N. Engl. J. Med.* 377:1602. doi: 10.1056/NEJMc1710379

Buchan, J. R., and Parker, R. (2009). Eukaryotic stress granules: the ins and outs of translation. *Mol. Cell* 36, 932–941. doi: 10.1016/j.molcel.2009.11.020

Buratti, E. (2018). TDP-43 post-translational modifications in health and disease. *Expert Opin. Ther. Targets* 22, 279–293. doi: 10.1080/14728222.2018.1439923

Butti, Z., and Patten, S. A. (2018). RNA dysregulation in amyotrophic lateral sclerosis. *Front. Genet.* 9:712. doi: 10.3389/fgene.2018.00712

Cammas, A., Pileur, F., Bonnal, S., Lewis, S. M., Léveque, N., Holcik, M., et al. (2007). Cytoplasmic relocalization of heterogeneous nuclear ribonucleoprotein A1 controls translation initiation of specific mRNAs. *Mol. Biol. Cell* 18, 5048–5059. doi: 10.1091/mbc.e07-06-0603

Cipolat Mis, M. S., Brajkovic, S., Frattini, E., Di Fonzo, A., and Corti, S. (2016). Autophagy in motor neuron disease: key pathogenetic mechanisms and therapeutic targets. *Mol. Cell. Neurosci.* 72, 84–90. doi: 10.1016/j.mcn.2016.01.012

Conlon, E. G., and Manley, J. L. (2017). RNA-binding proteins in neurodegeneration: mechanisms in aggregate. *Genes Dev.* 31, 1509–1528. doi: 10.1101/gad.304055.117

Couthouis, J., Hart, M. P., Erion, R., King, O. D., Diaz, Z., Nakaya, T., et al. (2012). Evaluating the role of the FUS/TLS-related gene EWSR1 in amyotrophic lateral sclerosis. *Hum. Mol. Genet.* 21, 2899–2911. doi: 10.1093/hmg/dds116

Couthouis, J., Hart, M. P., Shorter, J., DeJesus-Hernandez, M., Erion, R., Oristano, R., et al. (2011). A yeast functional screen predicts new candidate ALS disease genes. *Proc. Natl. Acad. Sci. U S A* 108, 20881–20890. doi: 10.1073/pnas.1109434108

Couthouis, J., Raphael, A. R., Daneshjou, R., and Gitler, A. D. (2014). Targeted exon capture and sequencing in sporadic amyotrophic lateral sclerosis. *PLoS Genet.* 10:e1004704. doi: 10.1371/journal.pgen.1004704

Crippa, V., Cicardi, M. E., Ramesh, N., Seguin, S. J., Ganassi, M., Bigi, I., et al. (2016). The chaperone HSPB8 reduces the accumulation of truncated TDP-43 species in cells and protects against TDP-43-mediated toxicity. *Hum. Mol. Genet.* 25, 3908–3924. doi: 10.1093/hmg/ddw232

Damrath, E., Heck, M. V., Gispert, S., Azizov, M., Nowock, J., Seifried, C., et al. (2012). ATXN2-CAG42 sequesters PABPC1 into insolubility and induces FBXW8 in cerebellum of old ataxic knock-in mice. *PLoS Genet.* 8:e1002920. doi: 10.1371/journal.pgen.1002920

De Marco, G., Lomartire, A., Calvo, A., Risso, A., De Luca, E., Mostert, M., et al. (2017). Monocytes of patients with amyotrophic lateral sclerosis linked to gene mutations display altered TDP-43 subcellular distribution. *Neuropathol. Appl. Neurobiol.* 43, 133–153. doi: 10.1111/nan.12328

DeJesus-Hernandez, M., Mackenzie, I. R., Boeve, B. F., Boxer, A. L., Baker, M., Rutherford, N. J., et al. (2011). Expanded GGGGCC hexanucleotide repeat in noncoding region of C9ORF72 causes chromosome 9p-linked FTD and ALS. *Neuron* 72, 245–256. doi: 10.1016/j.neuron.2011.09.011

Deng, H. X., Zhai, H., Bigio, E. H., Yan, J., Fecto, F., Ajroud, K., et al. (2010). FUS-immunoreactive inclusions are a common feature in sporadic and non-SOD1 familial amyotrophic lateral sclerosis. *Ann. Neurol.* 67, 739–748. doi: 10.1002/ana.22051

Deshaies, J. E., Shkreta, L., Moszczynski, A. J., Sidibé, H., Semmler, S., Fouillen, A., et al. (2018). TDP-43 regulates the alternative splicing of hnRNP A1 to yield an aggregation-prone variant in amyotrophic lateral sclerosis. *Brain* 141, 1320–1333. doi: 10.1093/brain/awy062

Deshpande, D., Higelin, J., Schoen, M., Vomhof, T., Boeckers, T. M., Demestre, M., et al. (2019). Synaptic FUS localization during motoneuron development and its accumulation in human ALS synapses. *Front. Cell. Neurosci.* 13:256. doi: 10.3389/fncel.2019.00256

Donnelly, C. J., Zhang, P. W., Pham, J. T., Haeusler, A. R., Mistry, N. A., Vidensky, S., et al. (2013). RNA toxicity from the ALS/FTD C9ORF72 expansion is mitigated by antisense intervention. *Neuron* 80, 415–428. doi: 10.1016/j.neuron.2013.10.015

Dormann, D., Rodde, R., Edbauer, D., Bentmann, E., Fischer, I., Hruscha, A., et al. (2010). ALS-associated fused in sarcoma (FUS) mutations disrupt Transportin-mediated nuclear import. *EMBO J.* 29, 2841–2857. doi: 10.1038/emboj.2010.143

Elden, A. C., Kim, H. J., Hart, M. P., Chen-Plotkin, A. S., Johnson, B. S., Fang, X., et al. (2010). Ataxin-2 intermediate-length polyglutamine expansions are associated with increased risk for ALS. *Nature* 466, 1069–1075. doi: 10.1038/nature09320

Fang, M. Y., Markmiller, S., Vu, A. Q., Javaherian, A., Dowdle, W. E., Jolivet, P., et al. (2019). Small-molecule modulation of TDP-43 recruitment to stress granules prevents persistent TDP-43 accumulation in ALS/FTD. *Neuron* 103, 802.e11–819.e11. doi: 10.1016/j.neuron.2019.05.048

Farg, M. A., Soo, K. Y., Warraich, S. T., Sundaramoorthy, V., Blair, I. P., and Atkin, J. D. (2013). Ataxin-2 interacts with FUS and intermediate-length polyglutamine expansions enhance FUS-related pathology in amyotrophic lateral sclerosis. *Hum. Mol. Genet.* 22, 717–728. doi: 10.1093/hmg/dds479

François-Moutal, L., Felemban, R., Scott, D. D., Sayegh, M. R., Miranda, V. G., Perez-Miller, S., et al. (2019). Small molecule targeting TDP-43's RNA recognition motifs reduces locomotor defects in a *Drosophila* model of amyotrophic lateral sclerosis (ALS). *ACS Chem. Biol.* 14, 2006–2013. doi: 10.1021/acschembio.9b00481

Franzmann, T. M., and Alberti, S. (2019). Prion-like low-complexity sequences: key regulators of protein solubility and phase behavior. *J. Biol. Chem.* 294, 7128–7136. doi: 10.1074/jbc.tm118.001190

Fratta, P., Sivakumar, P., Humphrey, J., Lo, K., Ricketts, T., Oliveira, H., et al. (2018). Mice with endogenous TDP-43 mutations exhibit gain of splicing function and characteristics of amyotrophic lateral sclerosis. *EMBO J.* 37:e98684. doi: 10.15252/embj.201798684

Freibaum, B. D., Lu, Y., Lopez-Gonzalez, R., Kim, N. C., Almeida, S., Lee, K. H., et al. (2015). GGGGCC repeat expansion in C9orf72 compromises nucleocytoplasmic transport. *Nature* 525, 129–133. doi: 10.1038/nature14974

Gallego-Iradi, M. C., Clare, A. M., Brown, H. H., Janus, C., Lewis, J., and Borchelt, D. R. (2015). Subcellular localization of matrin 3 containing mutations associated with ALS and distal myopathy. *PLoS One* 10:e0142144. doi: 10.1371/journal.pone.0142144

Gallego-Iradi, M. C., Strunk, H., Crown, A. M., Davila, R., Brown, H., Rodriguez-Lebron, E., et al. (2019). N-terminal sequences in matrin 3 mediate phase separation into droplet-like structures that recruit TDP43 variants lacking RNA binding elements. *Lab. Invest.* 99, 1030–1040. doi: 10.1038/s41374-019-0260-7

Gilpin, K. M., Chang, L., and Monteiro, M. J. (2015). ALS-linked mutations in ubiquilin-2 or hnRNPA1 reduce interaction between ubiquilin-2 and hnRNPA1. *Hum. Mol. Genet.* 24, 2565–2577. doi: 10.1093/hmg/ddv020

Guo, L., Kim, H. J., Wang, H., Monaghan, J., Freyermuth, F., Sung, J. C., et al. (2018). Nuclear-import receptors reverse aberrant phase transitions of RNA-binding proteins with prion-like domains. *Cell* 173, 677.e20–692.e20. doi: 10.1016/j.cell.2018.03.002

Haines, J. D., Herbin, O., de la Hera, B., Vidaurre, O. G., Moy, G. A., Sun, Q., et al. (2015). Nuclear export inhibitors avert progression in preclinical models of inflammatory demyelination. *Nat. Neurosci.* 18, 511–520. doi: 10.1038/nn.3953

Hasegawa, M., Arai, T., Nonaka, T., Kametani, F., Yoshida, M., Hashizume, Y., et al. (2008). Phosphorylated TDP-43 in frontotemporal lobar degeneration and amyotrophic lateral sclerosis. *Ann. Neurol.* 64, 60–70. doi: 10.1002/ana.21425

Hoell, J. I., Larsson, E., Runge, S., Nusbaum, J. D., Duggimpudi, S., Farazi, T. A., et al. (2011). RNA targets of wild-type and mutant FET family proteins. *Nat. Struct. Mol. Biol.* 18, 1428–1431. doi: 10.1038/nsmb.2163

Hofweber, M., and Dormann, D. (2019). Friend or foe-Post-translational modifications as regulators of phase separation and RNP granule dynamics. *J. Biol. Chem.* 294, 7137–7150. doi: 10.1074/jbc.tm118.001189

Hofweber, M., Hutten, S., Bourgeois, B., Spreitzer, E., Niedner-Boblenz, A., Schifferer, M., et al. (2018). Phase separation of FUS is suppressed by its nuclear import receptor and arginine methylation. *Cell* 173, 706.e13–719.e13. doi: 10.1016/j.cell.2018.03.004

Iguchi, Y., Katsuno, M., Niwa, J., Takagi, S., Ishigaki, S., Ikenaka, K., et al. (2013). Loss of TDP-43 causes age-dependent progressive motor neuron degeneration. *Brain* 136, 1371–1382. doi: 10.1093/brain/awt029

Jackrel, M. E., DeSantis, M. E., Martinez, B. A., Castellano, L. M., Stewart, R. M., Caldwell, K. A., et al. (2014). Potentiated Hsp104 variants antagonize diverse proteotoxic misfolding events. *Cell* 156, 170–182. doi: 10.1016/j.cell.2013.11.047

Johnson, J. O., Pioro, E. P., Boehringer, A., Chia, R., Feit, H., Renton, A. E., et al. (2014). Mutations in the Matrin 3 gene cause familial amyotrophic lateral sclerosis. *Nat. Neurosci.* 17, 664–666. doi: 10.1038/nn.3688

Jovicic, A., Mertens, J., Boeynaems, S., Bogaert, E., Chai, N., Yamada, S. B., et al. (2015). Modifiers of C9orf72 dipeptide repeat toxicity connect nucleocytoplasmic transport defects to FTD/ALS. *Nat. Neurosci.* 18, 1226–1229. doi: 10.1038/nn.4085

Kabashi, E., Valdmanis, P. N., Dion, P., Spiegelman, D., McConkey, B. J., Vande Velde, C., et al. (2008). TARDBP mutations in individuals with sporadic and familial amyotrophic lateral sclerosis. *Nat. Genet.* 40, 572–574. doi: 10.1038/ng.132

Kamelgarn, M., Chen, J., Kuang, L., Jin, H., Kasarskis, E. J., and Zhu, H. (2018). ALS mutations of FUS suppress protein translation and disrupt the regulation of nonsense-mediated decay. *Proc. Natl. Acad. Sci. U S A* 115, E11904–E11913. doi: 10.1073/pnas.1810413115

Kapeli, K., Martinez, F. J., and Yeo, G. W. (2017). Genetic mutations in RNA-binding proteins and their roles in ALS. *Hum. Genet.* 136, 1193–1214. doi: 10.1007/s00439-017-1830-7

Kim, H. J., and Taylor, J. P. (2017). Lost in transportation: nucleocytoplasmic transport defects in ALS and other neurodegenerative diseases. *Neuron* 96, 285–297. doi: 10.1016/j.neuron.2017.07.029

Kim, H. J., Kim, N. C., Wang, Y. D., Scarborough, E. A., Moore, J., Diaz, Z., et al. (2013). Mutations in prion-like domains in hnRNPA2B1 and hnRNPA1 cause multisystem proteinopathy and ALS. *Nature* 495, 467–473. doi: 10.1038/nature11922

Kosturko, L. D., Maggipinto, M. J., Korza, G., Lee, J. W., Carson, J. H., and Barbarese, E. (2006). Heterogeneous nuclear ribonucleoprotein (hnRNP) E1 binds to hnRNP A2 and inhibits translation of A2 response element mRNAs. *Mol. Biol. Cell* 17, 3521–3533. doi: 10.1091/mbc.e05-10-0946

Kwiatkowski, T. J. Jr., Bosco, D. A., Leclerc, A. L., Tamrazian, E., Vanderburg, C. R., Russ, C., et al. (2009). Mutations in the FUS/TLS gene on chromosome 16 cause familial amyotrophic lateral sclerosis. *Science* 323, 1205–1208. doi: 10.1126/science.1166066

Lagier-Tourenne, C., Polymenidou, M., Hutt, K. R., Vu, A. Q., Baughn, M., Huelga, S. C., et al. (2012). Divergent roles of ALS-linked proteins FUS/TLS and TDP-43 intersect in processing long pre-mRNAs. *Nat. Neurosci.* 15, 1488–1497. doi: 10.1038/nn.3230

Liachko, N. F., McMillan, P. J., Guthrie, C. R., Bird, T. D., Leverenz, J. B., and Kraemer, B. C. (2013). CDC7 inhibition blocks pathological TDP-43 phosphorylation and neurodegeneration. *Ann. Neurol.* 74, 39–52. doi: 10.1002/ana.23870

Liachko, N. F., McMillan, P. J., Strovas, T. J., Loomis, E., Greenup, L., Murrell, J. R., et al. (2014). The tau tubulin kinases TTBK1/2 promote accumulation of pathological TDP-43. *PLoS Genet.* 10:e1004803. doi: 10.1371/journal.pgen.1004803

Liachko, N. F., Saxton, A. D., McMillan, P. J., Strovas, T. J., Currey, H. N., Taylor, L. M., et al. (2016). The phosphatase calcineurin regulates pathological TDP-43 phosphorylation. *Acta Neuropathol.* 132, 545–561. doi: 10.1007/s00401-016-1600-y

Ling, S. C. (2018). Synaptic paths to neurodegeneration: the emerging role of TDP-43 and FUS in synaptic functions. *Neural Plast.* 2018:8413496. doi: 10.1155/2018/8413496

Ling, J. P., Pletnikova, O., Troncoso, J. C., and Wong, P. C. (2015). TDP-43 repression of nonconserved cryptic exons is compromised in ALS-FTD. *Science* 349, 650–655. doi: 10.1126/science.aab0983

Liu, Q., Shu, S., Wang, R. R., Liu, F., Cui, B., Guo, X. N., et al. (2016). Whole-exome sequencing identifies a missense mutation in hnRNPA1 in a family with flail arm ALS. *Neurology* 87, 1763–1769. doi: 10.1212/wnl.0000000000003256

Liu, T. Y., Chen, Y. C., Jong, Y. J., Tsai, H. J., Lee, C. C., Chang, Y. S., et al. (2017). Muscle developmental defects in heterogeneous nuclear Ribonucleoprotein A1 knockout mice. *Open Biol.* 7:160303. doi: 10.1098/rsob.160303

López-Erauskin, J., Tadokoro, T., Baughn, M. W., Myers, B., McAlonis-Downes, M., Chillon-Marinas, C., et al. (2018). ALS/FTD-linked mutation in FUS suppresses intra-axonal protein synthesis and drives disease without nuclear loss-of-function of FUS. *Neuron* 100, 816.e7–830.e7. doi: 10.1016/j.neuron.2018.09.044

Lutz, C. (2018). Mouse models of ALS: Past, present and future. *Brain Res.* 1693, 1–10. doi: 10.1016/j.brainres.2018.03.024

Mackenzie, I. R., Bigio, E. H., Ince, P. G., Geser, F., Neumann, M., Cairns, N. J., et al. (2007). Pathological TDP-43 distinguishes sporadic amyotrophic lateral sclerosis from amyotrophic lateral sclerosis with SOD1 mutations. *Ann. Neurol.* 61, 427–434. doi: 10.1002/ana.21147

Mackenzie, I. R., Nicholson, A. M., Sarkar, M., Messing, J., Purice, M. D., Pottier, C., et al. (2017). TIA1 mutations in amyotrophic lateral sclerosis and frontotemporal dementia promote phase separation and alter stress granule dynamics. *Neuron* 95, 808.e9–816.e9. doi: 10.1016/j.neuron.2017.07.025

Mackenzie, I. R., Rademakers, R., and Neumann, M. (2010). TDP-43 and FUS in amyotrophic lateral sclerosis and frontotemporal dementia. *Lancet Neurol.* 9, 995–1007. doi: 10.1016/s1474-4422(10)70195-2

Malik, A. M., Miguez, R. A., Li, X., Ho, Y. S., Feldman, E. L., and Barmada, S. J. (2018). Matrin 3-dependent neurotoxicity is modified by nucleic acid binding and nucleocytoplasmic localization. *Elife* 7:e35977. doi: 10.7554/elife.35977

Mandrioli, J., Crippa, V., Cereda, C., Bonetto, V., Zucchi, E., Gessani, A., et al. (2019). Proteostasis and ALS: protocol for a phase II, randomised, double-blind, placebo-controlled, multicentre clinical trial for colchicine in ALS (Co-ALS). *BMJ Open* 9:e028486. doi: 10.1136/bmjopen-2018-028486

Marko, M., Vlassis, A., Guialis, A., and Leichter, M. (2012). Domains involved in TAF15 subcellular localisation: dependence on cell type and ongoing transcription. *Gene* 506, 331–338. doi: 10.1016/j.gene.2012.06.088

Marrone, L., Drexler, H. C. A., Wang, J., Tripathi, P., Distler, T., Heisterkamp, P., et al. (2019). FUS pathology in ALS is linked to alterations in multiple ALS-associated proteins and rescued by drugs stimulating autophagy. *Acta Neuropathol.* 138, 67–84. doi: 10.1007/s00401-019-01998-x

Martinez, F. J., Pratt, G. A., Van Nostrand, E. L., Batra, R., Huelga, S. C., Kapeli, K., et al. (2016). Protein-RNA networks regulated by normal and ALS-associated mutant HNRNPA2B1 in the nervous system. *Neuron* 92, 780–795. doi: 10.1016/j.neuron.2016.09.050

McCampbell, A., Cole, T., Wegener, A. J., Tomassy, G. S., Setnicka, A., Farley, B. J., et al. (2018). Antisense oligonucleotides extend survival and reverse decrement in muscle response in ALS models. *J. Clin. Invest.* 128, 3558–3567. doi: 10.1172/jci99081

McGurk, L., Gomes, E., Guo, L., Mojsilovic-Petrovic, J., Tran, V., Kalb, R. G., et al. (2018). Poly(ADP-ribose) prevents pathological phase separation of TDP-43 by promoting liquid demixing and stress granule localization. *Mol Cell* 71, 703.e9–717.e9. doi: 10.1016/j.molcel.2018.07.002

Miller, T. M., Pestronk, A., David, W., Rothstein, J., Simpson, E., Appel, S. H., et al. (2013). An antisense oligonucleotide against SOD1 delivered intrathecally for patients with SOD1 familial amyotrophic lateral sclerosis: a phase 1, randomised, first-in-man study. *Lancet Neurol.* 12, 435–442. doi: 10.1016/S1474-4422(13)70061-9

Mitra, J., Guerrero, E. N., Hegde, P. M., Liachko, N. F., Wang, H., Vasquez, V., et al. (2019). Motor neuron disease-associated loss of nuclear TDP-43 is linked to DNA double-strand break repair defects. *Proc. Natl. Acad. Sci. U S A* 116, 4696–4705. doi: 10.1073/pnas.1818415116

Molliex, A., Temirov, J., Lee, J., Coughlin, M., Kanagaraj, A. P., Kim, H. J., et al. (2015). Phase separation by low complexity domains promotes stress granule assembly and drives pathological fibrillization. *Cell* 163, 123–133. doi: 10.1016/j.cell.2015.09.015

Moloney, C., Rayaprolu, S., Howard, J., Fromholt, S., Brown, H., Collins, M., et al. (2018). Analysis of spinal and muscle pathology in transgenic mice overexpressing wild-type and ALS-linked mutant MATR3. *Acta Neuropathol. Commun.* 6:137. doi: 10.1186/s40478-018-0631-0

Morriss, G. R., and Cooper, T. A. (2017). Protein sequestration as a normal function of long noncoding RNAs and a pathogenic mechanism of RNAs containing nucleotide repeat expansions. *Hum. Genet.* 136, 1247–1263. doi: 10.1007/s00439-017-1807-6

Naruse, H., Ishiura, H., Mitsui, J., Date, H., Takahashi, Y., Matsukawa, T., et al. (2018). Molecular epidemiological study of familial amyotrophic lateral sclerosis in Japanese population by whole-exome sequencing and identification of novel HNRNPA1 mutation. *Neurobiol. Aging* 61, 255.e9–255.e16. doi: 10.1016/j.neurobiolaging.2017.08.030

Naumann, M., Pal, A., Goswami, A., Lojewski, X., Japtok, J., Vehlow, A., et al. (2018). Impaired DNA damage response signaling by FUS-NLS mutations leads to neurodegeneration and FUS aggregate formation. *Nat. Commun.* 9:335. doi: 10.1038/s41467-017-02299-1

Neelagandan, N., Gonnella, G., Dang, S., Janiesch, P. C., Miller, K. K., Kuchler, K., et al. (2019). TDP-43 enhances translation of specific mRNAs linked to neurodegenerative disease. *Nucleic Acids Res.* 47, 341–361. doi: 10.1093/nar/gky972

Neumann, M., Bentmann, E., Dormann, D., Jawaid, A., DeJesus-Hernandez, M., Ansorge, O., et al. (2011). FET proteins TAF15 and EWS are selective markers that distinguish FTLD with FUS pathology from amyotrophic lateral sclerosis with FUS mutations. *Brain* 134, 2595–2609. doi: 10.1093/brain/awr201

Neumann, M., Sampathu, D. M., Kwong, L. K., Truax, A. C., Micsenyi, M. C., Chou, T. T., et al. (2006). Ubiquitinated TDP-43 in frontotemporal lobar degeneration and amyotrophic lateral sclerosis. *Science* 314, 130–133. doi: 10.1126/science.1134108

Nguyen, H. P., Van Broeckhoven, C., and van der Zee, J. (2018). ALS genes in the genomic era and their implications for FTD. *Trends Genet.* 34, 404–423. doi: 10.1016/j.tig.2018.03.001

Nonaka, T., Suzuki, G., Tanaka, Y., Kametani, F., Hirai, S., Okado, H., et al. (2016). Phosphorylation of TAR DNA-binding protein of 43 kDa (TDP-43) by truncated casein kinase 1δ triggers mislocalization and accumulation of TDP-43. *J. Biol. Chem.* 291, 5473–5483. doi: 10.1074/jbc.m115.695379

Nussbacher, J. K., Tabet, R., Yeo, G. W., and Lagier-Tourenne, C. (2019). Disruption of RNA metabolism in neurological diseases and emerging therapeutic interventions. *Neuron* 102, 294–320. doi: 10.1016/j.neuron.2019.03.014

Polymenidou, M., Lagier-Tourenne, C., Hutt, K. R., Huelga, S. C., Moran, J., Liang, T. Y., et al. (2011). Long pre-mRNA depletion and RNA missplicing contribute to neuronal vulnerability from loss of TDP-43. *Nat. Neurosci.* 14, 459–468. doi: 10.1038/nn.2779

Pozzi, S., Thammisetty, S. S., Codron, P., Rahimian, R., Plourde, K. V., Soucy, G., et al. (2019). Virus-mediated delivery of antibody targeting TAR DNA-binding protein-43 mitigates associated neuropathology. *J. Clin. Invest.* 129, 1581–1595. doi: 10.1172/jci123931

Qamar, S., Wang, G., Randle, S. J., Ruggeri, F. S., Varela, J. A., Lin, J. Q., et al. (2018). FUS phase separation is modulated by a molecular chaperone and methylation of arginine cation-pi interactions. *Cell* 173, 720.e15–734.e15. doi: 10.1016/j.cell.2018.03.056

Qiu, H., Lee, S., Shang, Y., Wang, W. Y., Au, K. F., Kamiya, S., et al. (2014). ALS-associated mutation FUS-R521C causes DNA damage and RNA splicing defects. *J. Clin. Invest.* 124, 981–999. doi: 10.1172/jci72723

Rayman, J. B., and Kandel, E. R. (2017). TIA-1 is a functional prion-like protein. *Cold Spring Harb. Perspect. Biol.* 9:a023671. doi: 10.1101/cshperspect.a023671

Renton, A. E., Majounie, E., Waite, A., Simon-Sanchez, J., Rollinson, S., Gibbs, J. R., et al. (2011). A hexanucleotide repeat expansion in C9ORF72 is the cause of chromosome 9p21-linked ALS-FTD. *Neuron* 72, 257–268. doi: 10.1016/j.neuron.2011.09.010

Russo, A., Scardigli, R., La Regina, F., Murray, M. E., Romano, N., Dickson, D. W., et al. (2017). Increased cytoplasmic TDP-43 reduces global protein synthesis by interacting with RACK1 on polyribosomes. *Hum. Mol. Genet.* 26, 1407–1418. doi: 10.1093/hmg/ddx035

Ryan, V. H., Dignon, G. L., Zerze, G. H., Chabata, C. V., Silva, R., Conicella, A. E., et al. (2018). Mechanistic view of hnRNPA2 low-complexity domain structure, interactions and phase separation altered by mutation and arginine methylation. *Mol. Cell* 69, 465.e7–479.e7. doi: 10.1016/j.molcel.2017.12.022

Sareen, D., O'Rourke, J. G., Meera, P., Muhammad, A. K., Grant, S., Simpkinson, M., et al. (2013). Targeting RNA foci in iPSC-derived motor neurons from ALS patients with a C9ORF72 repeat expansion. *Sci. Transl Med.* 5:208ra149. doi: 10.1126/scitranslmed.3007529

Scekic-Zahirovic, J., Oussini, H. E., Mersmann, S., Drenner, K., Wagner, M., Sun, Y., et al. (2017). Motor neuron intrinsic and extrinsic mechanisms contribute to the pathogenesis of FUS-associated amyotrophic lateral sclerosis. *Acta Neuropathol.* 133, 887–906. doi: 10.1007/s00401-017-1687-9

Sharma, A., Lyashchenko, A. K., Lu, L., Nasrabady, S. E., Elmaleh, M., Mendelsohn, M., et al. (2016). ALS-associated mutant FUS induces selective

motor neuron degeneration through toxic gain of function. *Nat. Commun.* 7:10465. doi: 10.1038/ncomms10465

Shelkovnikova, T. A., An, H., Skelt, L., Tregoning, J. S., Humphreys, I. R., and Buchman, V. L. (2019). Antiviral immune response as a trigger of FUS proteinopathy in amyotrophic lateral sclerosis. *Cell Rep.* 29, 4496.e4–4508.e4. doi: 10.1016/j.celrep.2019.11.094

Shi, K. Y., Mori, E., Nizami, Z. F., Lin, Y., Kato, M., Xiang, S., et al. (2017). Toxic PRn poly-dipeptides encoded by the C9orf72 repeat expansion block nuclear import and export. *Proc. Natl. Acad. Sci. U S A* 114, E1111–E1117. doi: 10.1073/pnas.1620293114

Sivakumar, P., De Giorgio, F., Ule, A. M., Neeves, J., Nair, R. R., Bentham, M., et al. (2018). TDP-43 mutations increase HNRNP A1–7B through gain of splicing function. *Brain* 141:e83. doi: 10.1093/brain/awy260

Smith, R. A., Miller, T. M., Yamanaka, K., Monia, B. P., Condon, T. P., Hung, G., et al. (2006). Antisense oligonucleotide therapy for neurodegenerative disease. *J. Clin. Invest.* 116, 2290–2296. doi: 10.1172/jci25424

Sproviero, W., Shatunov, A., Stahl, D., Shoai, M., van Rheenen, W., Jones, A. R., et al. (2017). ATXN2 trinucleotide repeat length correlates with risk of ALS. *Neurobiol. Aging* 51, 178.e1–178.e9. doi: 10.1016/j.neurobiolaging.2016.11.010

Sreedharan, J., Blair, I. P., Tripathi, V. B., Hu, X., Vance, C., Rogelj, B., et al. (2008). TDP-43 mutations in familial and sporadic amyotrophic lateral sclerosis. *Science* 319, 1668–1672. doi: 10.1126/science.1154584

Taylor, J. P., Brown, R. H. Jr., and Cleveland, D. W. (2016). Decoding ALS: from genes to mechanism. *Nature* 539, 197–206. doi: 10.1038/nature20413

Ticozzi, N., Vance, C., Leclerc, A. L., Keagle, P., Glass, J. D., McKenna-Yasek, D., et al. (2011). Mutational analysis reveals the FUS homolog TAF15 as a candidate gene for familial amyotrophic lateral sclerosis. *Am. J. Med. Genet. B Neuropsychiatr. Genet.* 156B, 285–290. doi: 10.1002/ajmg.b.31158

Tollervey, J. R., Curk, T., Rogelj, B., Briese, M., Cereda, M., Kayikci, M., et al. (2011). Characterizing the RNA targets and position-dependent splicing regulation by TDP-43. *Nat. Neurosci.* 14, 452–458. doi: 10.1038/nn.2778

Tyzack, G. E., Luisier, R., Taha, D. M., Neeves, J., Modic, M., Mitchell, J. S., et al. (2019). Widespread FUS mislocalization is a molecular hallmark of amyotrophic lateral sclerosis. *Brain* 142, 2572–2580. doi: 10.1093/brain/awz217

Van Deerlin, V. M., Leverenz, J. B., Bekris, L. M., Bird, T. D., Yuan, W., Elman, L. B., et al. (2008). TARDBP mutations in amyotrophic lateral sclerosis with TDP-43 neuropathology: a genetic and histopathological analysis. *Lancet Neurol.* 7, 409–416. doi: 10.1016/S1474-4422(08)70071-1

van der Spek, R. A., van Rheenen, W., Pulit, S. L., Kenna, K. P., Ticozzi, N., Kooyman, M., et al. (2018). Reconsidering the causality of TIA1 mutations in ALS. *Amyotroph. Lateral Scler. Frontotemporal. Degener.* 19, 1–3. doi: 10.1080/21678421.2017.1413118

van Es, M. A., Hardiman, O., Chio, A., Al-Chalabi, A., Pasterkamp, R. J., Veldink, J. H., et al. (2017). Amyotrophic lateral sclerosis. *Lancet* 390, 2084–2098. doi: 10.1016/S0140-6736(17)31287-4

Vance, C., Rogelj, B., Hortobagyi, T., De Vos, K. J., Nishimura, A. L., Sreedharan, J., et al. (2009). Mutations in FUS, an RNA processing protein, cause familial amyotrophic lateral sclerosis type 6. *Science* 323, 1208–1211. doi: 10.1126/science.1165942

Vanneste, J., Vercruysse, T., Boeynaems, S., Sicart, A., Van Damme, P., Daelemans, D., et al. (2019). C9orf72-generated poly-GR and poly-PR do not directly interfere with nucleocytoplasmic transport. *Sci. Rep.* 9:15728. doi: 10.1038/s41598-019-52035-6

Wang, H., Guo, W., Mitra, J., Hegde, P. M., Vandoorne, T., Eckelmann, B. J., et al. (2018). Mutant FUS causes DNA ligation defects to inhibit oxidative damage repair in Amyotrophic Lateral Sclerosis. *Nat. Commun.* 9:3683. doi: 10.1038/s41467-018-06111-6

Wang, I. F., Guo, B. S., Liu, Y. C., Wu, C. C., Yang, C. H., Tsai, K. J., et al. (2012). Autophagy activators rescue and alleviate pathogenesis of a mouse model with proteinopathies of the TAR DNA-binding protein 43. *Proc. Natl. Acad. Sci. U S A* 109, 15024–15029. doi: 10.1073/pnas.1206362109

Wu, L. S., Cheng, W. C., and Shen, C. K. (2012). Targeted depletion of TDP-43 expression in the spinal cord motor neurons leads to the development of amyotrophic lateral sclerosis-like phenotypes in mice. *J. Biol. Chem.* 287, 27335–27344. doi: 10.1074/jbc.m112.359000

Xiao, A., Wong, J., and Luo, H. (2010). Viral interaction with molecular chaperones: role in regulating viral infection. *Arch. Virol.* 155, 1021–1031. doi: 10.1007/s00705-010-0691-3

Yang, C., Wang, H., Qiao, T., Yang, B., Aliaga, L., Qiu, L., et al. (2014). Partial loss of TDP-43 function causes phenotypes of amyotrophic lateral sclerosis. *Proc. Natl. Acad. Sci. U S A* 111, E1121–E1129. doi: 10.1073/pnas.1322641111

Zhang, K., Daigle, J. G., Cunningham, K. M., Coyne, A. N., Ruan, K., Grima, J. C., et al. (2018). Stress granule assembly disrupts nucleocytoplasmic transport. *Cell* 173, 958.e17–971.e17. doi: 10.1016/j.cell.2018.03.025

Zhang, K., Donnelly, C. J., Haeusler, A. R., Grima, J. C., Machamer, J. B., Steinwald, P., et al. (2015). The C9orf72 repeat expansion disrupts nucleocytoplasmic transport. *Nature* 525, 56–61. doi: 10.1038/nature14973

Zhang, X., Yamashita, S., Hara, K., Doki, T., Tawara, N., Ikeda, T., et al. (2019). A mutant MATR3 mouse model to explain multisystem proteinopathy. *J. Pathol.* 249, 182–192. doi: 10.1002/path.5289

Conflict of Interest: The authors declare that the research was conducted in the absence of any commercial or financial relationships that could be construed as a potential conflict of interest.

frontiers in Molecular Neuroscience

ORIGINAL RESEARCH
published: 23 June 2020
doi: 10.3389/fnmol.2020.00102

Circulating microRNAs Profile in Patients With Transthyretin Variant Amyloidosis

Gian Luca Vita[1†], M'Hammed Aguennouz[2,3†], Francesca Polito[2], Rosaria Oteri[2], Massimo Russo[2], Luca Gentile[2], Cristina Barbagallo[4], Marco Ragusa[4,5], Carmelo Rodolico[2], Rosa Maria Di Giorgio[2], Antonio Toscano[2], Giuseppe Vita[1,2] and Anna Mazzeo[2]*

[1] Nemo Sud Clinical Centre for Neuromuscular Disorders, Messina, Italy, [2] Unit of Neurology and Neuromuscular Diseases, Department of Clinical and Experimental Medicine, University of Messina, Messina, Italy, [3] Mohammed VI University of Health Sciences, Casablanca, Morocco, [4] Molecular, Genome and Complex Systems BioMedicine Unit, Department of Biomedical and Biotechnological Sciences, University of Catania, Catania, Italy, [5] Oasi Research Institute IRCCS, Troina, Italy

Transthyretin variant amyloidosis (ATTRv) is a rare autosomal dominant disease characterized by the accumulation of amyloid in many organs, mostly causing a sensory-motor neuropathy, cardiomyopathy, and dysautonomia. The aim of the study was to report microRNAs (miRNAs) expression profile identified in the blood of ATTRv patients. Ten ATTRv patients, 10 asymptomatic carriers of transthyretin variant (TTRv), 10 patients with Charcot-Marie-Tooth (CMT) disease, and 10 healthy controls were studied. Human Schwann cells cultures were used to study the regulatory effects of miR-150-5p on the expression of cAMP response element-binding protein (CREB), brain-derived neurotrophic factor (BDNF), and nerve growth factor (NGF). ATTRv patients had 33 miRNAs up-regulated and 48 down-regulated versus healthy controls; 9 miRNAs were up-regulated and 30 down-regulated versus CMT patients; 19 miRNAs were up-regulated and 38 down-regulated versus asymptomatic TTRv carriers. Twelve out of the 19 upregulated miRNAs had a fold increase higher than 100. The validation experiment indicated miR-150-5p as a valuable biomarker to differentiate ATTRv patients from asymptomatic TTRv carriers (AUC: 0.9728; $p < 0.0001$). Schwann cells culture model demonstrated that miR-150-5p is a powerful negative regulator of CREB, BDNF, and NGF genes. Identification of deregulated miRNAs can help in understanding the complex pathomechamism underlying the development of ATTRv and related multisystemic pathology. Further investigations are needed on the role of circulating miR-150-5p to predict the shift of TTRv carriers from an asymptomatic status to symptoms appearance.

Keywords: transthyretin, amyloidosis, microRNAs, miR-150-5p, CREB, BDNF, NGF

OPEN ACCESS

Edited by:
Stefano Carlo Previtali, San Raffaele Scientific Institute (IRCCS), Italy

Reviewed by:
Kleopas A. Kleopa, The Cyprus Institute of Neurology & Genetics, Cyprus
John Svaren, University of Wisconsin–Madison, United States

****Correspondence:***
Giuseppe Vita
vitag@unime.it

† These authors share first authorship

Received: *08 March 2020*
Accepted: *12 May 2020*
Published: *23 June 2020*

Citation:
Vita GL, Aguennouz M, Polito F, Oteri R, Russo M, Gentile L, Barbagallo C, Ragusa M, Rodolico C, Di Giorgio RM, Toscano A, Vita G and Mazzeo A (2020) Circulating microRNAs Profile in Patients With Transthyretin Variant Amyloidosis. Front. Mol. Neurosci. 13:102. doi: 10.3389/fnmol.2020.00102

INTRODUCTION

Transthyretin (TTR) variant amyloidosis (ATTRv) is an autosomal dominant disease characterized by the formation and storage of amyloid aggregates in many organs, mostly causing an axonal sensory-motor neuropathy, cardiomyopathy, gastrointestinal dysfunction, and dysautonomia. More than 120 TTR variants (TTRv) are known with several thousand cases worldwide, and organ

involvement and clinical symptoms widely depend on the type of mutation (Adams et al., 2017). A staging system classifies patients into three stages based on severity of symptoms and the extent of disease progression, being stage 1 for symptomatic subjects with unimpaired walking, stage 2 for need of mono- or bilateral walking assistance, and stage 3 for patients relying on a wheelchair to move around. Stage 0 is an asymptomatic stage for subjects who have a TTRv but do not show yet any symptoms of the disease (Adams et al., 2016). Based on phase 3 clinical trials, the effectiveness of current treatment options is limited to stage 1 and 2 ATTRv patients (Vita et al., 2019), so that regular follow-ups are done in asymptomatic carriers to monitor the appearance of the first symptoms and to start treatment (Obici et al., 2016). Several neurophysiological and cardiological markers of early damage have been recently proposed (Jonker et al., 2018; Luigetti et al., 2018; Zouari et al., 2019). At the moment, no biomarker is available to document the progression from an asymptomatic to symptomatic status.

MicroRNAs (miRNAs) are small (20–25 nucleotides), evolutionary conserved, non-coding RNAs which negatively regulate gene expression by binding to the 3'-untranslated region of target mRNAs in a sequence-specific manner, leading to either mRNA degradation or translational repression. They can also positively regulate gene expression by repression of several negative regulators (Kong et al., 2012). They are expressed specifically in different tissues but circulating miRNAs have been recognized in human plasma and serum, since they are passively leaked or actively transported from cells. More specifically, miRNAs play key roles in vital biological processes such as cell division and death, metabolism, intracellular signaling, immunity, and cell movement (Baltimore et al., 2008; Png et al., 2011; Rayner et al., 2011; Ng et al., 2012). In the last years, circulating miRNAs emerged as an interesting new class of biomarkers, being easily measured using common laboratory techniques, with potential clinical relevance for diagnosis and prognosis, to predict responders from non-responders to a given treatment, or even as therapeutic targets (Huang et al., 2017; Molasy et al., 2017; Li et al., 2019; Fattahi et al., 2020). We performed a pilot study to determine whether circulating miRNAs could be identified in the blood of ATTRv patients and if so, whether they are linked to disease stage.

MATERIALS AND METHODS

Blood samples were obtained from 10 ATTRv patients (stage 1 or 2), 10 asymptomatic carriers of TTRv, 5 patients with axonal-type Charcot-Marie-Tooth (CMT) disease type 2 and 5 patients with CMT type 1A as pathological controls, and 10 healthy controls (HC) (**Table 1**). The ATTRv patients and the asymptomatic subjects carried the following TTR mutations: Glu89Gln (n. 4 and n. 4, respectively), Phe64Leu (n. 4 and n. 4), Thr49Ala (n. 2 and n. 2) (Mazzeo et al., 2015). All 10 symptomatic patients presented neuropathy, 5/10 had cardiopathy, and 7/10 had dysautonomia. All were on treatment with tafamidis. Patients had no concomitant major disease, such as diabetes, hypertension, ischemic heart disease, neoplasm, cerebrovascular disease, etc. Local ethics committee approved the study and all subjects gave written informed consent.

TABLE 1 | Populations studied.

	ATTRv patients	Asymptomatic TTRv carriers	CMT patients	Healthy controls
Discovery set				
No.	10	10	10	10
Male/female	5/5	4/6	6/4	5/5
Age (years)	52.8 ± 6.3	44.0 ± 7.0	43.5 ± 18.7	48.0 ± 7.5
Disease duration (years)	6.7 ± 4.0	NA	17.0 ± 14.8	NA
Validation set				
No.	24	23	–	–
Male/female	15/9	10/13	–	–
Age (years)	63.7 ± 12.1	49.1 ± 8.3	–	–
Disease duration (years)	7.7 ± 4.9	NA	–	–

Mean ± SD; NA, not applicable.

Blood samples were withdrawn by venipuncture into BD Vacutainer tubes with a gel separating serum from blood cells. The samples were centrifuged at 3500 RPM for 15 min at 4°C. Supernatant was isolated and centrifuged again to remove circulating cells or debris. Aliquots of serum were stored at −80°C, until analysis.

RNA Isolation

Eight hundred microliter serum samples were used to extract total RNA using Qiagen miRNeasy Mini Kit (Qiagen, GmbH, Hilden, Germany), according to Qiagen Supplementary Procedure for the purification of RNA, including small RNAs. Obtained RNA was eluted in 200 μl RNAse-free water and then precipitated adding 20 μg glycogen, 0.1 volumes 3 M sodium acetate, and 2.5 volumes ice cold 100% ethanol. Following overnight incubation at −80°C, RNA was centrifuged and twice washed in ice cold 75% ethanol and resuspended in 7 μl RNAse-free water. RNA was quantified by Nanodrop.

Circulating miRNA Profiling

Serum miRNA expression profile was done by nCounter Human v3 miRNA Expression Assay Kit (NanoString Technologies; Seattle, WA, United States) in an nCounter FLEX (Prep Station and Digital Analyzer) (NanoString Technologies), according to manufacturer procedures. Three microliter, containing about 100 ng of total RNA, were utilized for sample preparation. Data analysis was made through nSolver 2.6 software (NanoString Technologies). MiRNAs used as endogenous controls were chosen through global median normalization method: we computed Pearson correlation between the count means for each lane and the counts of each miRNA, identifying those miRNAs whose expression was closer to the count mean of the cartridge (miR-23a-3p, miR-1285-5p, miR-451a) (Di Pietro et al., 2018).

Single miRNA qRT validation analysis was performed on 20 ng of total RNA by using single TaqMan® MicroRNA Assays

TABLE 2 | Differentially expressed miRNAs.

	ATTRv patients vs HC		ATTRv patients vs CMT patients		ATTRv patients vs TTRv carriers	
	Fold change	***p*-value**	**Fold change**	***p*-value**	**Fold change**	***p*-value**
hsa-let-7d-5p	2.61	0.003	–	–	1.38	0.02
hsa-let-7i-5p	2.21	0.002	–	–	−50.13	2.51E-09
hsa-miR-10a-5p	–	–	−1.43	0.01	–	–
hsa-miR-15a-5p	–	–	–	–	−1.54	0.02
hsa-miR-19a-3p	−2.43	0.0006	–	–	–	–
hsa-miR-20a-5p + hsa-miR-20b-5p	3.09	0.0006	–	–	–	–
hsa-miR-21-5p	3.5	0.001	2.34	0.006	77.57	0.0001
hsa-miR-22-3p	2.28	0.003	–	–	–	–
hsa-miR-25-3p	−2.03	0.005	–	–	–	–
hsa-miR-26b-5p	2.6	0.001	–	–	2.26	0.0008
hsa-miR-28-5p	–	–	2.68	0.0001	–	–
hsa-miR-30a-5p	−2.38	0.01	–	–	–	–
hsa-miR-33a-5p	−2.42	0.0005	–	–	–	–
hsa-miR-34a-5p	1.74	0.03	–	–	106.74	0.00008
hsa-miR-93-5p	−2.31	0.001	–	–	–	–
hsa-miR-96-5p	1.98	0.03	–	–	−75.21	0.00000253
hsa-miR-107	1.84	0.0006	–	–	104.9	1.69E-08
hsa-miR-124-3p	−2.37	0.002	–	–	–	–
hsa-miR-125a-3p	2.79	0.0006	–	–	–	–
hsa-miR-126-3p	–	–	−3.32	0.001	–	–
hsa-miR-132-3p	−2.09	0.01	–	–	–	–
hsa-miR-133b	−2.22	0.001	–	–	–	–
hsa-miR-138-5p	–	–	−1.85	0.01	–	–
hsa-miR-141-3p	−2.54	0.0004	–	–	–	–
hsa-miR-142-3p	–	–	–	–	−2.25	0.003
hsa-miR-144-3p	−2.15	0.001	−7.97	0.0001	–	–
hsa-miR-146a-5p	1.71	0.01	–	–	−50.56	0.000000411
hsa-miR-146b-5p	–	–	−2.05	0.006	–	–
hsa-miR-147a	−2.61	0.001	–	–	–	–
hsa-miR-150-5p	1.6	0.02	1.7	0.03	109.23	0.00000111
hsa-miR-181a-5p	–	–	−1.61	0.003	–	–
hsa-miR-181b-2-3p	–	–	−2.23	0.0006	–	–
hsa-miR-184	–	–	–	–	−50.41	0.00000111
hsa-miR-188-5p	−1.78	0.001	−1.87	0.001	–	–
hsa-miR-190a-3p	−1.91	0.004	–	–	–	–
hsa-miR-196a-5p	–	–	−1.77	0.001	–	–
hsa-miR-199a-3p + hsa-miR-199b-3p	−2.68	0.008	–	–	–	–
hsa-miR-200a-3p	–	–	−1.69	0.0003	–	–
hsa-miR-206	1.58	0.008	–	–	−50.33	0.00000183
hsa-miR-208b-3p	2	0.0004	–	–	68.44	0.0000031
hsa-miR-210-3p	−2.15	0.003	–	–	–	–
hsa-miR-215-5p	2.13	0.006	–	–	101.96	0.000000688
hsa-miR-216a-5p	−1.74	0.002	–	–	–	–
hsa-miR-216b-5p	–	–	−1.92	0.0005	–	–
hsa-miR-219b-3p	−2.43	0.0002	–	–	−53.14	0.00000127
hsa-miR-223-3p	1.98	0.002	–	–	–	–
hsa-miR-224-5p	–	–	−1.37	0.006	–	–
hsa-miR-302e	−2.18	0.003	–	–	−50.21	0.00000535
hsa-miR-320a	−2.14	0.003	–	–	–	–

(Continued)

TABLE 2 | Continued

	ATTRv patients vs HC		ATTRv patients vs CMT patients		ATTRv patients vs TTRv carriers	
	Fold change	***p*-value**	**Fold change**	***p*-value**	**Fold change**	***p*-value**
hsa-miR-320e	−2.33	0.02	–	–	–	–
hsa-miR-323b-3p	−5.09	0.0008	−2.1	0.0002	−70.23	0.000002
hsa-miR-328-5p	2.52	0.002	–	–	–	–
hsa-miR-335-5p	2.04	0.009	–	–	–	–
hsa-miR-339-5p	–	–	−1.8	0.0005	–	–
hsa-miR-363-5p	1.81	0.04	–	–	65.44	0.0001
hsa-miR-376a-3p	–	–	−1.92	0.04	–	–
hsa-miR-378d	–	–	−1.95	0.01	–	–
hsa-miR-378i	2.2	0.0001	–	–	−70.11	0.000006
hsa-miR-411-5p	−2.14	0.02	–	–	−2.01	0.004
hsa-miR-422a	−2.42	0.0002	–	–	–	–
hsa-miR-450a-2-3p	−2.24	0.0005	–	–	−50.19	0.00001
hsa-miR-452-5p	−2.27	0.002	–	–	–	–
hsa-miR-495-3p	1.79	0.03	–	–	−50.28	0.00006
hsa-miR-497-5p	2.27	0.01	–	–	51.81	0.00000106
hsa-miR-514b-5p	–	–	–	–	−52.12	0.00000956
hsa-miR-518c-3p	−3.17	0.001	–	–	–	–
hsa-miR-518d-3p	−2.87	0.0002	–	–	–	–
hsa-miR-526a + hsa-miR-518c-5p + hsa-miR-518d-5p	–	–	–	–	−71.41	0.00000121
hsa-miR-548ad-3p	−1.74	0.0008	−2.06	0.0009	−71.2	0.000000891
hsa-miR-548ah-5p	−2.04	0.01	–	–	−51.94	0.00006
hsa-miR-548ar-3p	−1.76	0.0008	–	–	−50.16	0.00007
hsa-miR-566	–	–	–	–	−70.31	0.000000465
hsa-miR-575	2.02	0.01	3.24	0.001	108.57	0.0001
hsa-miR-584-5p	–	–	2.62	0.008	–	–
hsa-miR-585-3p	1.76	0.01	–	–	−1.7	0.0003
hsa-miR-587	2.44	0.006	–	–	102.39	0.00003
hsa-miR-593-3p	–	–	−1.89	0.0001	–	–
hsa-miR-598-3p	−2.02	0.002	–	–	–	–
hsa-miR-603	2.49	0.03	–	–	–	–
hsa-miR-607	−2.11	0.01	–	–	–	–
hsa-miR-612	−2.06	0.0002	−1.71	0.0001	–	–
hsa-miR-637	−2	0.0006	–	–	–	–
hsa-miR-663a	–	–	–	–	−72.96	0.00000086
hsa-miR-758-5p	−2.72	0.01	–	–	–	–
hsa-miR-802	–	–	–	–	−71.52	0.00000551
hsa-miR-873-3p	−2.44	0.005	−1.43	0.0004	−71	8.67E-08
hsa-miR-876-3p	1.53	0.009	–	–	121.29	0.00001
hsa-miR-877-5p	−2.03	0.0005	–	–	117.34	0.0001
hsa-miR-887-5p	8.68	0.0002	–	–	–	–
hsa-miR-889-3p	1.75	0.001	2.11	0.0002	112.77	9.41E-14
hsa-miR-891b	−1.51	0.001	–	–	66.38	0.000000747
hsa-miR-922	−2.21	0.03	–	–	−57.32	0.00000241
hsa-miR-933	–	–	−1.51	0.003	–	–
hsa-miR-936	−2.09	0.0001	–	–	−50.35	0.000000841
hsa-miR-941	–	–	−1.85	0.002	–	–
hsa-miR-1185-1-3p	−2.1	0.005	–	–	–	–
hsa-miR-1185-2-3p	−2.8	0.0001	–	–	−2.32	0.003
hsa-miR-1261	−2.36	0.01	–	–	–	–

(Continued)

TABLE 2 | Continued

	ATTRv patients vs HC		ATTRv patients vs CMT patients		ATTRv patients vs TTRv carriers	
	Fold change	***p*-value**	**Fold change**	***p*-value**	**Fold change**	***p*-value**
hsa-miR-1268b	−2.21	0.0005	–	–	−53.52	0.000000168
hsa-miR-1277-3p	2.75	0.01	–	–	–	–
hsa-miR-1279	3.07	0.006	–	–	119.18	0.00001
hsa-miR-1285-3p	–	–	–	–	−2.18	0.003
hsa-miR-1287-5p	1.8	0.009	2.53	0.002	104.7	0.000000611
hsa-miR-1296-3p	5.93	0.001	–	–	−61.1	4.61E-17
hsa-miR-1304-3p	–	–	−2.05	0.0003	–	–
hsa-miR-1304-5p	−2.28	0.001	2.03	0.01	102.09	0.0005
hsa-miR-1322	−2.37	0.006	–	–	–	–
hsa-miR-1827	–	–	1.73	0.03	−1.96	0.001
hsa-miR-1972	–	–	–	–	−52.55	9.26E-08
hsa-miR-2117	–	–	−2.1	0.03	–	–
hsa-miR-3168	–	–	–	–	−73.46	7.01E-08
hsa-miR-3614-5p	–	–	–	–	−1.81	0.0004
hsa-miR-3615	–	–	−1.86	0.002	–	–
hsa-miR-3928-3p	–	–	−1.59	0.0004	–	–
hsa-miR-4421	–	–	−1.5	0.02	−59.22	0.00000135
hsa-miR-4454 + hsa-miR-7975	−2.17	0.005	–	–	−2.2	0.04
hsa-miR-4516	–	–	–	–	−1.67	0.01
hsa-miR-4536-5p	−2.03	0.001	–	–	–	–
hsa-miR-4787-5p	–	–	–	–	−70.66	0.000000199
hsa-miR-5010-3p	–	–	−1.52	0.002	–	–
hsa-miR-6720-3p	–	–	−2.1	0.0002	–	–
hsa-miR-6721-5p	–	–	−1.54	0.0006	–	–

(Applied Biosystems) in a 7300 Real time PCR instrument (Thermo Fisher Scientific, Waltham, MA, United States), according to the manufacturer's instructions. Expression fold changes were calculated by the $2^{-\Delta\Delta CT}$ method by using RNU6 as reference genes. All assays were performed in triplicate.

Gene Ontology and Pathway Enrichment Analysis

To investigate the effects of the deregulation of miRNAs, a gene ontology (GO) analysis was performed following two parallel approaches. Experimentally validated targets of upregulated miRNAs were retrieved from TarBase v7.0[1]. The resulting list of mRNA targets was used as input for the TopGO v2.24.0 package, which analyzes the GO database. Moreover, upregulated miRNAs were submitted to the tool DIANA mirPath v3.0[2], which performed a pathway enrichment analysis according to the Kyoto Encyclopedia of Genes and Genomes (KEGG). DIANA mirPath was performed on experimentally validated miRNA targets retrieved from Tarbase v7.0 by appling FDR correction ($p < 0.05$, MicroT < 0.8) and Fisher's Exact Test (Hypergeometric Distribution).

[1]http://www.microrna.gr/tarbase

[2]http://snf-515788.vm.okeanos.grnet.gr/

Cell Culture

Human primary Schwann cells (SCs) (ABM Good, Richmond, Canada) were cultured in Prigrow X series medium (ABM Good) containing 10% fetal bovine serum (Gibco, Gaithersburg, MD, United States), 100 μg/ml streptomycin, and 100 IU/ml penicillin (Sigma, St. Louis, MO, United States) at 37°C in a 5% CO_2 humidified atmosphere. The cells were subcultured every 2–3 days.

miRNA Transfections

miR-150-5p mimic/inhibitor (ID MC10070/MH10070; Thermo Fisher Scientific) were transfected into human primary SCs using siPORT Lipid Transfection Reagent (Thermo Fisher Scientific) according to the manufacturer's procedure. Cells were transfected with 50 nmol of oligonucleotide per well (0.5×10^6 cells). Transfected cells were assayed 24 and 48 h after the transfection.

Western Blot Analysis

SCs samples were processed in lysis buffer (25 mM Tris/HCL, pH 7.4, 1.0 mM EGTA, 1.0 mM ethylen diamine tetraacetic acid (EDTA), protease, and phosphatase inhibitors) and total proteins concentration was determined using the Bio-Rad protein assay kit (Bio-Rad, Richmond, CA, United States).

TABLE 3 | GO analysis of targets of upregulated miRNAs found in ATTRv patients vs TTRv carriers.

Category	Term	Count	*p*-value	FDR
Biological process	GO:0007399~nervous system development	175	7.89E-12	1.75E-08
	GO:0065008~regulation of biological quality	174	6.25E-11	6.78E-09
	GO:0023051~regulation of signaling	176	4.12E-12	6.81E-09
	GO:0007167~enzyme linked receptor protein signaling pathway	105	2.33E-11	4.26E-08
	GO:0010604~positive regulation of macromolecule metabolic process	198	2.72E-11	5.34E-08
	GO:0010646~regulation of cell communication	148	2.22E-09	2.23E-09
Molecular function	GO:0070491~repressing transcription factor binding	124	2.54E-11	6.57E-09
	GO:0061659~ubiquitin-like protein ligase activity	118	3.12E-10	3.21E-09
	GO:0019899~enzyme binding	122	0.00000179	1.18E-09
	GO:0019904~protein domain specific binding	108	0.00000358	1.26E-08
	GO:0005057~receptor signaling protein activity	48	2.98E-08	0.0000451
	GO:0140096~catalytic activity, acting on a protein	57	3.01E-08	3.23E-09
Cellular components	GO:0070062~extracellular exome	178	2.98E-11	2.88E-09
	GO:0044451~nucleoplasm part	122	0.00000184	1.21E-09
	GO:0044424~intracellular part	52	0.00000181	1.18E-08
	GO:0005057~receptor signaling protein activity	68	2.11E-08	0.0000374

TABLE 4 | KEGG pathway analysis of targets of upregulated miRNAs found in ATTRv patients vs TTRv carriers.

KEGG pathways	Count	*p*-value	FDR
hsa04360: Axon guidance	78	0.0000083	0.0000531
hsa04010: MAPK signaling pathway	58	0.0000287	0.0000019
hsa04068: FoxO signaling pathway	62	0.0000482	0.0000021

Thirty micrograms of proteins were resolved by SDS-PAGE, separated by electrophoresis, and blotted onto PVDF membrane (Amersham Bioscience, Amersham, United Kingdom). Membranes were incubated with specific antibodies against cAMP response element-binding protein (CREB) (1:200; catalog #sc-240; Santa Cruz Biotechnology, CA, United States), brain-derived neurotrophic factor (BDNF) (1:200; catalog #sc-65514; Santa Cruz Biotechnology), or nerve growth factor (NGF) (1:500; catalog #MA5-32067; Invitrogen, Waltham, MA, United States). Equal loading of protein was assessed on stripped blots by immunodetection of β-actin (1:500; Abcam, Cambridge, MA, United States). For all primary antibodies, a peroxidase-conjugated goat anti-rabbit immunoglobulin G secondary antibody was used at concentration of 1:10,000 (catalog #G-21234; Pierce, Chester, United Kingdom). Signals were detected using Amersham ECL Plus Western Blotting Detection Reagents (Amersham Bioscience). Computer-assisted densitometry (UN-SCAN-IT gel version 6.1; Silk Scientific, Inc., Orem, UT, United States) was used to perform semi-quantitative analysis of protein expression detected by immunoblotting. Different times of exposure were used for each blot. β-actin signal was used to normalize protein levels. Integrated density values were expressed as a percentage of densitometric levels using arbitrary densitometric units (Vita et al., 2018).

Real Time-Quantitative Polymerase Chain Reaction (RT-qPCR)

Total RNA was isolated with Trizol Reagent (Invitrogen) according to the manufacturer's protocol. Five micrograms of RNA from each sample were reversely transcribed using High-Capacity cDNA Archive Kit (Applied Biosystems, Foster City, CA, United States). Generated cDNA was used as a template for RT-qPCR analysis. Briefly, for each reaction, 4 μl of cDNA in a total volume of 50 μl were used. 7300 Sequence Detection System apparatus (Applied Biosystems) was managed to quantitatively compare the mRNA levels; 20X target primer and probe (BDNF: HS02718934; NGF: HS00171458; CREB: HS00231713) were processed, and human β-actin (Cod.4326315E) was used as a house-keeping gene (Thermo Fisher Scientific). RT-qPCR was done in duplicate with 2 × TaqMan Universal PCR Master Mix. The thermal cycling conditions were as following: 10′ at 25°C, 120′ at 37°C, and then hold at 4°C. The comparative cycle threshold (Ct) procedure (Applied Biosystems) was used to analyze the data by generating relative values of target cDNA level. Relative quantification (RQ) was expressed as fold change over control, and calculated by the ΔΔCt method, with control samples as calibrators.

Statistical Analysis

For NanoString analysis, fold change (FC) expression changes between two groups were calculated by using nSolver v2.5 (NanoString Technologies) ratio data, based on normalized count data. *p* values between two groups were generated using a two-tailed t-test. Statistical analysis was done through Significance of Microarrays Analysis[3], using a *p* value based on 100 permutations; imputation engine: K-nearest neighbors (10 neighbors); false discovery rate (FDR) <0.05. Quantitative

[3]http://www.tm4.org

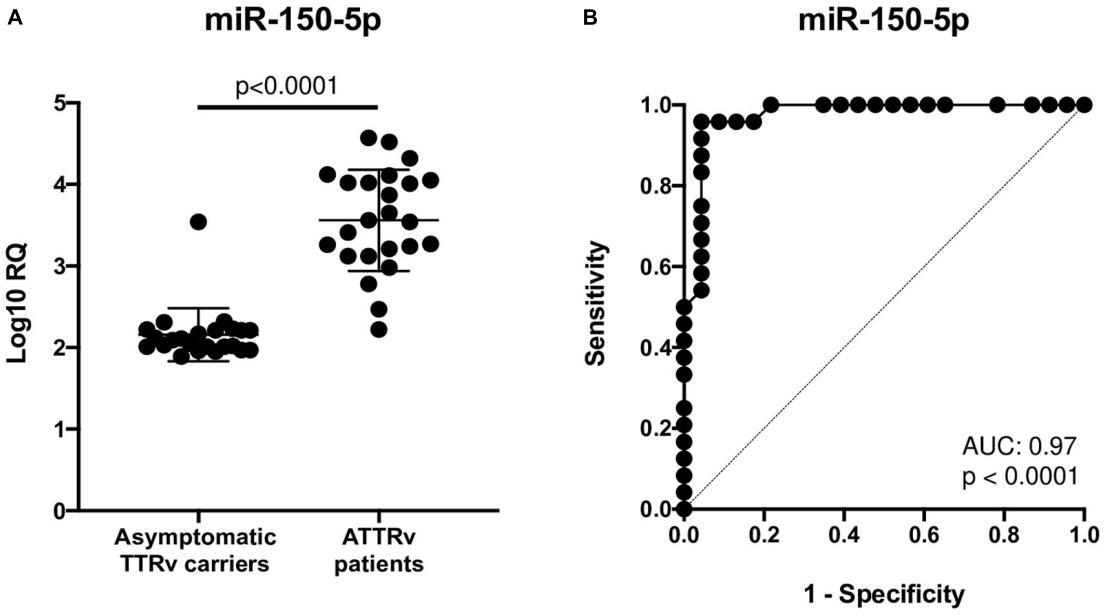

FIGURE 1 | Expression levels of circulating miR-150-5p in 23 asymptomatic TTRv carriers and 24 ATTRv patients **(A)**. Receiver operating characteristic (ROC) curve analysis of miR-150-5p **(B)**. AUC resulted 0.9728 (95% CI: 0.9285–1.000). At the cutoff value of 2.395, sensitivity and specificity were 95.8 and 95.6%, respectively.

RT-qPCR microRNA expression was assessed using SDS v2.4 software (Thermo Fisher Scientific) and analyzed using GraphPad Prism version 8.3.0. Results are expressed as mean ± standard deviation (SD). Receiver operating characteristic (ROC) analysis was used to assess the performance of miRNA as a binary expression status in symptomatic and asymptomatic carriers of TTRv. The area under the ROC curve (AUC) was also determined. Statistical multiple comparison between groups was performed by Kruskal-Wallis non-parametric ANOVA test. Comparison between groups was performed by Mann-Whitney test for unpaired non-parametric data. A level of significance of $p < 0.05$ was considered.

RESULTS

Among up to 800 biologically relevant miRNAs, 33 miRNAs were found significantly up-regulated and 48 down-regulated in the serum of ATTRv patients versus HC. Nine miRNAs were significantly up-regulated and 30 down-regulated in ATTRv patients versus CMT patients. With the aim to find differences between ATTRv patients versus asymptomatic carriers of TTRv, expression analysis led to identify 19 miRNAs significantly up-regulated and 38 miRNAs down-regulated in patients versus asymptomatic carriers. Twelve out of the 19 upregulated miRNAs had a fold increase higher than 100 (**Table 2**; GEO Series accession number GSE149665).

Bioinformatic analysis of upregulated miRNAs found in ATTRv patients vs TTRv carriers revealed that the target genes were involved in a variety of cellular functions. The top significantly related GO terms are listed in **Table 3**. The KEGG analysis showed the involvement of the upregulated target genes in important pathways such as axon guidance, the mitogen-activated protein kinase (MAPK) cascade, and the forkhead box O (FOXO) family of transcription factors, the last two being involved in proliferation, apoptosis, differentiation, and cell-cycle control (**Table 4**).

After a database search and literature review of the twelve most up-regulated miRNAs in ATTRv patients versus asymptomatic carriers of TTRv, miR-150-5p was selected for further validation. miR-150-5p expression was measured by RT-qPCR in the serum of n. 24 ATTRv patients and n. 23 asymptomatic carriers of TTRv (**Table 1**). The results revealed that miR-150-5p was significantly up-regulated in patients compared with asymptomatic carriers (**Figure 1A** and **Supplementary Table S1**). ROC curve analysis indicated that miR-150-5p was a valuable serum biomarker for differentiating with an AUC of 0.9728 (95% CI: 0.9285–1.000). At the cutoff value of 2.395, sensitivity and specificity were 95.8 and 95.6%, respectively (**Figure 1B**).

Since in ATTRv mutated transthyretin aggregates and forms amyloid fibrils in target organs, chiefly the peripheral nervous system and the heart, the expression of three regulators of neuronal growth, differentiation, survival and regeneration, such as CREB, BDNF and NGF, which are also involved in cardiac dysfunction, were investigated in human SCs cultures transfected by miR-150-5p mimic/inhibitor. Treatment with miR-150-5p mimic markedly increased the miR-150-5p expression by around 30-fold when compared to control ($p < 0.0001$), whereas treatment with miR-150-5p inhibitor suppressed its expression ($p < 0.0001$) (**Figure 2**). CREB protein and mRNA levels decreased after transfection of miR-150-5p mimic by almost 6-fold ($p < 0.0001$) and almost 4-fold ($p < 0.0001$), respectively

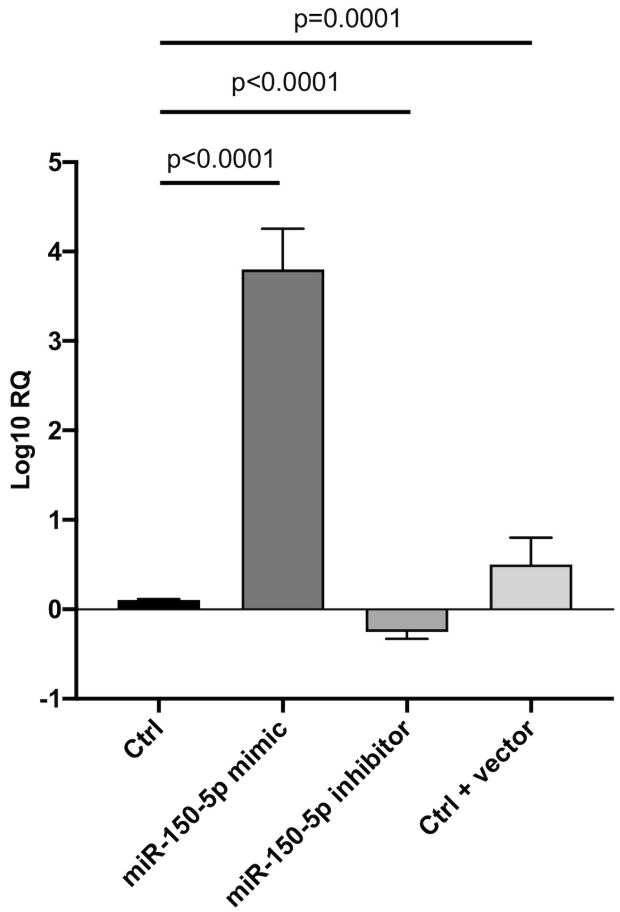

FIGURE 2 | Transfection of miR-150-5p mimic and inhibitor into human primary Schwann cells and its effect on miR-150-5p expression. Non-parametric ANOVA Kruskal-Wallis test $p < 0.0001$.

(**Figure 3**). BDNF protein and mRNA levels were decreased after transfection of miR-150-5p mimic by almost 4-fold ($p < 0.0001$) and almost 4-fold ($p < 0.0001$), respectively (**Figure 4**). NGF protein and mRNA levels reduced after transfection of miR-150-5p mimic by 2-fold ($p < 0.0001$) and 2-fold ($p < 0.0001$), respectively (**Figure 5**). Data from SCs culture experiments are listed in **Supplementary Table S2**.

DISCUSSION

Protein TTR misfolding and tissue deposition of amyloid start many years before the appearance of the first symptoms in ATTRv (Arbustini and Merlini, 2014; Adams et al., 2019). This phenomenon leads to the opportunity and the need to identify novel biomarkers to detect earlier phases of the disease and to permit prompter disease treatment. Since several studies have reported the presence of inflammation in ATTRv nerve biopsies, some inflammatory markers have been recently investigated in serum. TNF-α, IFN-β, IL-1β, IL-8, IL-10, and IL-33 were found increased in patients versus healthy controls, but high levels of IL-33, IL-1β, and IL-10 were already seen in stage 0 asymptomatic carriers. Although it is unclear whether such a pattern of inflammatory cytokines is primarily related to the disease pathogenesis or is a secondary effect of tissue damage or to circulating oligomers, it confirms that the body is reacting to the disease much before amyloid deposition or tissue damage take place (Azevedo et al., 2019).

Circulating miRNAs have been investigated in patients with ATTRv and wild type ATTR (ATTRwt) cardiomyopathy. Validation experiments led to the identification of up-regulated miR-339-3p only in ATTRwt but not in patients with heart failure of other origin or with ATTRv, supporting it as a potential candidate biomarker for ATTRwt (Derda et al., 2018). Our pilot study was performed with the main aim to distinguish miRNAs profile between stage 0 and stage 1–2 in subjects carrying a TTR mutation. We found many candidates deregulated in ATTRv patients versus healthy controls, versus CMT patients and versus asymptomatic carriers of TTRv. Our attention was drawn on 12 miRNAs significantly up-regulated with a fold increase higher than 100 in ATTRv patients versus asymptomatic TTRv carriers. Among them, we focused on miR-150-5p and aimed to validate our results and to look for possible pathomechanisms.

MiR-150-5p is expressed in many tissues, with greater distribution in pancreas, lymph nodes, spleen, vascular system, respiratory system, prostate, esophagus, kidney, thyroid, and also in peripheral nerves and myocardium (Ludwig et al., 2016). It regulates various immune cell functions via apoptosis, survival, and proliferation, controlling immune response and inflammatory cytokines, and also plays an important role in the pathogenesis of both solid and hematological cancers (Wu et al., 2010; Jiang et al., 2012; Sang et al., 2016). No data are so far available in the literature about miR-150-5p expression either in different components of normal nerves, i.e., the axon-myelin unit, or in nerves and heart from ATTRv patients or animal models. The miR-150-5p up-regulation found in this study was tested in a larger separate validation cohort and ROC analysis allowed to confirm the discrimination ability of miR-150-5p to differentiate ATTRv patients from asymptomatic carriers of TTRv, with high sensitivity and specificity. Some studies have investigated the different ability of laboratory and instrumental tests to detect early heart involvement and predict clinical worsening in subjects carrying a TTRv but yet completely asymptomatic who have been serially followed-up (Glaudemans et al., 2014; Hutt et al., 2017; Minutoli et al., 2019). Similarly, the discovery of a non-invasive sensitive biomarker specific for ATTRv patients, as supported by present results, needs now to be further validated longitudinally in a large cohort of asymptomatic carriers of TTRv to identify the time of increased expression of serum miR-150-5p and to verify its possible capability to anticipate the appearance of clinical symptoms. If the latter will be confirmed, this could be a strong argument in favor of an early start of now available innovative treatments (Vita et al., 2019) in still asymptomatic carriers.

How increased expression of miR-150-5p could play a pathophysiological role in ATTRv is lacking in the scientific literature, although some findings have been reported regarding

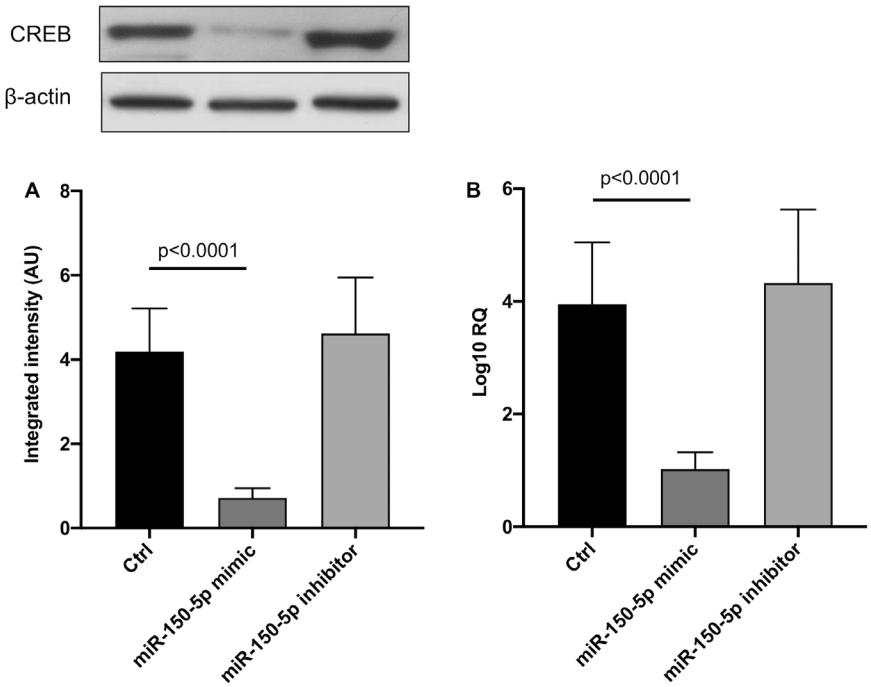

FIGURE 3 | CREB protein **(A)** and mRNA **(B)** levels in transfected human primary Schwann cells. **(A)** Lower panel shows graph with quantitative data; upper panel shows representative autoradiograms. Independent experiments were performed in triplicate. Non-parametric ANOVA Kruskal-Wallis test $p < 0.0001$ in both experiments.

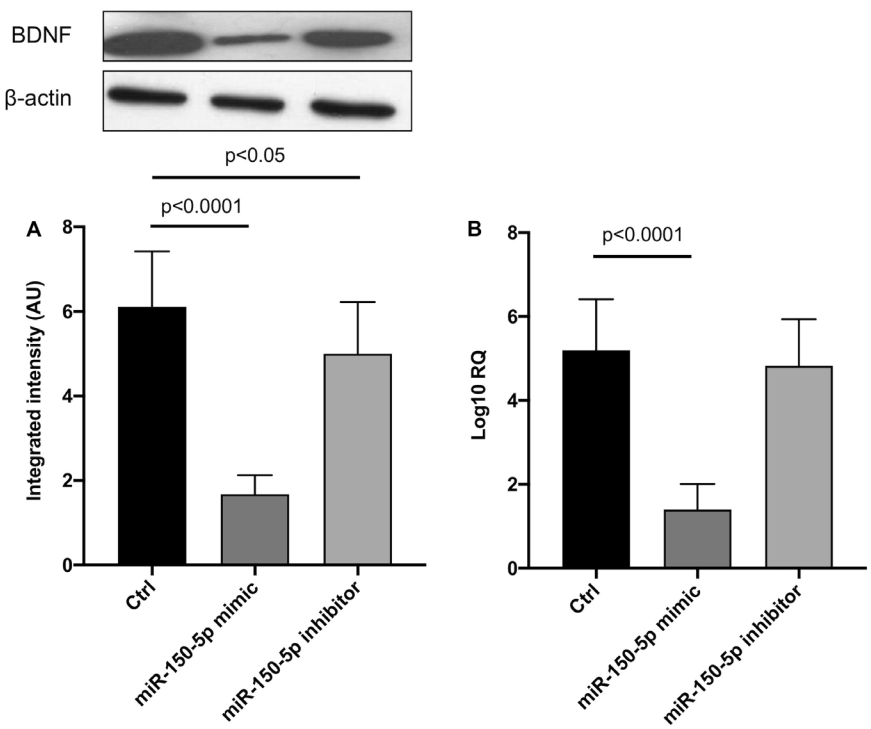

FIGURE 4 | BDNF protein **(A)** and mRNA **(B)** levels in transfected human primary Schwann cells. **(A)** Lower panel shows graph with quantitative data; upper panel shows representative autoradiograms. Independent experiments were performed in triplicate. Non-parametric ANOVA Kruskal-Wallis test $p < 0.0001$ in both experiments.

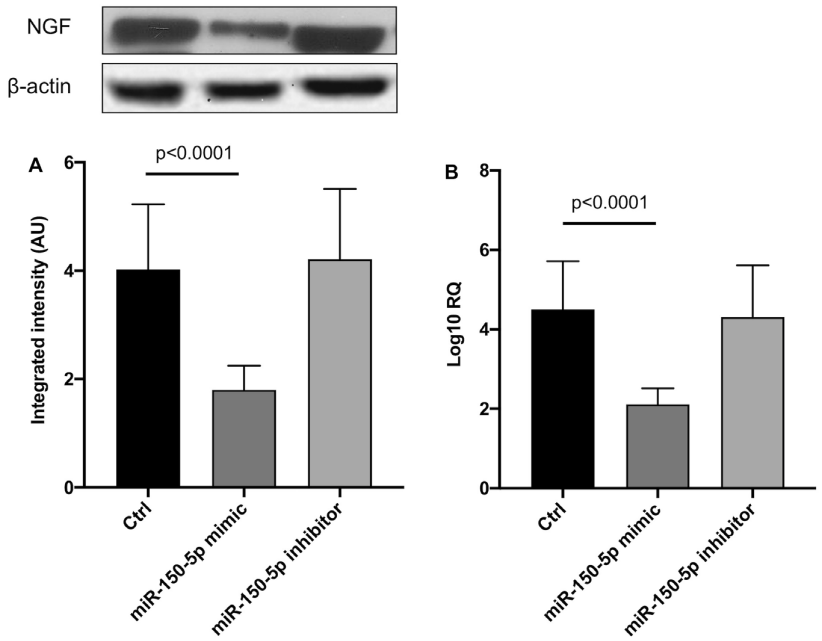

FIGURE 5 | NGF protein **(A)** and mRNA **(B)** levels in transfected human primary Schwann cells. **(A)** Lower panel shows graph with quantitative data; upper panel shows representative autoradiograms. Independent experiments were performed in triplicate. Non-parametric ANOVA Kruskal-Wallis test $p < 0.0003$ and $p < 0.0005$, respectively.

other neurodegenerative and cardiac diseases. Decreased plasma miR-150-5p levels have been found in patients with Alzheimer disease (AD) versus healthy controls (Lugli et al., 2015). Increased levels were observed in hippocampal neurons of prion-infected mice and in synaptoneurosomes from prion-infected mouse forebrain, both at terminal stage of the disease (Majer et al., 2012; Boese et al., 2016). Evidences were provided that increased miR-150 levels found in Purkinje neurons of the mouse model of spinocerebellar ataxia type 1 may modulate disease pathogenesis by targeting the expression of RGS8 and VEGFA genes (Rodriguez-Lebron et al., 2013). Moreover, circulating miR-150 was up-regulated in workers with carbon disulfide neuropathy (Guo et al., 2015), and miR-150-5p down-regulated in patients with advanced heart failure (Scrutinio et al., 2017). So, we decided to investigate the possible crosstalk between miR-150-5p and three different factors, CREB, BDNF, and NGF, whose roles in central and peripheral nervous systems and in the heart are known, using a cell culture model. Human primary SCs cultures were chosen as an easy model on the evidence of miR-150-5p expression in nerves (Ludwig et al., 2016). Although peripheral nerve involvement occurring in ATTRv is mainly an axonal type of neuropathy, SCs are known to participate with an active role during axonal degeneration, although through still poorly understood molecular and cellular mechanisms (Wong et al., 2017).

CREB has a multifaceted role in the nervous system, mostly in neurodevelopment, synaptic plasticity, and neuroprotection (Sakamoto et al., 2011). Recent evidences have been presented supporting the possibility that a dysregulation of CREB signaling is associated to cerebral amyloidosis, formation of tangle-like structures and microglial clustering, and cognitive decline in AD and its animal model (Kempf et al., 2016; Bartolotti and Lazarov, 2019). Moreover, CREB protein family of transcription factors is involved in cardiac growth, ventricular remodeling, and heart failure (Kobrinsky et al., 2011; Kreusser and Backs, 2014; Zhou et al., 2018).

BDNF plays a key role in neurogenesis and synaptic repair and is implicated in numerous neurodegenerative disorders (Bawari et al., 2019). Low plasma BDNF levels have been found significantly associated with brain amyloid burden measured with Pittsburg Compound B in AD and mild cognitive impairment patients, supporting a pathogenic and a peripheral signature role of BDNF (Hwang et al., 2015). Equally BDNF is a focal growth factor which regulates the response of cardiovascular system to acute and chronic injury, modulating contractility, neoangiogenesis, apoptosis and survival of cardiac myocytes, vascular muscle cells, and endothelial cells (Kermani and Hempstead, 2019).

Finally, NGF is the firstly discovered and best characterized neurotrophic factor, able to stimulate neuronal growth and differentiation in central, peripheral, and sympathetic nervous systems (Freed, 1976; Aloe et al., 2015). Likewise, NGF plays a role in cardiac physiopathology. Its levels increase following myocardial injury, most likely leading to sympathetic nerve sprouting, but decrease when heart failure develops, an event that may participate to defective innervation and cardiac failure (Govoni et al., 2011).

MiRNAs are important post-transcriptional regulators which participate to axonal guidance in the central nervous system, and to proliferation and migration of SCs and axonal growth in the

peripheral nervous system (Wang et al., 2019). Our SCs culture model allowed to demonstrate for the first time that miR-150-5p is a powerful negative regulator of CREB gene, BDNF gene, and, to a lesser extent, NGF gene expression, providing an additional basis for further investigations of their role in neurodegeneration and specifically in ATTRv pathogenesis.

This pilot study has some limits. One is the small sample size, but we have to consider that ATTRv amyloidosis is a rare disease and an exclusion criterion was the presence of concomitant major disease. Moreover, 12 miRNAs were found up-regulated with a fold increase higher than 100 in ATTRv patients versus asymptomatic TTRv carriers. However, we concentrated on one of them, miR-150-5p, in this study, with the aim to validate it and to look for associated pathophysiology. Nevertheless, all the others miRNAs have a translational potential and may point to future directions in the analysis of this emerging class of biomarkers. Furthermore, the biological basis of our observations in SCs culture needs to be confirmed in other experimental models.

In conclusion, identification of dysregulated miRNAs can help in understanding the complex pathomechamism underlying the development of ATTRv and related multisystemic pathology. The current results showed that some miRNAs are up-regulated and other down-regulated in stage 1-2 ATTRv patients versus stage 0 subjects. Serum level of miR-150-5p were able to well discriminate stage 1-2 versus stage 0. Our SCs culture model demonstrated that miR-150-5p may modulate the expression of CREB, BDNF and NGF genes, supporting their role in ATTRv pathogenesis. Further investigations on the role of circulating miR-150-5p to predict the shift of TTRv carriers from stage 0 to stage 1 are needed. Moreover, another future line of investigation should examine whether miR-150-5p circulating levels are responsive to the innovative treatments now available.

DATA AVAILABILITY STATEMENT

The datasets generated for this study are available on request to the corresponding author.

ETHICS STATEMENT

The study was approved by Comitato Etico di Messina, AOU Policlinico "G. Martino", Messina, Italy. The patients/participants provided their written informed consent to participate in this study.

AUTHOR CONTRIBUTIONS

GLV, M'HA, CR, RD, AT, GV, and AM contributed to the conception and design of the study. GLV, M'HA, FP, RO, MRu, LG, CB, MRa, RD, GV, and AM contributed to the acquisition and analysis of data. GLV, M'HA, FP, RO, MRu, LG, CB, MRa, CR, RD, AT, GV, and AM contributed to drafting the text and preparing the figures. All authors approved the final version.

FUNDING

The present study was supported by a Research Grant to University of Messina from Pfizer Inc. Pfizer Inc. had no role in the study design, data analysis, and results interpretation of the present study.

SUPPLEMENTARY MATERIAL

The Supplementary Material for this article can be found online at: https://www.frontiersin.org/articles/10.3389/fnmol.2020.00102/full#supplementary-material

List of miRNAs expressed in the single subjects has been deposited in NCBI's Gene Expression Omnibus and is accessible through GEO Series accession number GSE149665 (https://www.ncbi.nlm.nih.gov/geo/query/acc.cgi?acc~=~GSE149665).

TABLE S1 | Data from validation set.

TABLE S2 | Data from Schwann cells culture experiments.

REFERENCES

Adams, D., Cauquil, C., and Labeyrie, C. (2017). Familial amyloid polyneuropathy. *Curr. Opin. Neurol.* 30, 481–489. doi: 10.1097/WCO.0000000000000476

Adams, D., Koike, H., Slama, M., and Coelho, T. (2019). Hereditary transthyretin amyloidosis: a model of medical progress for a fatal disease. *Nat. Rev. Neurol.* 15, 387–404. doi: 10.1038/s41582-019-0210-4

Adams, D., Suhr, O. B., Hund, E., Obici, L., Tournev, I., Campistol, J. M., et al. (2016). First European consensus for diagnosis, management, and treatment of transthyretin familial amyloid polyneuropathy. *Curr. Opin. Neurol.* 29(Suppl. 1), S14–S26. doi: 10.1097/WCO.0000000000000289

Aloe, L., Rocco, M. L., Balzamino, B. O., and Micera, A. (2015). Nerve growth factor: a focus on neuroscience and therapy. *Curr. Neuropharmacol.* 13, 294–303. doi: 10.2174/1570159x13666150403231920

Arbustini, E., and Merlini, G. (2014). Early identification of transthyretin-related hereditary cardiac amyloidosis. *JACC Cardiovasc. Imaging* 7, 511–514. doi: 10.1016/j.jcmg.2014.03.007

Azevedo, E. P., Guimaraes-Costa, A. B., Bandeira-Melo, C., Chimelli, L., Waddington-Cruz, M., Saraiva, E. M., et al. (2019). Inflammatory profiling of patients with familial amyloid polyneuropathy. *BMC Neurol.* 19:146. doi: 10.1186/s12883-019-1369-4

Baltimore, D., Boldin, M. P., O'Connell, R. M., Rao, D. S., and Taganov, K. D. (2008). MicroRNAs: new regulators of immune cell development and function. *Nat. Immunol.* 9, 839–845. doi: 10.1038/ni.f.209

Bartolotti, N., and Lazarov, O. (2019). CREB signals as PBMC-based biomarkers of cognitive dysfunction: a novel perspective of the brain-immune axis. *Brain Behav. Immun.* 78, 9–20. doi: 10.1016/j.bbi.2019.01.004

Bawari, S., Tewari, D., Argüelles, S., Sah, A. N., Nabavi, S. F., Xu, S., et al. (2019). Targeting BDNF signaling by natural products: novel synaptic repair therapeutics for neurodegeneration and behavior disorders. *Pharmacol. Res.* 148:104458. doi: 10.1016/j.phrs.2019.104458

Boese, A. S., Saba, R., Campbell, K., Majer, A., Medina, S., Burton, L., et al. (2016). MicroRNA abundance is altered in synaptoneurosomes during prion disease. *Mol. Cell. Neurosci.* 71, 13–24. doi: 10.1016/j.mcn.2015.12.001

Derda, A. A., Pfanne, A., Bär, C., Schimmel, K., Kennel, P. J., Xiao, K., et al. (2018). Blood-based microRNA profiling in patients with cardiac amyloidosis. *PLoS One* 13:e0204235. doi: 10.1371/journal.pone.0204235

Di Pietro, V., Porto, E., Ragusa, M., Barbagallo, C., Davies, D., Forcione, M., et al. (2018). Salivary microRNAs: diagnostic markers of mild traumatic brain injury in contact-sport. *Front. Mol. Neurosci.* 11:290. doi: 10.3389/fnmol.2018.00290

Fattahi, M., Eskandari, N., Sotoodehnejadnematalahi, F., Shaygannejad, V., and Kazemi, M. (2020). Comparison of the expression of miR-326 between interferon beta responders and non-responders in relapsing-remitting multiple sclerosis. *Cell J.* 22, 92–95. doi: 10.22074/cellj.2020.6486

Freed, W. J. (1976). The role of nerve-growth factor (NGF) in the central nervous system. *Brain Res. Bull.* 1, 393–412. doi: 10.1016/0361-9230(76)90033-2

Glaudemans, A. W., van Rheenen, R. W., van den Berg, M. P., Noordzij, W., Koole, M., Blokzijl, H., et al. (2014). Bone scintigraphy with (99m)technetium-hydroxymethylene diphosphonate allows early diagnosis of cardiac involvement in patients with transthyretin-derived systemic amyloidosis. *Amyloid* 21, 35–44. doi: 10.3109/13506129.2013.871250

Govoni, S., Pascale, A., Amadio, M., Calvillo, L., D'Elia, E., Cereda, C., et al. (2011). NGF and heart: is there a role in heart disease? *Pharmacol. Res.* 63, 266–277. doi: 10.1016/j.phrs.2010.12.017

Guo, L., Luo, C., Fan, J., Hou, Z., Ji, X., Chen, F., et al. (2015). Serum miRNA profiling identifies miR-150/30a as potential biomarker for workers with damaged nerve fibers from carbon disulfide. *Ind. Health* 53, 38–47. doi: 10.2486/indhealth.2014-0120

Huang, Z., Zhang, L., Zhu, D., Shan, X., Zhou, X., Qi, L. W., et al. (2017). A novel serum microRNA signature to screen esophageal squamous cell carcinoma. *Cancer Med.* 6, 109–119. doi: 10.1002/cam4.973

Hutt, D. F., Fontana, M., Burniston, M., Quigley, A. M., Petrie, A., Ross, J. C., et al. (2017). Prognostic utility of the Perugini grading of 99mTc-DPD scintigraphy in transthyretin (ATTR) amyloidosis and its relationship with skeletal muscle and soft tissue amyloid. *Eur. Heart J. Cardiovasc. Imaging* 18, 1344–1350. doi: 10.1093/ehjci/jew325

Hwang, K. S., Lazaris, A. S., Eastman, J. A., Teng, E., Thompson, P. M., Gylys, K. H., et al. (2015). Plasma BDNF levels associate with Pittsburgh compound B binding in the brain. *Alzheimers Dement.* 1, 187–193. doi: 10.1016/j.dadm.2015.01.005

Jiang, X., Huang, H., Li, Z., Li, Y., Wang, X., Gurbuxani, S., et al. (2012). Blockade of miR-150 maturation by MLL-fusion/MYC/LIN-28 is required for MLL-associated leukemia. *Cancer Cell* 22, 524–535. doi: 10.1016/j.ccr.2012.08.028

Jonker, D. L., Hazenberg, B. P. C., Nienhuis, H. L. A., Slart, R. H. J. A., Glaudemans, A. W. J. M., and Noordzij, W. (2018). Imaging cardiac innervation in hereditary transthyretin (ATTRm) amyloidosis: a marker for neuropathy or cardiomyopathy in case of heart failure? *J. Nucl. Cardiol.* [Epub ahead of print]. doi: 10.1007/s12350-018-01477-y

Kempf, S. J., Metaxas, A., Ibáñez-Vea, M., Darvesh, S., Finsen, B., and Larsen, M. R. (2016). An integrated proteomics approach shows synaptic plasticity changes in an APP/PS1 Alzheimer's mouse model. *Oncotarget* 7, 33627–33648. doi: 10.18632/oncotarget.9092

Kermani, P., and Hempstead, B. (2019). BDNF actions in the cardiovascular system: roles in development, adulthood and response to injury. *Front. Physiol.* 10:455. doi: 10.3389/fphys.2019.00455

Kobrinsky, E., Duong, S. Q., Sheydina, A., and Soldatov, N. M. (2011). Microdomain organization and frequency-dependence of CREB-dependent transcriptional signaling in heart cells. *FASEB J.* 25, 1544–1555. doi: 10.1096/fj.10-176198

Kong, Y. W., Ferland-McCollough, D., Jackson, T. J., and Bushell, M. (2012). microRNAs in cancer management. *Lancet Oncol.* 13, e249–e258. doi: 10.1016/S1470-2045(12)70073-6

Kreusser, M. M., and Backs, J. (2014). Integrated mechanisms of CaMKII-dependent ventricular remodeling. *Front. Pharmacol.* 5:36. doi: 10.3389/fphar.2014.00036

Li, X., Teng, C., Ma, J., Fu, N., Wang, L., Wen, J., et al. (2019). miR-19 family: a promising biomarker and therapeutic target in heart, vessels and neurons. *Life Sci.* 232:116651. doi: 10.1016/j.lfs.2019.116651

Ludwig, N., Leidinger, P., Becker, K., Backes, C., Fehlmann, T., Pallasch, C., et al. (2016). Distribution of miRNA expression across human tissues. *Nucleic Acids Res.* 44, 3865–3877. doi: 10.1093/nar/gkw116

Lugli, G., Cohen, A. M., Bennett, D. A., Shah, R. C., Fields, C. J., Hernandez, A. G., et al. (2015). Plasma exosomal miRNAs in persons with and without Alzheimer disease: altered expression and prospects for biomarkers. *PLoS One* 10:e0139233. doi: 10.1371/journal.pone.0139233

Luigetti, M., Bisogni, G., Romano, A., Di Paolantonio, A., Barbato, F., Primicerio, G., et al. (2018). Sudoscan in the evaluation and follow-up of patients and carriers with TTR mutations: experience from an Italian Centre. *Amyloid* 25, 242–246. doi: 10.1080/13506129.2018.1545640

Majer, A., Medina, S. J., Niu, Y., Abrenica, B., Manguiat, K. J., Frost, K. L., et al. (2012). Early mechanisms of pathobiology are revealed by transcriptional temporal dynamics in hippocampal CA1 neurons of prion infected mice. *PLoS Pathog.* 8:e1003002. doi: 10.1371/journal.ppat.1003002

Mazzeo, A., Russo, M., Di Bella, G., Minutoli, F., Stancanelli, C., Gentile, L., et al. (2015). Transthyretin-related familial amyloid polyneuropathy (TTR-FAP): a single-center experience in Sicily, an Italian endemic area. *J. Neuromuscul. Dis.* 2, S39–S48. doi: 10.3233/JND-150091

Minutoli, F., Di Bella, G., Mazzeo, A., Laudicella, R., Gentile, L., Russo, M., et al. (2019). Serial scanning with 99mTc-3, 3-diphosphono-1, 2-propanodicarboxylic acid (99mTc-DPD) for early detection of cardiac amyloid deposition and prediction of clinical worsening in subjects carrying a transthyretin gene mutation. *J. Nucl. Cardiol.* [Epub ahead of print]. doi: 10.1007/s12350-019-01950-2

Molasy, M., Walczak, A., Szaflik, J., Szaflik, J. P., and Majsterek, I. (2017). MicroRNAs in glaucoma and neurodegenerative diseases. *J. Hum. Genet.* 62, 105–112. doi: 10.1038/jhg.2016.91

Ng, R., Song, G., Roll, G. R., Frandsen, N. M., and Willenbring, H. (2012). A microRNA-21 surge facilitates rapid cyclin D1 translation and cell cycle progression in mouse liver regeneration. *J. Clin. Invest.* 122, 1097–1108. doi: 10.1172/JCI46039

Obici, L., Kuks, J. B., Buades, J., Adams, D., Suhr, O. B., Coelho, T., et al. (2016). Recommendations for presymptomatic genetic testing and management of individuals at risk for hereditary transthyretin amyloidosis. *Curr. Opin. Neurol.* 29(Suppl. 1), S27–S35. doi: 10.1097/WCO.0000000000000290

Png, K. J., Halberg, N., Yoshida, M., and Tavazoie, S. F. (2011). A microRNA regulon that mediates endothelial recruitment and metastasis by cancer cells. *Nature* 481, 190–194. doi: 10.1038/nature10661

Rayner, K. J., Esau, C. C., Hussain, F. N., McDaniel, A. L., Marshall, S. M., van Gils, J. M., et al. (2011). Inhibition of miR-33a/b in non-human primates raises plasma HDL and lowers VLDL triglycerides. *Nature* 478, 404–407. doi: 10.1038/nature10486

Rodriguez-Lebron, E., Liu, G., Keiser, M., Behlke, M. A., and Davidson, B. L. (2013). Altered Purkinje cell miRNA expression and SCA1 pathogenesis. *Neurobiol. Dis.* 54, 456–463. doi: 10.1016/j.nbd.2013.01.019

Sakamoto, K., Karelina, K., and Obrietan, K. (2011). CREB: a multifaceted regulator of neuronal plasticity and protection. *J. Neurochem.* 116, 1–9. doi: 10.1111/j.1471-4159.2010.07080.x

Sang, W., Wang, Y., Zhang, C., Zhang, D., Sun, C., Niu, M., et al. (2016). MiR-150 impairs inflammatory cytokine production by targeting ARRB-2 after blocking CD28/B7 costimulatory pathway. *Immunol. Lett.* 172, 1–10. doi: 10.1016/j.imlet.2015.11.001

Scrutinio, D., Conserva, F., Passantino, A., Iacoviello, M., Lagioia, R., and Gesualdo, L. (2017). Circulating microRNA-150-5p as a novel biomarker for advanced heart failure: a genome-wide prospective study. *J. Heart Lung Transplant.* 36, 616–624. doi: 10.1016/j.healun.2017.02.008

Vita, G., Vita, G. L., Stancanelli, C., Gentile, L., Russo, M., and Mazzeo, A. (2019). Genetic neuromuscular disorders: living the era of a therapeutic revolution. Part 1: peripheral neuropathies. *Neurol. Sci.* 40, 661–669. doi: 10.1007/s10072-019-03778-7

Vita, G. L., Polito, F., Oteri, R., Arrigo, R., Ciranni, A. M., Musumeci, O., et al. (2018). Hippo signaling pathway is altered in Duchenne muscular dystrophy. *PLoS One* 13:e0205514. doi: 10.1371/journal.pone.0205514

Wang, X., Chen, Q., Yi, S., Liu, Q., Zhang, R., Wang, P., et al. (2019). The microRNAs let-7 and miR-9 down-regulate the axon-guidance genes Ntn1 and Dcc during peripheral nerve regeneration. *J. Biol. Chem.* 294, 3489–3500. doi: 10.1074/jbc.RA119.007389

Wong, K. M., Babetto, E., and Beirowski, B. (2017). Axon degeneration: make the Schwann cell great again. *Neural Regen. Res.* 12, 518–524. doi: 10.4103/1673-5374.205000

Wu, Q., Jin, H., Yang, Z., Luo, G., Lu, Y., Li, K., et al. (2010). MiR-150 promotes gastric cancer proliferation by negatively regulating the pro-apoptotic gene EGR2. *Biochem. Biophys. Res. Commun.* 392, 340–345. doi: 10.1016/j.bbrc.2009.12.182

Zhou, H., Li, N., Yuan, Y., Jin, Y. G., Guo, H., Deng, W., et al. (2018). Activating transcription factor 3 in cardiovascular diseases: a potential therapeutic target. *Basic Res. Cardiol.* 113:37. doi: 10.1007/s00395-018-0698-6

Zouari, H. G., Ng Wing Tin, S., Wahab, A., Damy, T., and Lefaucheur, J. P. (2019). Assessment of autonomic innervation of the foot in familial amyloid polyneuropathy. *Eur. J. Neurol.* 26:94-e10. doi: 10.1111/ene.13774

Conflict of Interest: The authors declare that the research was conducted in the absence of any commercial or financial relationships that could be construed as a potential conflict of interest.

Advantages of publishing in Frontiers

OPEN ACCESS
Articles are free to read for greatest visibility and readership

FAST PUBLICATION
Around 90 days from submission to decision

HIGH QUALITY PEER-REVIEW
Rigorous, collaborative, and constructive peer-review

TRANSPARENT PEER-REVIEW
Editors and reviewers acknowledged by name on published articles

Frontiers
Avenue du Tribunal-Fédéral 34
1005 Lausanne | Switzerland

Visit us: www.frontiersin.org
Contact us: frontiersin.org/about/contact

REPRODUCIBILITY OF RESEARCH
Support open data and methods to enhance research reproducibility

DIGITAL PUBLISHING
Articles designed for optimal readership across devices

FOLLOW US
@frontiersin

IMPACT METRICS
Advanced article metrics track visibility across digital media

EXTENSIVE PROMOTION
Marketing and promotion of impactful research

LOOP RESEARCH NETWORK
Our network increases your article's readership